The Synthesis and Characterisation of Novel Rhodium(III) Heteroleptic Complexes.

By

Helen M. Burke, B.Sc. (Hons) A.M.R.S.C.

A Thesis presented to Dublin City University for the degree of Doctor of Philosophy.

Supervisor Prof. J.G. Vos,

School of Chemical Sciences,

Dublin City University.

2003

To my parents and Richard

I hereby certify that this material, which I now submit for assessment on the programme of study leading to the award of Doctor of Philosophy by Research and Thesis is entirely my own work and has not been taken from the work of others save and to the extent that such work has been cited and acknowledged within the text of my work.

Signed: Helen Ryelce

ID No.: 9791070O

Date: 19:09:03

Anybody who has been seriously engaged in scientific work of any kind realizes that over the entrance to the gates of the temple of science are written the words:

'Ye must have faith.'

It is a quality which the scientist cannot dispense with.

Max Planck (1858 - 1947)

"The trouble with the world is that the stupid are cocksure and the intelligent full of doubt."

Bertrand Russell.

ACKNOWLEDGEMENTS

Finally, the time has come for me to relinquish my student card and acknowledge those who nudged, helped and in some cases booted me to this stage!

Firstly I would like to thank Prof. Han Vos for his guidance, support and patience over the years. Thanks for all the advice on writing this thesis, however, the English lessons can now stop! I guess there's really only one thing left to say ..... where's the Christmas dinner going to be this year?!?

I would also like to thank Prof. Franco Scandola and Prof. Maria Teresa Indelli for helping me to get started in the world of rhodium chemistry and Anna Prodi for all her help during my time at Ferrara.

I owe particular thanks to the all of the technicians and especially to Mick who has the uncanny ability to do ten things at once and be in two places at the same time - without your generosity with NMR tubes I would be still be running experiments! My thanks also to Maurice for helping me out with my mass specs and of course there's my paper supplier Ambrose!

And now to the postgrads!! It's difficult to know where to begin but I guess the HVRG is the best place to start. There's the golden oldies - Sporty Spice Scott, Adrian (you'll always be New Boy!), Marco (the style guru), Dec, Auntie Anthea, Egbert, Stefano, Christine, Luke, Frances and the new recruits Fiona I, Fiona II, Noel, Bill, Clare and Stefania - my thanks for all the laughs and the memories. My particular thanks go to Wesley for all his help and support and in particular for knowing so much about photophysics.....you saved me a lot of time!!! From the far side there's the CLRG, Peter, Bronagh, Kieran, Karl, Johnny, Jennifer and Kevin – thanks for having your side of the lab stocked when our side ran out! To the members of the RFRG thanks for

letting me invade your lab and in particular to Johan for sharing his electrochemistry trade secrets!

And now to the girls! Carol, Davnat, Mairead, Jenni, Edel and I guess I can include Ger and Neil as honorary girlies!! Thank you all so much for all the laughs through the years and for being there in good times and bad. I guess from now on we'll have to arrange to have our tea breaks elsewhere!!

I owe a huge amount of thanks to my parents, Linda and Angela for all their patience support and encouragement down the years. At this point I am happy to say that life can return to normal, that you can finally turn the stereo on high again Dad and Angela you can have it in writing to I will be coming to visit you soon! To members of the extended family you can now stop asking me if I am still a student……I have a job!

And finally, but by no means least, my thanks to Richard for his support over the years. To your relief I will now stop talking chemistry and actually be free at weekends!! Thanks for always being there to keep me sane, to cheer me up and to put a smile on my face! Thanks mostly for just being you!

ABSTRACT

It is the aim of the work that will be discussed in the following thesis to contribute to the field of Rh(III) polypyridyl chemistry. A series of heteroleptic Rh(III) polypyridyl complexes have been synthesised and characterised from the perspective of studying the effect of ligand variation and it was also hoped that it would be possible to develop dinuclear Ru(II)-Rh(III) complexes in which both the electron donor and the electron acceptor would be photoexcitable units.

A series of complexes of the form $[Rh(L)_2(L')]^{n+}$ where L = bpy or phen, L' = a pyridine triazole / pyrazine triazole/ triazine or imidazo based ligand and n = 2 or 3 have been synthesised and characterised. Chapter 3 focuses upon the synthesis, purification and structural characterisation of the complexes incorporating pyridine triazole ligands whereas Chapter 5 details the synthesis and structural characterisation of the complexes incorporating pyrazine, triazine, imidazole and triazole based ligands. Whilst particular emphasis was placed on the synthesis and structural characterisation of these complexes, their photophysical and electrochemical properties were also studied and Chapters 4 and 6 detail the results of these studies. The complexes all contain ligands with different σ-donor and π-acceptor properties and their characterisation aims to determine if the variation of these ligand properties influences their photophysical and electrochemical properties. Their behaviour is compared with that of the tris homoleptic complexes $[Rh(phen)_3]^{3+}$ and $[Rh(bpy)_3]^{3+}$ and where possible with analogous Ru(II) complexes. Chapter 7 details the numerous synthetic approaches which were taken in attempts to synthesise Rh(III)/Ru(II) dinuclear complexes and also discusses the difficulties which were encountered. Chapter 8 aims to take the results discussed throughout the thesis into consideration and discusses the issues of coordination modes, protonation states and the photophysical and electrochemical properties of all of the complexes synthesised, with particular emphasis being placed upon their behaviour in relation to their ligand σ-donor and π-acceptor strengths. Having analysed the results obtained, Chapter 8 also proposes avenues through which this research can progress.

TABLE OF CONTENTS

Chapter **Page No.**

Abbreviation	
bpy	2,2'-bipyridine
TEOA	triethanolamine
phen	1,10-phenanthroline
phi	9,10-phenanthrenequinone diimine
ppy	2-phenylpyridine
thpy	2-(2-thienyl)pyridine
tpy	2,2':6'2''-terpyridine
biq	2,2'-biquinoline
TAP	1,4,5,8-tetraazaphenanthrene
pq	2-(2'-pyridyl)quinoline
dpb	2,3-bis(2-pyridyl)-benzoquinoxaline
Hbpt	3,5-bis(pyridin-2-yl)-1,2,4-triazole
NH_2bpt	4-amino-3,5-bis(pyridin-2-yl)-4H-1,2,4-triazole
bpm	2,2'-bipyrimidine
HAT	1,4,5,8,9,12-hexaazatriphenylene
dpp	2,3-bis(2-pyridyl)pyrazine
dpq	2,3-bis(2-pyridyl)-quinoxaline
MC	metal centred
LC	ligand centred
LMCT	ligand to metal charge transfer
MLCT	metal to ligand charge transfer
CTTS	charge transfer to solvent
LLCT	ligand to ligand charge transfer
py	pyridine
CT	charge transition
FWHM	full width at half maximum
5,6-Mephen	5,6-dimethyl-1,10-phenanthroline

Abbreviation	
ODMR	optically detected magnetic resonance
zfs	zero field splitting
4-Mephen	4-methyl-1,10-phenanthroline
4,7-Me_2phen	4,7-dimethyl-1,10-phenanthroline
3,4,7,8-Me_4phen	3,4,7,8-tetramethyl-1,10-phenanthroline
dp-phen	4,7-diphenyl-phenanthroline
TEAP	tetraethylammonium-perchlorate
SCE	saturated calomel electrode
E_{pa}	anodic peak potential
E_{pc}	cathodic peak potential
$E_{½}$	half wave potential
DMF	dimethylformamide
TBAH	tetra-*n*-butylammonium hexafluorophosphate
TFMS	trifluoromethanesulphonate anion
bzq	benzo[h]quinoline
ptpy	2-(*p*-tolyl)pyridine
mppy	3-methyl-2-phenylpyridine
bpca	bis(2-pyridylcarbonyl)amide
dppt	5,6-diphenyl-3-(pyridin-2-yl)-1,2,4-triazine
FID	free induction decay
***d_6*-DMSO**	d_6-dimethylsulphoxide
TMS	trimethylsilane
COSY	correlation spectroscopy
HMQC	heteronuclear multiple quantum coherence
TCSPC	time correlated single photon counter
TAC	time-to-amplitude converter

Abbreviation	
MCA	multichannel analyser
$TBABF_4$	tetrabutylammonium-fluoroborate
CV	cyclic voltammetry
DPV	differential pulse voltammetry
IUPAC	International Union of Pure and Applied Chemistry
Hpytr	3-(pyridin-2-yl)-1,2,4-triazole
HPLC	high performance liquid chromatography
tfb	tetrafluorobenzobicyclo-[2,2,2]octatriene
cod	1,5-cyclooctadiene
nbd	bicyclo[2,2,1]heptadiene
4Mpytr	4-methyl-3-(pyridin-2-yl)-1,2,4-triazole
1M3pytr	1-methyl-3-(pyridin-2-yl)-1,2,4-triazole
HPhpytr	3-phenyl-5-(pyridin-2-yl)-1,2,4-triazole
Hpt	3-(2-phenol)-5-(pyridin-2-yl)-1,2,4-triazole
(d)	doublet
(dd)	double doublet
(s)	singlet
m/z	mass to charge ratio
EI-MS	electrospray ionisation mass spectrometry
Amu	atomic mass units
3,3'-dmbpy	3,3'-dimethyl-2, 2'-bipyridine
sh	shoulder
LUMO	lowest unoccupied molecular orbital

Abbreviation	
HOMO	highest occupied molecular orbital
Ox/red	oxidation/reduction
i_{pa}	anodic peak current
i_{pc}	cathodic peak potential
i_p	peak current
ΔE_p	pulse amplitude
Fc	ferrocene
Hppt	3-(pyridin-2-yl)-5-(pyrazine-2-yl)-1,2,4-triazole
Hpztr	3-(pyrazin-2-yl)-1,2,4-triazole
Hbpzt	3,5-bis(pyrazin-2-yl)-1,2,4-triazole
HPhpztr	3-phenyl-5-(pyrazin-2-yl)-1,2,4-triazole
PIP	1-pyridin-2-yl-imadazo-[1,5-a]-pyridine
MePIP	3-methyl-pyridin-2-yl-imadazo-[1,5-a]-pyridine
PTP	3-pyridin-2-yl-triazolo-[4,3-a]-pyridine
tptz	2,4,6-tris(pyridin-2-yl)-1,3,5-triazine
tpt	3,4,6-tris(pyridin-2-yl)-1,2,5-triazine
dmpt	5,6-dimethyl-3-(pyridin-2-yl)-1,2,4-triazine
PMD	photochemical molecular device
***p*-pytbzpyt**	1,4 -bis(5-(pyridin-2-yl)-1,2,4-triazol-3-yl)benzene
***m*-pytbzpyt**	1,3-bis(5-(pyridin-2-yl)-1,2,4-triazol-3-yl)benzene
***p*-Mepytbzpyt**	1,4-bis(5-(pyridin-2-yl)-1,2,4-triazol-3-yl)benzene

Chapter 1 - Introduction

"Things should be made as simple as possible, but not any simpler."

Albert Einstein

Abstract: In the field of polypyridyl transition metal complexes a great deal of emphasis has been placed upon ruthenium(II) complexes, particularly $[Ru(bpy)_3]^{2+}$, whereas relatively little attention has been paid to the analogous rhodium(III) complexes. This thesis aims to contribute to the development and further understanding of Rh(III) polypyridyl complexes. The following chapter aims to provide a synopsis of developments to date in this area. Whilst the occurrence and applications of rhodium are introduced, the discussion focuses primarily on developments with respect to the synthesis and characterisation of Rh(III) polypyridyl complexes with particular emphasis being placed upon their photophysical and electrochemical behaviour.

1.1 Introduction – Occurrence and Applications of Rhodium

Rhodium is a fairly soft, ductile, silver-white metal and was first discovered in 1803 by William Hyde Wollaston. It has an abundance of approximately $4x10^{-4}$ppm in the earth's crust and along with ruthenium, osmium, iridium, palladium and platinum is referred to as a platinum metal. Rhodium has several potential oxidation states the most important of which are I and III with the latter being the most common. Other oxidation states are rare. Table 1.1 illustrates the possible rhodium oxidation states and examples are given.[1,2]

Table 1.1 Possible rhodium oxidation states.[1]

Oxidation State	Examples
Rh(-I)	$[Rh(CO)_4]^-$, $[Rh(CO)_2(PPh_3)_2]^-$
Rh(0)	$Rh_4(CO)_{12}$, $Rh_6(CO)_{16}$
Rh(I)	$[Rh(CO)_2Cl]_2$, $[Rh(C_2H_4)_2Cl]_2$
Rh(II)	$[Rh(OAc)_2]_2$,
Rh(III)	$[Rh(NH_3)_6]^{3+}$,
Rh(IV)	$K_2[RhF_6]$
Rh(V)	$[RhF_5]_4$
Rh(VI)	RhF_6

Rhodium is predominantly used for catalytic purposes in particular in the hydroformylation of olefins and the carbonylation of methanol in the production of acetic acid. A number of systems have also been reported where $[Rh(bpy)_3]^{3+}$, bpy = 2,2'-bipyridyl, has been used as relays and redox catalysts in the photochemical evolution of H_2 from water.[3,4,5] Mann *et. al.* reported the production of hydrogen by 546 nm irradiation of a dinuclear rhodium(I) complex in acidic aqueous solution and Brown *et. al.* described the mechanism of the formation of dihydrogen from the photoinduced reactions of $[Ru(bpy)_3]^{2+}$ and $[Rh(bpy)_3]^{3+}$.[3,4] They found that visible irradiation of aqueous solutions of $[Ru(bpy)_3]^{2+}$ and $[Rh(bpy)_3]^{3+}$, TEOA/$TEOAH^+$ (pH 8.1) where TEOA = triethanolamine and K_2PtCl_4 yielded dihydrogen as the end product of a series of electron transfer reactions:

Irradiation with visible light gives rise to $^{*}[Ru(bpy)_3]^{2+}$ which in turn is oxidised by $[Rh(bpy)_3]^{3+}$ to produce $[Ru(bpy)_3]^{3+}$ and $[Rh(bpy)_3]^{2+}$. TEOA reduces $[Ru(bpy)_3]^{3+}$ and the Rh(II) in the presence of platinum can either disproportionate or yield dihydrogen or in the absence of platinum disproportionates to give Rh(III) and Rh(I).[4] Creutz *et. al.* reported the formation of dihydrogen from photoinduced reactions of polypyridine ruthenium(II) and polypyridine rhodium (III) complexes the outline of which can be seen in Figure 1.1.[6]

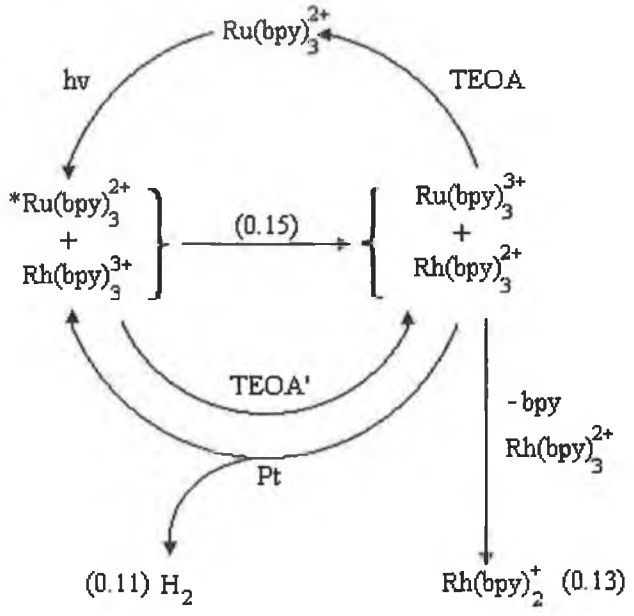

Figure 1.1 Outline of reaction pathways leading to the production of H_2. [6]

Lehn *et. al.* have also outlined a photochemical system for the generation of hydrogen by water reduction by either sunlight or UV-VIS light which consists of two catalytic processes, a ruthenium cycle and a rhodium cycle.[7,8] Rhodium has been used as a minor constituent of platinum alloys in the production of nitric acid, glass and glass fibre materials and in thermocouples. Recent developments have also seen an increase in interest in rhodium complexes for biological and medicinal purposes.[9,10,11] A number of reviews deal with progress in the field of rhodium coordination chemistry such as those by Housecroft, Hannon and DeWit.[12,13,14,15] For the purpose of this discussion it is necessary to focus upon rhodium polypyridyl complexes rather than the development of rhodium systems for catalytic purposes.

A vast amount of research has been dedicated to the study of the synthesis and characterisation of Ru(II) polypyridyl complexes, in particular $[Ru(bpy)_3]^{2+}$, whereas relatively little attention has been paid to the analogous Rh(III) complexes.[16] It is the aim of the following discussion to give a brief overview of the field of rhodium polypyridyl chemistry to date, focusing primarily upon the synthesis, the photophysical and the electrochemical properties of rhodium(III) systems with a brief discussion of Rh(II) and Rh(I) systems.

From a ligand perspective the ligand 2,2'-bipyridine (bpy) is the one most predominantly integrated into transition metal polypyridyl complexes and is considered to be the "parent ligand".[17] The bpy ligand has generated extensive interest as a metal chelating ligand because of its robust redox stability and due to the ease of functionalisation of the ligand. The fact that the ligand itself is neutral also allows for the formation of charged complexes with metal cations.[17] The properties of transition metal polypyridyl complexes are governed by the σ-donor and π-acceptor properties of the ligands and these may be divided into one of two classes upon comparison with the "parent" ligand, bpy. The first class, Class I type ligands, are weaker σ-donors and stronger π-acceptors than bpy and the second class, Class II type ligands, are stronger σ-donors and weaker π-acceptors than bpy. Class II ligands donate much electron density into the metal d orbitals thus lowering oxidation potentials and causing more negative reduction potentials whereas Class I ligands stabilise the filled d-orbitals giving rise to high oxidation potentials and low reduction potentials.

Table 1.2 ***Examples of Class I and Class II Type Ligands.***

Class I Type Ligands	**Class II Type Ligands**
2,2'-bipyrazine	Imidazole
2,2'-bipyrimidine	Pyrazole
2,2'-biquinoline	1,2,4-triazole

Thus it can be seen that based upon a judicious choice of ligands it is possible to control the redox potentials and the energies of the emission and absorption bands. The ligands, which will be discussed in this chapter, can be seen in Figure 1.2 and Figure 1.3.

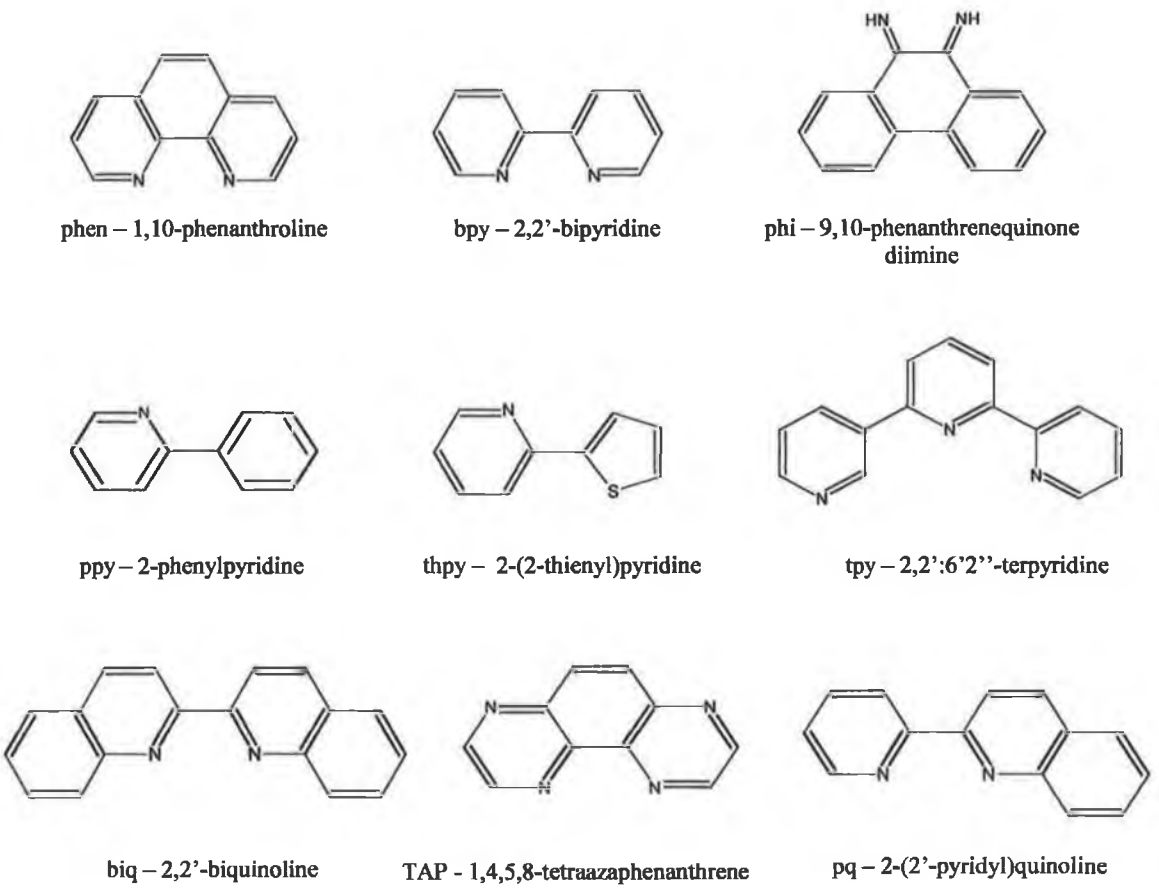

Figure 1.2 Structures of chelating ligands cited in the following discussion.

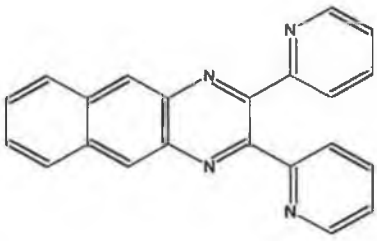

dpb – 2,3-bis(2-pyridyl)benzoquinoxaline

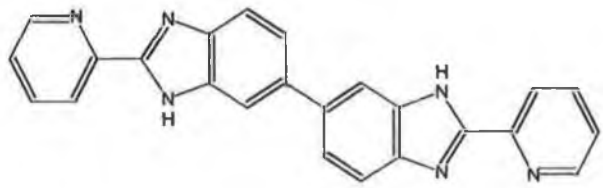

2,2'-bis(2-pyridyl)-6,6'-bibenzimidazole

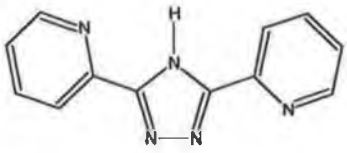

Hbpt – 3,5-bis(pyrdin-2-yl)-1,2,4-triazole

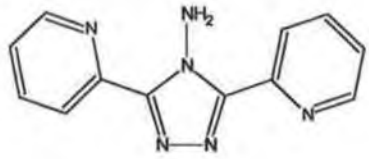

NH_2bpt – 4-amino-3,5-bis(pyrdin-2-yl)-4H-1,2,4-triazole

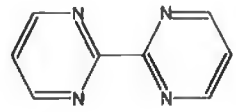

bpm – 2,2'-bipyrimidine

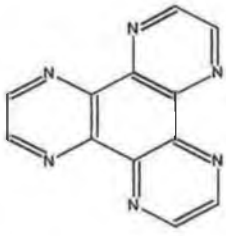

HAT - 1,4,5,8,9,12-hexaazatriphenylene

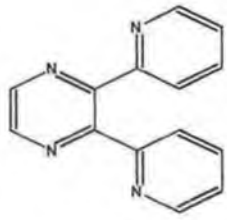

dpp – 2,3-bis(2-pyridyl)pyrazine

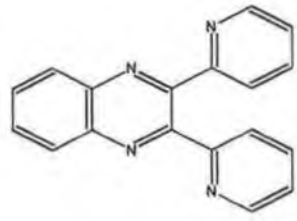

dpq – 2,3-bis(2-pyridyl)-quinoxaline

Figure 1.3 Structures of potential bridging ligands cited in following discussion.

1.2 Synthetic Aspects of Rhodium(III) Polypyridyl Complexes

In the synthesis of rhodium compounds $RhCl_3 \cdot xH_2O$ is predominantly used as a starting material. This starting material is obtained by dissolving Rh_2O_3 in HCl. Evaporation of the solution gives rise to the dark red deliquescent $RhCl_3 \cdot xH_2O$ material that is soluble in alcohols and water. Figure 1.4 outlines some of the reactions in which $RhCl_3 \cdot xH_2O$ is employed.[18]

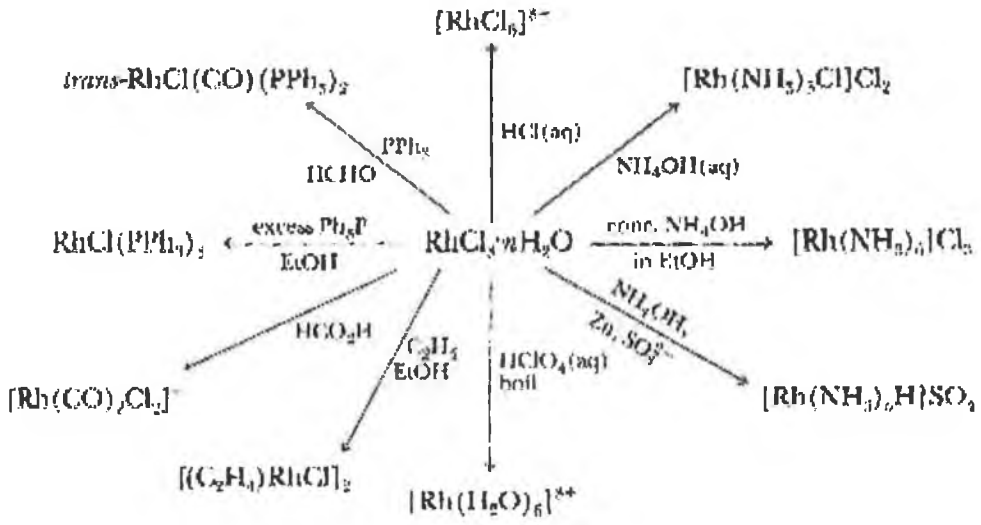

Figure 1.4 Reactions of $RhCl_3 \cdot xH_2O$.[18]

From the perspective of the synthesis of bis- and tris-homoleptic rhodium polypyridyl complexes, the synthetic route reported by Gillard *et. al.* is generally applied.[19] By this method it is possible to synthesise complexes $[Rh(L)_2Cl_2]Cl$ where L is a polypyridyl ligand such as bpy or 1,10-phenanthroline (phen) by boiling $RhCl_3.xH_20$ with either ligand in the ratio 1mmol : 2.2mmol in ethanol : water 1:1.5 for approximately 10 minutes. At this time the addition of a catalytic amount of hydrazinium monochloride gives rise to a pale yellow solution which upon cooling gives rise to $[Rh(L)_2Cl_2]Cl$, where L = bpy / phen, with a yield of approximately 70%.[19] In theory $[Rh(bpy)_2Cl_2]Cl$ and $[Rh(phen)_2Cl_2]Cl$ may assume either of two possible geometrical isomers but only a single isomer has ever been observed. It was initially thought that the product obtained assumed a *trans*-octahedral geometry but this was later shown to be incorrect by McKenzie and Plowman.[20,21] They characterised three polymorphs of $[Rh(phen)_2Cl_2]Cl \cdot xH_2O$, one of which was found

to be isomorphous with the previously studied $[Co(phen)_2Cl_2]Cl{\cdot}3H_2O$ and based upon this it was concluded that the *cis* form of both complexes, $[Rh(bpy)_2Cl_2]Cl$ and $[Rh(phen)_2Cl_2]Cl$, was exclusively formed. One possible reason for the exclusive formation of the *cis* isomers of $[Rh(bpy)_2Cl_2]Cl$ and $[Rh(phen)_2Cl_2]Cl$ is that if formed, the *trans* form of the complexes would experience a marked steric interaction between the α-hydrogen atoms of the opposite chelating ligands.[22,23,24]

The syntheses of tris-homoleptic and heterotrischelated complexes tend to require extended reflux times and / or more rigorous reaction conditions.[19,20,25] The synthesis of tris-homoleptic complexes are possible via the method reported by Gidney *et. al.* using a 3.3mmol:1mmol ratio of ligand : $RhCl_3.xH_20$ and again using hydrazinium monochloride as a catalyst. In contrast to the syntheses of the bis complexes, which required heating for 10 minutes, the tris complexes required boiling for 30 minutes.[19] The heterotrischelated complexes are generally synthesised by addition of the required ligand to the bis complex. The synthesis of $[Rh(tpy)(bpy)(py)](ClO_4)_3{\bullet}H_2O$,where tpy is 2,2':6'2''-terpyridine, for example is carried out using the bis complex $[Rh(tpy)(bpy)Cl](ClO_4)_2{\bullet}3H_2O$ and by refluxing this in ethanol for 10 hours in the presence of pyridine.[26] It is known that complexes such as $[Rh(phen)_2Cl_2]Cl$ do not readily displace coordinated chloride ligands for a third bidentate ligand. This problem may be circumvented in some situations by forming the corresponding aqua complex, which tends to be more reactive. Barton *et. al.* have reported the synthesis of $[Rh(phen)_2(phi)]Cl_3$, where phi is 9,10-phenanthrenequinone diimine, using this approach.[27]

The purification of rhodium(III) polypyridyl complexes has been carried out by various chromatographic methods. Both ion exchange chromatography (Sephadex C-25) and particle size exclusion (Sephadex LH-20) have been employed. In the case of C-25 column chromatography NaCl, HCl and $NaHCO_3$ have been used as eluents, whereas, LH-20 generally uses either methanol or a methanol-acetonitrile mixture as eluent.[28,29,30,31,32] Purification on both silica and alumina has also been reported. Methanol is normally used for alumina columns whereas the mixture of acetonitrile:water: KNO_3 in the ratio 40:10:1 has proven to be effective on silica.[33]

1.3 Photophysical Properties of Rh(III) Polypyridyl Complexes

1.3.1 Concepts in Photophysics

Transition metal complexes have attracted a great deal of interest in recent years particularly due to their photochemical and photophysical properties. The development of various bridging ligands has allowed for the creation of numerous polynuclear complexes which have been used in the study of electron transfer processes, in attempts to mimic biological electron transfer processes and in the development of molecular devices.[34] If a photon of light, be it from the visible or the ultraviolet region, is absorbed by a metal complex M, then the metal complex will be transformed into an electronically excited state M*. When in an upper excited state level the molecule is usually also vibronically excited and rapid relaxation to the lowest excited state occurs in a few picoseconds or less. From this point M* may be involved in a number of processes; it may undergo a non radiative relaxation to a state of similar multiplicity i.e. an internal conversion, it may undergo a non radiative relaxation to a state of different multiplicity i.e. intersystem crossing, it may return to the ground state by either radiative means or by nonradiative means i.e. fluorescence or phosphorescence or a chemical pathway may be followed in which the complex is converted to product(s). It should be noted that fluorescence is the radiative deactivation pathway between states of the same multiplicity whereas phosphorescence involves states of different multiplicity.[35,36] A Jablonski diagram is the means usually used to illustrate the possible excited states, their relative energy ordering and possible interconversions for a complex. Figure 1.5 illustrates the Jablonski diagram for $[Rh(NH_3)_6]^{3+}$.[37] Information regarding the excited state of a complex can be obtained by several approaches. Spectroscopic analysis of the absorption of the ground state molecule in conjunction with theoretical models can give information regarding to energy levels, the state/configuration and symmetry of the possible excited state(s). The study of the luminescence observed from the excited state yields allows for the determination of the lifetime and yields of the excited state. Direct monitoring of the excited state may be achieved by using time resolved absorption and resonance Raman techniques.[16,18,36]

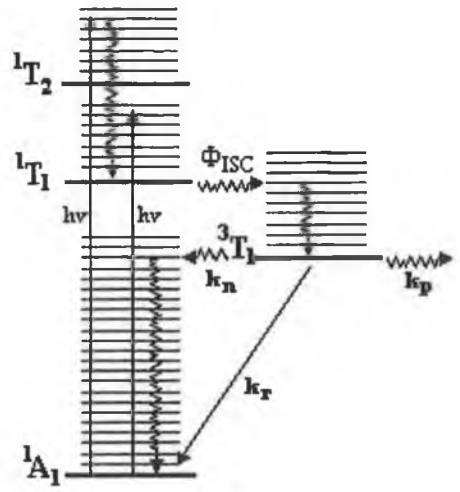

Figure 1.5 Jablonski diagram for $[Rh(NH_3)_6]^{3+}$ where Φ_{ISC} is the efficiency of the intersystem crossing from singlet states to lower energy triplet states, k_n and k_r are the nonradiative and radiative deactivation rate constants respectively and k_p is the rate constant for reactive deactivation to products.[37]

With respect to theoretical models, the first theory of electronic structure to be developed was crystal field theory. In crystal field theory a ligand lone pair is considered as a single point negative charge (or as the partial negative charge of an electric dipole) that repels electrons in the d orbitals of the central metal ion. Upon coordination, the energies of the d electrons of the metal ion are raised but it should be noted that when we consider the geometry of the d electrons of the core metal ion, those that reside on d orbitals that are directed toward the ligands (the e_g set) are repelled more than those directed between the ligands (t_{2g} set). [18,36] This means that not all of the d electrons are destabilised to the same extent and this difference in the destabilisation energy, known as Δ_0 (where the subscript O stands for octahedral), gives rise to splitting of the d-orbital energies. Several factors control the magnitude of the crystal field splitting parameter, Δ_0. The chemical nature of the ligands has been seen to contribute to Δ_0. The following series represents ligands in order of increasing energy of transitions that occur when present in a complex:

$$I^- < Br^- < S^{2-} < SCN^- < Cl^- < NO_3^- < F^- < OH^- < C_2O_4^{2-} < H_2O < NCS^- CH_3CN < NH_3 < en < bpy < phen < NO_2^- < PPh_3 < CN^- < CO$$

As ligands are varied across the series there is an increase in the energy of the lowest energy electronic transition and accordingly in Δ_0 with this variation being seen irrespective of the metal centre. The metal centre is also a factor in the determination of Δ_0 as Δ_0 increases with increasing oxidation number and increases down a group.[36]

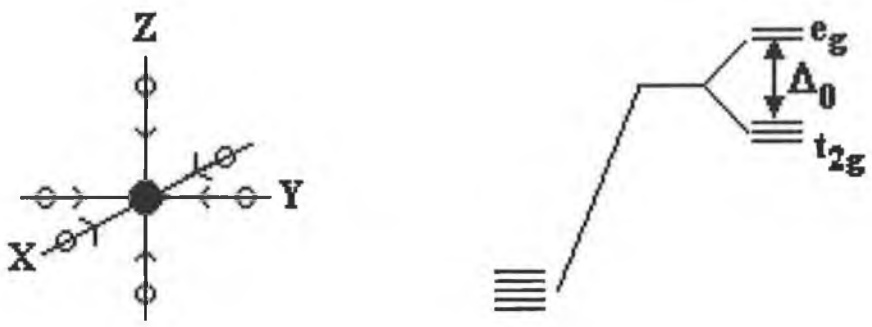

Figure 1.6 Illustration of the splitting of metal d orbitals in an octahedral ligand field.[16]

Whereas crystal field theory provides a simple and easy to envisage theory of electronic structure, ligand field theory focuses on the role of the d orbitals on the metal ion and their overlap with ligand orbitals.[18,36] When attempting to develop a composite electronic model to describe a complex using ligand field theory it is necessary to take all of the electrons involved in bonding localised both on the metal ion and on the ligand into consideration in two separate sets. Based upon this it is then possible to combine the molecular orbital diagrams of both the metal and the ligand to create a model representative of the system as a whole as may be seen in the energy level diagram in Figure 1.7.[34] Energy level diagrams such as the one seen in Figure 1.7 are dependent upon the nature of the metal orbitals and ligand orbitals in question and thus upon the nature of the complex. Derived from the fact that the relative disposition of both the metal and ligand orbitals can vary it is possible for several orbital arrangements to arise.

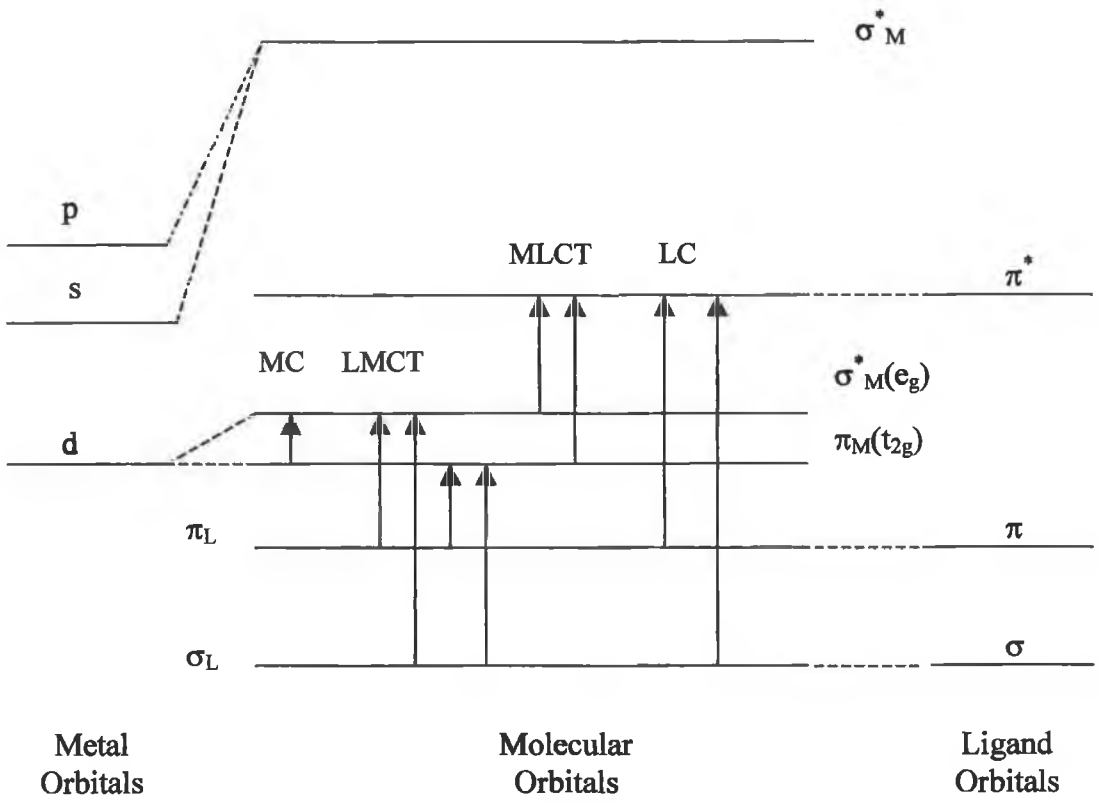

Figure 1.7 Energy level diagram for an octahedral transition metal complex.[34]

The various transitions, which may be observed in Figure 1.7, are as follows:

MC: transitions between molecular orbitals predominantly localised on the metal i.e. metal based

LC: transitions between orbitals predominantly localised on the ligand i.e. ligand centred transitions

LMCT: ligand-metal-charge-transfer

MLCT: metal-ligand-charge-transfer

Other transitions, which may be observed, are

CTTS: charge-transfer-to-solvent

LLCT: ligand-ligand-charge-transfer (this is possible if different ligands are present).[34]

1.3.2 Rh(III) Bis-polypyridyl Complexes – $[Rh(L)_2(X)_2]^+$, L = bpy/phen, X= Cl, Br, I

1.3.2.1 Absorption and Emission Properties

Of the bis-polypyridyl complexes studied to date the complexes $[Rh(bpy)_2Cl_2]Cl$ and $[Rh(phen)_2Cl_2]Cl$ have received the most attention. A number of bands may be identified in the absorption spectra of these complexes; a π-π^* band associated with the ligands may be seen below 333 nm, a split band around 289 nm can be attributed to interactions between the bpy/phen ligands and a weak visible band at approximately 405 nm has been attributed to the lowest ^{1}d-d* state.[16,38] As can be seen from Figure 1.8 these complexes exhibit a broad structureless emission at 77K.

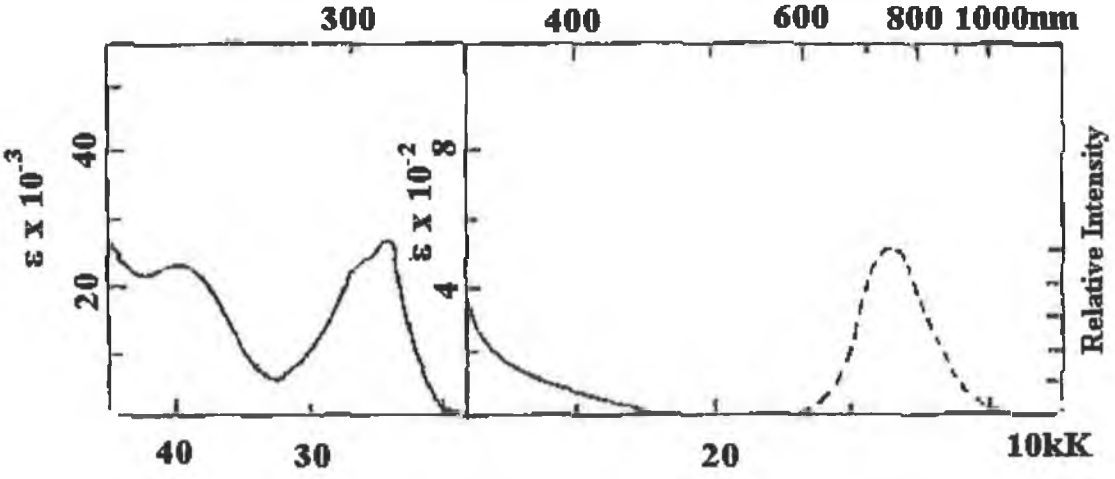

Figure 1.8 Absorption and emission spectra of $[Rh(bpy)_2Cl_2]Cl$. The absorption was measured in water at room temperature and the emission spectrum was measured in a water:ethanol glass (1:4) at 77K. [38]

A number of studies have been carried out in order to determine the origin of the emission observed for these complexes with early work indicating that emission originated from a $^3T_{1g}$(d-d) parent octahedral state and Carstens and Crosby attributed luminescence from these types of bis complexes to a d-d triplet-singlet transition.[38] This was subsequently borne out by another study carried out by Crosby *et. al.*[39] They focused on a series of complexes of the form *cis*-$[Rh(L)_2(L')_2]^+$ where

L = bpy or phen and L' = Cl, Br, I and *trans*-$[Rh(py)_4Br_2]Br$ where py = pyridine. In each instance, an intrinsic lifetime τ_0 was calculated using Equation 1.1.

$$k_r = \frac{1}{\tau_0} = \frac{Q}{\phi_{isc}\tau} \qquad \textbf{Equation 1.1}$$

Where k_r = a radiative rate constant,

τ_0 = the intrinsic lifetime,

Q = the absolute quantum yield upon excitation to a singlet state,

τ = the measured luminescence lifetime,

ϕ_{isc} = the intersystem-crossing yield.

A radiative rate constant k_r and a quenching rate constant k_q were also calculated for each. Crosby *et. al.* presented evidence for near unity intersystem crossing in each case and assigned the luminescence of each to a spin forbidden process.[39] This spin forbidden process was inferred from a number of observations the first of which was the analysis of the intrinsic lifetimes obtained for the complexes. The relevant data may be seen in Table 1.3.[39]

Table 1.3 Quantum yield and lifetimes for rhodium complexes. All measurements were carried out in an alcohol glass at 77K unless otherwise stated.[39]

Complex	Quantum Yield Q, ± std dev	Lifetime τ, μsec	Intrinsic lifetime τ_0,[a] μsec
cis-$[Rh(bpy)_2Cl_2]Cl$	0.0369 ± 0.0017	31.8 ± 0.5	862
cis-$[Rh(phen)_2Cl_2]Cl$	0.0417 ± 0.0014	33.9 ± 0.6	813
cis-$[Rh(bpy)_2Br_2]NO_3$	0.177 ± 0.011	18.0 ± 0.3	102
cis-$[Rh(phen)_2Br_2]NO_3$	0.194 ± 0.018	16.0 ± 0.1	82.5
cis-$[Rh(bpy)_2Cl_2]I$	0.55[c]	9.7[b]	17.5[c]
cis-$[Rh(phen)_2Cl_2]I$	0.46[c]	10.8[b]	23.7[c]
trans-$[Rh(py)_2Br_2]Br$	0.0806 ± 0.005	499 ± 2	6200

[a] Calculated using Equation 1.1. [b] Measured in methanol-water glass (4:1 v/v) at 77K. [c] Estimated values.

From Table 1.3 it can be seen that the intrinsic lifetimes of the *cis* chloro and bromo complexes are of the order of 0.1 ms or longer and in the case of *trans*-$[Rh(py)_2Br_2]Br$ τ_0 is ~6 ms. Dawson *et. al.* observed similar intrinsic lifetimes for a series of complexes of terbium and europium, both of which are elements having free ion, spin orbit coupling constants comparable to rhodium.[40] Because these rare-earth complexes were known to exhibit a spin and a Laporte-forbidden luminescence Crosby *et. al.* proposed that a spin forbidden process was also occurring for the rhodium complexes.[39] It can also be seen from Table 1.3 that upon halide variation in the *cis* complexes, i.e. by changing from chloro to bromo to iodo, a significant decrease (40 fold) in the intrinsic lifetime occurs. Such a large decrease is indicative of phosphorescence, as halide substitution generally causes no detectable effect upon the intrinsic fluorescent lifetimes. Both these factors in conjunction with the presence of a weak band ($\varepsilon \sim 3$) in the low temperature absorption spectrum of *trans*-$[Rh(py)_4Br_2]Br$ attributed to a $S_o \rightarrow T_1$, d-d transition led Crosby *et. al.* to the conclusion that a spin forbidden transition was occurring. Demas and Crosby also presented experimental evidence for rapid relaxation between states of different orbital configuration as follows; $\pi - \pi^* \rightarrow (d - \pi^*) \rightarrow d - d$.[39] It should be noted though that Ohashi *et. al.* have subsequently found evidence that suggested that direct energy transfer $^1(\pi - \pi^*) \rightarrow {}^3(\pi - \pi^*) \rightarrow {}^3(d - d)$ occurs.[41] Ohashi *et. al.* reported that for the complexes $[Rh(bpy)_2(L)_2]L$, where L = Cl or Br, the emission maxima shifts toward shorter wavelengths and the intensity decreases with increasing temperature.[41] The decrease in the intensity of the emission observed was caused by an increase in the nonradiative decay from the lowest triplet state upon increasing temperature. It was more difficult to account for the observed peak shifts in the emission spectra but one possible cause could be that with increasing temperature the difference in the positions of the potential minima between the ground state and the excited state decreases resulting in a peak shift in the emission spectrum to a higher frequency.[41]

A multiple emission is an interesting feature of the photophysics of rhodium complexes and is derived from excited states of different multiplicity and / or different orbital parentage i.e. emission from singlets and triplets and / or

simultaneous emission from LC, MC and CT excited states. It should be noted that careful analysis of the complex in such a case is required in order to verify the purity of the complex thus ruling out impurities as a source of the multiple emission.[16] Ohno *et. al.* have also reported a dual ^{3}(d-d) emission from both $[Rh(bpy)_2Cl_2](PF_6)$ and $[Rh(phen)_2Cl_2](PF_6)$ in a crystal in the temperature range of 77-536K. [42] Figure 1.9 illustrates the temperature dependent emission spectra of $[Rh(bpy)_2Cl_2](PF_6)$ and $[Rh(phen)_2Cl_2](PF_6)$ crystals in the temperature range 77K to 536K.[42]

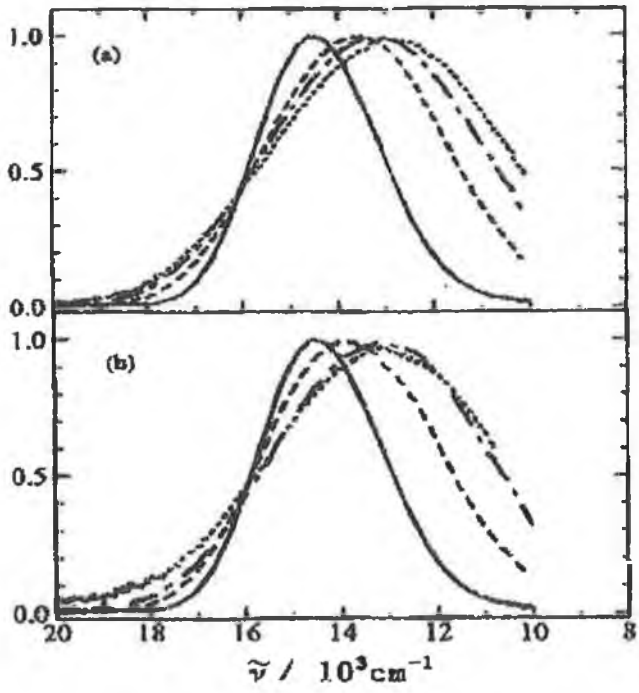

Figure 1.9 The temperature dependence of the emission spectra of Rh(III) complexes: (a) $[Rh(bpy)_2Cl_2](PF_6)$ (i) — 77K, (ii) - - - 297K,(iii) - • - 441K and (iv)•••536K and (b) $[Rh(phen)_2Cl_2](PF_6)$ (i) — 77K, (ii) - - - 298K,(iii) - • - 436K and (iv)•••528K. [42]

It can be seen from Figure 1.9 – (a) that the spectrum of $[Rh(bpy)_2Cl_2](PF_6)$ displays a shift in peak energy from approximately 14 600 cm^{-1} to 12 800 cm^{-1} and an increase in the full width at half maximum (FWHM) from about 2850 cm^{-1} to 5450 cm^{-1} with increasing temperature. The spectra obtained over the same temperature range for $[Rh(phen)_2Cl_2](PF_6)$, Figure 1.9 - (b), displayed a similar behaviour but the emission bandwidths were found to be narrower than for $[Rh(bpy)_2Cl_2](PF_6)$. It was proposed that this behaviour was due to the presence of two ^{3}(d-d) emitting states.[42]

1.3.3 Rh(III) Tris-polypyridyl Complexes

1.3.3.1 Absorption and Emission Properties

In contrast to ruthenium complexes of the type $[Ru(L)_3]^{2+}$, whose electronic properties result from metal-to-ligand-transitions (MLCT),[43] $[Rh(L)_3]^{3+}$ complexes, where L = bpy or phen, have a lowest excited state which may be classified as a ligand localised π-π^* transition. The UV spectra of $[Rh(phen)_3]^{3+}$ and $[Rh(bpy)_3]^{3+}$ are π-π^* in nature with no clear evidence for either CT bands or d-d bands.[38] Rh(III) polypyridyl complexes are typically nonemissive at room temperature due to radiationless deactivation from the excited MC state. At 77K, the MC state is not accessible and an emission is observed which is LC in nature. There have, however, been conflicting findings regarding emission from $[Rh(phen)_3]^{3+}$ at room temperature. Bolletta *et. al.* reported the presence of a very weak ($\Phi \approx 10^{-5}$) emission from $[Rh(phen)_3]^{3+}$ in acetonitrile at room temperature and assigned this as metal-centred d-d phosphorescence but the emission was later attributed to impurities by Watts *et. al.*[44,45]

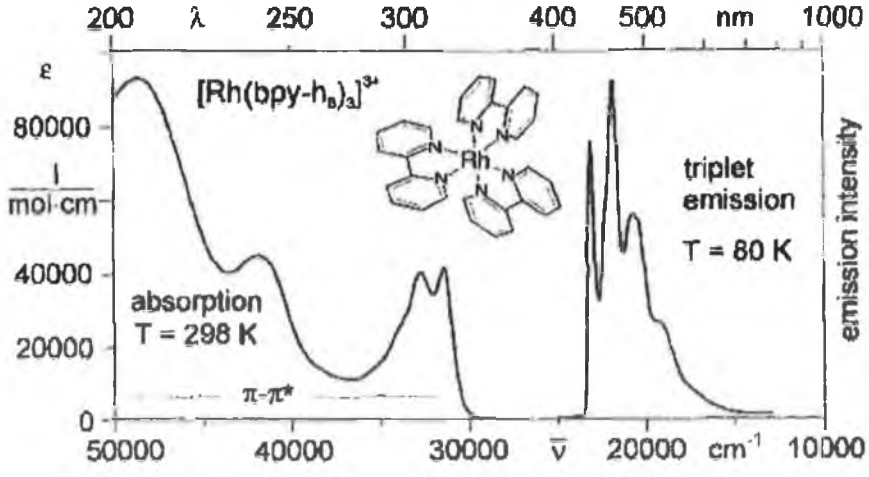

Figure 1.10 Emission and absorption spectrum of $[Ru(bpy)_3]^{3+}$ in ethanol.[46]

The classification of the lowest excited state of these types of Rh(III) polypyridyl complexes as a ligand localised π-π^* transition was originally made because of the similarity with respect to the location and structure of the

phosphorescence band observed from a glass at 77K of $[Rh(bpy)_3]^{3+}$ and $[Rh(phen)_3]^{3+}$ in comparison to the phosphorescence observed for the free ligands. Figure 1.10 illustrates the structured phosphorescence observed for $[Rh(bpy)_3]^{3+}$ in an ethanol:methanol 4:1 glass at 80K.[46] It is possible to verify the localised nature of the emitting state by studying mixed ligand complexes. These types of studies were carried out by G.A. Crosby and W.H. Elfring in their study of the photoluminescence and proton magnetic resonance measurements on complexes of the type $[M(bpy)_m(phen)_n]Cl_x$ where m = 3-n and n = 0,1,2,3 and when M = Rh(III), x = 3 whereas when M = Ru(II), x = 2.[47] Figure 1.11 shows the absorption spectra of the rhodium(III) chelates in ethanol:methanol 4:1 at room temperature and in these spectra we can see the bpy bands of $[Rh(bpy)_3]^{3+}$ are being progressively replaced by an absorption band characteristic of 1,10-phenanthroline as the number of phen ligands in the complex increases (b to d).[47]

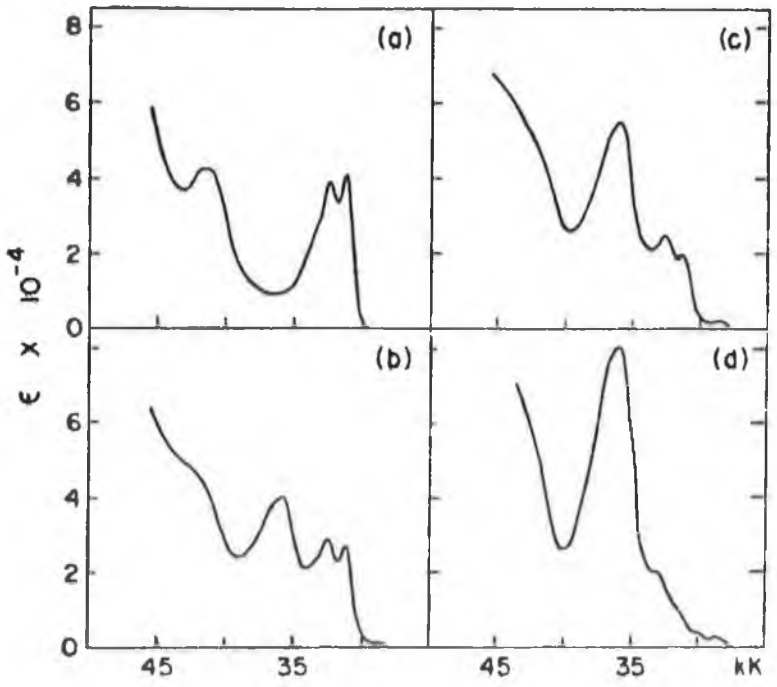

Figure 1.11 The absorption spectra of Rh(III) chelates in 4:1 ethanol:methanol at room temperature: (a) $[Rh(bpy)_3]Cl_3$, (b) $[Rh(bpy)_2(phen)]Cl_3$,(c) $[Rh(bpy)(phen)_2]Cl_3$ and (d) $[Rh(phen)_3]Cl_3$.[47]

The emission spectra showed a similar trend but the differences in the spectra were subtle and the decay time of the observed phosphorescence was single

exponential for both $[Rh(bpy)_3]^{3+}$ and $[Rh(phen)_3]^{3+}$ and multi exponential for the complexes $[Rh(bpy)_2(phen)]^{3+}$ and $[Rh(bpy)(phen)_2]^{3+}$ as was previously reported by DeArmond *et. al.*[48] Crosby *et. al.* observed long lifetimes for all the complexes studied (> ms) thus implying that the amount of singlet character mixed into the lowest triplet state to be very small. Their results led to the conclusion that the coordinated ligands were virtually isolated from one another and effectively decaying independently.[47]

Watts and Van Houten later carried out an emission study using three different groups of complexes.[49] The groups were as follows:

Group A	$[Rh(bpy)_n(phen)_{3-n}]^{3+}$
Group B	$[Rh(bpy)(5,6\text{-Mephen})_2]^{3+}$
Group C	$[Rh(phen)(5,6\text{-Mephen})_2]^{3+}$

Their work showed that the mixed ligand complexes of group A displayed non-exponential decay curves with the short component of the decay being due to the localised $^3\pi\text{-}\pi^*$ emission of bpy whilst the longer component was a result of a localised $^3\pi\text{-}\pi^*$ emission of the phen ligand. The conclusion by Watts and Van Houten that the non-exponential decays observed were as a result of localised $^3\pi\text{-}\pi^*$ emissions on bpy and phen was supported by time resolved luminescence spectroscopy.[49] The $^3\pi\text{-}\pi^*$ emissions of both $[Rh(bpy)_3]^{3+}$ and $[Rh(phen)_3]^{3+}$ are derived from nearly the same energies but it should be noted that the vibrational intensity distributions of these two complexes are different. Due to the difference in their vibrational intensity distribution it was possible to relate intensity variations in the vibrational structure with time via time resolution of the non-exponential emissions of $[Rh(bpy)_2(phen)]^{3+}$ and $[Rh(bpy)(phen)_2]^{3+}$. As can be seen in Figure 1.12 variation in the vibrational intensity distribution was observed for both complexes and on a short time scale the spectra observed were similar to that of $[Rh(bpy)_3]^{3+}$ whilst spectra obtained on a longer time scale were similar to the luminescence spectrum of $[Rh(phen)_3]^{3+}$.[49]

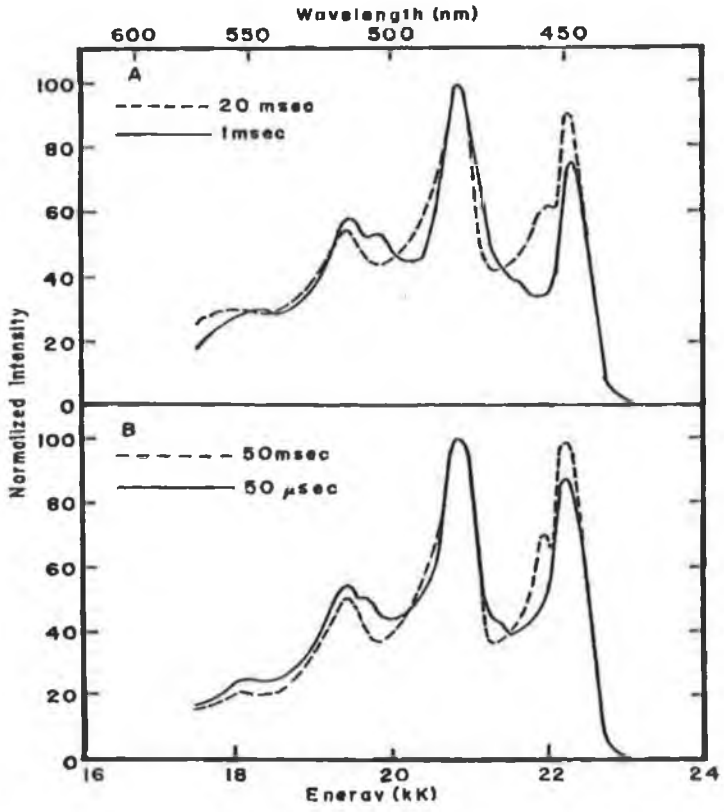

Figure 1.12 Time resolved luminescence of (A) $[Rh(bpy)_2(phen)]^{3+}$ and (B) $[Rh(bpy)(phen)_2]^{3+}$ in methanol-water at 77K.[49]

Watts and Van Houten found no evidence for multi exponential decay in the complexes of group B. Both complexes in group B showed exponential decays with their lifetimes and their emission spectra being almost identical to that of $[Rh(5,6\text{-Mephen})_3]^{3+}$, where 5,6-Mephen = 5,6-dimethyl-1,10-phenanthroline, hence leading to the conclusion that energy transfer from the $^3\pi\text{-}\pi^*$ of bpy to the $^3\pi\text{-}\pi^*$ of 5,6-Mephen occurs on a shorter timescale than the emission from the $^3\pi\text{-}\pi^*$ of bpy.[49] For complexes in the C category it was found that the lifetimes of $[Rh(phen)_3]^{3+}$ and $[Rh(5,6\text{-Mephen})_3]^{3+}$ were practically identical and their emission spectra easily resolved in energy but not so in relation to time. When the emission spectra of the complex $[Rh(phen)(5,6\text{-Mephen})_2]^{3+}$ were studied a strong band associated with the 5,6-Mephen ligand was observed whilst a weak band, attributed to a $[Rh(phen)_3]^{3+}$ impurity was also detected. It was concluded that energy transfer from the phen ligand to the 5,6-Mephen ligand within the complex $[Rh(phen)(5,6\text{-Mephen})_2]^{3+}$ occurred at a much faster rate than emission from the phen ligand.[49]

The nature of the emissive state of complexes incorporating the ligands phen and phi was investigated by Barton *et. al.*[50] The complexes reported were $[Rh(phi)_2(phen)]^{3+}$ and $[Rh(phi)_2(bpy)]^{3+}$ and these were found to have long lived excited states which appeared to be intra-ligand in nature. In the case of the complex $[Rh(phi)_2(phen)]^{3+}$ two emissive states were observed corresponding to emission from both the phen and the phi ligands. It was found that the low temperature lifetimes of $[Rh(phi)_2(phen)]^{3+}$ were shorter that those observed for the complex $[Rh(phen)_3]^{3+}$ thus indicating that another mechanism was attributing to the deactivation of the $^3\pi$-π^* state. The additional deactivation of the $^3\pi$-π^* state was found to occur via the ILCT state. The excited states of $[Rh(phi)_2(phen)]^{3+}$ may be seen schematically in Figure 1.13.[50]

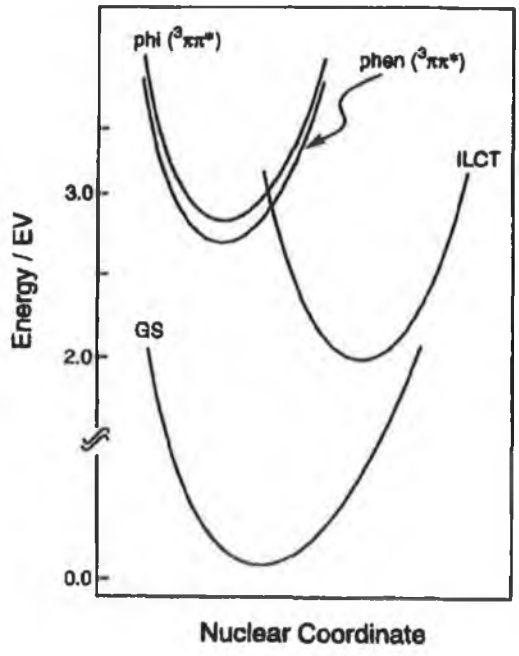

Figure 1.13 Schematic diagram of the excited states of $[Rh(phi)_2(phen)]^{3+}$.[50]

From these three studies it can be seen that the localised nature of the emitting state in these types of complexes can be determined with relative ease but the determination of other triplet properties of $[Rh(bpy)_3]^{3+}$ and $[Rh(phen)_3]^{3+}$ was more difficult, for example, the extent of the zero-field splitting (zfs) parameters for these complexes was ambiguous and also, in contrast to the similarities observed between the phosphorescent spectra of $[Rh(bpy)_3]^{3+}$ and $[Rh(phen)_3]^{3+}$ and of their respective free ligands, their lifetimes were found to be significantly shorter than those

determined for the respective free ligands. In an attempt to clarify some of these issues Komada *et. al.* carried out a phosphorescence and zero-field optically detected magnetic resonance (ODMR) study of the lowest excited states of both $[Rh(bpy)_3]^{3+}$ and $[Rh(phen)_3]^{3+}$.[51] Their work represented the first successful ODMR experiments to be carried out on Rh complexes. They concluded that the lowest excited triplet state, T_1, of the complexes is π-π^* in nature and excitation is localised on a single ligand based upon the vibrational structure of the emission spectra and the magnitude of the zfs. They attributed the shortening of the triplet lifetime in rhodium complexes to the existence of ^{3,1}d-π^* states and as opposed to previous predictions of a large zfs Komada *et. al.* found the zfs to be very small and similar to the zfs of the free ligands.[51]

Humbs and Yersin later confirmed that excitation of $[Rh(bpy)_3]^{3+}$ led to an excited state which was localised on one ligand by means of highly resolved emission and excitation spectra.[52] They studied complexes of the form $[Rh(bpy\text{-}h_8)_n(bpy\text{-}d_8)_{3-n}]^{3+}$ and it is interesting to note that when the deuterated complex $[Rh(bpy\text{-}h_8)_2(bpy\text{-}d_8)]^{3+}$ was analysed, Humbs and Yersin observed emission only from the protonated ligands even when the deuterated ligand was selectively excited. This behaviour was attributed to an efficient energy transfer from the deuterated to the protonated ligands thus excluding the possibility of dual emission.[52]

Having been used successfully by Komada *et. al.* as a method of studying the nature of the emitting state the technique of ODMR has been utilised in a number of other studies. Giesbergen *et. al.* have studied the complexes $[Rh(thpy)_2(bpy)]^+$ and $[Rh(thpy)(phpy)(bpy)]^+$ where thpy = 2,2'-thienylpyridine and ppy = 2-phenylpyridine.[53] In this instance the emissive state was again determined to be $^3\pi$-π^* in nature which was found to be localised on one of the thienylpyridine ligands. Brozik *et. al.* used ODMR studies in an attempt to determine the role of metal d-orbitals in modifying the spin sublevels of the $^3\pi$-π^* emitting state of phen, $[Rh(phen)_3]^{3+}$ and $[Rh(CN)_2(phen)_2]^+$ and using the effect of ligand field strength on the radiative properties of the ligand localised $^3\pi$-π^* state of the aforementioned

rhodium complexes proposed a model which postulated that configurational mixing of the emitting triplet state $^3\pi$-π^* with d-d and d-π excited states occurred.[54]

Most of the complexes outlined so far contain the ligands bpy, phen and 5,6-Mephen but various other ligands have been incorporated in rhodium(III) polypyridyl systems. Complexes of Rh(III) with ligands such as biq - 2,2'-biquinoline and pq - 2-(2'-pyridyl)quinoline have been reported by Zaghal *et. al.* and Brewer *et. al.* have developed a series of bis chelate complexes with the ligands bpm – 2,2'-bipyrimidine; dpp – 2,3-bis(2-pyridyl)pyrazine; dpq - 2,3-bis(2-pyridyl)quinoxaline; dpb - 2,3-bis(2-pyridyl)benzoquinoxaline [55,56,57] Terpyridine ligands are another group of ligands with which a number of Rh(III) complexes have been synthesised and characterised. An interesting example of a mononuclear terpyridine complex was reported by Ford *et. al.* who described the synthesis and excited state properties a series the rhodium(III) complexes $[Rh(tpy)_2]^{3+}$, $[Rh(tpy)(bpy)(py)]^{3+}$ and $[Rh(tpy)(bpy)Cl]^{2+}$ where tpy is 2,2':6'2''-terpyridine.[26] The absorption spectrum of each of these displayed intraligand π_L- π_L^* transitions – Figure 1.14.

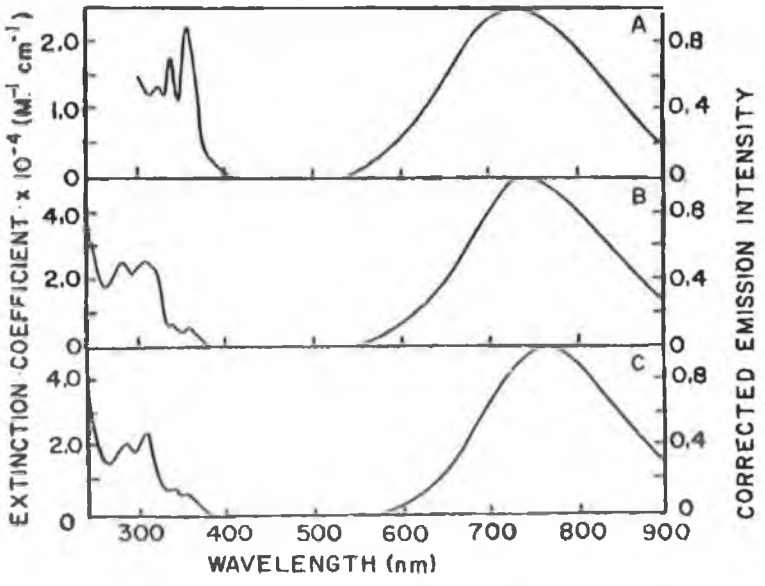

Figure 1.14 Absorption spectra (left) in aqueous solution at 298K and emission spectra at 77K in an ethanol glass of (A) $[Rh(tpy)_2]^{3+}$,(B) $[Rh(tpy)(bpy)(py)]^{3+}$and (C) $[Rh(tpy)(bpy)Cl]^{2+}$.[26]

Emission was observed for these complexes at both 77K and at ambient temperature and, unusually, resulted from the lowest triplet ligand field state $^3MC^*$ as opposed to being from a ligand centred state which is the case for analogous complexes such as $[Rh(bpy)_3]^{3+}$ and $[Rh(phen)_3]^{3+}$.[26]

From the previous discussion, it can be seen that the nature of the emitting state is dependent upon, among other things, the nature of the ligands incorporated into the complex. It should therefore, be possible to fine-tune the emitting properties of a system by varying the ligands present. Such a study was conducted by Indelli and Scandola whereby the possibility of a crossover from metal-centred to ligand centred emission in rhodium(III) polypyridine complexes was demonstrated.[30] Ancillary ligands were used in an effort to alter the energy of the MC states in a predictable manner without substantially varying the energy of the LC state. The study demonstrated that it is possible to tune the MC-LC energy gap by judiciously selecting ancillary ligands making it possible to go from MC emitters, for example $[Rh(phen)_2Cl_2]^+$ and $[Rh(phen)_2(NH_3)Cl]^{2+}$, to LC emitters, for example $[Rh(phen)_2(CN)_2]^+$ via complexes that, in an appropriate temperature range, are capable of exhibiting dual LC-MC emission e.g. $[Rh(phen)_2(NH_3)_2]^{3+}$.[30] Figure 1.15 illustrates the dual emitting nature of $[Rh(phen)_2(NH_3)_2]^{3+}$ with spectrum (a) being the emission detected at 77K. It can be seen that this exhibits both a structured emission between 425 nm and 440 nm which is assigned as a ligand centred emission and a broad shoulder between 440 nm an 650 nm assigned as a metal based emission. The spectra in Figure 1.15b and c illustrate the individual components of the emission spectrum seen in Figure 1.15a.[30]

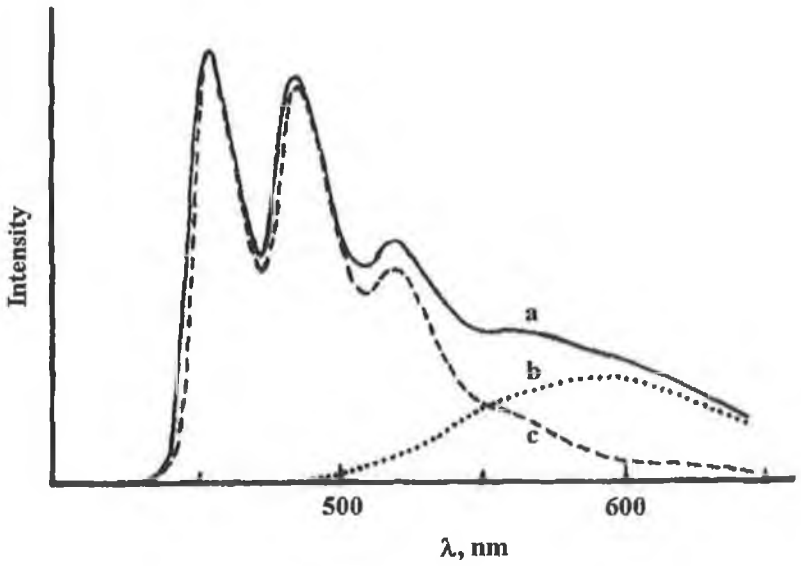

Figure 1.15 Emission spectra of (a) $[Rh(phen)_2(NH_3)_2]^{3+}$ at 77K, the MC and LC components of which can be seen in (b) and (c).[30]

1.3.3.2 Photochemical reactions of Rh(III) polypyridyl complexes

Whilst the photophysical properties of these complexes are usually dominated by the lowest triplet excited state it should be noted that these are often perturbed by close lying upper excited levels. These states not only provide static perturbations but as the temperature is increased, these thermally accessible upper excited states may be responsible for changes in the photophysical properties of the complex. This not only results in a reduction of luminescent intensity with increasing temperature but may also be responsible for competing photochemical reactions. An example of this was reported by Indelli and Scandola when they observed phosphorescence which was $^3\pi$–π^*→gs in nature at 77K in a 1:1 ethylene glycol:water glass for the complex $[Rh(phen)_2(NH_3)_2]^{3+}$. When the temperature was increased, a ^{3}d-d→gs luminescence was observed. Brozik and Crosby have investigated the thermal activation of a triplet d-d level from a triplet π-π^* manifold.[58] They studied a series of Rh(III) complexes with the ligands phen, 4-Mephen = 4-methyl-1,10-phenanthroline , 4,7-Me_2phen = 4,7-dimethyl-1,10-phenanthroline and 3,4,7,8-Me_4phen = 3,4,7,8-tetramethyl-1,10-phenanthroline in solid glycerol matrices. It was observed that in a rigid glycerol glass, below 150K, the complexes studied displayed a $^3\pi$-π^*

phosphorescence attributable to the phen substituted ligands. Above 150K but below the melting point of glycerol a temperature dependent first order photoinduced reaction was observed. Reactions of this nature are generally attributed to the thermal redistribution of energy from a chemically inert $^3\pi$-π^* level to a higher lying ^{3}d-d level which results in the immediate formation of a photoproduct. In this case Brozik *et. al.* proposed that one octahedral site on the metal was occupied by a glyceroxide moiety which was bonded to the rhodium atom via the oxygen atom as can be seen in Figure 1.16.[58]

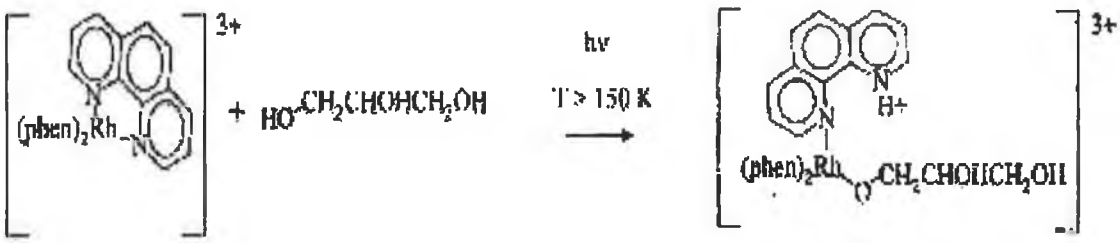

Figure 1.16 Photochemical reaction proposed by Brozik and Crosby.[58]

1.3.3.3 A comparison of the nature of low lying electronic states of $[Rh(bpy)_3]^{3+}$ $[Pt(bpy)_3]^{2+}$, $[Ru(bpy)_3]^{2+}$ and $[Os(bpy)_3]^{2+}$

A comparative study of the low-lying electronic states of $[Rh(bpy)_3]^{3+}$, $[Pt(bpy)_3]^{2+}$ and $[Ru(bpy)_3]^{2+}$ was carried out by Humbs and Yersin.[46] In the study they reported a series of trends, Table 1.4, which were related to an increase of metal-d or MLCT character in the lowest triplet states. Firstly in relation to the transition energies (specified in column 1 of Table 1.4) it was found that the transition energies are red shifted with respect to the free ligand 2,2'-bipyridine. This stabilisation occurs as a result of (i) complex formation and (ii) from increasing d-d* and / or MLCT admixtures to the lowest ^{3}LC states of $[Rh(bpy)_3]^{3+}$, $[Pt(bpy)_3]^{2+}$ whereas for the complexes $[Ru(bpy)_3]^{2+}$ and $[Os(bpy)_3]^{2+}$ the MLCT character becomes dominant. A decrease in the lifetimes of the complexes was observed and attributed to the fact that the spin selection rules are weakened with increasing d-admixture and spin orbit coupling. Approximate classifications of the transitions discussed may be seen in the final column.

Table 1.4 Comparison of the spectroscopic properties of $[Rh(bpy)_3]^{3+}$, $[Pt(bpy)_3]^{2+}$ and $[Ru(bpy)_3]^{2+}$.[46]

Complex	Lowest electronic transition (cm^{-1})	Emission Lifetime (μs)	Nature of the electronic transition
Bpy in *n*-heptane	23504	4×10^6	$^3\pi\pi^*$
$[Rh(bpy)_3]^{3+}$ in $[Zn(bpy)_3](ClO_4)_2$	22757	4.6×10^3	$^3LC(^3\pi\pi^*)$ + small dd^* admixtures
$[Pt(bpy)_3]^{2+}$ in $[Pt(bpy)_2](ClO_4)_2$	21237	50	$^3LC(^3\pi\pi^*)$ + small MLCT admixtures
$[Ru(bpy)_3]^{2+}$ in $[Zn(bpy)_3](ClO_4)_2$	17684	230	^{3} MLCT ($d\pi^*$)
$[Os(bpy)_3]^{2+}$ in $[Zn(bpy)_3](ClO_4)_2$	14223	22	^{3} MLCT ($d\pi^*$)

1.3.4 Excited State Absorption Spectroscopy of Rh(III) Complexes

Rh(III) polypyridyl complexes are typically non emissive at room temperature however, it is possible to examine the excited state processes by means of studying the transient absorption corresponding to the formation and the decay of the excited state. Studies involving laser flash photolysis have enabled a number of groups to observe excited state absorption of moderate intensity for a number of Rh(III) polypyridyl complexes. One such example was reported by Indelli *et. al.* for $[Rh(phen)_3]^{3+}$.[59] In this instance a broad transient absorption was observed with a maximum at 490nm in both aqueous solution at room temperature and in a 1:1 water:ethylene glycol glass at 77K. The transient absorption observed was assigned as an excited state absorption associated with the ligand centred π-π^* triplet state based on comparison with emission lifetimes measured under the same conditions. Figure 1.17 illustrates the excited state absorption spectrum of $[Rh(phen)_3]^{3+}$ obtained by Indelli *et. al.*[59]

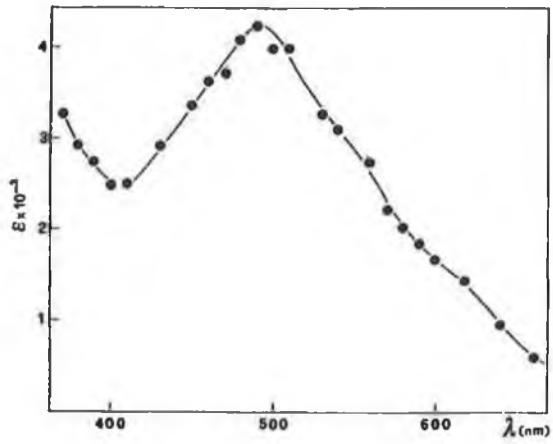

Figure 1.17 Excited-state absorption spectrum of $[Rh(phen)_3]^{3+}$.[59]

Room temperature excited state absorption and phosphorescence of Rh(III) compounds incorporating phenanthroline based ligands have also been studied by Ohno *et. al.*[60] Figure 1.18 illustrates the excited state absorption spectra obtained for $[Rh(phen)_2Cl_2]^+$ and $[Rh(dp\text{-}phen)_2Cl_2]^+$ where dp-phen is 4,7-diphenyl-phenanthroline.

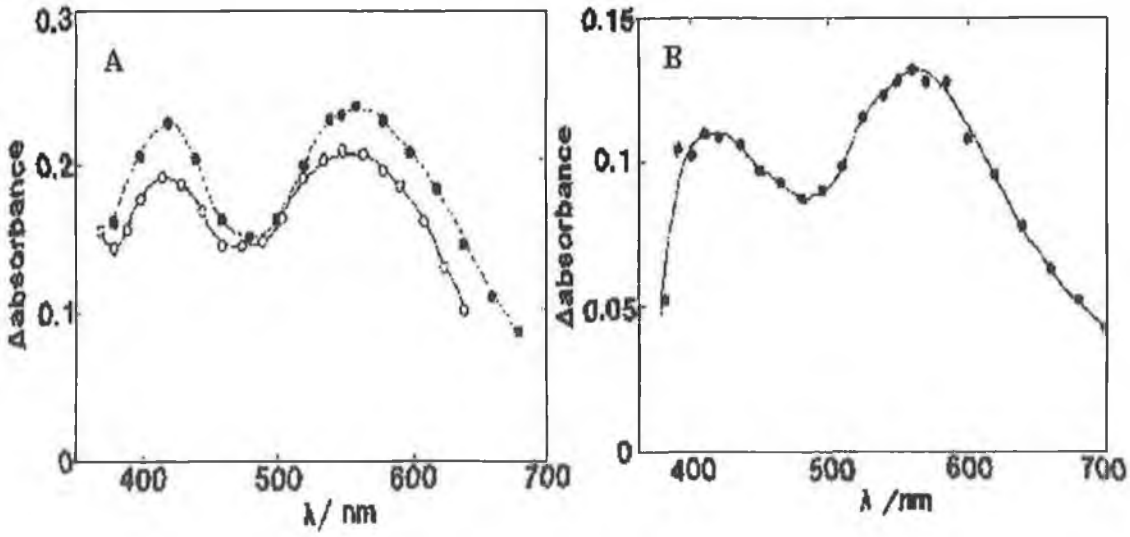

Figure 1.18 Transient absorption spectra of (A) $[Rh(phen)_2Cl_2]^+$ (200μM) in acetonitrile:water (1:1) (open circle) and acetonitrile (closed circle) and (B) $[Rh(dp\text{-}phen)_2Cl_2]^+$ (50μM) in acetonitrile.[60]

The excited state lifetimes were found to be strongly solvent dependent and when the excited state lifetimes were measured at 77K and at room temperature it was found that the tris complexes exhibited a stronger temperature dependence than the bis complexes. These temperature effects were possibly as a result of coupling of the low lying (emitting) π-π^* states with a nearby d-d* state. [60]

1.4 Electrochemical Properties of Rhodium (III) Complexes

The redox chemistry of tris-rhodium(III) polypyridyl complexes is made difficult due to irreversibility and the loss of a polypyridyl ligand upon reduction. Equations 1.2 and 1.3 illustrate a one electron reduction of $[Rh(bpy)_3]^{3+}$.

$$[Rh^{III}(bpy)_3]^{3+} + e^- \leftrightharpoons [Rh^{II}(bpy)_3]^{2+} \qquad \textbf{Equation 1. 2}$$

$$[Rh^{II}(bpy)_3]^{2+} \leftrightharpoons [Rh^{II}(bpy)_2]^{2+} + bpy \qquad \textbf{Equation 1. 3}$$

The electrochemical behaviour of the Rh(III) polypyridine complexes was first probed by DeArmond *et. al.* who initially studied the electrochemistry of rhodium bipyridyl complexes and phen complexes.[61,62] In each case acetonitrile was used in conjunction with tetraethylammonium perchlorate (TEAP) as a base electrolyte and a platinum electrode. In the case of $[Rh(bpy)_3]^{3+}$ the first one electron reduction was followed by a moderately fast elimination of a bipyridyl ligand. A second one electron transfer yielded a Rh(I) species and was followed by two further stepwise reversible one electron transfers giving $[Rh(bpy)_2]^0$ and $[Rh(bpy)_2]^-$. Figure 1.19 illustrates the cyclic voltammograms obtained for $[Rh(bpy)_3]^{3+}$.[61] As with the bipyridyl complexes the bis and tris 1,10-phenanthroline complexes displayed four one electron processes. For the complexes $[Rh(phen)_3]^{3+}$, $[Rh(phen)_2(bpy)]^{3+}$ and $[Rh(phen)(bpy)_2]^{3+}$ a quasi-reversible one electron cathodic wave was observed at -0.7V to -0.9V vs. SCE. This was followed by a chemical reaction, thought to be ligand loss, with a rate constant of ~0.1 s^{-1}. About ~0.1V negative of the first wave

a second cathodic wave was observed and a rapid chemical reaction was subsequently observed.[62]

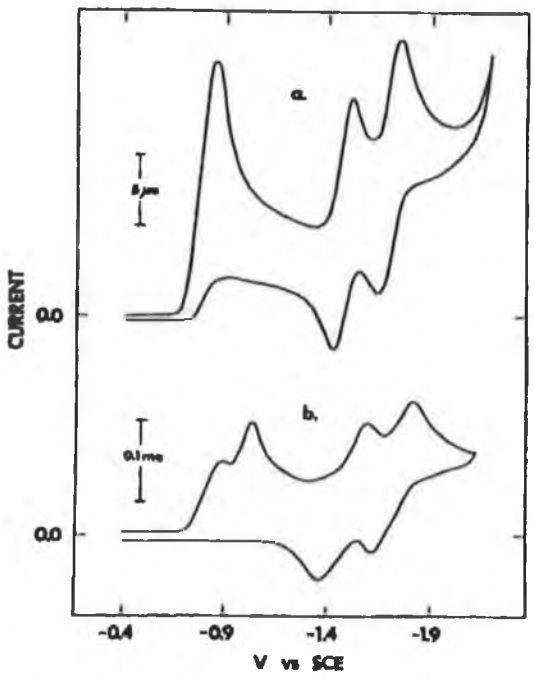

Figure 1.19 Cyclic voltammogram of $[Rh(bpy)_3]^3$, 1.08 x 10^{-4}M where (a) v = 0.1. V/sec and (b) v = 31.2 V/sec.[61]

Creutz *et. al.* carried out a study of the electrochemical behaviour of $[Rh(bpy)_3]^{3+}$, $[Rh(phen)_3]^{3+}$ and $[Rh(bpy)_2(OH)_2]^+$ on a pyrolytic graphite electrode in 0.05M NaOH at 25°C.[6] In the case of $[Rh(phen)_3]^{3+}$ Creutz *et. al.* found no reversible features when the sweep range was from +0.24 V to – 1.06 V and at a sweep rate of $200mVs^{-1}$ but upon reversal of the sweep range at –0.76 V the anodic partner of the –0.703 V reduction wave was detectable at –0.633 V. It was observed that at faster sweep rates this anodic wave became more prominent. Meyer *et. al* have also reported upon the electrochemical behaviour of rhodium(III) and iridium(III) 2,2'-bipyridine complexes.[63] Cyclic voltammetric data obtained by Meyer *et. al.* can be seen in Table 1.5.

***Table 1.5 Cyclic voltammetric data obtained by Meyer et. al.*[63]**

Complex	E_{pa}, V	E_{pc}, V	$E_{½}$, V
$[Rh(bpy)_2Cl_2][ClO_4]$	-0.40	-0.92	
	-1.30	-1.39	-1.35
	-1.58	-1.72	-1.65
$[Rh(bpy)_2(TFMS)_2][TFMS]$ [a b]	-0.36	-0.84	
	-1.18	-1.26	-1.22
	-1.45	-1.55	-1.51
$[Rh(bpy)_2(TFMS)_2][TFMS]$ [c]	-0.17	-0.36	
	-1.23	-1.34	
	-1.52	-1.60	
$[Rh(4,4'(t\text{-}Bu)_2bpy)_2][PF_6]$ [c, b]	-0.29	-0.99	
	-1.35	-1.45	-1.40
	-1.64	-1.73	-1.68

[a] C-button working electrode, [b] DMF with 0.1M TBAH as supporting electrolyte, [c]Irreversible oxidation. TFMS = trifluoromethanesulphonate anion and TBAH = tetra-*n*-butylammonium hexafluorophosphate.

Based on their results and results obtained by DeArmond *et. al.* Meyer and co-workers summarised the pattern of reactions which appeared to occur during the reduction of rhodium(III) complexes can be seen in equations 1.4 - 1.7.

$$cis\text{-}[Rh(bpy)_2X_2]^+ \underset{2e^-}{\overset{2e^-}{\rightleftharpoons}} [Rh(bpy)_2X_2]^- \qquad \textbf{Equation 1.4}$$

$$[Rh(bpy)_2X_2]^- \xrightarrow{fast} [Rh(bpy)_2]^+ + 2X^- \qquad \textbf{Equation 1.5}$$

$$[Rh(bpy)_2]^+ \underset{e^-}{\overset{e^-}{\rightleftharpoons}} [Rh(bpy)_2] \qquad \textbf{Equation 1.6}$$

$$[Rh(bpy)_2] \underset{e^-}{\overset{e^-}{\rightleftharpoons}} [Rh(bpy)_2]^- \qquad \textbf{Equation 1.7}$$

The electrochemical behaviour of rhodium polypyridyl complexes will be discussed further in chapters 4 and 6.

1.5 Rh(III) Cyclometalated Complexes

In the cases of polypyridyl complexes containing rhodium, iridium, platinum and palladium there is also the possibility of the formation of an orthometalated isomer in addition to the N – N bonded isomer.

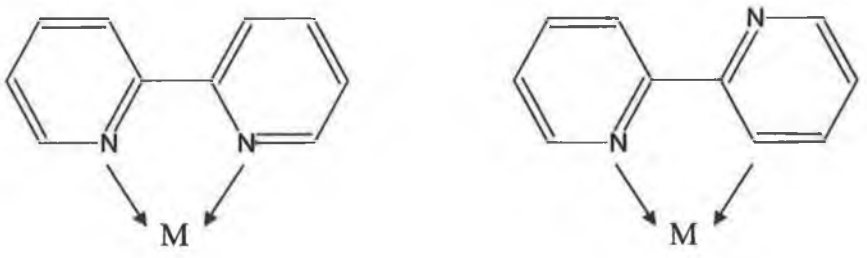

N-N isomer orthometalated isomer

Figure 1.20 Mode of chelation for the N-N bound isomer and the orthometalated isomer.[16]

These orthometalated complexes are quite stable and a number of examples of these complexes may be found in the literature. Sandrini *et. al.* have reported the spectroscopic and electrochemical properties of mixed ligand orthometalated rhodium(III) complexes with the ligands phen; biq = 2,2'- biquinoline; ppy and thpy = 2-(2-thienyl)pyridine respectively.[64,65] They found that the complexes $[Rh(ppy)_2(L)]^+$ and $[Rh(thpy)_2(L)]^+$, where L = phen, bpy and biq, behaved quite differently from their ruthenium(II) counterparts. A study of the luminescence of these complexes led to the conclusion that the lowest energy excited state was predominantly ligand centred. When L = bpy or phen the lowest energy excited state was based on the NC-orthometalating ligands and when L = biq the lowest energy excited state was based on the NN-coordinating ligands.[65] The results from cyclic voltammetry indicated that the NN-coordinating ligands were easier to reduce than the NC-metalating ligands indicative of the lowest unoccupied molecular orbital (LUMO) being a π^* orbital based on the NN-coordinating ligands. In contrast to this, the absorption spectra showed that the lowest energy MLCT band involved the NC-metalating ligands rather than the NN-coordinating ligands which are more easily

reducible.[65] The temperature dependence of the luminescence of these complexes were also investigated by Sandrini *et. al.* [66]

Complexes with ligands 1,4,5,8,9,12-hexaazatriphenylene (HAT) and 1,4,5,8-tetraazaphenanthrene (TAP) were investigated by Didier *et. al.*[67] Unusually for these types of complexes, $[Rh(ppy)_2(HAT)]^+$ and $[Rh(ppy)_2(TAP)]^+$ both display a structureless emission spectrum at room temperature and in glass matrices. They exhibit large blue shifts upon cooling from room temperature to 77K which is characteristic of a distorted CT state to the HAT or the TAP ligand.[67] This behaviour is in contrast with that of $[Rh(ppy)_2(bpy)]^+$ which exhibits a highly structured emission both at room temperature and at 77K and displays no shift of the emission upon cooling. In the case of $[Rh(ppy)_2(bpy)]^+$ emission is due to a $^3\pi$-π^* excited state localised on the ppy ligand.[68,69] Didier *et. al.* have more recently extended their studies with the HAT and TAP ligands and have studied dinuclear complexes of rhodium(III), iridium(III) and ruthenium(II) with the HAT ligand.[29]

Colombo *et. al.* have related the synthesis, structure and optical spectroscopic properties of cyclometalated complex *fac*-$[Rh(ppy)_3]$.[70] Again in this complex the lowest excited state was a $^3\pi$-π^* transition. It was also found that the lifetime of the tris complex studied was shorter than that of the corresponding bis complex which was thought to give credence to the idea that the MLCT states may lowered as the number of coordinating C^- atoms is increased.[70] The photophysical effects of metal-carbon σ bonds in complexes of the type $[Rh(ppy)_2Cl]_2$ and $[Rh(bzq)_2Cl]_2$ where bzq is the ligand benzo[h]quinoline have been studied by Watts *et. al.*[71]. Watts *et. al.* have also reported the ^1H and ^{13}C NMR assignments with coordination induced shift calculations for a series of rhodium(III) and iridium(III) complexes incorporating the ligands ppy; ptpy - 2-(*p*-tolyl)pyridine; mppy - 3-methyl-2-phenylpyridine and bpy.[72]

Triazole ligands are of particular interest as much of the work that will be discussed in the following chapters incorporates triazole ligands. As with the benzimidazole ligands the triazole ligands are asymmetric thus allowing for different

modes of coordination within the complex and contain a labile NH moiety. Transition metal complexes incorporating 1,2,4-triazole based ligands generally feature either ruthenium(II) or osmium(II) as metal centres but a number of rhodium(III) cyclometalated complexes with 1,2,4-triazoles have been reported. Vos *et. al.* have reported the synthesis and characterisation of a series of Rh(III) cyclometalated complexes of the form $[Rh(ppy)_2(L)](PF_6)$ where L = 3-(pyridin-2-yl)-1,2,4-triazole, 1-methyl-5-(pyridin-2-yl)-1,2,4-triazole, 1-methyl-3-(pyridin-2-yl)-1,2,4-triazole, 4-methyl-3-(pyridin-2-yl)-1,2,4-triazole, 3-methyl-5-(pyridin-2-yl)-1,2,4-triazole, 3-(pyridin-2-yl)-5-phenyl-1,2,4-triazole, 3-(pyridin-2-yl)-5-(3-nitrophenyl)-1,2,4-triazole, 3-(pyridin-2-yl)-5-(2-thienyl)-1,2,4-triazole.[73]

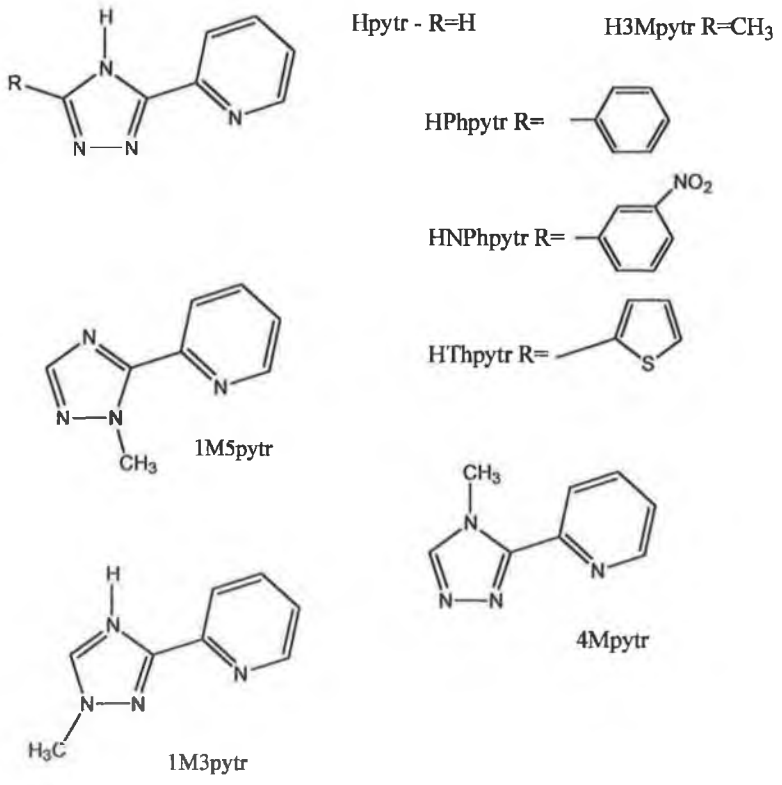

Figure 1.21 Structures of triazole ligands reported by Vos et. al.[73]

NMR spectroscopy allowed the characterisation of the coordination mode of these complexes and it was found that coordination predominantly occurred via the N4 of the triazole ring. Analysis of the absorption spectra showed that the lowest energy absorption of these complexes was a Rh → ppy transition that was insensitive to the nature of the incorporated triazole ligand. At 77K, all complexes showed a highly structured emission spectrum at 450 nm, which was independent of the nature of the incorporated triazole ligand and was assigned as a ppy based π-π* emission.[73]

In an extension of this work, the electrochemical and photophysical properties of triazole bridged heterobimetallic ruthenium-rhodium and ruthenium-iridium complexes. In this case the bridging ligand used was the ligand 3,5-bis(pyridin-2-yl)-1,2,4-triazole (Hbpt) and the complexes studied were $[(bpy)_2Ru(bpt)Rh(ppy)_2]^{2+}$, $[Rh(ppy)_2(bpt)]^+$, and the iridium complexes $[(bpy)_2Ru(bpt)Ir(ppy)_2]^{2+}$, $[Ir(ppy)_2(bpt)]^+$.[74]

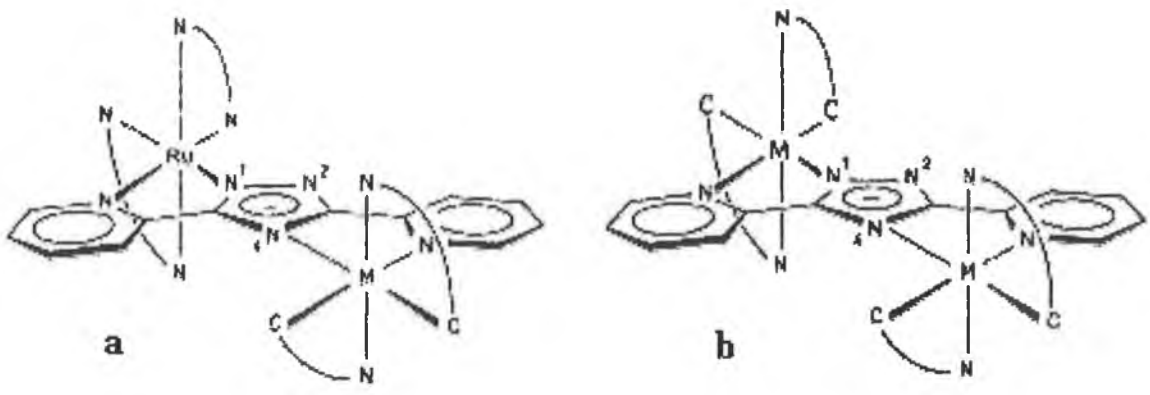

Figure 1.22 Schematic representation of the structures of the complexes (a) $[(bpy)_2Ru(bpt)M(ppy)_2]^{2+}$ where M = Rh or Ir and (b) $[(M(ppy)_2(bpt)]^+$ where M = Rh or Ir.[74]

In the case of the complex $[(Rh(ppy)_2)_2(bpt)]^+$ the emission observed at 77K was resultant from a ligand centred excited state whereas for $[(Ir(ppy)_2)(bpt)]^+$ a charge transfer emission that involved the bpt^- was observed. The mixed metal complexes studied exhibited efficient energy transfer from higher energy excited states centred on the $M(ppy)_2$ moiety, where M = Rh/Ir, to a MLCT level that was localised on the

$Ru(bpy)_2$ component.[74] The mononuclear complexes $[Rh(ppy)_2(dpt\text{-}NH_2)](PF_6)$ and $[Ir(ppy)_2(dpt\text{-}NH_2)](PF_6)$ have also been reported by Campagna *et. al.*.[75]

1.6 Rh(II) and Rh(I) Complexes

Very few Rh(II) complexes have been reported and those which have been reported have been primarily diamagnetic dimers which incorporate a Rh-Rh bond. The stability of Rh(II) monomers is dependent upon the ligands contained in the system and ligands such as tertiary phosphines, porphyrins and crown thioethers have been utilised.[15] When Rh(III) complexes are reduced to Rh(II) the result tends to be ligand loss followed by dimerisation or disproportionation to Rh(III) and Rh(I) complexes.[4,61,62,76] Dimerisation and disproportionation were observed by Schwarz and Creutz in their study of the reactions of tris and bis-(2,2'-bipyridine)rhodium(II) complexes in aqueous solution.[76] The complexes were generated in solution by one electron reduction of $[Rh(bpy)_3]^{3+}$ and $[Rh(bpy)_2(OH)_2]^{+}$ by either e^- or $R\bullet$ = $(CH_3)_2\dot{C}OH$ and studied by pulse-radiolytic methods.

Paul *et. al.* reported the synthesis, spectroscopic and structural characterisation of rhodium(II) complexes with the ligand bis(2-pyridylcarbonyl)amide or bpca.[77]

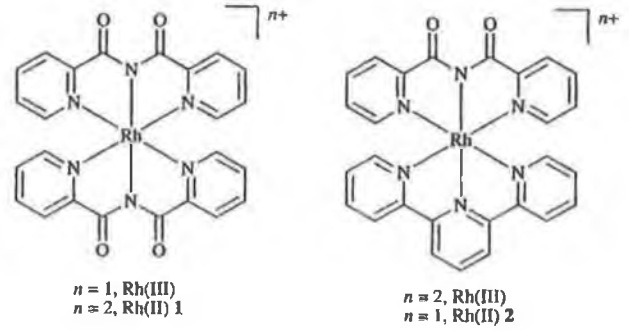

Figure 1.23 Rh(II) complex reported by P. Paul et. al.[77]

The synthesis reported by Paul *et. al.* yielded a mixture of Rh(III) and Rh(II) complexes with the Rh(II) complexes being and the required Rh(II) products were isolated by column chromatography. Both the Rh(II) complexes displayed absorption bands between 545nm and 600nm which were not present in the

analogous Rh(III) complexes. From an electrochemical viewpoint the complexes $[Rh(bpca)_2]\cdot 3H_2O$ (1) and (2) $[Rh(bpca)(tpy)]Cl\cdot 8H_2O$ exhibited a metal based reduction, $Rh^{II} \rightarrow Rh^{I}$ at –1.13 and -0.72V respectively followed by two ligand based redox couples.[77]

As with Rh(III) complexes Rh(II) complexes have been studied for medicinal purposes.[9,10,78] The Rh(II) complexes, seen in Figure 1.24, were developed by Bień *et. al.* and have exhibited antibacterial activity against many *Staphylococcus* strains which are resistant to commonly used antibiotics.[78]

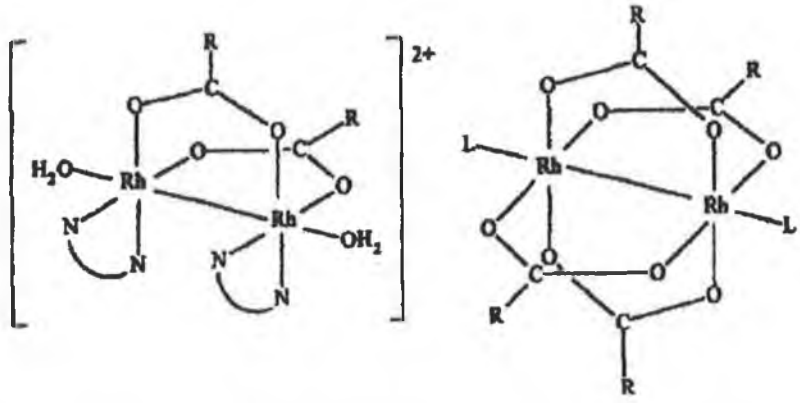

Figure 1.24 Structure of $[Rh_2(OOCR)_2(N\text{-}N)_2(H_2O)_2](OOCR)_2$ and $[Rh_2(OOCR)_4L_2]$ where N-N = 2,2'-bipyridine or 1,10-phenanthroline and R = Ph, Bu^n or Pr^n.[78]

Oro *et. al.* have developed a number of rhodium(I) complexes containing triazole ligands a number of which may be seen in Figure 1.25.[79] Complexes with the ligands Hbpt and NH_2-bpt of the form $[Rh^{(I)}(L)Cl]$ where L is a diolefin or $(CO)(PPh_3)$ have also been synthesised and characterised but these complexes will be discussed in Chapter 3.[80,81]

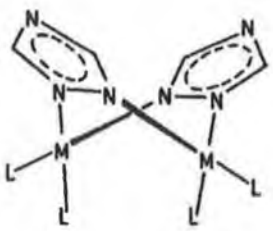

	M	L_2
(1)	Rh	cod
(2)	Rh	nbd
(3)	Rh	tfbb
(4)	Rh	tmtfbb
(5)	Rh	$(CO)_2$
(6)	Rh	$(CO)(PPh_3)$
(7)	Ir	cod
(8)	Ir	$(CO)_2$
(9)	Ir	$(CO)(PPh_3)$
(10)	Pd	η^3-C_3H_5
(11)	Pd	η^3-C_4H_7

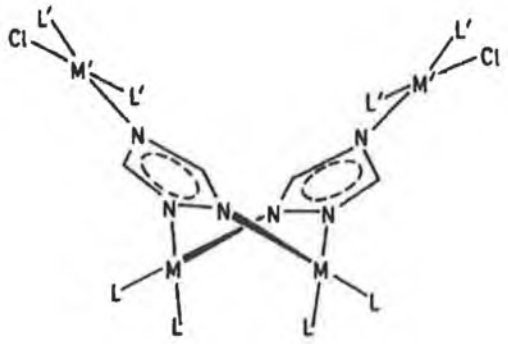

	M	L_2	M′	L'_2
(12)	Rh	cod	Rh	cod
(13)	Rh	cod	Rh	$(CO)_2$
(14)	Rh	$(CO)_2$	Rh	$(CO)_2$
(15)	Rh	cod	Ir	cod
(16)	Pd	η^3-C_3H_5	Rh	$(CO)_2$
(17)	Pd	η^3-C_4H_7	Rh	$(CO)_2$

Figure 1.25 Triazolate complexes prepared by Oro et. al. [79]

Other examples of rhodium(I) complexes are the homo- and heteronuclear-bridged bimetallic complexes of Rh(I), Ir(I), Pt(I), Au(I) whose excited states were investigated by Crosby *et. al.* and the one dimensional Rh(I)-Rh(II) complex $[Rh_2(OOCMe)_2(phen)_2]_n \cdot 0.5n Me_2CHOH$ which behaves as a molecular wire reported by Pruchnik *et. al.* [82,83]

1.7 Scope of Thesis

It is the aim of the work that will be discussed in the following chapters to contribute to the field of Rh(III) polypyridyl chemistry. A series of heteroleptic Rh(III) polypyridyl complexes have been synthesised and characterised from the perspective of studying the effect of ligand variation upon the excited state and it was also hoped that it would be possible to develop dinuclear Ru(II)-Rh(III) complexes in which both the electron donor and the electron acceptor would be photoexcitable units.

A series of complexes of the form $[Rh(L)_2(L')]^{n+}$ where L = bpy or phen, L' = a pyridine triazole / pyrazine triazole / triazine or imidazo based ligand and n = 2 or 3 have been synthesised and characterised. The instrumentation and techniques used to characterise these complexes are detailed in Chapter 2. Chapter 3 focuses

upon the synthesis, purification and structural characterisation of the complexes incorporating pyridine triazole ligands whereas Chapter 5 details the synthesis and structural characterisation of the complexes incorporating pyrazine, triazine, imidazole and triazole based ligands. X-ray crystallography and in particular NMR spectroscopy are discussed in detail in these chapters and it will be seen that the technique of ligand deuteration is a powerful tool in the analysis of ^{1}H NMR spectra. The formation of structural isomers is an issue for several of the complexes synthesised and NMR spectroscopic techniques in conjunction with ligand deuteration have been employed in an attempt to determine their mode of coordination. Whilst particular emphasis was placed on the synthesis and structural characterisation of these complexes, their photophysical and electrochemical properties were also studied and Chapters 4 and 6 detail the results of these studies. The complexes all contain ligands with varying σ-donor and π-acceptor properties and their characterisation aims to determine if the variation of these ligand properties influences their photophysical and electrochemical properties. Their behaviour is compared with that of the tris homoleptic complexes $[Rh(phen)_3]^{3+}$ and $[Rh(bpy)_3]^{3+}$ and where possible with analogous Ru(II) complexes.

Chapter 7 concentrates on Rh(III) dinuclear complexes and developments to date in this area are detailed here. The chapter details the numerous synthetic approaches which were taken in attempts to synthesise Rh(III)/Ru(II) dinuclear complexes and also discusses the difficulties which were encountered.

Whilst conclusions are drawn at the end of each chapter it is the final chapter, Chapter 8, which aims to take the results discussed throughout the thesis into consideration. It is in this chapter that the issues of coordination modes, protonation states and the photophysical and electrochemical properties of all of the complexes synthesised will be addressed, with particular emphasis being placed upon their behaviour in relation to their ligand σ-donor and π-acceptor strengths. Having analysed the results obtained, Chapter 8 also proposes avenues through which this research can progress.

References:

1 F.R. Hartly, *Chemistry of the Platinum Group Metals – Recent Developments*, **1991,** Elservier, Amsterdam; New York.

2 J.C. Bailar, H.J. Emeléus, R. Nyholm, A.F.Trotman-Dickenson, Eds, *Comprehensive Inorganic Chemistry*, Volume 3, **1973,** Perganom Press Ltd, Oxford.

3 K.R. Mann, N.S. Lewis, V.M. Miskowski, D.K. Erwin, G.S. Hammond, H.B. Gray, *J. Am. Chem. Soc.*, **1977**, *99*, 5525-5526.

4 G.M. Brown, S.F. Chan, C. Creutz, H.A. Schwarz, N. Sutin, *J. Am. Chem. Soc.*, **1979**, *101*, 7638-7640.

5 M. Kirch, J.M. Lehn, J.P. Sauvage, *Helv. Chim. Acta.*, **1979**, *1*, 449-451.

6 S.F. Chan, M. Chou, C. Creutz, T. Matsubara, N. Sutin, *J. Am. Chem. Soc.*, **1981**, *103*, 369-379.

7 J.M. Lehn, J.P. Sauvage, *Nouv. J. Chim.*, **1977**, *1*, 449-451.

8 M. Kirch, J.M. Lehn, J.P. Sauvage, *Helv. Chim. Acta*, **1979**, *62*, 1345-1384.

9 M.F. Sadiq, M.H. Zaghal, *Polyhedron*, **1997**, *16*, 1483-1486.

10 G. Mestroni, E. Alessio, A. Sessanta o Santi, S. Geremia, A. Bergamo, G. Sava, A. Boccarelli, A. Schettino, M. Coluccia, *Inorg. Chim. Acta*, **1998**, *273*, 62-71.

11 F.P. Pruchnik, P. Jakimowicz, Z. Ciunik, J Zakrzewska-Czerwińska, A. Opolski, J. Wietrzyk, E. Wojdat, *Inorg. Chim. Acta*, **2002**, *334*, 59-66.

12 C.E. Housecroft, *Coord. Chem. Rev.*, **1995**, *146*, 235-267.

13 C.E. Housecroft, *Coord. Chem. Rev.*, **1996,** *152*, 107-139.

14 M.J. Hannon, *Coord. Chem. Rev.*, **1997**, *162*, 477-494.

15 D.G. DeWit, *Coord. Chem Rev.*, **1996**, *147*, 209-246.

16 K. Kalyanasundaram, *Photochemistry of Polypyridine and Porphyrin Complexes*, **1992**, Academic Press, London.

17 C. Kaes, A. Katz, M.W. Hosseini, *Chem. Rev.*, **2000**, *100*, 3553-3590.

18 F.A. Cotton, G. Wilkinson, P.L. Gaus, *Basic Inorganic Chemistry, 3rd Ed.*, **1995**, Wiley & Sons Inc., New York.

19 R.D. Gillard, J.A. Osborn, G. Wilkinson, *J. Chem. Soc.*, **1965**, 1951-1965.

20 E.D. McKenzie, R.A. Plowman, *J. Inorg. Nucl. Chem.*, **1970**, *32*, 199-212.

21 E.D. McKenzie, *Coord. Chem. Rev.*, **1971**, *6*, 187-216.

22 J.A. Broomhead, W. Grumley, *Inorg. Chem.*, **1971**, *10*, 2002-2009.

23 P.M. Gidney, R.D. Gillard, B.T. Heaton, *J. Am. Chem. Soc.*, **1972**, 2621-2628.

24 D.E. Schwab, J.V. Rund, *J. Inorg. Nucl. Chem.*, **1970**, *32*, 3949-3950.

25 C.M. Harris, E.D. McKenzie, *J. Inorg. Nucl. Chem.*, **1963**, *25*, 171-174.

26 M.E. Frink, S.D. Sprouse, H.A. Goodwin, R.J. Watts, P.C. Ford, *Inorg. Chem.*, **1988**, *27*, 1283-1286.

27 A.M. Pyle, M.Y. Chiang, J.K. Barton, *Inorg. Chem.*, **1990**, *29*, 4487-4495.

28 M.T. Indelli, C.A. Bignozzi, A. Harriman, R.J. Schoonover, F. Scandola, *J. Am. Chem. Soc.*, **1994**, *116*, 3768-3779.

29 I. Ortmans, P. Didier, A. Kirsch-De Mesmaeker, *Inorg. Chem.*, **1995**, *34*, 3695-3704.

30 M.T. Indelli, F. Scandola, *Inorg. Chem.*, **1990**, *29*, 3056-3058.

31 M. Haga, T. Ano, T. Ishizaki, K. Kano, K. Nozaki, T. Ohno, *J. Chem. Soc., Dalton Trans.*, **1994**, 263-272.

32 J. Lee, L.M. Vrana, E.R. Bullock, K.J. Brewer, *Inorg. Chem.*, **1998**, *37*, 3575-3580.

33 M.T. Indelli, F. Scandola, J.P. Collin, J.P. Sauvage, A. Sour, *Inorg. Chem.*, **1996**, *35*, 303-312.

34 V. Balzani, A. Juris, M. Venturi, S. Campagna, S. Serroni, *Chem. Rev.*, **1996**, *96*, 759-833.

35 J.R. Lakowicz, *Principles of Fluorescence Spectroscopy*, **1984**, Plenum Press, New York.

36 D.F. Schriver, P.W. Atkins, C.H. Langford, *Inorganic Chemistry, Second Edition*, **1994**, Oxford University Press, New York.

37 P.C. Ford, *J. Chem. Ed.*, **1983**, *60*, 829-833.

38 D.H.W. Carstens, G.A. Crosby, *J. Mol. Spectrosc.*, **1970**, *34*, 113-135.

39 J.N. Demas, G.A. Crosby, *J. Am. Chem. Soc.*, **1970**, *92*, 7762-7270.

40 W. Dawson, J.L. Kropp, M.W. Windsor, *J. Chem. Phys.*, **1966**, *45*, 2410-2418.

41 Y. Ohashi, K. Yoshihara, S. Nagakura, *J. Mol. Spectrosc.*, **1971**, *38*, 43-52.

42 A. Islam, N. Ikeda, K. Nozaki, T. Ohno, *J. Photochem Photobiol A: Chem.*, **1997**, *106*, 61-66.

43 F.E. Lytle, D.M. Hercules, *J. Am. Chem. Soc.*, **1969**, *91*, 253-257.

44 F. Bolletta, A. Rossi, F. Barigelletti, S. Dellonte, V. Balzani, *Gazz. Chim. Ital.*, **1981**, *111*, 155.

45 M. Nishizawa, T.M. Suzuki, S. Sprouse, R.J. Watts, P.C. Ford, *Inorg.Chem.*, **1984**, *23*, 1837-1841.

46 H. Yersin, W. Humbs, J. Strasser, *Coord. Chem Rev.*, **1997**, *159*, 325-358.

47 G.A. Crosby, W.H. Elfring Jr., *J. Phys. Chem.*, **1976**, *80*, 2206-2211.

48 M.K. DeArmond, J.E. Hillis, *J. Chem. Phys.*, **1971**, *54*, 2247-2253.

49 R.J. Watts, J. Van Houten, *J. Am. Chem. Soc.*, **1978**, *100*, 1718-1721.

50 C. Turro, A. Evenzahav, S.H. Bossmann, J.K. Barton, N.J. Turro, *Inorg. Chim. Acta*, **1996**, *243*, 101-108.

51 Y. Komada, S. Yamauchi, N. Hirota, *J. Phys. Chem.*, **1986**, *90*, 6425-6430.

52 W. Humbs, H. Yersin, *Inorg. Chem.*, **1996**, *35*, 2220-2228.

53 Giesbergen, M. Glasbeek, *J. Phys. Chem.*, **1993**, *97*, 9942-9946.

54 H. Miki, M. Shimada, T. Azumi, J.A. Brozik, G.A. Crosby, *J. Phys. Chem.*, **1993**, *97*,11175-11179.

55 M. Zaghal, H.A. Qaseer, *Trans. Metal Chem.*, **1991**, *16*, 39-44.

56 M. Zaghal, B.F. Ali, *Polyhedron*, **1995**, *14*, 1011-1019.

57 S.C. Rasmussen, M.M. Richter, E. Yi, H. Place, K.J. Brewer, *Inorg. Chem.*, **1990**, *29*, 3926-3932.

58 J.A. Brozik, G.A. Crosby, *J. Phys. Chem.*, **1998**, *102*, 45-50.

59 M.T. Indelli, A. Carioli, F. Scandola, *J. Phys. Chem.*, **1984**, *88*, 2685-2686.

60 T. Ohno, S. Kato, *Bull. Chem. Soc. Jpn.*, **1984**, *57*, 3391-3394.

61 G. Kew, K. DeArmond, K. Hanck, *J. Phys. Chem.*, **1974**, *78*, 727-734.

62 G. Kew, K. Hanck, K. DeArmond, *J. Phys. Chem.*, **1975**, *79*, 1828-1835.

63 C.M. Bolinger, N. Story, B.P. Sullivan, T.J. Meyer, *Inorg. Chem.*, **1988**, *27*, 4582-4587.

64 M.Maestri, D. Sandrini, V. Balzani, U. Maeder, A. von Zelewsky, *Inorg. Chem.*, **1987**, *26*, 1323-1327.

65 D. Sandrini, M. Maestri, V. Balzani, U. Maeder, A. von Zelewsky, *Inorg. Chem.*, **1988**, *27*, 2640-2643.

66 F Bargelletti, D. Sandrini, M. Maestri, V. Balzani, A. von Zelewsky, L. Chassot, P. Jolliet, U. Maeder, *Inorg. Chem.*, **1988**, *27*, 3644-3647.

67 P. Didier, I. Ortmans, A. K. Mesmaeker, R.J. Watts, *Inorg. Chem.*, **1993**, *32*, 5239-5245.

68 Y. Ohsawa, S. Sprouse, K.A. King, M.K. DeArmond, K.W. Hanck, R.J. Watts, *J. Phys. Chem.*, **1987**, *91*, 1047-1054.

69 G. Frei, A. Zilian, A. Raselli, H.U. Güdel, H.B. Bürgi, *Inorg. Chem.*, **1992**, *31*, 4766-4773.

70 M.G. Colombo, T. C. Brunold, T. Riedener, H.U. Güdel, M. Förtsch, H.B. Bürgi, *Inorg. Chem.*, **1994**, *33*, 545-550.

71 S. Sprouse, K.A. King, P.J. Spellane, R.J. Watts, *J. Am. Chem. Soc.*, **1984**, *106*, 6647-6653.

72 F.O. Garces, R.J. Watts, *Magn. Reson. in Chem.*, **1993**, *31*, 529-536.

73 J.H. Van Diemen, J.G. Haasnoot, R. Hage, J. Reedijk, J.G. Vos, R. Wang, *Inorg. Chem.*, **1991**, *30*, 4038-4043.

74 J.H. Van Diemen, R. Hage, J.G. Haasnoot, H.E.B. Lempers, J. Reedijk, J.G. Vos, L.De Cola, F. Barigelletti, V. Balzani, *Inorg. Chem.*, **1992**, *31*, 3518-3522.

75 G. Calogero, G. Giuffrida, S. Serroni, V. Ricevuto, S. Campagna, *Inorg. Chem.*, **1995**, *34*, 541-545.

76 H.A. Schwarz, C. Creutz, *Inorg. Chem.*, **1983**, *22*, 707-713.

77 P. Paul, B. Tyagi, A.K. Bilakhiya, M.M. Bhadbhade, E. Suresh, *J. Chem. Soc., Dalton Trans.*, **1999**, 2009-2014.

78 M. Bień, F.Pruchnik, A. Seniuk, T.M. Lachowicz, P. Jakimowicz, *J. Inorg. Biochem.*, **1999**, *73*, 49-55.

79 L.A. Oro, M.T. Pinillos, C. Tejel, C. Foces-Foces, F.H. Cano, *J. Chem. Soc., Dalton Trans.*, **1986**, 1087-1094.

80 M.P. Garciá, J.A. Manero, L.A. Oro, C. Apreda, F.H. Cano, C. Foces-Foces, J.G. Haasnoot, R. Prins, J. Reedijk, *Inorg. Chim. Acta*, **1986**, *122*, 235-241.

81 M.P. Garciá, M. Martin, L.A. Oro, *Inorg. Chim. Acta*, **1992**, *191*, 221-225.

82 D.R. Striplin, G.A. Crosby, *J. Phys. Chem.*, **1995**, *99*, 7977-7984.

83 F.P. Pruchnik, P. Jakimowicz, Z. Ciunik, *Inorg. Chem. Commum.*, **2001**, *4*, 726-729.

Chapter 2 - Experimental Procedures

"Every revolutionary idea seems to evoke three stages of reaction. They may be summed up by the phrases: (1) It's completely impossible. (2) It's possible, but it's not worth doing. (3) I said it was a good idea all along."

Arthur C. Clarke

Abstract: The following chapter describes the experimental procedures that were followed throughout the course of this study. Steps, which were taken to ensure reproducibility of results, especially in the case of the electrochemical analysis, have also been detailed. The instrumentation that was used in the characterisation of the complexes has been detailed and where it was felt necessary the techniques used have been explained. Also included are the methods by which data were analysed and conventions which were followed in the presentation of data throughout this thesis.

2.1 Reagents and Materials

All synthetic reagents and solvents were of commercial grade and no further purification was carried out unless otherwise stated. 2,2'-bipyridine, 1,10-phenanthroline, $RhCl_3xH_2O$, hydrazine monohydrate and the ligands NH_2bpt = 4-amino-3,5-bis(pyridin-2-yl)-4H-1,2,4-triazole and dppt = 5,6-diphenyl-3-(pyridin-2-yl)-1,2,4-triazine were purchased from Aldrich whilst electrochemical grade tetrabutylammoniumfluoroborate was purchased from Lennox. The solvents used for the spectroscopic measurements were of spectrophotometric grade and were purchased from Lennox and the solvents used for electrochemical measurements were of spectrophotometric grade and were purchased from Aldrich.

2.2 Column Chromatography

Two different systems were used in order to purify the rhodium(III) complexes.

- The first involved a column being run on silica using a mobile phase of acetonitrile:water:potassium nitrate in the ratio 40:10:1.

- The second type utilised an ion exchange resin. In this type of chromatography the column packing has a charge bearing functional group attached to the polymer matrix. The functional groups are permanently bonded ionic groups associated with counterions of the opposite charge. The most common retention mechanism in these instances is the simple exchange of sample ions and mobile-phase ions with the charged group of the stationary phase. In this particular case the carboxy-resin Sephadex C-25 was used and various concentrations of NaCl were used as the mobile phase. The carboxy resin is a weak acid and is therefore a weak cation exchanger that functions in the pH region 6-13. The Sephadex C-25 was prepared by being placed in distilled water for at least 24 hours prior to the running of the column.

2.3 Nuclear Magnetic Resonance

A Bruker AC400 instrument was used in order to obtain both ^{1}H (400MHz) and ^{13}C (100MHz) nuclear magnetic resonance spectra. The free induction decay (FID) profiles obtained were processed using the software package XWIN-NMR. The solvent used to carry out the NMR measurements was d_6-dimethyl sulphoxide (d_6-DMSO) for both complexes and ligands unless otherwise stated. Chemical shifts were measured relative to TMS. Temperature dependent NMR experiments were carried out in the range 19° - 59°C.

The 2D Correlated spectroscopy (COSY) experiment is used to identify nuclei that share a scalar (J) coupling. The presence of off-diagonal peaks (cross-peaks) in the spectrum directly correlates the coupled partners. The COSY experiments carried out involved the accumulation of 128 FID's each of 16 scans. Digital filtering was sine-bell squared and the FID was zero filled in the F1 dimension. Acquisition parameters were F1 = ± 500Hz, F2 = 1000Hz and $t_{½}$ = 0.001s. The cycle delay time was 1.5s.

Heteronuclear Multiple Quantum Coherence (HMQC) NMR experiments were carried out in order to assign ^{13}C NMR spectra. This is a 2D experiment used to correlate directly bonded carbon-proton nuclei. This process utilises proton detection and has very high sensitivity (and can be quicker to acquire than a 1D carbon spectrum). The correlations can be used to map known proton assignments onto their directly attached carbons. The 2D spectrum can also prove useful in the assignment of the proton spectrum itself by dispersing the proton resonances along the ^{13}C dimension and so reducing proton multiplet overlap. It also provides a convenient way of identifying diastereotopic geminal protons (which are sometimes difficult to distinguish unambiguously, even in COSY) since only these will produce two correlations to the same carbon.[1]

2.4 Absorption Spectroscopy

UV-VIS spectra were obtained using a Shimadzu UV-3100 spectrophotometer connected to an Elonex 466/1 PC and were analysed using the UV-VIS data manager. A 1cm pathlength quartz cell was used for all measurements and spectra were obtained in both acetonitrile and ethanol:methanol 4:1.

2.5 Photochemical Studies

Photolysis experiments were carried out in acetonitrile using a 1cm pathlength quartz cell and were followed by UV-VIS absorption spectroscopy. A slide projector, Kodak Carousel S-AV2020, using a 20 W Tungsten filament source was used as a light source.

2.6 Emission Spectroscopy

Emission spectra were obtained using a Perkin Elmer LS50B luminescence spectrophotometer attached to an Elonex 5200/1 PC. All measurements were carried out at 77K in an ethanol:methanol 4:1 glass. Measurements were carried out using either an Oxford Instruments liquid nitrogen cooled cryostat model 39426 (80K) and the custom made quartz cell or in a glass NMR tube inserted into a liquid nitrogen filled glass cryostat (77K). When using the Oxford Instruments liquid nitrogen cooled cryostat samples were allowed to equilibrate at 77K for approximately 20 minutes before measurements were carried out. The slit widths for all the 77K measurements were set at either 10nm or 15nm unless otherwise stated and all spectra are uncorrected for photomultiplier response. It is important to note that the luminescence spectrophotometer used can be adjusted to measure fluorescence, phosphorescence or bioluminescence. This was of particular importance as many of the complexes studied were dual emitting and exhibited a π-π^* based emission with a lifetime in the region of 0.91-27.3 ms and a d-d* emission with lifetimes in the region of 1.5-21 μs. The difference in the lifetimes of these two processes meant that when the instrument was set to measure phosphorescence, i.e. emission processes

longer than 1ms, only the π-π^* based emission was detected. In order to obtain the emission spectra associated with the d-d* emission it was necessary to set the instrument to measure fluorescence. As a result all compounds were analysed using both methods.

2.7 Excited State Lifetime Measurements

Two different systems were utilised in the determination of the lifetimes of the complexes being studied. The first system used was an Edinburgh Instruments Time Correlated Single Photon Counter (TCSPC) and measurements using this approach were carried out with the assistance of Wesley Browne. This system, an Edinburgh Instruments FL900 with an nf900 ns flashlamp and CD900 TAC (time to amplitude converter), is detailed in Figure 2.1. TCSPC is a digital counting technique, counting photons that are time correlated in relation to the excitation light pulse. The heart of this technique is a time-to-amplitude converter (TAC). By this method the sample is repetitively excited using a pulsed light source. Each pulse is optically monitored to produce a start signal, which in turn is used to trigger the voltage ramp of the TAC. When the first photon from the sample is detected the voltage ramp is halted. The TAC provides an output pulse whose voltage is proportional to the time between the start and stop signals. A multichannel analyser (MCA) converts this voltage to a time channel. Summing over many pulses the MCA builds up a probability histogram of counts versus time channels.[3] Figure 2.2 illustrates a schematic configuration for time correlated single photon counting.

The TCSPC allowed for the measurement of lifetimes within the range of 2ns to 30μs hence it was necessary to use a different system in order to measure the lifetimes in the ms region. A Spectron Laser Systems SL801 Q-switched Nd-Yag laser capable of generating both the third (λ = 355nm; 30 mJ) and fourth (λ = 266nm; 40 mJ) harmonic of the fundamental wavelength (pulse duration 20ns) was used by Dr. Mary Pryce to carry out these measurements. The monitoring system, arranged in a crossbeam configuration, consisted of an F/3.4 monochromator and a five-stage photomultiplier supplied by Applied Photophysics. The signals were captured using

a Hewlett-Packard 54510A digitising oscilloscope, and the data reduction was carried out using a software program developed in house.[2]

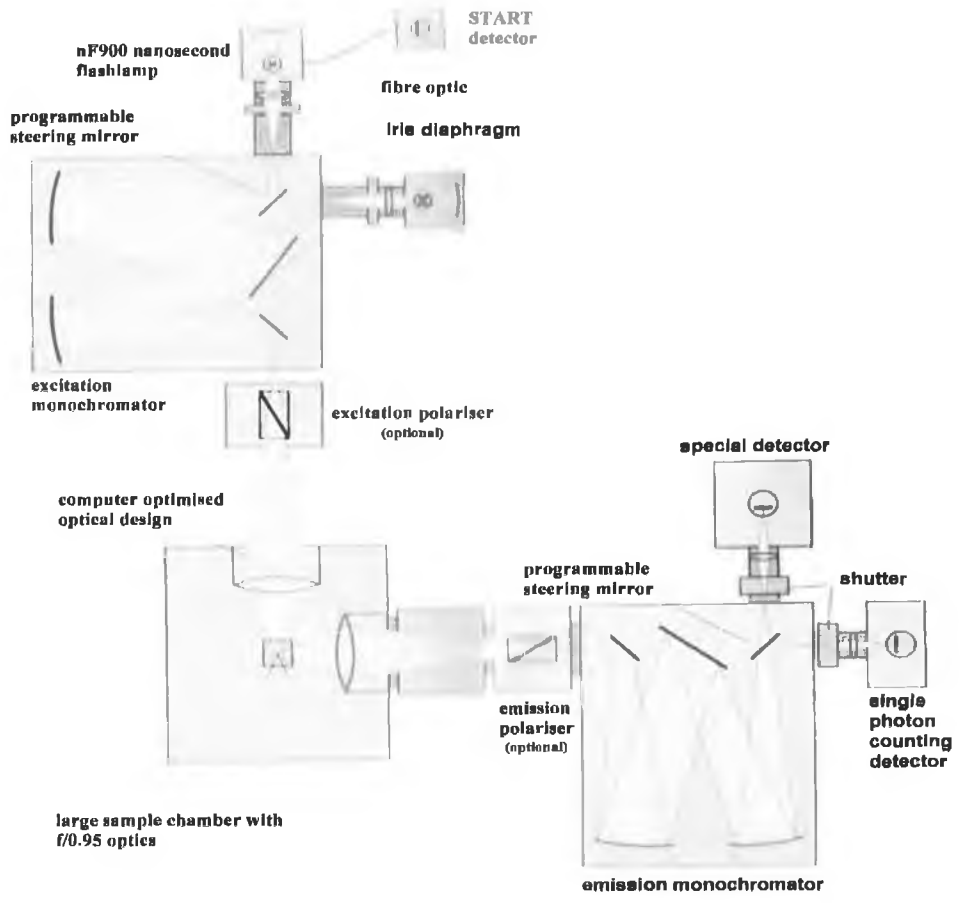

Figure 2.1 Schematic diagram of the Edinburgh Instruments FL900 Time Correlated Single Photon Counter (TCSPC).[3]

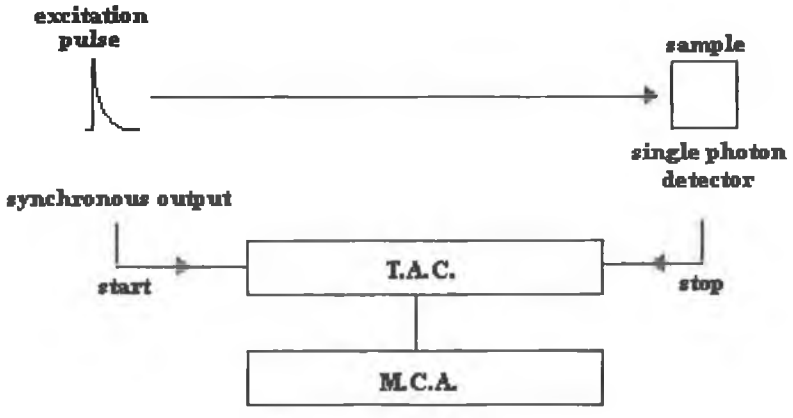

Figure 2.2 Schematic configuration for time correlated single photon counting.[3]

All lifetime measurements were carried out in an ethanol:methanol 4:1 glass at 77K using 337 nm as the excitation wavelength. Measurements were carried out using a glass cryostat and the sample was contained in an NMR tube. It should be noted that each NMR tube was washed thoroughly and, prior to lifetime measurements being carried out, the emission spectra of each sample tube containing just the solvent was obtained to make sure that there were no impurities present in the NMR tube which would influence the lifetime measurements.

2.8 Electrochemical Measurements

Electrochemical measurements were carried out using a CH Instruments Model C440 potentiostat. A conventional three electrode cell was used with a platinum electrode functioning as the working electrode, a platinum wire as the auxiliary electrode and a Ag/Ag^+ (acetonitrile with 10mM $AgNO_3$ and 0.1 M $TBABF_4$) half-cell was used as the reference electrode. All measurements were carried out in anhydrous acetonitrile with 0.1M tetrabutylammoniumfluoroborate ($TBABF_4$) as the supporting electrolyte.

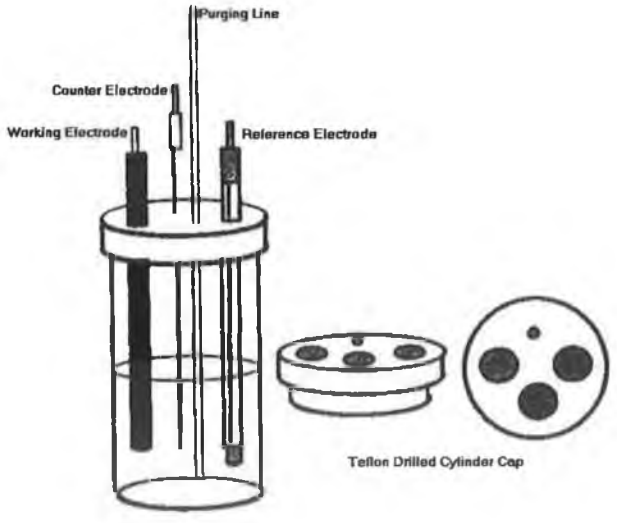

Figure 2.3 Illustration of the three electrode cell used for measurements.[4]

Two types of electrochemical experiments were carried out. The first technique, cyclic voltammetry (CV) involves the cycling of the potential of a

stationary electrode immersed in a quiescent solution and measuring the resulting current. The second technique, differential pulse voltammetry (DVP), involves a series of potential pulses of fixed, but small, amplitude (10-100mV) is superimposed on a dc voltage ramp. The current is first measured before applying the potential pulse and again late into the pulse. For each cycle the first current value is instrumentally subtracted from the second and a plot of this current applied (dc ramp) potential produces a stepped peak-shaped incremental derivative voltammogram. [5]

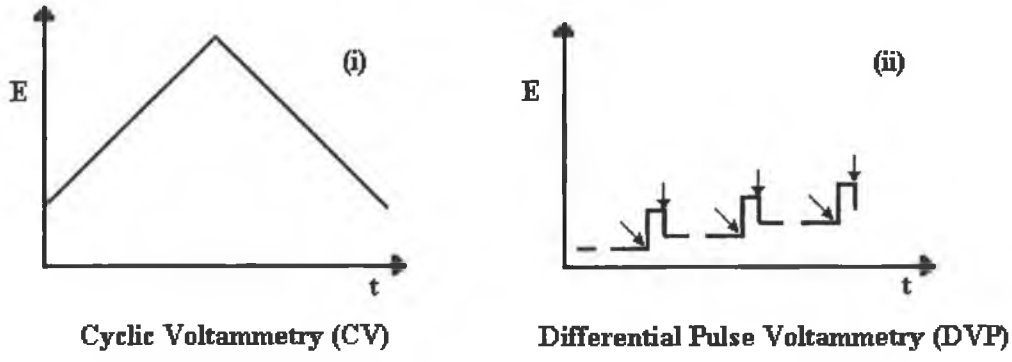

Figure 2.4 Potential excitation functions for cyclic voltammetry (CV) and differential pulse voltammetry. The arrows in (ii) indicate the measuring points. [4]

Particular care was taken in the preparation of samples for analysis. All glassware, which was used in these experiments, was left to dry overnight in a vacuum oven at 80°. The $TBABF_4$ was also dried in the vacuum oven. The working electrodes used were polished on a soft polishing pad with aqueous slurry of 0.3 micron alumina and sonicated for at least 5 min in deionised water before use. The electrode was then rinsed with acetone and air dried before being used. The auxiliary electrode was either flamed before use or washed thoroughly with acetone making sure that it was dried before being used. The acetonitrile used in these experiments was stored under argon and the 0.1M $TBABF_4$ solutions were prepared in either $2.5cm^3$ or $5cm^3$, using a calibrated glass syringe, for immediate use. All solutions were degassed for 5 minutes and kept under a blanket of either nitrogen or argon throughout the experiments. CV's were obtained at a scan rate of 0.1V/s and DPV's were obtained with a step height of 50 mV, at an increment of 4 mV with a pulse duration of 60 ms

and a sampling interval of 20 ms with a frequency of 5 Hz. The reference electrode was calibrated versus ferrocene on a daily basis.[6] It should also be noted that all CV's and DPV's detailed in this thesis observe IUPAC conventions i.e. anodic current is positive and positive potentials are right hand plotted and the cyclic voltammograms are drawn ''clockwise''as illustrated by Figure 2.5.[7]

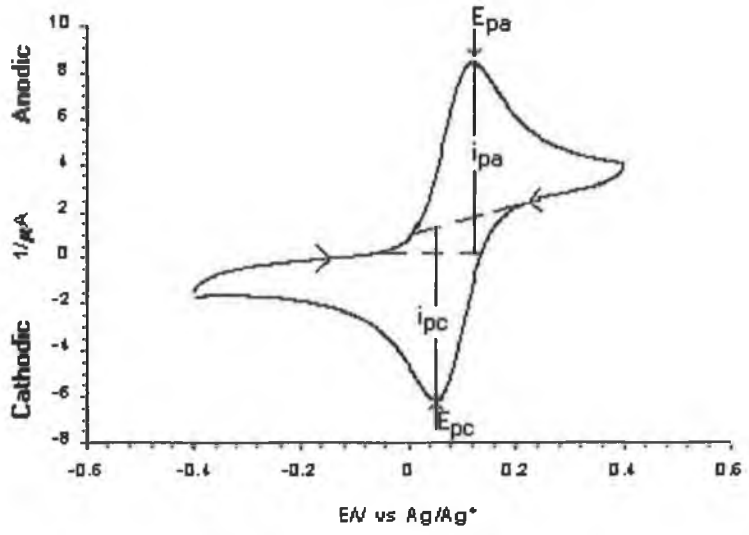

Figure 2.5 Illustration of IUPAC conventions for cyclic voltammograms using a CV of ferrocene where E_{pa} = the anodic peak potential, E_{pc} = the cathodic peak potential, i_{pa} = the anodic peak current and i_{pc} = the cathodic peak potential.

2.9 Mass Spectrometry

Mass spectrometry was carried out using a Bruker-Esquire LC-00050 electrospray ionisation mass spectrometer. The measurements were carried out at a positive polarity with a cap-exit voltage of 167V. The spectra obtained were an average of 30 scans and were recorded in the scan range of 50-2200 m/z with an acquisition time of between 300 and 900ms and a potential of between 30 and 70V. All measurements were carried out in spectrophotometric grade acetonitrile. Samples were prepared by dissolving ~2mg of sample in 1ml of acetonitrile. 50μL of this solution was then taken and diluted by the addition of 1ml of acetonitrile and this solution was then used to acquire the mass spectrum.

2.10 Deuteration

Deuterated Hpytr and Hbpt, H-d_4-pytr and d_8-bpt, were obtained from Christine O'Connor and d_8-bpy was obtained from Wesley Browne.[8]

2.11 Elemental Analysis

Elemental analysis on C, H, and N was carried out at the Microanalytical Laboratory of University College Dublin using an Exetor analytical CE440 instrument. It should be noted that when calculating the overall mass of deuterated complexes the additional mass of the deuterium was included but when calculating the percentage of hydrogen and deuterium in the sample all protons and deuterons were treated as protons. Generally

$$\%E = [Mass_E \div MW_C] \times 100 \qquad \text{where E = element and C = complex}$$

therefore the % H in bpy and d_8-bpy is calculated as follows;

bpy $\%H = [\mathbf{(8x1)} \div \{(10x12) + \mathbf{(8 \times 1)} + (2 \times 14)\}] \times 100 = 5.16$ whereas

d_8-bpy $\%H = [\mathbf{(8x1)} \div \{(10x12) + \mathbf{(8 \times 2)} + (2 \times 14)\}] \times 100 = 4.91.$

2.12 X-ray crystallography

X-ray crystallography was carried out by Dr. John Gallagher at Dublin City University. The data was collected using a Bruker P4 diffractometer using the XSCANS software with graphite monochromated Mo-Kα radiation.[9] The structures were solved using direct methods and refined with the SHELXL-97 program and the non-hydrogen atoms were refined with anisotropic thermal methods.[10] CCDC reference number for the crystal structure of $[Rh(phen)_2(NHbpt)](PF_6)_2 \cdot 0.767\ CH_3CN \cdot 0.28\ H_2O$ is 201151.

References:

1 W.R. Croasmun, R.M.K. Carlson, *Two-Dimensional NMR Spectroscopy – Applications for Chemists and Biochemists, Second Edition,* **1994,** VCH Publishers Inc., New York.

2 B. Crocock, *PhD. Thesis*, Dublin City University, **1992**.

3 *Edinburgh Analytical Instruments FL900 Time Correlated Single Photon Counter (TCSPC) product guide*, Edinburgh Instruments LTD, Scotland.

4 A.E. Kaifer, M. Gomez-Kaifer, *Supramolecular Electrochemistry*, **1999**, Wiley-VCH, Weinheim (Federal Republic of Germany).

5 H.H. Willard, L.L. Merritt Jr., J.A. Dean, F.A. Settle Jr., *Instrumental Methods of Analysis*, *Seventh Edition*, **1988**, Wadsworth Inc., California.

6 V.V. Pavlishchuk, A.W. Addison, *Inorg. Chim. Acta*, **2000**, *298*, 97-102.

7 G.Gritzner, J. Kůta, *Pure and Appl. Chem.*, **1984**, *56*, 461-466.

8 W.R. Browne, J.G. Vos, *Coord. Chem. Rev.*, **2001**, *219-221*, 761-787.

9 J.Fait, *XSCANS-Program for Data Collection and Processing*, **1993**, Brucker, Madison, WI.

10 SHELXS-97 (Sheldrick, 1990) and SHELXL-97 (Sheldrick, 1997), University of Göttingen, Göttingen 1997.

Chapter 3 - Synthesis and Structural Characterisation of Rh(III) complexes with pyridyl triazole ligands.

"The most exciting phrase to hear in science, the one that heralds new discoveries, is not 'Eureka!' (I found it!) but 'That's funny...."

Isaac Asimov

Abstract: The following chapter outlines in detail the synthesis and structural characterisation of a series of complexes of the form $[Rh(L)_2(L')]^{n+}$ where L is either 2,2'-bipyridine (bpy) or 1,10-phenanthroline (phen), L' is a pyridyl triazole based ligand and n is either 2 or 3 depending upon the nature of the pyridyl triazole ligand. The synthesis, purification and structural behaviour of these types of complexes are considered in relation to analogous ruthenium(II) complexes. The structural characterisation of the Rh(III) complexes studied involved several techniques including X-ray crystallography, NMR spectroscopy and mass spectrometry. Confirmation of the purity of the complexes was obtained by elemental analysis and complexes were also analysed by mass spectrometry. Only two crystals were obtained which were suitable for analysis via X-ray crystallography and both are detailed in this chapter with supplementary data being included in Appendix II.

3.1 Introduction

Polypyridine complexes with d^6 transition metal ions have generated widespread interest in recent years due to their photophysical and photochemical properties and their potential as photocatalysts and photosensitisers. These complexes have the ability to play the role of light absorption sensitisers and / or light emission sensitisers for the interconversion between light energy and chemical energy via electron transfer reactions involving electronically excited states and they have been used as a basis for studying electron transfer processes with the aim of creating model compounds that mimic energy transfer or electron transfer processes in natural processes.[1] Complexes with d^6 metals such as Ru(II), Os(II) and Fe(II) have been studied extensively whilst complexes incorporating Rh(III), Ir(III), Pt(IV) and Pd(IV) have been researched to a lesser degree.[2,3] The properties of these complexes tend to be controlled by the σ-donor and π-acceptor properties of the ligands. Ligands such as py, bpy and phen are regularly used in the development of polypyridyl transition metal complexes. A common feature of all these ligands is the presence of an empty π^* orbital that can accept electron density from the metal ion to form a type of π bonding that supplements the σ bonding arising from the donation of lone pairs of electrons. This in turn results in the stabilisation of the metal complex even in complexes with metal ions in low oxidation states. In this manner the high electron density on the metal is delocalised onto the ligands. It should be noted that a ligand that is a weaker σ-donor but a stronger π-acceptor than bpy is referred to as a Class I type ligand and one which is a weak π-acceptor but a strong σ-donor in comparison to bpy is referred to as a Class II ligand. Examples of each class of ligand may be seen in Figure 1.2. Strong π-acceptor ligands stabilise the filled metal orbitals and as a result high oxidation potentials and low reduction potentials are observed whereas strong σ-donor ligands donate much electron density into the d-orbitals thus giving rise to lower oxidation potentials and more negative reduction potentials. It should also be noted that the difference in energy between the filled d-orbitals and the lowest empty ligand based orbital is related to the absorption and emission energy of the complexes. From this it can be seen that by judicious choice of metal atom, oxidation state and coordinating ligands it is possible

to fine-tune not only the redox potentials but also the absorption and emission bands of a complex.[4]

The 1,2,4-triazoles and their derivatives have generated a sizeable amount of interest in recent years in the development of polypyridyl transition metal complexes.[5] This attention has stemmed from the strong σ-donor properties of these ligands and from the fact that the two coordinating nitrogen atoms are not equivalent with the N2' coordination site being a better σ-donor than the N4' site. Figure 3.1 illustrates not only the structure of the ligand Hpytr but also the labelling that will be referred to throughout this discussion.

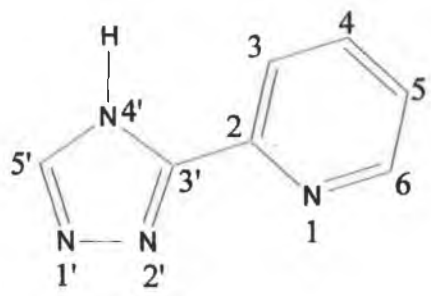

Figure 3.1 Hpytr ligand with numbering

The 1,2,4-triazoles are considered to be Class II ligands i.e. they are stronger σ-donors and weaker π-acceptors than 2,2'-bipyridine. The introduction of substituents onto various positions of the triazole ring makes it possible to control which coordination mode is obtained, for example, if a methyl group is present at the N4' position then coordination is only possible via the N2' position.

A substantial amount of research has been dedicated to the study of ruthenium(II) complexes which incorporate these 1,2,4-triazoles and their derivatives and to a lesser extent osmium(II) and rhodium(III) complexes have been studied.[6] The first ruthenium(II) polypyridyl complex that contained a 1,2,4-triazole ligand was reported in 1983 by Vos *et. al.*[7] Since that time numerous ruthenium(II) mononuclear complexes containing 1,2,4-triazoles have been synthesised and

characterised.[8,9,10,11,12] From a characterisation point of view ^{1}H NMR studies have been particularly important in determining modes of coordination whereas HPLC studies have made it possible to isolate the coordination isomers of these complexes making it feasible to study the effect of coordination geometry upon the spectroscopic and the acid-base properties of the complex.[10,11] Mononuclear systems have been extended to include ligands such as Hbpt that are capable of forming homo- and hetero-bimetallic species and even ligands capable of forming hexanuclear complexes, such as the tris(pyrazyltriazole)benzene ligand seen in Figure 3.2, have been developed. [13,14]

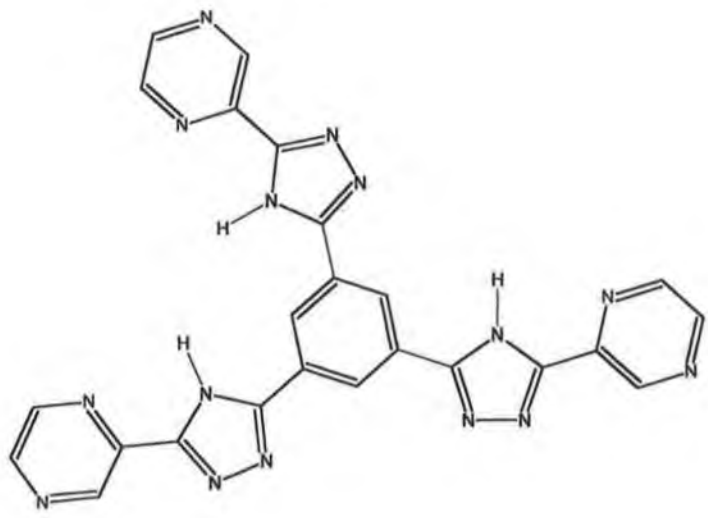

Figure 3.2 Structure of the ligand 1,3,5-tris(5-(pyrazin-2-yl-1,2,4-triazole)benzene.[14]

A more limited number of polypyridyl complexes containing 1,2,4-triazole ligands have been reported in which the metal centres rhodium(I) and rhodium(III) have been incorporated. Oro *et. al.* reported rhodium(I) complexes with 1,2,4-triazolate ligands (Section 1.6) and have since reported Rh(I) complexes with the ligands 4-amino-3,5-bis(pyridin-2-yl)-1,2,4-triazole (NH_2bpt) and 3,5-bis(pyridin-2-yl)-1,2,4-triazole (Hbpt).[15,1617] When Oro *et. al.* prepared a series of complexes incorporating diolefins and the NH_2bpt ligand the carbonyl complex $[Rh(CO)_2(NH_2bpt)]ClO_4$ yielded crystals that were suitable for analysis and it was found that the rhodium ion was coordinated via a nitrogen of the pyridine ring and a

nitrogen of the triazole ring.[17] Figure 3.3 illustrates the mode of coordination observed for the cationic complex $[Rh(CO)_2(NH_2bpt)]ClO_4$.

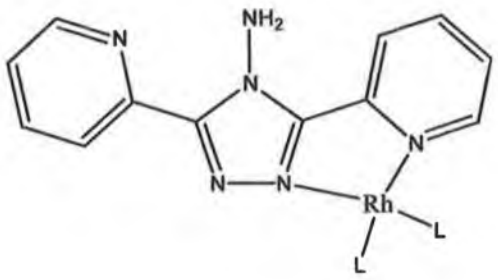

Figure 3.3 Illustration of method of coordination for the complex $[Rh(NH_2bpt)(L)_2]ClO_4$ where L = CO.

In contrast to the mode of coordination observed for the cationic complex $[Rh(CO)_2(NH_2bpt)]ClO_4$, ^1H NMR spectroscopy of the neutral complexes of the form $[Rh(NHbpt)(CO)(PPh_3)]$ and [Rh(NHbpt)(L)] where L = tetrafluorobenzobicyclo[2,2,2]octatriene (tfb), 1.5-cyclooctadiene (cod) and bicyclo[2,2,1]heptadiene (nbd) suggested that the rhodium ion was in a square-planar arrangement and was bound via the amine nitrogen and one of the pyridine nitrogens as shown in Figure 3.4.[17]

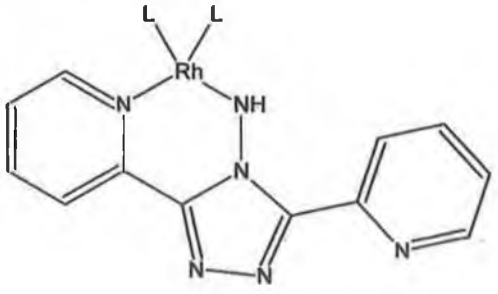

Figure 3.4 Illustration of proposed method of chelation for the complex $[Rh(NHbpt)(CO)(PPh_3)]$.[17]

Oro *et. al.* later reported the synthesis of mononuclear and dinuclear complexes with the ligand Hbpt. They prepared neutral mononuclear complexes of the type [Rh(L)(bpt)] where L = tfb, cod or $(CO)(PPh_3)$ and cationic mononuclear complexes

of the type $[Rh(L)_2(Hbpt)]^+$ where L = tfb, cod, nbd, $(CO)(PPh_3)$ or $(CO)_2$ but were not able to determine if coordination occurred via the N2' of the N4' positions.[18]

Two groups have reported rhodium complexes again with the ligands Hbpt and NH_2bpt as bridging ligands but in both these cases the complexes discussed contained Rh(III) metal centres, as opposed to the Rh(I) complexes studied by Oro *et. al.*, and the cyclometalated ligand ppy. [19,20]

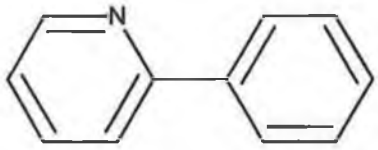

Figure 3.5 Structure of the ligand 2-phenylpyridine (ppy).

Van Diemen *et. al.* have synthesised and characterised a series of heterobimetallic ruthenium-rhodium and ruthenium-iridium complexes in which Hbpt was used as the bridging ligand.[19] The dinuclear species was obtained from the Ru(II) mononuclear complex in which the $Ru(bpy)_2$ moiety was bound to the bridging ligand via the N2' of the triazole ring. The second metal centre, either $Rh(ppy)_2$ or $Ir(ppy)_2$ was subsequently introduced and was bound via the N4' of the triazole ring. Campagna *et. al.* reported cyclometalated iridium(III) and rhodium(III) mononuclear complexes with the ligand NH_2bpt. These complexes were prepared by the cleavage of the appropriate dichloro-bridged dimer with NH_2bpt.[20]

As has been discussed in Chapter 1 one of the aims of this thesis is to develop the synthesis and characterisation of a series of mixed ligand rhodium(III) complexes, and for this purpose a series of complexes containing pyridyl triazole ligands have been synthesised. This chapter deals with the synthesis and structural characterisation, using NMR spectroscopy, X-ray crystallography and mass spectrometry of a series of mononuclear rhodium(III) complexes containing various pyridyl-triazole ligands. The complexes are of the form $[Rh^{III}(L)_2(L')](PF_6)_n$ where

L = bpy or phen, L' is a pyridyl triazole ligand and n = 2 or 3. The ligands which will be referred to in this chapter can be seen in Figure 3.6.

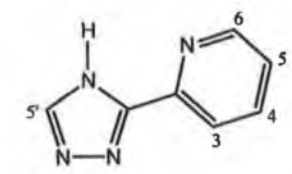

Hpytr - 3-(pyridin-2-yl)-1,2,4-triazole

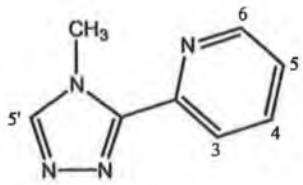

4Mpytr - 4-methyl-3-(pyridin-2-yl)-1,2,4-triazole

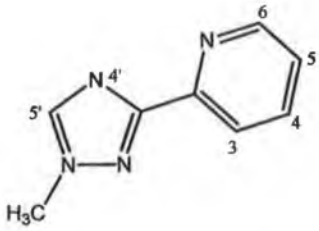

1M3pytr - 1-methyl-3-(pyridin-2-yl)-1,2,4-triazole

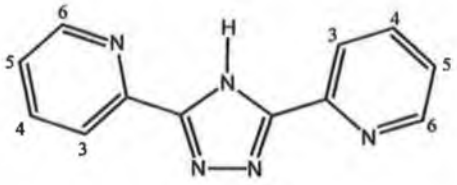

Hbpt - 3,5-bis(pyridin-2-yl)-1,2,4-triazole

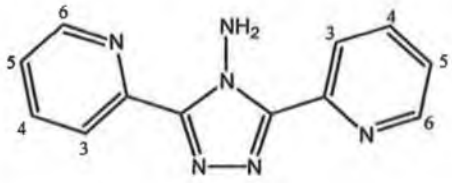

NH_2bpt - 4-amino-3,5-bis(pyridin-2-yl)-1,2,4-triazole

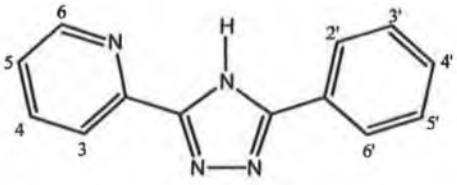

HPhpytr- 3-phenyl-5-(pyridin-2-yl)-1,2,4-triazole

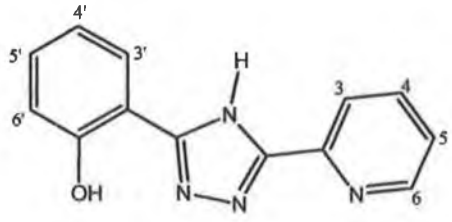

Hpt- 3-(2-phenol)-5-(pyridin-2-yl)-1,2,4-triazole

Figure 3.6 Ligands cited in the following discussion.

As can be seen in Figure 3.6 the protons of both pyridyl rings in the ligands Hbpt, NH_2bpt and HPhpytr are referred to as H3, H4, H5 and H6 however when a metal centre is coordinated to one pyridyl ring these protons will be differentiated between by referring to one set as being associated with ring A, the metal bound ring whilst the second set of protons, those associated with the uncoordinated ring, will be referred to as being associated with ring B.

3.2 Experimental

3.2.1 Preparation of Rhodium(III) Complexes

***cis*-[Rh(bpy)$_2$Cl$_2$]Cl**

$RhCl_3.(xH_20)$ (1mmol, 0.266g) was dissolved in 5cm^3 of water with gentle heating 2,2'-bipyridyl (2.2mmol, 0.344g) was dissolved in 4cm^3 of ethanol again with gentle heating. Both solutions were heated till the $RhCl_3.(xH_20)$ and 2,2'-bipyridyl had fully dissolved. At this point the $RhCl_3.(xH_20)$ was added to the 2,2'-bipyridyl . This was allowed to heat for a few minutes (2/3mins) and to this 0.1mmol (57μL) of hydrazine hydrate was added. Upon the addition of the hydrazine a yellow solution was observed and a precipitate was formed. This was heated for 10 minutes (covered using a clock glass). It was then heated further and the ethanol was allowed to evaporate off. Once the ethanol had evaporated the solution was allowed to cool on ice. The pale yellow precipitate obtained was filtered, washed repeatedly with water and dried. Yield 0.444g (85%).[21]

***cis*-[Rh(phen)$_2$Cl$_2$]Cl**

$RhCl_3.(xH_20)$ (264mg, 1mmol) was dissolved in 5cm^3 of water with gentle heating. O-phenanthroline (436mg, 2.2mmol) was dissolved in 4cm^3 of ethanol again with gentle heating. Both solutions were heated till the $RhCl_3.(xH_20)$ and o-phenanthroline had fully dissolved. At this point the $RhCl_3.(xH_20)$ was added to the o-phenanthroline. This was allowed to heat for five and to this 0.1mmol (57μL) of hydrazine hydrate was added. Upon the addition of the hydrazine a yellow solution was observed and a precipitate was formed. This was heated for 10 minutes (covered using a clock glass). It was then heated further and the ethanol was allowed to evaporate off. Once the ethanol had evaporated the solution was allowed to cool on ice. The pale yellow precipitate obtained was filtered, washed repeatedly with water and dried. Yield 0.394g (69%).[21]

$[Rh(phen)_2(pytr)][PF_6]_2 \cdot NaCl$

0.088g (0.6mmol) of 3-(pyridin-2-yl)-1,2,4-triazole (Hpytr) were dissolved in 30cm^3 water:ethanol 2:1 and to this, over a period of an hour, 0.110g (0.2mmol) of $[Rh(phen)_2Cl_2]Cl$ were added. This reaction mixture was then heated to reflux for 24 hours. The ethanol was then evaporated off and the remaining solution was loaded onto a Sephadex C-25 ion exchange column. Excess ligand was eluted using distilled water and the required complex was eluted with 0.2M NaCl. The 0.2M was fraction was then reduced to approximately 15cm^3 and the complex was then isolated as a PF_6^- salt by adding aqueous NH_4PF_6. A white powder was obtained with a yield of 0.112g (61%). Analysis found: C, 38.90; H, 2.17; N, 11.57. Calculated for $[Rh(phen)_2(pytr)][PF_6]_2.NaCl$: C, 38.91; H, 2.21; N, 11.71.

$[Rh(bpy)_2(pytr)][PF_6]_2$

0.087g (0.6mmol) of 3-(pyridin-2-yl)-1,2,4-triazole (Hpytr) were dissolved in 15cm^3 water:ethanol 2:1 and to this, over a period of an hour, 0.094g of $[Rh(bpy)_2Cl_2]Cl$ (0.2mmol) were added and this reaction mixture was then heated to reflux for 24 hours. The ethanol was then evaporated off and the remaining solution was loaded onto a C-25 column. Excess ligand was eluted using distilled water and the required complex was eluted with 0.1M NaCl. The 0.1M fraction was then reduced to approximately 15cm^3 and the complex was isolated as a PF_6^- salt by adding aqueous NH_4PF_6. A white powder was obtained with a yield of 0.090g (59%). Analysis found: C, 38.02; H, 2.42; N, 12.93. Calculated for $[Rh(bpy)_2(pytr)][PF_6]_2$: C, 38.14; H, 2.49; N, 13.18.

$[Rh(phen)_2(4Mpytr)][PF_6]_3$

0.061g (0.4mmol) of 4-methyl-3-(pyridin-2-yl)-1,2,4-triazole (4Mpytr) were dissolved in 15cm^3 water:ethanol 2:1 and to this, over a period of 1½ hours, 0.113g (0.2mmol) of $[Rh(phen)_2Cl_2]Cl$ were added. This reaction mixture was then heated to reflux overnight. The ethanol was then evaporated off and the remaining solution

was loaded onto a C-25 column. Excess ligand was eluted using distilled water and the required complex was eluted with 0.2M NaCl. The 0.2M fraction was reduced to approximately 15cm^3 and the complex was then isolated as a PF_6^- salt by adding aqueous NH_4PF_6. A white powder was obtained with a yield of 0.107g (50%). Analysis found C, 36.11; H, 2.23; N, 10.50. Calculated for $[Rh(phen)_2(4Mpytr)][PF_6]_3$ C, 36.31; H, 2.29; N, 10.50.

$[Rh(bpy)_2(4Mpytr)][PF_6]_3 \cdot H_2O$

0.045g (0.3mmol) of 4-methyl-3-(pyridin-2-yl)-1,2,4-triazole (4Mpytr) were dissolved in 20cm^3 water:ethanol 3:1 and to this, over a period of an hour, 0.077g (0.15mmol) of $[Rh(bpy)_2Cl_2]Cl$ were added. This reaction mixture was then heated to reflux overnight. After cooling the ethanol was evaporated off and the remaining solution was loaded onto a C-25 column. Excess ligand was eluted using distilled water and the required complex was eluted with 0.2M NaCl. The 0.2M fraction was then reduced to approximately 15cm^3 and the complex was isolated as a PF_6^- salt by adding aqueous NH_4PF_6. A white powder was obtained with a yield of 0.122g (80%). Analysis found C, 32.58; H, 2.33; N, 11.24. Calculated for $[Rh(bpy)_2(4Mpytr)][PF_6]_3 \cdot H_2O$: C, 32.70; H, 2.55; N, 10.90.

$[Rh(phen)_2(1M3pytr)][PF_6]_3$

0.061g (0.4mmol) of 1-methyl-3-(pyridin-2-yl)-1,2,4-triazole (1M3pytr) were dissolved in 15cm^3 water:ethanol 2:1 and to this, over a period of 1½ hours, 0.114g (0.2mmol) of $[Rh(phen)_2Cl_2]Cl$ were added. This reaction mixture was then heated to reflux for overnight. The ethanol was then evaporated off and the remaining solution was loaded onto a C-25 column. Excess ligand was eluted using distilled water and the required complex was eluted with 0.2M NaCl. The 0.2M fraction was reduced to approximately 15cm^3 and the complex was then isolated as a PF_6^- salt by adding aqueous NH_4PF_6. A white powder was obtained with a yield of 0.056g (26%). Analysis found C, 36.27; H, 2.18; N, 10.45. Calculated for $[Rh(phen)_2(1M3pytr)][PF_6]_3$ C, 36.31; H, 2.29; N, 10.50.

$[Rh(bpy)_2(1M3pytr)][PF_6]_3 \cdot 2NaCl$

0.053g (0.3mmol) of 1-methyl-3-(pyridin-2-yl)-1,2,4-triazole (1M3pytr) were dissolved in 15cm^3 water:ethanol 2:1 and to this, over a period of 1½ hours, 0.073g (0.15mmol) of $[Rh(bpy)_2Cl_2]Cl$ were added. This reaction mixture was then heated to reflux overnight. The ethanol was then evaporated off and the remaining solution was loaded onto a C-25 column. Excess ligand was eluted using distilled water and the required complex was eluted with 0.1M NaCl. The 0.1M fraction was then reduced to approximately 10cm^3 and the complex was then isolated as a PF_6^- salt by adding aqueous NH_4PF_6. A white powder was obtained with a yield of 0.032g (16%). Analysis found: C, 30.00; H, 2.15; N, 10.26. Calculated for $[Rh(bpy)_2(1M3pytr)][PF_6]_3 \cdot 2NaCl$: C,29.83; H,2.15; N,9.94.

$[Rh(phen)_2(bpt)](PF_6)_2 \cdot NaCl$

0.068g (0.3mmol) of 3,5-bis(pyridin-2-yl)-1,2,4-triazole (Hbpt) were dissolved in 25cm^3 ethanol:water 4:1 and to this, over a period of an hour, 0.085g (0.15mmol) of $[Rh(phen)_2Cl_2]Cl$ were added. This reaction mixture was then heated to reflux for 48 hours. The reaction mixture was allowed to cool and was loaded directly onto a C-25 column. Excess ligand was eluted using distilled water and the required complex was eluted with 0.2M NaCl. The 0.2M fraction was then reduced to approximately 15cm^3 and the complex was then isolated as a PF_6^- salt by adding aqueous NH_4PF_6. A pale pink powder was obtained with a yield of 0.021g (14%). Analysis found C, 41.96; H, 2.61; N, 12.62: Calculated for $[Rh(phen)_2(bpt)](PF_6)_2 \cdot NaCl$: C,41.82 ; H,2.34 ; N,12.19.

$[Rh(bpy)_2(bpt)](PF_6)_2 \cdot 3NaCl$

0.089g (0.4mmol) of 3,5-bis(pyridin-2-yl)-1,2,4-triazole (Hbpt) were dissolved in 25cm^3 ethanol:water 4:1 and to this, over a period of an hour, 0.105g (0.2mmol) of $[Rh(bpy)_2Cl_2]Cl$ were added. This reaction mixture was then heated to reflux for 48 hours. The reaction mixture was allowed to cool and was loaded directly onto a C-

25 column. Excess ligand was eluted using distilled water and the required complex was eluted with 0.2M NaCl. The 0.2M fraction was then reduced to approximately 15cm^3 and the complex was then isolated as a PF_6^- salt by adding aqueous NH_4PF_6. A pale pink powder was obtained with a yield of Yield 0.072g (32%). Analysis found C, 34.78; H, 2.07; N, 11.42: Calculated for $[Rh(bpy)_2(bpt)](PF_6)_2 \cdot 3NaCl$: C, 34.85; H, 2.19; N, 11.43.

$[Rh(phen)_2(NHbpt)](PF_6)_2 \cdot NaCl$

0.072g (0.3mmol) of 4-amino-3,5-bis(pyridin-2-yl)-1,2,4-triazole (NH_2bpt) were dissolved in 15cm^3 basic water pH 9 and to this, over a period of an hour, 0.078g (0.14mmol) of $[Rh(phen)_2Cl_2]Cl$ were added. This reaction mixture was then heated to reflux for 4 hours. The reaction mixture was allowed to cool and any unreacted ligand that precipitated was filtered off. The remaining solution was loaded directly onto a C-25 column. Excess ligand was eluted using distilled water and the required complex was eluted with 0.2M NaCl. The 0.2M fraction was then reduced to approximately 15cm^3 and the complex was then isolated as a PF_6^- salt by adding aqueous NH_4PF_6. A bright yellow powder was obtained with a yield of 0.110g (77%). Analysis found C, 41.10; H, 2.45; N, 13.09: Calculated for $[Rh(phen)_2(NHbpt)](PF_6)_2 \cdot NaCl$: C, 41.22; H, 2.40; N,13.35.

$[Rh(phen)_2(NH_2bpt)](PF_6)_3$

0.071g (0.3mmol) of 4-amino-3,5-bis(pyridin-2-yl)-1,2,4-triazole (NH_2bpt) were dissolved in 15cm^3 water:ethanol 3:1 and to this, over a period of an hour, 0.085g (0.15mmol) of $[Rh(phen)_2Cl_2]Cl$ were added. This reaction mixture was then heated to reflux for 10 days. The reaction mixture was allowed to cool and was loaded directly onto a C-25 column. Excess ligand was eluted using distilled water and the fraction which was eluted with 0.2M NaCl was then reduced to approximately 15cm^3 and then precipitated as a PF_6^- salt by adding aqueous NH_4PF_6. However, ^{1}H NMR spectroscopy showed that the pure complex had not been isolated thus elemental analysis was not carried out.

$[Rh(bpy)_2(NHbpt)](PF_6)_2 \cdot 2NaCl \cdot H_2O$

0.070g (0.3mmol) of 4-amino-3,5-bis(pyridin-2-yl)-4H-1,2,4-triazole (NH_2bpt) were dissolved in 20cm^3 H_2O pH 9 with refluxing and to this, over a period of an hour, 0.075g (0.15mmol) of $[Rh(bpy)_2Cl_2]Cl$ were added. This reaction mixture was then heated to reflux for 5 hours. The reaction mixture was allowed to cool, filtered to remove some unreacted ligand that had precipitated and loaded directly onto a C-25 column. Remaining excess ligand was eluted using distilled water and the required complex was eluted with 0.2M NaCl. The 0.2M fraction was then reduced to approximately 15cm^3 and the complex was then isolated as a PF_6^- salt by adding aqueous NH_4PF_6. A bright yellow powder was obtained with a yield of 0.091g (59%). Analysis found: C, 35.26; H, 2.29; N, 12.97%. Calculated for $[Rh(bpy)_2(NHbpt)](PF_6)_2 \cdot 2NaCl \cdot H_2O$: C, 35.68 ; H, 2.53; N, 13.00%.

$[Rh(bpy)_2(NH_2bpt)](PF_6)_3 \bullet NaCl$

0.092g (0.4mmol) of 4-amino-3,5-bis(pyridin-2-yl)-4H-1,2,4-triazole (NH_2bpt) were dissolved in 15cm^3 water:ethanol 2:1 and to this, over a period of 2 hours, 0.152g (0.3mmol) of $[Rh(bpy)_2Cl_2]Cl$ were added. This reaction mixture was then heated to reflux for 24 hours. The ethanol was then evaporated off and the remaining solution was loaded onto a C-25 column. Excess ligand was eluted using distilled water and the required complex was eluted with 0.2M NaCl. The 0.2M fraction was then reduced to approximately 15cm^3 and the complex was then isolated as a PF_6^- salt by adding aqueous NH_4PF_6. A pale yellow powder was obtained with a yield of 0.066g (20%). Analysis found: C, 33.64; H, 2.30; N, 12.13%. Calculated for $[Rh(bpy)_2(NH_2bpt)](PF_6)_3 \bullet NaCl$: C, 33.51; H, 2.28; N, 12.21%.

$[Rh(phen)_2(Phpytr)](PF_6)_2$

0.072g of (Phpytr) (0.3mmol) were dissolved in 15cm^3 water:ethanol 1:1 and to this, over a period of an hour, 0.132g (0.2mmol) of $[Rh(phen)_2Cl_2]Cl$ were added. This reaction mixture was then heated to reflux for 12 hours. The solvent was then

evaporated off and the residue was dissolved in $10cm^3$ of water and the complex was then isolated as a PF_6^- salt by adding aqueous NH_4PF_6. The solid obtained was filtered and dried and purification was carried out on a silica column using acetonitrile: water: KNO_3 in the ratio 40:10:1 as eluent. A white powder was obtained with a yield of 0.162g (83%). Analysis found C, 45.48; H, 2.63; N, 11.44%. Calculated for $[Rh(phen)_2(Phpytr)](PF_6)_2$: C, 45.60; H, 2.59; N, 11.50%.

$[Rh(bpy)_2(Phpytr)](PF_6)_2 \cdot H_2O$

0.043g (0.2mmol) of (Phpytr) were dissolved in $20cm^3$ water:ethanol 1:1 and to this, over a period of 2 hours, 0.049g (0.1mmol) of $[Rh(bpy)_2Cl_2]Cl$ were added. This reaction mixture was then heated to reflux for 12 hours. The solvent was then evaporated off and the residue was dissolved in $10cm^3$ of water and the complex was then isolated as a PF_6^- salt by adding aqueous NH_4PF_6. The solid obtained was filtered and dried and purification was carried out on a silica column using acetonitrile: water: KNO_3 in the ratio 40:10:1 as eluent. A white powder was obtained with a yield of 0.079g (84%) which yielded crystals upon recrystallisation in acetonitrile:toluene 7:3. Analysis found C, 42.28; H, 2.64; N, 11.92%. Calculated for $[Rh(bpy)_2(Phpytr)](PF_6)_2 \cdot H_2O$: C, 41.97; H, 2.88; N, 11.86%.

3.2.2 Preparation of Deuterated Rh(III) Complexes

It should be noted that deuterated Hpytr and Hbpt, H-d_4-pytr and d_8-bpt, were obtained from Christine O'Connor and d_8-bpy was obtained from Wesley Browne.

***cis*-$[Rh(d_8\text{-bpy})_2Cl_2]_2$**

$RhCl_3.(xH_20)$ (1mmol, 0.266g) was dissolved in $5cm^3$ of water with gentle heating 2,2-bipyridyl (2.2mmol, 0.362g) was dissolved in $4cm^3$ of ethanol again with gentle heating. Both solutions were heated till the $RhCl_3.(xH_20)$ and 2,2-dipyridyl had fully dissolved. At this point the $RhCl_3.(xH_20)$ was added to the 2,2'-bipyridyl. This was allowed to heat for a few minutes (2/3mins) and to this 0.1mmol (57μL) of hydrazine hydrate was added. Upon the addition of the hydrazine a yellow solution

was observed and a precipitate was formed. This was heated for 10 minutes (covered using a clock glass). It was then heated further and the ethanol was allowed to evaporate off. Once the ethanol had evaporated the solution was allowed to cool on ice. The pale yellow precipitate obtained was filtered, washed repeatedly with water and dried. Yield 0.332g (62%).[21]

$[Rh(phen)_2(d_4\text{-pytr})][PF_6]_2$

0.096g (0.6mmol) of d_4-pytr were dissolved in 30cm^3 water:ethanol 2:1 and to this, over a period of an hour, 0.110g (0.2mmol) of $[Rh(phen)_2Cl_2]Cl$ were added. This reaction mixture was then heated to reflux for overnight. The ethanol was then evaporated off and the remaining solution was loaded onto a Sephadex C-25 ion exchange column. Excess ligand was eluted using distilled water and the required complex was eluted with 0.2M NaCl. The 0.2M was fraction was then reduced to approximately 15cm^3 and the complex was then isolated as a PF_6^- salt by adding aqueous NH_4PF_6. A white powder was obtained with a yield of 0.058g (32%). Analysis Found: C, 39.65; H, 2.22; N, 12.86%. Calculated for $[Rh(phen)_2(d_4\text{-pytr})][PF_6]_2.1\frac{1}{2}H_2O$: C, 40.06; H, 2.60; N, 12.06%.

$[Rh(bpy)_2(d_4\text{-pytr})][PF_6]_2 \cdot H_2O \cdot NaCl$

0.076g (0.5mmol) of d_4-pytr were dissolved in 15cm^3 water:ethanol 2:1 and to this, over a period of an hour, 0.132g (0.25mmol) of $[Rh(bpy)_2Cl_2]Cl$ were added. This reaction mixture was then heated to reflux for 24 hours. The ethanol was then evaporated off and the remaining solution was loaded onto a C-25 column. Excess ligand was eluted using distilled water and the required complex was eluted with 0.1M NaCl. The 0.1M fraction was then reduced to approximately 15cm^3 and the complex was then isolated as a PF_6^- salt by adding aqueous NH_4PF_6. A white powder was obtained with a yield of 0.046g (20%). Analysis found: C, 34.58; H, 2.30; N, 11.85%. Calculated for $[Rh(bpy)_2(d_4\text{-pytr})][PF_6]_2 \cdot H_2O \cdot NaCl$ C, 34.84; H, 2.49; N, 12.04%.

$[Rh(phen)_2(d_8\text{-bpt})](PF_6)_2 \cdot 3NaCl$

0.070g (0.3mmol) of d_8-bpt were dissolved in $15cm^3$ basic water pH 9 and to this, over a period of an hour, 0.088g (0.15mmol) of $[Rh(phen)_2Cl_2]Cl$ were added. This reaction mixture was then heated to reflux for 24 hours. The reaction mixture was allowed to cool and was loaded directly onto a C-25 column. Excess ligand was eluted using distilled water and the required complex was eluted with 0.2M NaCl. The 0.2M fraction was then reduced to approximately $15cm^3$ and the complex was then isolated as a PF_6^- salt by adding aqueous NH_4PF_6. A white powder was obtained with a yield of 0.047g (26%). Analysis found: C, 37.38; H, 2.10; N, 10.59%. Calculated for $[Rh(phen)_2(d_8\text{-bpt})](PF_6)_2 \cdot 3NaCl$ C, 37.31; H, 2.09; N, 10.88%.

$[Rh(bpy)_2(d_8\text{-bpt})](PF_6)_2 \cdot 2NaCl$

0.101g (0.45mmol) of (d_8-bpt) were dissolved in $15cm^3$ water:ethanol 2:1 and to this, over a period of one hour, 0.151g (0.3mmol) of $[Rh(bpy)_2Cl_2]Cl$ were added. This reaction mixture was then heated to reflux for 24 hours. The ethanol was then evaporated off and the remaining solution was loaded onto a C-25 column. Excess ligand was eluted using distilled water and the required complex was eluted with 0.2M NaCl. The 0.2M fraction was then reduced to approximately $15cm^3$ and the complex was then isolated as a PF_6^- salt by adding aqueous NH_4PF_6. A white powder was obtained with a yield of 0.087g (29%). Analysis found: C, 38.53; H, 2.47; N, 12.63%. Calculated for $[Rh(bpy)_2(d_8\text{-bpt})](PF_6)_2 \cdot 2NaCl$: C, 38.67; H, 2.43; N, 12.68%.

$[Rh(d_8\text{-bpy})_2(NH_2bpt)](PF_6)_3 \cdot 2NaCl$

0.092g (0.4mmol) of (NH_2bpt) were dissolved in $15cm^3$ water:ethanol 2:1 and to this, over a period of an hour, 0.100g (0.2mmol) of $[Rh(d_8\text{-bpy})_2Cl_2]Cl$ were added. This reaction mixture was then heated to reflux for 24 hours. The ethanol was then evaporated off and the remaining solution was loaded onto a C-25 column. Excess

ligand was eluted using distilled water and the required complex was eluted with 0.2M NaCl. The 0.2M fraction was then reduced to approximately 15cm^3 and the complex was then isolated as a PF_6^- salt by adding aqueous NH_4PF_6. A yellow powder was obtained with a yield of 0.087g (38%). Analysis found: C, 31.36; H, 2.13; N, 11.41%. Calculated for $[Rh(d_8\text{-bpy})_2(NH_2bpt)](PF_6)_3 \cdot 2NaCl$: C,31.47; H, 2.15; N, 11.47%.

$[Rh(d_8\text{-bpy})_2(NHbpt)](PF_6)_2$

0.025g (0.1mmol) of (NH_2bpt) were dissolved in 15cm^3 water at pH 9 and to this, over a period of an hour, 0.050g (0.1mmol) of $[Rh(d_8\text{-bpy})_2Cl_2]Cl$ were added. This reaction mixture was then heated to reflux for 48 hours. The ethanol was then evaporated off and the remaining solution was loaded onto a C-25 column. Excess ligand was eluted using distilled water and the required complex was eluted with 0.1M NaCl. The 0.1M fraction was then reduced to approximately 15cm^3 and the complex was then isolated as a PF_6^- salt by adding aqueous NH_4PF_6. A yellow powder was obtained with a yield of 0.022g (23%).

Note: method used for calculating C,H,N values of deuterated complexes is discussed in 2.11.

3.3 Results and Discussion

3.3.1 Synthesis and Purification

Rhodium(III) bis complexes such as $[Rh(bpy)_2Cl_2]Cl$ and $[Rh(phen)_2Cl_2]Cl$ can be synthesised with relative ease but the synthesis of the tris complexes is not as simple and often requires extended reflux times.[21] As can be seen from the section 3.2 all of the complexes that have been developed were synthesised in water:ethanol 2:1 with the exception of the 1,10-phenanthroline complex with the ligand NH_2bpt. The required reaction times vary depending upon the ligands being used with reactions involving the Hbpt ligand generally requiring the longest reflux times and reactions with NH_2bpt in basic water necessitating comparatively short reaction times. The syntheses of complexes containing the NH_2bpt ligand were carried out under two different conditions. Initial attempts to obtain the phen complex with NH_2bpt were carried out in water:ethanol 3:1 but with little success. The second medium used was basic water and this proved to be more conducive to complex formation. The nature of the complexes formed will be discussed in Section 3.3.3.6. The bpy ligand proved to be more reactive than phen with NH_2bpt in water:ethanol but the yield for this reaction remained low. In basic water, comparable reaction times to $[Rh(phen)_2(bpt)]^{2+}$ were observed whereas lower yields were obtained. Ru(II) analogues of several of the Rh(III) complexes which will be discussed in this chapter have previously been reported and it is of interest to compare the two series of complexes with respect to reaction times and % yields.[22,23,24] Table 3.1 allows for just such a comparison wherever possible. It can be seen from Table 3.1 that reaction times of 4 hours are standard in the synthesis of Ru(II) mononuclear complexes of this type. These reactions times are considerably shorter than those required for the analogous Rh(III) complexes studied in this instance. It can also be seen from Table 3.1 that yields of the ruthenium complexes also tend to be slightly higher than those observed for the rhodium complexes.[22,23,24]

Table 3.1 ***Reaction times and yields for both Rh(III) and Ru(II) complexes containing pyridyl triazole based ligands.***

Complex	Reaction Time EtOH:H_2O	Reaction Time Basic Water	% Yield	Complex	Reaction Time EtOH:H_2O	% Yield
$[Rh(phen)_2(pytr)]^{2+}$	24	-	61	$[Ru(phen)_2(pytr)]^{+}$ [a]	4	77
$[Rh(bpy)_2(pytr)]^{2+}$	24	-	59	$[Ru(bpy)_2(pytr)]^{+}$ [b]	4	60
$[Rh(phen)_2(4Mpytr)]^{2+}$	12	-	50	$[Ru(phen)_2(4Mpytr)]^{+}$ [a]	4	77
$[Rh(bpy)_2(4Mpytr)]^{2+}$	12	-	80	$[Ru(bpy)_2(4Mpytr)]^{+}$ [b]	4	90
$[Rh(phen)_2(1M3pytr)]^{2+}$	12	-	26	$[Ru(phen)_2(1M3pytr)]^{+}$ [a]	4	78
$[Rh(bpy)_2(1M3pytr)]^{2+}$	12	-	16	$[Ru(bpy)_2(1M3pytr)]^{+}$ [b]	4	85
$[Rh(phen)_2(bpt)]^{2+}$	48	-	14	$[Ru(phen)_2(bpt)]^{+}$	-	-
$[Rh(bpy)_2(bpt)]^{2+}$	48	-	33	$[Ru(bpy)_2(bpt)]^{+}$ [b]	6	30
$[Rh(phen)_2(NHbpt)]^{2+}$	-	4	77	-	-	-
$[Rh(bpy)_2(NHbpt)]^{2+}$	-	5	59	-	-	-
$[Rh(phen)_2(NH_2bpt)]^{3+}$	10 days	-	*	-	-	-
$[Rh(bpy)_2(NH_2bpt)]^{3+}$	24	-	20	-	-	-
$[Rh(phen)_2(Phpytr)]^{2+}$	12	-	83	$[Ru(phen)_2(Phpytr)]^{+}$	-	-
$[Rh(bpy)_2(Phpytr)]^{2+}$	12	-	84	$[Ru(bpy)_2(Phpytr)]^{+}$ [c]	4	55

a = ref. 22, b = ref. 23, c = 24, * = pure complex was not isolated.

With respect to purification, all of the complexes were purified on a Sephadex C-25 column with the exception of $[Rh(bpy)_2(Phpytr)](PF_6)_2$ and $[Rh(phen)_2(Phpytr)](PF_6)_2$. Initial attempts were made to purify these complexes on a C-25 column but a good separation was not observed and it was decided to try an alternative method of purification. The PF_6 salts of these complexes were then taken and purified on a silica column using 40:10:1 acetonitrile:water:KNO_3 as the mobile phase. This method of purification proved to be successful but proved suitable only

for the complexes $[Rh(bpy)_2(Phpytr)](PF_6)_2$ and $[Rh(phen)_2(Phpytr)](PF_6)_2$ as when attempts were made to purify complexes with the other ligands in the same manner a mixture of unreacted ligand and complex was obtained.

As previously discussed the pyridine triazole ligands are capable of coordinating a metal centre via either the N2' or the N4' of the triazole ring and studies of Ru(II) complexes incorporating the ligands Hpytr, HPhpytr and Hbpt have shown the formation of both of these isomers.[23] In contrast to this ^1H NMR analysis of the complexes detailed in 3.2.1 showed no evidence for the formation of two isomers. Where suitable crystals for x-ray crystallography were not obtained it was not possible to determine unambiguously the mode of coordination exhibited by these complexes but, as will be discussed in Chapter 8, evidence was found to support the theory that coordination occurs via the N2' position in almost all cases. Exceptions to this were the complexes with the ligand 1M3pytr and complexes with the NH_2bpt ligand where the synthesis was carried in basic water. The coordination modes exhibited in these cases will be discussed in sections 3.3.2 and 3.3.3. It should also be noted that complexes with the ligands Hpytr, HPhpytr and Hbpt were isolated in their deprotonated forms as evidenced by the results of their elemental analysis. This is of importance as it has been shown that for Ru(II) pyridine triazole complexes that the σ-donor strengths of these ligands, and thus the properties of their complexes, have been shown to vary depending upon their protonation state.[23]

3.3.2 X-ray Crystallography

Crystals of suitable for x-ray crystallography were obtained for two of the complexes studied, $[Rh(bpy)_2(Phpytr)](PF_6)_2.0.1H_2O$ and $[Rh(phen)_2(NHbpt)](PF_6)_2 \cdot 0.767\ CH_3CN \cdot 0.28\ H_2O$, and the relevant crystal data is summarised in Table 3.2. In both cases, crystals were obtained when the complexes were recrystallised in acetonitrile:toluene 7:3. Dr. John Gallagher at the School of Chemical Sciences, DCU, carried out the x-ray crystallography.

Table 3.2 Crystal data for $[Rh(phen)_2(NHbpt)](PF_6)_2 \cdot 0.767\ CH_3CN \cdot 0.28\ H_2O$ and $[Rh(bpy)_2(Phpytr)](PF_6)_2.0.1H_2O$.

Chem formula	$C_{36}\ H_{25}\ F_{12}\ N_{10}\ P_2\ Rh,\ 0.767\ CH_3CN,\ 0.28\ H_2O$	$C_{33}\ H_{25}\ F_{12}\ N_8\ P_2\ Rh,\ H_2O$
Fw	1027.06	928.26
a (Å)	13.2334(12)	13.3893(13)
b (Å)	20.507(3)	18.740(2)
c (Å)	16.0732(15)	14.2650(12)
β (°)	103.620(6)	95.587(5)
Z	4	4
Volume ($Å^3$)	4239.3(8)	3562.3(6)
System, space group	monoclinic, $P2_1/m$	monoclinic, $P2_1/m$
Crystal size	0.43 x 0.10 x 0.08	0.28 x 0.17 x 0.13
Temperature	297(2) K	297(2) K
F(000)	2055	1852
Radiation, λ (Å)	MoK_α, 0.71073	MoK_α,
d_{cald}, $g.cm^{-3}$	1.609	1.612
abs coeff, μ (mm^{-1})	0.575	0.672
abs corr T (min, max)	0.792, 0.958	0.837, 0.921
θ range for data collection	1.87to 25.57°	1.8 to 26°
Reflections collected	8528	8278
Unique, $>2\sigma(I)$	8164, 5460	8278/6947
Parameters	705	642
Restraints	288	231
$R(F_o)$	0.062	0.054
$R_w(F_o)$	0.149	0.083
Residual electron density	+0.76, -0.68	+0.36, -0.30

3.3.2.1 $[Rh(bpy)_2(Phpytr)](PF_6)_2.0.1H_2O$.

As has been previously discussed it is necessary when working with ligands like the pyridyl triazoles to be able to identify which isomers are present. ^1H NMR has proven to be a powerful aid in structural elucidation of complexes of this type but x-ray crystallography definitively identifies the coordinating mode of the complex.[23] The molecular structure of the cation of $[Rh(bpy)_2(Phpytr)](PF_6)_2.0.1H_2O$ can be seen in Figure 3.7.

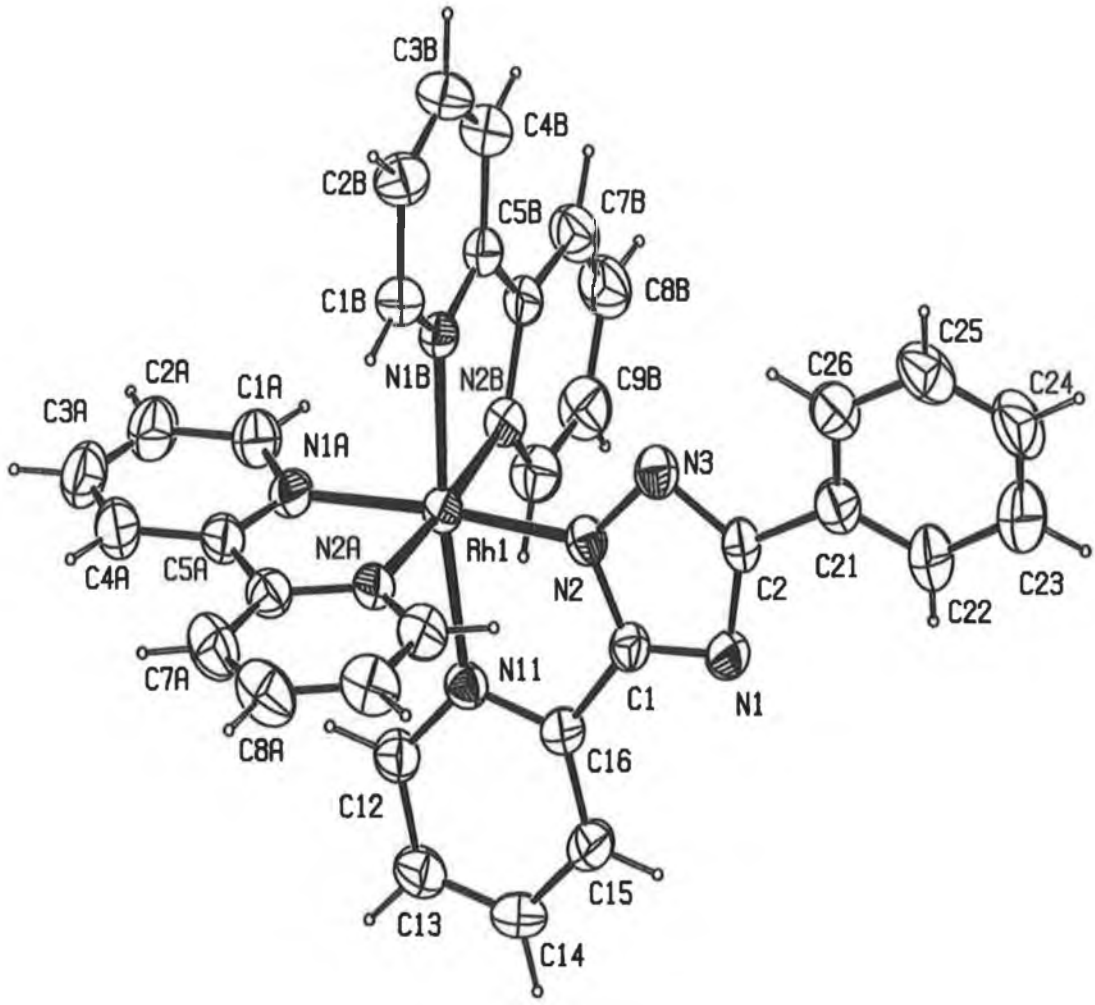

Figure 3.7 Molecular structure of the cation in $[Rh(bpy)_2(Phpytr)](PF_6)_2.0.1H_2O$. Counter ions and the solvent molecules have been omitted for clarity.

The crystal structure of $[Rh(bpy)_2(Phpytr)](PF_6)_2.0.1H_2O$ shows that the $Rh(bpy)_2$ moiety is bound via the N2' of the triazole ring in this instance. The rhodium atom is coordinated by one pyridyl triazole and two bipyridine molecules. Two (PF_6) counter ions and a partial site occupancy water molecule (0.01) complete the crystal structure (not included in figure). Selected bond lengths can be seen in Table 3.3.

Table 3.3 ***Selected bond lengths (Å) for [Rh(bpy)$_2$(Phpytr)](PF$_6$)$_2$.0.1H$_2$O, Ru(bpy)$_2$(bpt)](PF$_6$). ½H$_2$O and Ru(bpy)$_2$(pt)](PF$_6$). CH$_3$COCH$_3$.***

	[Rh(bpy)$_2$(Phpytr)]. (PF$_6$)$_2$. 0.1H$_2$O.	[Ru(bpy)$_2$(bpt)](PF$_6$). ½H$_2$O.	[Ru(bpy)$_2$(pt)](PF$_6$). CH$_3$COCH$_3$.
Rh(1)–N(2)	1.985(4)	2.03(2)	2.051(3)
Rh(1)–N(11)	2.064(4)	2.11(2)	2.085(3)
Rh(1)–N(1A)	2.044(4)	2.04(2)	2.056(3)
Rh(1)–N(2A)	2.013(4)	2.05(2)	2.056(3)
Rh(1)–N(1B)	2.024(4)	2.06(2)	2.063(3)
Rh(1)–N(2B)	2.044(4)	2.04(2)	2.049(3)

The Rh–N bond lengths are all within their expected range.[25,26,27,28] Typical Rh-N bond lengths of 2.036(3) Å and 2.054(3) Å have been reported by Kim *et. al.* for the complex [Rh(tpy)(bpy))(Cl)](ClO$_4$)$_2$ and 2.044(6) Å and 2.055(6) Å in the complex [Rh(tpy)(phen))(Cl)](PF$_6$)$_2$. In these instances the bond lengths refer to distances between the rhodium metal centre and the bipyridine and phenanthroline ligands. Bond lengths of 2.049(3) Å, 1.954(3) Å and 2.045(3) Å were found to be typical of Rh-N of the terpyridine ligand.[25] A number of crystal structures of ruthenium(II) pyridyl triazole complexes have been obtained but the complexes [Ru(bpy)$_2$ (3-(2-phenol)-5-(pyridine-2-yl)-1,2,4-triazole)](PF$_6$) and [Ru(bpy)$_2$(3,5-bis(pyridin-2-yl)-1,2,4-triazole)(PF$_6$) have been chosen for comparison purposes in this discussion.[23] The ligands 3-(2-phenol)-5-(pyridine-2-yl)-1,2,4-triazole (Hbpt) and 3,5-bis(pyridin-2-yl)-1,2,4-triazole (Hbpt) may be seen in Figure 3.6. Table 3.3 also shows the Ru-N bond lengths observed for the complexes [Ru(bpy)$_2$(bpt)](PF$_6$).½H$_2$O and [Ru(bpy)$_2$(pt)](PF$_6$). CH$_3$COCH$_3$. It can be seen that the Rh-N of the triazole ring is slightly shorter than the Ru-N of the triazole ring at 1.985(4) Å as compared to 2.03(2) Å and 2.051(3) Å for the ruthenium complexes [Ru(bpy)$_2$(bpt)](PF$_6$).½H$_2$O and [Ru(bpy)$_2$(pt)](PF$_6$).CH$_3$COCH$_3$ respectively. It can be seen from Table 3.3 that the Rh(1)-N(1A) and Rh(1)-N(2B) bond lengths are comparable to the corresponding

bond lengths observed in the ruthenium complexes $[Ru(bpy)_2(bpt)](PF_6).\ ½H_2O$ and $[Ru(bpy)_2(pt)](PF_6).CH_3COCH_3$. The distances observed for Rh(1)-N(2A) and Rh(1)-N(1B), 2.013(4) Å and 2.024(4) Å respectively, are however slightly shorter than similar bonds lengths in the complexes $[Ru(bpy)_2(bpt)](PF_6).½H_2O$ and $[Ru(bpy)_2(pt)](PF_6).CH_3COCH_3$. Selected bond angles for the complex $[Rh(bpy)_2(Phpytr)](PF_6)_2.0.1H_2O$ are given in Table 3.4.

Table 3.4 Selected bond angles (°) for $[Rh(bpy)_2(Phpytr)](PF_6)_2.0.1H_2O$.

Bond Angle	(°)	Bond Angle	(°)
N(2)–Rh(1)–N(2A)	96.12 (16)	**N(11)–Rh(1)–N(1A)**	97.40 (15)
N(2)–Rh(1)–N(1B)	94.64 (15)	**N(2A)–Rh(1)–N(1B)**	96.54 (16)
N(2)–Rh(1)–N(2B)	86.38 (15)	**N(2A)–Rh(1)–N(2B)**	175.93 (15)
N(2)–Rh(1)–N(1A)	175.08 (16)	**N(2A)–Rh(1)–N(1A)**	80.38 (18)
N(2)–Rh(1)–N(11)	78.76 (16)	**N(1B)–Rh(1)–N(2B)**	80.12 (17)
N(11)–Rh(1)–N(2A)	87.26 (15)	**N(1B)–Rh(1)–N(1A)**	89.34 (15)
N(11)–Rh(1)–N(1B)	172.75 (15)	**N(2B)–Rh(1)–N(1A)**	97.18 (17)
N(11)–Rh(1)–N(2B)	96.31 (15)		

The complex $[Rh(bpy)_2(Phpytr)](PF_6)_2.0.1H_2O$ does deviate slightly from an octahedral geometry with angles of 175.08(16)° and 175.93(15)° for N1A-Rh1-N2 and N2A-Rh1-N2B respectively and 172.75(15) ° for N11-Rh1-N1B. Bite angles of 80.38(18)° and 80.12(17)° are observed between the rhodium centre and the two bipyridine rings whereas the bite angle between the rhodium centre and the triazole was determined to be 78.76(16)°. The aforementioned complexes $[Rh(tpy)(bpy)(Cl)](ClO_4)_2$ and $[Rh(tpy)(phen))(Cl)](PF_6)_2$ displayed bite angles of 79.74(11)° and 80.8(3)° between the rhodium metal centres and the bpy and phen ligands respectively. Between the terpyridine ligand and the rhodium atom the angles 80.28(11)° and 80.72(11)° were found for $[Rh(tpy)(bpy)(Cl)](ClO_4)_2$ and

80.8(3)° and 81.5(2)° were found for [Rh(tpy)(phen))(Cl)]$(PF_6)_2$.[25] The bite angles observed for [Rh$(bpy)_2$(Phpytr)]$(PF_6)_2$ are also comparative with those observed for Ru(II) pyridyl triazole complexes with bite angles of 78-79° being reported.[23]

3.3.2.2 [Rh(phen)$_2$(NHbpt)](PF$_6$)$_2$·0.767 CH$_3$CN·0.28 H$_2$O.

A single crystal x-ray investigation yielded the molecular structure of [Rh$(phen)_2$(NHbpt)]$(PF_6)_2$·0.767 CH_3CN·0.28 H_2O, the cation of which is depicted in Figure 3.8. Two disordered PF_6^- counter ions and partial site occupancy acetonitrile (0.767) water solvent molecules (0.28) complete the crystal structure (not depicted). Selected bond lengths and angles for [Rh$(phen)_2$(NHbpt)]$(PF_6)_2$·0.767 CH_3CN·0.28 H_2O can be seen in Table 3.5 and Table 3.6.

Table 3.5 Selected bond lengths (Å) for [Rh(phen)$_2$(NHbpt)](PF$_6$)$_2$·0.767 CH$_3$CN·0.28 H$_2$O.

Bond	Bond Length (Å)	Bond	Bond Length (Å)
Rh1–N99	2.012(4)	Rh1–N11	2.086(5)
Rh1–N1A	2.033(4)	Rh1–N2A	2.106(4)
Rh1–N2B	2.036(5)	N1–N99	1.406(6)
Rh1–N1B	2.040(5)		

Table 3.6 Selected Bond Angles (°) for [Rh(phen)$_2$(NHbpt)](PF$_6$)$_2$·0.767 CH$_3$CN·0.28 H$_2$O.

Bond Angle	(°)	Bond Angle	(°)
N99–Rh1–N1A	91.30(19)	N1A–Rh1–N2A	80.62(19)
N99–Rh1–N2A	171.30(19)	N1A–Rh1–N2B	174.11(19)
N99–Rh1–N1B	88.53(19)	N1A–Rh1–N1B	93.54(19)
N99–Rh1–N2B	91.70(2)	N1B–Rh1–N2B	81.40(2)
N99–Rh1–N11	86.850(19)	N1B–Rh1–N11	174.73(18)
Rh1– N99–N1–C1	57.10(6)	N1– N99–Rh1	110.30(3)

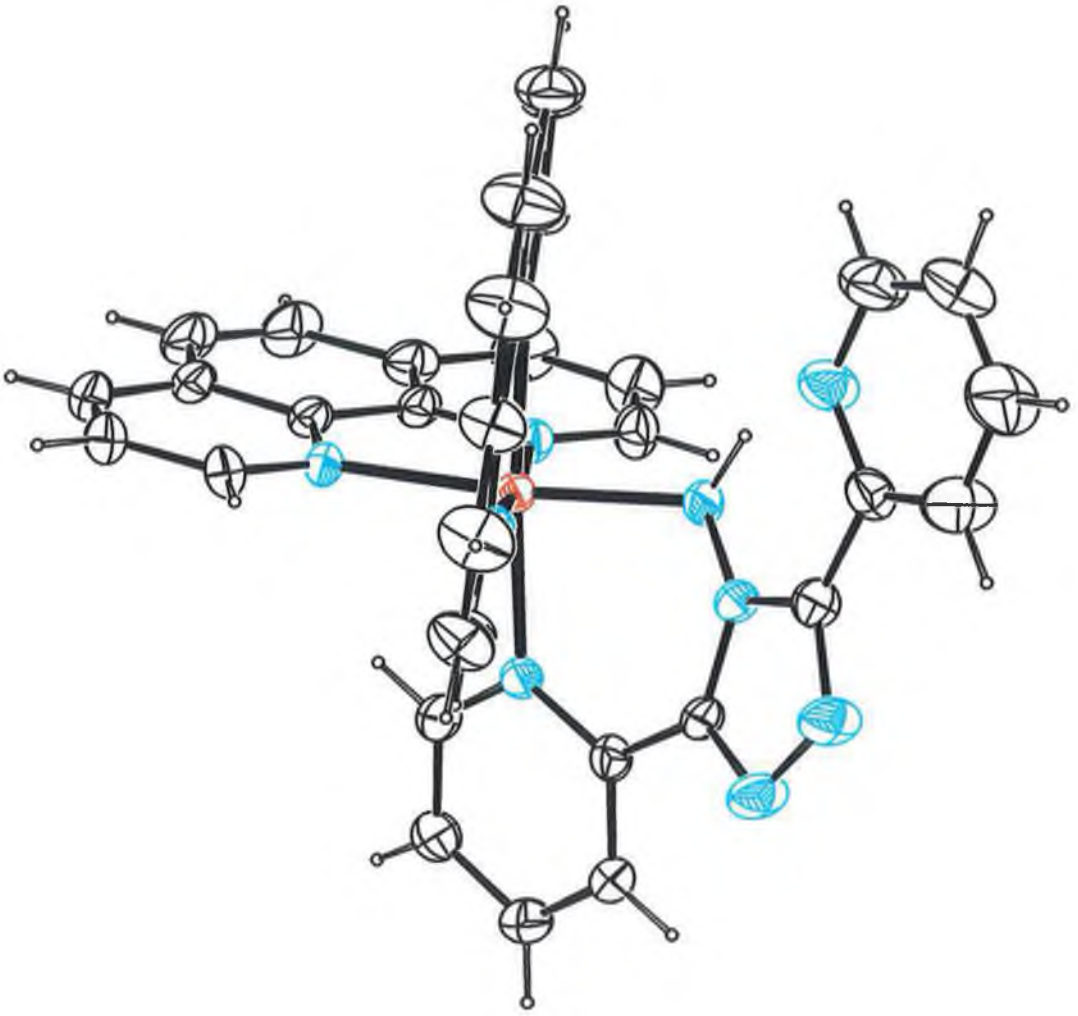

Figure 3.8 Molecular structure of the cation in $[Rh(phen)_2(NHbpt)](PF_6)_2 \cdot 0.767\ CH_3CN \cdot 0.28\ H_2O$. Hydrogen atoms, counter ions and the solvent molecules have been omitted for clarity.

It can be seen clearly from Figure 3.8 that coordination of the metal centre in the complex $[Rh(phen)_2(NHbpt)]^{2+}$ occurs via the amine nitrogen and a nitrogen of a pyridine ring. Although a crystal structure was not obtained a similar mode of coordination was indicated from ^1H NMR studies carried out by Oro *et. al.* for the complex $[Rh^I(CO)_2(NHbpt)]$. Whilst coordination in this manner was proposed for the neutral complex $[Rh^I(CO)_2(NHbpt)]$ it was found from x-ray crystallography that for the cationic complex $[Rh^I(CO)_2(NH_2bpt)]^+$ coordination occurred via the N2' of the triazole ring and a nitrogen of a pyridine ring.[18]

The phenanthroline chelating angles observed for the complex $[Rh(phen)_2(NHbpt)](PF_6)_2 \cdot 0.767\ CH_3CN \cdot 0.28\ H_2O$ are 80.62(19)° and 81.40(2)° which are comparable to those reported by Kim *et. al.*[25] It is interesting to examine the effect of complexation in this instance by comparison of the angles N1-C2-C21 and N1-C1-C16. It should be noted that the angles N1-C2-C21 and N1-C1-C16 relate only to the crystal structure seen in Figure 3.8. N1-C2-C21 relates to the angle between the triazole ring and the free pyridine ring whereas N1-C1-C16 relates to the angle between the triazole ring and the bound pyridine ring. In complexes with pyridine triazole ligands where binding of the metal centre to the pyridine triazole occurs via the N2' or the N4' of the triazole ring and a nitrogen of a pyridine ring coordination generally causes the angle comparable to N1-C1-C16 of the bound pyridine ring to be smaller than N2-C1-C16. For example the complex $[Ru(bpy)_2(pytr)]^{2+}$ has been studied where the corresponding angles were found to be 117° and 132.1°, the crystal structure of the complex $[Rh(CO)_2(NH_2bpt)]ClO_4$ displayed angles of 119.3(6)° and 132.9(5)° for the analogous angles and the complex $[Rh(bpy)_2(Phpytr)](PF_6)_2$ previously discussed exhibited angles of 115.6(4)° and 132.5(4)° for corresponding angles.[29,18] In contrast to the complexes previously observed, which, it should be noted form a five membered ring upon coordination, binding via the amino group gives rise to the formation of a six membered ring and the effect of this may be seen when the molecular structure in Figure 3.8 is studied. Unlike the behaviour observed when coordination gave rise to a five membered ring it was found that the angles N1-C1-C16 and N1-C2-C21 were almost identical, 124.70(5)° and 124.80(6)° respectively, and the angle N1-C1-C16, 124.70(5)°, was

almost identical to the angle exhibited by N2-C1-C16 of 124.20(6)°. Thus it can be seen that coordination in this particular manner, i.e. via the amino group, does not give rise to any decrease in the magnitude of the N1-C1-C16 bond angle. It would be expected that if binding occurred via the N2' of the triazole ring and a nitrogen of a pyridine ring a five membered ring would be formed which would behave in a similar manner to $[Rh(bpy)_2(Phpytr)](PF_6)_2$ but it was not possible to obtain any such crystals.

It is important to note that N99 of the molecular structure seen in Figure 3.8 was originally interpreted to be an oxygen atom as detailed in reference 30, Appendix I. Subsequent preparation of a full series of deuterated and non-deuterated complexes with the Hbpt ligand were prepared and revealed inconsistencies, which cast doubt over the original interpretation. It was thought possible that the crystals obtained were in fact those of the complex $[Rh(phen)_2(NHbpt)](PF_6)_2$ which may have been formed due to the presence of an impurity in the Hbpt ligand as the NH_2bpt ligand is a precursor to Hbpt. This possibility was verified when the NH_2bpt ligand, purchased from Aldrich, was reacted with the $[Rh(phen)_2Cl_2]Cl$ under the same reaction conditions used previously and in a very short reaction time and with a very high yield bright yellow crystals were obtained. ^{1}H NMR spectroscopy proved to be a suitable a method for the analysis of both complexes and verified that the original crystals were in fact $[Rh(phen)_2(NHbpt)](PF_6)_2$ as the ^{1}H NMR spectra of the complexes were identical.

3.3.3 ^{1}H NMR Spectroscopy

The vast majority of research conducted in the area of rhodium polypyridyl complexes has been focused upon the photochemical behaviour of these complexes with a very minimal amount of work being carried out in analysis of the ^{1}H and ^{13}C spectroscopic behaviour of these complexes.[31] The elucidation of the mode of coordination of N-heterocycles to metal ions is of significant importance and this is particularly evident in complexes containing moieties such as triazoles where two different modes of coordination are available so that the properties of these

complexes may be fully assessed. ^{1}H NMR spectroscopy, coupled to ^{13}C NMR and 2-dimensional NMR techniques such as ^{1}H-^{1}H and ^{13}C-^{1}H correlation spectroscopy, have previously been shown to be invaluable in the structural determination of ruthenium(II) polypyridyl complexes containing 1,2,4-triazole moieties. In the case of ruthenium(II) complexes such as $[Ru(bpy)_2(pytr)]^+$ it has been shown that when the ligand is bound via the N4' nitrogen of the triazole ring the H5' proton is in close proximity to an adjacent bpy.[23]

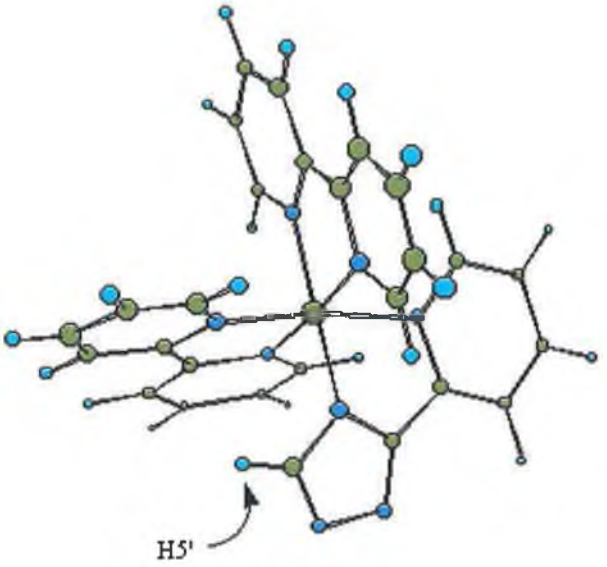

Figure 3.9 Illustration of $[Rh(bpy)_2(pytr)]^{2+}$ demonstrating the position of the H5' proton in relation to the bpy ligands.

The ring current of the bpy ring thus causes a large upfield shift of H5'. In contrast to this when coordination is via N2' of the triazole ring the pyridine ring has no influence upon the triazole ring therefore the H5' proton is not shifted. Another feature of these complexes, which must be taken into consideration, is the protonation state of the complex. It has been found that the H5' proton of ruthenium(II) complexes containing the ligand Hpytr exhibits a downfield shift upon protonation of the complex.[23]

In order to facilitate the elucidation of the structure of the complexes developed deuteration was undertaken in order to simplify their ^{1}H NMR spectra.[32] It is possible to deuterate a wide variety of ligands and it is also possible to control the degree of deuteration of the ligand. The effects of deuteration upon the photophysical properties of transition metal polypyridyl complexes will be discussed in Chapter 4 but there is another property that may be affected by the introduction of deuterium that is of interest here. Exchange of C-H with C-D may be observed in the ^{13}C spectra of the complex, a fact that was first reported by Echols *et. al.*[33] They used deuteration as a method to fully assign the ^{13}C NMR spectrum of vitamin B and noted a substantial decrease in the height of the carbon signal where C-H to C-D exchange has occurred and to a lesser degree for the adjacent carbons. This effect of deuteration upon the ^{13}C spectrum is due to the fact that when a proton bearing carbon is selectively deuterated the ^{13}C spin lattice relaxation time (T_1) of that carbon increases. The increase of T_1 is a consequence of the deuterium nucleus having a smaller magnetic moment than that of the proton. Another contributing factor to the decrease in signal intensity is thought to be the decrease in the nuclear Overhauser effect to the carbon centres. The effect of deuteration on the ^{13}C NMR spectra of the complexes detailed in Section 3.2 will be discussed in Section 3.3.4.

3.3.3.1 $[Rh(phen)_2(pytr)]^{2+}$ and $[Rh(bpy)_2(pytr)]^{2+}$

Of the series of complexes incorporating pyridyl triazole ligands those that incorporate the ligand Hpytr will be discussed first. The ^{1}H NMR spectra of such complexes tend to be complicated and difficult to assign. It is in situations like these that the technique of deuteration is particularly useful in simplifying spectra and thus allowing for complete assignment. Figure 3.10 shows the ^{1}H NMR spectra of both the deuterated complex $[Rh(phen)_2(d_4\text{-pytr})]^{2+}$ (red) and the non-deuterated $[Rh(phen)_2(pytr)]^{2+}$ (black) complexes. It should be noted that when the ligand H-d_4-pytr is referred to it is the H3, H4, H5 and H6 protons of the pyridine ring which have been deuterated.

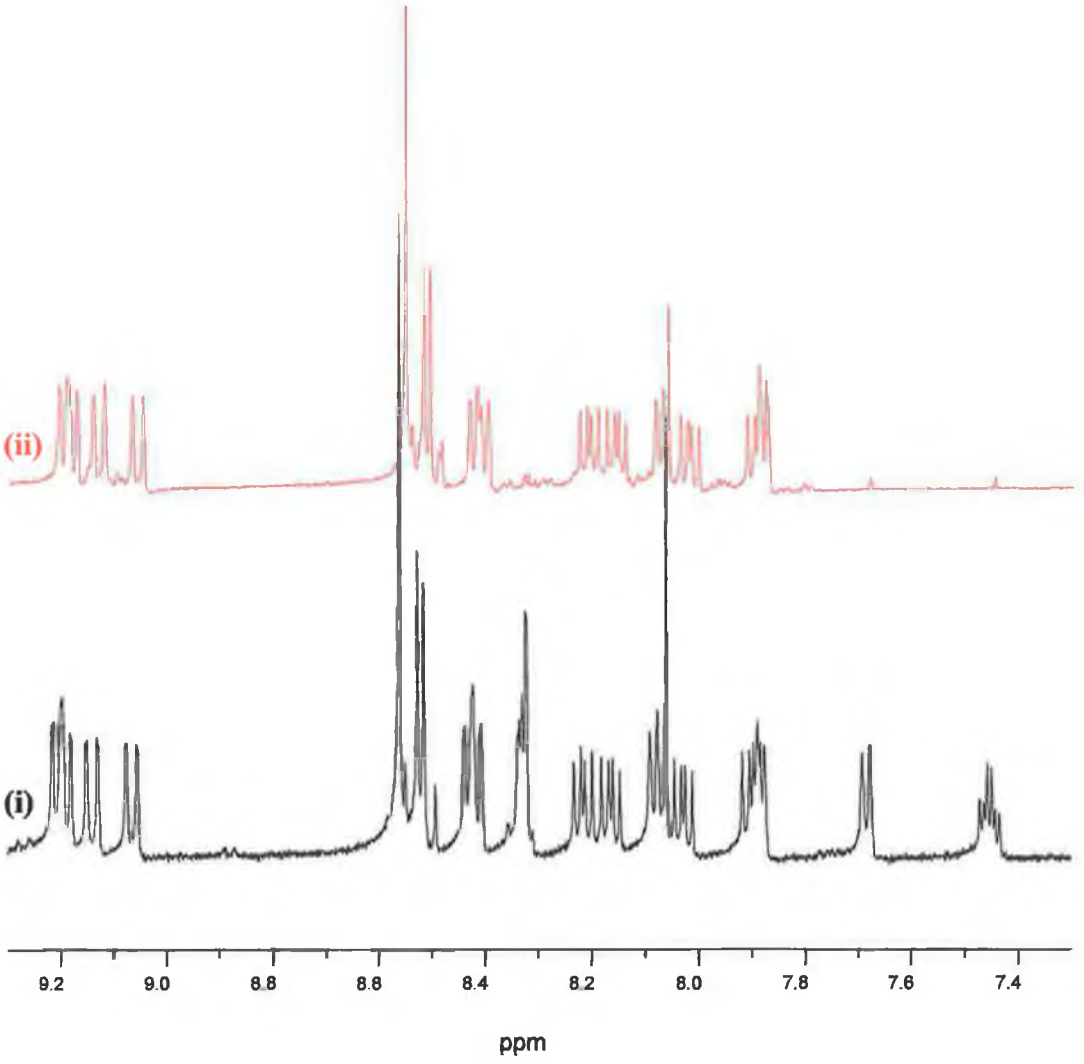

Figure 3.10 ^{1}H NMR spectra of (i) [Rh(phen)$_2$(pytr)]$^{2+}$ (——) and (ii) [Rh(phen)$_2$(d$_4$-pytr)]$^{2+}$ (——) in d$_6$-DMSO.

From Figure 3.10 it is immediately possible to distinguish the pyridyl triazole protons from those of the phenanthroline with pyridyl triazole resonances at 7.46 ppm - 1H, 7.68 ppm - 1H, 8.33 ppm - 1H and a multiplet at 8.33 ppm - 2H. The singlet associated with H5' of the triazole ring can be clearly observed at 8.07 ppm. The ^{1}H-^{1}H COSY spectrum of the non-deuterated complex [Rh(phen)$_2$(pytr)]$^{2+}$ which can be seen in Figure 3.11 was used to elucidate the coupling within the complex.

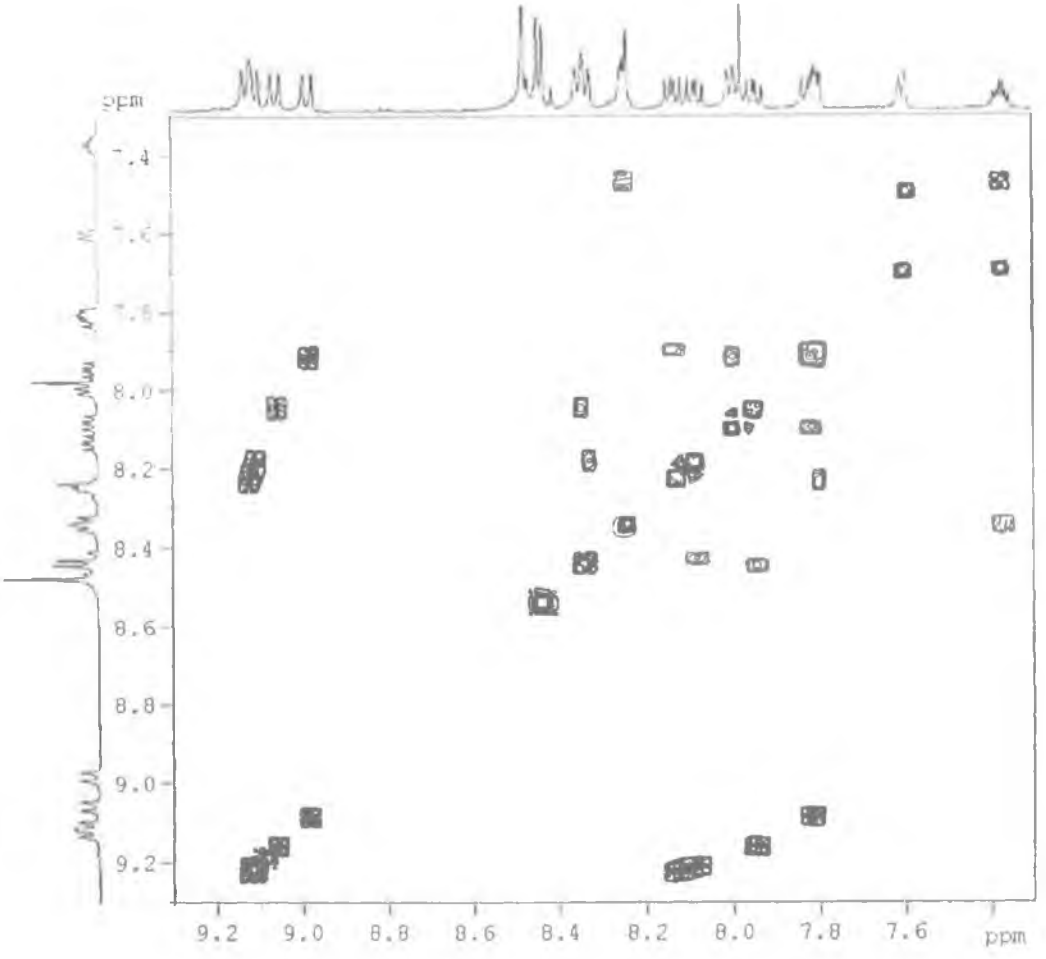

Figure 3.11 ^{1}H-^{1}H COSY NMR spectrum of $[Rh(phen)_2(pytr)]^{2+}$ in d_6-DMSO.

^{1}H NMR spectroscopy is an effective tool in observing the presence of isomers for complexes such as those that will be discussed here, a fact that is illustrated by Figure 3.12. Here the ^{1}H NMR spectra of both the N4' and the N2' isomers of the complex $[Ru(bpy)_2(pytr)]^{2+}$ can be seen and the influence of the mode of coordination is particularly evident for the H5' proton.[8,23]

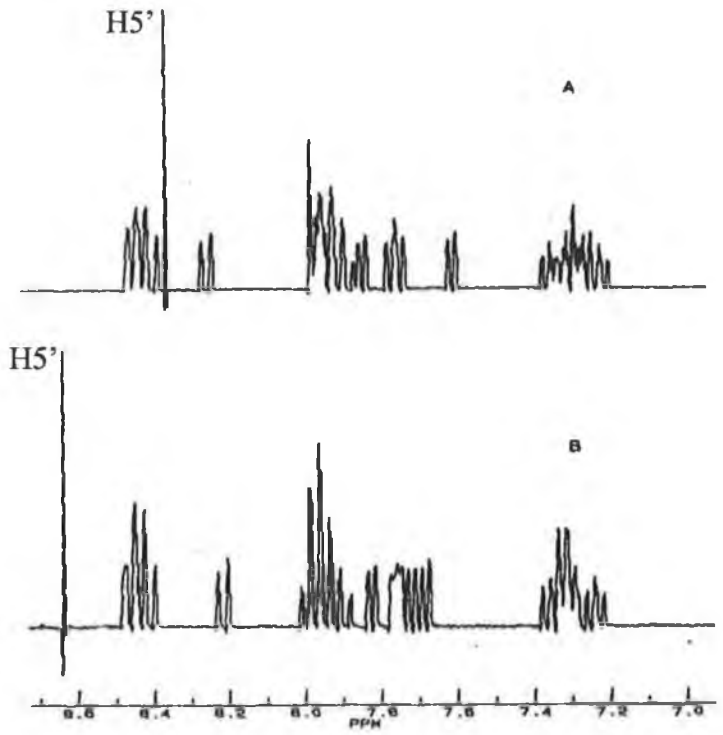

Figure 3.12 ^{1}H NMR spectra of (A) the N4' isomer of [Ru(bpy)$_2$(Hpytr)]$^{2+}$ and (B) the N2' isomer of [Ru(bpy)$_2$(Hpytr)]$^{2+}$ measured in (CD$_3$)$_2$CO.[8]

When the ^{1}H NMR spectrum of [Rh(phen)$_2$(pytr)]$^{2+}$, Figure 3.10, was studied carefully no evidence was found to indicate the presence of a second isomer. The spectrum integrates to 21 protons with the H5' singlet being readily observed at 8.07 ppm. If a second isomer was indeed present it should be possible to identify a second H5' singlet as was seen in Figure 3.12. Another singlet may be seen in the spectrum of [Rh(phen)$_2$(pytr)]$^{2+}$ at 8.58 ppm but this integrates to two protons and was identified as being associated with the phenanthroline ligand.

The ^{1}H spectrum obtained for [Rh(bpy)$_2$(pytr)]$^{2+}$ can be seen in Figure 3.13. As was the case with [Rh(phen)$_2$(pytr)]$^{2+}$ only one isomer is observed for the complex [Rh(bpy)$_2$(pytr)]$^{2+}$. The singlet at 8.14 ppm may be attributed to the proton in the H5' position of the Hpytr ligand. Once again deuteration was employed to fully assign the ^{1}H NMR spectrum. The spectrum of the deuterated complex [Rh(bpy)$_2$(d_4-pytr)]$^{2+}$ may be seen in Figure 3.13 (red) and may be directly compared

with the non deuterated complex (black) $[Rh(bpy)_2(pytr)]^{2+}$. Using the ^1H NMR spectrum of the deuterated and the non-deuterated complexes in conjunction with the ^1H-^1H COSY spectrum of the non-deuterated complex, Appendix III, it was possible to assign the following pytr resonances: H3 – 8.30 ppm, H4 – 8.36 ppm, H5 – 7.58 ppm and H6 – 7.74 ppm.

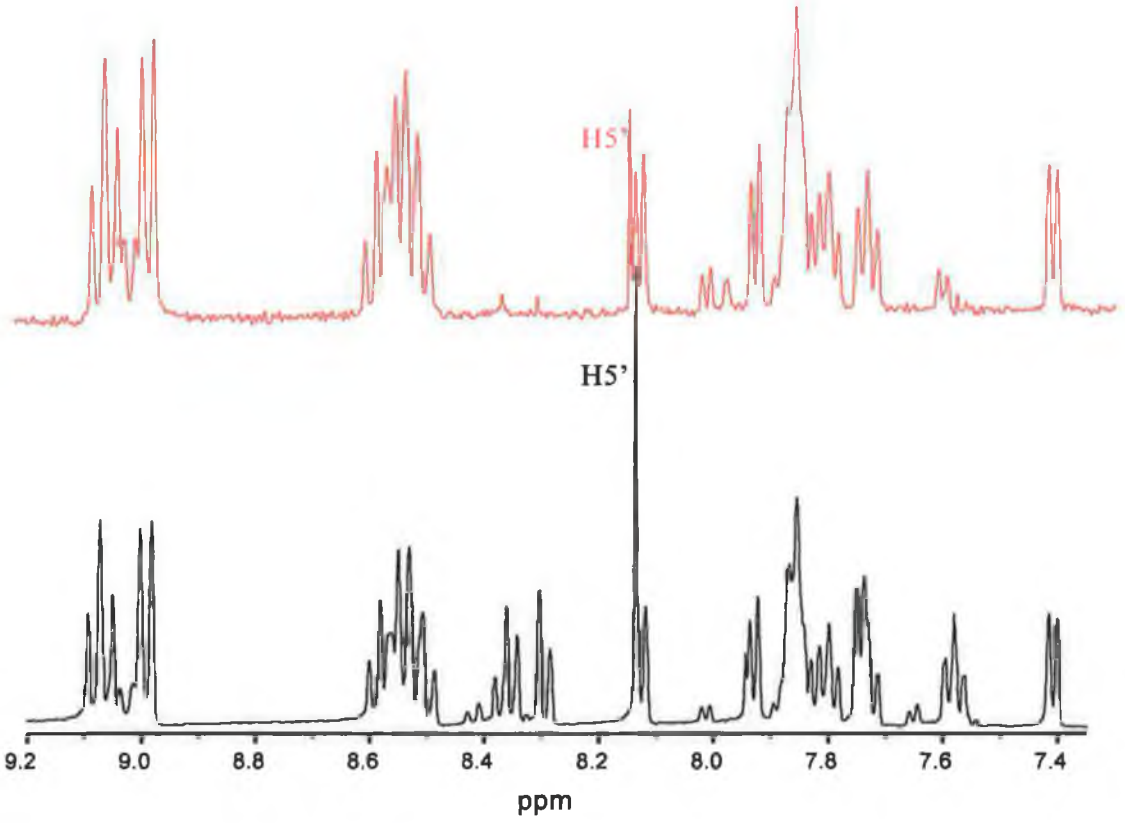

Figure 3.13 ^1H NMR spectrum of $[Rh(bpy_2(pytr)]^{2+}$ (——) and $[Rh(bpy_2(d_4\text{-}pytr)]^{2+}$ (——) in d_6–DMSO.

Due to the absence of crystals of $[Rh(phen)_2(pytr)]^{2+}$ and $[Rh(bpy)_2(pytr)]^{2+}$ suitable for analysis, it was not possible to determine their mode of coordination. In contrast to this both the N2' and the N4' isomers were isolated for the analogous complexes $[Ru(bpy)_2(pytr)]^{+}$ and $[Ru(bpy)_2(Hpytr)]^{2+}$ and the determination of their coordination modes was achieved by analysis and comparison of their ^1H NMR spectra.[23] A series of complexes containing the ligands 4Mpytr and 1M3pytr were synthesised, as the coordination of a metal centre to these ligands is influenced by the location of the methyl group. It was hoped that analysis of their ^1H NMR spectra

would help establish which isomers of $[Rh(phen)_2(pytr)]^{2+}$ and $[Rh(bpy)_2(pytr)]^{2+}$ were being obtained.

3.3.3.2 $[Rh(phen)_2(4Mpytr)]^{2+}$ and $[Rh(bpy)_2(4Mpytr)]^{2+}$

It has been found that ruthenium pyridyl triazole complexes incorporating the ligands 4Mpytr and 1M3pytr give rise to the formation of a single isomer. In the case of $[Ru(bpy)_2(1M3pytr)]^{2+}$ coordination is possible via either the N2' or the N4' of the triazole ring but it was found only to coordinate via the N4' of the triazole ring whereas the complex $[Ru(bpy)_2(4Mpytr)]^{2+}$ has only the N2' coordination site free and as a result the N2' isomer is the only possible isomer which can be formed.[23] From these studies with ruthenium pyridyl triazoles it was expected that similar coordination trends would be observed for the analogous rhodium(III) complexes. The ^1H NMR spectrum of $[Rh(phen)_2(4Mpytr)]^{3+}$ in d_6-DMSO can be seen in Figure 3.14.

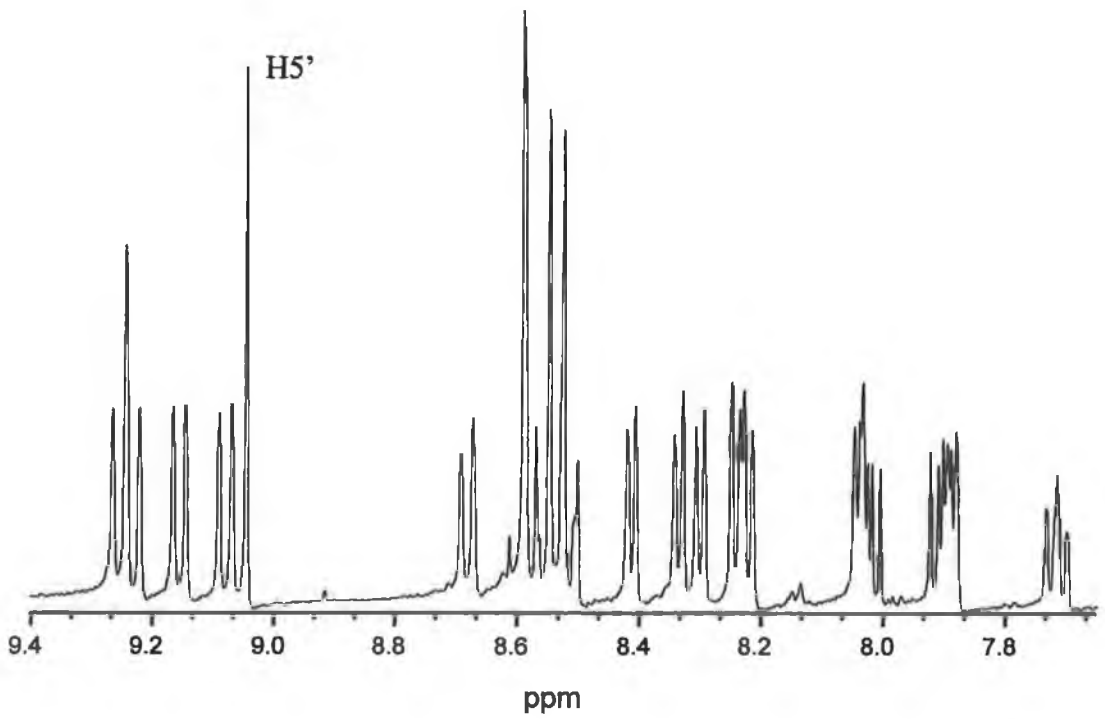

Figure 3.14 ^1H NMR spectrum of $[Rh(phen)_2(4Mpytr)]^{3+}$ in d_6–DMSO.

The singlet due to H5' of the triazole ring can be clearly seen at 9.05 ppm in this instance. When the NMR in Figure 3.14 above is compared with that of $[Rh(phen)_2(pytr)]^{2+}$, Figure 3.10, it can be seen that the double doublet and two doublets at 9.24 ppm, 9.16 ppm and 9.08 ppm are very clear features of the 1,10-phenanthroline ligands. From this knowledge it was possible to study the ^1H-^1H COSY spectrum of this complex and to assign the doublet at 8.67 ppm to H3 of the ligand 4Mpytr, H4 was found to appear at 8.54 ppm (m), H5 at 7.72 ppm (dd) and H6 at 7.90 ppm (m). The methyl group appeared at 4.22 ppm. The ^1H NMR and the ^1H-^1H NMR spectra of $[Rh(bpy)_2(4Mpytr)]^{2+}$ may be seen in Appendix III and the spectral assignment is detailed in Table 3.7.

3.3.3.3 $[Rh(phen)_2(1M3pytr)]^{3+}$ and $[Rh(bpy)_2(1M3pytr)]^{3+}$

Figure 3.15 illustrates the ^1H NMR spectrum of $[Rh(phen)_2(1M3pytr)]^{3+}$ and H5' is clearly visible at 9.06 ppm.

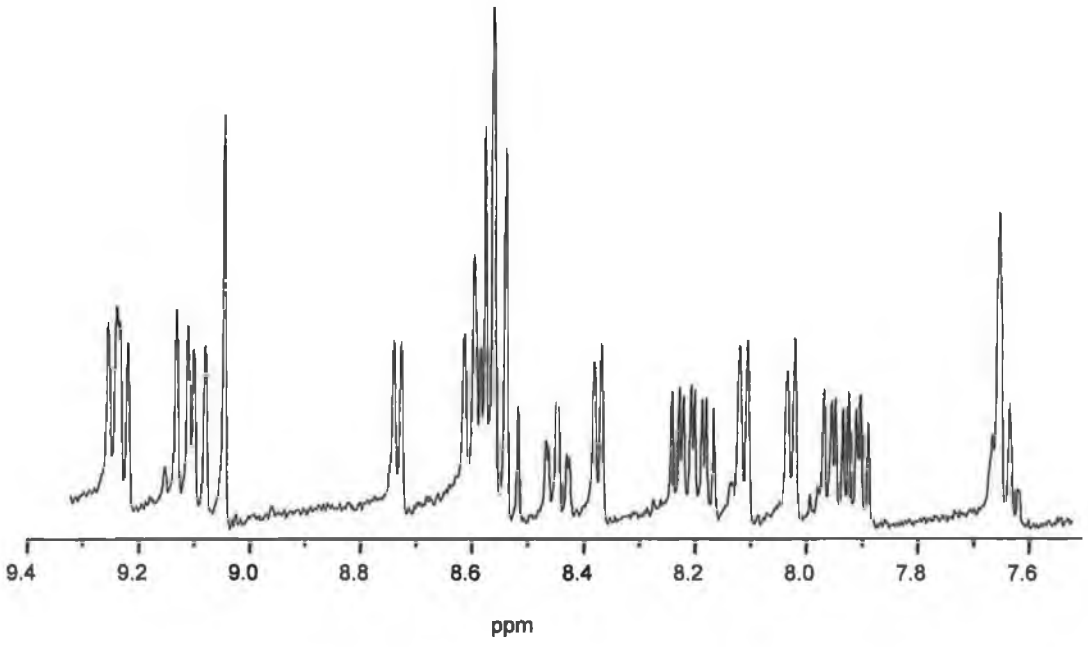

Figure 3.15 ^1H NMR spectrum of $[Rh(phen)_2(1M3pytr)]^{3+}$ in d_6–DMSO.

From comparison of the 1,10-phenanthroline containing complexes discussed earlier, the pair of double doublets at 9.26 ppm and 9.13 ppm may be ascribed to the 1,10-

phenanthroline ligands. From this the other 1,10-phenanthroline protons may be attributed by study of the ^{1}H-^{1}H COSY spectrum of the complex (see Appendix III) and thus the triazole protons were determined to be H3 – 8.62 ppm (part of multiplet), H4 – 8.47 ppm (dd), H5 and H6 overlap in the multiplet observable at 7.67 ppm.

Very little information can be gathered from the spectrum of $[Rh(bpy)_2(1M3pytr)]^{3+}$ seen in Appendix III. It was possible however to see the H5' signal occurring at 9.27 ppm. In this instance the methyl group was apparent at 4.00 ppm. Table 3.7 summarises the ^{1}H NMR results discussed containing the ligands Hpytr, 4Mpytr and 1M3pytr measured in d_6–DMSO.

Table 3.7 ***^{1}H NMR data for complexes containing the ligands Hpytr, 4Mpytr and 1M3pytr. All spectra were obtained in d_6-DMSO.***

	H3	H4	H5	H6	R- H5'	R – CH_3
Hpytr	8.09 (d)	7.98 (dd)	7.51 (dd)	8.70 (d)	8.27 (s)	-
$[Rh(phen)_2(pytr)]^{2+}$	8.33 (m)	8.33 (m)	7.46 (dd)	7.68 (d)	8.07 (s)	-
$[Rh(bpy)_2(pytr)]^{2+}$	8.30 (d)	8.36 (dd)	7.58 (dd)	7.74 (m)	8.10 (s)	-
4Mpytr	8.11 (d)	7.95 (dd)	7.47 (dd)	8.66 (d)	8.62 (s)	3.99 (s)
$[Rh(phen)_2(4Mpytr)]^{3+}$	8.67 (d)	8.54 (m)	7.72 (dd)	7.90 (m)	9.05 (s)	4.22 (s)
$[Rh(bpy)_2(4Mpytr)]^{3+}$	8.97 (d)	8.42 (m)	7.67 (m)	7.80 (d)	9.63 (s)	4.07 (s)
1M3pytr	8.16 (d)	7.91 (dd)	7.43 (dd)	8.66 (d)	8.61 (s)	3.97 (s)
$[Rh(phen)_2(1M3pytr)]^{3+}$	8.62 (m)	8.47 (dd)	7.67 (m)	7.67 (m)	9.06 (s)	3.97 (s)
$[Rh(bpy)_2(1M3pytr)]^{3+}$	-	-	-	-	9.27 (s)	4.00 (s)

The assignment of the mode of coordination for the complexes $[Rh(phen)_2(4Mpytr)]^{3+}$ and $[Rh(bpy)_2(4Mpytr)]^{3+}$ is indisputable, only the N2' isomer may be formed. It should be noted that the CH_3 moiety was shifted downfield with respect to the free ligand by 0.23 ppm and 0.08 ppm for

$[Rh(phen)_2(4Mpytr)]^{3+}$ and $[Rh(bpy)_2(4Mpytr)]^{3+}$ respectively. For the complexes $[Rh(phen)_2(1M3pytr)]^{3+}$ and $[Rh(bpy)_2(1M3pytr)]^{3+}$ two isomers in theory are possible but no evidence was observed to suggest that two isomers were being formed. From a steric viewpoint it is unlikely that the N2' isomer would be formed preferentially. The signal of the CH_3 moiety was virtually unaffected by coordination it was concluded that the N4' isomer was being formed in these cases (N2' coordination causes a downfield shift of the methyl group as was observed for $[Rh(phen)_2(4Mpytr)]^{3+}$ and $[Rh(bpy)_2(4Mpytr)]^{3+}$. Having established the mode of coordination for complexes incorporating methylated pyridine triazole ligands their ^1H NMR data was studied in order to determine if they could be used to identify the mode of coordination in $[Rh(phen)_2(pytr)]^{2+}$ and $[Rh(bpy)_2(pytr)]^{2+}$. However, when the ^1H NMR data for complexes with the ligands Hpytr, 4Mpytr and 1M3pytr were compared, Table 3.7, it was not possible identify any definitive trends and therefore the mode of coordination of $[Rh(phen)_2(pytr)]^{2+}$ and $[Rh(bpy)_2(pytr)]^{2+}$ could not be identified. The issue of coordination isomers will be addressed further in Chapter 8 where it will be discussed in relation to the photophysical and electrochemical behaviour of these complexes.

3.2.3.4 $[Rh(phen)_2(Phpytr)]^{2+}$ and $[Rh(bpy)_2(Phpytr)]^{2+}$

The ^1H NMR spectrum of $[Rh(phen)_2(Phpytr)]^{2+}$ may be seen below and the ^1H NMR spectrum of $[Rh(bpy)_2(Phpytr)]^{2+}$ may be seen in Appendix III. Comparison of the spectra of these two complexes with those obtained for the complexes $[Rh(phen)_2(pytr)]^{2+}$ and $[Rh(bpy)_2(pytr)]^{2+}$ shows that the phenyl ring has little influence on the positions of the protons of the pyridine ring of the HPhpytr ligand with H3, H4, H5, H6 being found in practically the same positions for the complexes $[Rh(phen)_2(Phpytr)]^{2+}$ and $[Rh(bpy)_2(Phpytr)]^{2+}$ as they were for the complexes $[Rh(phen)_2(pytr)]^{2+}$ and $[Rh(bpy)_2(pytr)]^{2+}$. No evidence for the formation of two isomers was detected for either $[Rh(phen)_2(Phpytr)]^{2+}$ or $[Rh(bpy)_2(Phpytr)]^{2+}$ and when the ^1H NMR spectra of the crude products were analysed only trance amounts of excess ligand were detected and once this ligand impurity was removed the spectra integrated to 25 protons as expected. As was detailed in Section 3.3.2.1

crystals of $[Rh(bpy)_2(Phpytr)]^{2+}$ were obtained which were suitable for x-ray analysis and it was found that binding occurred via N2' of the triazole.

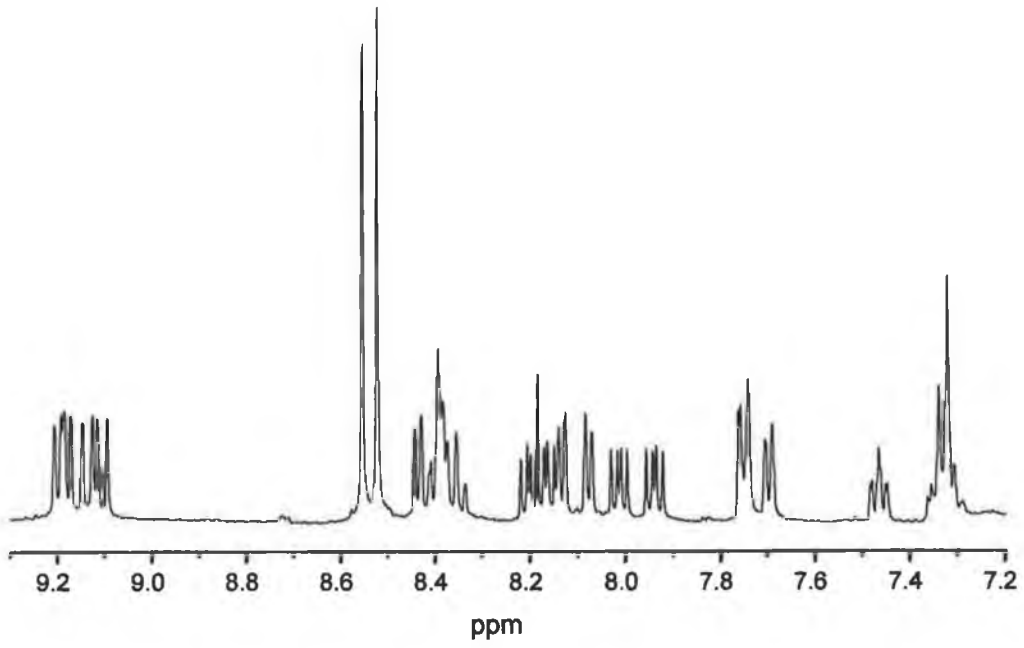

Figure 3.16 ^1H NMR spectrum of $[Rh(phen)_2(Phpytr)]^{2+}$ in d_6-DMSO.

Table 3.8 ***^1H NMR data for $[Rh(phen)_2(Phpytr)]^{2+}$ and $[Rh(bpy)_2(Phpytr)]^{2+}$ and $[Rh(phen)_2(pytr)]^{2+}$ and $[Rh(bpy)_2(pytr)]^{2+}$ measured in d_6-DMSO.***

	H3	H4	H5	H6	H5'
HPhpytr	8.10 (d)	8.02 (dd)	7.49 (dd)	8.73 (d)	-
$[Rh(phen)_2(Phpytr)]^{2+}$	8.36 (m)	8.36 (m)	7.47 (dd)	7.69 (d)	-
$[Rh(bpy)_2(Phpytr)]^{2+}$	8.37 (m)	8.37 (m)	7.56 (dd)	7.75 (d)	-
Hpytr	8.09 (d)	7.98 (dd)	7.51 (dd)	8.70 (dd)	8.27(s)
$[Rh(phen)_2(pytr)]^{2+}$	8.33 (m)	8.33 (m)	7.46 (dd)	7.68 (d)	8.56 (s)
$[Rh(bpy)_2(pytr)]^{2+}$	8.30 (d)	8.36 (dd)	7.58 (dd)	7.74 (d)	8.10 (s)

3.3.3.5 *$[Rh(phen)_2(bpt)]^{2+}$ and $[Rh(bpy)_2(bpt)]^{2+}$*

Having studied complexes containing chelating ligands the next stage was to introduce ligands that have the capacity to bind two metal centres. Two pyridyl triazole ligands were selected for this purpose. The first was the ligand 3,5-bis(pyridin-2-yl)-1,2,4-triazole (Hbpt). This ligand was chosen primarily for its similarity to the Hpytr ligand. It was felt that a comparison between the complexes $[Rh(phen)_2(pytr)]^{2+}$ and $[Rh(phen)_2(bpt)]^{2+}$ and $[Rh(bpy)_2(bpt)]^{2+}$ and $[Rh(bpy)_2(pytr)]^{2+}$ should allow complete assignment of ^1H NMR spectra. It was of importance to isolate and assign isomers of these mononuclear complexes from the perspective of the synthesis and characterisation of dinuclear species in particular hetero-dinuclear complexes.

Figure 3.17 illustrates this mode of binding with ring A being the pyridine ring coordinated to the metal centre and ring B being the free or uncoordinated ring. Two distinct sets of signals associated with the ligand were anticipated.

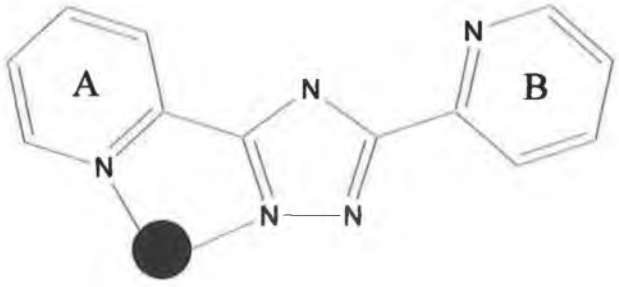

Figure 3.17 Illustration of N2' isomer with Hbpt ligand.

The first set, associated with ring A, was expected to be comparable to H3, H4, H5 and H6 of the bound pyridine ring of $[Rh(L)_2(pytr)]^{2+}$ where L = bpy /phen, Table 3.9. The second set, from ring B, was expected to behave in a similar fashion to the free ligand. The ^1H NMR spectra of these complexes are, as expected, more complicated than those discussed so far and as can be seen in Figure 3.18 deuteration was again necessary. It is evident from Figure 3.18 that deuteration greatly simplifies the task of assigning spectra. The doublets at 8.50 ppm and 7.71 ppm and the double doublets at 7.85 ppm, 7.49 ppm and 7.37 ppm of spectrum (i) are clearly resonances associated with the Hbpt ligand. When the spectra of Hbpt and

$[Rh(phen)_2(pytr)]^{2+}$ were taken into consideration the spectrum of $[Rh(phen)_2(bpt)]^{2+}$ was assigned as outlined in Table 3.9. Complexation of the metal centre gives rise to an upfield shift of ring B, the uncoordinated ring and the signals of the bound ring, ring A, are comparable to those of $[Rh(phen)_2(pytr)]^{2+}$. It should be noted that the H6 proton of the bound ring has been shifted significantly upfield to 7.71 ppm (-0.96 ppm). This particular proton feels the ring current of an adjacent phen ligand and as a result is shifted to higher field. Evidence was only observed for the presence of a single isomer and, in the absence of suitable crystals for analysis, it was not possible to unambiguously identify the mode of coordination occurring. As stated previously this issue will be discussed further in Chapter 8.

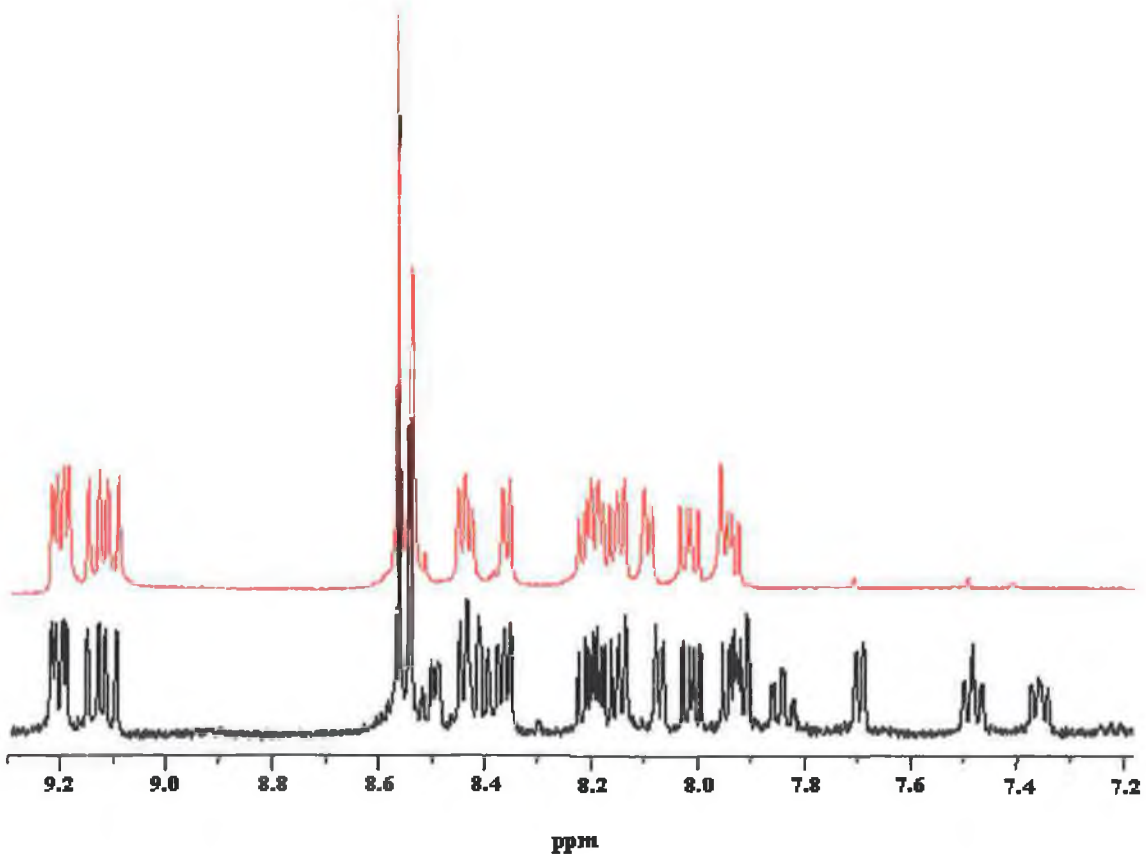

Figure 3.18 ^1H NMR spectra of (i) $[Rh(phen)_2(bpt)]^{2+}$(——) and (ii) $[Rh(phen)_2(d_8\text{-}bpt)]^{2+}$(——) in d_6–DMSO.

Figure 3.19 illustrates the ^1H NMR spectra of $[Rh(bpy)_2(bpt)]^{2+}$ and $[Rh(bpy)_2(d_8\text{-}pytr)]^{2+}$. Assignment of the non-deuterated complex, Figure 3.19 (i), in this case was complicated by the fact the most of the Hbpt resonances coincided with bpy

resonances occurring as multiplets. By analysis of the integration of these spectra and by comparison with the free ligand and $[Rh(bpy)_2(pytr)]^{2+}$ it was possible to assign the spectrum of $[Rh(bpy)_2(bpt)]^{2+}$ as detailed in Table 3.9. Again only evidence for the single isomer was observed and as before assignment of the coordination mode was not possible.

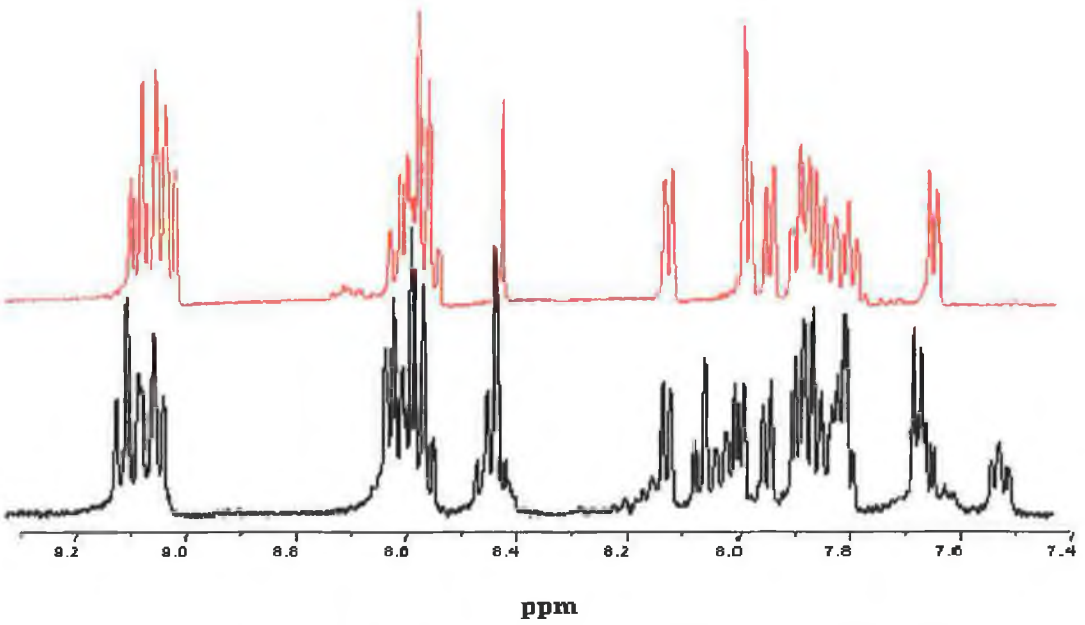

Figure 3.19 ^{1}H NMR spectra of (i) $[Rh(bpy)_2(bpt)]^{2+}$(——) and (ii) $[Rh(bpy)_2(d_8\text{-}bpt)]^{2+}$(——) in d_6–DMSO.

Table 3.9 ^{1}H NMR data for Rh(III) complexes with Hbpt and Hpytr measured in d_6-DMSO and $[Ru(bpy)_2(bpt)]^+$ measured in d_6-Acetone.

		H3 (ppm)	H4 (ppm)	H5 (ppm)	H6 (ppm)
Hbpt		8.15 (d)	8.00 (dd)	7.52 (dd)	8.67 (d)
$[Rh(phen)_2(pytr)]^{2+}$		8.33 (m)	8.33 (m)	7.46 (dd)	7.68 (d)
$[Rh(phen)_2(bpt)]^{2+}$	**Ring A**	8.46-8.36 (m)	8.46-8.36 (m)	7.49 (dd)	7.70 (d)
	Ring B	7.96-7.92 (m)	7.85 (dd)	7.37 (dd)	8.50 (d)
$[Rh(bpy)_2(pytr)]^{2+}$		8.30 (d)	8.36 (dd)	7.58 (dd)	7.74 (d)
$[Rh(bpy)_2(bpt)]^{2+}$	**Ring A**	8.45-8.39 (m)	8.45-8.39 (m)	7.64-7.63 (m)	7.87-7.82(m)
	Ring B	7.98 (m)	8.03 (dd)	7.50 (dd)	8.61-8.52 (d)
$[Ru(bpy)_2(bpt)]^{+}$ [a]	**Ring A**	8.23	8.01	7.26	7.74
	Ring B	8.06	7.74	7.20	8.45

Ring A – pyridine ring coordinated to the metal centre Ring B – free pyridine ring a – from ref 29.

3.3.3.6 *$[Rh(phen)_2(NHbpt)]^{2+}$, $[Rh(phen)_2(NH_2bpt)]^{3+}$, $[Rh(bpy)_2(NHbpt)]^{2+}$ and $[Rh(bpy)_2(NH_2bpt)]^{3+}$*

The ligand NH_2bpt differs from the Hbpt ligand in that an amino group replaces the proton of the N4' position of the triazole ring thus allowing coordination via either the amino group or via the N2' position of the triazole ring and a nitrogen of a pyridine ring. As outlined in the experimental section of this chapter, Section 3.2, the syntheses of complexes with this particular ligand were carried out under two different sets of conditions. These reactions yielded two sets of complexes and ^1H NMR spectroscopy proved very effective in the analysis of their spectra. The first complex to be discussed here was synthesised in basic water and it was for this that suitable crystals were obtained for analysis, Section 3.3.2.2. The ^1H NMR of this complex, $[Rh(phen)_2(NHbpt)]^{2+}$, can be seen in Figure 3.20. The crystal structure of the complex is also included in Figure 3.20 and the 1,10-phenanthroline moieties are labelled in the manner in which they will be referred to in the following discussion.

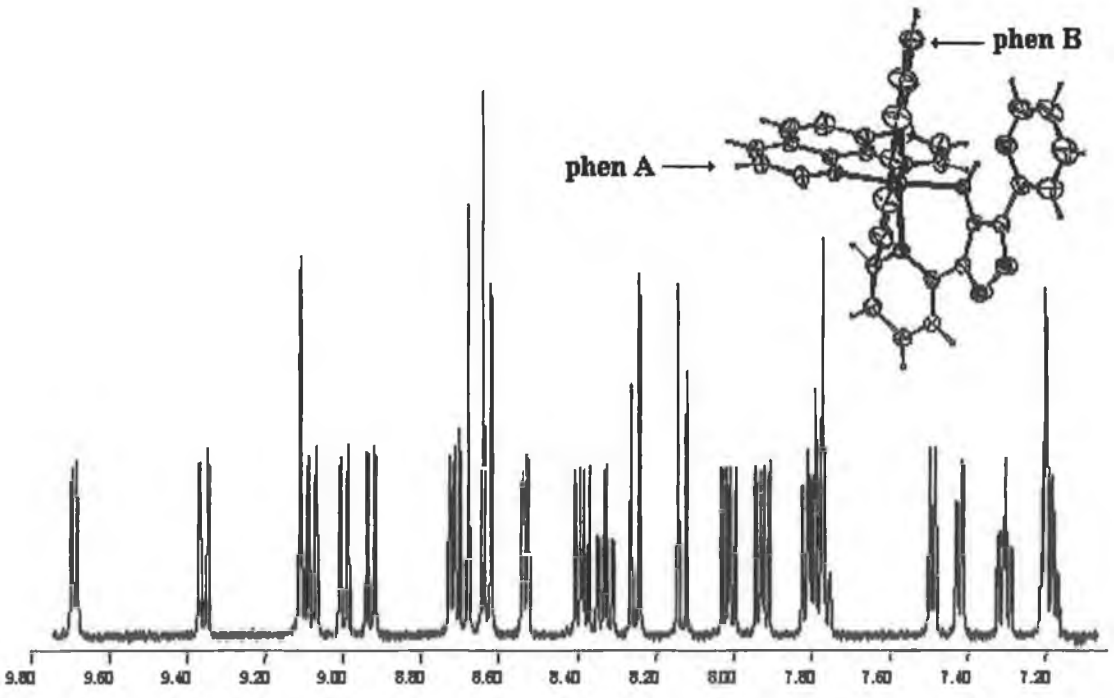

Figure 3.20 ^1H NMR spectrum of $[Rh(phen)_2(NHbpt)]^{2+}$ in d_6–DMSO.

As detailed in Section 3.3.2.2 coordination of the metal centre in this instance occurs via the amine nitrogen and a nitrogen of a pyridine ring. The formation of this complex is assumed to be facilitated by the reaction conditions i.e. basic water in this case. These conditions allow for the deprotonation of the ligand thus promoting complex formation in the manner observed. The ^{1}H NMR spectrum shown in Figure 3.20, integrating to 25 protons, clearly indicates the presence of only one species, indicative of the absence of linkage isomers. Although certain elements of the spectrum could easily be identified as being indicative of phenanthroline such as the doublets at 8.14 ppm and 8.24 ppm the ^{1}H-^{1}H COSY spectrum was instrumental in the assignment of the spectrum, Figure 3.21.

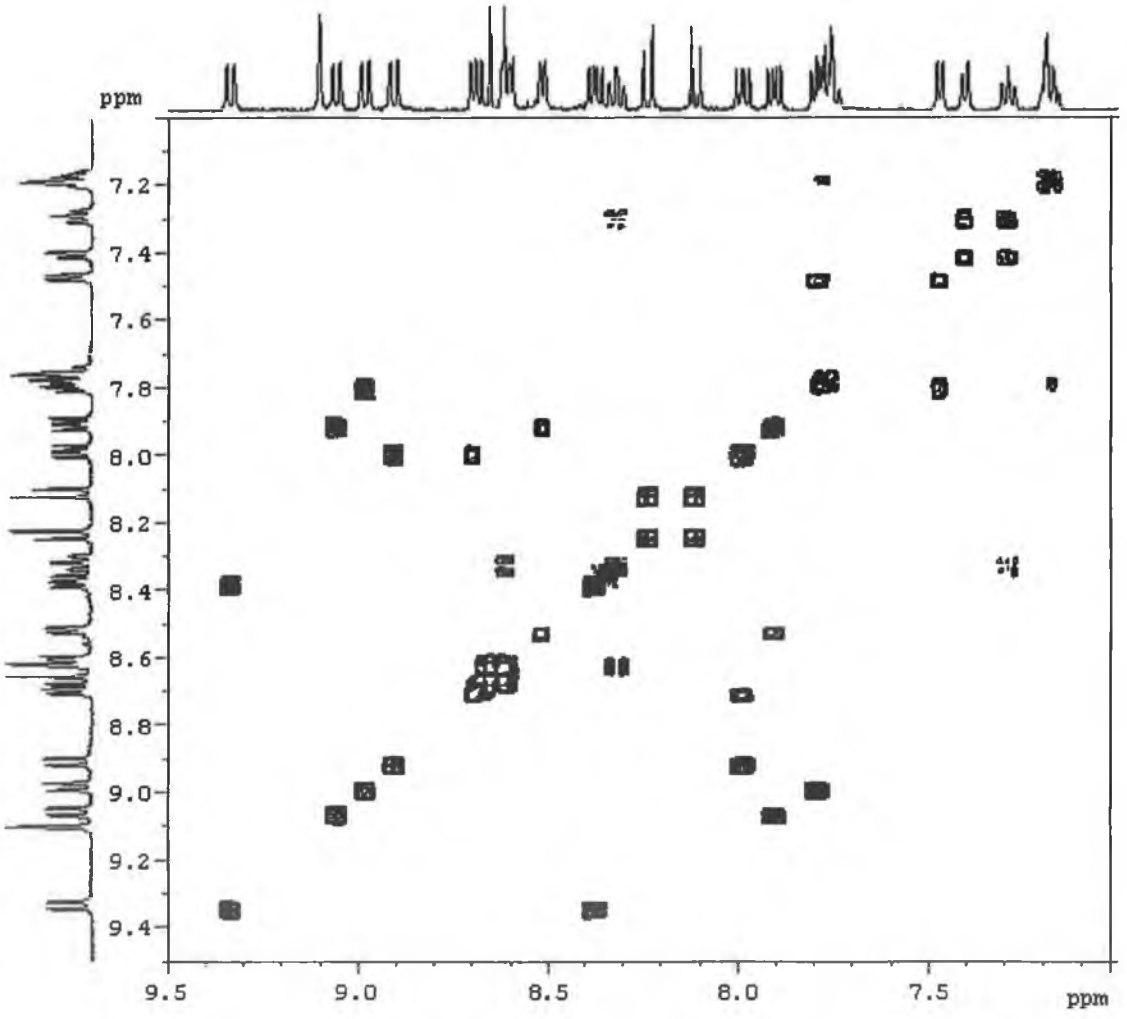

Figure 3.21 ^{1}H-^{1}H COSY NMR spectrum of $[Rh(phen)_2(NHbpt)]^{2+}$ in d_6–DMSO.

It should be noted that the spectrum of $[Rh(phen)_2(NHbpt)]^{2+}$ was also obtained in d_3–acetonitrile. Changing solvents can alter chemical shifts but it can also influence coupling and linewidths and in this case was found to be particularly useful in the analysis of the region between 9.00 ppm and 8.60 ppm. The doublets observed at 9.75 ppm and 9.42 ppm can be attributed to protons of the phenanthroline ring A. These resonances are downfield with respect to the resonances observed for equivalent protons in the $[Rh(phen)_3]^{3+}$ complex and this can be attributed to the influence of the NH moiety of the NH_2bpt ligand. The singlet at 9.11 ppm is attributed to the amino NH and is shifted significantly downfield with respect to the free ligand and indicative of coordination via the amine group. By comparison of the two ^1H NMR spectra and from the close analysis of the ^1H-^1H COSY NMR spectrum of $[Rh(phen)_2(NHbpt)]^{2+}$ it was possible to assign the signals associated with the NH_2bpt ligand as detailed in Table 3.10.

Table 3.10 ***^1H NMR data for NH_2bpt and $[Rh(phen)_2(NHbpt)]^{2+}$ in d_6-DMSO.***

	H3 (ppm)	H4 (ppm)	H5 (ppm)	H6 (ppm)	NH_2 (ppm)	NH
NH_2bpt	8.23 (d)	8.06 (dd)	7.58 (dd)	8.77 (d)	7.82 (s)	-
$[Rh(phen)_2(NHbpt)]^{2+}$						
Ring A	8.63-8.61 (m)	8.32 (dd)	7.30 (dd)	7.41 (d)	-	9.11 (s)
Ring B	7.78 (m)	7.78 (m)	7.20 (m)	7.20 (m)		

Ring A – metal bound ring Ring B – free ring

It should be noted that a temperature dependent study of $[Rh(phen)_2(NHbpt)]^{2+}$ was carried out in d_6-DMSO with spectra being obtained over the temperature range 19-59°C but no changes were observed in the spectrum of $[Rh(phen)_2(NHbpt)]^{2+}$ over this temperature range. When DCl is added to $[Rh(phen)_2(NHbpt)]^{2+}$ the spectrum seen here in Figure 3.22 is observed. It can be seen that the singlet at 9.17 ppm in Figure 3.20 is not present in the spectrum above and that the doublet, which was at 9.75 ppm, has now been shifted downfield to 10.00 ppm. This particular doublet was attributed to the phen Ring A in Figure 3.20 and the fact that it has been shifted further downfield and broadened upon the addition of DCl may be attributed to its proximity to the amino nitrogen.

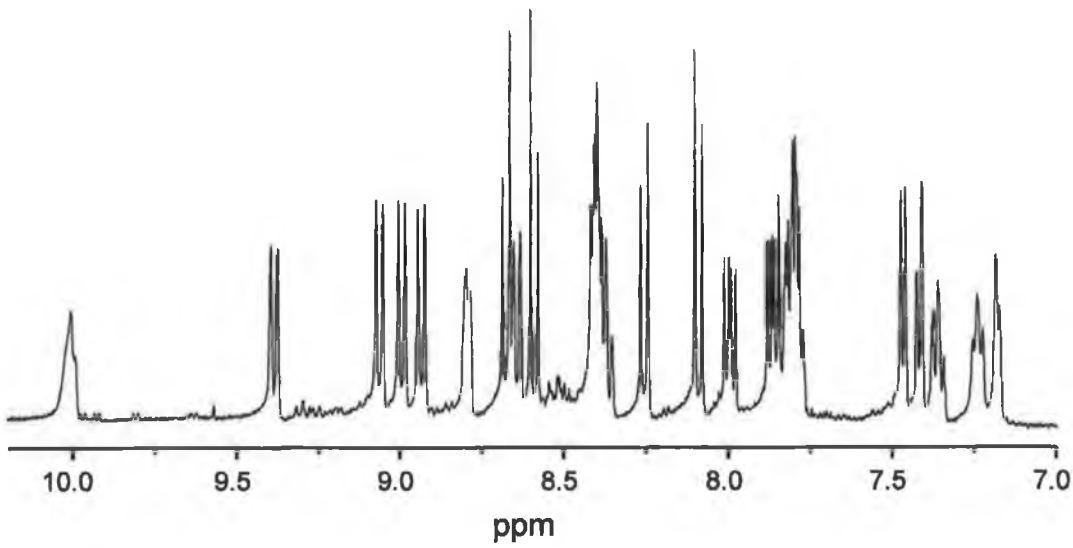

Figure 3.22 ^{1}H NMR spectrum of [Rh(phen)$_2$(NHbpt)]$^{2+}$ with DCl added in d_6–DMSO.

The reaction with the NH_2bpt ligand and $[Rh(phen)_2Cl_2]Cl$ was also carried out in water:ethanol and was allowed to reflux for 10 days. The reaction was very slow with a very poor yield and when passed through the C-25 column only enough complex was obtained to get the ^{1}H NMR spectrum that can be seen in Figure 3.23. Although still containing unreacted starting materials it can be seen from Figure 3.23 that the complex obtained from the ethanol:water synthesis is markedly different from that obtained in basic water, Figure 3.20. The peak at 9.75 ppm which was present in the spectrum of $[Rh(phen)_2(NHbpt)]^{2+}$, and assigned as a resonance associated with a proton of the phen ring A, is not present in the major product in this particular case. It was previously concluded that the signal at 9.75 ppm was shifted downfield due to the influence of the amino nitrogen and its absence in the spectrum in Figure 3.2 indicates that in this instance binding occurs not via the nitrogen of the amine moiety but rather through the N2' of the triazole ring and a nitrogen of a pyridine ring. The presence of a singlet at 7.88 ppm may be considered to be further evidence of binding via the N2' of the triazole ring. If binding does occur via the N2' of the triazole ring then it would be expected that the NH_2 moiety would, from a ^{1}H NMR perspective, behave in a similar fashion to the free ligand and in fact the protons associated with the NH_2 of the free ligand are found at 7.82 ppm.

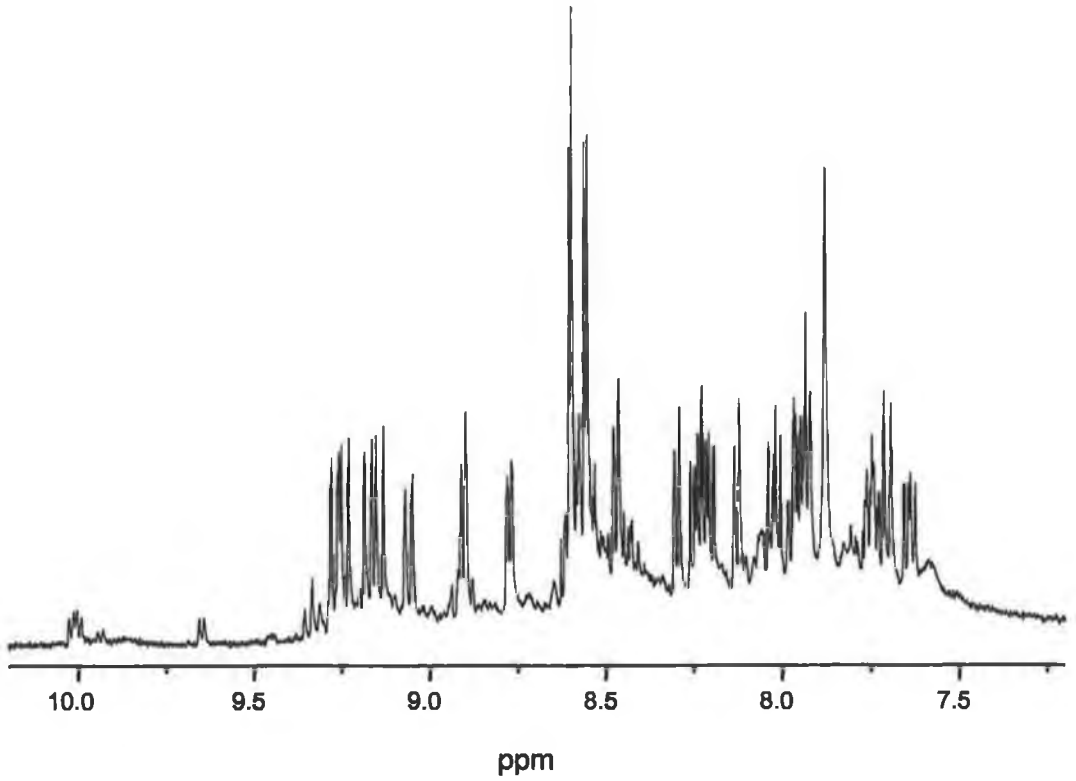

Figure 3.23 ^{1}H NMR spectrum of $[Rh(phen)_2(NH_2bpt)]^{3+}$ synthesised in ethanol:water in d_6–DMSO.

Figure 3.2 illustrates the possible modes of coordination of a metal centre to the NH_2bpt ligand.

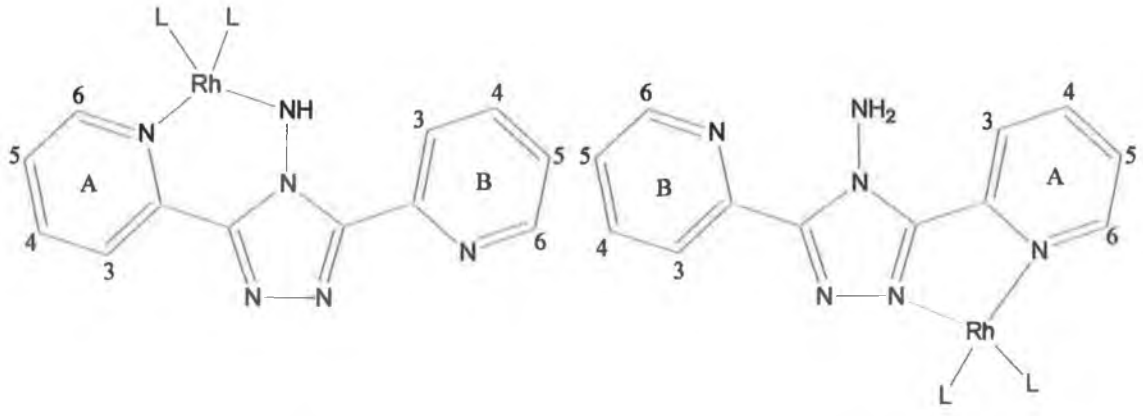

Isomer I Isomer II

Figure 3.24 The two possible modes of coordination of a metal centre to the NH_2bpt ligand where L = bpy / phen.

As mentioned in Section 3.1, Oro *et. al.* observed a similar behaviour with the complexes for $[Rh^{I}(CO)_2(NHbpt)]$ and $[Rh^{I}(CO)_2(NH_2bpt)]^+$ whereby the neutral complex $[Rh^{I}(CO)_2(NHbpt)]$ coordinated through the amine moiety and the cationic complex $[Rh^{I}(CO)_2(NH_2bpt)]^+$ coordinated through the N2' of the triazole ring.[18] Rheingold *et. al.* have also reported both modes of coordination in their study of two coordination isomers of $[Ru(CO)_2(NH_2bpt)Cl_2]$.[34] Thus it can be seen that for this particular ligand, that is NH_2bpt, it is possible to selectively synthesise isomers by varying the reaction conditions. When in basic water the ligand is deprotonated and coordination occurs via the amine moiety giving isomer I and when in ethanol:water the ligand is protonated and gives rise to the formation of isomer II although much longer reaction times are required and yields are lower than for isomer I.

The ^{1}H NMR spectrum seen in Figure 3.25 is that of the complexes obtained when NH_2bpt is reacted with $[Rh(bpy)_2Cl_2]Cl$ and $[Rh(d_8\text{-bpy})_2Cl_2]Cl$ in basic water. Under these reaction conditions it would be expected that the ligand is deprotonated and that coordination occurs via the nitrogen of the amine group giving the complexes $[Rh(bpy)_2(NHbpt)]^{2+}$ and $[Rh(d_8\text{-bpy})_2(NHbpt)]^{2+}$.

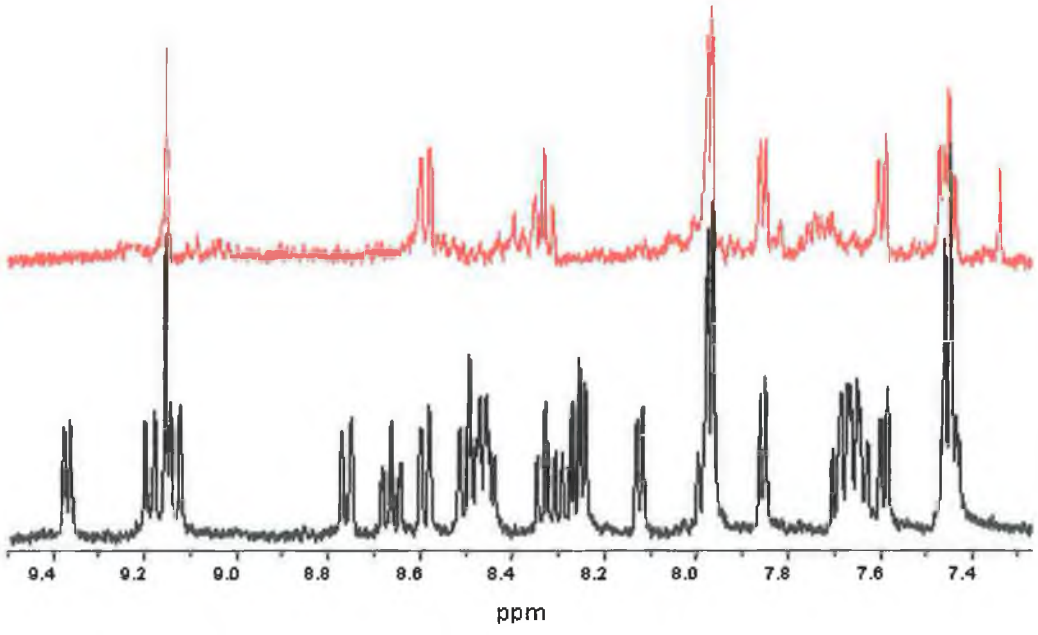

Figure 3.25 ^{1}H NMR spectra of (i) $[Rh(bpy)_2(NHbpt)]^{2+}$ (——) and (ii) $[Rh(d_8\text{-bpy})_2(NHbpt)]^{2+}$ (——) in d_6-DMSO.

Deuteration of the bpy ligand greatly assists the assignment of the ^{1}H NMR spectrum of $[Rh(bpy)_2(NHbpt)]^{2+}$ and the clear presence of a singlet at 9.16 ppm indicates that coordination in this instance does indeed occur via the amine group and a nitrogen of a pyridine ring.

The ^{1}H NMR spectrum that can be seen in Figure 3.26 is that of the complex obtained when NH_2bpt is reacted with $[Rh(bpy)_2Cl_2]Cl$ in ethanol:water. Under these reaction conditions it would be expected that the ligand is protonated and that coordination occurs via the N2' of the triazole ring and a nitrogen of a pyridine ring giving the complex $[Rh(bpy)_2(NH_2bpt)]^{3+}$.

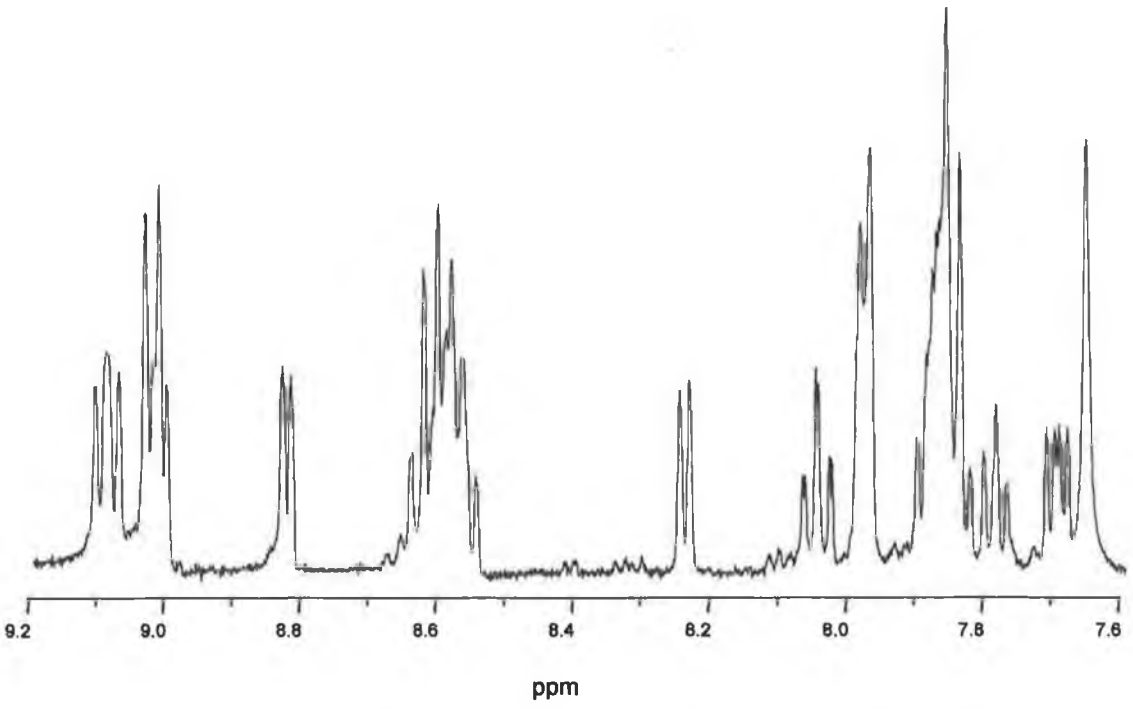

Figure 3.26 ^{1}H NMR spectrum of $[Rh(bpy)_2(NH_2bpt)]^{3+}$ in d_6-DMSO.

The singlet observable at 7.66 ppm can be attributed to the protons associated with the amine moiety. It was seen in the case of the complexes $[Rh(phen)_2(NHbpt)]^{2+}$ and $[Rh(bpy)_2(NHbpt)]^{2+}$ that this particular signal was shifted significantly downfield when the amine group was directly involved in the coordination of the metal centre, 9.11 ppm and 9.16 ppm respectively. In contrast, when the amine group is not directly involved in coordination, it can be seen that a singlet is present at 7.88 ppm in the spectrum of $[Rh(phen)_2(NH_2bpt)]^{3+}$ (Figure 3.23). Based upon

the behaviour observed for the phen complexes it can be concluded that for the complex whose spectrum is seen in Figure 3.26 is coordinated via the N2 of the triazole ring and a pyridine nitrogen. As was the case for the phen complexes only a single isomer is observed via both reaction conditions. Table 3.11 contains the ^{1}H NMR data for complexes with the NH_2bpt ligand.

Table 3.11 ^{1}H NMR data for complexes with NH_2bpt measured in d_6-DMSO.

	H3 (ppm)	H4 (ppm)	H5 (ppm)	H6 (ppm)	NH_2 / NH (ppm)
Hbpt	8.15 (d)	8.00 (dd)	7.52 (dd)	8.67 (d)	-
$[Rh(phen)_2(bpt)]^{2+}$					
Ring A	8.46-8.36 (m)	8.46-8.36 (m)	7.49 (dd)	7.70 (d)	-
Ring B	7.96-7.92 (m)	7.85 (dd)	7.37 (dd)	8.50 (d)	-
$[Rh(bpy)_2(bpt)]^{2+}$					
Ring A	8.45-8.39 (m)	8.45-8.39 (m)	7.64-7.63 (m)	7.87-7.82 (m)	-
Ring B	7.98 (m)	8.03 (dd)	7.50 (dd)	8.61-8.52 (m)	-
NH_2bpt	8.23 (d)	8.06 (dd)	7.58 (dd)	8.77 (d)	7.82 NH_2(s)
$[Rh(phen)_2(NHbpt)]^{2+}$					
Ring A	8.63-8.61 (m)	8.32 (dd)	7.30 (dd)	7.41 (d)	9.11 NH (s)
Ring B	7.78 (m)	7.78 (m)	7.20 (m)	7.20 (m)	
$[Rh(bpy)_2(NHbpt)]^{2+}$					
Ring A	8.59 (d)	8.33 (dd)	7.48-7.44 (m)	7.60 (d)	9.16 NH (s)
Ring B	7.98 (m)	7.98 (m)	7.48-7.44 (m)	7.86 (d)	
$[Rh(bpy)_2(NH_2bpt)]^{3+}$					
Ring A	9.02 (m)	8.65-8.55 (m)	7.90-7.83 (m)	7.98 (m)	7.66 NH_2(s)
Ring B	7.98 (m)	8.05 (dd)	7.69 (dd)	8.82 (d)	

Ring A – pyridine ring coordinated to the metal centre
Ring B – free pyridine ring

3.3.4 ^{13}C NMR Spectroscopy

^{13}C NMR measurements are regularly used in structural elucidation. In comparison to the ^{1}H nucleus the ^{13}C nucleus has a low sensitivity and also it has quite a low natural abundance (1.1%) resulting in a very low absolute sensitivity (the absolute sensitivity in this instance refers to the product of the natural abundance and the relative sensitivity). As a result of this ^{13}C NMR experiments not only require longer measurement times but also more concentrated samples. It should also be noted that in comparison to the ^{1}H NMR spectra the signal to noise ratio is greater in the ^{13}C spectrum. Due to the fact that the syntheses carried out were microscale in nature, difficulties were experienced in some cases in obtaining enough sample to obtain a good ^{13}C spectrum but experiments involving up 10,000 scans resulted in spectra suitable for analysis. 2-dimensional NMR techniques were required to determine the C-H correlations within each complex. These data were obtained using the heteronuclear multiple quantum coherence or HMQC method. The advantage of using this measurement technique is that it is more sensitive than the normal C,H-COSY and the accumulation time required is shorter. The increased sensitivity of the HMQC method was of particular importance with respect to the complexes being studied, as very little sample was available for analysis.

As has been discussed earlier, Section 3.3.3, deuteration has been known to have an effect on the ^{13}C spectra in organic chemistry.[33] A decrease in the height of the carbon signal where C-H to C-D has occurred has previously been observed for ruthenium(II) pyridyl triazole complexes and it was of interest to determine if a similar effect could be observed for rhodium(III) pyridyl triazole complexes.[29] The ^{13}C spectra for the complexes $[Rh(phen)_2(pytr)]^{2+}$ and $[Rh(phen)_2(d_4\text{-pytr})]^{2+}$ in d_6-DMSO can be seen in Figure 3.27 and Figure 3.28.

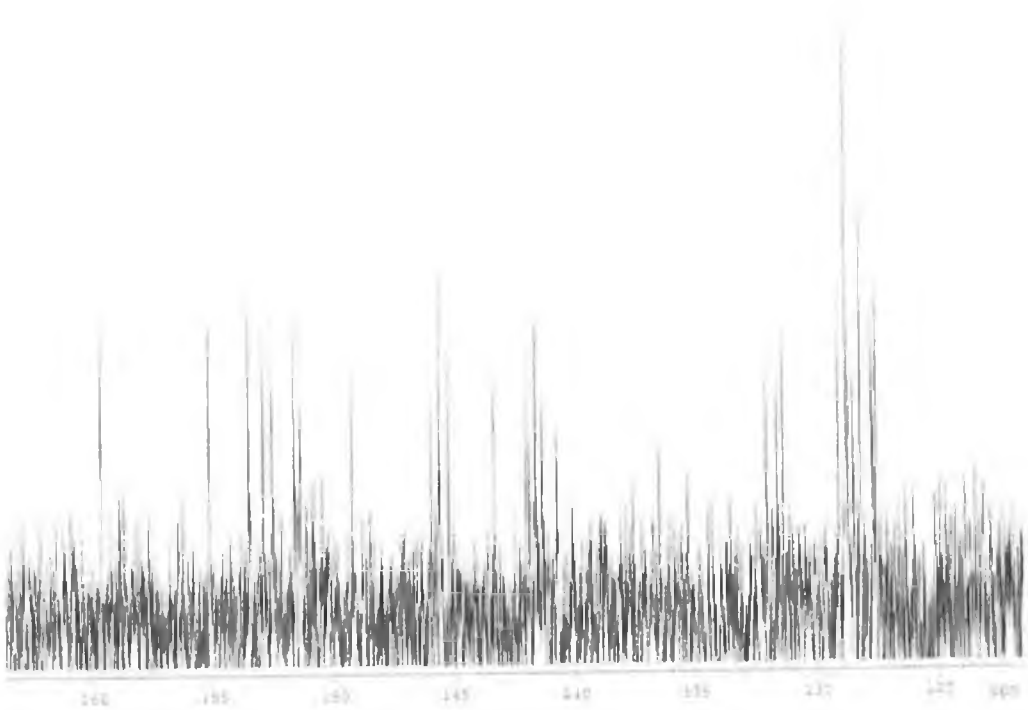

Figure 3.27 ^{13}C NMR spectrum of $[Rh(phen)_2(pytr)]^{2+}$ in d_6-DMSO.

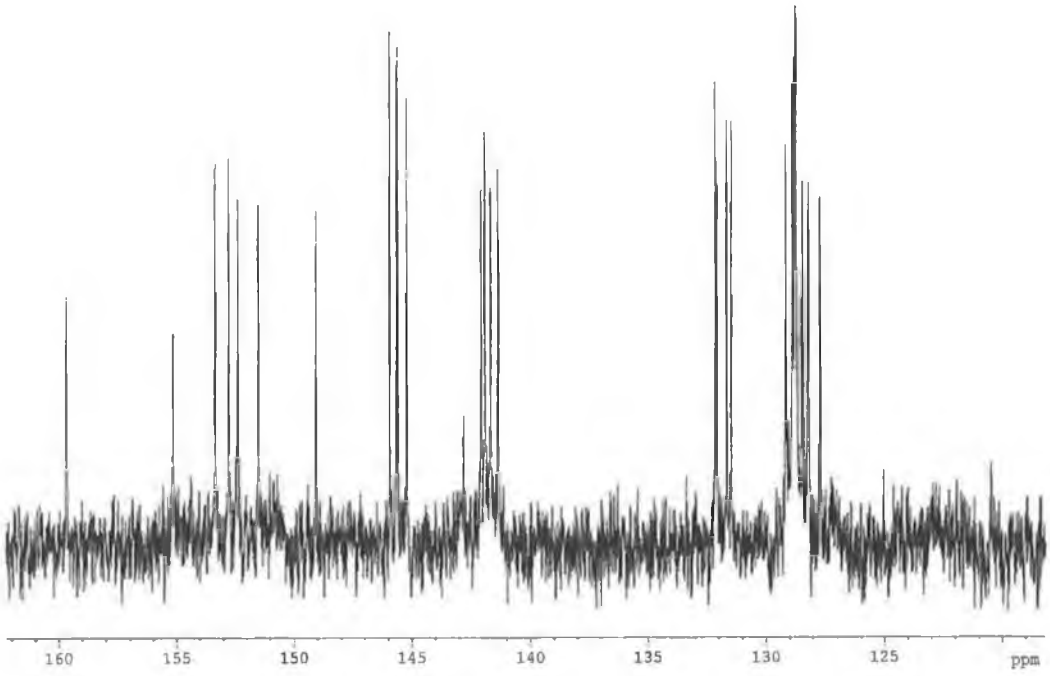

Figure 3.28 ^{13}C NMR spectrum of $[Rh(phen)_2(d_4\text{-}pytr)]^{2+}$ in d_6-DMSO.

The positions of the carbons of the pyridyl ring of the Hpytr ligand could be determined by HMQC and CH correlation based upon knowledge obtained from the comparison of the NMR spectra of $[Rh(phen)_2(pytr)]^{2+}$ and $[Rh(phen)_2(d_4\text{-pytr})]^{2+}$. From the analysis of the HMQC the carbons of the Hpytr ring are expected in the vicinity of 123.50 ppm, 128.00 ppm, 143.90 ppm and 152.00 ppm. An initial comparison of the two spectra shows that the peaks at 123.34 ppm and 127.56 ppm are absent in the deuterated spectrum and upon a more careful comparison it was also found that peaks at 143.35 ppm and 151.38 ppm were absent.

Figure 3.29 and Figure 3.30 show the ^{13}C spectra for the complexes $[Rh(bpy)_2(pytr)]^{2+}$ and $[Rh(bpy)_2(d_4\text{-pytr})]^{2+}$ in d_6-DMSO. The protons of the pyridyl rings were determined by studying the ^1H NMR spectra of $[Rh(bpy)_2(pytr)]^{2+}$ and $[Rh(bpy)_2(d_4\text{-pytr})]^{2+}$ and then from the HMQC of $[Rh(bpy)_2(pytr)]^{2+}$ it was possible to identify the carbons associated with these protons. From the HMQC, carbons are expected at approximately 123.00 ppm, 128.00 ppm, 143.00 ppm and 151.00 ppm. It can immediately be seen that the peak at 123.38 ppm in the non-deuterated spectrum is not present in the deuterated spectrum. Upon a closer comparison of the two spectra it was found that peaks at 127.93 ppm, 143.53 ppm and 150.61 ppm are not present in the deuterated spectrum. The peak at 155.21 ppm is also absent in the deuterated complex. From the HMQC of $[Rh(bpy)_2(pytr)]^{2+}$ this carbon was found to be associated with the H5' of the triazole ring. Interestingly it can be seen that the peak at 148.51 ppm has decreased in intensity in the spectrum of the deuterated complex. This carbon does not appear to couple to anything in the HMQC spectrum and as a result it is thought that this carbon is adjacent to a C-D bond with the decrease in its intensity being as a result of its proximity to the C-D bond.

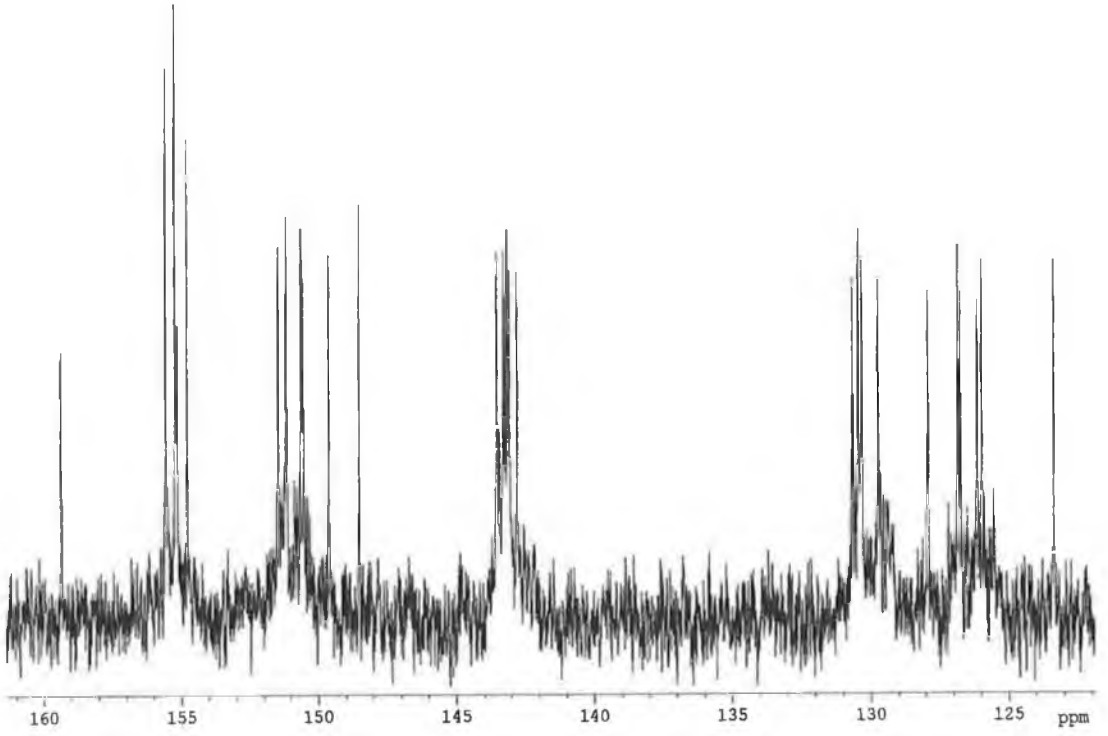

Figure 3.29 ^{13}C NMR spectrum of $[Rh(bpy)_2(pytr)]^{2+}$ in d_6-DMSO.

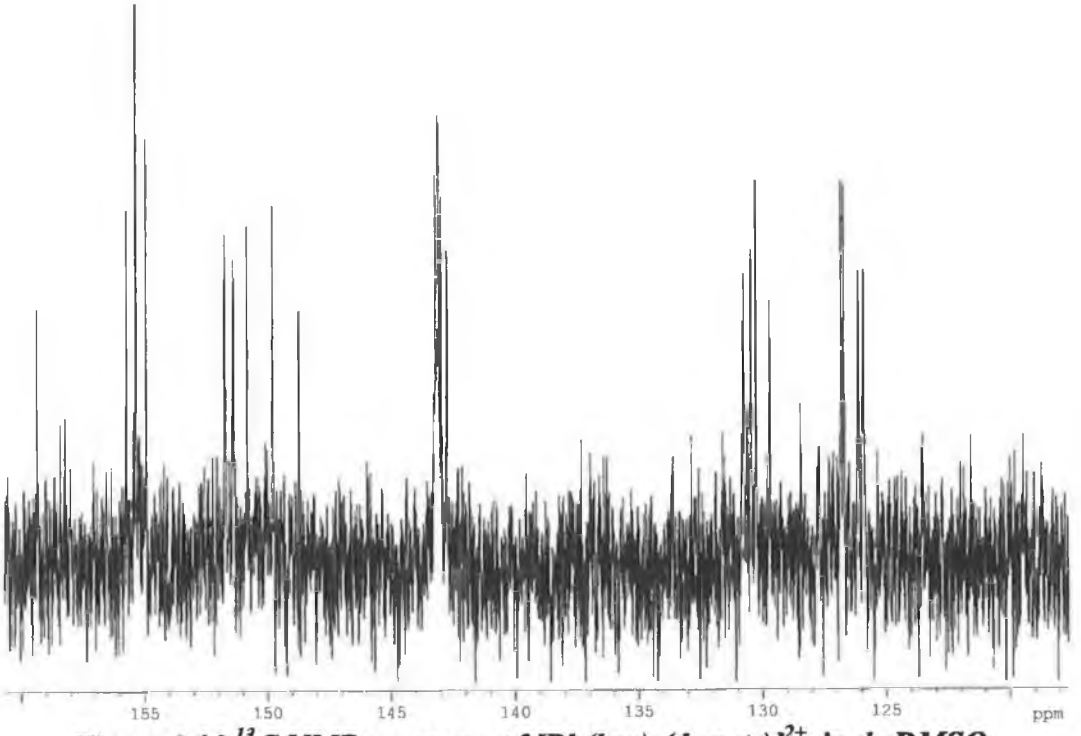

Figure 3.30 ^{13}C NMR spectrum of $[Rh(bpy)_2(d_4\text{-}pytr)]^{2+}$ in d_6-DMSO.

As discussed, the relevant C-H correlations were obtained by consulting the previously assigned ^{1}H NMR spectra followed by detailed analysis of the pertinent HMQC NMR spectrum. Figure 3.31 illustrates the HMQC NMR spectrum of $[Rh(phen)_2(NHbpt)](PF_6)_2$ as an example of the type of spectrum acquired.

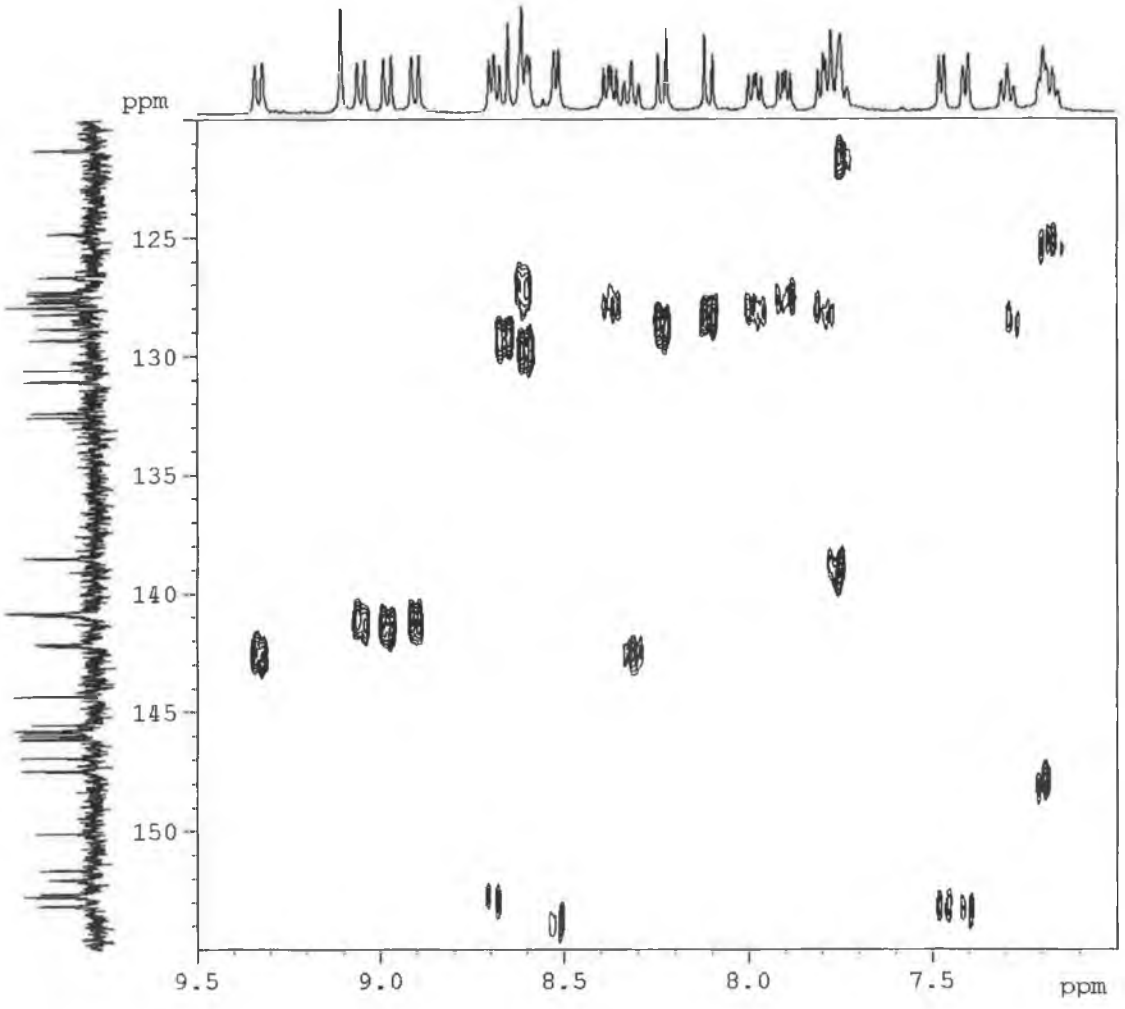

Figure 3.31 HMQC NMR spectrum of $[Rh(phen)_2(NHbpt)](PF_6)_2$ in d_6-DMSO.

Table 3.12 summarises, where possible, the ^{1}H and ^{13}C NMR spectroscopic data for the pyridine triazole complexes discussed in this chapter. Whilst some variation between the occurrence of the ^{13}C resonances of the H3, H4, H5 and H6 protons of the various complexes detailed in Table 3.12 does occur definite trends can be seen. In particular the carbons associated with the H3 and H5 protons are found upfield of

the H4, H5 and H5' protons. Analysis of the ^{13}C spectra proved to be particularly useful in this study as they served to compliment the ^{1}H NMR assignments made.

Table 3.12 Summary of ^{1}H and ^{13}C NMR spectroscopic data for pyridine triazole complexes discussed in this chapter measured in d_6-DMSO.

$[Rh(phen)_2(pytr)]^{2+}$	**^{1}H chemical**	**^{13}C chemical shift (ppm)**	**$[Rh(bpy)_2(pytr)]^{2+}$**	**^{1}H chemical shift (ppm)**	**^{13}C chemical shift (ppm)**
3	8.33	123.34	3	8.30	123.38
4	8.33	143.35	4	8.36	143.53
5	7.46	127.56	5	7.58	127.93
6	7.68	151.38	6	7.74	150.61
5'	8.07	*	5'	8.10	155.21
$[Rh(phen)_2(4Mpytr)]^{3+}$	**^{1}H chemical**	**^{13}C chemical shift (ppm)**	**$[Rh(bpy)_2(4Mpytr)]^{3+}$**	**^{1}H chemical shift (ppm)**	**^{13}C chemical shift (ppm)**
3	8.67	127.1	3	8.97	127.0-125.5
4	8.54	*	4	8.34-8.46	143.8-141.2
5	7.72	*	5	7.72	129.33
6	7.90	154.9	6	8.04	151.38
5'	9.05	151.2	5'	9.63	150.1
$[Rh(phen)_2(Phpytr)]^{2+}$	**^{1}H chemical**	**^{13}C chemical shift (ppm)**	**$[Rh(bpy)_2(Phpytr)]^{2+}$**	**^{1}H chemical shift (ppm)**	**^{13}C chemical shift (ppm)**
3	8.36	123.42	3	8.37	123.47
4	8.36	143.36	4	8.37	143.50-142.80
5	7.47	127.83	5	7.56	127.76
6	7.69	151.79	6	7.75	150.81
$[Rh(phen)_2(NHbpt)]^{2+}$ Bound py	**^{1}H chemical**	**^{13}C chemical shift (ppm)**	**$[Rh(phen)_2(NHbpt)]^{2+}$ Free py**	**^{1}H chemical shift (ppm)**	**^{13}C chemical shift (ppm)**
3	8.63-8.61	126.67	3	7.78	121.29
4	8.32	142.21-142.13	4	7.78	138.51
5	7.30	129.50-128.00	5	7.20	124.82
6	7.41	152.77	6	7.20	147.47
$[Rh(bpy)_2(NH_2bpt)]^{3+}$ Bound py	**^{1}H chemical**	**^{13}C chemical shift (ppm)**	**$[Rh(bpy)_2(NH_2bpt)]^{3+}$ Free py**	**^{1}H chemical shift (ppm)**	**^{13}C chemical shift (ppm)**
3	9.02	127.15-126.30	3	7.98	131.15-130.84
4	8.65-8.55	144.57-143.35	4	8.05	138.92
5	7.90-7.83	*	5	7.69	127.15-126.30
6	7.98	153.36-151.32	6	8.82	149.76

* - ^{13}C chemical shift could not be determined unambiguously

3.3.5 Mass Spectrometry

Mass spectrometry is a powerful tool in determining the molecular weight of a compound and uses either electric and / or magnetic fields to ionise and separate ions in space according to their mass-to-charge (m/z) ratio. In this instance electrospray ionisation mass spectrometry was carried out, where possible, on all complexes discussed. EI-MS provides a gentle ionisation and as a result is particularly suited to the study of inorganic transition metal complexes.

The mass spectra of the complexes $[Rh(bpy)_2(pytr)]^{2+}$ and $[Rh(bpy)_2(d_4\text{-pytr})](PF_6)_2$ can be seen in Figure 3.32 and Figure 3.33. No attempt was made to determine the entire fragmentation pattern for these complexes but a number of important fragments may be assigned in each instance. The exchange of four of the protons of the Hpytr ligand with deuterium leads to an increase in molecular weight of 4.02 amu of the deuterated complex with respect to the non-deuterated complex. The two spectra can be compared and fragments containing the d_4-pytr can be easily distinguished as they differ from peaks in the non-deuterated complex by m/z of 4. In the case of the non-deuterated complex the fragment $[[Rh(bpy)_2(pytr)](PF_6)]^+$, resulting from the loss of one PF_6 salt, is responsible for m/z 704.9. In the case of the deuterated complex the fragment $[[Rh(bpy)_2(d_4\text{-pytr})](PF_6)]^+$, can be quite clearly seen at m/z 708.9 which is as expected. It is important to also note in the case of the deuterated complex that nothing is observed at m/z 704. This shows that only the deuterated form of the complex is present in this instance. The mass spectrum of the deuterated complex is also useful in interpreting the non-deuterated spectra as it can be used as a method to establish the presence or absence of the pytr ligand in a fragment. When the two spectra are compared, any fragments, which differ by 4 amu, can be assumed to contain the Hpytr ligand. If, upon comparison of the deuterated and non-deuterated spectra, two identical fragments can be seen it can be presumed that the Hpytr ligand is not present in this case.

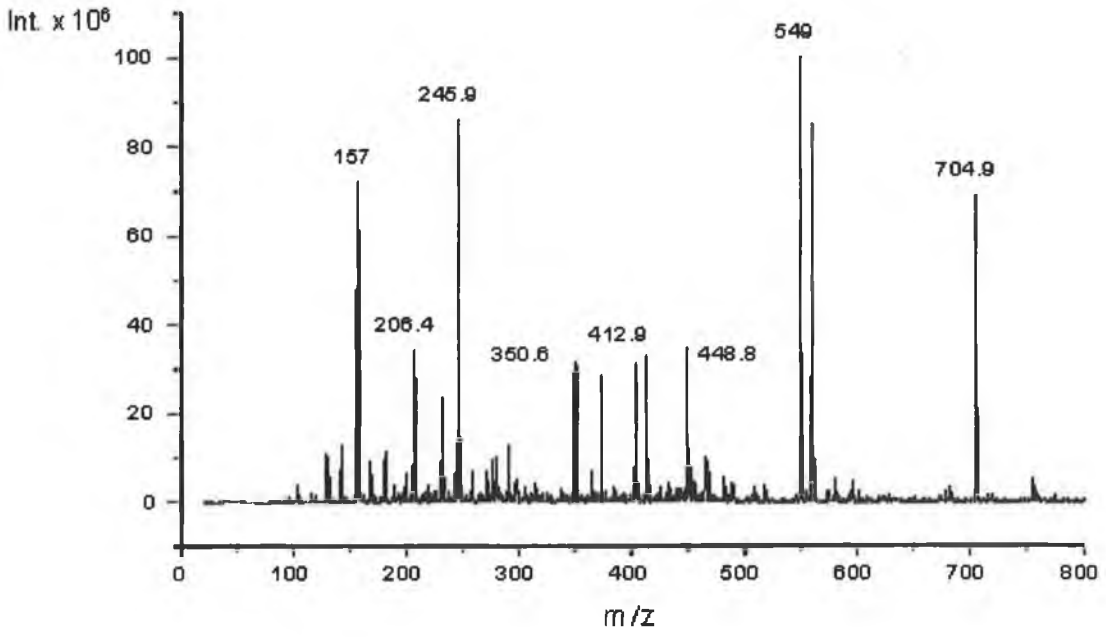

Figure 3.32 Mass spectrum of [Rh(bpy)$_2$(pytr)](PF$_6$)$_2$ measured in acetonitrile.

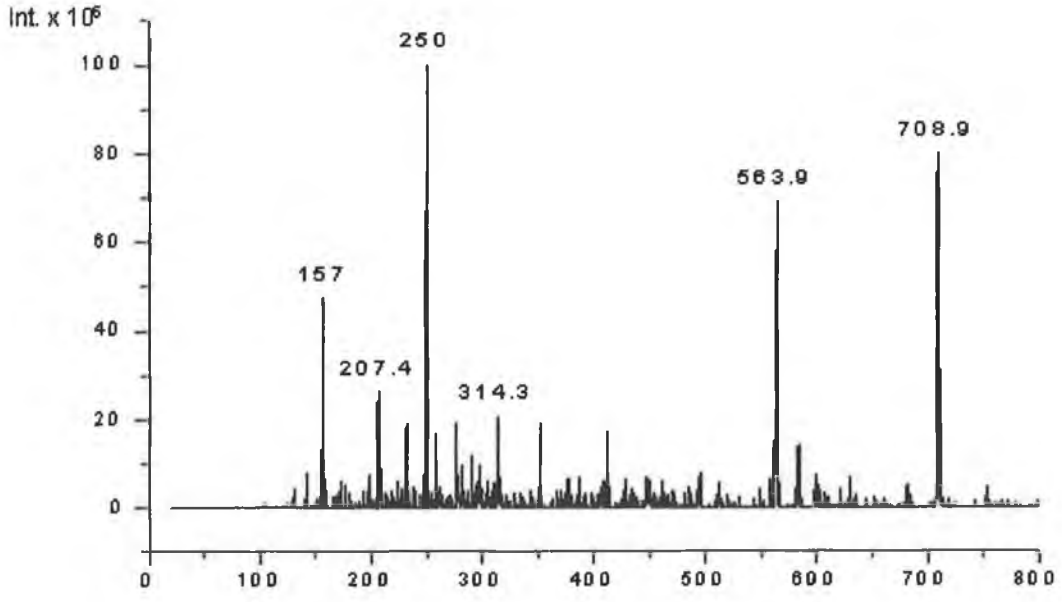

Figure 3.33 Mass spectrum of [Rh(bpy)$_2$(d_4-pytr)](PF$_6$)$_2$ measured in acetonitrile.

Figure 3.34 and Figure 3.35 show the spectra obtained for the complexes [Rh(phen)$_2$(pytr)](PF$_6$)$_2$ and [Rh(phen)$_2$(d_4-pytr)](PF$_6$)$_2$. Again the two spectra can be compared in order to determine which fragments contain the ligand pytr and d_4-pytr. The fragments [Rh(phen)$_2$(pytr)](PF$_6$)$^+$ and [Rh(phen)$_2$(d_4-pytr)](PF$_6$)$^+$ can be seen at m/z 752.9 and m/z 756.9 respectively.

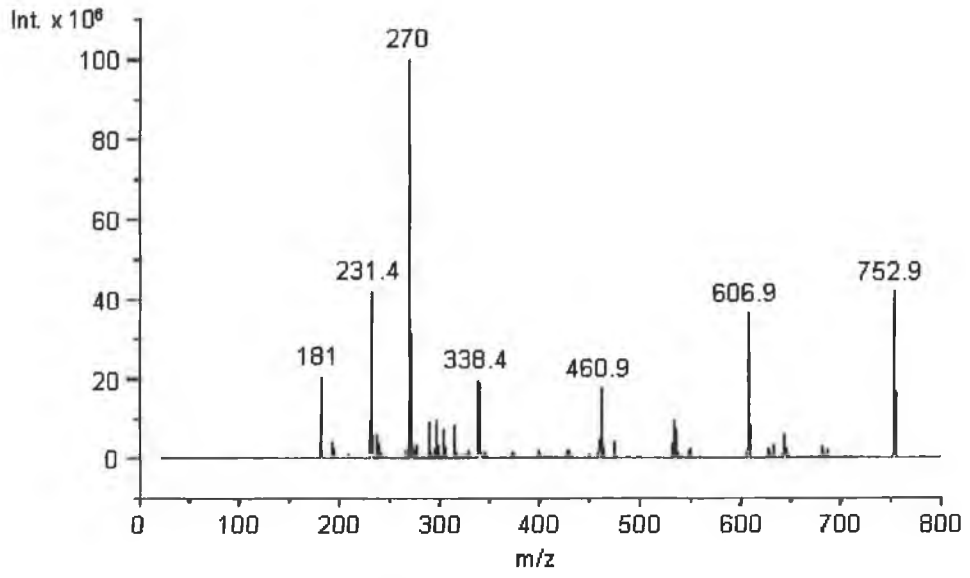

Figure 3.34 Mass spectrum of [Rh(phen)$_2$(pytr)](PF$_6$)$_2$ measured in acetonitrile.

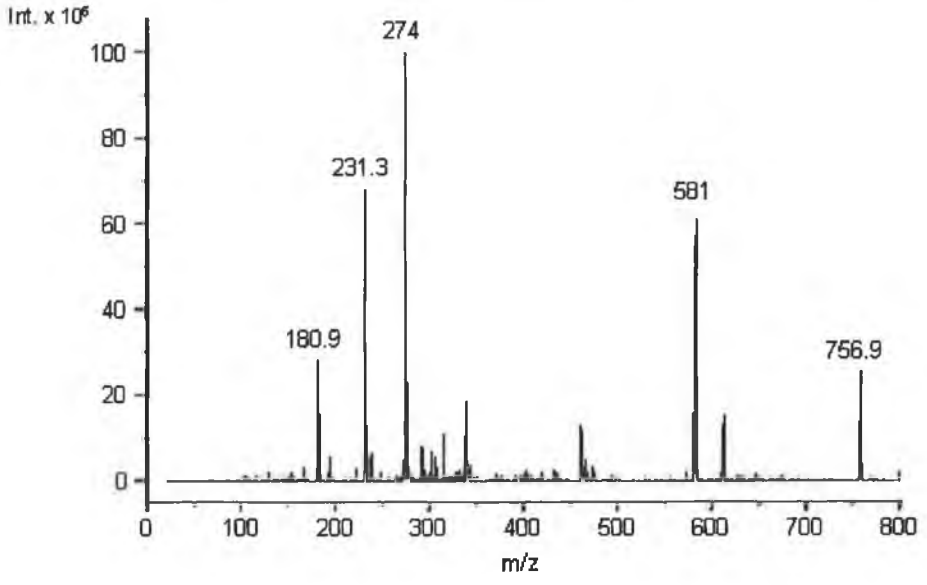

Figure 3.35 Mass spectrum of [Rh(phen)$_2$(d_4-pytr)](PF$_6$)$_2$ measured in acetonitrile.

Mass spectra were also obtained for the complexes [Rh(phen)$_2$(bpt)](PF$_6$)$_2$ and [Rh(phen)$_2$(d_8-bpt)](PF$_6$)$_2$. As can be seen in Table 3.13 the fragments m/z 830.1 and m/z 838.0 correspond to [[Rh(phen)$_2$(bpt)](PF$_6$)]$^+$ and [[Rh(phen)$_2$(d_8-bpt)]-(PF$_6$)]$^+$. The region of particular interest in the mass spectrum of [Rh(phen)$_2$(NHbpt)](PF$_6$)$_2$ can be seen in Figure 3.36.

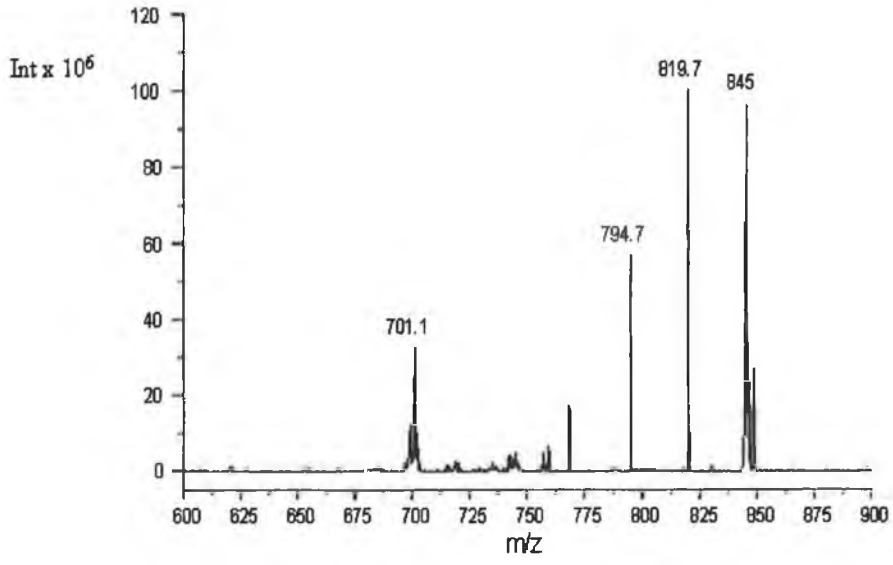

Figure 3.36 Mass spectrum of [Rh(phen)$_2$(NHbpt)](PF$_6$)$_2$.

The fragments at m/z 845.0 and m/z 701.1 are resultant from the fragments of $[Rh(phen)_2(NHbpt)](PF_6)^+$ and $[Rh(phen)_2(NHbpt)+H]^+$ respectively. Observation of fragments in these positions confirm that the complex formed in basic water is $[Rh(phen)_2(NHbpt)](PF_6)_2$. It was not possible to obtain the mass spectrum of $[Rh(phen)_2(NH_2bpt)](PF_6)_3$, as the pure complex was not isolated, but the spectra of both $[Rh(bpy)_2(NHbpt)](PF_6)_2$ and $[Rh(bpy)_2(NH_2bpt)](PF_6)_3$ were obtained and can be seen in Figure 3.37 and Figure 3.38.

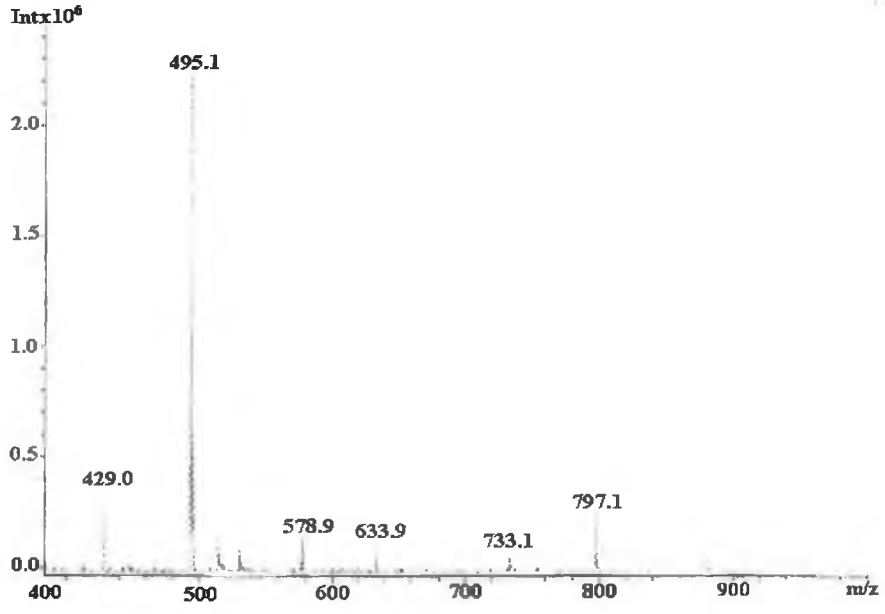

Figure 3.37 Mass spectrum [Rh(bpy)$_2$(NHbpt)](PF$_6$)$_2$ obtained in acetonitrile.

In this instance the fragment observable at m/z 797.1 corresponds to the fragment $[[Rh(bpy)_2(NHbpt)](PF_6)]^+$ whereas in the spectrum of $[Rh(bpy)_2(NH_2bpt)](PF_6)_3$, seen in Figure 3.38, peaks can be seen at m/z 943.0 and m/z 797.1. The fragment at m/z 943.0 relates to the fragment $[[Rh(bpy)_2(NH_2bpt)](PF_6)_2]^+$ and it is important to note that this peak is not a feature of the spectrum in Figure 3.37. This behaviour demonstrates the charge difference between the complexes $[Rh(bpy)_2(NHbpt)](PF_6)_2$ and $[Rh(bpy)_2(NH_2bpt)](PF_6)_3$ and confirms the conclusion reached based upon ^1H NMR interpretation that two different complexes are formed when the ligand NH_2bpt is reacted with $[Rh(L)_2Cl_2]^+$ with $[Rh(bpy)_2(NHbpt)](PF_6)_2$ being the exclusive product of the synthesis in basic water and $[Rh(bpy)_2(NH_2bpt)](PF_6)_3$ being formed solely in an ethanol:water mixture.

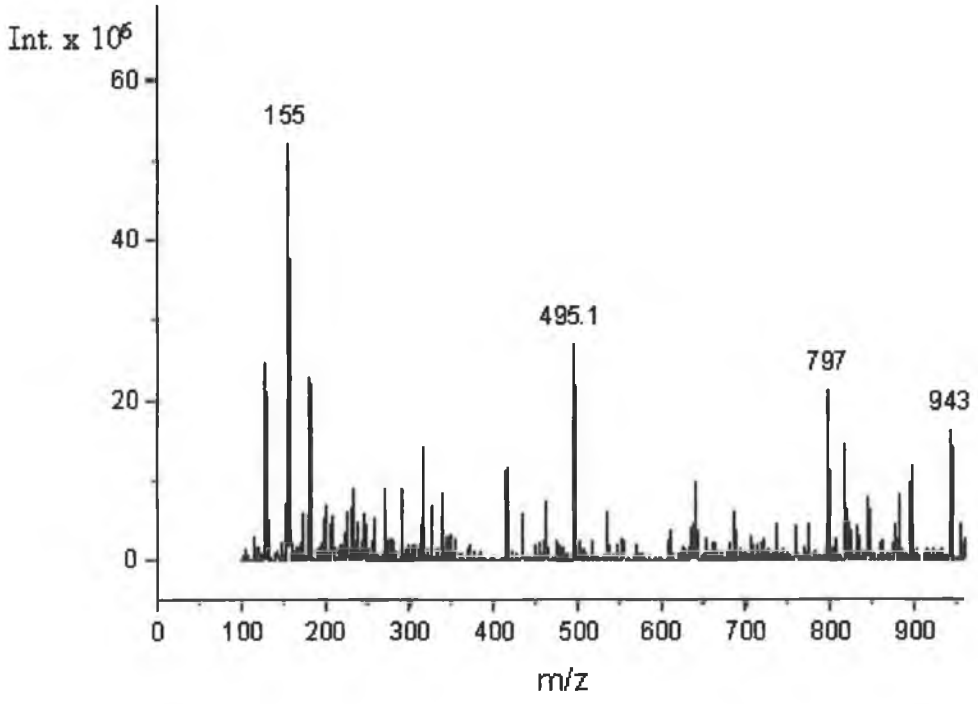

Figure 3.38 Mass spectrum $[Rh(bpy)_2(NH_2bpt)](PF_6)_3$ obtained in acetonitrile.

Table 3.13 summarises, where possible, the mass spectroscopic data of the complexes discussed in this chapter.

Table 3.13 ***Summary of a selection of the mass spectroscopic data for the complexes detailed in this chapter. All measurements were carried out in acetonitrile.***

	Fragment	Calculated m/z	Observed m/z
$[Rh(phen)_2(pytr)](PF_6)_2$	$[[Rh(phen)_2(pytr)](PF_6)]^+$	753.1	752.9
	$[Rh(phen)_2(pytr) - H^+]^+$	607.1	606.9
	$[phen + H]^+$	181.1	181.0
$[Rh(phen)_2(d_4\text{-pytr})](PF_6)_2$	$[Rh(phen)_2(d_4\text{-pytr})(PF_6)]^+$	757.1	756.9
	$[Rh(phen)_2(d_4\text{-pytr}) - H^+]^+$	611.1	610.9
$[Rh(bpy)_2(pytr)](PF_6)_2$	$[[Rh(bpy)_2(pytr)](PF_6)]^+$	705.1	704.9
	$[Rh(bpy)_2(pytr) - H^+]^+$	559.1	558.9
	$[bpy + H]^+$	157.1	157.0
$[Rh(bpy)_2(d_4\text{-pytr})](PF_6)_2$	$[[Rh(bpy)_2(d_4\text{-pytr})](PF_6)]^+$	709.1	708.9
	$[Rh(bpy)_2(d_4\text{-pytr}) - H^+]^+$	563.1	563.9
$[Rh(phen)_2(4Mpytr)](PF_6)_3$	$[[Rh(phen)_2(4Mpytr)](PF_6)_2]^+$	913.0	912.9
$[Rh(phen)_2(1M3pytr)](PF_6$	$[[Rh(phen)_2(1M3pytr)](PF_6)_2]^+$	913.0	912.9
	$[[Rh(phen)_2(1M3pytr)](PF_6) - H^+]^+$	767.1	766.9
	$[phen + H]^+$	181.1	181.1
$[Rh(bpy)_2(1M3pytr)](PF_6)_3$	$[[Rh(bpy)_2(1M3pytr)](PF_6) - H^+]^+$	719.1	718.9
	$[bpy + H]^+$	157.1	156.9
$[Rh(phen)_2(bpt)](PF_6)_2$	$[[Rh(phen)_2(bpt)](PF_6)]^+$	830.1	830.1
	$[Rh(phen)_2(bpt) - H^+]^+$	684.1	684.0
$[Rh(phen)_2(d_8\text{-bpt})](PF_6)_2$	$[[Rh(phen)_2(d_8\text{-bpt})](PF_6)]^+$	838.1	838.0
	$[Rh(phen)_2(d_8\text{-bpt}) - H^+]^+$	692.1	692.0
$[Rh(bpy)_2(bpt)](PF_6)_2$	$[[Rh(bpy)_2(bpt)](PF_6)]^+$	782.1	782.1
$[Rh(phen)_2(NHbpt)](PF_6)_2$	$[[Rh(phen)_2(NHbpt)](PF_6)]^+$	845.1	845.0
	$[[Rh(phen)_2(NHbpt) - H^+]^+$	701.1	701.1
	$[phen + H]^+$	181.1	181.1
$[Rh(bpy)_2(NHbpt)](PF_6)_2$	$[[Rh(bpy)_2(NHbpt)](PF_6)]^+$	797.1	797.1
$[Rh(bpy)_2(NH_2bpt)](PF_6)_3$	$[[Rh(bpy)_2(NH_2bpt)](PF_6)_2]^+$	943.1	943.0
	$[[Rh(bpy)_2(NHbpt)](PF_6) - H^+]^+$	797.1	797.0
$[Rh(bpy)_2(Phpytr)](PF_6)_2$	$[[Rh(bpy)_2(Phpytr)](PF_6)]^+$	781.1	781.0

3.4 Conclusions

In this chapter the synthesis and structural characterisation of a series of complexes $[Rh(L)_2(L')]^{n+}$ where L = bpy or phen, L' = a pyridyl triazole ligand and n = 2 or 3. It was found that the synthesis of such complexes required longer reaction times and afforded lower yields than analogous Ru(II) complexes. Elemental analysis was used to confirm the nature and purity of complexes and, as can be seen from Section 3.1.1 several of the complexes contain NaCl, which is a remnant of the purification process. It should be noted that a substantial amount of eluent was required to remove complexes from the column (300-600 cm^3) over the course of 1-2 days and that after the required fractions were reduced and precipitated as PF_6 salts they were washed with copious amounts of water. Due to the fact that the complexes were synthesised on a small scale there was typically an insufficient amount of the complexes for recrystallisation thus the ^1H NMR spectra of all of the complexes and their mass spectra also became important in confirming the purity of these complexes. It should also be noted that problems with excess salts remaining after purification have also been observed with some Ru(II) complexes.[29] All of the complexes were analysed using several techniques including X-ray crystallography, NMR spectroscopy and mass spectrometry with mass spectrometry proving useful in identifying complexes and in determining the extent of ligand deuteration.

The issues of coordination and protonation are of particular importance for the complexes detailed in this chapter. The protonation state of the complexes detailed in this chapter was determined from the results of the elemental analysis and it was found that all of the complexes were isolated in their deprotonated state. The coordination mode of these complexes could not however be established as easily. For the Ru(II) complexes studied by Hage *et. al.* it was possible to determine the mode of coordination using NMR spectroscopic techniques, as both the N2' and N4' isomers of these Ru(II) complexes were isolated which allowed for comparative studies.[23] In contrast the Rh(III) complexes detailed in this chapter yielded only a single isomer and in the absence of suitable crystals for analysis it was not possible to determine the mode of coordination for complexes incorporating the ligands Hpytr

and Hbpt. Complexes incorporating the 4Mpytr ligand may only coordinate via the N2' position and those with 1M3pytr are expected to coordinate via the N4' position for steric reasons. X-ray crystallography established the metal centre was coordinated via the N2' position in $[Rh(bpy)_2(Phpytr)]^{2+}$, which is to be expected due to the presence of the phenyl group in the 5 position of the 1,2,4-triazole ring and also established the unusual binding mode of the metal centre in the complex $[Rh(phen)_2(NHbpt)]^{2+}$. The nature of the complex formed with the NH_2bpt ligand was found to depend upon the reaction conditions with ^1H NMR spectroscopy proving particularly useful in identifying whether complexes were bound via the amine moiety or via the N2' position of the triazole ring. It was established that when the reaction was carried out in basic water the metal centre coordinated via the amine moiety and a singlet, associated with the NH group were observed at 9.11 ppm and 9.16 ppm in the ^1H NMR spectra of $[Rh(phen)_2(NHbpt)]^{2+}$and $[Rh(bpy)_2(NHbpt)]^{2+}$. In contrast when the reaction was carried out in ethanol:water the metal centre was coordinated via the N2' of the triazole ring whilst the resonance associated with the NH_2 moiety was observed at 7.66 ppm in the spectrum of $[Rh(bpy)_2(NH_2bpt)]^{3+}$. The issue of coordination will again be examined in Chapter 8 where it will be considered taking the photophysical and electrochemical properties exhibited by these complexes into account. The following chapter details the photophysical and electrochemical properties of all the complexes discussed in this chapter.

References:

1 V. Balzani, A. Juris, M. Venturi, S. Campagna, S. Serroni, *Chem. Rev.*, **1996**, *96*, 759-833.

2 J.P. Sauvage, J.P. Collin, J.C. Chambron, S. Guillerez, C. Coudret, *Chem. Rev.*, **1994**, *94*, 993-1019.

3 J.H. van Diemen, J.G. Haasnoot, R. Hage, E. Müller, J. Reedijk, *Inorg. Chim Acta*, **1991**, *181*, 245-251.

4 S. Fanni, T.E. Keyes, C.M. O'Connor, H. Hughes, R. Wang, J.G. Vos, *Coord. Chem. Rev.*, **2000**, *208*, 77-86.

5 J.G. Haasnoot, *Coord. Chem. Rev.*, **2000**, *200-202*, 131-185.

6 F. Barigelletti, L. De Cola, V. Balzani, R. Hage, J.G. Haasnoot, J. Reedijk, J.G.Vos, *Inorg. Chem.*, **1991**, *30*, 641-645.

7 J.G. Vos, J.G. Haasnoot, G. Vos, *Inorg. Chim. Acta*, **1983**, *71*, 155-162.

8 B.E. Buchanan, R. Wang, J.G. Vos, R. Hage, J.G. Haasnoot, J. Reedijk, *Inorg. Chem.*, **1990**, *29*, 3263-3265.

9 T.E. Keyes, J.G. Vos, J.A. Kolnaar, J.G. Haasnoot, J. Reedijk, R. Hage, *Inorg. Chim. Acta*, **1996**, *245*, 237-242.

10 H.A. Nieuwenhuis, J.G. Haasnoot, R. Hage, J. Reedijk. T.L. Snoeck, D.J. Stufkens, J.G. Vos, *Inorg. Chem.*, **1991**, *30*, 48-54.

11 R. Hage, J.G. Haasnoot, H.A. Nieuwenhuis, J. Reedijk, R. Wang, J.G. Vos, *J. Chem. Soc. Dalton Trans.*, **1991**, 3271-3275.

12 B.E. Buchanan, J.G. Vos, M. Kaneko, W.J.M. van der Putten, J.M. Kelly, R. Hage, R.A.G de Graaff, R. Prins, J.G. Haasnoot, J. Reedijk, *J. Chem. Soc. Dalton Trans.*, **1990**, 2425-2431.

13 R. Hage, A.H.J. Dijkhuis, J.G. Haasnoot, R. Prins, J. Reedijk, B.E. Buchanan, J.G. Vos, *Inorg. Chem.*, **1988**, *27*, 2185-2189.

14 H.E.B. Lempers, J.G. Haasnoot, J. Reedijk, R. Hage, F.M. Weldon, J.G. Vos, *Inorg. Chim. Acta*, **1994**, *225*, 67-74.

15 L.A. Oro, M.T. Pinillos, C. Tejel, C. Foces-Foces, F.H Cano, *J. Chem. Soc. Dalton Trans.*, **1986**, 1087-1094.

16 L.A. Oro, M.T. Pinillos, C. Tejel, C. Foces-Foces, F.H Cano, *J. Chem. Soc. Dalton Trans.*, **1986**, 2193-2200.

17 M.P. García, J.A. Manero, L.A. Oro, M.C. Apreda, F.H. Cano, C. Foces-Foces, J.G. Haasnoot, R. Prins,J. Reedijk, *Inorg. Chim. Acta*, **1986**, *122*, 235-241.

18 M.P. García, M. Martin, L.A. Oro, *Inorg. Chim. Acta*, **1992**, *191*, 221-225.

19 J.H. Van Diemen, R. Hage, J.G. Haasnoot, H.E.B. Lempers, J. Reedijk, J.G. Vos, L. De Cola, F. Barigelletti, V. Balzani, *Inorg. Chem.*, **1992**, *31*, 3518-3522.

20 G. Calogero, G. Giuffrida, S. Serroni, V. Ricevuto, S. Campagna, *Inorg. Chem.*, **1995**, *34*, 541-545.

21 P.M. Gidney, R.D. Gillard, B.T. Heaton, *J. Chem. Soc., Dalton Trans.*, **1972**, 2621-2628.

22 E.M. Ryan, *Ph.D. Thesis*, Dublin City University, **1991**.

23 R. Hage, *Ph.D. Thesis*, Leiden University, The Netherlands, **1991**.

24 W. Browne, *Ph.D. Thesis*, Dublin City University, **2002**.

25 M.Y. Kim, W.K. Seok, Y. Dong, H. Yun, *Inorg. Chim. Acta*, **2001**, *319*, 194-198.

26 Z.D. Matovíc, S.R. Trifunovíc, G. Ponticelli, L.P. Battaglia, G. Pelizzi, I.A. Efimenko, D.J. Randanovíc, *Inorg. Chim. Acta*, **1988**, *278*, 209-216.

27 N. Rahmouni, A.A. Bahsoun, M.T. Youinou, J.A. Osborn, J. Fischer, A. Ezzamarty, *Polyhedron,* **1998**, *17*, 3083-3088.

28 M.Y. Kim, W.K. Seok, H.N. Lee, S.H. Han,Y. Dong, H. Yun, *Zeitschrift fur Naturfirschung Section A – A J. of Chem. Sci.*, **2001**, *56*, 747-752.

29 C. M. O'Connor, *Ph.D. Thesis*, Dublin City University, **1999**.

30 H.M. Burke, J.G. Gallagher, M.T. Indelli, F. Scandola, J.G. Vos, *Eur. J. Inorg. Chem.*, **2002**, *2002*, 846-849.

31 F.O. Garces, R.J. Watts, *Magn. Reson. Chem.*, **1993**, *31*, 529-536.

32 S. Chirayil, R.P. Thummel, *Inorg. Chem.*, **1989**, *28*, 813-814.

33 R. Echols, G. Levy, *J. Organ. Chem.*, **1974**, *39*,1321-1322.

34 A.L. Rheingold, P. Saisuwan, N.C. Thomas, *Inorg. Chim. Acta*, **1993**, *214*, 41-45.

Chapter 4 - Photophysical and Electrochemical properties of Rh(III) complexes with pyridyl triazole ligands.

"The trouble with doing something right the first time is that nobody appreciates how difficult it was."

Anonymous

Abstract: Having studied the synthesis and structural characterisation of Rh(III) complexes incorporating pyridyl triazole ligands, as detailed in Chapter 3, an investigation of the photophysical and electrochemical properties of these complexes was carried out. Luminescence studies yielded particularly interesting results with a dual emission being observed for all complexes with the exception of those where the metal centre was bound via the amine group of the NH_2bpt ligand. All complexes exhibited a π–π^* based emission at 77K which was independent of the incorporated triazole ligand. In contrast the d-d* emission observed at 77K was dependent upon the σ-donor strength of the triazole ligand. Throughout this chapter the behaviour of the Rh(III) complexes in question is compared with the that of the tris-homoleptic complexes $[Rh(phen)_3]^{3+}$ and $[Rh(bpy)_3]^{3+}$ and where possible with analogous Ru(II) pyridyl triazole complexes.

4.1 Introduction

Polypyridyl transition metal complexes have attracted a substantial amount of interest with studies to date focusing primarily upon their photochemical, photophysical and electrochemical properties. The photophysical processes, which are relevant to this chapter, are described briefly in the following discussion.

The absorption of light by a fluorophore gives rise to a number of processes, which are illustrated in Figure 4.1. In Figure 4.1 S_0, S_1 and S_2 refer to the ground state and the first and second singlet excited states respectively, each of which has a number of vibrational levels in which the excited electron can exist. If we consider the processes occurring in Figure 4.1 it can be seen that following the absorption of light the electron is usually excited into an excited vibrational level of either S_1 or S_2 which subsequently relaxes to the lowest vibrational level of S_1 via internal conversion.[1]

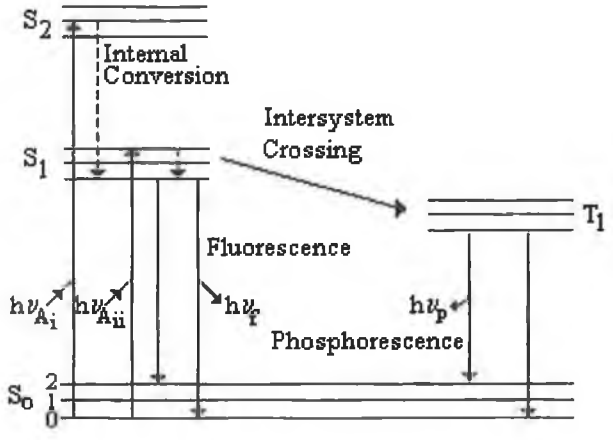

Figure 4.1 Jablonski diagram [1]

From here there are two distinct radiative emission processes that may occur. Emission may occur from the lowest vibrational level of S_1 to the S_0 ground state or a process of intersystem crossing may occur whereby a triplet state is populated and is subsequently followed by emission to the ground state. It is important to note that in polyatomic molecules, luminescence is observed almost exclusively from the lowest excited state of any given multiplicity even though many electronically

excited states are possible. This is known as Kasha's rule and does not mean that emissions from these upper excited states do not occur but simply that their quantum yields are very low and as a result are usually undetectable.[1,2] It is possible to differentiate between these two emission processes (i.e. emission from S_1 to S_0 and from T_1 to S_0) by considering the change in the spin quantum number between the initial and final states. In the first instance where the transition occurring is a singlet-singlet transition, the quantum numbers remain constant and $\Delta S = 0$. As $\Delta S = 0$ this type of transition is spin allowed and is termed fluorescence. In the case of emission from the triplet state, a change in the quantum number means that $\Delta S \neq 0$ and as a result this is referred to as a spin forbidden process and emission of this type is referred to as phosphorescence. These two types of emission differ in their kinetics with fluorescence being short-lived in comparison to phosphorescent lifetimes, which range from 1 ms to many seconds or even minutes.[1] The means by which the spin forbidden process of phosphorescence occurs is provided by spin orbit coupling. The process occurs due to the compensation of two simultaneous changes in angular momentum represented by the orbital quantum number L and the spin quantum number S, the sum of which J remains constant while S and L vary in opposite directions. Spin orbit coupling provides the link between S and L and increases with atomic number as electrons move faster around nuclei that carry large positive charges. As a result the interaction between the electron currents and the related magnetic fields increases with atomic number. This behaviour is the basis of the effect known as the heavy atom effect, which enhances the rates of formally forbidden radiative and non-radiative transitions.[1,2]

It can be seen from Figure 4.1 that the electronic transition from the excited state, S_1, to the ground state S_0 can also result in population of higher vibronic levels of S_0 before reaching the ground state, an equilibrium process that takes approximately 10^{-12} seconds. As a result it can be said that an absorption spectrum reflects the vibrational levels of the electronically excited states whilst the emission process reflects the vibrational processes of the ground electronic state. These two types of spectra tend to mirror each other however the emission spectrum generally occurs at longer wavelengths (i.e. a loss of energy) with respect to the absorption

spectrum.[1] This effect is referred to as the Stokes' shift. Several processes contribute to the loss of energy in these cases with the rapid decay to the lowest vibrational level of S_1 being a common cause. Energy is also lost when fluorophores decay to excited vibrational levels of S_0 with other processes such as excited state reactions and solvent effects also being possible contributory factors. Figure 4.2 demonstrates how the absorption and emission spectra relate to electronic energy levels and illustrates the mirror image effect, which is regularly observed.[1] Deviation from this mirror image relationship implies the occurrence of a process in which a different geometric arrangement of nuclei in the excited state occurs as compared to the ground state. It should also be noted that phosphorescent emission is generally shifted to longer wavelengths / lower energy with respect to fluorescence.[1]

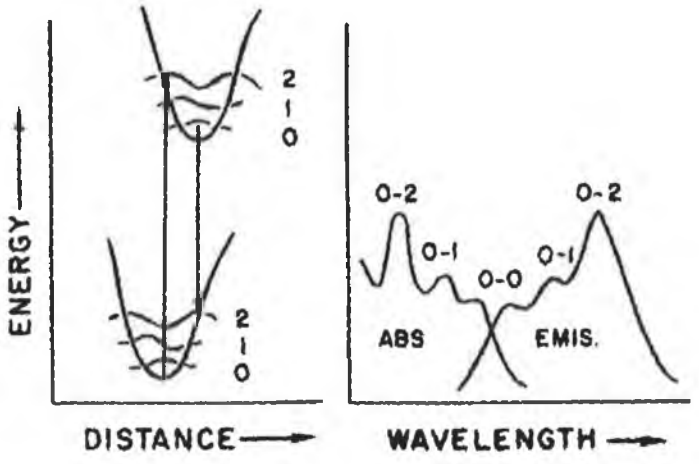

Figure 4.2 Illustration of the mirror image effect.[1]

Another important aspect of the study of transition metal complexes is the determination of the average amount of time the molecule remains in the excited state prior to its return to the ground state otherwise known as the excited state lifetime of the complex. Depending upon the type of substance, the measurement of the excited state lifetime can reveal important information about the rate of energy transfer and the rate of excited state reactions. Fluorescence quantum yields are also regularly investigated. The fluorescence quantum yield is the ratio of the number of photons emitted to the number of photons absorbed. [1,2]

The following chapter aims to provide a detailed description of the photophysical and electrochemical properties of the Rh(III) complexes introduced in Chapter 3. The complexes detailed in Chapter 3 are heterotrischelated complexes of the form $[Rh(L)_2(L')]^{n+}$ where L = bpy or phen and L' = Hpytr, 4Mpytr, 1M3pytr, HPhpytr, Hbpt and NH_2bpt. The properties of the tris complexes $[Rh(bpy)_3]^{3+}$ and $[Rh(phen)_3]^{3+}$ have been discussed in Chapter 1 and it is with these and analogous Ru(II) complexes that the behavior of the Rh(III) pyridyl triazole complexes will be compared. The electronic properties of the complexes have been probed by means of UV-VIS absorption spectroscopy and emission spectroscopy, low temperature lifetimes have been studied and, where possible the electrochemical properties of the complexes examined.

4.2 Results

4.2.1 Absorption Spectroscopy

The absorption and emission properties of Rh(III) tris-polypyridyl complexes have been outlined in Chapter 1 but to summarise, complexes such as these typically have a lowest excited state which is classified as being associated with a ligand localised π-π^* transition. The UV absorption spectra of the complexes $[Rh(phen)_3]^{3+}$ and $[Rh(bpy)_3]^{3+}$ are both π-π^* in nature and do not exhibit any clear evidence for either CT bands, which generally lie at relatively high energies for Rh(III) complexes of this nature, or d-d* bands. The UV spectra of the complexes $[Rh(phen)_2(pytr)]^{2+}$ and $[Rh(bpy)_2(pytr)]^{2+}$, which are typical of the spectra obtained for the complexes discussed in this chapter, may be seen in Figure 4.3.

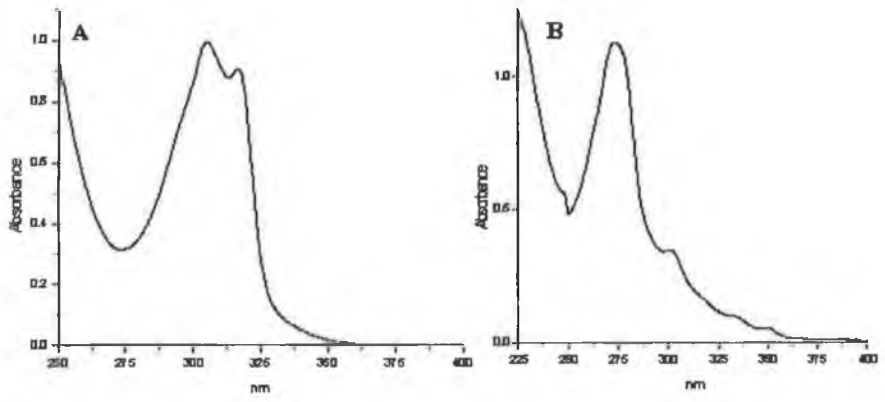

Figure 4.3 Absorption spectra of (A) $[Rh(bpy)_2(pytr)]^{2+}$ and (B) $[Rh(phen)_2(pytr)]^{2+}$ measured in acetonitrile at room temperature.

The complex $[Rh(bpy)_2(pytr)]^{2+}$ exhibits an intense band in the region 275-350 nm and $[Rh(phen)_2(pytr)]^{2+}$ exhibits bands in the region 250-375 nm, with one intense band at 275nm and a progression to lower energies of four weaker bands. The spectra observed in Figure 4.3 are very similar to those obtained for the analogous tris-homoleptic complexes $[Ru(phen)_3]^{3+}$ and $[Ru(bpy)_3]^{3+}$.[3] This similarity allows for the assignment of the main features observed in Figure 4.3 to π-π^* transitions with each displaying absorptions characteristic of their respective π-electron systems. As expected, the spectra of complexes and their deuterated analogous were found to be the same. Table 4.1 details the absorption data obtained for all complexes discussed here.

Table 4.1 ***Absorption data for $[Rh(phen)_3]^{3+}$, $[Rh(bpy)_3]^{3+}$ and pyridyl triazole complexes measured in acetonitrile.***

Complex	Absorption (nm) (log ε)	Complex	Absorption (nm) (log ε)
$[Rh(phen)_3]^{3+}$	334 (3.10)[a]	$[Rh(bpy)_3]^{3+}$	307 (36.3)[a]
	351 (4.18)[a]		321 (38.3)[a]
$[Rh(phen)_2(pytr)]^{2+}$	301 (4.32)	$[Rh(bpy)_2(pytr)]^{2+}$	306 (4.37)
	331 (3.78)		317 (4.34)
	350 (3.50)		
$[Rh(phen)_2(4Mpytr)]^{3+}$	301 (4.19)	$[Rh(bpy)_2(4Mpytr)]^{3+}$	307 (4.47)
	333 (3.30)		316 (4.39)
	350 (3.12)		
$[Rh(phen)_2(1M3pytr)]^{3+}$	301 (4.16)	$[Rh(bpy)_2(1M3pytr)]^{3+}$	306 (4.45)
	333 (3.25)		320 (4.46)
	350 (3.09)		
$[Rh(phen)_2(Phpytr)]^{2+}$	301 (5.18)	$[Rh(bpy)_2(Phpytr)]^{2+}$	304 (4.51)
	333 (4.79)		317 (4.53)
	349 (4.73)		340 sh (3.83)
$[Rh(phen)_2(bpt)]^{2+}$	300	$[Rh(bpy)_2(bpt)]^{2+}$	304
	332		316
	347		340 sh
$[Rh(phen)_2(NHbpt)]^{2+}$	300 (4.47)	$[Rh(bpy)_2(NHbpt)]^{2+}$	305 (4.56)
			316 (4.56)
		$[Rh(bpy)_2(NH_2bpt)]^{3+}$	306
			319

a – values taken from ref 3.

As can be seen from Table 4.1 the complexes $[Rh(bpy)_2(Phpytr)]^{2+}$ and $[Rh(bpy)_2(bpt)]^{2+}$ exhibit a shoulder in the region of 340 nm whilst the absorption spectrum of $[Rh(bpy)_2(NH_2bpt)]^{3+}$ shows some indications of a shoulder at 335 nm when compared with $[Rh(bpy)_2(pytr)]^{2+}$. The remaining bpy complexes do not exhibit such absorption bands, which suggests that the intense absorption bands associated with the π-π* transitions mask them. Figure 4.4A illustrates the UV spectra of $[Rh(bpy)_2(Phpytr)]^{2+}$, $[Rh(bpy)_2(bpt)]^{2+}$ and $[Rh(bpy)_2(pytr)]^{2+}$. Also

included in Figure 4.4 are the UV spectra of $[Rh(bpy)_2(bpt)]^{2+}$ and the Hbpt ligand (B) and $[Rh(bpy)_2(pytr)]^{2+}$ and the Hpytr ligand (C).

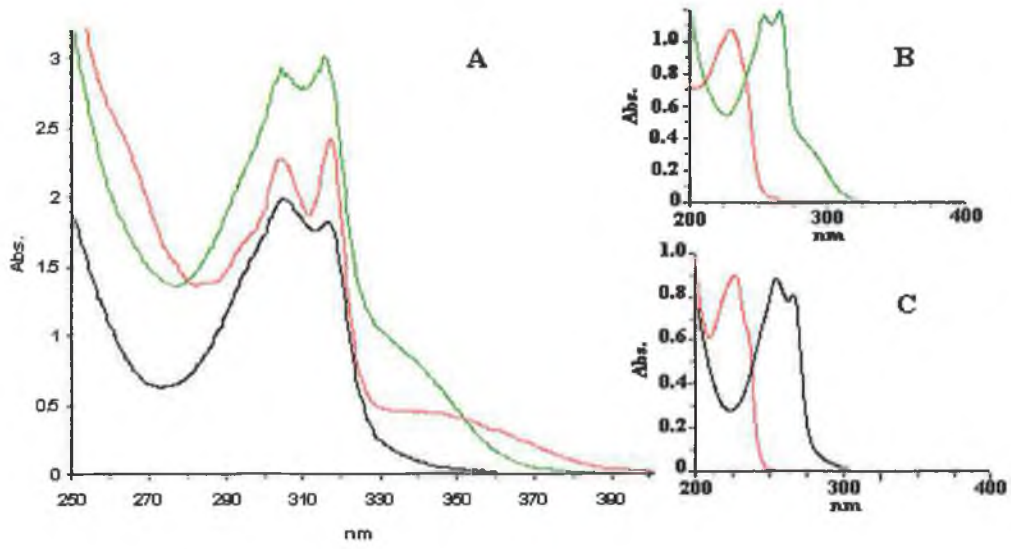

Figure 4.4 Absorption spectra of (A) $[Rh(bpy)_2(pytr)]^{2+}$(——), $[Rh(bpy)_2(Phpytr)]^{2+}$ (——) and $[Rh(bpy)_2(bpt)]^{2+}$ (——), (B) $[Rh(bpy)_2(bpt)]^{2+}$ (——) and Hbpt (——) and (C) $[Rh(bpy)_2(pytr)]^{2+}$(——) and Hpytr (——) measured in acetonitrile.

The bands observed in the spectrum of $[Rh(bpy)_2(pytr)]^{2+}$ at 306 nm and 317 nm are assigned to π-π^* transitions based upon the their similarity with the same region of the spectrum of $[Rh(bpy)_3]^{3+}$.[3] The absorbance bands in the spectra of $[Rh(bpy)_2(Phpytr)]^{2+}$ and $[Rh(bpy)_2(bpt)]^{2+}$ at $\lambda > 330$nm are more difficult to assign with a number of possible transitions needing to be considered i.e. (i) π-π^* transitions associated with the incorporated triazole based ligand (ii) d-d* transitions and (iii) CT transitions. Moderate absorption bands, or shoulders, have been observed for many Rh(III) bis complexes including $[Rh(bpy)_2Cl_2]^+$ in the same region, whereas as in the case of the tris complexes it is generally felt that these possible d-d* and CT transitions are obscured by the intense absorption bands associated with the π-π^* transitions.[4] The fact that the bands in question are quite weak indicates that a spin forbidden process is occurring. Thus these bands are tentatively assigned as d-d* transitions.[5] Further studies are however needed to determine the nature of these transitions unambiguously, for example, the charge

transfer nature of a transition is most often demonstrated by solvatochromism. Polar solvents stabilise CT states more so than nonpolar solvents and by varying the solvent used, the energy of the observed emission varies also whereas solvent effects are insignificant for non-CT transitions.[6] Resonance Raman would also be an effective technique in assigning these transitions.

Having analysed the absorption spectra of $[Rh(bpy)_2(Phpytr)]^{2+}$ and $[Rh(bpy)_2(bpt)]^{2+}$ the spectra of the complexes $[Rh(phen)_2(Phpytr)]^{2+}$ and $[Rh(phen)_2(bpt)]^{2+}$ were examined and compared with the spectrum observed for $[Rh(phen)_3]^{3+}$ as can be seen in Figure 4.5. Unlike $[Rh(bpy)_3]^{3+}$ the absorption spectrum of $[Rh(phen)_3]^{3+}$ exhibits bands in the region 320-370 nm making it difficult to observe absorption bands associated with d-d* or CT transitions. However, if the intensity of these bands between 320 nm and 370 nm is compared it can be seen that these bands are more intense in the spectra of the $[Rh(phen)_2(Phpytr)]^{2+}$ and $[Rh(phen)_2(bpt)]^{2+}$. This observation would indicate that the moderately intense bands observed in the absorption spectra of $[Rh(bpy)_2(Phpytr)]^{2+}$ and $[Rh(bpy)_2(bpt)]^{2+}$ are also present in the phen complexes. When compared with $[Rh(phen)_3]^{3+}$ several of the phen complexes exhibited a similar behaviour, (Figure 4.6).

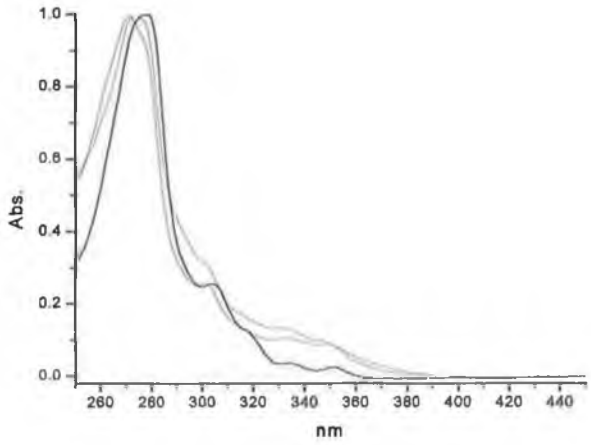

Figure 4.5 Absorption spectra of $[Rh(phen)_3]^{3+}$(——), $[Rh(phen)_2(Phpytr)]^{2+}$ (——) and $[Rh(phen)_2(bpt)]^{2+}$ (——).

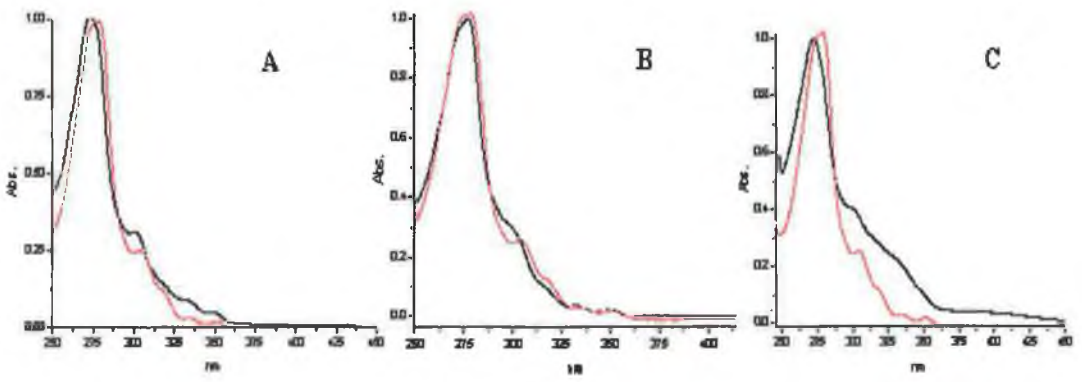

Figure 4.6 Absorption spectra of (A) $[Rh(phen)_2(pytr)]^{2+}$ (——), (B) $[Rh(phen)_2(1M3pytr)]^{3+}$ (——) and (C) $[Rh(phen)_2(NH_2bpt)]^{3+}$(——) in each case vs. $[Rh(phen)_3]^{3+}$ (——) measured in acetonitrile.

4.2.2 Emission Spectroscopy

In contrast to ruthenium complexes of the type $[Ru(L)_3]^{2+}$, whose electronic properties result from metal-to-ligand-transitions (MLCT), $[Rh(L)_3]^{3+}$ complexes, where L = bpy or phen, only emit at 77K and have a lowest excited state which may be classified as a ligand localised π-π^* transition. The photophysical properties of Rh(III) heteroleptic complexes can be quite intricate with dual emissions being distinctly possible. Crosby *et. al.* and Watts *et. al.* both observed multiple emissions from $[Rh(bpy)_2(phen)]^{3+}$ and $[Rh(bpy)(phen)_2]^{3+}$ at 77K which were assigned as π-π* states localised on phen and bpy.[7,8] When studied almost all of the complexes detailed in Chapter 3 exhibited multiple emissions. The only exceptions to this behaviour were complexes in which the metal centre was coordinated via the NH moiety of the NH_2bpt ligand. Unlike the multiple emissions observed by Crosby *et. al.*, Watts *et. al.* and Islam *et. al.*, where both emissions were either ligand based or metal based, the emissions observed for the Rh(III) pyridyl triazole compounds were assigned to π-π* and d-d* excited states. Whilst not a common feature, dual LC and MC emissions have been reported previously for $[Rh(phen)_2(NH_3)_2]^{3+}$ by Indelli *et.*

al. and for $[Rh(dmbpy)_3]^{3+}$ by Ford *et. al.*[9,10] The nature of these multiple emission will be considered in the following discussion.

The relaxation, either radiative or nonradiative, of excited electronic states in complex polyatomic molecules is determined by the spacing and electron configurations of the lowest two or three excited states and the ground state.[3] The potential energy curves illustrated in Figure 4.7 are representative of the potential energy curves for Rh(III) polypyridine complexes with the energy ordering of LC and the MC state depending upon the nature of the ligands and demonstrates the distorted nature of the MC state in comparison with the LC state.[9]

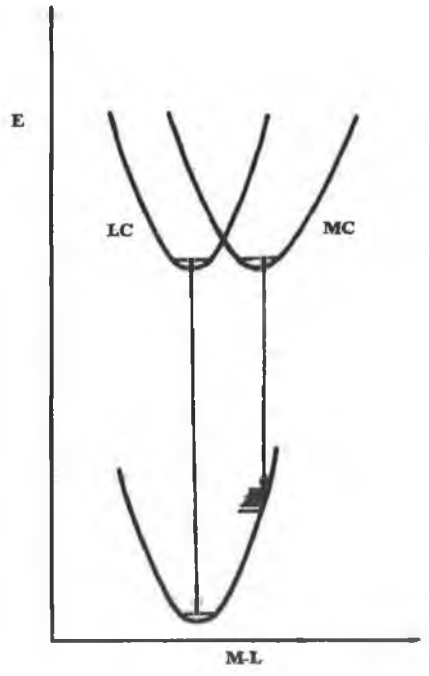

Figure 4.7 Potential energy curves for a Rh(III) polypyridine complex with the relative energy ordering of LC and the MC state depending upon the nature of the complex.[9]

As outlined in 1.3.3.1, Watts and Van Houten studied the effect of the energy gap between the $^3\pi$-π^* of the coordinated ligands on multiple emissions in heterotris-chelated Rh(III) complexes.[11] They estimated that the $^3\pi$-π^* of the phen ligand lay about 100 cm^{-1} below that of bpy in the mixed complexes $[Rh(bpy)_n(phen)_{3-n}]^{3+}$ where n = 1,2. In the case of the complexes of the type $[Rh(bpy)_n(5,6\text{-Mephen})_{3-n}]^{3+}$

and $[Rh(phen)_n(5,6\text{-}Mephen)_{3-n}]^{3+}$ it was determined that the $^3\pi\text{-}\pi^*$ of the 5,6-Mephen ligand lay well below that of the bpy and phen and the energy gap was estimated to be approximately 1600 cm^{-1}. The emission spectra and the excited state lifetimes of the mixed complexes incorporating the bpy and phen ligands exhibited characteristics associated with both ligands whereas the complexes incorporating the methylated phen ligand only displayed characteristics of 5,6-Mephen. The behaviour observed for these complexes suggested that a slow radiationless transition occurs when the energy gap between the states lay in the range 100 - 400 cm^{-1}; whilst at energy gaps of 1600 cm^{-1} the transitions occur rapidly.[11]

Ford *et. al.* later studied ligand steric effects on the photophysics of Rh(III) bis and tris homoleptic complexes of incorporating the bpy ligand.[10] It was observed that when complexed, the two pyridine rings of 3,3'-Me_2bpy, where 3,3'-Me_2bpy = 3,3'-dimethyl-2,2'-bipyridine, were not coplanar when coordinated owing to the steric repulsion between the methyl groups. [10] A crystallographic study showed that the dihedral angle between the two pyridine planes of individual (3,3'-Me_2bpy) ligands to be approximately 30°. Ford *et. al.* showed that subtle steric hindrances introduced on the ligand can influence ligand-metal interactions so as to affect the relative location of various types of low lying excited states. The bis complexes $[Rh(3,3'\text{-}Me_2bpy)_2Cl_2]^+$ and $[Rh(bpy)_2Cl_2]^+$ exhibited similar characteristics whereas in contrast the tris complexes $[Rh(3,3'\text{-}Me_2bpy)_3]^{3+}$ and $[Rh(bpy)_3]^{3+}$ behaved quite differently. In an alcoholic glass the tris complex $[Rh(3,3'\text{-}Me_2bpy)_3]^{3+}$ showed an intense, broad band at low energies with a lifetime of 75μs, which was assigned to a d-d* emission. Examination of the high-energy edge of the emission spectra showed a second structured emission. The two types of emission could be resolved by time resolved measurements with the metal-centred emission being the dominant luminescent feature at 77K whilst the ligand-centred emission was enhanced relative to the metal centred one in fluidic solutions. [10]

The behaviour of $[Rh(3,3'\text{-}Me_2bpy)_3]^{3+}$ indicates that the two excited states, i.e. the d-d* and $\pi\text{-}\pi^*$ states, are quite close in energy with the presence of two independent emission spectra indicating an inability of the two states to interconvert

efficiently at lower temperatures. It was suggested that this might have been associated with geometric differences between the two states and in the structures of the associated solvation spheres. Solvent effects can result in large viscosity-dependent activation barriers for the non-radiative transitions between these two states. Thus, once the d*-d and π*-π excited states are populated by competing internal conversion / intersystem crossing / vibrational relaxation pathways from the upper states formed by initial excitation, the rates of internal conversion between them are slower than the independent deactivation processes to the ground state. At higher temperatures and lower viscosities, solvent reorganisational barriers are reduced and the thermal energy of the system becomes sufficient to overcome the remaining activation barriers.[10] Figure 4.8 illustrates a schematic energy level diagram for the low lying excited states of various types of Rh(III) polypyridyl complexes.

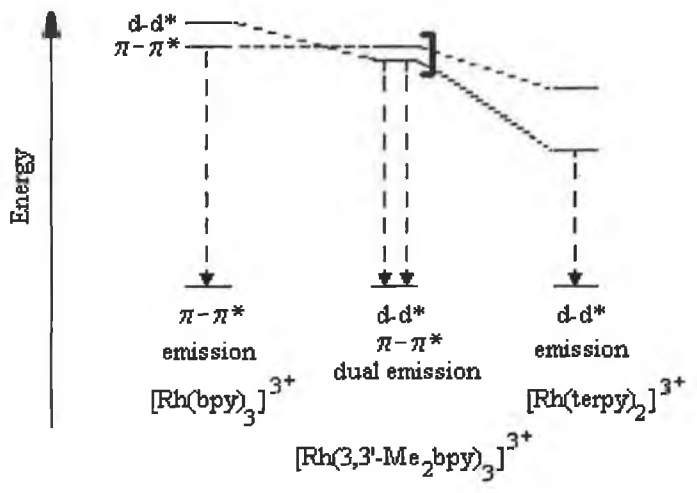

Figure 4.8 Schematic energy level diagram for the low lying excited states of Rh(III) polypyridyl complexes.[12]

It is important to detail the manner in which emission spectra were obtained in this study. As discussed in Chapter 2 the luminescence spectrophotometer used could be set to measure either phosphorescence or fluorescence. When set to measure phosphorescence the instrument observed a 1ms time delay time after excitation before emission was measured. This time delay is particularly important for the Rh(III) complexes being studied as, when the excited state lifetimes of the

two emitting states were studied a significant difference was observed between the two. Thus arose the problem that when the instrument was set to detect phosphorescence (τ > 1ms) the emission with a short excited state lifetime was not detected and when set to detect fluorescence the emission with a long lived excited state was not detected. Therefore it was necessary to analyse all complexes under both sets of conditions. It should be noted that all experiments were carried out at 77K. When studying the luminescence of the complexes detailed in Chapter 3 on with a lifetime >1 ms the complexes was studied over the wavelength range 285 nm to 350 nm but unless otherwise stated all of the spectra shown were obtained with a λ_{ex} of 305nm. The emission detected on a shorter timescale was studied using a λ_{ex} of 337 nm.

The results obtained for the Rh(III) pyridyl triazole compounds differ significantly from the behaviour of $[Rh(phen)_3]^{3+}$ and $[Rh(bpy)_3]^{3+}$ with multiple emissions being a common feature. Figure 4.9 and Figure 4.10 represent the emission spectra obtained for the complexes $[Rh(phen)_2(pytr)]^{2+}$ and $[Rh(bpy)_2(pytr)]^{2+}$ respectively.

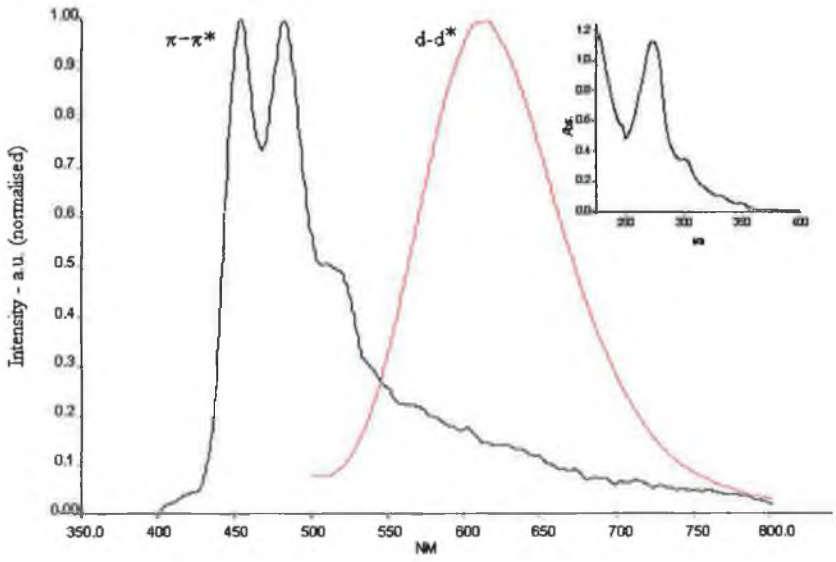

Figure 4.9 Emission spectra of $[Rh(phen)_2(pytr)]^{2+}$ measured in ethanol:methanol 4:1 at 77K. Inset shows the UV spectrum of $[Rh(phen)_2(pytr)]^{2+}$.

As can be seen there are two different types of emission spectra for both $[Rh(phen)_2(pytr)]^{2+}$ and $[Rh(bpy)_2(pytr)]^{2+}$. If we first consider the spectra obtained for $[Rh(phen)_2(pytr)]^{2+}$, Figure 4.9, it can be seen that one of the emissions exhibits a fine structure with maxima at 454 nm and 484 nm while the second emission observed is a broad structureless emission at a lower energy with a maximum of 612 nm. If the structured emission in Figure 4.9 is compared with that of $[Rh(phen)_3]^{3+}$, Appendix IV, it can be seen that they are almost identical with $[Rh(phen)_3]^{3+}$ having maxima at 454 nm and 483 nm whilst both spectra exhibit a shoulder in the region of 512 nm. Based upon this observation it is proposed that the structured emission exhibited by $[Rh(phen)_2(pytr)]^{2+}$ is a ligand π-π^* transition based on the phen ligand.

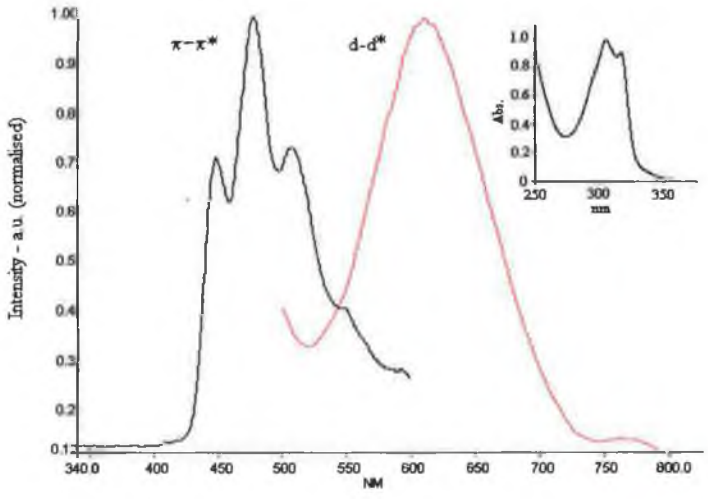

Figure 4.10 Emission spectra of $[Rh(bpy)_2(pytr)]^{2+}$ measured in ethanol:methanol 4:1 at 77K. Inset shows the UV spectrum of $[Rh(bpy)_2(pytr)]^{2+}$.

Whilst the observation of two distinct sets of emissions indicates that this is a dual emitting species such an assignment is generally met with a certain amount of scepticism due to the possibility that impurities are the cause of the dual emission. Hence it is necessary to rule out the possibility of the presence of impurities. As detailed in Chapter 3 the purity of all of these complexes has been checked by elemental analysis whilst NMR studies have shown no indication that any starting materials are present in the complexes in question. A factor which serves to preclude the possibility that this is an emission associated with an impurity is that whilst a

broad structureless emission has been previously reported for the complex $[Rh(phen)_2Cl_2]^+$, which was used as a starting material here, its emission has a maximum at 709 nm with a lifetime of 41.5μs.[3] In contrast the broad structureless emission in Figure 4.9 has a maximum at 612 nm a lifetime of 8.6μs. It is also interesting to note that the dual emitting nature of the complex $[Rh(3,3'\text{-}Me_2\text{-}bpy)_3]^{3+}$ has already been established and in this instance a broad structureless emission was observed at 610 nm and assigned as a d-d* based emission.[10] Thus the broad Gaussian shaped emission observed for $[Rh(phen)_2(pytr)]^{2+}$ is assigned as a d-d* transition.

In order to account for the behaviour of the pyridyl triazole complexes it is necessary to consider the σ-donor properties of the ligands. It has been shown that the pyridyl triazole ligands are much stronger σ-donors than bpy and phen consequently it is expected that this would cause an increase in the energy of the ^{3}MC state. The potential energy curves in Figure 4.11 illustrate this situation.

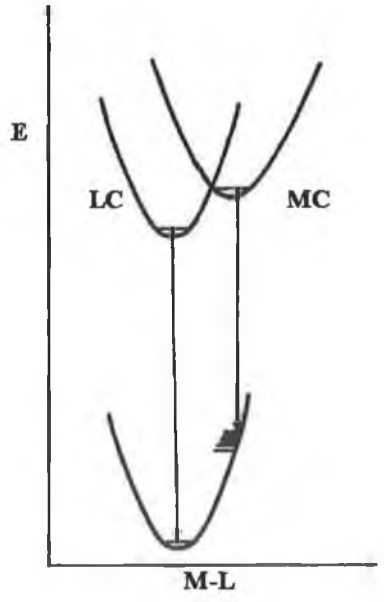

Figure 4.11 Potential energy diagram for $[Rh(phen)_2(pytr)]^{2+}$ and $[Rh(bpy)_2(pytr)]^{2+}$.

The observation of emission from both a $^3\pi$-π^* and a d-d* emitting state for $[Rh(phen)_2(pytr)]^{2+}$ and $[Rh(bpy)_2(pytr)]^{2+}$ would indicate that the rate of internal

conversion between these two states is slower than the independent deactivation processes to the ground state.

The emission spectra of the complexes $[Rh(phen)_2(4Mpytr)]^{3+}$, $[Rh(bpy)_2(4Mpytr)]^{3+}$, $[Rh(phen)_2(1M3pytr)]^{3+}$and $[Rh(bpy)_2(1M3pytr)]^{3+}$can be seen in Appendix IV. Again all of these complexes exhibit two independent emitting states. Figure 4.12 and Figure 4.13 illustrate the emission spectra obtained for $[Rh(phen)_2(Phpytr)]^{2+}$ and $[Rh(bpy)_2(Phpytr)]^{2+}$. The d-d* emission of $[Rh(phen)_2(Phpytr)]^{2+}$ is quite poor in comparison to those seen previously and, whilst quantitative analysis was not carried out, the broad structureless emission in this case was quite weak.

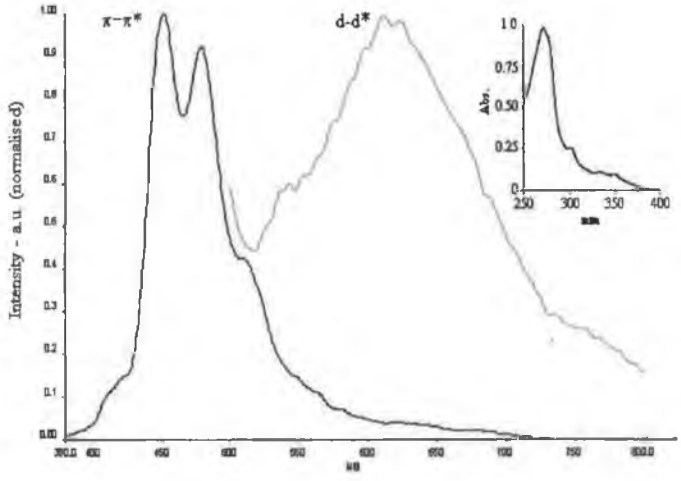

Figure 4.12 Emission spectra of $[Rh(phen)_2(Phpytr)]^{2+}$ measured in ethanol: methanol 4:1 at 77K. Inset shows the UV spectrum of $[Rh(phen)_2(Phpytr)]^{2+}$.

$[Rh(bpy)_2(Phpytr)]^{2+}$ also exhibited a weak d-d* emission whilst the π-π* based emission was found to be wavelength dependent. As can be seen from Figure 4.13, when the exciting wavelength was changed from 285 nm to 310 nm the structure of the emission associated with the π-π* state varied. This wavelength dependency would indicate that either an inter- or an intraligand process is occurring, the exact nature of which is not however known.

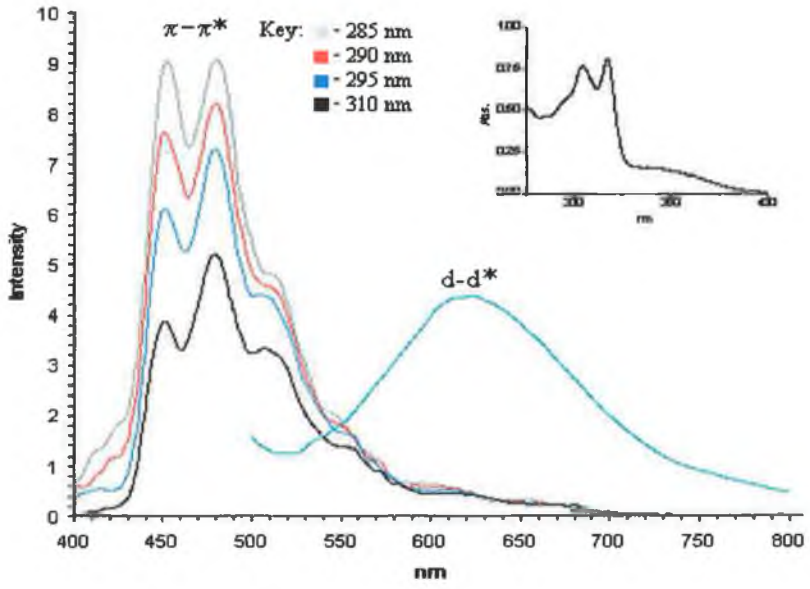

Figure 4.13 Emission spectra of $[Rh(bpy)_2(Phpytr)]^{2+}$ measured in ethanol:methanol 4:1 at 77K. Inset shows the UV spectrum of $[Rh(bpy)_2(Phpytr)]^{2+}$.

The fact that only a quite weak d-d* based emission was observed for these complexes might be due to the fact that the HPhpytr ligand is a weaker sigma donor than Hpytr and would have as a result a lower ^{3}MC level. This might result in some crossing between the ^{3}MC state and the π-π* emitting state thus resulting in a diminished d-d* emission.

For $[Rh(phen)_2(bpt)]^{2+}$ a broad Gaussian emission spectrum was observed on a short timescale (<1ms) while the longer lived structured π-π* emission which had been observed for the earlier complexes was barely detectable between 420 nm and 600 nm. The intensity of this π-π* emission improved marginally upon the addition of a drop of sodium methoxide, Figure 4.14. These emission spectra were obtained on a timescale longer than 1ms and this complex behaves quite differently to the complexes already discussed, showing a much broader emission spectrum, which also exhibits a wavelength dependence.

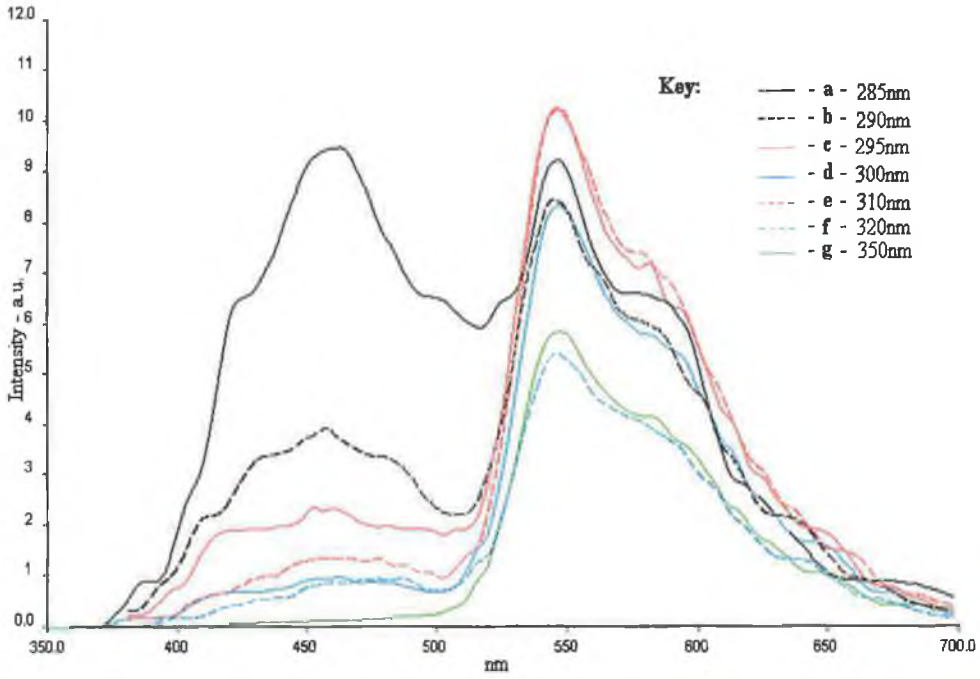

Figure 4.14 Emission spectra of $[Rh(phen)_2(bpt)]^{2+}$ with a drop of sodium methoxide added measured in ethanol:methanol 4:1 at 77K.

If we first consider the spectrum obtained at 285 nm, Figure 4.15 a, it appears that two emission processes are occurring i.e. one in the region of 400 nm to 525 nm and the second in the region 500 nm to 650 nm. Although it is not structurally defined and quite weak, the emission between 400 nm and 525 nm is coincident with the π-π* based emission exhibited by $[Rh(phen)_3]^{3+}$ and is assigned as such. As the excitation wavelength is varied from 285 nm to 350 nm the emission in the region of 400 nm to 525 nm decreases until at 350 nm it is no longer observed. The intensity of the emission at 546 nm has decreased slightly but the structure remains essentially unchanged and is comparable to that of the emission at λ_{ex} 285 nm. The emission at 546 nm (λ_{ex} 350 nm) is also attributed to a π-π* based transition due to the fact that it is similar in intensity to the emission at 461 nm, which was assigned as a ligand based π-π* based transition, and due to the fact that it exhibits a degree of structure. The exact nature of this emission is not however known, as it is possible that it is associated with either a phen ligand or the bpt ligand. Figure 4.15 illustrates the UV spectrum of the complex $[Rh(phen)_2(bpt)]^{2+}$ and the emission spectra obtained using excitation wavelengths of 285 nm (A) and 350 nm (B) for $[Rh(phen)_2(bpt)]^{2+}$ with a drop of sodium methoxide added. Also included in this diagram is the d-d* based

emission obtained for $[Rh(phen)_2(bpt)]^{2+}$ when measurements were carried out on a timescale < 1 ms (C). It should be noted that the d-d* emission was present both in the presence and absence of sodium methoxide although it was red shifted, from 634 nm to 652 nm, when sodium methoxide was added.

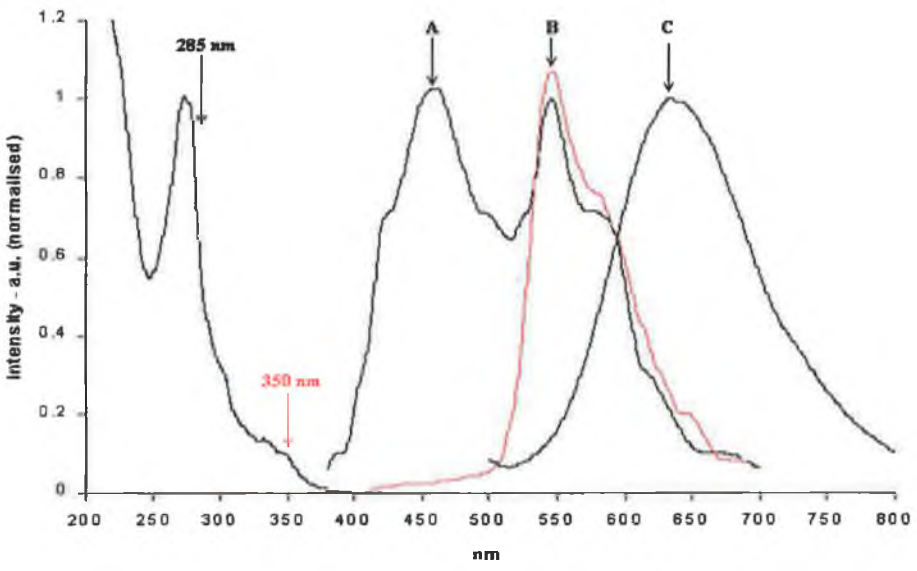

Figure 4.15 UV spectrum of $[Rh(phen)_2(bpt)]^{2+}$ measured in ethanol:methanol 4:1(——), the ligand based emission spectra of $[Rh(phen)_2(bpt)]^{2+}$ with a drop of sodium methoxide obtained with an excitation wavelength of 285 nm (A) and 350 nm (B) and the metal based emission of $[Rh(phen)_2(bpt)]^{2+}$ (C).

For $[Rh(bpy)_2(bpt)]^{2+}$ the bpy based emission was again found to be weak and poorly defined. It was found that upon the addition of sodium methoxide the π-π* based emission became more resolved although it was still quite weak and in contrast to the behaviour of $[Rh(phen)_2(bpt)]^{2+}$, the ligand based emission of $[Rh(bpy)_2(bpt)]^{2+}$ did not exhibit a wavelength dependency. Once again the d-d* based emission was observed both in the presence and absence of sodium methoxide. In the absence of sodium methoxide emission was observed at 625 nm and in the presence of base at 635 nm.

The emission spectrum obtained for the complex $[Rh(phen)_2(NHbpt)]^{2+}$ can be seen in Appendix IV. It is particularly interesting to note that this complex does not show a dual emission. The spectrum was found to be similar to that seen for $[Rh(phen)_3]^{3+}$ and may be assigned as a π–π* emission based on the phen ligand. Only a structured emission, associated with a ligand π–π* emission, was detected for $[Rh(bpy)_2(NHbpt)]^{2+}$ also. However unlike $[Rh(bpy)_2(NHbpt)]^{2+}$, the complex $[Rh(bpy)_2(NH_2bpt)]^{3+}$ did exhibit a broad Gaussian shaped emission spectrum with a lifetime <1ms. Figure 4.16 illustrates the emission spectra obtained for this compound.

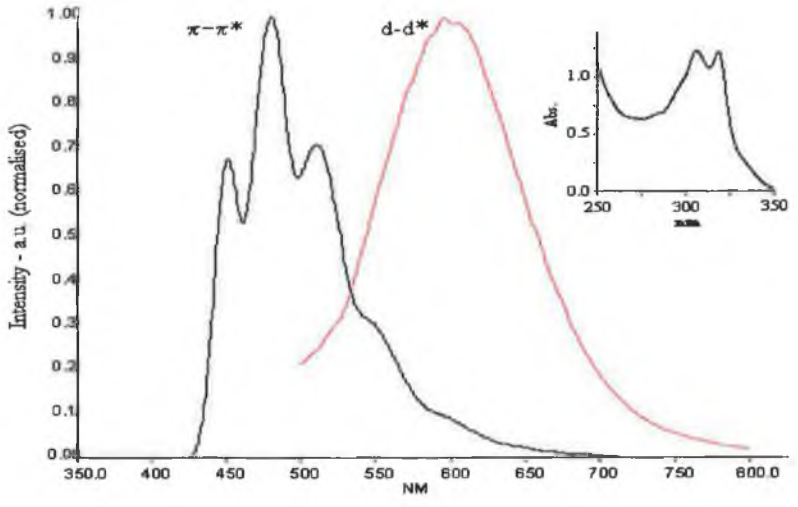

Figure 4.16 Emission spectrum of $[Rh(bpy)_2(NH_2bpt)]^{3+}$ measured in ethanol:methanol 4:1 at 77K. Inset shows the UV spectrum of $[Rh(bpy)_2(NH_2bpt)]^{3+}$.

The differing behaviour of $[Rh(bpy)_2(NHbpt)]^{2+}$ and $[Rh(bpy)_2(NH_2bpt)]^{3+}$, i.e. The absence of the broad d-d* based emission for $[Rh(bpy)_2(NHbpt)]^{2+}$, is striking. As was discussed in detail in Chapter 3, these complexes differ in their charge and in their mode of coordination. The metal centre of $[Rh(bpy)_2(NHbpt)]^{2+}$ is bound via the amino group and a nitrogen of a pyridine ring whereas, $[Rh(bpy)_2(NH_2bpt)]^{3+}$ exhibits the more conventional method of binding to a pyridyl triazole based ligand by binding via the N2' of the triazole ring and a nitrogen of a pyridine ring. The crystal structure of $[Rh(bpy)_2(NHbpt)]^{2+}$ demonstrated that in comparison to all of the complexes discussed previously, which formed a 5-coordinate ring upon

coordination, the Rh(III) metal centre binding via the NH-grouping gives rise to a six membered ring, Figure 3.8. As already discussed steric effects have been shown to influence the photophysics of Rh(III) polypyridyl complexes with the lowering of the MC excited state of $[Rh(3,3'\text{-}Me_2bpy)_3]^{3+}$ being attributed by Ford *et. al.* to ligand out of plane distortions which caused a decrease in the overlap between metal and ligand σ orbitals. It is likely here that it is the unusual mode of coordination of the metal centre to the NH_2bpt ligand in $[Rh(bpy)_2(NHbpt)]^{2+}$ which contributes to the behaviour observed by this complex although further study is required.[10]

Table 4.2 details the emission data for $[Rh(phen)_3]^{3+}$, $[Rh(bpy)_3]^{3+}$ and for the pyridyl triazole complexes studied. Whilst the emission maxima for the π-π* do not vary to any great extent the same cannot be said for the d-d* emission maxima. These maxima vary from 597 nm to 634 nm depending upon the nature of the pyridyl triazole ligand incorporated into the complex. Complexes incorporating the ligands 4Mpytr, 1M3Mpytr and NH_2bpt exhibit emission maxima at higher energies than those incorporating the Hpytr, Hbpt and Phpytr ligands. This behaviour can be attributed to the nature of the triazole ring in the complexes i.e. whether or not a negative charge resides on the triazole ring. When the triazole ring is deprotonated, as in the case of the Hpytr, Hbpt and Phpytr complexes, the negatively charged triazole moiety is a stronger σ donor than when the triazole moiety is neutral, donating more electron density into the d orbitals thus causing a shift of the emission spectra to lower energies. In cases where the triazole ring has been methylated or aminated as is the case with the ligands 4Mpytr, 1M3Mpytr and NH_2bpt the coordinated ligand becomes a weaker σ donor and a stronger π acceptor thus causing a shift of the emission to higher energies. The observation of such trends strengthens the argument that these complexes are demonstrating authentic dual emitting behaviour as, if the broad Gaussian spectra were associated with impurities it would be expected that they would exhibit the same emission maxima. The investigation of the behaviour of these complexes over a wide temperature range was not possible due to time constraints but it should be noted that at room temperature neither the structured nor the Gaussian type emissions were observed for either $[Rh(phen)_2(pytr)]^{2+}$ or $[Rh(bpy)_2(pytr)]^{2+}$.

Table 4.2 ***Emission data for $[Rh(phen)_3]^{3+}$, $[Rh(bpy)_3]^{3+}$ and pyridyl triazole complexes.***

Complex	Emission (nm)	Complex	Emission (nm)
$[Rh(phen)_3]^{3+}$		$[Rh(bpy)_3]^{3+}$	
(π–π^*)	454, 483, 512 sh	(π–π^*)	450, 483, 510 [a]
(d-d*)	-	(d-d*)	-
$[Rh(phen)_2(pytr)]^{2+}$		$[Rh(bpy)_2(pytr)]^{2+}$	
(π–π^*)	454, 482, 514 sh	(π–π^*)	450, 479, 509
(d-d*)	612	(d-d*)	609
$[Rh(phen)_2(d_6\text{-pytr})]^{2+}$		$[Rh(bpy)_2(d_6\text{-pytr})]^{2+}$	
(π–π^*)	454, 481, 514 sh	(π–π^*)	448, 478, 508
(d-d*)	623	(d-d*)	616
$[Rh(phen)_2(4Mpytr)]^{3+}$		$[Rh(bpy)_2(4Mpytr)]^{3+}$	
(π–π^*)	452, 481, 511 sh	(π–π^*)	470, 497
(d-d*)	597	(d-d*)	597
$[Rh(phen)_2(1M3pytr)]^{3+}$		$[Rh(bpy)_2(1M3pytr)]^{3+}$	
(π–π^*)	454, 482, 514 sh	(π–π^*)	450, 481, 511
(d-d*)	600	(d-d*)	598
$[Rh(phen)_2(Phpytr)]^{2+}$		$[Rh(bpy)_2(Phpytr)]^{2+}$	
(π–π^*)	452, 479, 509 sh	(π–π^*)	452, 479, 510
(d-d*)	618	(d-d*)	620
$[Rh(phen)_2(bpt)]^{2+}$		$[Rh(bpy)_2(bpt)]^{2+}$	
(π–π^*)	461, 546 †	(π–π^*)	449, 478, 507
(d-d*)	634	(d-d*)	625
$[Rh(phen)_2(NHbpt)]^{2+}$		$[Rh(bpy)_2(NHbpt)]^{2+}$	
(π–π^*)	453, 482, 512 sh	(π–π^*)	455, 482, 506
(d-d*)	–	(d-d*)	–
		$[Rh(bpy)_2(NH_2bpt)]^{3+}$	
		(π–π^*)	451, 481, 511
		(d-d*)	600

a- taken from ref. 3 sh – shoulder † - dual emitting

4.2.3 Excited State Lifetimes

The instrumentation that was used to carry out excited state lifetime measurements has been detailed in Chapter 2. Using TCSPC it was possible to measure excited state lifetimes in the region of 2ns to 30μs and laser flash photolysis potentially allowed for the measurement of lifetimes in the ms region. The pyridyl triazole compounds do not however absorb at 355 nm, the excitation wavelength of the laser, meaning that it was not possible to measure the excited state lifetimes of π-π^* emissions which had been detected on a time scale >1 ms. The Nd-Yag laser is also capable of generating the fourth harmonic where λ = 266 nm. The pyridyl triazole compounds do absorb in this region and it would be possible to measure these long lived excited states at this excitation wavelength however at this wavelength it would be necessary to use a quartz cell and a cryostat with quartz windows. Measurements using this apparatus are quite time consuming and as a result could not be attempted. Thus, all excited state lifetimes reported in this chapter refer to the excited state of the d-d* based emissions measured at 77K with an excitation wavelength of 337 nm using TCSPC.

When the samples were initially measured all showed some multi-exponential behaviour. In order to verify this behaviour as being associated to the complexes and not being related to an excited state build up, the lifetimes were measured again under the same conditions with the exception of the repetition rate of the laser. Excited state build up is found to occur when the system is being pulsed at a faster rate than the decay of the excited state. Thus if when the pulse repetition rate is reduced and the bi-exponential behaviour is seen to be notably affected by this repetition change then it can be assumed that the emission is not multi-exponential. If a decay is truly multi-exponential then varying the repetition rate would not alter the lifetime decay. When the complexes in question here were reanalysed at a lower repetition rate, i.e. 3000 Hz as opposed to 10,000 Hz, all of them displayed mono-exponential behaviour with the exception $[Rh(phen)_2(Phpytr)]^{2+}$. The results obtained can be seen in Table 4.3.

Table 4.3 ***77K lifetimes for $[Rh(phen)_3]^{3+}$ and $[Rh(bpy)_3]^{3+}$ and for pyridyl triazole complexes.***

Complex	τ (μs)	Complex	τ (μs)
$[Rh(phen)_3]^{3+}$		$[Rh(bpy)_3]^{3+}$	
(π–π*)	48400 [a]	(π–π*)	2210 [a]
(d-d*)	-	(d-d*)	-
$[Rh(phen)_2(pytr)]^{2+}$		$[Rh(bpy)_2(pytr)]^{2+}$	
(π–π*)	*	(π–π*)	*
(d-d*)	8.6	(d-d*)	6
$[Rh(phen)_2(d_4\text{-pytr})]^{2+}$		$[Rh(bpy)_2(d_4\text{-pytr})]^{2+}$	
(π–π*)	*	(π–π*)	*
(d-d*)	10.5	(d-d*)	9.3
$[Rh(phen)_2(4Mpytr)]^{3+}$		$[Rh(bpy)_2(4Mpytr)]^{3+}$	
(π–π*)	*	(π–π*)	*
(d-d*)	18	(d-d*)	c
$[Rh(phen)_2(1M3pytr)]^{3+}$		$[Rh(bpy)_2(1M3pytr)]^{3+}$	
(π–π*)	*	(π–π*)	*
(d-d*)	21.0	(d-d*)	14
$[Rh(phen)_2(Phpytr)]^{2+}$		$[Rh(bpy)_2(Phpytr)]^{2+}$	
(π–π*)	*	(π–π*)	*
(d-d*)	2.7, 18	(d-d*)	2.3
$[Rh(phen)_2(bpt)]^{2+}$		$[Rh(bpy)_2(bpt)]^{2+}$	
(π–π*)	*	(π–π*)	*
(d-d*)	4	(d-d*)	7
$[Rh(phen)_2(NHbpt)]^{2+}$		$[Rh(bpy)_2(NHbpt)]^{2+}$	
(π–π*)	*	(π–π*)	*
(d-d*)	-	(d-d*)	-
$[Rh(phen)_2(NH_2bpt)]^{3+}$	b	$[Rh(bpy)_2(NH_2bpt)]^{3+}$	
		(π–π*)	*
		(d-d*)	13

— = not observed * = could not be measured using conditions available a = values taken from ref 3 and 12. b = complex not isolated in pure form c = complex not available

It should be noted that all excited state lifetimes reported here are ± 5% and that two methods were used for analysing the quality of the data acquired – a χ^2 goodness of fit test and analysis of the residuals plot. A χ^2 value as close as possible to but not below 1 is ideal and χ^2 values between 1 and 1.2 were obtained for all data reported.

Typical decay profiles are seen in Figure 4.17 and Figure 4.18. Figure 4.17 illustrates the decay profile of $[Rh(phen)_2(4Mpytr)]^{3+}$ measured in an ethanol:methanol glass at 77K.

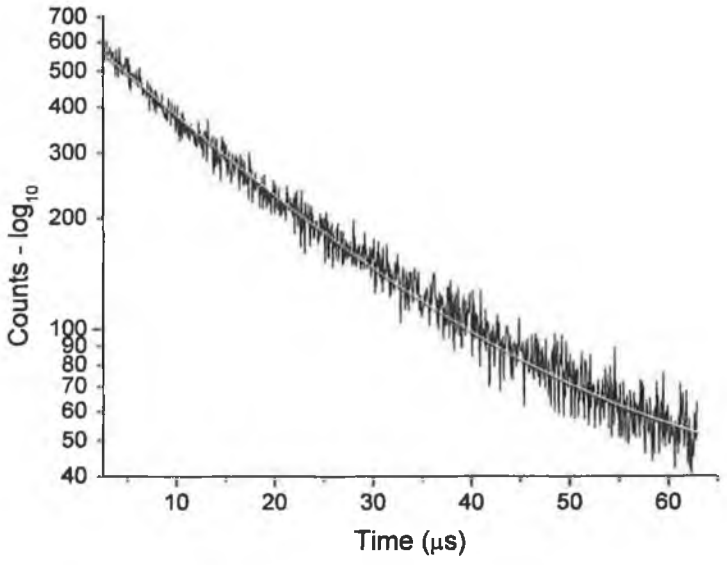

Figure 4.17 The decay profile of $[Rh(phen)_2(4Mpytr)]^{3+}$ measured in an ethanol:methanol glass at 77K.

The main component of this particular decay profile is mono-exponential with a lifetime of 18μs. It can however be seen that the decay is not completely linear and this is attributed to a build up of the excited state. Since all the lifetimes obtained here are in the μs timescale these decays can be attributed to being d-d* in nature as ligand based lifetimes for complexes of this nature are generally in the ms region.[12]

Figure 4.18 illustrates the decay profile of $[Rh(phen)_2(Phpytr)]^{2+}$ and as already stated, this complex exhibits a definite bi-exponential behaviour, which is unaltered by variation of the pulse repetition rate. The lifetimes in this case were determined to be 2.7 μs and 18 μs. It was found that the lifetime of the analogous bpy complex $[Rh(bpy)_2(Phpytr)]^{2+}$ was 2.3 μs which is coincident with the lifetime

of the short component of the decay of $[Rh(phen)_2(Phpytr)]^{2+}$. It is not known what process is associated with the 18 μs decay observed for $[Rh(phen)_2(Phpytr)]^{2+}$.

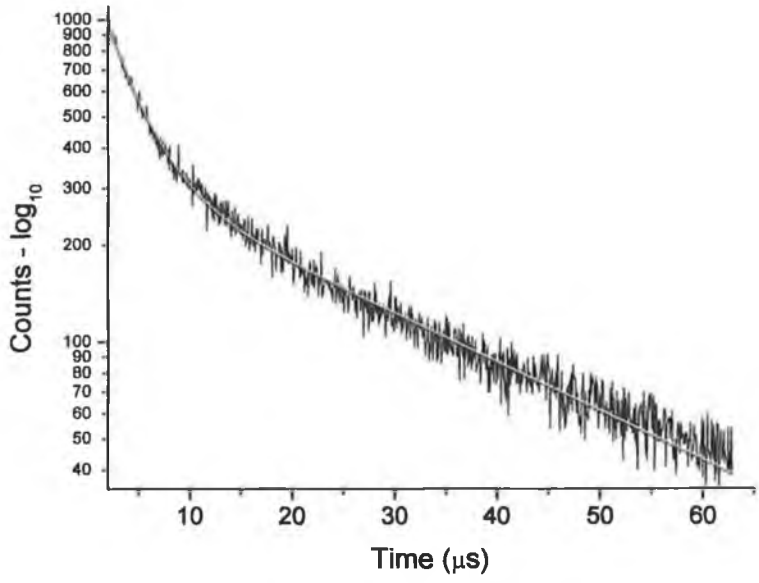

Figure 4.18 The decay profile of $[Rh(phen)_2(Phpytr)]^{2+}$ measured in an ethanol:methanol glass at 77K.

The application of deuteration has been discussed in Chapter 3 in relation to its contribution in assigning ^1H NMR spectra. Deuteration is also a useful tool in photophysical studies.[13] Deuteration has the effect of reducing both the amplitude and the frequency of vibrational modes and as a result C-D vibrations are of lower frequency and amplitude than the equivalent C-H vibrations. Thus the vibrational overlap between two states will be diminished for the same energy gap and as non-radiative deactivation is less effective in the deuterated case it results in an increase in the observed lifetime of the electronically excited state. It has been shown that this observation may be used for the determination of the location of the excited state in heteroleptic complexes. Figure 4.19 compares vibrational levels and overlap for C-D and C-H vibrational modes.[13]

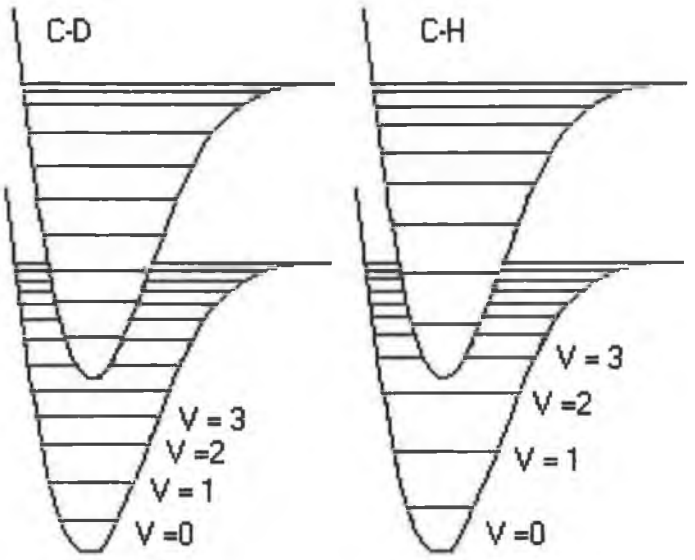

Figure 4.19 Comparison of vibrational levels and overlap for C-D and C-H vibrational modes.[13]

Thus if the excited state is localised on a deuterated ligand for example on d_4-pytr in $[Rh(phen)_2(d_4\text{-pytr})]^{2+}$ it would be expected that the lifetime of $[Rh(phen)_2(d_4\text{-pytr})]^{2+}$ would be significantly longer than that of $[Rh(phen)_2(pytr)]^{2+}$. It can be seen from Table 4.3 that the lifetimes of the deuterated complexes do differ from their non-deuterated analogues with lifetimes of 8.6 μs and 10.5 μs being observed for $[Rh(phen)_2(pytr)]^{2+}$ and $[Rh(phen)_2(d_4\text{-pytr})]^{2+}$ and 6 μs and 9.3 μs being observed for $[Rh(bpy)_2(pytr)]^{2+}$ and $[Rh(bpy)_2(d_4\text{-pytr})]^{2+}$ respectively. This variation in the excited state lifetimes would indicate that, mixing of the metal and ligand excited states is occurring to some degree. Evidence for mixing of the emitting π-π^* triplet with d-d and d-π^* excited states has been observed previously by Crosby *et. al.*, Yersin *et. al.* and Glasbeek *et. al.*[14,15]

4.2.4 Electrochemical Properties

Electrochemical analysis is another method by which the electronic properties of complexes may be studied. Reduction potentials are an indication of the location of the lowest excited states. In the reduction process an electron is added to the Lowest Unoccupied Molecular Orbital (LUMO) whereas in an oxidation process an electron is removed from the Highest Occupied Molecular Orbital (HOMO).[16] As was discussed earlier, Section 1.4, the electrochemistry of Rh(III) polypyridyl complexes is complicated by irreversibility, with ligand loss upon reduction being common. For a redox reaction to be reversible, the concentrations of the oxidised and reduced species at the electrode surface must be maintained at the values required by the Nernst equation. Each half-reaction responds to the interfacial potential difference at the corresponding electrode. The potential of any electrode for an oxidation / reduction system (*ox* / *red*) where $ox + ne^- = red$ may be given in the generalised form the Nernst equation which is as follows [17]

$$E = E^0 - \frac{RT}{nF}\ln\frac{a_{red}}{a_{ox}} = E^0 - \frac{2.3026RT}{nF}\log\frac{a_{red}}{a_{ox}} \qquad \textbf{Equation 4.1}$$

where

E^0	=	the standard electrode potential
R	=	the molar gas constant
T	=	the absolute temperature
n	=	the number of electrons transferred in the electrode reaction
F	=	Faraday constant
a_{ox}	=	the activity of the oxidised forms involved in the electrode reaction
a_{red}	=	the activity of the reduced forms involved in the electrode reaction

If we take Equation 4.1 and substitute concentrations for activity, common logarithms for natural logarithms and insert numerical data for the constants whilst assuming the temperature is 298K the Nernst equation may be expressed as Equation

4.2 where $E^{0'}$ is the formal electrode potential defined in terms of concentration rather than activities.

$$E = E^{0'} - \frac{0.05916}{n} \log \frac{[red]}{[ox]} \qquad \textbf{Equation 4.2}$$

A change of one unit in the logarithmic term changes the value of E by $59.16/n$ mV. [17,18] Thus the theoretical peak potential difference for a reversible system is 59.16 mV with 60-70mV generally being accepted. For all of the complexes that will be discussed here both the E_{pa} and the E_{pc} values will be given where E_{pa} and E_{pc} are the anodic and cathodic peak potentials respectively. Reversibility is not only dependent upon the peak potential separation but also upon the peak current ratio (i_{pa}/i_{pc}) being equal to 1 at all scan rates and the peak current function $i_p/\nu^{1/2}$ (ν = scan rate) being independent of ν. The peak current is given by the Randles-Sevcik equation [19,17,18]

$$i_p = (2.69 \times 10^5) n^{3/2} A C D^{1/2} \nu^{1/2} \qquad \textbf{Equation 4.3}$$

where

n = the number of electrons transferred/molecule

A = the electrode surface area (cm^2)

C = the concentration (mol cm^{-3}) and

D = the diffusion coefficient ($cm^2\ s^{-1}$).

Slow electron transfer kinetics and chemical reactions are the two major reasons for deviations from the ideal Nernstian reversible behaviour leading to systems which can be classified as quasi-reversible or irreversible.[16,17,18] The details of the criteria that will be applied in the following discussion to categorise a system are as follows;

System Type	ΔE_p (mV)
reversible	55-60
quasi-reversible	60-100
irreversible	>100

The electrochemical techniques that were employed in this study were cyclic voltammetry (CV) and differential pulse voltammetry (DPV). DPV significantly diminishes background current and this is part of the reason for the increased sensitivity of DPV with respect to CV, with 10^{-8} M being the lowest detection limit of DPV. The basic principles of these methods have been outlined in Chapter Two, Section 2.8, together with the method employed. It is important to emphasise that all experiments were carried out at least twice using a clean working electrode in each case and that the results obtained were reproducible. It was found that, in concert, CV and DPV allowed for an comprehensive study of the electrochemical behaviour of these Rh(III) complexes.

The results that will be detailed in the following discussion generally involve both the CV and DPV spectra being integrated into the same figure for comparison purposes. It is important to note that the DPV's are purely for comparison proposes and are not to scale. In almost all cases the CV's illustrated are the third of three scans and any deviation from this is detailed. All spectra and tabulated data are presented versus Fc/Fc^+ with values vs. SCE being converted to Fc/Fc^+ using conversion constants reported by Addison *et. al.*[20] It is important to note that in differential pulse voltammetry the actual differential current value may be determined from Equation 4.3.

$$E_{max} = E_{\frac{1}{2}} - \frac{\Delta E_p}{2} \qquad \textbf{Equation 4.4}$$

where

E_{max} = the maximum differential current value

$E_{½}$ = the half-wave potential

ΔE_p = pulse amplitude

with ΔE_p values being negative in cathodic scans and positive in anodic scans. All scans were carried out using a pulse amplitude of 50mV thus it was necessary to compensate for a -25mV shift by adding 25mV to the potential axis for anodic scans and –25mV for cathodic scans.

The voltammetry of Rh(III) phen and bpy complexes and was studied by DeArmond *et. al.* Figure 4.20 illustrates the proposed reactions for phen bis and tris species.[21,22] It was found that for the tris complexes $[Rh(phen)_3]^{3+}$ and $[Rh(bpy)_3]^{3+}$ the first one electron reduction was followed by a moderately fast elimination of a phen/bpy ligand and that a second one electron transfer producing a Rh(I) species was followed by a chemical reaction.[21,22] These reduction waves were observed at -1.171V and -1.343V for $[Rh(phen)_3]^{3+}$ and a two electron wave was observed at –1.21 V for $[Rh(bpy)_3]^{3+}$. When the scan rate was increased from 0.10 V/sec to 31.2 V/sec the wave at –1.21V became more resolved and two separate peaks were observed at -1.24V and -1.38V respectively. DeArmond *et. al.* observed two further reductions which were attributed to the formation of $[Rh(phen)_2]^0$ at -1.87V and $[Rh(phen)_2]^{-1}$ at -2.015V and for the analogous tris bpy complexes these reduction waves were found at -1.84V for the formation for the species $[Rh(bpy)_2]^0$ and -2.05V for $[Rh(bpy)_2]^{-1}$.

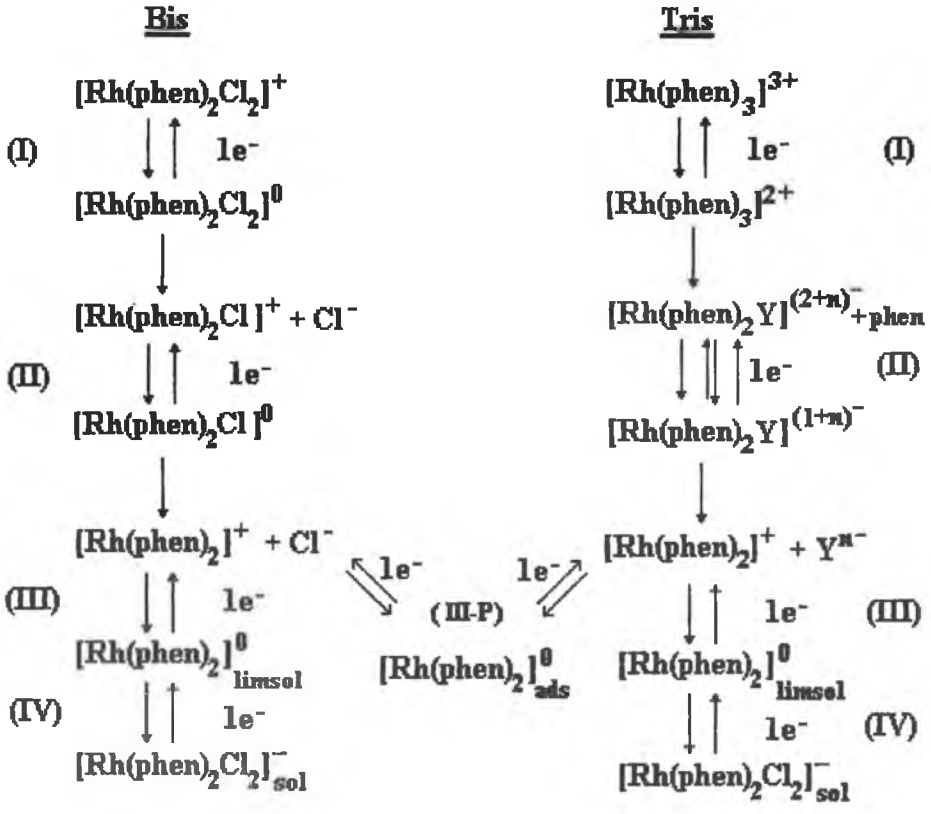

Figure 4.20 Proposed reaction sequences for $[Rh(phen)_2Cl_2]^+$ and $[Rh(phen)_3]^{3+}$ [21]

The electrochemical results obtained for the pyridyl triazole complexes are detailed in Table 4.4 and Table 4.5.

Table 4.4 ***Electrochemical data obtained for $[Rh(phen)_3]^{3+}$ and for the complexes $[Rh(phen)_2(L)]^{n+}$ where L = pyridyl triazole ligand and x = 2 or 3 measured in acetonitrile with 0.1M $TBABF_4$.***

Complex	E_{pc}, V	E_{pa}, V
$[Rh(phen)_3]^{3+}$		
CV	-1.171, -1.343, -1.87, -2.015 [a]	-1.107 [a]
$[Rh(phen)_2(pytr)]^{2+}$		
CV	-1.37, -1.79, -2.04	-1.52, -1.94
DPV	-1.33, -1.81, -2.00	-0.19, -0.80, -1.33, -1.55, -1.98
$[Rh(phen)_2(d_4\text{-pytr})]^{2+}$		
CV	-1.37, -1.80, -2.07	-1.49, -1.90
DPV	-1.31, -1.48, -1.80, -1.87, -2.00	-1.27, -1.33, -1.57, -1.87, -2.01
$[Rh(phen)_2(1M3pytr)]^{3+}$		
CV	-1.11, -1.82, -2.05	-
DPV	-1.05, -1.81, -1.89, -2.00	-0.84, -1.06, -1.54, -1.98
$[Rh(phen)_2(Phpytr)]^{2+}$		
CV	-1.36, -1.72, -2.06	-1.52, -1.94
DPV	-1.32, -1.70, -1.97	-0.87, -1.33, -1.53, -1.97
$[Rh(phen)_2(bpt)]^{2+}$		
CV	-1.36, -1.74, -2.08	-1.95
DPV	-0.95, -1.32, -1.77, -2.00	-
$[Rh(phen)_2(NHbpt)]^{2+}$		
CV	-1.37, -1.46, -1.69, -1.83 -2.06	0.77
DPV	+0.71, -1.33, -1.43, -1.65, -1.89, -2.02	+0.71, -0.87, -1.55

a= values taken from ref 21 and converted from V vs. SCE to V vs. Fc/Fc^+ using ref 20.

It is important to note that DPV is much more sensitive than CV and as a result more peaks tend to be apparent in the DPV. A number of the peaks in the DPV data

detailed in Table 4.4 and Table 4.5 are associated with quite weak reduction / oxidation processes.

Table 4.5 ***Electrochemical data obtained for $[Rh(bpy)_3]^{3+}$ and for the complexes $[Rh(bpy)_2(L)]^{n+}$ where L = pyridyl triazole ligand and x = 2 or 3 measured in acetonitrile with 0.1M $TBABF_4$.***

Complex	E_{pc}, V	E_{pa}, V
$[Rh(bpy)_3]^{3+}$		
CV	-1.21, -1.84, -1.67 [a]	-1.78, -1.99 [a]
$[Rh(bpy)_2(pytr)]^{2+}$		
CV	-1.34, -2.03	-1.95
DPV	-0.96, -1.31, 1.65, -2.00	-0.98, -1.32, -1.98
$[Rh(bpy)_2(d_4\text{-pytr})]^{2+}$		
CV	-1.21, -1.34, -1.71, -2.01	-1.95
DPV	-0.96, -1.21, -1.31, -1.66, -2.00	-1.31, -1.69, -1.98
$[Rh(bpy)_2(4Mpytr)]^{3+}$		
CV	-1.24, -1.69, -2.03	-0.76, -1.33, -1.58
DPV	-1.20, -1.64, -2.00	-0.80, -1.21, -1.34, -1.56, -1.69, -1.99
$[Rh(bpy)_2(1M3pytr)]^{3+}$		
CV	-1.12, -1.75, -2.02	-1.66, -1.94
DPV	-1.07, -1.71, -1.98	-1.03, -1.26, -1.74, -2.00
$[Rh(bpy)_2(Phpytr)]^{2+}$		
CV	-1.35, -2.01	-0.71, -1.94
DPV	-1.31, -1.97	-1.32, -1.97
$[Rh(bpy)_2(bpt)]^{2+}$		
CV	-1.27, -1.33, -2.01	-1.92
DPV	-0.73, -1.02, -1.30, -1.95, -2.02	-1.31, -1.97
$[Rh(bpy)_2(NHbpt)]^{2+}$		
CV	+0.67, -1.44, -2.15	+0.78
DPV	-1.41, -1.75, -2.10	-0.91, -1.33, -1.91
$[Rh(bpy)_2(NH_2bpt)]^{3+}$		
CV	-1.11, -1.22, -1.76, -2.03	-1.94, -1.66, -0.75
DPV	-1.08, -1.43, -1.90	-2.08, -1.89, -1.67, -1.74, -1.27

a= values taken from ref 22 and converted from V vs. SCE to V vs. Fc/Fc^+ using ref 20.

The CV (a) and DPV's (b) of $[Rh(phen)_2(pytr)]^{2+}$ may be seen in Figure 4.21.

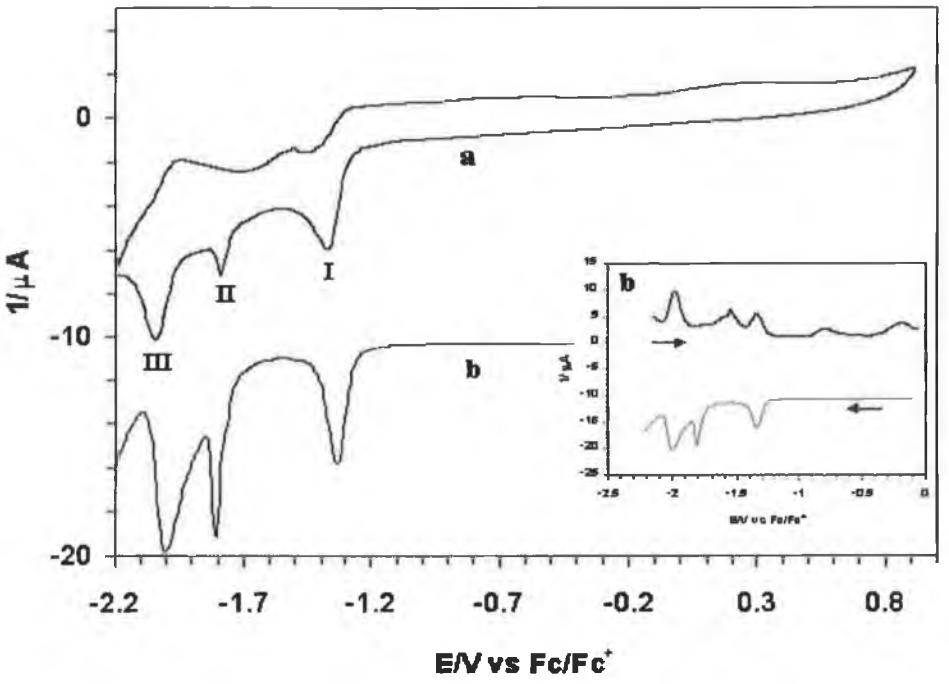

Figure 4.21 CV (a) and DPV's (b) of $[Rh(phen)_2(pytr)]^{2+}$ measured in acetonitrile with 0.1M $TBABF_4$.

The CV of $[Rh(phen)_2(pytr)]^{2+}$, Figure 4.21, exhibits three quite well defined reduction waves at -1.37V, -1.79V and -2.04V. Based upon the behaviour of $[Rh(phen)_3]^{3+}$ and $[Rh(bpy)_3]^{3+}$ this first wave can be assigned as the reduction of Rh(III) to Rh(II) and it is expected that this reduction is followed by ligand dissociation.[21,22] It is this tendency to dissociate, when the metal centre is in the Rh(I) oxidation state, which leads to the irreversible nature of rhodium electrochemistry. When the reverse scan, started at -2.2V, is studied there is no evidence for the presence of a corresponding oxidation wave for the reduction wave observed at -1.37V making this an irreversible process. The third reduction wave occurs at -2.04V and the corresponding oxidation wave is found at -1.94V. The peak potential separation in this case is 100mV and is this is deemed to be quasi-reversible. DPV is much more sensitive than CV and it can be seen that the DPV obtained by scanning in the negative direction is the same as the observed CV. Based upon the behaviour of previously reported Rh(III) tris homoleptic complexes

it is assumed that the reduction wave (I) is a composite wave i.e. comprised of more than one reduction wave. It would appear due to the broadness of (III) that this is also a composite wave but further study is required to establish this definitively. It is interesting to note that for the complex $[Ru(phen)_2(bpt)]^+$ ligand based reduction waves were found at -1.85V and -2.17V respectively.[23] Thus it is feasible that ligand based reductions are contributing to the reduction waves observed in Figure 4.21. The CV and DPV of $[Rh(phen)_2(d_4\text{-pytr})]^{2+}$ can be seen in Appendix (IV). Similar reduction waves are observed for both the deuterated and non-deuterated complexes. The DPV of the deuterated complex shows a slight variation from that of the non-deuterated complex but the extra waves observed are most probably due to the adsorption and desorption of dissociated material onto the surface of the working electrode.

Figure 4.22 illustrates the CV (a) and DPV's (b) of $[Rh(bpy)_2(pytr)]^{2+}$ measured in acetonitrile with 0.1M $TBABF_4$. In this case only two reduction waves are observed, the first of which shows no corresponding oxidation peak.

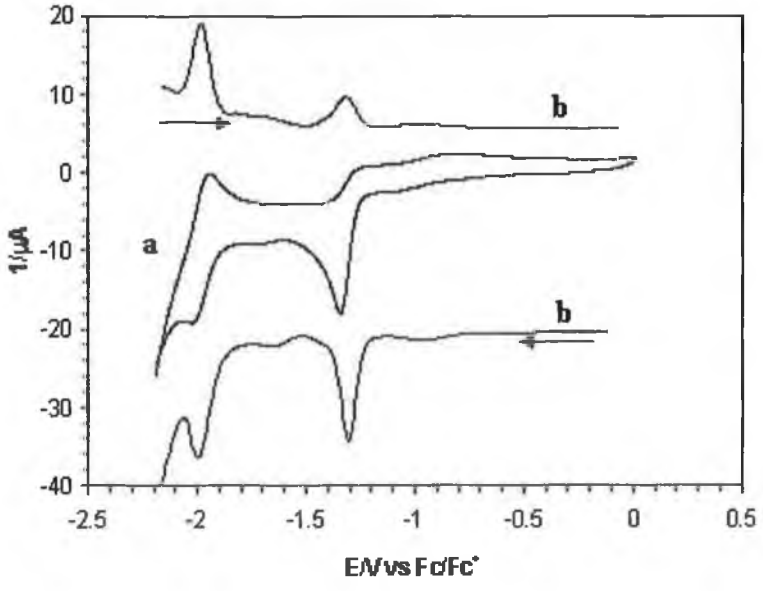

Figure 4.22 CV (a) and DPV's (b) of $[Rh(bpy)_2(pytr)]^{2+}$ measured in acetonitrile with 0.1M $TBABF_4$.

The second reduction wave does have a corresponding oxidation wave and with a peak separation of 80mV this reduction is deemed to be quasi-reversible. It is difficult to establish conclusively whether these are one or two electron processes based on the results obtained and when the analogous deprotonated ruthenium(II) complex $[Ru(bpy)_2(pytr)]^+$, coordinated via the N2' of the triazole ring, was studied ligand based reductions were observed at-1.85V, -2.10V and -2.63V respectively.[23]

When Hage studied the behaviour of ruthenium(II) polypyridyl complexes incorporating pyridyl triazole based ligands it was found that methylation of the Hpytr ligand in the 4 position of the triazole ring gave rise to more positive reduction potentials with ligand based reductions being detected at -1.77V, -1.99V and -2.32V respectively. Hage attributed the first two ligand based reductions to the bpy ligands based on the electrochemical behaviour of $[Ru(bpy)_3]^{2+}$ and found that the third, more negative, reduction was located at the pyridyl triazole ligand.[23] Figure 4.23 illustrates the CV's (a) and DPV's (b) obtained when the complex $[Rh(bpy)_2(4Mpytr)]^{3+}$ was analysed. The CV exhibits reduction peaks at -1.24V, -1.69V and -2.03V. If these reduction potentials are compared with the complex $[Rh(bpy)_2(pytr)]^{2+}$, found at -1.34V and -2.40V, it can be seen that, as expected, Rh(III) complexes display a behaviour comparable to that exhibited by the analogous Ru(II) complexes upon methylation of the Hpytr ligand.[23]

If we again consider the CV of $[Rh(bpy)_2(4Mpytr)]^{3+}$ it can be seen that as the potential approaches –2.20V a large peak can be seen to develop in the cathodic scan due to the presence of water. This very intense water peak is more prominent in the DPV obtained when the potential was scanned in the negative direction and it can be seen that this obscures any reduction waves associated with the complex. Whilst the cathodic scan results in three reduction waves the anodic scan is more complicated with a number of waves being observed. In particular two sharp peaks can be seen in the anodic scan at –1.33V and –0.76V. The reversibility of the reduction wave at -1.24V was probed by switching the potential at -1.3V rather than -2.2V and the resultant CV can be seen in red in Figure 4.23. In this range the peak, which had previously been observed at -0.76V in the anodic scan, is no longer

detected. This observation confirms that the reduction wave observed at -1.24V is in fact irreversible. The sharp peak observed at -0.76V is most likely to be the result of desorption of material that had been deposited onto the working electrode after complex dissociation has occurred. Although it was not probed it is expected that a similar behaviour would be observed for the sharp peak observed at –1.33V in the anodic scan.

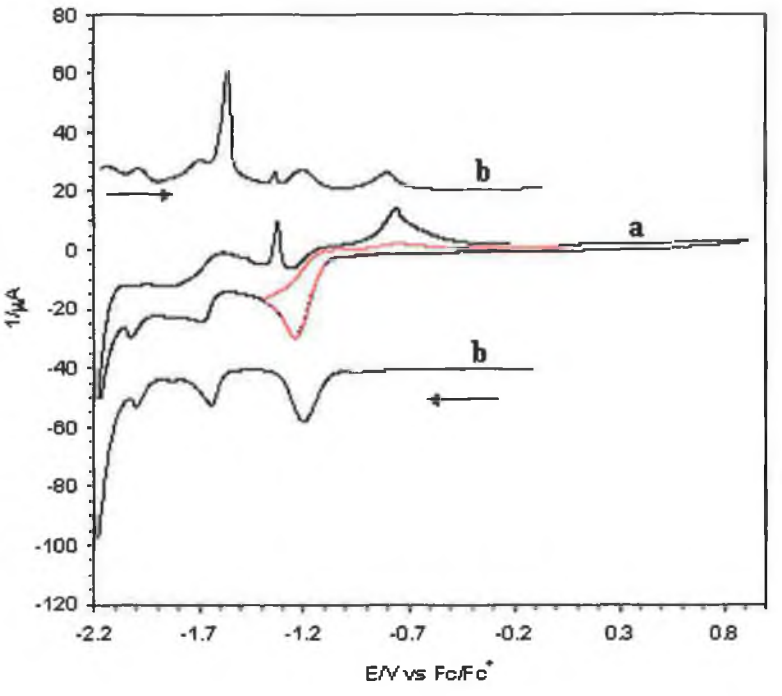

Figure 4.23 CV's (a) and DPV's (b) of $[Rh(bpy)_2(4Mpytr)]^{3+}$ measured in acetonitrile with 0.1M $TBABF_4$.

Figure 4.24 portrays the CV (a) and DPV's (b) obtained for the complex $[Rh(phen)_2(1M3pytr)]^{3+}$. In the CV of $[Rh(phen)_2(1M3pytr)]^{3+}$ the first reduction wave can be seen at –1.11 V with two further waves occurring at –1.82V and –2.05V. It is interesting to examine the corresponding DPV as it is not clear from the CV if the wave at –1.82V is a result of a one or a two electron process. The shape of this wave in the corresponding DPV indicates that this is in fact a composite wave and also shows the presence of a prewave at –1.81V. All of the reduction waves observed by cyclic voltammetry were found to be irreversible in this case and it should be noted that the sharp peak observed at –1.54V in the anodic DPV scan is

again attributed to the desorption of material from the surface of the working electrode.

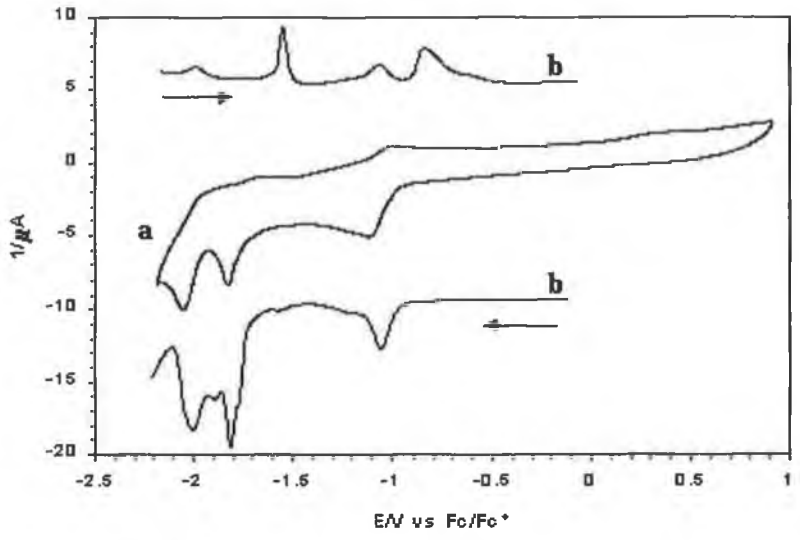

Figure 4.24 CV (a) and DPV's (b) of $[Rh(phen)_2(1M3pytr)]^{3+}$ measured in acetonitrile with 0.1M $TBABF_4$.

Figure 4.25 represents the CV (a) and DPV's (b) obtained for the complex $[Rh(bpy)_2(1M3pytr)]^{3+}$. Unlike $[Rh(phen)_2(1M3pytr)]^{3+}$ shown above, the CV of $[Rh(bpy)_2(1M3pytr)]^{3+}$ demonstrates a degree of reversibility and the shape of reduction waves I and III indicate that these are composite waves. Reduction potentials in this case occur at -1.12V (I), -1.75V (II), and -2.02V (III). The reduction waves II and III were found to be quasi-reversible with peak potentials separations of 90mV and for 80mV being observed respectively. When the reduction potentials of the complexes incorporating the 1M3pytr ligand are compared with those of $[Rh(bpy)_2(pytr)]^{2+}$ it can be seen that they behave similarly to the 4Mpytr complex with more positive reduction potentials with respect to those of $[Rh(bpy)_2(pytr)]^{2+}$. This difference in the first reduction potential exhibited by complexes with Hpytr and 4Mpytr and 1M3pytr is related to the σ-donating strengths of the ligands. When complexed, the Hpytr ligand is deprotonated ($pytr^-$) thus a negative charge resides on the triazole ring whereas the 4Mpytr and 1M3pytr ligands are neutral when complexed. It has been shown that the triazole ligands are stronger σ donors when deprotonated and donate more electron density into the d obitals thus

resulting in more negative oxidation and reduction potentials.[23] Table 4.6 compares the behaviour of Rh(III) and Ru(II) complexes incorporating the ligands Hpytr, 4Mpytr and 1M3pytr.

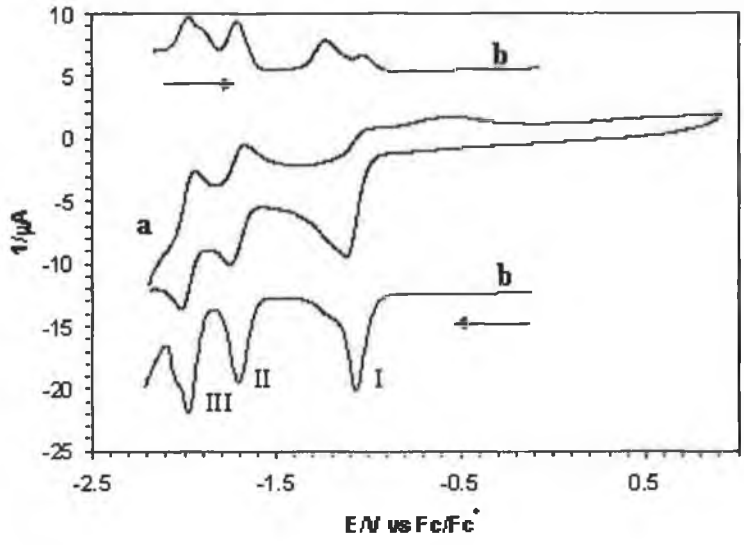

Figure 4.25 CV (a) and DPV's (b) of $[Rh(bpy)_2(1M3pytr)]^{3+}$ measured in acetonitrile with 0.1M $TBABF_4$.

Table 4.6 Comparison of the reduction potentials of $[Rh(bpy)_2(pytr)]^{3+}$, $[Rh(bpy)_2(4Mpytr)]^{3+}$ and $[Rh(bpy)_2(1Mp3ytr)]^{3+}$ measured in acetonitrile with 0.1M $TBABF_4$ with the analogous Ru(II) complexes.

Complex	E_{pc} V vs. Fc/Fc^+	Complex	E_{pc} V vs. Fc/Fc^+
$[Rh(bpy)_2(pytr)]^{2+}$	-1.34, -2.40	$[Ru(bpy)_2(pytr)]^{+}$	-1.85, -2.10, -2.63 [a]
$[Rh(bpy)_2(4Mpytr)]^{3+}$	-1.24, -1.69, -2.03	$[Ru(bpy)_2(4Mpytr)]^{2+}$	-1.77, -1.99, -2.32 [a]
$[Rh(bpy)_2(1M3pytr)]^{3+}$	-1.12, -1.75, -2.02	$[Ru(bpy)_2(1M3pytr)]^{2+}$	-1.77, -1.99, 2.43 [a]
$[Rh(phen)_2(1M3pytr)]^{3+}$	-1.11, -1.82, -2.05	$[Ru(phen)_2(1M3pytr)]^{2+}$	-

a = values taken from ref 23. Note: values quoted in ref 23 were obtained using differential pulse voltammetry and are quoted vs. SCE. Conversion constants given in ref 20 were used to convert SCE values to V Fc/Fc^+.

The CV's (a) and DPV's (b) obtained for the complexes $[Rh(phen)_2(Phpytr)]^{2+}$ and $[Rh(bpy)_2(Phpytr)]^{2+}$ can be seen in Figure 4.26 and Figure 4.27.

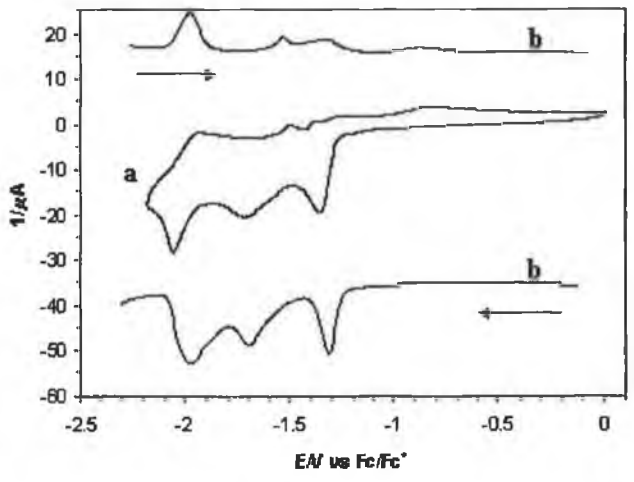

Figure 4.26 CV (a) and DPV (b) of $[Rh(phen)_2(Phpytr)]^{2+}$ measured in acetonitrile with 0.1M $TBABF_4$.

The CV of $[Rh(phen)_2(Phpytr)]^{2+}$ again shows three reduction waves all of which are irreversible. The CV of $[Rh(bpy)_2(Phpytr)]^{2+}$ is much more clearly defined and the second reduction wave is quasi reversible in nature with a peak potential separation of 70mV.

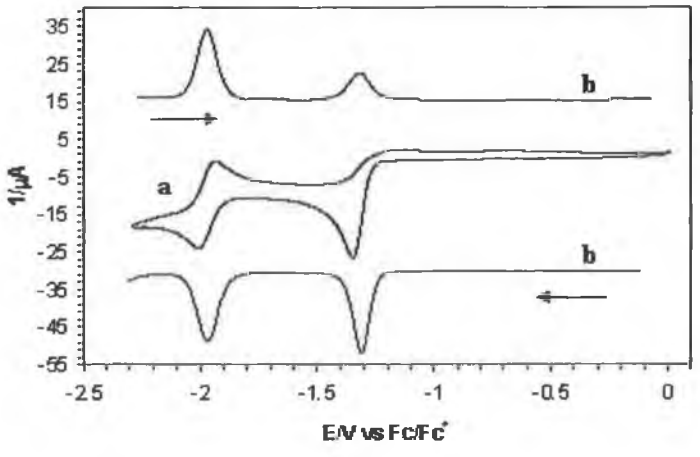

Figure 4.27 CV (a) and DPV (b) of $[Rh(bpy)_2(Phpytr)]^{2+}$ measured in acetonitrile with 0.1M $TBABF_4$.

The behaviour of $[Rh(bpy)_2(Phpytr)]^{2+}$ is quite similar to that of $[Rh(bpy)_2(pytr)]^{2+}$ with only two reduction waves being observed in both cases whereas it was possible to detect a third reduction wave in the case of the methylated complexes. It is anticipated that this third reduction wave occurs for $[Rh(bpy)_2(Phpytr)]^{2+}$ and $[Rh(bpy)_2(Phpytr)]^{2+}$ at a more negative potential which was not possible to measure under the conditions used.

Figure 4.28 illustrates the CV's (a) and DPV (b) obtained for the complex $[Rh(phen)_2(bpt)]^{2+}$. It should be noted that the main picture in Figure 4.28 was obtained from the first scan and the inset demonstrates the changes observed for three successive scans.

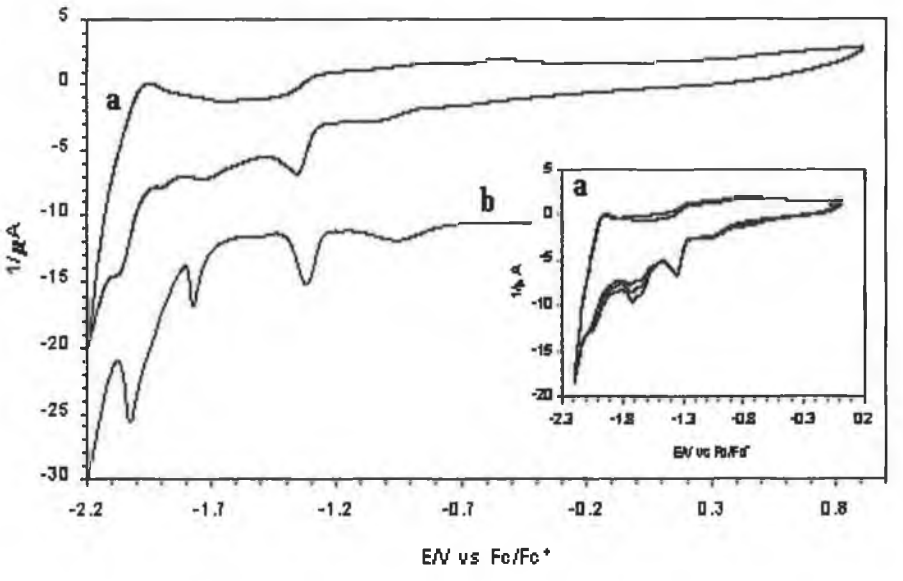

Figure 4.28 CV's (a) and DPV (b) of $[Rh(phen)_2(bpt)]^{2+}$ measured in acetonitrile with 0.1M $TBABF_4$. Inset shows CV's of $[Rh(phen)_2(bpt)]^{2+}$ with successive scanning.

In Figure 4.28 the first two reduction waves of the CV are irreversible and whilst the third reduction wave does appear to have a corresponding oxidation wave in the reverse scan but the peak potential separation was found to be 130mV and therefore this reduction is also deemed to be irreversible. It can be seen that the CV changes with successive scanning with what appears to be two waves at -1.66V and -1.72V

become more prominent with each scan. It is not known what species is responsible for this behaviour. The reduction potentials for $[Rh(phen)_2(bpt)]^{2+}$ are detailed in Table 4.4.

The CV (a) and DPV's (b) obtained for $[Rh(bpy)_2(bpt)]^{2+}$ can be seen in Figure 4.29. Again the CV exhibited here was the first of three scans.

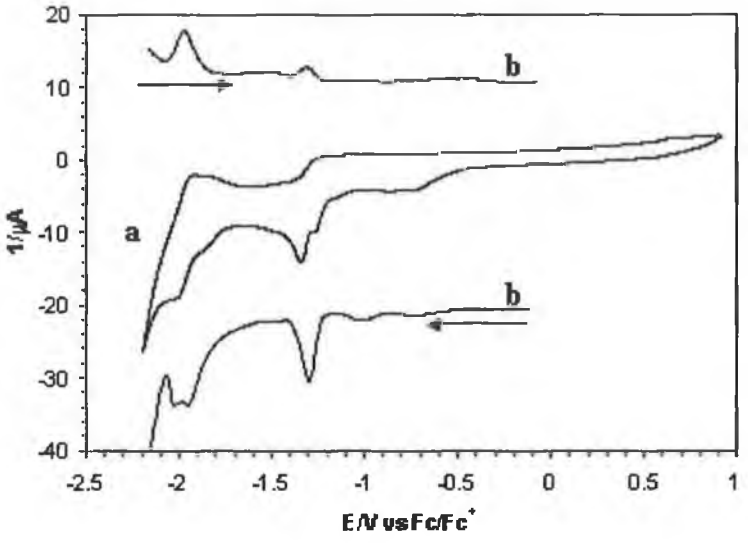

Figure 4.29 CV (a) and DPV's (b) of $[Rh(bpy)_2(bpt)]^{2+}$ measured in acetonitrile with 0.1M $TBABF_4$.

In this, the first scan, the first reduction wave appears to consist of two waves with some degree of resolution being seen between the two waves. In subsequent scans the smaller wave cannot be seen and it is assumed that the wave observed in these cases are composite waves. Analysis of the CV in the region –1.80V to –2.10V reveals signs of two further reduction waves although they are not very well defined.

Figure 4.30 illustrates CV (a) and DPV's (b) obtained for $[Rh(phen)_2(NHbpt)]^{2+}$. In comparison to the CV's discussed so far, where many of the reduction waves observed were thought to be composite waves, the CV of $[Rh(phen)_2(NHbpt)]^{2+}$ exhibits reduction waves at -1.37V, -1.46V, -1.69V, -1.83V and -2.06V . Unlike any of the complexes discussed previously there appears to be an oxidation wave present in the CV of $[Rh(phen)_2(NHbpt)]^{2+}$ at 0.77V the presence

of which is more evident in the DPV of the complex. Such an oxidation wave is also present in the analogous bpy complex $[Rh(bpy)_2(NHbpt)]^{2+}$, Appendix IV, but is not present for the complex $[Rh(bpy)_2(NH_2bpt)]^{3+}$. The exact nature of these waves is not understood however it is likely that there are associated with the NH_2 moiety with oxidation of the free ligand NH_2bpt having been observed previously at 1.42V.[24]

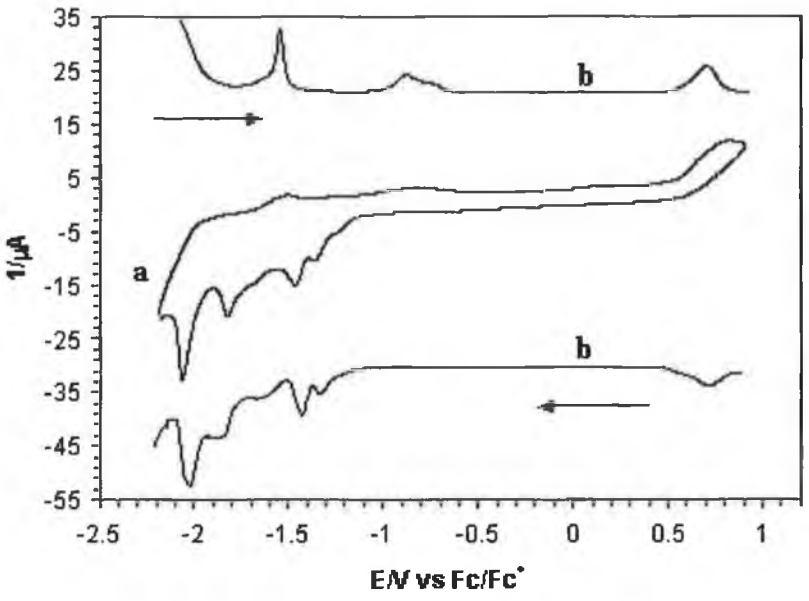

Figure 4.30 CV (a) and DPV's (b) of $[Rh(phen)_2(NHbpt)]^{2+}$ measured in acetonitrile with 0.1M $TBABF_4$.

Whilst the CV of $[Rh(bpy)_2(NHbpt)]^{2+}$, Appendix IV, is not as well defined as that of its phen analogue and it can be seen that both reduction waves detected are irreversible and it can be seen that a second oxidation wave is present when scanned to a higher potential. As detailed in Chapter 3, it was not possible to isolate $[Rh(phen)_2(NH_2bpt)]^{3+}$ but it was possible to isolate the bpy analogue and the CV of $[Rh(bpy)_2(NH_2bpt)]^{3+}$ can be seen in Figure 4.31. Four reduction waves can easily be identified at -1.11V (I), -1.22V (II), -1.76V (III), and -2.03V (IV). As was seen for $[Rh(bpy)_2(bpt)]^{2+}$ the first two irreversible reduction waves of $[Rh(bpy)_2(NH_2bpt)]^{3+}$, (I) and (II) in Figure 4.31, appear quite closely spaced and partially overlap. All of the bpy based complexes discussed so far, with the exception of $[Rh(bpy)_2(bpt)]^{2}$,

showed only a single wave in this region that was thought to be a composite wave. The resolution to some extent of these two waves in the CV's of $[Rh(bpy)_2(bpt)]^{2+}$ and $[Rh(bpy)_2(NH_2bpt)]^{3+}$ here confirms this conclusion. Both reduction waves (III) and (IV) have corresponding oxidation waves in the reverse scan and these reduction processes are quasi-reversible with peak potential separations of 100mV and 92mV being observed between the cathodic and anodic peaks of (III) and (IV) respectively.

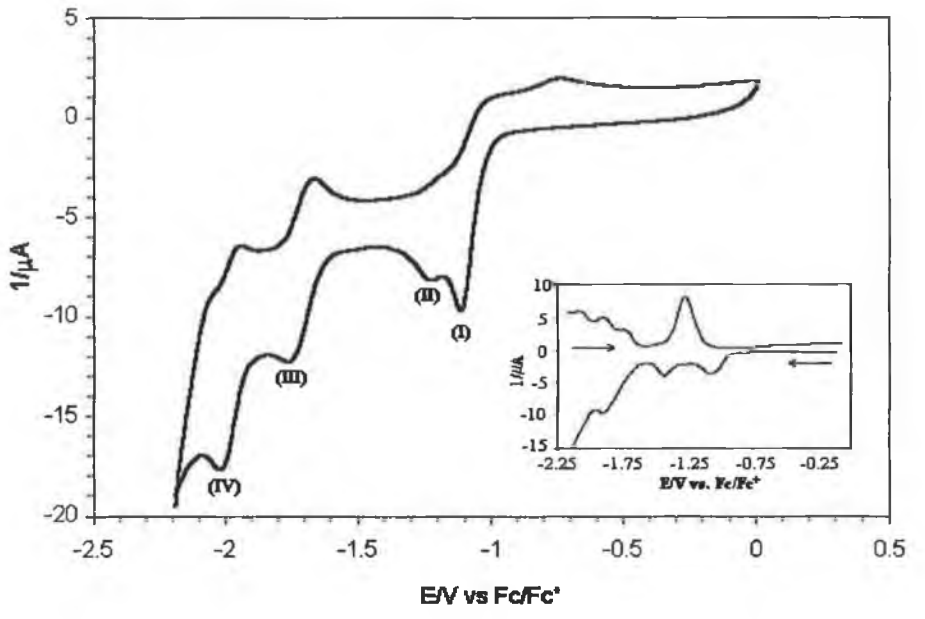

Figure 4.31 CV and inset the DPV's of $[Rh(bpy)_2(NH_2bpt)]^{3+}$ measured in acetonitrile with 0.1M $TBABF_4$.

4.3 Conclusions

The photophysical and electrochemical properties of the pyridine triazole complexes introduced in Chapter 3 have been investigated in this chapter. From a photophysical viewpoint these complexes have demonstrated very interesting properties particularly with respect to their emissive behaviour. Analysis of their absorption spectra indicated, in addition to the very apparent π-π^* transitions indicative of these types of complexes, that weak absorption bands were also present for several of the complexes studied. These weak absorption bands were tentatively assigned as d-d* transitions but further analysis of these is necessary. The emissive behaviour of the pyridine triazole complexes differed from that exhibited by the tris homoleptic complexes $[Rh(phen)_3]^{3+}$ and $[Rh(bpy)_2]^{3+}$ with almost all complexes exhibiting a dual emission with the difference between the excited state lifetimes of the emitting state being sufficient to allow the acquisition of well resolved spectra. The dual emitting behaviour was found to be related to the increasing σ strength of the pyridyl triazole ligands with respect to the bpy and phen ligands and the emitting states were attributed to π-π^* and d-d* based transitions. Evidence was found to show that these d-d* emissions were influenced by the charge of the triazole moiety with emissions being shifted to lower energies when a negative charge was located on the triazole moiety. The influence of the pyridyl triazole ligands upon these d-d* states was also apparent from analysis of their excited state lifetimes as an increase in their excited state lifetimes was observed when the triazole ligand was deuterated. Of the complexes studied only the complex $[Rh(phen)_2(NHbpt)]^{2+}$ did not exhibit a metal based emission. This particular complex was shown to be quite different structurally from the other complexes and it is probable that the absence of a metal based emission in this case is related to this.

From an electrochemical viewpoint it was generally found that complexes incorporating pyridine triazole ligands have more negative reduction potentials than their related tris homoleptic complexes. This is due to the greater σ donor strength of the pyridine triazole ligands particularly when deprotonated. The effect of the negative charge on the triazole ring can be seen when the reduction potentials of the

Hpytr complexes are compared with those of the 4Mpytr, 1M3pytr and NH_2bpt where the metal centre is coordinated via the N2' position of the triazole ring. These complexes exhibit more positive reduction potentials than the deprotonated complexes. Studies of the electrochemical behaviour of Ru(II) pyridyl triazole complexes found evidence that the pyridine triazole ligands act as better σ donors when the metal centre is bound via the N2' position as opposed to N4' coordination. A similar behaviour was observed as when compared $[Rh(bpy)_2(4Mpytr)]^{3+}$, which is coordinated via the N2' position, exhibits a reduction potential 120mV more negative than $[Rh(bpy)_2(1M3pytr)]^{3+}$ which is coordinated via the N4' position of the triazole ring.

It can be seen form these studies that the properties of these types of complexes are strongly dependent upon the σ donor / π acceptor properties of the incorporated ligands. The following chapters will detail how this behaviour was explored further by synthesising complexes of the form $[Rh(L)_2(L')]^{n+}$ where L = phen / bpy, L' = pyrazine, triazine, imidazole and triazole ligands with varying σ donor / π acceptor properties and n = 2/3. The behaviour of the pyridine triazole complexes detailed in this chapter will be discussed further in Chapter 8 where they will also be compared with the pyrazine, triazine, imidazole based complexes which will be discussed in Chapters 5 and 6.

References:

1 J.R. Lakowicz, *Principles of Fluorescence Spectroscopy*, **1984**, Plenum Press, New York.

2 P.Suppan, *Chemistry and Light*, **1994**, The Royal Society of Chemistry, Cambridge.

3 M.K. DeArmond, J.E. Hillis, *J. Chem. Phys.*, **1971**, *54*, 2247-2253.

4 D.H.W. Carstens, G.A. Crosby, *J. Mol. Spec.*, **1970**, *34*, 113-135.

5 M. Gerloch, E.C. Constable, *Transition Metal Chemistry – The Valence Shell in d-Block Chemistry,* **1994,** VCH Publishers, Weinheim & New York.

6 E. Kober, B. P. Sullivan and T. J. Meyer, *Inorg. Chem.*, **1984**, *23*, 2098-2014.

7 G.A. Crosby, W.H. Elfring Jr., *J. Phys. Chem.*, **1976**, *80*, 2206-2211.

8 R.J. Watts, J. Van Houten, *J. Am. Chem. Soc.*, **1978**, *100*, 1718-1721.

9 M.T. Indelli, F. Scandola, *Inorg. Chem.*, **1990**, *29*, 3056-3058.

10 M. Nishizawa, T.M. Suzuki, S. Sprouse, R.J. Watts, P.C. Ford, *Inorg. Chem.*, **1984**, *23*, 1837-1841.

11 R.J. Watts, J. Van Houten, *J. Am. Chem. Soc.*, **1978**, *100*, 1718-1721.

12 K. Kalyanasundaram, *Photochemistry of Polypyridine and Porphyrin Complexes*, **1992**, Academic Press, London.

13 W.R. Browne, J.G. Vos, *Coord. Chem. Rev.*, **2001**, *219-221*, 761-787.

14 H. Miki, M. Shimada, T. Azumi, J.A. Brozik, G.A. Crosby, *J. Phys. Chem.*, **1993**, *97*,11175-11179.

15 W. Humbs, H. Yersin, *Inorg. Chem.*, **1996**, *35*, 2220-2228, Giesbergen, M. Glasbeek, *J. Phys. Chem.*, **1993**, *97*, 9942-9946.

16 **Website;** chem.ch.huji.ac.il/~eugeniik/faq.htm.

17 C.M.A. Brett, A.M.O. Brett, *Electrochemistry – Principles, Methods and Applications*, **1993**, Oxford University Press, New York.

18 H.H. Willard, L.L. Merritt Jr., J.A. Dean, F.A. Settle Jr., *Instrumental Methods of Analysis*, *Seventh Edition*, **1988**, Wadsworth Inc., California.

19 A.E. Kaifer, M. Gomez-Kaifer, *Supramolecular Electrochemistry*, **1999**, Wiley-VCH, Weinheim (Federal Republic of Germany).

20 V.V. Pavlishchuk, A.W. Addison, *Inorg. Chim. Acta*, **2000**, *298*, 97-102.

21 G. Kew, K. Hanck, K. DeArmond, *J. Phys. Chem.*, **1975**, *79*, 1828-1835.

22 G. Kew, K. DeArmond, K. Hanck, *J. Phys. Chem.*, **1974**, *78*, 727-734.

23 R. Hage, *Ph.D. Thesis*, Leiden University, The Netherlands, **1991**.

24 G. Calegero, G. Giuffrida, S. Serroni, V. Ricevuto, S. Campagna, *Inorg. Chem.*, **1995**, *34*, 541-545.

Chapter 5 - Synthesis and of Rh(III) complexes with Pyrazine, Triazine and Imidazole Ligands.

"Science is a wonderful thing if one does not have to earn one's living at it."
Albert Einstein

Abstract: Having developed the synthesis of Rh(III) complexes incorporating pyridyl triazole ligands it was of interest to see how variation of these ligands would affect the behaviour of these complexes. The following chapter details the synthesis, purification and characterisation of a series of complexes incorporating not only pyrazine triazole based ligands but also triazine and imidazole based ligands. From a synthetic viewpoint complexes incorporating triazine and imidazole based ligands required shorter reaction times and gave higher yields than pyridine or pyrazine based complexes. NMR spectroscopy proved to be invaluable in the characterisation of these complexes particularly for complexes incorporating the 3-(pyrazin-2-yl)-5-(pyridin-2yl)-1,2,4-triazole (Hppt) ligand. For Hppt, coordination is possible via either the N2′ or the N4′ of either the pyridine ring or the pyrazine ring. Analysis of the ^{1}H NMR spectra of Hppt complexes established that coordination occurs predominantly via the pyridine ring.

5.1 Introduction

Fine-tuning, of the ground state and the excited state properties of rhodium(III) polypyridyl complexes, by modification of the π-acceptor and σ-donor properties of ligands was introduced in Chapters 1 and 3. Chapter 3 focused on heteroleptic complexes of the form $[Rh(L)_2(L')]^{n+}$ where L = bpy or phen, n = 2 or 3 and L' was a pyridine triazole based ligand which was comprised of a combination of a Class I and a Class II ligand. It was of interest to determine the effects on the ground state and excited state properties upon modification of the L' ligand and with this in mind a series of complexes were studied incorporating ligands with various Class I and Class II ligands, Figure 5.1. The first approach undertaken to modify the properties of the complexes studied in Chapter 3 was to replace the pyridine ring of the pyridine triazole ligand with a pyrazine ring. Bipyrazine is known to be a weaker σ-donor than bipyridine and as a result it is expected that the there would be significant differences between the properties of complexes containing pyridine triazole ligands and pyrazine triazole ligands.[1] As in the case of the pyridyl triazole ligands the analogous pyrazine triazole ligands display both better π-acceptor properties which are resultant from the pyrazine ring and good σ-donating properties due to the presence of the triazole ring.

The issue of coordination modes arises once again with the pyrazine triazole complexes. In the case of the ruthenium bpy complex with the unsubstituted 3-(pyrazin-2-yl)-1,2,4-triazole (Hpztr) ligand, only a single isomer was initially isolated but a later report established the formation of both the N2' and the N4' isomers in the approximate ratio 1:1.[2,3] From a ^{1}H NMR perspective significant differences have been observed in the spectra of the N2' and N4' isomers of $[Ru(bpy)_2(pztr)]^+$. As was the case for the analogous pyridine triazole complexes, when the metal ion is bound via the N4' of the triazole ring the H5' is in the vicinity of an adjacent bpy ligand thus giving rise to an upfield shift. In contrast when the metal is coordinated via the N2' of the triazole ring the H5' proton is no longer affected by a bpy ligand. Thus identification of the H5' proton within the ^{1}H NMR spectrum can allow for the determination of the mode of coordination within the

complex. The ligands, which will be cited in the following discussion, can be seen in Figure 5.1.

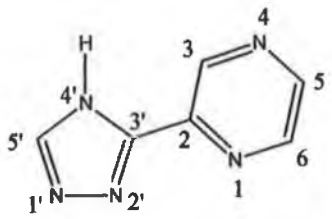

Hpztr - 3-(pyrazin-2-yl)-1,2,4-triazole

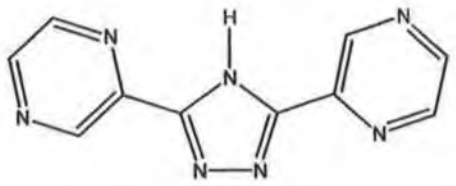

Hbpzt - 3,5-bis(pyrazin-2-yl)-1,2,4-triazole

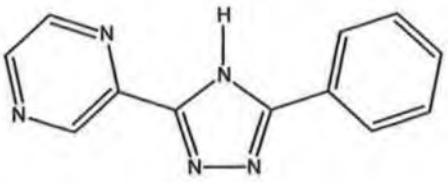

HPhpztr - 3-phenyl-5-(pyrazin-2-yl)-1,2,4-triazole

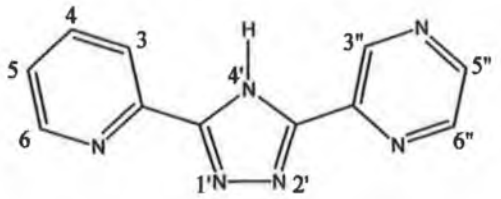

Hppt - 3-(pyrazin-2-yl)-5-(pyridin-2-yl)-1,2,4-triazole

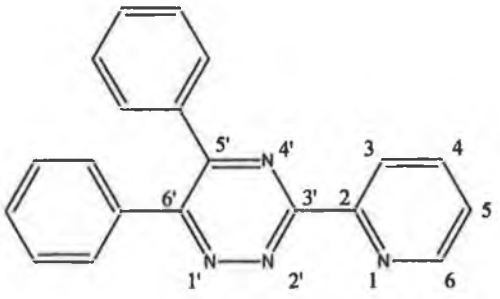

dppt - 5,6-diphenyl-3-(pyridin-2-yl)-1,2,4-triazine

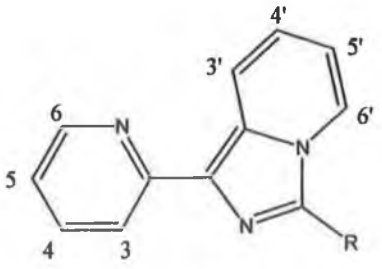

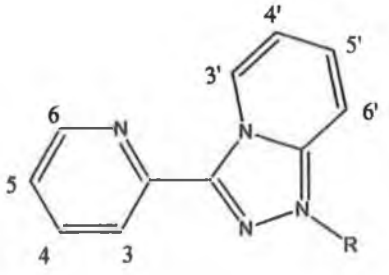

PIP - R=H, 1-pyridin-2-yl-imadazo-[1,5-a]-pyridine
MePIP - R=CH_3, 3-methyl-pyridin-2-yl-imadazo-[1,5-a]-pyridine

PTP - 3-pyridin-2-yl-triazolo-[4,3-a]-pyridine

Figure 5.1 Ligands cited in this chapter.

Triazine based ligands are known to be stronger π – acceptors and weaker σ-donors than bpy and Rh(III) complexes incorporating ligands such as tptz = 2,4,6-tris(pyridin-2-yl)-1,3,5-triazine and tpt = 3,4,6-tris(pyridin-2-yl)-1,2,5-triazine have been studied previously.[4,5,6,7,8] The ligand dppt - 5,6-diphenyl-3-(pyridin-2-yl)-1,2,4-triazine was selected for this study as Ru(II) analogues had previously been prepared and characterised.[8,9] ^{1}H NMR spectra of complexes with dppt are quite complicated and as a result complexes with the deuterated ligand d_{10}-dppt were also prepared. It should be noted that for the ligand d_{10}-dppt it is the protons of the phenyl rings which have been deuterated. It can be seen in Figure 5.1 that the dppt ligand has two possible coordination sites. Although the metal centre may coordinate via either the N2' or the N4' of the triazine ring and the nitrogen of the pyridine ring it is expected that the N2' isomer is formed for steric reasons.

Imidazole based ligands are further examples of strongly σ-donating ligands and whilst several ruthenium(II) biimidazole and bibenzimidazole complexes have been reported in recent years, very few rhodium complexes incorporating such ligands have been developed. One such case will be discussed in Chapter 7 where dinuclear complexes of Ru, Rh and Os containing the ligand 2,2'-bis(2-pyridyl)-6,6'-bibenzimidazole were investigated.[10] For the purpose of this study a series of complexes were prepared using the novel ligands PIP, MePIP and PTP, the structures of which can be seen in Figure 5.1. It can be seen that both PIP and MePIP are imidazole based whereas the ligand PTP is structurally similar to PIP and MePIP but the imidazole ring has been replaced with a triazole moiety. It is expected that the behaviour of complexes with the PTP ligand will differ significantly from those with PIP and MePIP and it is also of interest to compare the behaviour of the complexes with the PTP ligand with those incorporating pyridine triazole based ligands.

The following chapter is devoted to the synthesis and the structural characterisation of complexes of the type $[Rh(L)_2(L')]^{n+}$ where L = bpy or phen, L' = Hpztr – 3-(pyrazine-2-yl)-1,2,4-triazole, Hbpzt – 3,5-bis(pyrazine-2-yl)-1,2,4-triazole, HPhpztr – 3-phenol-5-(pyrazine-2-yl)-1,2,4-triazole, Hppt – 3-(pyrazin-2-

yl)-5-(pyridin-2-yl)-1,2,4-triazole n = 2 and when M = dppt – 5,6-diphenyl-3-(pyridin-2-yl)-1,2,4-triazine, PIP – 1-pyridin-2-yl-imidazo-[1,5-a]-pyridine, MePIP – 3-methyl-pyridin-2yl-imidazo-[1,5-a]-pyridine and PTP 3-pyridin-2-yl-triazolo-[4,3-a]-pyridine n = 3.

5.2 Experimental

It should be noted that Prof. Manfred Doering kindly provided the ligands PIP, MePIP and PTP.

5.2.1 Preparation of Rhodium(III) Complexes

$[Rh(phen)_2(pztr)][PF_6]_2$

0.053 g (0.4mmol) of 3-(pyrazin-2-yl)-1,2,4-triazole (Hpztr) were dissolved in 30cm^3 water:ethanol 2:1 and to this, over a period of an hour, 0.099g (0.2mmol) of $[Rh(phen)_2Cl_2]Cl$ were added. This reaction mixture was then heated to reflux for 72 hours. The ethanol was then evaporated off and the remaining solution was loaded onto a Sephadex C-25 ion exchange column. Excess ligand was eluted using distilled water and the required complex was eluted with 0.2M NaCl. The 0.2M was fraction was then reduced to approximately 15cm^3 and the product was then isolated as a PF_6^- salt by adding aqueous NH_4PF_6. A white powder was obtained with a yield of 0.018g (14%) but when analysed proved not to be the pure complex. The synthesis was repeated but the pure complex was not isolated.

$[Rh(bpy)_2(pztr)][PF_6]_2 \cdot H_2O \cdot NaCl$

0.057g (0.4mmol) of 3-(pyrazin-2-yl)-1,2,4-triazole (Hpztr) were dissolved in 30cm^3 water:ethanol 2:1 and to this, over a period of an hour, 0.101g (0.2mmol) of $[Rh(bpy)_2Cl_2]Cl$ were added. This reaction mixture was then heated to reflux for 24 hours. The ethanol was then evaporated off and the remaining solution was loaded onto a Sephadex C-25 ion exchange column. Excess ligand was eluted using

distilled water and the required complex was eluted with 0.1M NaCl. The 0.1M fraction was then reduced to approximately 15cm^3 and the complex was then isolated as a PF_6^- salt by adding aqueous NH_4PF_6. A white powder was obtained with a yield of 0.111g (62%). Analysis found: C, 33.52; H, 2.24; N, 13.70. Calculated for $[Rh(bpy)_2(pztr)][PF_6]_2 \cdot H_2O \cdot NaCl$: C,33.66; H,2.39; N,13.59.

$[Rh(phen)_2(bpzt)][PF_6]_2 \cdot 2H_2O$

0.089g (0.4mmol) of 3,5-bis(pyrazin-2-yl)-1,2,4-triazole (Hbpzt) were dissolved in 20cm of water pH ~9 and to this, over a period of an hour, 0.098g (0.17 mmol) of $[Rh(phen)_2Cl_2]Cl$ were added. This reaction mixture was then heated to reflux for 48 hours and the reaction mixture was then allowed to cool and some excess ligand precipitated. The reaction mixture was then filtered and loaded onto a Sephadex C-25 ion exchange column. Remaining excess ligand was eluted using distilled water and the required complex was eluted with 0.2M NaCl. The 0.2M was fraction was then reduced to approximately 15cm^3 and the complex was then isolated as a PF_6^- salt by adding aqueous NH_4PF_6. A white powder was obtained with a yield of 0.062g (36%). Analysis found: C, 40.53; H, 2.23; N, 15.22. Calculated for $[Rh(phen)_2(bpzt)][PF_6]_2 \cdot 2H_2O$: C, 40.29; H, 2.59; N, 15.20.

$[Rh(bpy)_2(bpzt)][PF_6]_2$

0.670g (0.mmol) of 3,5-bis(pyrazin-2-yl)-1,2,4-triazole (Hbpzt) were dissolved in 30cm^3 water:ethanol 2:1 and to this, over a period of an hour, 0.101g (0.mmol) of $[Rh(bpy)_2Cl_2]Cl$ were added. This reaction mixture was then heated to reflux for 48 hours after which it was allowed to cool to room temperature. The reaction mixture was then filtered and loaded onto a Sephadex C-25 ion exchange column. Excess ligand was eluted using distilled water and the main band was eluted with 0.2M NaCl. The 0.2M fraction was then reduced to approximately 15cm^3 and the complex was then isolated as a PF_6^- salt by adding aqueous NH_4PF_6. The pure complex was not however isolated.

$[Rh(phen)_2(Phpztr)][PF_6]_2 \cdot H_2O \cdot NaCl$

0.065g (0.3mmol) of 3-phenyl-5-(pyrazin-2-yl)-1,2,4-triazole (HPhpztr) were dissolved in 30cm^3 water:ethanol 2:1 and to this, over a period of an hour, 0.075g (0.13mmol) of $[Rh(phen)_2Cl_2]Cl$ were added. This reaction mixture was then heated to reflux overnight. The ethanol was then evaporated off and the remaining solution was loaded onto a Sephadex C-25 ion exchange column. Excess ligand was eluted using distilled water and the required complex was eluted with 0.2M NaCl. The 0.2M fraction was then reduced to approximately 15cm^3 and the complex was then isolated as a PF_6^- salt by adding aqueous NH_4PF_6. A yellow powder was obtained with a yield of 0.078g (56%). Analysis found: C, 40.94; H, 2.37; N, 11.65. Calculated for $[Rh(phen)_2(Phpztr)][PF_6]_2 \cdot H_2O \cdot NaCl$: C, 41.14; H, 2.40; N, 12.00.

$[Rh(bpy)_2(Phpztr)][PF_6]_2 \cdot H_2O$

0.392g (1.7mmol) of 3-phenyl-5-(pyrazin-2-yl)-1,2,4-triazole (HPhpztr) were dissolved in 30cm^3 water:ethanol 2:1 and to this, over a period of an hour, 0.302g (0.6mmol) of $[Rh(bpy)_2Cl_2]Cl$ were added. This reaction mixture was then heated to reflux overnight. The solvent was then evaporated off and the residue was dissolved in 10cm^3 of water and the complex was then isolated as a PF_6^- salt by adding aqueous NH_4PF_6. The solid obtained was filtered and dried and purification was carried out on a silica column using acetonitrile: water: KNO_3 in the ratio 40:10:1 as eluent. A yellow powder was obtained with a yield of 0.365g (65%). Analysis found: C, 40.48; H, 2.60; N, 13.25. Calculated for $[Rh(bpy)_2(Phpztr)][PF_6]_2 \cdot H_2O$: C, 40.65; H, 2.77; N, 13.33.

$[Rh(phen)_2(dppt)][PF_6]_3 \cdot 3NaCl$

0.122g (0.4mmol) of 5,6-diphenyl-3-(pyridin-2-yl)-1,2,4-triazine (dppt) were dissolved in 25cm^3 water:ethanol 4:1 and to this, over a period of an hour, 0.106g (0.2mmol) of $[Rh(phen)_2Cl_2]Cl$ were added. This reaction mixture was then heated to reflux overnight. The ethanol was then evaporated off and the remaining solution

was loaded onto a Sephadex C-25 ion exchange column. Excess ligand was eluted using distilled water and the required complex was eluted with 0.2M NaCl. The 0.2M fraction was then reduced to approximately 15cm^3 and the complex was then isolated as a PF_6^- salt by adding aqueous NH_4PF_6. A yellow powder was obtained with a yield of 0.177g (66%). Analysis found: C, 36.31; H, 1.97; N, 7.47. Calculated for $[Rh(phen)_2(dppt)][PF_6]_3 \cdot 4NaCl$: C,36.64 ; H,2.10 ; N,7.77.

$[Rh(bpy)_2(dppt)][PF_6]_3 \cdot 2H_2O$

0.128g (0.4mmol) of 5,6-diphenyl-3-(pyridin-2-yl)-1,2,4-triazine (dppt) were dissolved in 25cm^3 water:ethanol 4:1 and to this, over a period of an hour, 0.103g (0.2mmol) of $[Rh(bpy)_2Cl_2]Cl$ were added. This reaction mixture was then heated to reflux overnight. The solution was allowed to cool and the excess ligand was allowed to precipitate. The solution was filtered and tlc indicated that only the product complex was present. The solution was then reduced to approximately 15cm^3 and the complex was then isolated as a PF_6^- salt by adding aqueous NH_4PF_6. A yellow powder was obtained with a yield of 0.199g (85%). Analysis found: C, 39.96; H, 2.39; N, 9.19. Calculated for $[Rh(bpy)_2(dppt)][PF_6]_3 \cdot 2H_2O$: C,40.15; H, 2.86; N, 9.36.

$[Rh(phen)_2(ppt)][PF_6]_2 \cdot NaCl$

0.079g (0.35mmol) of 3-(pyridin-2-yl)-5-(pyrazine-2-yl)-1,2,4-triazole (Hppt) were dissolved in 25cm^3 water:ethanol 3:1 and to this, over a period of an hour, 0.101g (0.17mmol) of $[Rh(phen)_2Cl_2]Cl$ were added. This reaction mixture was then heated to reflux for 24 hours. The reaction was allowed to cool and the ethanol was then evaporated off and the remaining solution was loaded onto a Sephadex C-25 ion exchange column. Excess ligand was eluted using distilled water and the required complex was eluted with 0.2M NaCl. The 0.2M fraction was then reduced to approximately 15cm^3 and the complex was then isolated as a PF_6^- salt by adding aqueous NH_4PF_6. A white powder was obtained with a yield of 0.062g (34%).

Analysis found: C, 40.13; H, 2.26; N,13.37. Calculated for $[Rh(phen)_2(ppt)][PF_6]_2 \cdot NaCl$ C, 40.31; H, 2.22; N, 13.43.

$[Rh(bpy)_2(ppt)][PF_6]_2 \cdot NaCl$

0.078g (0.35mmol) of 3-(pyridin-2-yl)-5-(pyrazine-2yl)-1,2,4-triazole (Hppt) were dissolved in 30cm^3 water:ethanol 2:1 and to this, over a period of an hour, 0.091g (0.17mmol) of $[Rh(bpy)_2Cl_2]Cl$ were added. This reaction mixture was then heated to reflux for 24 hours. The ethanol was then evaporated off and the remaining solution was loaded onto a Sephadex C-25 ion exchange column. Excess ligand was eluted using distilled water and the required complex was eluted with 0.2M NaCl. The 0.2M was fraction was then reduced to approximately 15cm^3 and the complex was then isolated as a PF_6^- salt by adding aqueous NH_4PF_6. A white powder was obtained with a yield of 0.78g (45%). Analysis found: C, 37.11; H, 2.41; N, 13.95. Calculated for $[Rh(bpy)_2(ppt)][PF_6]_2 \cdot NaCl$: C, 37.42; H, 2.33; N, 14.08.

$[Rh(phen)_2(PIP)][PF_6]_3 \cdot NaCl$

0.060 (0.3mmol) of 1-pyridin-2-yl-imidazo-[1,5-a]-pyridine (PIP) were dissolved in 25cm^3 water:ethanol 4:1 and to this, over a period of an hour, 0.087g (0.15mmol) of $[Rh(phen)_2Cl_2]Cl$ were added. This reaction mixture was then heated to reflux for 3 hours. The ethanol was then evaporated off and the remaining solution was loaded onto a Sephadex C-25 ion exchange column. Excess ligand was eluted using distilled water and the required complex was eluted with 0.2M NaCl. The 0.2M was fraction was then reduced to approximately 15cm^3 and the complex was then isolated as a PF_6^- salt by adding aqueous NH_4PF_6. A pale yellow powder was obtained with a yield of 0.124g (72%). Analysis found: C, 37.35; H, 2.12; N, 8.47. Calculated for $[Rh(phen)_2(PIP)][PF_6]_3 \cdot NaCl$: C, 37.54 ; H, 2.19; N, 8.51.

$[Rh(bpy)_2(PIP)][PF_6]_2 \cdot 3NaCl$

0.101g (0.5mmol) of 1-pyridin-2-yl-imidazo-[1,5-a]-pyridine (PIP) were dissolved in 25cm^3 water:ethanol 4:1 and to this, over a period of an hour, 0.134g (0.25mmol) of

$[Rh(bpy)_2Cl_2]Cl$ were added. This reaction mixture was then heated to reflux for 3 hours. The ethanol was then evaporated off and the remaining solution was loaded onto a Sephadex C-25 ion exchange column. Excess ligand was eluted using distilled water and the required complex was eluted with 0.2M NaCl. The 0.2M fraction was then reduced to approximately $15cm^3$ and the complex was then isolated as a PF_6^- salt by adding aqueous NH_4PF_6. A pale yellow powder was obtained with a yield of 0.231g (74%). Analysis found: C, 31.02; H, 2.12; N, 7.81. Calculated for $[Rh(bpy)_2(PIP)][PF_6]_3 \cdot 3NaCl$: C, 31.28; H, 2.05; N, 7.98.

$[Rh(phen)_2(MePIP)][PF_6]_3 \cdot 2H_2O$

0.065g (0.2mmol) of 3-methyl-pyridin-2yl-imidazo-[1,5-a]-pyridine (MePIP) were dissolved in $25cm^3$ water:ethanol 4:1 and to this, over a period of an hour, 0.079g (0.14mmol) of $[Rh(phen)_2Cl_2]Cl$ were added. This reaction mixture was then heated to reflux for 3 hours. The solution was allowed to cool and the excess ligand was allowed to precipitate. The solution was filtered and tlc indicated that only the product complex was present. The solution was then reduced to approximately $15cm^3$ and the complex was then isolated as a PF_6^- salt by adding aqueous NH_4PF_6. A yellow powder was obtained with a yield of 0.125g (79%). Analysis found: C, 38.70; H, 2.28; N, 8.64. Calculated for $[Rh(phen)_2(MePIP)][PF_6]_3 \cdot 2H_2O$: C, 38.86; H, 2.73; N, 8.57.

$[Rh(bpy)_2(MePIP)][PF_6]_3 \cdot 2H_2O$

0.112g (0.4mmol) of 3-methyl-pyridin-2yl-imidazo-[1,5-a]-pyridine (MePIP) were dissolved in $25cm^3$ water:ethanol 4:1 and to this, over a period of an hour, 0.100g (0.2mmol) of $[Rh(bpy)_2Cl_2]Cl$ were added. This reaction mixture was then heated to reflux for 3 hours. The solution was allowed to cool and the excess ligand was allowed to precipitate. The solution was filtered and tlc indicated that only the product complex was present. The solution was then reduced to approximately $15cm^3$ and the complex was then isolated as a PF_6^- salt by adding aqueous NH_4PF_6. A yellow powder was obtained with a yield of 0.191g (91%). Analysis found: C,

35.99; H, 2.36; N, 8.97. Calculated for $[Rh(bpy)_2(PTP)][PF_6]_3 \cdot 2H_2O$: C, 36.18; H, 2.85; N, 8.95.

$[Rh(phen)_2(PTP)][PF_6]_3 \cdot NaCl$

0.196g (0.3mmol) of 3-pyridin-2-yl-triazolo-[4,3-a]-pyridine (PTP) were dissolved in 25cm^3 water:ethanol 4:1 and to this, over a period of an hour, 0.088g (0.15mmol) of $[Rh(phen)_2Cl_2]Cl$ were added. This reaction mixture was then heated to reflux for 3 hours. The ethanol was then evaporated off and the remaining solution was loaded onto a Sephadex C-25 ion exchange column. Excess ligand was eluted using distilled water and the required complex was eluted with 0.2M NaCl. The 0.2M fraction was then reduced to approximately 15cm^3 and the complex was then isolated as a PF_6^- salt by adding aqueous NH_4PF_6. A white powder was obtained with a yield of 0.127g (71%). Analysis found: C, 35.93; H, 1.95; N, 9.63. Calculated for $[Rh(phen)_2(PTP)][PF_6]_3 \cdot NaCl$: C, 35.90; H, 2.25; N, 9.57.

$[Rh(bpy)_2(PTP)][PF_6]_3 \cdot 2NaCl$

0.098g (0.5mmol) of 3-pyridin-2-yl-triazolo-[4,3-a]-pyridine (PTP) were dissolved in 25cm^3 water:ethanol 4:1 and to this, over a period of an hour, 0.131g (0.25mmol) of $[Rh(bpy)_2Cl_2]Cl$ were added. This reaction mixture was then heated to reflux overnight. The ethanol was then evaporated off and the remaining solution was loaded onto a Sephadex C-25 ion exchange column. Excess ligand was eluted using distilled water and the required complex was eluted with 0.2M NaCl. The 0.2M fraction was then reduced to approximately 15cm^3 and the complex was then isolated as a PF_6^- salt by adding aqueous NH_4PF_6. A white powder was obtained with a yield of 0.132g (45%). Analysis found: C, 31.54; H, 2.14; N, 9.48. Calculated for $[Rh(bpy)_2(PTP)][PF_6]_3 \cdot 2NaCl$: C, 31.79; H, 2.07; N, 9.57.

5.2.2 Preparation of Deuterated Rh(III) Complexes

It should be noted that deuterated dppt, d_{10}-dppt, was obtained from Ronald Hage and that it was the protons of the phenyl ring which were selectively deuterated.

$[Rh(phen)_2(d_{10}\text{-dppt})][PF_6]_3 \cdot NaCl$

0.057g (0.18mmol) of 5,6-diphenyl-3-(pyridin-2-yl)-1,2,4-triazine (d_{10}-dppt) were dissolved in 30cm^3 water:ethanol 2:1 and to this, over a period of an hour, 0.079g (0.14mmol) of $[Rh(phen)_2Cl_2]Cl$ were added. This reaction mixture was then heated to reflux overnight. The ethanol was then evaporated off and the remaining solution was loaded onto a Sephadex C-25 ion exchange column. Excess ligand was eluted using distilled water and the required complex was eluted with 0.2M NaCl. The 0.2M fraction was then reduced to approximately 15cm^3 and the complex was then isolated as a PF_6^- salt by adding aqueous NH_4PF_6. A yellow powder was obtained with a yield of 0.095g (54%). Analysis found: C, 41.58; H, 2.44; N, 8.58. Calculated for $[Rh(phen)_2(d_{10}\text{-dppt})][PF_6]_3 \cdot NaCl$: C, 41.71; H, 2.39; N, 8.84.

$[Rh(bpy)_2(d_{10}\text{-dppt})][PF_6]_3 \cdot NaCl$

0.050g (0.16mmol) of 5,6-diphenyl-3-(pyridin-2-yl)-1,2,4-triazine (d_{10}-dppt) were dissolved in 30cm^3 water:ethanol 2:1 and to this, over a period of an hour, 0.069g (0.13mmol) of $[Rh(bpy)_2Cl_2]Cl$ were added. This reaction mixture was then heated to reflux overnight. The ethanol was then evaporated off and the remaining solution was loaded onto a Sephadex C-25 ion exchange column. Excess ligand was eluted using distilled water and the required complex was eluted with 0.2M NaCl. The 0.2M was fraction was then reduced to approximately 15cm^3 and the complex was then isolated as a PF_6^- salt by adding aqueous NH_4PF_6. A yellow powder was obtained with a yield of 0.127g (78%). Analysis found: C, 39.74; H, 2.44; N, 9.18. Calculated for $[Rh(bpy)_2(d_{10}\text{-dppt})][PF_6]_3 \cdot NaCl$: C, 39.41; H, 2.48; N, 9.19.

[Rh(d_8-bpy)$_2$(PIP)][PF$_6$]$_3$

0.038g (0.02mmol) of 1-pyridin-2-yl-imidazo-[1,5-a]-pyridine (PIP) were dissolved in 25cm^3 water:ethanol 4:1 and to this, over a period of an hour, 0.51g (0.1mmol) of [Rh(d_8-bpy)$_2$Cl$_2$]Cl were added. This reaction mixture was then heated to reflux overnight. The ethanol was then evaporated off and the remaining solution was loaded onto a Sephadex C-25 ion exchange column. Excess ligand was eluted using distilled water and the required complex was eluted with 0.2M NaCl. The 0.2M fraction was then reduced to approximately 15cm^3 and the complex was then isolated as a PF_6^- salt by adding aqueous NH_4PF_6. A yellow powder was obtained with a yield of 0.060g (57%).

Note: method used for calculating C, H, N values of deuterated complexes is discussed in 2.11.

5.3 Results and Discussion

5.3.1 Synthetic Aspects

The starting materials $[Rh(bpy)_2Cl_2]Cl$ and $[Rh(phen)_2Cl_2]Cl$ were synthesised according to the literature as outlined in Chapter 3.[11] Section 5.2 showed that all of the complexes discussed in this chapter were synthesised in various ratios of water and ethanol. In general, when compared with the pyridine triazole complexes discussed earlier, the pyrazine triazole complexes required longer reaction times and gave lower yields. A similar behaviour was observed when the reaction times and yields of the analogous Ru(II) pyridine and pyrazine triazole complexes were compared.[12] Repeated synthesis of $[Rh(phen)_2(pztr)]^{2+}$and $[Rh(bpy)_2(bpzt)]^{2+}$ gave very low yields and after column chromatography neither complex was isolated in its pure form. It should also be noted that elemental analysis indicated that all of the pyrazine based complexes isolated were deprotonated. As was the case for the related pyridine triazole compounds the formation of coordination isomers is an important consideration in the synthesis and the analysis of the pyrazine triazole complexes. All of the pyrazine triazole complexes studied can coordinate via either the N2' or the N4' of the triazole ring with a nitrogen of the pyrazine ring and in the case of the ligand Hppt two further isomers were possible with the option of binding via the triazole ring with either the pyridine ring or the pyrazine ring. It should be noted that once in the same protonation state all of the isomers have the same charge. Because these complexes were purified using ion exchange chromatography and as this method of isolation is only dependent upon the charge of the complex it would be expected that, if formed, both isomers should be eluted at the same time and analysis of the ^{1}H NMR spectra of $[Rh(phen)_2(ppt)]^{2+}$ and $[Rh(bpy)_2(ppt)]^{2+}$ showed that two isomers were in fact obtained. For the complexes containing the ligands HPhpztr and Hbpzt studied only one isomer was observable in the ^{1}H NMR spectra whereas the presence of two isomers was clearly visible in the ^{1}H NMR spectra of the complexes $[Rh(phen)_2(ppt)]^{2+}$ and $[Rh(bpy)_2(ppt)]^{2+}$. The issue of isomer formation will be discussed in more detail in the Section 5.3.2.

Hage *et. al.* have previously reported a series of ruthenium(II) bpy complexes containing various substituted 3-(pyridin-2-yl)-1,2,4-triazines.[8] The synthesis of these complexes was typically carried out in $50cm^3$ ethanol:water 1:1 with reflux times in the region of 6 hours and yields of between 60% and 80% being reported. The complexes with the ligands dppt and tptz yielded a mixture of isomers, the isolation of which was not possible.[8] Rhenium and molybdenum complexes have also been synthesised with tptz.[13,14,15,16,17] The syntheses of the Re and Mo complexes were carried out at room temperature, whereas reflux in ethanol:water for approximately 21 hours was required for the synthesis of the ruthenium complex $[Ru(bpy)_2(tptz)](PF_6)_2$.[4] Purification by means of ion exchange chromatography on a Sephadex C-25 column proved effective with various concentration of NaCl being used as mobile phase for $[Ru(bpy)_2(tptz)](PF_6)_2$. Yields of between 60% and 90% were observed for these types of complexes. For the dppt ligand, as detailed in Section 5.2, reflux times of approximately 15 hours were required and high yields were obtained which were comparable to the yields observed for Ru(II) complexes with the same ligand.[18]

The synthesis of complexes with the ligands PIP, MePIP and PTP proved relatively straightforward. Complexes with these ligands required only very short reflux times, 2-4 hours, with yields of up to 95% being achieved with no discernable differences being observed when the synthetic conditions and yields of Rh(III) complexes with PIP, MePIP and PTP were compared with the analogous Ru(II) complexes.[19]

All complexes with the exception of $[Rh(bpy)_2(Phpztr)]^{2+}$ were purified by means of ion exchange chromatography using a Sephadex C-25 column and various concentrations of NaCl as eluent. As was the case for the pyridine triazole complexes elemental analysis showed the presence of excess NaCl from column chromatography in several of the complexes detailed in this chapter. It is important to note however that these excess salts did not affect subsequent measurements. $[Rh(bpy)_2(Phpztr)]^{2+}$ was purified using a silica column and using acetonitrile:water:KNO_3 in the ratio 40:10:1 as eluent.

5.3.2 ^{1}H NMR Spectroscopy

5.3.2.1 Complexes with pyrazine triazole based ligands.

Chapter 3 demonstrated how ^{1}H NMR spectroscopy coupled with 2-dimensional NMR techniques are valuable in the structural assignment of pyridine triazole complexes. The same techniques may be applied when studying the analogous pyrazine triazole complexes. Whilst ligand deuteration was necessary for the assignment of the ^{1}H NMR spectra of the pyridine triazole complexes it was not generally required to elucidate the ^{1}H NMR spectra of the pyrazine triazole complexes. It was possible in nearly all cases to determine a number of the resonances associated with either the bpy or the phen ligands by comparison with the analogous pyridine triazole complexes studied in Chapter 3. Once this had been achieved it was possible to assign the entire spectrum by analysis of the ^{1}H-^{1}H correlation spectrum.

5.3.2.1.1 $[Rh(phen)_2(pztr)]^{2+}$ and $[Rh(bpy)_2(pztr)]^{2+}$

Although the synthesis of $[Rh(phen)_2(pztr)]^{2+}$ was carried out a number of times it was not possible to isolate a sample of pure $[Rh(phen)_2(pztr)]^{2+}$. In each instance a mixture was obtained, which comprised of approximately 75% product and 25% $[Rh(phen)_2Cl_2]Cl$, after purification on both Sephadex C-25 and on silica. Whilst the ^{1}H NMR spectrum obtained contained unreacted starting materials it was possible to identify the peaks associated with the complex $[Rh(phen)_2(pztr)]^{2+}$. H5' was identified as a singlet at 8.52 ppm, H3 at 9.52 ppm, H5 at 8.63 ppm and H6 was found at 7.77 ppm, see Figure 5.1 for relevant ligand numbering. As has been discussed, the formation of isomers is a possibility for complexes containing pyridine or pyrazine triazole ligands. In the case of the complexes outlined in Chapter 3 no evidence was found for the formation of two isomers, based upon the absence of any minor signals which could be attributed to the presence of a second isomer and upon analysis of the integration of the ^{1}H NMR spectra, and it was concluded that only a single isomer was present in each case. As the pure complex

$[Rh(phen)_2(pztr)]^{2+}$ was not isolated, it was not possible to determine if a second isomer was present in the ^1H NMR spectra or to identify the coordination mode of the crude product obtained.

Spectrum (i) of Figure 5.2, illustrates the ^1H NMR spectra obtained for the complex $[Rh(bpy)_2(pztr)]^{2+}$. The singlet, which is clearly observable at 8.23 ppm may be attributed to the H5' of the triazole ring.

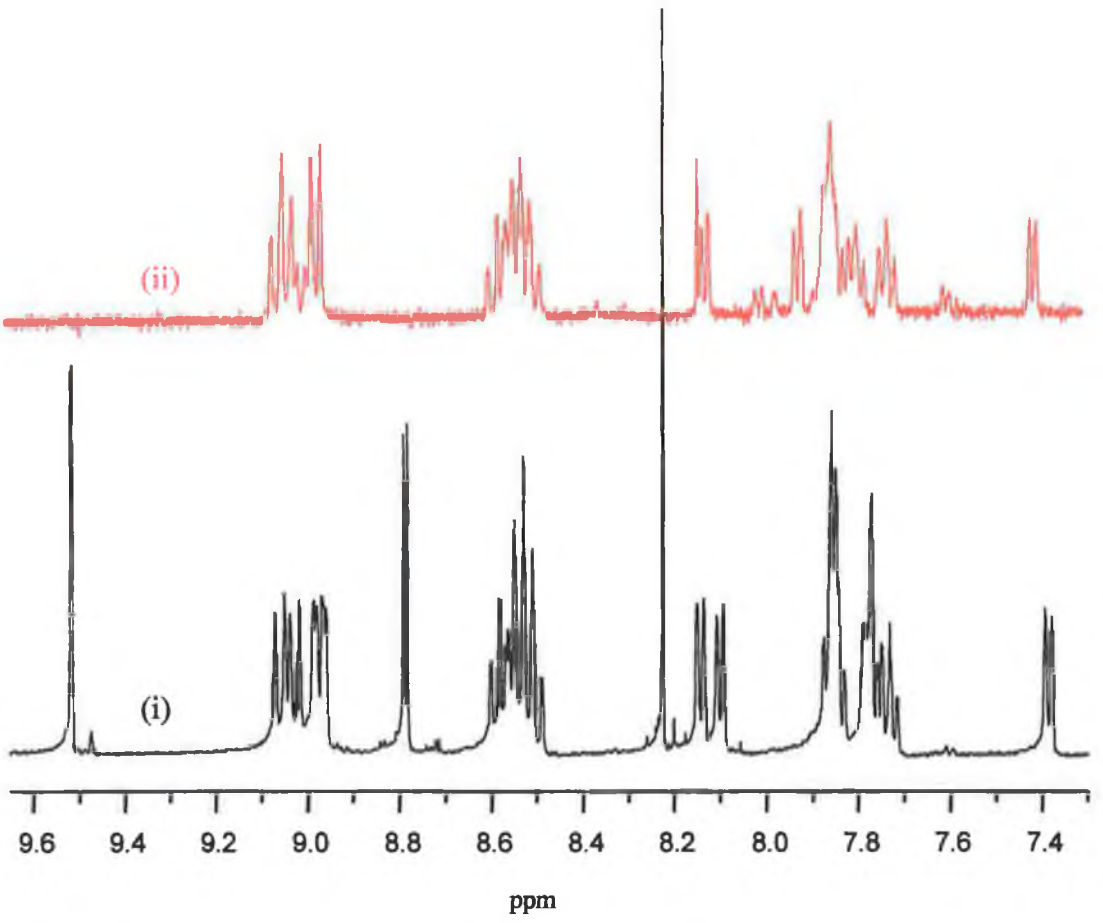

Figure 5.2 ^1H NMR spectra of (i) $[Rh(bpy)_2(pztr)]^{2+}$(——) and (ii) $[Rh(bpy)_2(d_4\text{-}pytr)]^{2+}$(——) in d_6-DMSO.

The assignment of the remainder of the spectrum was achieved through the study of the ^1H-^1H correlation spectrum of $[Rh(bpy)_2(pztr)]^{2+}$ and by comparison of the spectrum in Figure 5.2 with the analogous bpy pyridine triazole complexes discussed in Chapter 3. Deuteration of the complexes discussed in Chapter 3 allowed for the

unambiguous assignment of a number of bpy based complexes. It was found that the resonances of the bpy protons did not differ significantly between the complexes $[Rh(bpy)_2(pztr)]^{2+}$ and $[Rh(bpy)_2(pytr)]^{2+}$ as evidenced in Figure 5.2. In this instance the spectrum of $[Rh(bpy)_2(pztr)]^{2+}$ is compared with that of the analogous pyridine triazole complex $[Rh(bpy)_2(d_4\text{-pytr})]^{2+}$, Figure 5.2.

From Figure 5.2, the bpy protons can be readily identified making it possible to assign the H3, H5 and H6 protons of the pyrazine ring as follows; H3 - 9.52 ppm, H5 - 8.80 ppm (d) and H6 - 7.85 ppm (m). As was the case for $[Rh(phen)_2(pztr)]^{2+}$ a small peak can be seen in Figure 5.2 at 9.47 ppm. It is likely, however that the peak at 9.47 ppm is due to a ligand impurity as the H3 of the free ligand is expected at 9.47 ppm. There is also a peak at 8.71 ppm with a similar relative intensity to the peak at 9.47 ppm, which is the exact position where the peak of the H5 proton of the free ligand is expected.

5.3.2.1.2 $[Rh(phen)_2(Phpztr)]^{2+}$ and $[Rh(bpy)_2(Phpztr)]^{2+}$

Figure 5.3 and Figure 5.4 illustrate the ^1H NMR spectra of the complexes $[Rh(phen)_2(Phpztr)]^{2+}$ and $[Rh(bpy)_2(Phpztr)]^{2+}$. Both spectra integrate to 24 protons and no evidence was found to indicate the presence of a second isomer in either instance. The spectra were assigned as outlined in Table 5.1. Table 5.1 also allows the comparison of the complexes incorporating the ligands Hpztr and HPhpztr with those containing Hpytr and HPhpytr detailed in Chapter 3. It can be seen that the H3 proton is shifted downfield by 0.23 ppm with respect to the free ligand upon coordination for both $[Rh(phen)_2(Phpztr)]^{2+}$ and $[Rh(bpy)_2(Phpztr)]^{2+}$. In the case of the complex $[Rh(bpy)_2(Phpztr)]^{2+}$ the H5 proton is unaffected by binding of the metal centre whereas the same proton in $[Rh(phen)_2(Phpztr)]^{2+}$ is found 0.16 ppm upfield of the free ligand. As expected a significant upfield shift (approximately 1 ppm) of the H6 proton is observed upon coordination in both cases. In the absence of suitable crystals for x-ray crystallography it was not possible to determine which isomer was being formed in these cases.

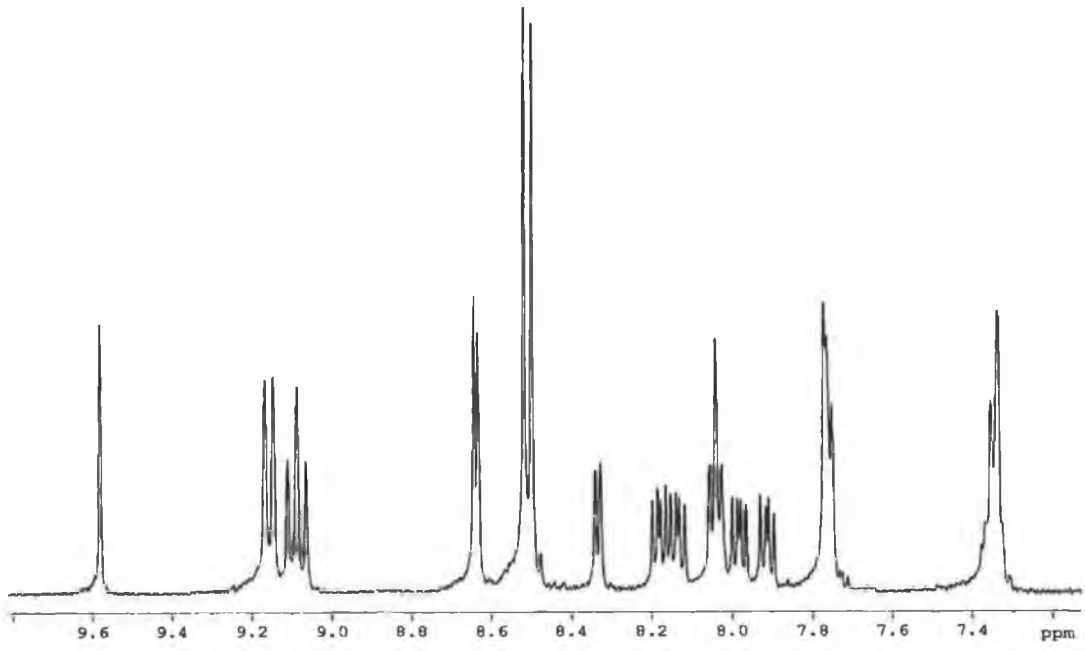

Figure 5.3 ^{1}H NMR spectrum of $[Rh(phen)_2(Phpztr)]^{2+}$ in d_6-DMSO.

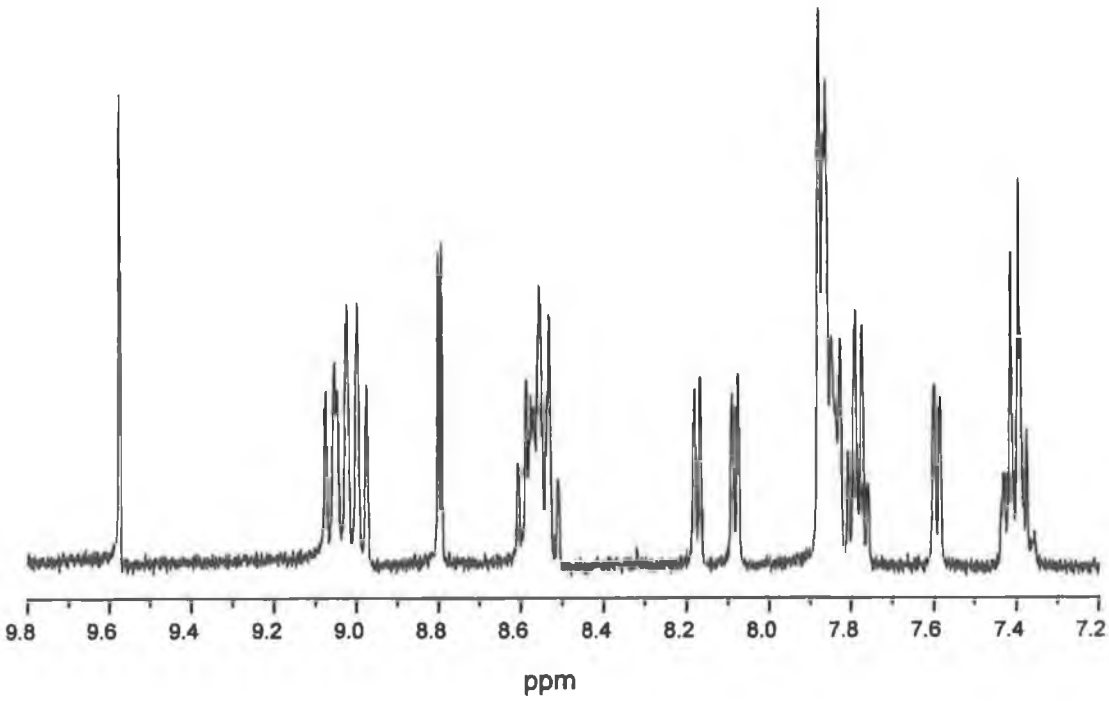

Figure 5.4 ^{1}H NMR spectrum of $[Rh(bpy)_2(Phpztr)]^{2+}$ in d_6-DMSO.

Table 5.1 ***^{1}H NMR data for the complexes $[Rh(L)_2(L')]^{2+}$,when L = phen, L' = Hpztr, Hpytr, HPhpztr and Phpytr and when L = bpy, L' = HPhpztr and Phpytr, and their related free ligands in d_6-DMSO.***

	H3 (ppm)	H4 (ppm)	H5 (ppm)	H6 (ppm)	H5'
Hpztr	9.27 (s)	-	8.76 (d)	8.72 (d)	8.58 (s)
$[Rh(phen)_2(pztr)]^{2+}$	9.52 (d)	-	8.63(m)	7.77(m)	8.52 (s)
Hpytr	8.09 (d)	7.98 (dd)	7.51 (dd)	8.70 (d)	8.27 (s)
$[Rh(phen)_2(pytr)]^{2+}$	8.33 (m)	8.33 (m)	7.46 (dd)	7.68 (d)	8.56 (s)
HPhpztr	9.35 (s)	-	8.80 (m)	8.77 (m)	-
$[Rh(phen)_2(Phpztr)]^{2+}$	9.58 (s)	-	8.64 (d)	7.77 (m)	-
$[Rh(bpy)_2(Phpztr)]^{2+}$	9.58 (s)	-	8.80 (d)	7.89-7.81(m)	-
HPhpytr	8.10 (d)	8.01 (dd)	7.49 (dd)	8.73 (d)	-
$[Rh(phen)_2(Phpytr)]^{+}$	8.36 (m)	8.36 (m)	7.47 (dd)	7.69 (d)	-
$[Rh(bpy)_2(Phpytr)]^{+}$	8.37 (m)	8.37 (m)	7.56 (dd)	7.75 (d)	-

5.3.2.1.3 *$[Rh(phen)_2(bpzt)]^{2+}$*

Figure 5.5 and Figure 5.6 illustrate the ^{1}H and ^{1}H-^{1}H COSY NMR spectra obtained for $[Rh(phen)_2(bpzt)]^{2+}$. By comparison with the phen complexes discussed in Chapter 3 it was possible to determine that the peaks at 9.20 ppm (d), 8.16-8.22 ppm (m), 8.01 ppm (dd) and 7.94 ppm (dd) were associated with the phen ligand. Close analysis of the ^{1}H-^{1}H correlation spectrum, seen in Figure 5.6, led to the assignment detailed in Table 5.2. It should also be noted that the spectrum of $[Rh(phen)_2(bpzt)]^{2+}$ integrates to 22 protons as expected and no evidence was found to suggest the formation of a second isomer in this case. The ^{1}H NMR data obtained for all of the pyrazine-based complexes can be seen in Table 5.2.

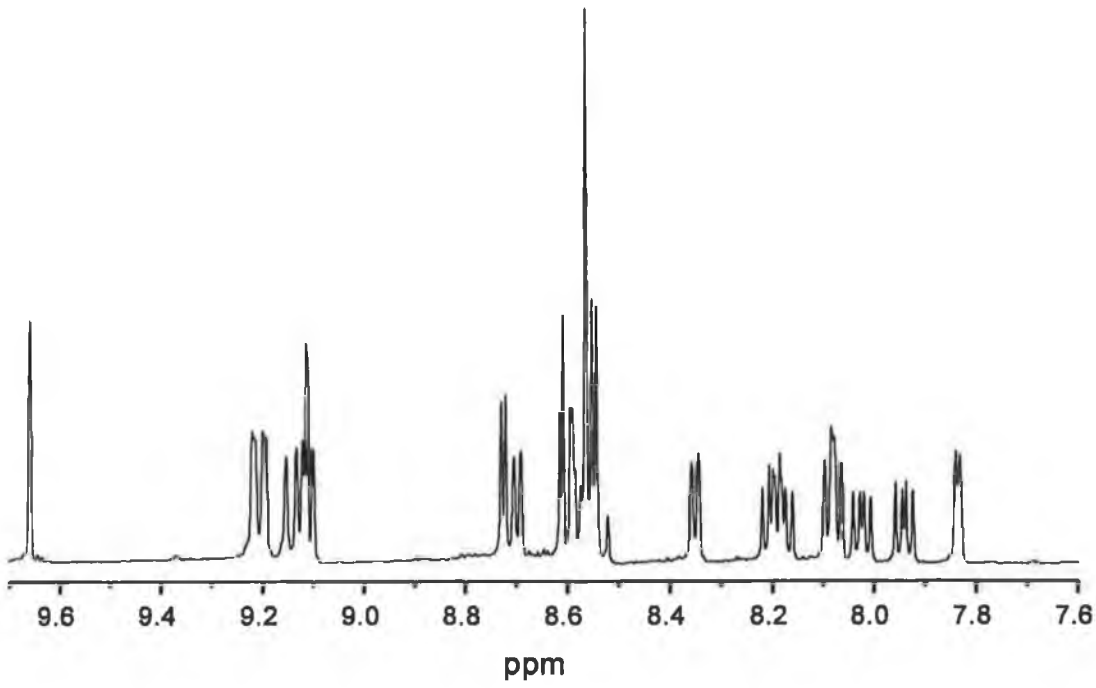

Figure 5.5 ^{1}H NMR spectrum of $[Rh(phen)_2(bpzt)]^{2+}$ in d_6-DMSO.

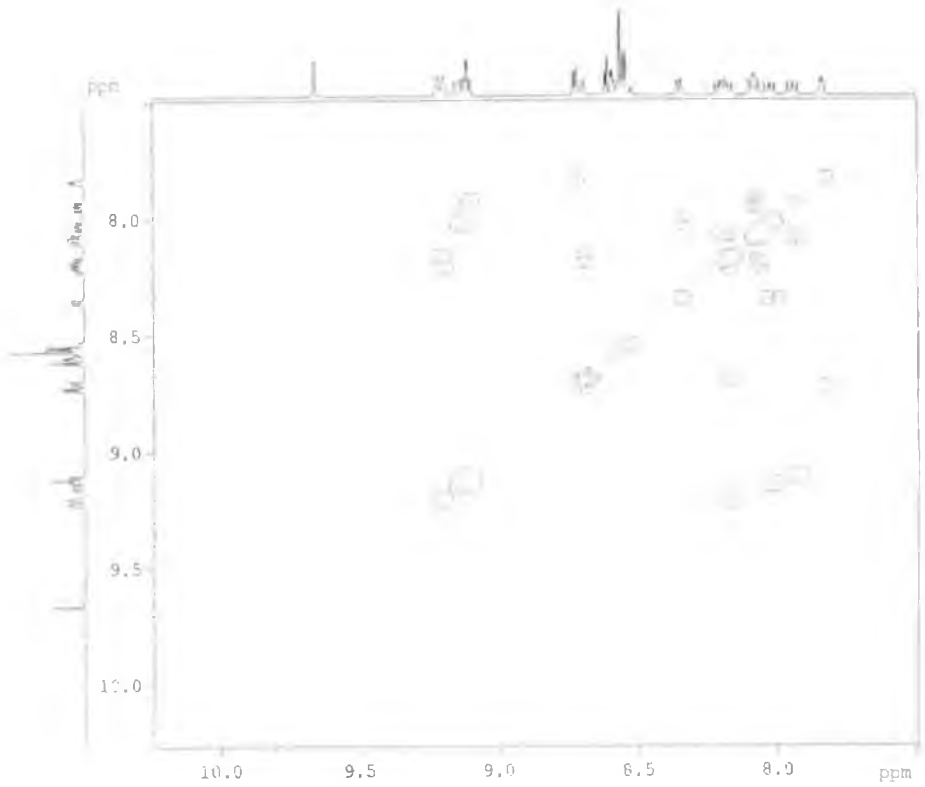

Figure 5.6 ^{1}H-^{1}H COSY NMR spectrum of $[Rh(phen)_2(bpzt)]^{2+}$ in d_6-DMSO.

Table 5.2 *^1H NMR data for all pyrazine triazole complexes measured in d_6-DMSO.*

		H3 (ppm)	H4 (ppm)	H5 (ppm)	H6 (ppm)	H5' (ppm)
Hpztr		9.27 (s)	-	8.76 (d)	8.72 (d)	8.58 (s)
$[Rh(phen)_2(pztr)]^{2+}$		9.52 (s)	-	8.63	7.77	8.52 (s)
$[Rh(bpy)_2(pztr)]^{2+}$		9.52 (s)	-	8.80 (d)	7.85 (m)	8.23(s)
HPhpztr		9.35 (s)	-	8.80 (m)	8.77 (m)	-
$[Rh(phen)_2(Phpztr)]^{2+}$		9.58 (s)	-	8.64 (d)	7.77 (m)	-
$[Rh(bpy)_2(Phpztr)]^{2+}$		9.58 (s)	-	8.80 (d)	7.89-7.81 (m)	-
Hbpzt		9.34 (s)		8.80-8.76 (m)	8.80-8.76 (m)	
$[Rh(phen)_2(bpzt)]^{2+}$	**Ring A**	9.66 (s)		8.72 (d)	7.84 (d)	
	Ring B	9.11 (s)		8.70 -8.50 (m)	8.70-9.50 (m)	

Ring A – pyrazine ring coordinated to the metal centre Ring B – free pyrazine ring.

5.3.2.1.4 *$[Rh(phen)_2(ppt)]^{2+}$ and $[Rh(bpy)_2(ppt)]^{2+}$*

In the case of the Hppt ligand four modes of coordination are possible. Figure 5.7 shows that coordination may occur in any of the following ways; (i) via N4' of the triazole ring and a nitrogen of the pyridine ring, (ii) via N4' of the triazole ring and a nitrogen of the pyrazine ring (iii) via N2' of the triazole ring and a nitrogen of the pyridine ring or (iv) via N2' of the triazole ring and a nitrogen of the pyrazine ring.

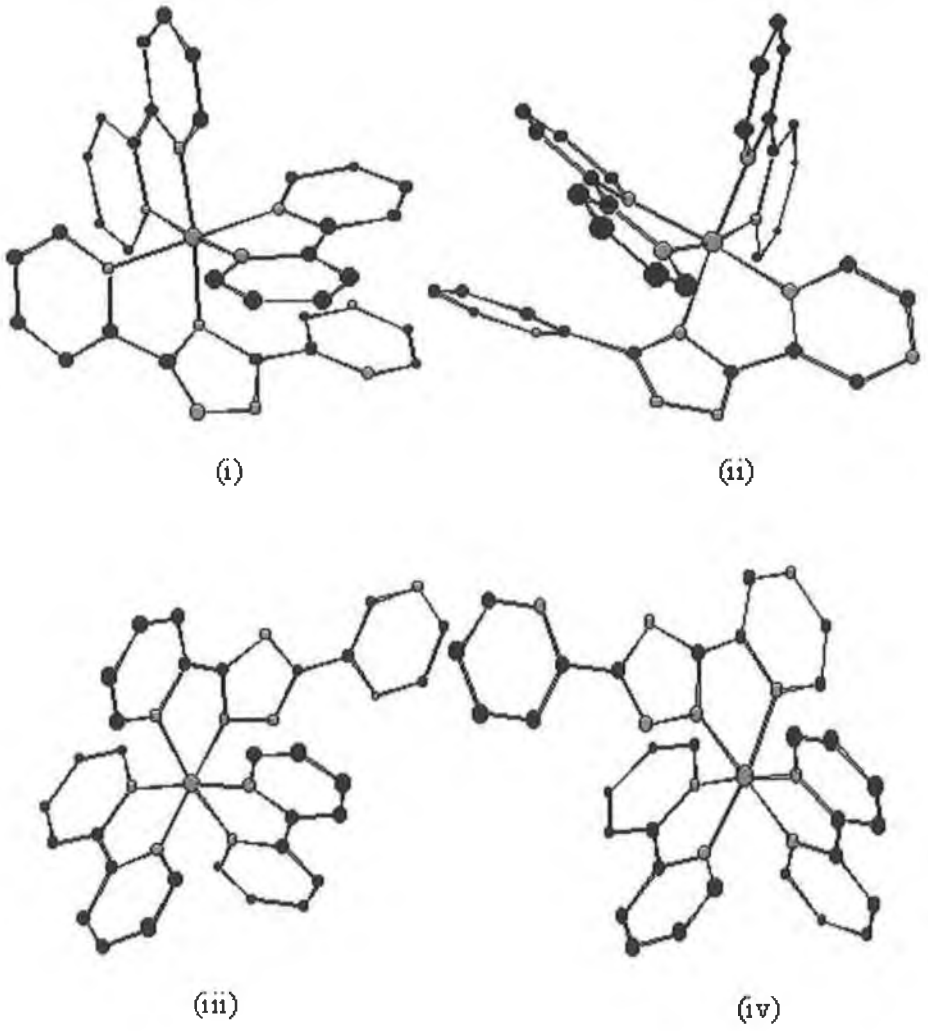

Figure 5.7 Illustration of the four possible modes of coordination of the ligand Hppt in complex $[Rh(bpy)_2(ppt)]^{2+}$.

All coordination modes of the Hppt ligand illustrated in Figure 5.7 were observed when the Ru(II) complexes $[Ru(phen)_2(ppt)]^+$ and $[Ru(bpy)_2(ppt)]^+$ were studied however the two isomers coordinated via the N4' of the triazole ring accounted for only 2-3% of the crude yield of both complexes. Of the two predominant isomers formed, the yield of the N2' pyridine bound isomer was higher than that of the pyrazine bound isomer after purification.[20] The ^1H NMR spectrum of $[Rh(phen)_2(ppt)]^{2+}$ can be seen in Figure 5.8.

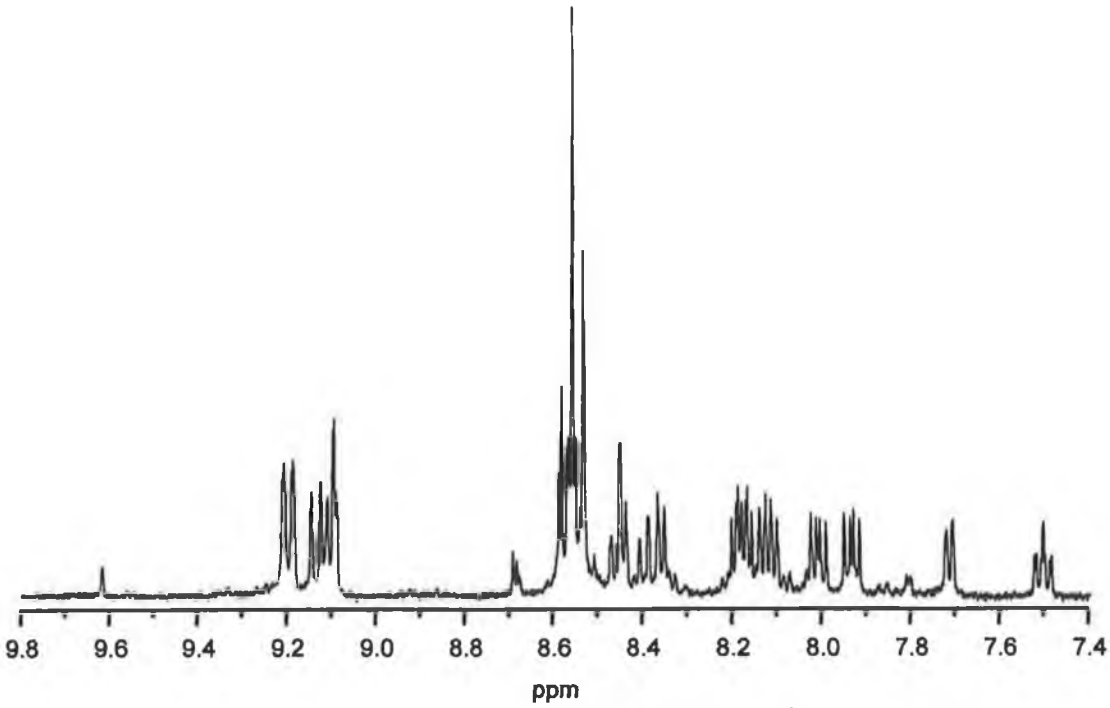

Figure 5.8 ^{1}H NMR spectrum of [Rh(phen)$_2$(ppt)]$^{2+}$ in d_6-DMSO.

In order to assign the spectrum of $[Rh(phen)_2(ppt)]^{2+}$ and to determine if coordination is taking place via the pyridine ring or the pyrazine ring it is necessary to take into account the chemical shifts observed for the free ligands Hpztr, Hpytr and Hppt and the complexes $[Rh(phen)_2(pytr)]^{2+}$ and $[Rh(phen)_2(pztr)]^{2+}$ as detailed in Table 5.3. In theory, if the metal centre is bound through the pyridine ring of the Hppt ligand then the chemical shifts for this bound pyridine ring should be similar to those observed for the complex $[Rh(phen)_2(pytr)]^{2+}$ and the unbound pyrazine ring should be similar to that of the free ligand. If on the other hand the metal centre is bound through the pyrazine ring then it should be possible to observe the chemical shifts for this pyrazine ring at similar positions to the bound pyrazine ring of the complex $[Rh(phen)_2(pztr)]^{2+}$ with the unbound pyridine ring exhibiting chemical shifts in the same region as that of the free ligand.

It is immediately clear in Figure 5.8 that two compounds are present as traces of a second compound can be seen at 9.62 ppm and 8.70 ppm. By comparison with the ^{1}H NMR data in Table 5.3 the double doublet and the doublet in Figure 5.8 at 7.51 ppm and 7.71 ppm coincide with that of H5 and H6 of the bound pyridine ring of $[Rh(phen)_2(pytr)]^{2+}$ thus indicating that the predominant product is the isomer in

which the metal centre is bound via the triazole and the pyridine ring. From this it can be predicted that the chemical shifts associated with the free pyrazine ring of $[Rh(phen)_2(ppt)]^{2+}$ would be expected to be similar to those of the free ligand. H3 can indeed be seen at 9.10 ppm.

Table 5.3 ***^1H NMR data for $[Rh(phen)_2(pytr)]^{2+}$, $[Rh(phen)_2(pztr)]^{2+}$, and $[Rh(phen)_2(ppt)]^{2+}$ and their free ligands measured in d_6-DMSO.***

		H3 (ppm)	H4 (ppm)	H5 (ppm)	H6 (ppm)	R (ppm)
Hpytr		8.09 (d)	7.98 (dd)	7.51 (dd)	8.70 (d)	8.27-H5' (s)
$[Rh(phen)_2(pytr)]^{2+}$		8.33 (m)	8.33 (m)	7.46 (dd)	7.68(d)	8.07-H5' (s)
Hpztr		9.27 (s)	-	8.76 (d)	8.72 (d)	8.58-H5' (s)
$[Rh(phen)_2(pztr)]^{2+}$		9.52	-	8.63	7.77	8.52-H5' (s)
Hppt	**py**	8.17 (d)	8.01 (dd)	7.54 (dd)	8.77 (d)	-
	pz	9.33 (s)	-	8.72 (m)	8.72 (m)	-
$[Rh(phen)_2(ppt)]^{2+}$						
Isomer I	**py**	8.45 (d)	8.39 (dd)	7.51 (dd)	7.71 (d)	-
	pz	9.10 (s)	-	8.60-8.50 (m)	8.60-8.50 (m)	-
$[Rh(phen)_2(ppt)]^{2+}$						
Isomer II	**py**	-	-	-	-	-
	pz	9.62 (s)	-	8.69 (d)	7.81(d)	-

py – pyridine ring, pz – pyrazine ring, Isomer I –metal centre bound via a nitrogen of the pyridine ring and the triazole ring, Isomer II –metal centre bound via a nitrogen of the pyrazine ring and the triazole ring.

This is shifted slightly upfield in comparison to the free ligand where H3 is observed at 9.33 ppm but this is expected due to the effect of the negatively charged triazole ring on the coordinated ppt^- ligand. This negative charge results in increased electron density on both the pyridine and the pyrazine rings thus causing an upfield shift of all the protons compared with the free ligand. H5 and H6 of the unbound pyrazine ring cannot be identified due to the presence of a number of multiplets between 8.50-8.70 ppm.

The ^{1}H NMR spectrum in Figure 5.8 exhibited signs of a second product with chemical shifts being observed at 9.62 ppm and 8.70 ppm. This could either be the second isomer of the pyridine bound complex or an isomer of the pyrazine bound complex. Thus it is necessary to examine the behaviour of $[Rh(phen)_2(pztr)]^{2+}$ where the metal can only bind via the triazole ring and the pyrazine ring. For $[Rh(phen)_2(pztr)]^{2+}$ H3 occurs at 9.52 ppm and H6 at 7.77 ppm and H5 at 8.63 ppm. The peak at 9.62 ppm may therefore be assigned as the H3 of the bound pyrazine ring and if the spectrum in Figure 5.8 is studied carefully other small peaks can be seen at 8.69 ppm and 7.81 ppm thus confirming that the minor product in this instance is the complex in which the metal centre is coordinated via the triazole ring and the pyrazine ring.

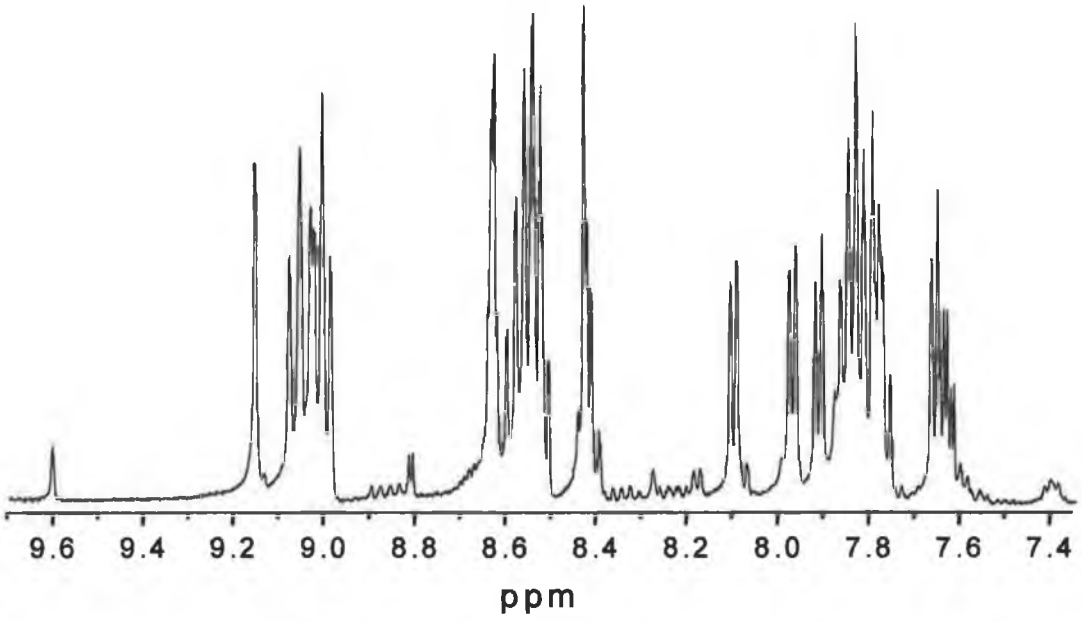

Figure 5.9 ^{1}H NMR spectrum of $[Rh(bpy)_2(ppt)]^{2+}$ in d_6-DMSO.

The ^{1}H NMR spectrum of $[Rh(bpy)_2(ppt)]^{2+}$ can be seen in Figure 5.9. As with the analysis of the complex $[Rh(phen)_2(ppt)]^{2+}$ it is necessary to compare $[Rh(bpy)_2(ppt)]^{2+}$, Figure 5.9, with $[Rh(bpy)_2(pytr)]^{2+}$ and $[Rh(bpy)_2(pztr)]^{2+}$ in order to determine which mode of coordination is being observed and Table 5.4 details the relevant ^{1}H NMR data.

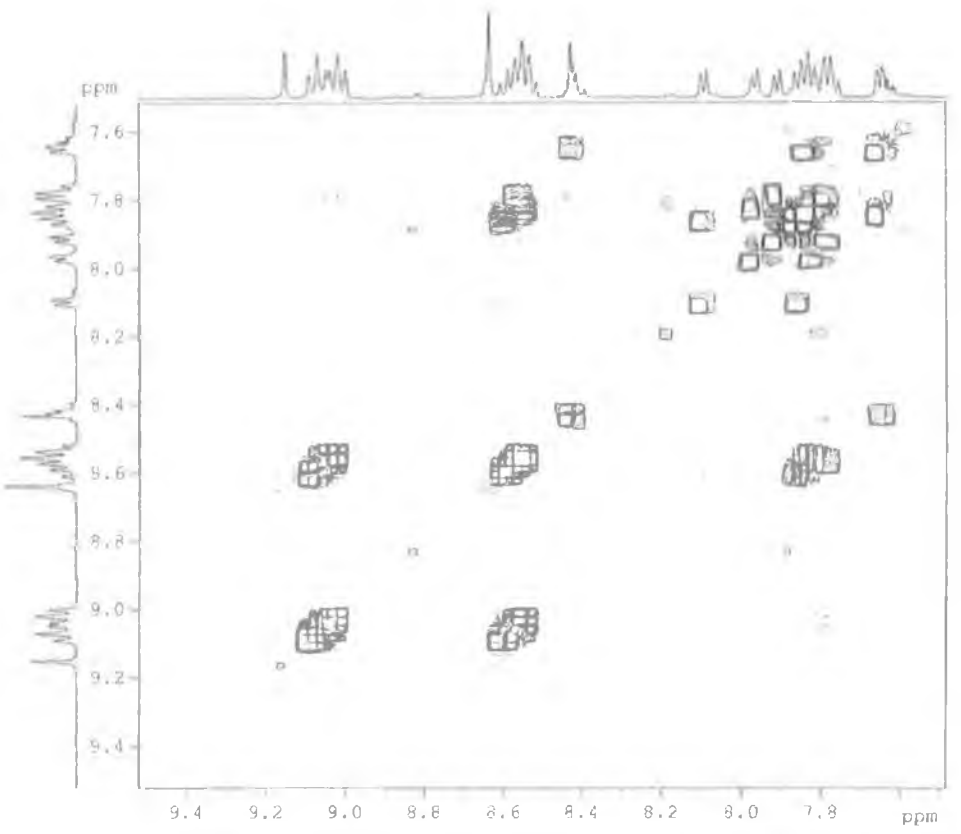

Figure 5.10 ^1H-^1H COSY NMR spectrum of $[Rh(bpy)_2(ppt)]^{2+}$ in d_6-DMSO.

Table 5.4 ^1H NMR data for $[Rh(bpy)_2(pytr)]^{2+}$, $[Rh(bpy)_2(pztr)]^{2+}$, $[Rh(bpy)_2(ppt)]^{2+}$ and related free ligands measured in d_6-DMSO.

		H3 (ppm)	H4 (ppm)	H5 (ppm)	H6 (ppm)	R (ppm)
Hpytr		8.09 (d)	7.98 (dd)	7.51 (dd)	8.70 (d)	8.27-H5' (s)
$[Rh(bpy)_2(pytr)]^{2+}$		8.30 (d)	8.36 (dd)	7.58 (dd)	7.74 (m)	8.10-H5' (s)
Hpztr		9.27 (s)	-	8.76 (d)	8.72 (d)	8.58-H5' (s)
$[Rh(bpy)_2(pztr)]^{2+}$		9.52 (s)	-	8.80 (d)	7.85 (m)	8.23-H5' (s)
Hppt		8.17 (d)	8.01 (dd)	7.54 (dd)	8.77 (d)	-
		9.33 (s)	-	8.72 (m)	8.72 (m)	-
$[Rh(bpy)_2(ppt)]^{2+}$						
Isomer I	**py**	8.41-8.45 (m)	8.41-8.45 (m)	7.61-7.68 (m)	7.70-7.90 (m)	-
	pz	9.13 (s)	-	8.62-8.64 (m)	8.62-8.64 (m)	-
$[Rh(bpy)_2(ppt)]^{2+}$						
Isomer II	**py**	8.17 (d)	-	7.40 (dd)	-	-
	pz	9.61(s)	-	8.82 (d)	-	-

Isomer I – isomer where metal centre bound via a nitrogen of the pyridine ring and the triazole ring.

Isomer II – isomer where metal centre bound via a nitrogen of the pyrazine ring and the triazole ring.

The first feature of the spectrum that can be easily identified is the singlet at 9.16 ppm. This can be attributed to H3 of the pyrazine ring and from Table 5.4 it can be seen that H3 in this position corresponds to H3 at 9.33 ppm of the free ligand. Once again this upfield shift upon complexation is anticipated due to the increased negative charge on the pyridine and pyrazine rings, which is a consequence of the deprotonation of the triazole ring upon coordination of the metal centre. If the major product observed in Figure 5.9 is due to coordination through the triazole ring and the nitrogen of the pyridine ring it should to an extent be possible to assign the spectrum in Figure 5.9 based upon the data summarized in Table 5.4. The multiplet at 8.41-8.45 ppm may be attributed to H3 and H4 of the bound pyridine ring with H5 and H6 occurring at 7.68-7.61 ppm (m) and 7.70-7.90 ppm (m) respectively. With respect to the unbound pyrazine ligand the H3 proton can be seen at 9.16 ppm and the multiplet at 8.64-8.62 ppm, which integrates to two protons can be attributed to the H5 and H6 protons of the pyrazine ring.

As was previously seen for $[Rh(phen)_2(ppt)]^{2+}$ a second H3 peak can be seen at 9.61 ppm which corresponds to the isomer in which the metal centre is bound via the triazole ring and a nitrogen of the pyrazine ring. Only a single isomer was obtained in the synthesis of $[Rh(bpy)_2(pztr)]^{2+}$ and as detailed in Table 5.4, H3 in this instance was observed at 9.52 ppm. If the spectrum in Figure 5.9 is studied further it is also possible to identify the peak associated with the H5 proton of the isomer bound via the pyrazine ring as expected at 8.82 ppm. Most of the other chemical shifts associated with this particular isomer cannot been seen as they are masked by the more dominant isomer but the H5 proton of the free pyridine ring can be seen at 7.40 ppm in Figure 5.9. Table 5.5 summarises the ^1H NMR data for all of the pyrazine based complexes discussed in this chapter. In the absence of suitable crystals for analysis and due to the fact that only a single isomer was obtained for all of the complexes studied it was not possible to determine whether the mode of coordination exhibited by the pyrazine triazole complexes detailed in this chapter. It should be noted that whilst two isomers were obtained for complexes incorporating the Hppt ligand, these corresponded to coordination via the (i) pyrazine ring and (ii) via the pyridine ring. The nature of this coordination i.e. whether they are

coordinated via the N2' or N4' positions of the pyridine/pyrazine rings cannot be established unambiguously. The issue of coordination in these complexes will be discussed in more detail in Chapter 8.

Table 5.5 ***^{1}H NMR data for all pyrazine based complexes measured in d_6-DMSO.***

		H3 (ppm)	H4 (ppm)	H5 (ppm)	H6 (ppm)	H5' (ppm)
$[Rh(phen)_2(pztr)]^{2+}$		9.52	-	8.63	7.77	9.52 (s)
$[Rh(bpy)_2(pztr)]^{2+}$		9.52 (s)	-	8.80 (d)	7.85 (m)	8.23 (s)
$[Rh(phen)_2(bpzt)]^{2+}$	(ring A)	9.66 (s)	-	8.72 (d)	7.84 (d)	-
	(ring B)	9.11 (s)	-	8.76-9.50 (m)	8.76-9.50 (m)	-
$[Rh(phen)_2(Phpztr)]^{2+}$		9.58 (s)	-	8.64 (d)	7.77 (m)	-
$[Rh(bpy)_2(Phpztr)]^{2+}$		9.58 (s)	-	8.80 (d)	7.89-7.81 (m)	-
$[Rh(phen)_2(ppt)]^{2+}$ Isomer I	py	8.45 (d)	8.39 (dd)	7.51 (dd)	7.71 (d)	-
	pz	9.10 (s)	-	8.60-8.50 (m)	8.60-8.50 (m)	-
$[Rh(phen)_2(ppt)]^{2+}$ Isomer II	py	-	-	-	-	-
	pz	9.62 (s)	-	8.69 (d)	7.81 (d)	-
$[Rh(bpy)_2(ppt)]^{2+}$ Isomer I	py	8.41-8.45 (m)	8.41-8.45 (m)	7.61-7.68 (m)	7.70-7.90 (m)	-
	pz	9.13 (s)		8.62-8.64 (m)	8.62-8.64 (m)	-
$[Rh(bpy)_2(ppt)]^{2+}$ Isomer II	py	8.17 (d)		7.40 (dd)	-	-
	pz	9.61 (s)	-	8.82 (d)	-	-

a – bound ring , b– free ring, Isomer I – metal centre bound via a nitrogen of the pyridine ring and the triazole ring, Isomer II – metal centre bound via a nitrogen of the pyrazine ring and the triazole ring.

5.3.2.2 Complexes with triazine based ligands.

A number of complexes incorporating triazine type ligands with metal centres such as ruthenium, osmium, rhenium, copper and rhodium have been reported with ^{1}H NMR analysis generally being a feature of their characterisation.[6,7,14,15,13] An example of which may be found with the synthesis and characterisation of rhodium complexes containing the tptz ligand and its metal promoted hydrolytic products reported by Paul *et. al.*.[13] Figure 5.11 outlines the reactions carried out by Paul *et. al.*

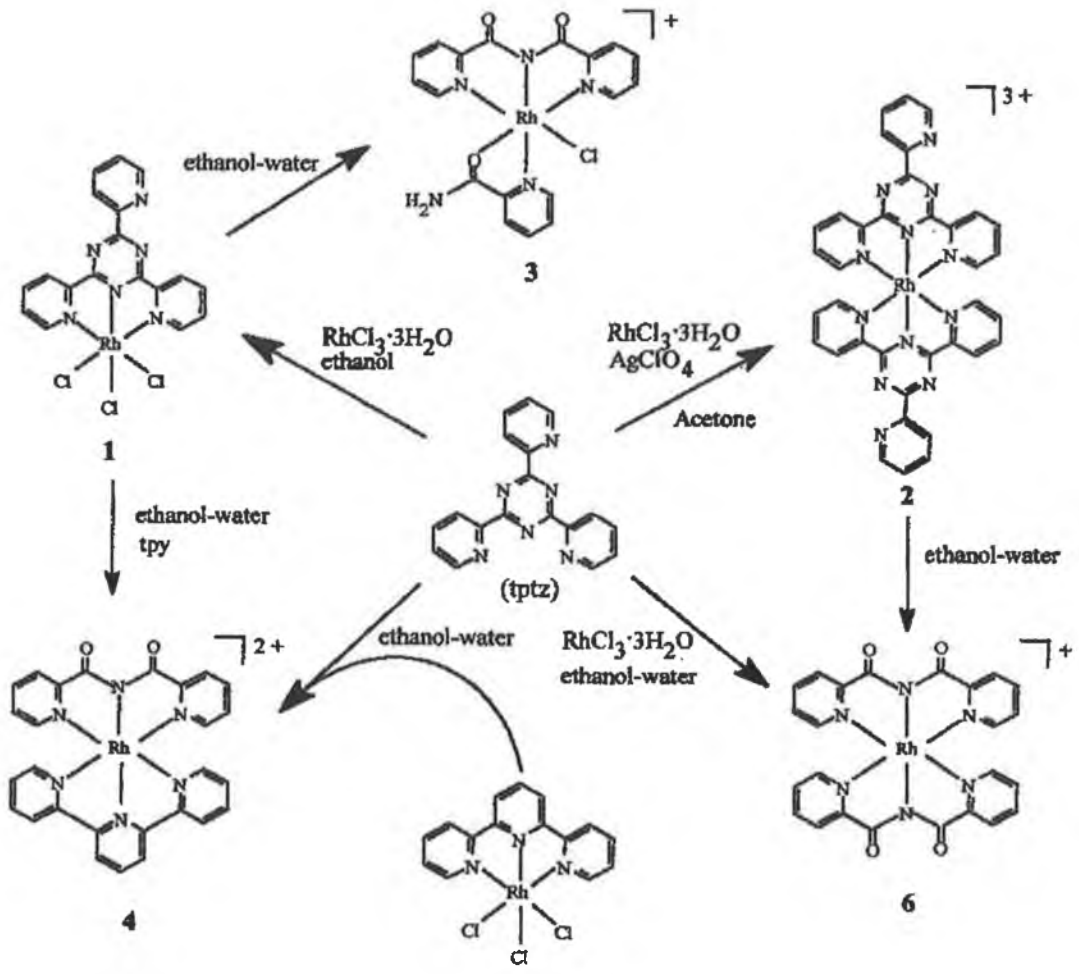

Figure 5.11 Schematic representation of the reactions carried out by Paul et. al.[13]

Figure 5.12 illustrates the ^{1}H NMR spectra for the free ligand tptz and complex **1.** A significant downfield shift (0.35-0.62 ppm) was observed for all protons of the metal-bound pyridyl with respect to the free ligand for the complexes outlined in Figure 5.11. This downfield shift is in contrast to the upfield shift observed upon coordination of a metal centre to triazole-based ligands that is explained by the negative charge on the triazole ring and with through space interactions also playing a role.

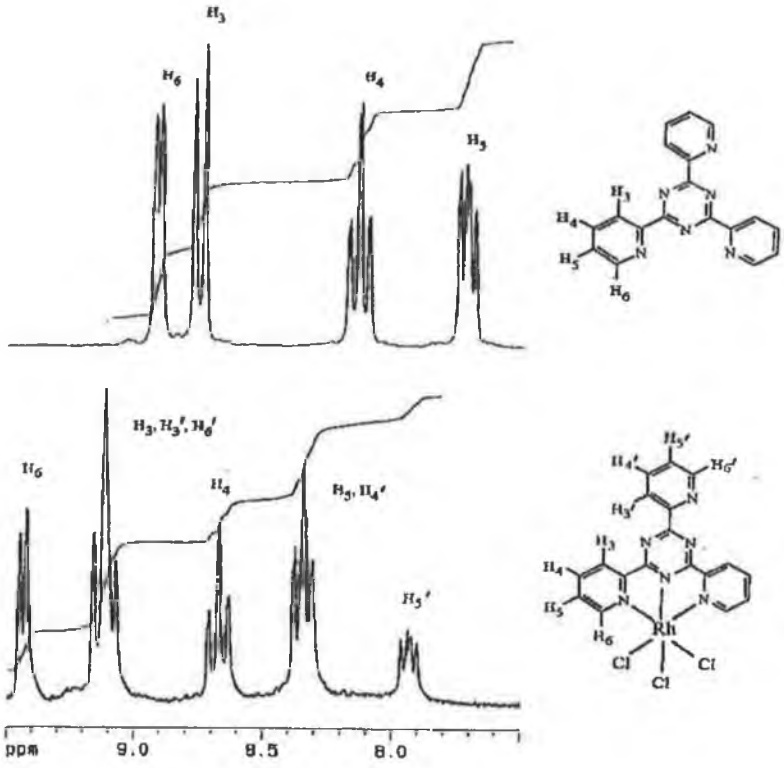

Figure 5.12 ^{1}H NMR spectra of the ligand tptz and complex 1 in d_6-DMSO with assignment of protons. [6]

In the case of complex **1** in Figure 5.11 the lowest field doublet was assigned to H_6 as H_6 is adjacent to the metal bound nitrogen atoms and is expected to experience the maximum deshielding effect. Comparison with the free ligand and J values was used to assign the spectrum of **1** completely. When the ^{1}H NMR spectra of **4** of Figure 5.11 was compared with that of the analogous Ru(II) complex a striking difference, almost 1 ppm, was observed between the chemical shifts of H_6 of the two complexes. Although the shielding effect caused by the ring current of the central pyridyl ring and the charge difference between Ru(II) and Rh(III) may have contributed slightly to the difference in chemical shifts observed, the main contributing factor was the π-back-bonding ability of Ru(II). This π-back-bonding ability increases electron density on the metal bound nitrogen and on adjacent atoms giving rise to an additional shielding effect for H_6. It should be noted however that no significant difference was observed between the resonances of the H6 protons of the Rh(III) complexes which will be detailed in the following discussion and their Ru(II) analogues.

5.3.2.2.1 $[Rh(phen)_2(dppt)]^{3+}$ and $[Rh(bpy)_2(dppt)]^{3+}$

The ^{1}H NMR spectrum of $[Rh(phen)_2(dppt)]^{3+}$ as seen in Figure 5.13 spectrum (i) is quite complex and it was decided to use deuteration to identify the peaks associated with the dppt ligand - see Figure 5.13. It should be noted that it was the protons of the two phenyl rings which were deuterated.

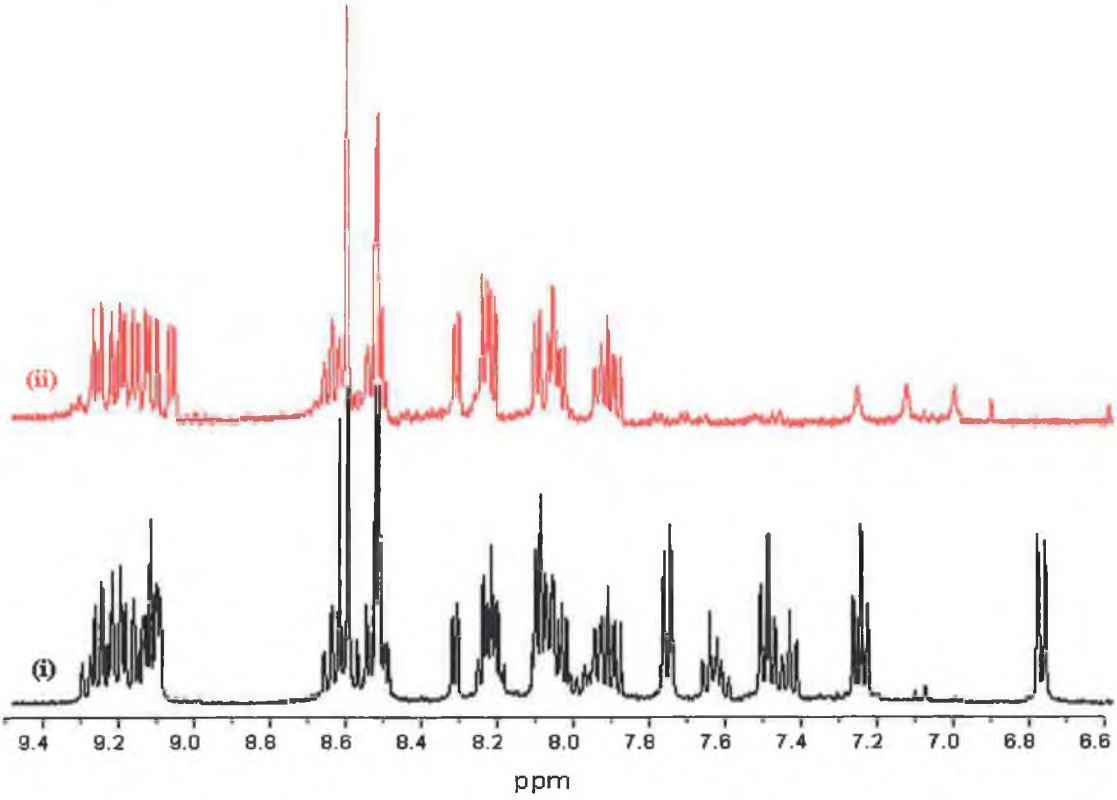

Figure 5.13 ^{1}H NMR spectra of (i) $[Rh(phen)_2(dppt)]^{3+}$(——) and (ii) $[Rh(phen)_2(d_{10}\text{-}dppt)]^{3+}$(——) in d_6-DMSO.

If we compare the spectra in Figure 5.13 it can easily be seen that the protons of the phenyl rings are located between 7.80 ppm and 6.70 ppm with one further proton at 8.10 ppm. It should be noted that the three small peaks at 7.23 ppm, 7.14 ppm, 7.02 ppm in the spectrum of $[Rh(phen)_2(d_{10}\text{-dppt})]^{3+}$ are due to the presence of excess ammonium hexafluorophosphate and in no way interfere with subsequent analysis. Close scrutiny of the ^{1}H NMR spectrum of the deuterated complex showed the presence of a double doublet at 8.66 ppm and this was assigned as the H4 proton of the pyridine ring with H3 at 9.25-9.10 ppm, H5 at 7.95 ppm and H6 at 8.05 ppm.

The ^{1}H NMR spectra of both $[Rh(bpy)_2(dppt)]^{3+}$ and $[Rh(bpy)_2(d_{10}\text{-dppt})]^{3+}$ can be seen in Figure 5.14.

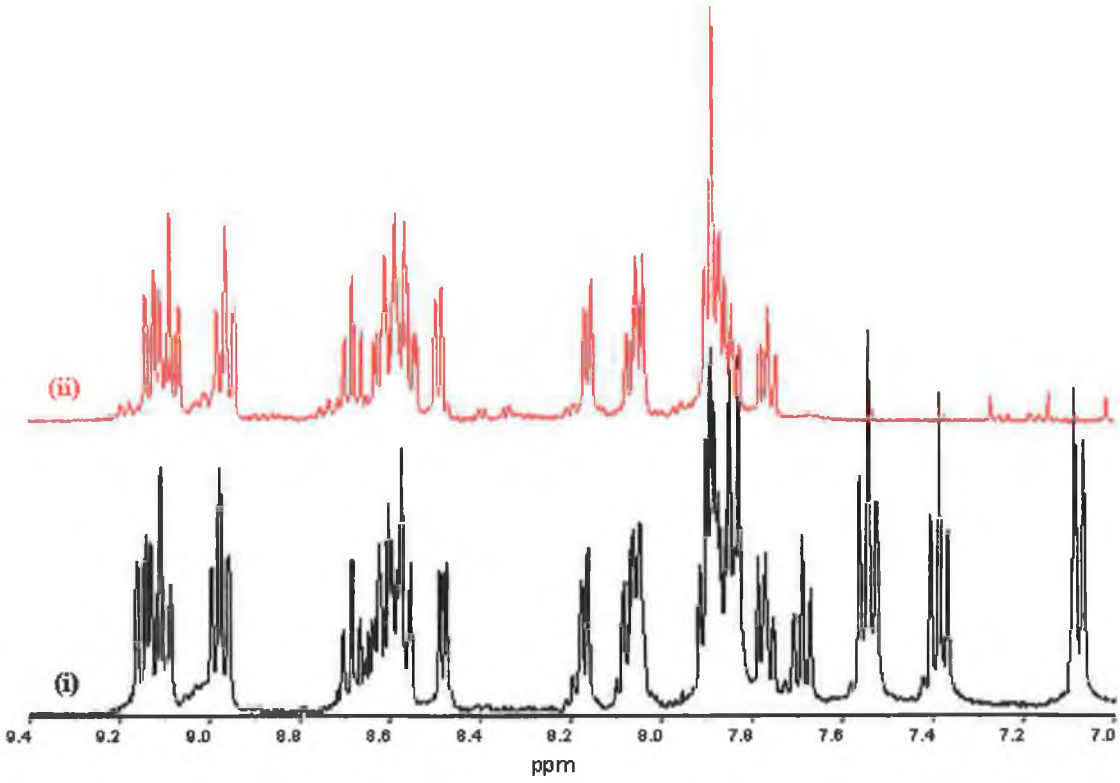

Figure 5.14 ^{1}H NMR spectra of (i) $[Rh(bpy)_2(dppt)]^{3+}$(——) and (ii) $[Rh(bpy)_2(d_{10}\text{-dppt})]^{3+}$(——) in d_6-DMSO.

As was the case with the previous spectrum, deuteration of the dppt ligand allows for the immediate identification of the protons of the phenyl rings, which it can be seen occur between 8.00 ppm and 7.00 ppm. The spectrum was tentatively assigned, using the ^{1}H-^{1}H COSY NMR spectrum seen in Figure 5.15, as detailed in Table 5.6. It would however be necessary to synthesise the complex $[Rh(d_8\text{-bpy})_2(dppt)]^{3+}$ to assign the H3, H4, H5 and H6 protons of the pyridine ring unambiguously.

It can be seen from Table 5.6 that resonances assigned to H3, H4 and H5 all demonstrate a downfield shift with only the H6 proton experiencing an upfield shift. Unlike complex (4) of Figure 5.11 and its analogous Ru(II) complex when the H6

protons of $[Rh(bpy)_2(dppt)]^{3+}$ and $[Ru(bpy)_2(dppt)]^{2+}$ are compared no significant difference between the signals of the H6 resonance is observed.

Table 5.6 ***^{1}H NMR data for complexes containing the dppt ligand measured in d_6-DMSO.***

	H3 (ppm)	H4 (ppm)	H5 (ppm)	H6 (ppm)
dppt	8.55 (d)	8.07(dd)	7.64 (dd)	8.85 (d)
$[Rh(phen)_2(dppt)]^{3+}$	9.25-9.10 (m)	8.66 (m)	7.95 (m)	8.05 (m)
$[Rh(bpy)_2(dppt)]^{3+}$	9.14-9.07 (m)	8.68 (dd)	8.17 (d)	8.07-8.03 (m)
$[Ru(bpy)_2(dppt)]^{2+}$ [a]	9.00	8.33	7.80	8.24

a - values taken from ref.8

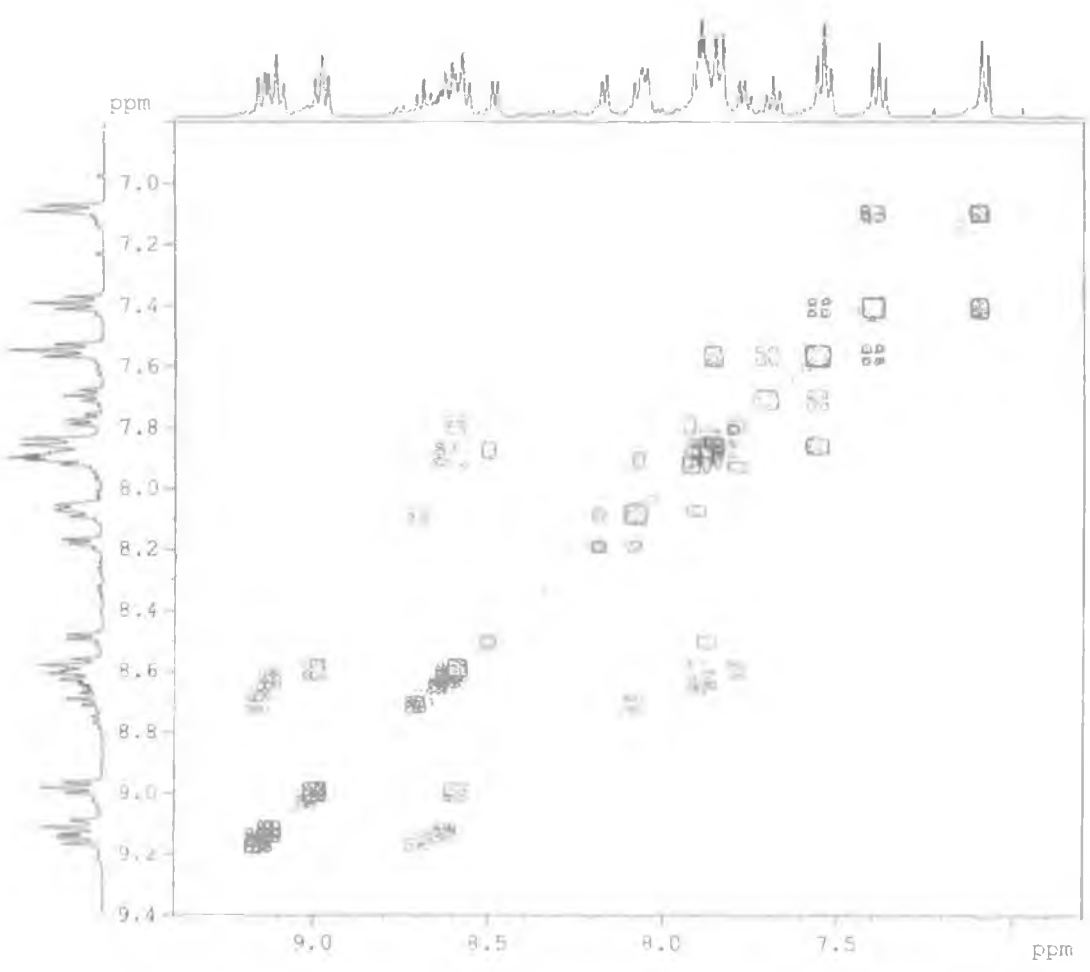

Figure 5.15 ^{1}H - ^{1}H COSY NMR spectrum of $[Rh(bpy)_2(dppt)]^{3+}$ in d_6-DMSO.

5.3.2.3 Complexes with imidazole and triazole based ligands.

The final series of complexes that have been investigated contain a core pyridine ring fused with a five membered ring so that the ligands are either imidazole (PIP and MePIP) or triazole (PTP) in nature depending upon the nature of the five membered ring. The ligands, with relevant numbering, may be seen in Figure 5.1. The ^{1}H NMR data obtained for the free ligands are summarised in Table 5.7. As is evident from Table 5.7 the H3' proton of PIP, MePIP and PTP occurs further downfield than all other signals because of a hydrogen bonding interaction between the H3' proton and the nitrogen of the pyridine ring. Substitution of the R proton of the PIP ligand with a methyl group results in the H3' signal being shifted 1.35 ppm further downfield and the H4', H5' and H6' protons are shifted slightly upfield. When the PTP and the PIP ligands are compared it can be seen that with the exception of the H6' proton all other protons of the PTP ligand occur downfield of the PIP ligand. This downfield shift is caused by the replacement of a carbon of the fused ring with another nitrogen. This alters the nature of the ligand from an imidazole based ligand to a triazole based ligand and in turn causes an electron withdrawing effect resulting in an overall downfield shift.

Table 5.7 ^{1}H NMR data for ligands PIP, MePIP and PTP in d_6-DMSO.

	PIP (ppm)	MePIP (ppm)	PTP (ppm)
H3	8.07 (d)	8.22 (d)	8.45 (d)
H4	7.80 (dd)	7.89 (dd)	8.10 (dd)
H5	7.17 (dd)	7.32 (dd)	7.60-7.55 (m)
H6	8.59 (d)	8.66 (d)	8.84 (d)
H3'	8.46 (d)	9.81 (d)	9.75 (d)
H4'	7.01 (dd)	6.93-6.83 (m)	7.23 (dd)
H5'	6.80 (dd)	6.93-6.83 (m)	7.60-7.55 (m)
H6'	8.43 (d)	7.70 (d)	7.99 (d)
R-H	8.48 (s)	-	-
R-CH_3	-	3.36 (s)	-

Note: see Figure 5.1 for ligand numbering

^{1}H NMR spectra of the complexes containing the ligands PIP, MePIP and PTP proved difficult to assign and as a result it was decided to synthesise [Rh(d_8-bpy)$_2$(PIP)]$^{3+}$ to unambiguously assign the signals associated with the PIP ligand. It was more prudent to synthesise a complex containing deuterated bpy than deuterated phen as certain features of the phen ligand can be discerned relatively easily in the ^{1}H NMR spectrum. In particular the occurrence of four double doublets associated with the phen ligand make it relatively easy to assign the remainder of the spectrum

5.3.2.3.1 [Rh(phen)$_2$(PIP)]$^{3+}$ and [Rh(bpy)$_2$(PIP)]$^{3+}$

The ^{1}H NMR spectrum of [Rh(phen)$_2$(PIP)]$^{3+}$ may be seen in Figure 5.16 below. The singlet at 8.62 ppm may be attributed to the proton in the R position of the PIP ligand. If it is assumed that the resonances at 9.22 ppm and 9.13 ppm are associated with the phenanthroline ring, as was seen in earlier spectra, for example Figures 3.10 and 3.20, then it is possible, with the aid of the ^{1}H-^{1}H COSY spectrum, to identify the chemical shifts associated with the PIP ligand.

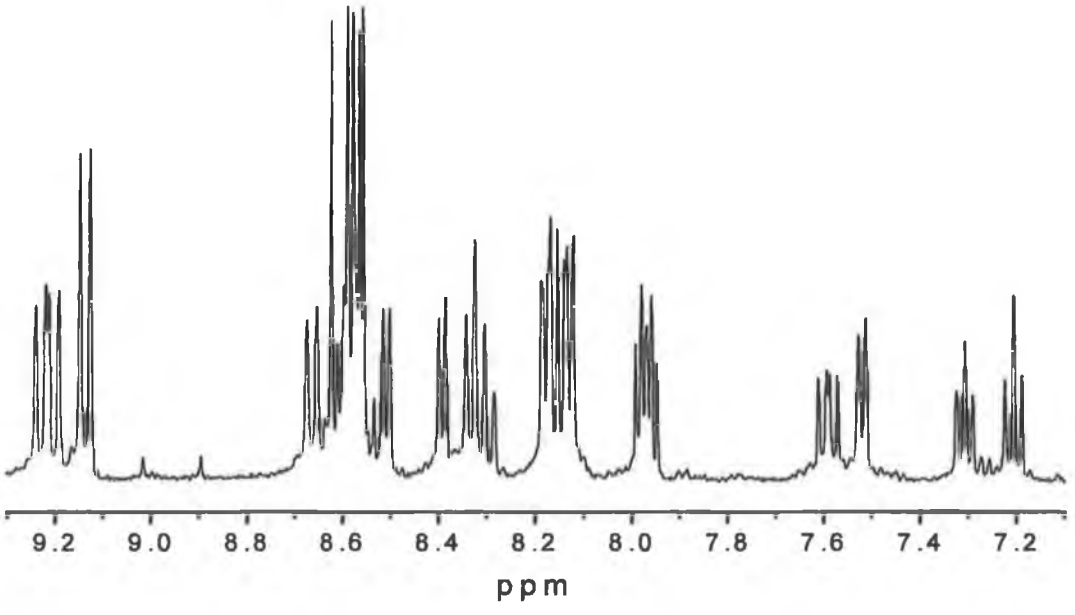

Figure 5.16 ^{1}H NMR spectrum of [Rh(phen)$_2$(PIP)]$^{3+}$ in d_6-DMSO.

The following chemical shifts were found associated with the PIP ligand; 8.66 ppm (d, 1H), 8.62 ppm (s, 1H), 8.50 ppm (d, 1H), 8.32 ppm (dd, 1H), 7.60 ppm (dd, 1H), 7.52 ppm (d, 1H), 7.31 ppm (dd, 1H), 7.21 ppm (dd, 1H). It would be expected that upon complexation a general downfield shift of the PIP protons with the exception of the H6 proton. As in the case of the pyridine triazole complexes it is expected that upon coordination this H6 proton would be directed above an adjacent phen ligand and as a result would be shifted upfield and as a result it can be assumed that the doublet at 7.52 ppm is that of H6. Based upon this, the spectrum has been assigned as shown in Table 5.8.

To aid in the analysis of the ^{1}H NMR spectrum of $[Rh(bpy)_2(PIP)]^{3+}$ deuteration of the bipyridyl ligands was carried out and the spectra of $[Rh(bpy)_2(PIP)]^{3+}$ and $[Rh(d_8\text{-bpy})_2(PIP)]^{3+}$ - see Figure 5.17.

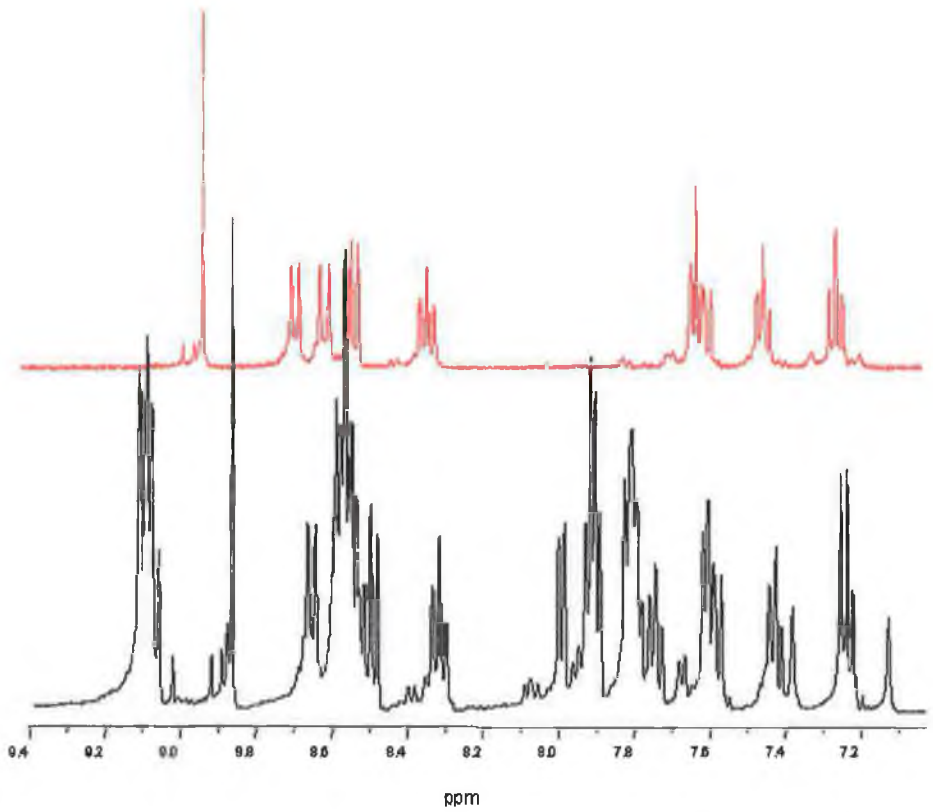

Figure 5.17 ^{1}H NMR spectra of (i) $[Rh(bpy)_2(PIP)]^{3+}$ (——) and (ii) $[Rh(d_8\text{-bpy})_2(PIP)]^{3+}$ (——) in d_6-DMSO.

The use of deuteration in this instance allowed for the immediate identification of the PIP protons. Once again the doublet shifted furthest upfield, to 7.64 ppm in this case, was attributed to the H6 of the pyridine ring. The ^{1}H-^{1}H COSY spectrum in Figure 5.18 was instrumental in the assignment of the ^{1}H NMR spectrum of [Rh(d_8-bpy)$_2$(PIP)]$^{3+}$ - Table 5.8.

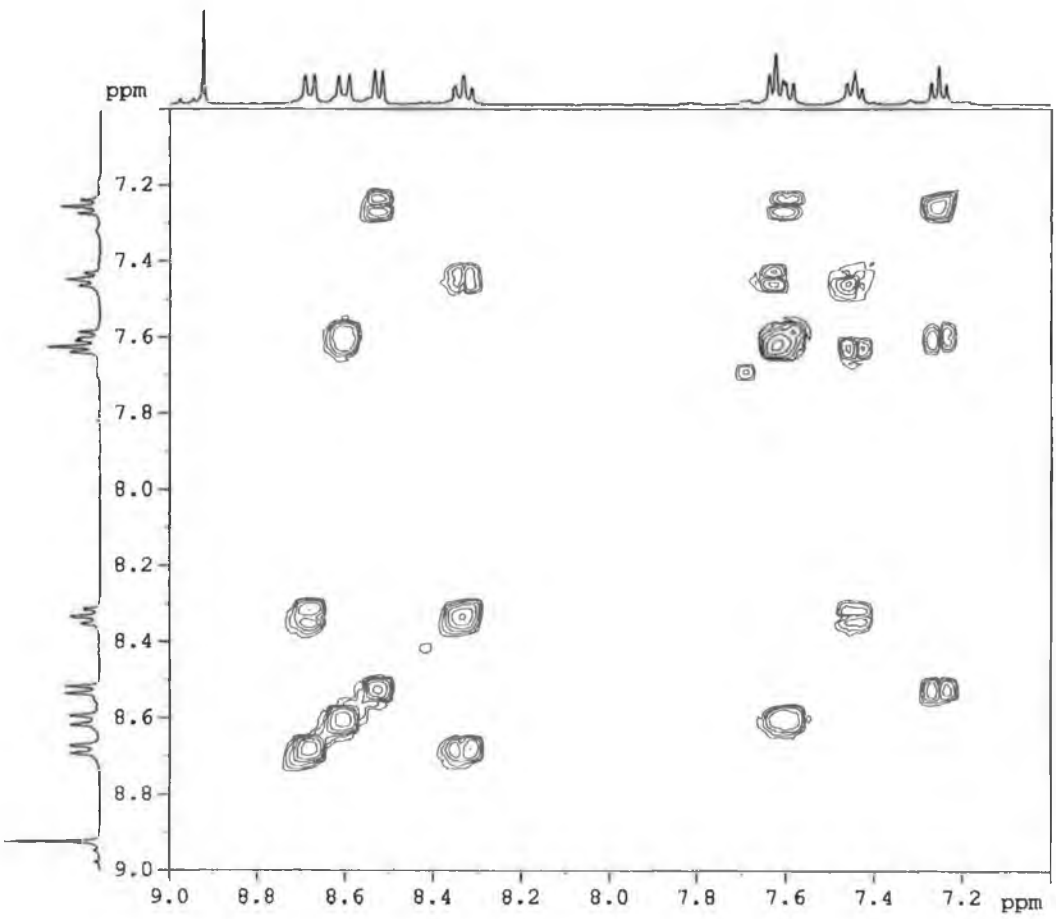

Figure 5.18 2-D ^{1}H-^{1}H COSY NMR spectrum of [Rh(d_8-bpy)$_2$(PIP)]$^{3+}$ in d_6-DMSO.

Table 5.8 details the ^{1}H NMR data obtained for all the complexes incorporating the PIP, MePIP and PTP ligands.

Table 5.8 ***^{1}H NMR data for complexes incorporating the ligands PIP, MePIP and PTP measured in d_6-DMSO.***

	$[Rh(phen)_2(PIP)]^{3+}$ (ppm)	$[Rh(phen)_2(MePIP)]^{3+}$ (ppm)	$[Rh(phen)_2(PTP)]^{3+}$ (ppm)
H3	8.66 (d)	8.86 (d)	9.10 (m)
H4	8.34-8.28 (m)	8.40 (dd)	8.62-8.58 (m)
H5	7.31 (dd)	7.47-7.36 (m)	7.70-7.63 (m)
H6	7.52 (d)	7.55 (d)	7.97-7.92 (m)
H3'	8.61-8.54 (m)	9.31 (d)	9.55 (d)
H4'	7.59 (dd)	7.47-7.36 (m)	7.72-7.63 (m)
H5'	7.21 (dd)	7.47-7.36 (m)	7.86 (dd)
H6'	8.34-8.28 (m)	8.02 (d)	8.07-8.01 (m)
R	8.62 - H (s)	1.37-CH_3 (s)	-
	$[Rh(bpy)_2(PIP)]^{3+}$ (ppm)	$[Rh(bpy)_2(MePIP)]^{3+}$ (ppm)	$[Rh(bpy)_2(PTP)]^{3+}$ (ppm)
H3	8.68 (d)	8.85 (d)	8.83-8.77 (m)
H4	8.33 (dd)	8.43 (dd)	8.37-8.45 (m)
H5	7.45 (m)	7.52 (dd)	7.76 (dd)
H6	7.64 (m)	7.67 (d)	8.18 (m)
H3'	8.60 (m)	9.29 (d)	9.87 (d)
H4'	7.61 (d)	7.48-7.40 (m)	7.42 (dd)
H5'	7.26 (m)	7.48-7.40 (m)	7.83 (m)
H6'	8.56 (m)	8.11 (m)	7.58-7.63 (m)
R	8.88 – H (s)	1.72-CH_3 (s)	-
	$[Ru(bpy)_2(PIP)]^{2+}$ [a] (ppm)	$[Ru(bpy)_2(MePIP)]^{2+}$ [a] (ppm)	$[Ru(bpy)_2(PTP)]^{2+}$ [a] (ppm)
H3	8.49 (8.18)	8.82 (8.17)	8.81 (7.85)
H4	8.06 (7.78)	8.18 (7.72)	8.19 (7.50)
H5	7.27 (7.14)	7.50 (7.14)	7.64 (7.14)
H6	7.83 (8.62)	8.08 (8.49)	8.17 (8.78)
H3'	8.40 (8.59)	8.18 (9.78)	8.13 (9.85)
H4'	7.48 (6.99)	8.18 (6.63)	8.14 (7.50)
H5'	7.09 (6.77)	7.36 (6.72)	7.53 (8.04)
H6'	8.40 (8.38)	7.91 (7.47)	8.05 (8.50)
R	8.49-H (8.37)	-	-

a – values taken from ref. 19 and measured in d_6-acetone. Values in parentheses = free ligand

5.3.2.3.2 *[Rh(phen)$_2$(MePIP)]$^{3+}$ and [Rh(bpy)$_2$(MePIP)]$^{3+}$*

The ^{1}H NMR spectrum of [Rh(phen)$_2$(MePIP)]$^{3+}$ can be seen below and [Rh(bpy)$_2$(MePIP)]$^{3+}$ can be seen in Appendix III and their assignment is detailed in Table 5.8. In the case of the MePIP ligand a methyl group has been introduced into the R position of the fused ring and the effect of this can be seen in Figure 5.19 where the ^{1}H NMR spectrum of [Rh(phen)$_2$(MePIP)]$^{3+}$ may be compared with the ^{1}H NMR spectrum [Rh(phen)$_2$(PIP)]$^{3+}$ with the positions of the pertinent protons being indicated in each spectrum. It can be seen that it is the H3' and the H6' protons that are affected most by the presence of the methyl moiety.

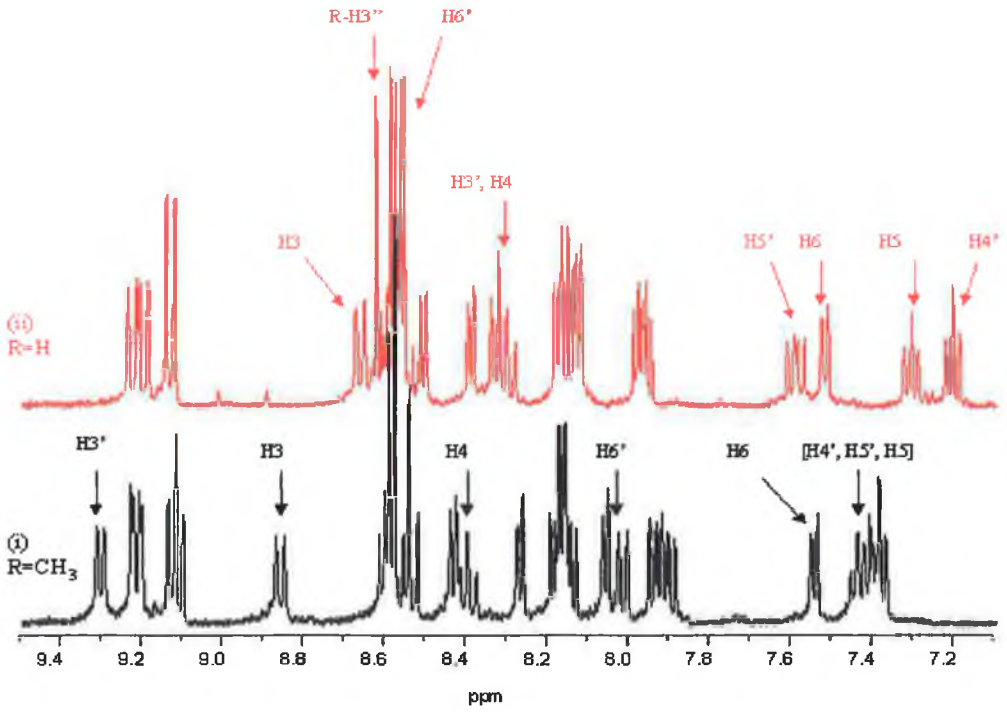

Figure 5.19 ^{1}H NMR spectrum of (i) [Rh(phen)$_2$(MePIP)]$^{3+}$ (——) and (ii) [Rh(phen)$_2$(PIP)]$^{3+}$(——) in d_6-DMSO.

5.3.2.3.3 $[Rh(phen)_2(PTP)]^{3+}$ and $[Rh(bpy)_2(PTP)]^{3+}$

As detailed in Table 5.7 the introduction of a third nitrogen into the fused ring has an electron withdrawing effect, which in turn leads to a downfield shift of the protons of the fused ring. The introduction of this third nitrogen into the fused ring means that unlike the PIP and MePIP ligands, which are imidazole based, the PTP ligand is a triazole based ligand. As a result complexes containing the PTP ligand are interesting intermediate complexes between the complexes containing triazole based ligands, which have been discussed previously in detail, and the series of complexes containing the PIP and MePIP ligands. Figure 5.20 and Figure 5.21 illustrate the ^1H NMR spectra of $[Rh(phen)_2(PTP)]^{3+}$ and $[Rh(bpy)_2(PTP)]^{3+}$ and Table 5.8 summarises the ^1H NMR data obtained.

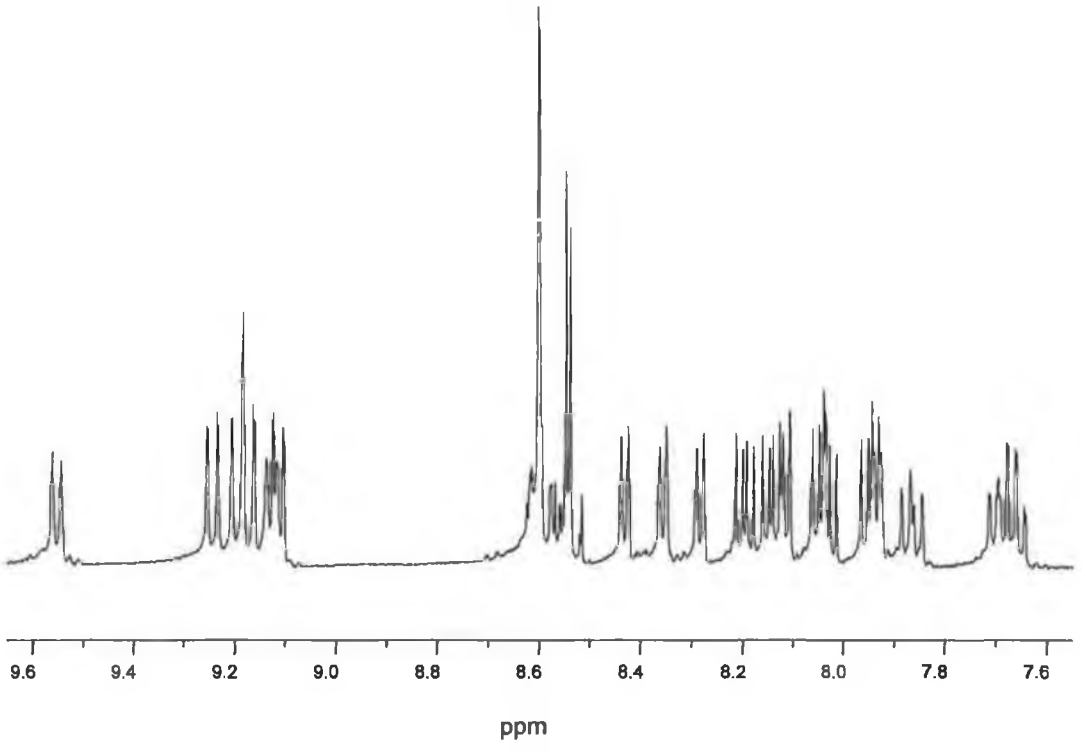

Figure 5.20 ^1H NMR spectrum of $[Rh(phen)_2(PTP)]^{3+}$ in d_6-DMSO.

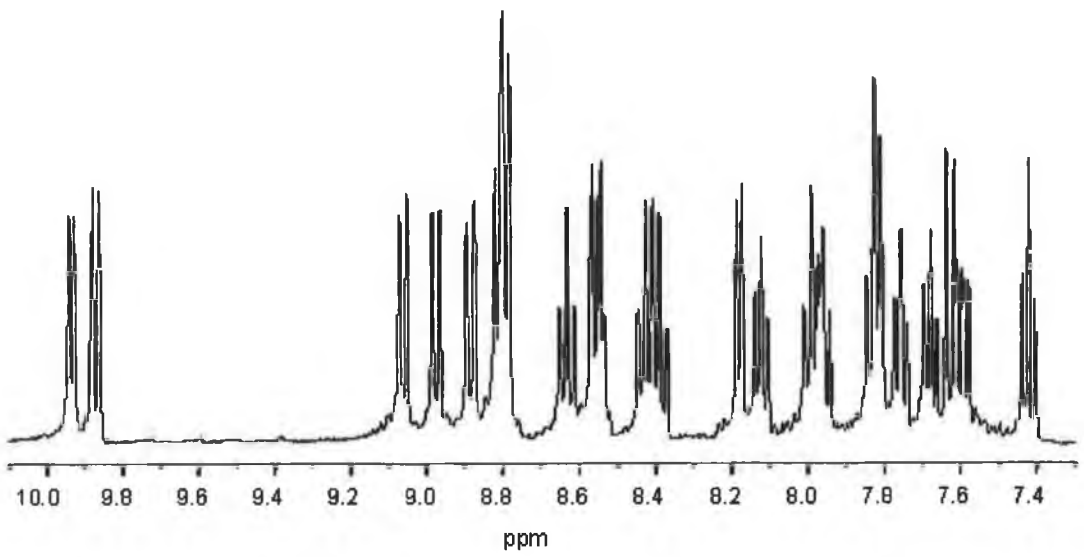

Figure 5.21 ^{1}H NMR spectrum of [Rh(bpy)$_2$(PTP)]$^{3+}$ in d_6-DMSO.

Table 5.8 allows for the comparison of complexes of the form $[M(bpy)_2(L)]^{n+}$, where L = PIP, MePIP or PTP and M = Rh x = 3 or M = Ru x = 2. It is important to note that the data cannot be directly compared as the spectra of the Ru(II) complexes were obtained in d_6-acetone and the Rh(III) in d_6-DMSO but in each case the values of the free ligands are given in the appropriate solvent and general behaviour of these complexes can be examined. It can be seen from this that, as expected, when the Rh(III) complexes are compared resonances associated with the complex incorporating the PTP ligand are found further downfield of the same protons of the in the complexes with the PIP and MePIP ligands.

It is also of interest to see how the PIP, MePIP and PTP complexes behave in comparison to the pyridyl triazole ligands previously discussed. Table 5.9 allows the direct comparison of bpy complexes containing the ligands PIP, MePIP, PTP, Hpytr, Hpztr, 4Mpytr, HPhpytr, HPhpztr, Hbpt and NH_2bpt. It should be noted that Table 5.9 only details the ^{1}H NMR data for the protons of the bound pyridine rings. Free pyridine rings and protons of fused rings such as in the case of the PIP, MePIP and PTP ligands have been omitted.

Table 5.9 ***^{1}H NMR data for the H3, H4, H5 and H6 protons of the bound pyridine rings for the complexes $[Rh(bpy)_2(L)]^{n+}$ where L=PIP, MePIP, PTP, Hpytr, Hpztr, 4Mpytr, HPhpytr, HPhpztr, Hbpt and NH_2bpt measured in d_6-DMSO.***

	H3	H4	H5	H6
$[Rh(bpy)_2(PIP)]^{3+}$	8.68 (d)	8.33 (dd)	7.45 (m)	7.64 (m)
$[Rh(bpy)_2(MePIP)]^{3+}$	8.85 (d)	8.43 (dd)	7.52 (dd)	7.67 (d)
$[Rh(bpy)_2(PTP)]^{3+}$	8.83-8.77 (m)	8.37-8.45 (m)	7.76 (dd)	8.18 (m)
$[Rh(bpy)_2(dppt)]^{3+}$	9.14-9.07 (m)	8.68 (dd)	8.17 (d)	8.07-8.03 (m)
$[Rh(bpy)_2(pytr)]^{2+}$	8.30 (d)	8.36 (dd)	7.58 (dd)	7.74 (m)
$[Rh(bpy)_2(pztr)]^{2+}$	9.52 (s)	-	8.80 (d)	7.85 (m)
$[Rh(bpy)_2(4Mpytr)]^{3+}$	8.97 (d)	8.34-8.46 (m)	7.72 (dd)	7.90 (d)
$[Rh(bpy)_2(Phpytr)]^{2+}$	8.37 (m)	8.37 (m)	7.56 (dd)	7.75 (d)
$[Rh(bpy)_2(Phpztr)]^{2+}$	9.58 (s)	-	8.80 (d)	7.89-7.81 (m)
$[Rh(bpy)_2(bpt)]^{2+}$	8.45-8.39 (m)	8.45-8.39 (m)	7.64-7.63(m)	7.87-7.82 (m)
$[Rh(bpy)_2(NHbpt)]^{2+}$	8.59 (d)	8.33 (dd)	7.48-7.44(m)	7.60 (d)
$[Rh(bpy)_2(NH_2bpt)]^{3+}$	9.02 (m)	8.65-8.55 (m)	7.90-7.83(m)	7.98 (m)

It can be seen from Table 5.9 that from a ^{1}H NMR perspective the protons of the coordinated pyridine rings appear to be comparable with a few exceptions. Due to their proximity to a nitrogen the H3 and the H5 protons of $[Rh(bpy)_2(pztr)]^{2+}$ and $[Rh(bpy)_2(Phpztr)]^{2+}$ occur downfield with respect to the H3 and the H5 protons of $[Rh(bpy)_2(pytr)]^{2+}$ and $[Rh(bpy)_2(Phpytr)]^{2+}$. It would appear that the H6 proton of $[Rh(bpy)_2(PTP)]^{3+}$ and the resonances associated with the bound pyridine ring of $[Rh(bpy)_2(NH_2bpt)]^{3+}$ are similarly affected.

^{13}C analysis was carried out where possible and the spectra of $[Rh(bpy)_2(ppt)]^{2+}$, $[Rh(bpy)_2(Phpztr)]^{2+}$ and $[Rh(phen)_2(PTP)]^{3+}$ and the data obtained can be seen in Appendix III.

5.3.4 Mass Spectrometry

Where possible, the complexes associated with this chapter were studied by means of mass spectrometry. The results were analysed with respect to verifying the presence of the desired product and for comparison of deuterated and non-deuterated complexes. For the complexes containing the ligands Hpztr, Hbpzt, HPhpztr and Hppt it was generally possible to see the complex with loss of one PF_6^- counter ion in each mass spectrum. In some cases the loss of the second counter ion could also be observed. Whereas no attempt was made to determine the entire fragmentation pattern of these complexes it was possible to pick out certain features in each mass spectrum. Table 5.10 details the results obtained for the following complexes; $[Rh(phen)_2(pztr)](PF_6)_2$, $[Rh(bpy)_2(pztr)](PF_6)_2$, $[Rh(phen)_2(bpzt)](PF_6)_2$, $[Rh(phen)_2(Phpztr)](PF_6)_2$, $[Rh(bpy)_2(Phpztr)](PF_6)_2$, $[Rh(phen)_2(ppt)](PF_6)_2$ and $[Rh(bpy)_2(ppt)](PF_6)_2$.

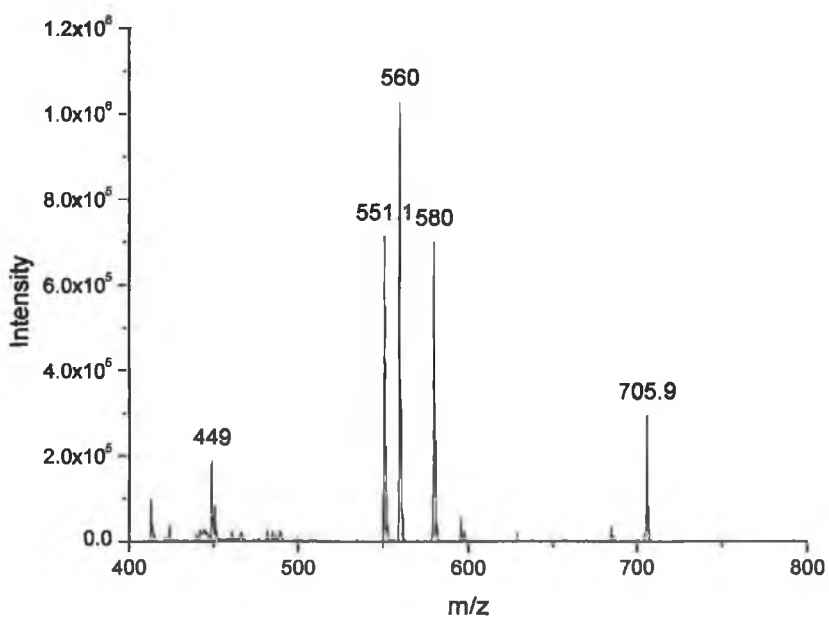

Figure 5.22 Mass spectrum $[Rh(bpy)_2(pztr)](PF_6)_2$ obtained in acetonitrile.

Table 5.10 ***Selection of mass spectrometry data obtained for complexes incorporating Hpztr, HPhpztr and Hppt measured in acetonitrile.***

	Fragment	Calculated m/z	Observed m/z
$[Rh(bpy)_2(pztr)](PF_6)_2$	$[[Rh(bpy)_2(pztr)](PF_6)]^+$	706.1	705.9
$[Rh(phen)_2(bpzt)](PF_6)_2$	$[[Rh(phen)_2(bpzt)](PF_6)]^+$	832.1	832.0
	$[phen+H]^+$	181.1	181.1
$[Rh(phen)_2(Phpztr)](PF_6)_2$	$[[Rh(phen)_2(Phpztr)](PF_6)]^+$	830.1	829.0
$[Rh(bpy)_2(Phpztr)](PF_6)_2$	$[[Rh(bpy)_2(Phpztr)](PF_6)]^+$	782.1	781.8
	$[Rh(bpy)_2(Phpztr)\text{-}H^+]^+$	636.1	635.9
	$[Rh(bpy)(Phpztr)]^+$	480.0	479.8
$[Rh(phen)_2(ppt)](PF_6)_2$	$[[Rh(phen)_2(ppt)](PF_6)]^+$	831.1	831.0
	$[Rh(phen)_2(ppt)\text{-}H^+]^+$	685.1	685.0

Although it was not possible to obtain mass spectra for the complexes $[Rh(phen)_2(dppt)](PF_6)_3$ and $[Rh(phen)_2(d_{10}\text{-dppt})](PF_6)_3$ spectra were obtained for $[Rh(bpy)_2(dppt)](PF_6)_3$ and $[Rh(bpy)_2(d_{10}\text{-dppt})](PF_6)_3$. Upon comparison of the mass spectra of $[Rh(bpy)_2(dppt)](PF_6)_3$ and $[Rh(bpy)_2(d_{10}\text{-dppt})](PF_6)_3$ it was found that a number of fragments differ by m/z 10 thus indicating that these fragments contained the ligands dppt and d_{10}-dppt and confirming that all 10 of the protons of the phenyl rings had been deuterated. It was not possible to assign all of the signals observed in the mass spectrum particularly in the case of the deuterated complex with fragments at m/z 529, m/z 604.9 and m/z 693.1 remaining unidentified. Table 5.11 summarises the fragments identified for the complexes $[Rh(bpy)_2(dppt)](PF_6)_3$ and $[Rh(bpy)_2(d_{10}\text{-dppt})](PF_6)_3$.

Table 5.11 Selection of mass spectrometry data for the complexes $[Rh(bpy)_2(dppt)](PF_6)_3$ and $[Rh(bpy)_2(d_{10}\text{-dppt})](PF_6)_3$.

	Fragment	Calculated m/z	Observed m/z
$Rh(bpy)_2(dppt)](PF_6)_3$	$[[Rh(bpy)_2(dppt)](PF_6)_2]^+$	1015.1	1014.9
	$[[Rh(bpy)_2(dppt)](PF_6)+H_2O\text{-}H^+]^+$	887.1	887.0
$Rh(bpy)_2(d_{10}\text{-dppt})](PF_6)_3$	$[[Rh(bpy)_2(d_{10}\text{-dppt})](PF_6)_2]^+$	1025.2	1025.0

The final series of complexes studied were those containing the ligands PIP, MePIP and PTP. The fragmentation patterns of these complexes were found to be less complicated than those already discussed and in most cases it was possible to identify all of the signals observed in the spectra obtained. Figure 5.23 and Figure 5.24 illustrate the mass spectra obtained for the complexes $[Rh(phen)_2(MePIP)](PF_6)_3$ and $[Rh(bpy)_2(MePIP)](PF_6)_3$. Table 5.12 summarises, where possible, the fragments identified in the spectra of the PIP, MePIP and PTP complexes.

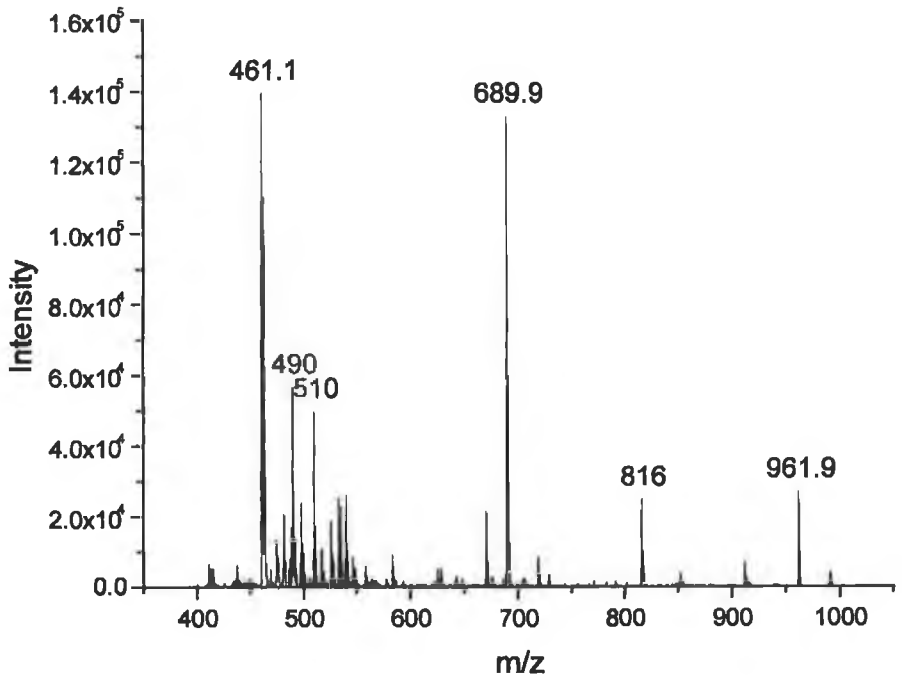

Figure 5.23 Mass spectrum [Rh(phen)$_2$(MePIP)](PF$_6$)$_3$ obtained in acetonitrile.

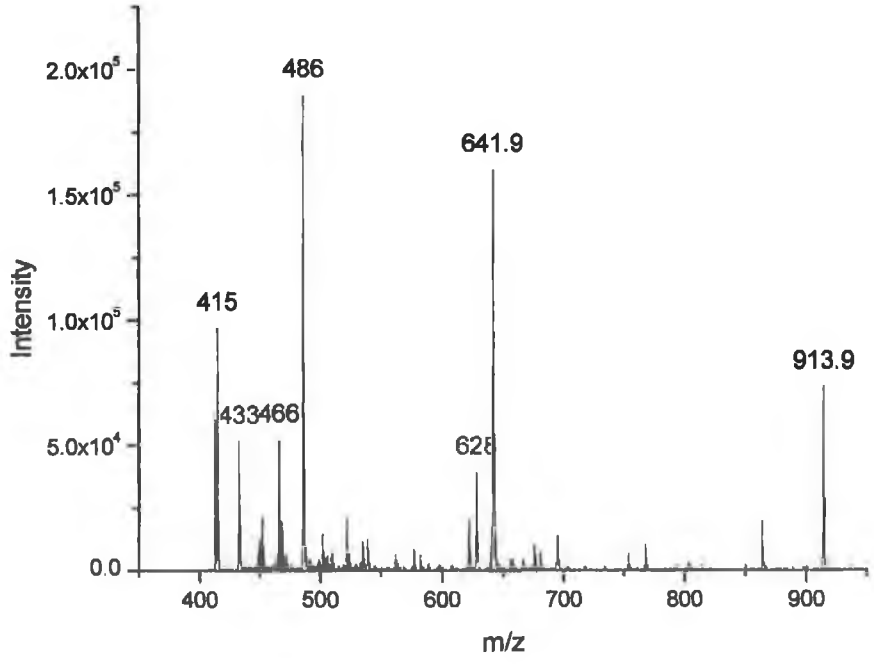

Figure 5.24 Mass spectrum [Rh(bpy)$_2$(MePIP)](PF$_6$)$_3$ obtained in acetonitrile.

Table 5.12 ***Selection of Mass spectrometry data for the following complexes with the ligands PIP, MePIP and PTP measured in acetonitrile.***

	Fragment	Calculated m/z	Observed m/z
$[Rh(phen)_2(PIP)](PF_6)_3$	$[[Rh(phen)_2(PIP)](PF_6)_2]^+$	948.1	947.9
	$[[Rh(phen)_2(PIP)](PF_6)–H^+]^+$	802.1	802.0
$[Rh(bpy)_2PIP](PF_6)_3$	$[[Rh(bpy)_2(PIP)](PF_6)_2]^+$	900.1	899.9
	$[[Rh(bpy)_2(PIP)](PF_6)-H^+]^+$	754.1	754.0
$[Rh(phen)_2(MePIP)](PF_6)_3$	$[[Rh(phen)_2(MePIP)](PF_6)_2]^+$	962.1	961.9
	$[[Rh(phen)_2(MePIP)](PF_6)-H^+]^+$	816.1	815.9
$[Rh(bpy)_2(MePIP)](PF_6)_3$	$[[Rh(bpy)_2(MePIP)](PF_6)_2]^+$	914.1	914.0
	$[[Rh(bpy)_2(MePIP)]+H_2O]^+$	642.1	641.9
	$[[Rh(bpy)(MePIP)]+H_2O]^+$	486.1	486.0
$[Rh(phen)_2(PTP)](PF_6)_3$	$[[Rh(phen)_2(PTP)](PF_6)_2]^+$	949.0	948.9
	$[[Rh(phen)_2(PTP)](PF_6)-H^+]^+$	803.1	803.0

5.4 Conclusions

In this chapter the synthesis and structural characterisation of a series of complexes $[Rh(L)_2(L')]^{n+}$ where L = bpy or phen, L' = a pyrazine, triazine, imidazole or triazole based ligand and n = 2 or 3. The pyrazine based complexes were found to require longer reactions times and gave lower yields than their pyridine triazole analogues which were discussed in Chapter 3 and as was the case for the pyridine triazole complexes all of the pyrazine based complexes isolated were found to be deprotonated. Generally it was not possible to determine the mode of coordination employed by these complexes but NMR spectroscopy proved particularly useful in elucidating the mode of coordination in complexes with the Hppt ligand and it was found that coordination occurs predominantly via the pyridine ring of the Hppt ligand. It was not possible however to determine if these isomers were bound via the N2' or the N4' positions of the pyridine ring. The issue of coordination modes will be addressed again Chapter 8, where it will be considered, taking the photophysical and electrochemical properties of these complexes into account.

Triazine and imidazole based complexes were also investigated and it was found that the synthesis of these types of complexes required much shorter reaction times and gave higher yields than the pyridine and pyrazine triazole complexes previously detailed. Unlike the pyridine and pyrazine triazole complexes isomer formation was not a concern with complexes incorporating these ligands. Some variations in the ^1H NMR spectra were observed and when compared, Table 5.9, it can be seen that the introduction of the second nitrogen into the pyridine ring giving a pyrazine based complex results in a downfield shift of the H3 and H5 protons. The triazine H3, H5 and H6 resonances are further downfield than almost all of the other complexes studied and this can be related to their σ donor / π acceptor properties as the dppt ligands are the weakest σ donors and strongest π acceptors of all the ligands studied. The resonances of the H3, H4, H5 and H6 protons of the imidazole based complexes do not differ significantly than those of the pyridine triazole based complexes however the H6 protons of $[Rh(phen)_2(PTP)](PF_6)_3$ and

$[Rh(bpy)_2(PTP)](PF_6)_3$ are shifted almost 0.50 ppm further downfield than the same protons of the PIP and MePIP complexes.

It is expected, due to the differing σ donor / π acceptor properties of the complexes discussed in this chapter that their photophysical and electrochemical properties will differ significantly and the following chapter concentrates on the study of these properties.

References:

1 R.J. Crutchley, A.B.P. Lever, *J. Am. Chem. Soc.*, **1980**, *102*, 7128-7129.

2 R. Hage, J.G. Haasnoot, H.A. Nieuwenhuis, J. Reedijk, R. Wang, J.G. Vos, *J. Chem. Soc., Dalton Trans.*, **1991**, 3271-3275.

3 H.A. Nieuwenhuis, J.G. Haasnoot, R. Hage, J. Reedijk. T.L. Snoeck, D.J. Stufkens, J.G. Vos, *Inorg. Chem.*, **1991**, *30*, 48-54.

4 R.M. Berger, D.D. Ellis II, *Inorg. Chim. Acta*, **1996**, *241*, 1-4.

5 R.M. Berger, J.R. Holcombe, *Inorg. Chim. Acta*, **1995**, *232*, 217-221.

6 P. Paul, B. Tyagi, M.M. Bhadbhade, E. Suresh, *J. Chem.Soc., Dalton Trans,* **1997**, 2273-2277.

7 P. Paul, B. Tyagi, A.K. Bilakhiya, M.M. Bhadbhade, E. Suresh, G. Ramachandraiah, *Inorg. Chem.*, **1998**, *37*, 5733-5742.

8 R. Hage, J.H. van Diemen, G. Ehrlich, J.G. Haasnoot, D.J. Stufkens, T.L. Snoeck, J.G. Vos, J. Reedijk, *Inorg. Chem.*, **1990**, *29*, 988-993.

9 T.E. Keyes, F. Weldon, E. Müller, P. Pechy, M. Grätzel, *J. Chem. Soc., Dalton Trans.*, **1995**, 2705-2706.

10 M. Hage, T. Ano, T. Ishizaki, K.Kano, K. Nozaki, *J. Chem. Soc., Dalton Trans*, **1994**, 263-272.

11 P.M. Gidney, R.D. Gillard, B.T. Heaton, *J. Chem. Soc., Dalton Trans.*, **1972**, 2621-2628.

12 R. Hage, *Ph.D. Thesis*, Leiden University, The Netherlands, **1991**.

13 P. Paul, B. Tyagi, A.K. Bilakhiya, P. Dastidar, E. Suresh, *Inorg. Chem.*, **2000**, *39*, 14-22.

14 J. Granifo, *Polyhedron*, **1999**, *18*, 1061-1066.

15 J. Granifo, *Polyhedron*, **1996**, *15*, 203-209.

16 R. Uma, M. Palaniandavar, R.J. Butcher, *J. Chem. Soc., Dalton Trans.*, **1996**, 2061-2066.

17 J. Granifo, *Polyhedron*, **1995**, *14*, 1593-1599.

18 R. Hage, J.H. van Diemen, G. Erlich, J.G. Haasnoot, D.J. Stufkens, T.L. Snoeck, J.G. Vos, J. Reedijk, *Inorg. Chem.*, **1990**, *29*, 988-993.

19 Adrian Guckian, *PhD. Thesis*, Dublin City University, 2002.

20 Christine O'Connor, *PhD. Thesis*, Dublin City University, 1999.

Chapter 6 – The Photophysical and Electrochemical properties of Rh(III) complexes incorporating pyrazine triazole, triazine and imidazo ligands.

"If you are out to describe the truth, leave elegance to the tailor."

Albert Einstein

Abstract: The photophysical and electrochemical properties of the complexes incorporating pyrazine triazole, triazine and imidazole based ligands are characterised in the same manner as those containing pyridine triazole ligands. The results of the analysis of the absorption and emission data of these complexes are outlined in the following chapter and again several of the complexes studied exhibited both π–π^* and d-d* based emissions but such dual emitting behaviour was not detected for any of the complexes incorporating triazine ligands or ligands incorporating a fused ring i.e. PIP, MePIP or PTP. Unlike the complexes incorporating pyridyl triazole ligands all of the complexes related in this chapter absorbed in the region of 355 nm thus making it possible to obtain low temperature lifetimes in both a μs and ms time range and the electrochemical behaviour of the complexes in question was again probed using cyclic voltammetry and differential pulse voltammetry. Throughout the following chapter the behaviour exhibited by these complexes is compared with the behaviour of tris homoleptic complexes $[Rh(phen)_2]^{3+}$ and $[Rh(bpy)_2]^{3+}$, the Rh(III) pyridyl triazole complexes discussed in Chapter 3 and 4 and where possible with analogous Ru(II) complexes.

6.1 Introduction

Chapter 4 discussed the photophysical behaviour of Rh(III) pyridyl triazole complexes and also outlined the processes associated with absorption and emission processes. In general these complexes exhibited a dual emitting behaviour whereby emission from both a π-π^* state, located on either the phen or the bpy ligand depending upon the nature of the complex, and a d-d* state was observed. It was only possible to obtain the lifetimes in the μs region for these complexes and lifetimes of between 4 and 21 μs were observed. Chapter 5 detailed the synthesis of three series of complexes, the properties of which will be discussed in this chapter. The first series of complexes detailed in Chapter 5 incorporated pyrazine triazole ligands. From a synthetic point of view the pyrazine complexes required longer reaction times than their pyridine triazole counterparts. It was anticipated that these complexes would behave differently from a photophysical point of view based upon the fact that bipyrazine is known to be a weaker σ-donor than bipyridine.[1] Analysis of complexes of the form $[Ru(bpy)_2(L)]^{n+}$, where L = pyrazine triazole based ligand and n = 1 or 2, found that when deprotonated these complexes exhibited a bpy based emission yet when protonated the emission was found to involve the Hpztr ligand. The protonation of the triazole ring resulted in the LUMO of the Hpztr ligand being situated just lower than that of the bpy ligand thus accounting for the shift from a bpy based emission in the deprotonated form to a pyrazine based emission in the protonated form.[2,3,4]

The second series of complexes studied incorporated the triazine based ligand dppt. Hage *et. al.* and studied the photophysical and electrochemical properties of complexes of the form $[Ru(bpy)_2(L)]^{2+}$ where L = dppt - 5,6-diphenyl-3-(pyridin-2-yl)-1,2,4-triazine, dmpt - 5,6-dimethyl-3-(pyridin-2-yl)-1,2,4-triazine and tpt - 3,5,6-tris(pyridin-2-yl)-1,2,4-triazine and $[Ru(L)_3]^{2+}$ where L = dppt or dmpt whilst the nature of the emitting state of $[Ru(bpy)_2(dppt)]^{2+}$ was studied by Keyes *et. al.*[5,6] Hage *et. al.* found that all of the complexes displayed emission at room temperature and at 77K and resonance Raman and electrochemical studies showed evidence to suggest that that the pyridyl triazine ligands have rather low lying LUMO levels.[5]

Keyes *et. al.* used the technique of deuteration to probe the excited state of $[Ru(bpy)_2(dppt)]^{2+}$ by comparing the behaviour of $[Ru(bpy)_2(dppt)]^{2+}$ and $[Ru(d_8\text{-}bpy)_2(dppt)]^{2+}$ with that of $[Ru(bpy)_2Phpytr]^{+}$ and $[Ru(d_8\text{-}bpy)_2Phpytr]^{+}$ from the perspective of their emission lifetimes. When studied it was found that the lifetime of $[Ru(d_8\text{-}bpy)_2Phpytr]^{+}$ was 410 ns whereas the lifetime of the non-deuterated complexes was 225 ns. This increase in the observed lifetimes upon deuteration of the bpy ligand implied that it was the bpy ligand that was involved in the excited state. In contrast the lifetimes of $[Ru(bpy)_2(dppt)]^{2+}$ and $[Ru(d_8\text{-}bpy)_2(dppt)]^{2+}$ were found to be 740 ns and 780 ns respectively. The absence of any significant difference between the lifetimes of the $[Ru(bpy)_2(dppt)]^{2+}$ and $[Ru(d_8\text{-}bpy)_2(dppt)]^{2+}$ indicated that in the triazine complex the emitting state is located upon the electron poor triazine ligand and as a result the vibrational modes affected by the deuteration are not available for a deactivation of the excited state.[6]

The final series of complexes, which are to be discussed here, are those that feature the ligands PIP, MePIP and PTP. Whereas both PIP and MePIP ligands are imidazo based PTP is a triazo-based ligand and as a result it is expected that it will exhibit different photophysical and electrochemical properties. Complexes of the form $[Ru(bpy)_2(X)]^{2+}$ where X = PIP, MePIP or PTP have previously be studied and the behaviour of the Rh(III) complexes will be compared what that exhibited by their Ru(II) analogues.[7]

In addition to studying the photophysical properties of the complexes related in Chapter 5 the electrochemical properties of these complexes have also been probed. By varying the types of the ligands, thus altering the σ donating properties, it is expected that behaviour of the complexes will vary and will be reflected in the photophysical and electrochemical properties of the complexes. Therefore it is of importance to consider the results obtained from the characterisation of these complexes in relation to the behaviour of the Rh(III) complexes detailed in Chapter 4 and with Ru(II) analogues.[2]

6.2 Results and Discussion

6.2.1 Absorption Spectroscopy

The UV absorption spectra of the complexes $[Rh(phen)_3]^{3+}$ and $[Rh(bpy)_3]^{3+}$ are both π-π^* in nature whilst the pyridine triazole complexes detailed in Chapter 4 demonstrated behaviour which was being predominantly π-π^* in nature evidence was also found to indicate that d-d* bands were also present. Figure 6.1 illustrates the UV spectrum obtained for $[Rh(bpy)_2(pztr)]^{2+}$ (——) and the spectrum of $[Rh(bpy)_2(pytr)]^{2+}$(——) is included for comparison purposes.

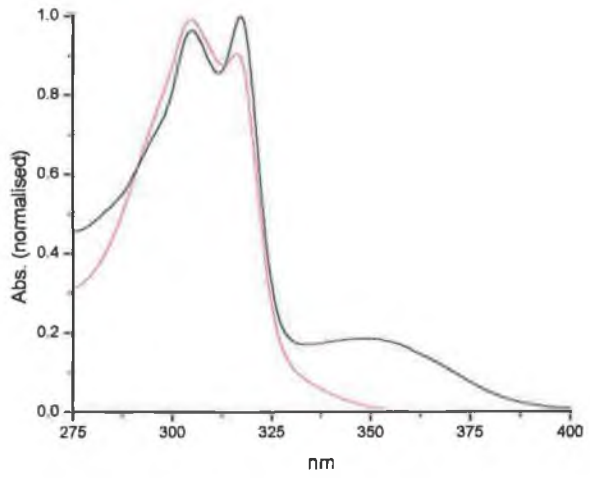

Figure 6.1 Absorption spectra of $[Rh(bpy)_2(pztr)]^{2+}$ (——) and $[Rh(bpy)_2(pytr)]^{2+}$ (——) measured in acetonitrile at room temperature.

When compared we can see a definite broad band in the spectrum of $[Rh(bpy)_2(pztr)]^{2+}$ as compared with that of $[Rh(bpy)_2(pytr)]^{2+}$. There are a number of possibilities for the origin of this band with it possibly being associated with a π-π^* transition associated with the pyrazine ring or with a d-d* or a charge transfer (CT) transition. As was the case for the pyridine triazole complexes, Section 4.2.1, this band is tentatively assigned as d-d* transition based upon its position and intensity. Table 6.1 details the absorption data for all of the complexes discussed in this chapter.

Table 6.1 ***Absorption data for $[Rh(phen)_3]^{3+}$, $[Rh(bpy)_3]^{3+}$ and complexes with the ligands Hpztr, HPhpztr, Hppt, dppt, PIP, MePIP and PTP measured in acetonitrile.***

Complex	Absorption (nm) (log ε)	Complex	Absorption (nm) (log ε)
$[Rh(phen)_3]^{3+}$	334 (3.10) 351 (4.18)	$[Rh(bpy)_3]^{3+}$	307 (36.3) [a] 321 (38.3) [a]
$[Rh(phen)_2(pztr)]^{2+}$	b	$[Rh(bpy)_2(pztr)]^{2+}$	242 (4.49) 305 (4.38) 317 (4.40) 349 sh (3.66)
$[Rh(phen)_2(Phpztr)]^{2+}$	273 (4.80) 302 sh (4.31) 336 sh (3.74) 352 sh (3.76)	$[Rh(bpy)_2(Phpztr)]^{2+}$	245(4.69) 306 (4.50) 319 (4.49) 378 sh (3.71)
$[Rh(phen)_2(bpzt)]^{2+}$	277 (4.89) 301 sh (4.49) 334 sh (3.86) 351 sh (3.91)	$[Rh(bpy)_2(bpzt)]^{2+}$	b
$[Rh(phen)_2(ppt)]^{2+}$	274 (4.83) 300 sh (4.47) 330 sh (4.08) 348 sh (3.85)	$[Rh(bpy)_2(ppt)]^{2+}$	301 (4.76) 313 (4.39)
$[Rh(phen)_2(dppt)]^{3+}$	276 (4.96) 300 sh, (4.63) 352 sh (4.18)	$[Rh(bpy)_2(dppt)]^{3+}$	306 (4.65) 319 (4.62) 343 sh (4.19)
$[Rh(phen)_2(PIP)]^{3+}$	277 (4.82) 302 (4.36) 353 sh (4.23) 369 (4.32) 386 (4.27)	$[Rh(bpy)_2(PIP)]^{3+}$	243 (4.72) 305 (4.56) 319 (4.55) 369 (4.33) 386 (4.28)
$[Rh(phen)_2(MePIP)]^{3+}$	277 (4.86) 301 sh (4.37) 334 (4.01) 351 (4.03) 393 sh (4.20) 414 (4.28)	$[Rh(bpy)_2(MePIP)]^{3+}$	242 (4.70) 306 (4.54) 319 (4.58) 394 sh (4.26) 415 (4.35)
$[Rh(phen)_2(PTP)]^{3+}$	277 (4.72) 302 (4.25) 340 (4.03) 352 (4.01)	$[Rh(bpy)_2(PTP)]^{3+}$	304 (4.63)

a = values takes from ref.8 b-pure complex not isolated

If we consider the spectra of $[Rh(phen)_2(Phpztr)]^{2+}$ and $[Rh(bpy)_2(Phpztr)]^{2+}$, as seen in Figure 6.2, then we can see that this band is again present. The absorption spectra

of the complexes incorporating the dppt ligand demonstrate similar characteristics (Appendix IV).

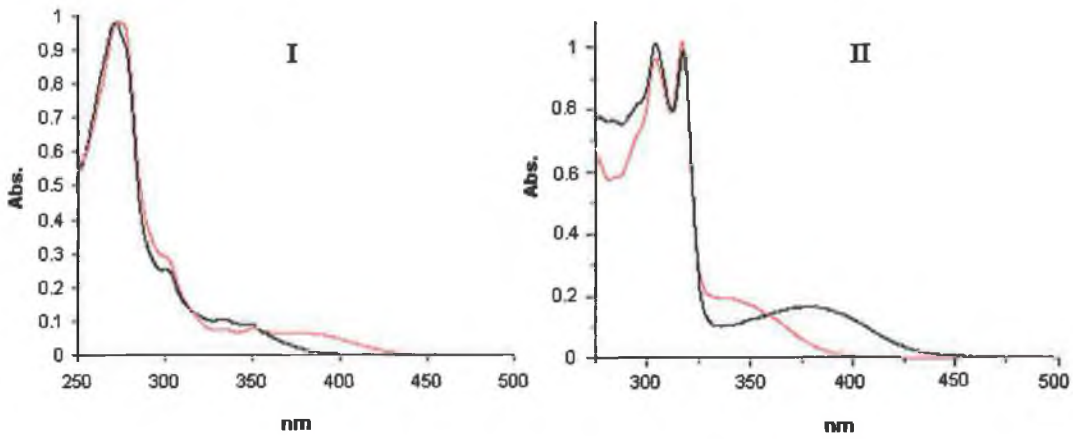

Figure 6.2 Absorption spectra of (I) $[Rh(phen)_2(Phpztr)]^{2+}$ (——) and $[Rh(phen)_2(Phpytr)]^{2+}$ (——) and (II) $[Rh(bpy)_2(Phpztr)]^{2+}$ (——) and $[Rh(bpy)_2(Phpytr)]^{2+}$ (——) measured in acetonitrile at room temperature.

The third series of complexes are those including the PIP, MePIP and PTP ligands. These ligands absorb at higher energies than the pyridine and pyrazine based complexes discussed previously. Absorption maxima for the free ligands are found at 225 nm, 282 nm, 325 nm and 357 nm for PIP, 248 nm and 358 nm for MePIP and 243 nm and 308 nm for PTP. Figure 6.3 illustrates the absorption spectra of the complexes $[Rh(phen)_3]^{3+}$, $[Rh(phen)_2(PIP)]^{3+}$, $[Rh(phen)_2(MePIP)]^{3+}$ and $[Rh(phen)_2(PTP)]^{3+}$. Complexes containing these ligands absorb over a broad wavelength with bands between 325 nm and 460 nm being attributed to the PIP, MePIP and PTP ligands. Figure 6.4 illustrates the spectra of $[Rh(bpy)_2(PIP)]^{3+}$, $[Rh(bpy)_2(MePIP)]^{3+}$ and $[Rh(bpy)_2(PTP)]^{3+}$ and again bands associated with the free ligands can be seen clearly. The differing behaviour of the PIP and the MePIP ligands as compared with the PTP ligand can clearly be seen here with $[Rh(phen)_2(PIP)]^{3+}$, $[Rh(phen)_2(MePIP)]^{3+}$, $[Rh(bpy)_2(PIP)]^{3+}$ and $[Rh(bpy)_2(MePIP)]^{3+}$ exhibiting strong absorption bands between 350 nm and 450 nm in comparison to the weaker absorption exhibited by $[Rh(phen)_2(PTP)]^{3+}$ and particularly $[Rh(bpy)_2(PTP)]^{3+}$ in this region.

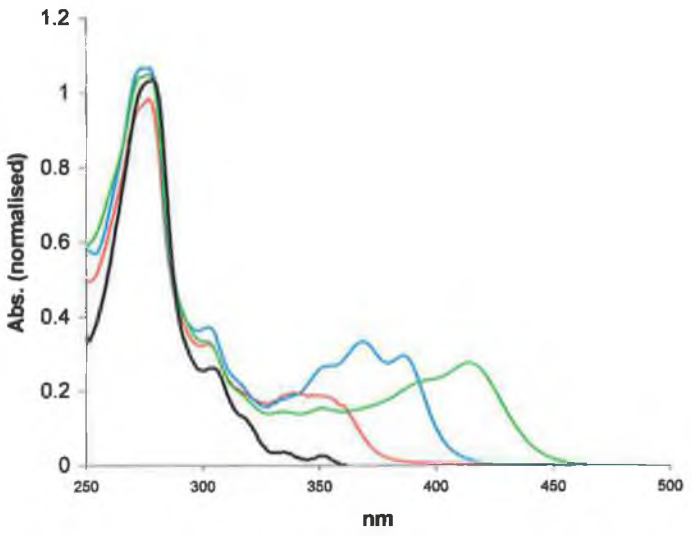

Figure 6.3 Absorption spectra of $[Rh(phen)_3]^{3+}$ (——), $[Rh(phen)_2(PIP)]^{3+}$ (——), $[Rh(phen)_2(MePIP)]^{3+}$ (——) and $[Rh(phen)_2(PTP)]^{3+}$ (——) measured in acetonitrile at room temperature.

All of the absorption bands exhibited by the complexes in Figure 6.3 are attributed to ligand based π-π^* transitions based on either the phen ligand (250nm -350 nm) or on the ligands containing a fused ring (350nm - 460nm). These assignments have been reached based upon comparisons with the tris homoleptic complex $[Rh(phen)_3]^{3+}$ and the free phen, PIP, MePIP and PTP ligands. Similarly, all of the absorption bands exhibited by the complexes $[Rh(bpy)_2(L)]^{3+}$ where L = PIP, MePIP or PTP in Figure 6.4 are attributed to ligand based π-π^* transitions based on either the bpy ligand (275nm -340 nm) or on the ligands containing a fused ring (340nm - 460nm). Table 6.1 details the absorption data obtained for the complexes $[Rh(phen)_3]^{3+}$ and $[Rh(bpy)_3]^{3+}$ and for complexes incorporating the ligands Hpztr, HPhpztr, Hbpzt, Hppt, dppt, PIP, MePIP, and PTP.

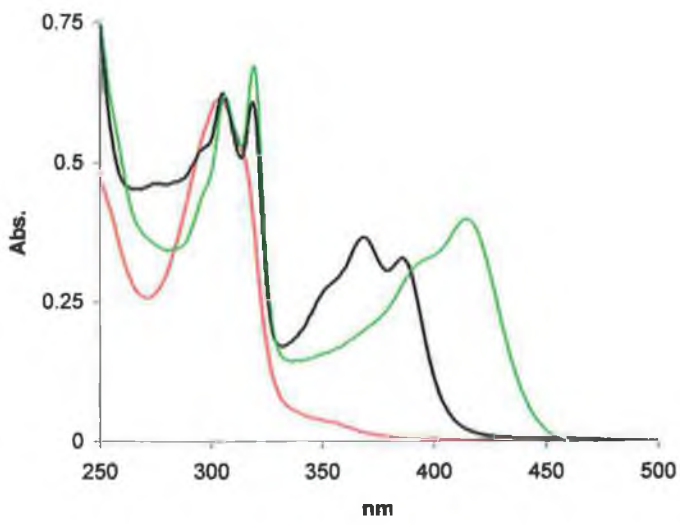

Figure 6.4 Absorption spectra of $[Rh(bpy)_2(PIP)]^{3+}$ (——), $[Rh(bpy)_2(MePIP)]^{3+}$ (——) and $[Rh(bpy)_2(PTP)]^{3+}$ (——) measured in acetonitrile at room temperature.

6.2.2 Emission Spectroscopy

It should be noted that all of these experiments were carried out at 77K. As was the case with the pyridine triazole complexes detailed in Chapter 4, when studying the luminescence of the pyrazine triazole complexes on with a lifetime >1 ms the complexes were studied over the wavelength range 285 nm to 350 nm but unless otherwise stated all of the spectra shown were obtained with a λ_{ex} of 305nm. When an emission was detected on a timescale < 1ms the spectrum was obtained using a λ_{ex} of 337 nm.

6.2.2.1 Complexes incorporating pyrazine triazole ligands

Figure 6.5 below illustrates the emission spectra obtained for $[Rh(bpy)_2(pztr)]^{2+}$ and it can be seen that this is a dual emitting complex with maxima at 492 nm and 614 nm. In contrast to the behaviour of $[Rh(bpy)_2(pytr)]^{2+}$ neither of the emissions exhibited by $[Rh(bpy)_2(pztr)]^{2+}$ are structured.

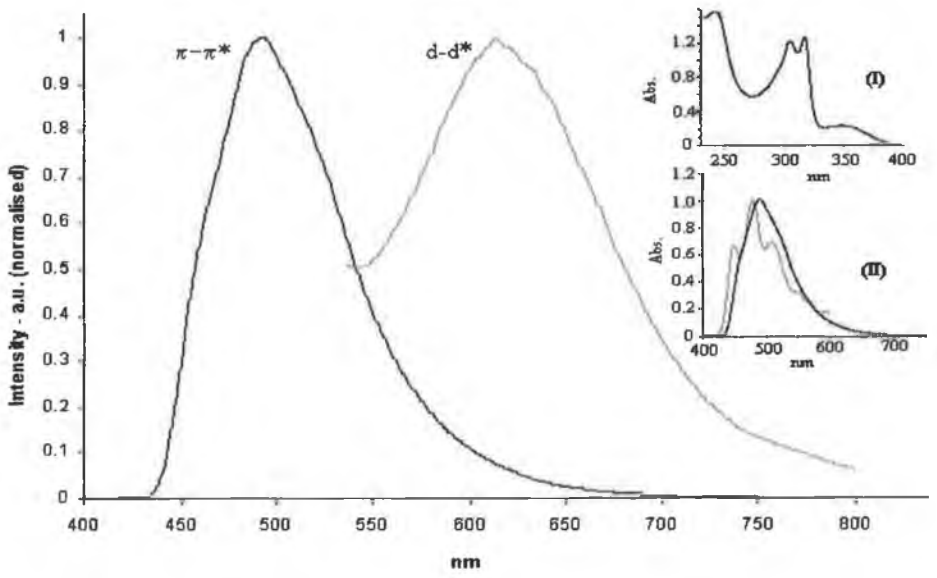

Figure 6.5 Emission spectra of $[Rh(bpy)_2(pztr)]^{2+}$ measured in ethanol:methanol 4:1 at 77K. Inset (I) shows the UV spectrum of $[Rh(bpy)_2(pztr)]^{2+}$ and inset (II) portrays the π–π* emission spectra of $[Rh(bpy)_2(pztr)]^{2+}$ (——) compared with $[Rh(bpy)_2(pytr)]^{2+}$ (——) measured in ethanol:methanol 4:1 at 77K.

Based upon the behaviour of the pyridine triazole complexes, the emission exhibited by $[Rh(bpy)_2(pztr)]^{2+}$ at 614 nm can be attributed to a d-d* based emission. The pyridine triazole complexes all exhibited a ligand based emission between 400 nm and 600 nm the structure of which was coincident with that of the appropriate tris homoleptic complex. $[Rh(bpy)_2(pztr)]^{2+}$ does exhibit an emission in this region, with a maximum at 492 nm, but the absence of any fine structure implies that this is a ligand based emission based not on the bpy ligand but on the pyrazine triazole ligand. The emission data for all of the complexes detailed in this chapter can be seen in Table 6.2.

Table 6.2 ***Emission data for $[Rh(phen)_3]^{3+}$, $[Rh(bpy)_3]^{3+}$ and complexes containing the ligands Hpztr, HPhpztr, Hbpzt, Hppt, dppt, PIP, MePIP and PTP measured in ethanol:methanol 4:1 at 77K.***

Complex	Emission (nm)	Complex	Emission (nm)
$[Rh(phen)_3]^{3+}$		**$[Rh(bpy)_3]^{3+}$**	
(π–π*)	454, 483, 512 sh [a]	**(π–π*)**	450, 483, 510[a]
(d-d*)	-	**(d-d*)**	-
$[Rh(phen)_2(pztr)]^{2+}$	b	**$[Rh(bpy)_2(pztr)]^{2+}$**	
(π–π*)	-	**(π–π*)**	492
(d-d*)	-	**(d-d*)**	614
$[Rh(phen)_2(Phpztr)]^{2+}$		**$[Rh(bpy)_2(Phpztr)]^{2+}$**	
(π–π*)	517	**(π–π*)**	493, 519
(d-d*)	620	**(d-d*)**	624
$[Rh(phen)_2(bpzt)]^{2+}$		**$[Rh(bpy)_2(bpzt)]^{2+}$**	b
(π–π*)	498	**(π–π*)**	-
(d-d*)	637	**(d-d*)**	-
$[Rh(phen)_2(ppt)]^{2+}$		**$[Rh(bpy)_2(ppt)]^{2+}$**	
(π–π*)	508	**(π–π*)**	509
(d-d*)	638	**(d-d*)**	629
$[Rh(phen)_2(dppt)]^{3+}$		**$[Rh(bpy)_2(dppt)]^{3+}$**	
(π–π*)	544	**(π–π*)**	473,516, 542
(d-d*)	-	**(d-d*)**	-
$[Rh(phen)_2(d_{10}\text{-dppt})]^{3+}$		**$[Rh(bpy)_2(d_{10}\text{-dppt})]^{3+}$**	
(π–π*)	542	**(π–π*)**	451, 476, 517, 540
(d-d*)	-	**(d-d*)**	-
$[Rh(phen)_2(PIP)]^{3+}$		**$[Rh(bpy)_2(PIP)]^{3+}$**	
(π–π*)	547, 591	**(π–π*)**	545, 589
(d-d*)	-	**(d-d*)**	-
$[Rh(phen)_2(MePIP)]^{3+}$		**$[Rh(bpy)_2(MePIP)]^{3+}$**	
(π–π*)	554, 594	**(π–π*)**	553, 589
(d-d*)	-	**(d-d*)**	-
$[Rh(phen)_2(PTP)]^{3+}$		**$[Rh(bpy)_2(PTP)]^{3+}$**	
(π–π*)	480, 515, 548 sh	**(π–π*)**	480, 512, 541
(d-d*)	-	**(d-d*)**	-

a – values taken from ref. 8 and 9 b – pure complex not isolated

The emission spectra of $[Rh(phen)_2(Phpztr)]^{2+}$ and $[Rh(bpy)_2(Phpztr)]^{2+}$ can be seen in Figure 6.6. Both the π-π* and the d-d* emissions have been normalised but it can be seen that even on a short timescale (<1ms, d-d* emission spectrum (——)) the emission is predominantly π-π* based, with the d-d* being evident as a shoulder. This is in contrast to the behaviour of the pyridine and pyrazine based complexes discussed previously in which the π-π* based emissions were dwarfed by the d-d* emission on this timescale (i.e.<1ms).

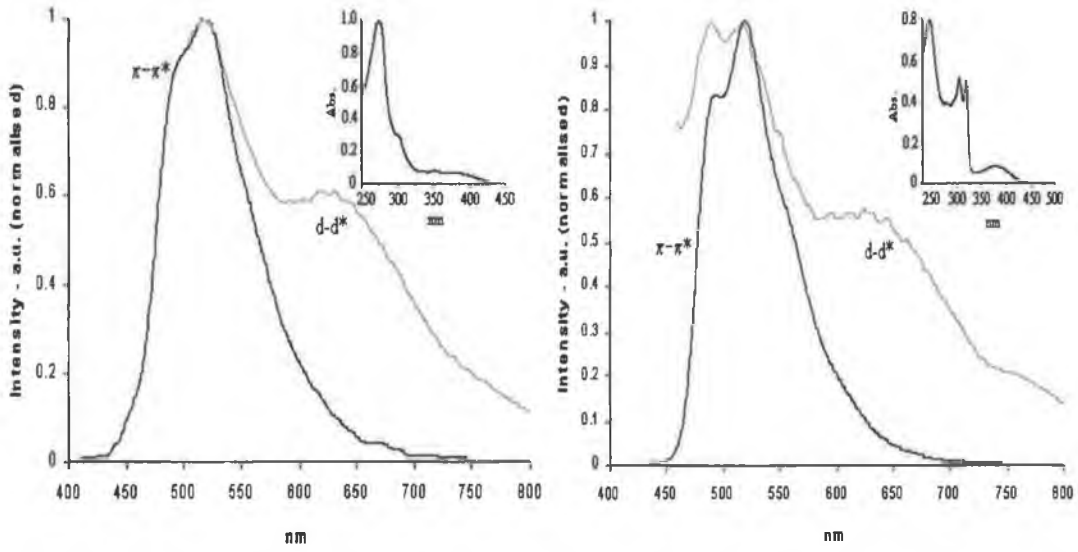

Figure 6.6 Emission spectra of (a) $[Rh(phen)_2(Phpztr)]^{2+}$ and (b) $[Rh(bpy)_2(Phpztr)]^{2+}$ measured in ethanol:methanol 4:1 at 77K. Inset shows the UV spectrum of (a) $[Rh(phen)_2(Phpztr)]^{2+}$ and (b) $[Rh(bpy)_2(Phpztr)]^{2+}$.

Figure 6.7 shows the emission spectra of $[Rh(phen)_2(bpzt)]^{2+}$. Once again emission associated with both π-π* and d-d* transitions is observed. The emission at 498 nm does appear to be structured to some degree and in contrast to $[Rh(phen)_2(Phpztr)]^{2+}$ the d-d* based emission here was readily detected and quite intense. From previous studies it is known that the pyrazine triazole ligands are weaker σ donors then the pyridine triazole ligand and it was shown in Chapter 4 that the metal based emission of these pyridine triazole complexes was dependent upon their σ donating properties.[2] As a result it might be expected that the d-d* based emissions exhibited by the pyrazine based complexes would be shifted to higher energies relative to their pyridine triazole analogues. However, when compared no

significant differences were found between the emission maxima with differences of ≤ 5 nm being observed. It was however observed that the metal based emission was particularly weak for complexes with the HPhpztr ligand.

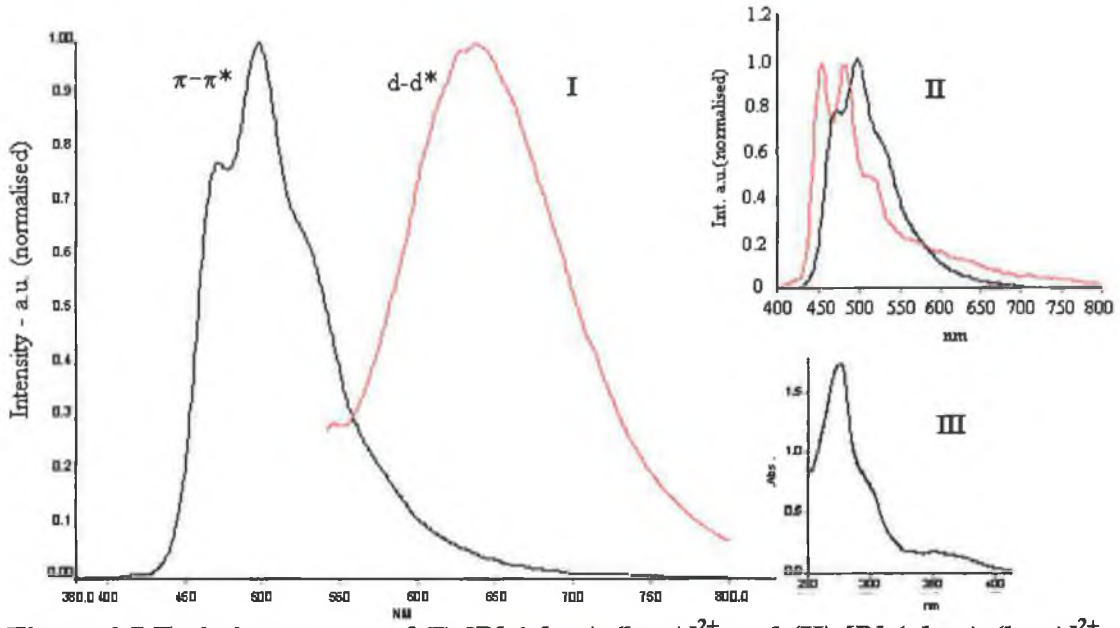

Figure 6.7 Emission spectra of (I) $[Rh(phen)_2(bpzt)]^{2+}$ and (II) $[Rh(phen)_2(bpzt)]^{2+}$ (——) and $[Rh(phen)_2(pytr)]^{2+}$(——)measured in ethanol:methanol 4:1 at 77K. The UV spectrum of $[Rh(phen)_2(bpzt)]^{2+}$ is shown in (III).

Of the pyrazine triazole ligands studied this is the weakest σ donor due to the presence of the phenyl ring and would thus have the lowest ^{3}MC state. It would appear from the intensity of the metal based emission that conversion between the d-d* and the π-π* states is occurring to some degree. As the ligands are varied from Hpztr to Hbpzt to Hppt the σ donor strength increases and this is reflected in the increasing intensity of the metal based emissions detected. Hbpzt is a stronger σ donor than Hpztr due to the presence of a second pyrazine ring and Hppt is stronger again due to the influence of the pyridine ring. Complexes incorporating the Hppt ligand again exhibited both a d-d* based emission and a π-π* based emission. Based upon the results obtained, the π-π* based emission exhibited by $[Rh(phen)_2(ppt)]^{2+}$ and $[Rh(bpy)_2(ppt)]^{2+}$ was assigned as being located upon the Hppt ligand. This assignment was based upon the hyperfine structure and λ_{max} exhibited by these complexes. The π-π* based emission exhibited of $[Rh(bpy)_2(ppt)]^{2+}$ can be seen in Appendix IV (Figure AIV.5).

6.2.2.2 *Complexes incorporating triazine ligands*

The emission spectrum of $[Rh(phen)_2(dppt)]^{3+}$ can be seen in Figure 6.8 and that of $[Rh(bpy)_2(dppt)]^{3+}$ in Figure 6.9. Unlike the complexes with pyrazine triazole ligands neither $[Rh(phen)_2(dppt)]^{3+}$ nor $[Rh(bpy)_2(dppt)]^{3+}$ demonstrated a d-d* based emission. The triazine ligands are much stronger π-acceptors than the pyridine and pyrazine triazole ligands and would thus have a lower π* level than the complexes previously discussed.[2,5] The absence of a d-d* based emission for these complexes implies that conversion between the d-d* state and the π-π* state occurs at a rate much faster than emission from the d-d* state. $[Rh(phen)_2(dppt)]^{3+}$ exhibited a structureless emission with a maximum at 544 nm. This emission is at lower energies than and structurally different from an emission associated with the phen ligand thus indicating that the emission was not a phen based in this instance but based on the dppt ligand instead.

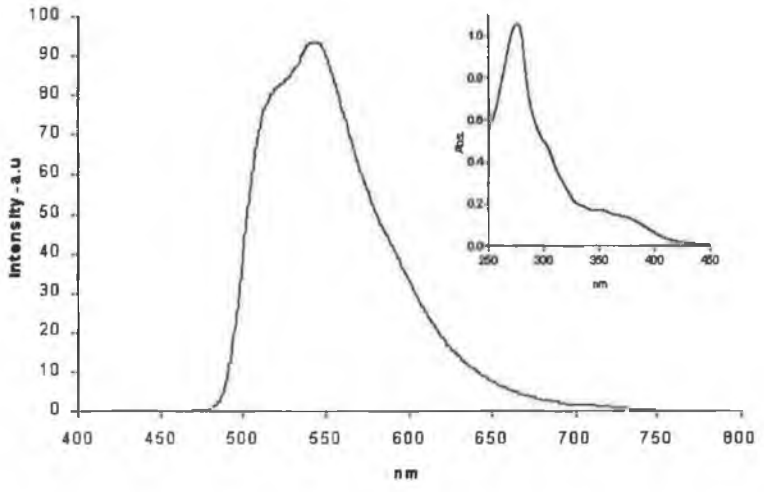

Figure 6.8 Emission spectrum of $[Rh(phen)_2(dppt)]^{3+}$ measured in ethanol:methanol 4:1 at 77K, λ_{ex} 305nm . Inset shows the UV spectrum of $[Rh(phen)_2(dppt)]^{3+}$.

In contrast, the emission exhibited by $[Rh(bpy)_2(dppt)]^{3+}$ was found to be wavelength dependent. The emission exhibited at 350 nm is identical to that of $[Rh(phen)_2(dppt)]^{3+}$ which was assigned as a ligand based π-π* transition associated with the dppt ligand whereas at an excitation wavelength of 280 nm the emission, whilst poorly defined, appears to be bpy based. Figure 6.10 compares the emission

spectrum obtained for $[Rh(bpy)_2(d_{10}\text{-dppt})]^{3+}$ at λ_{ex} = 280 nm with that of the bpy based emission of $[Rh(bpy)_2(pytr)]^{2+}$. Although the emission spectrum of $[Rh(bpy)_2(d_{10}\text{-dppt})]^{3+}$ is poorly defined structurally it can be seen that emission spectrum of $[Rh(bpy)_2(d_{10}\text{-dppt})]^{3+}$ observed at λ_{ex} = 280 nm is coincident with that of $[Rh(bpy)_2(pytr)]^{2+}$.

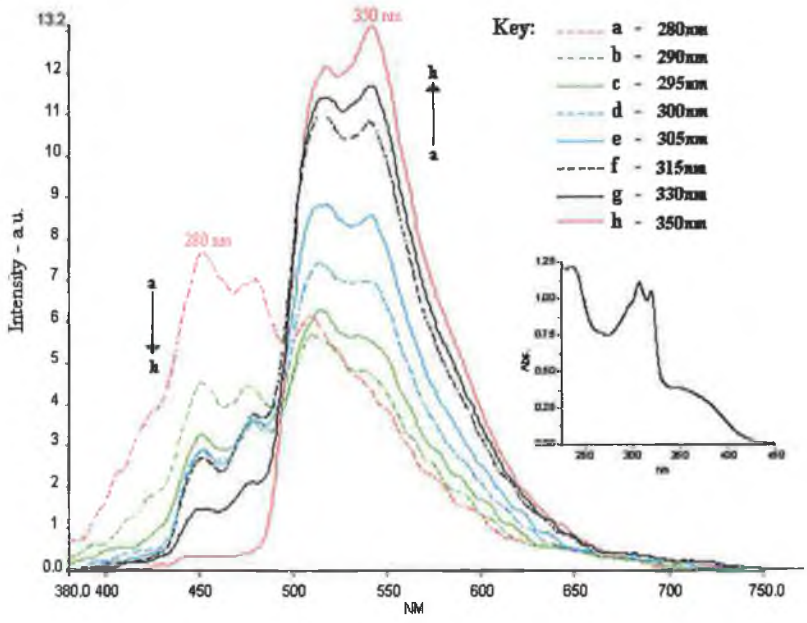

Figure 6.9 Emission spectra of $[Rh(bpy)_2(d_{10}\text{-dppt})]^{3+}$, λ_{ex} 280nm-350nm, measured in ethanol:methanol 4:1 at 77K. Inset shows the UV spectrum of $[Rh(bpy)_2(d_{10}\text{-dppt})]^{3+}$.

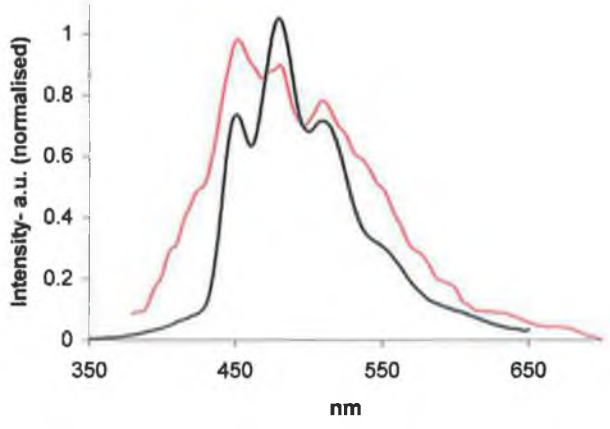

Figure 6.10 Emission spectra of $[Rh(bpy)_2(d_{10}\text{-dppt})]^{3+}$ at λ_{ex} = 280 nm (——) and $[Rh(bpy)_2(pytr)]^{2+}$ (——) measured in ethanol:methanol 4:1 at 77K.

Such behaviour was observed for $[Rh(phen)_2(bpt)]^{2+}$ and $[Rh(bpy)_2(Phpytr)]^{2+}$, Section 4.1.2, whereby the emission assigned as a ligand based π-π^* transition varied with excitation wavelength but in these cases the origin of the second ligand based emission was unclear. Based upon comparisons between the ligand based π-π^* transitions exhibited by $[Rh(phen)_2(dppt)]^{3+}$ and $[Rh(bpy)_2(pytr)]^{2+}$ it is relatively easy to establish that $[Rh(bpy)_2(d_{10}\text{-dppt})]^{3+}$ exhibits a ligand based emission associated with the dppt ligand at λ_{ex} = 350 nm and a ligand based emission associated with the bpy ligand at λ_{ex} = 280 nm. Such intraligand behaviour was observed by Barton *et. al* when they studied the complex $[Rh(phi)_2(phen)]^{3+}$.[10] They observed two emissive states for $[Rh(phi)_2(phen)]^{3+}$ which were assigned as emission from both the phen and the phi ligands, see Section 1.3.3.1.

6.2.2.3 Complexes incorporating fused ligands

The emission spectra of $[Rh(phen)_2(PIP)]^{3+}$, $[Rh(phen)_2(MePIP)]^{3+}$ and $[Rh(phen)_2(PTP)]^{3+}$ can be seen in Figure 6.11. Only a single emission was detected for all of these complexes and no wavelength dependency was observed.

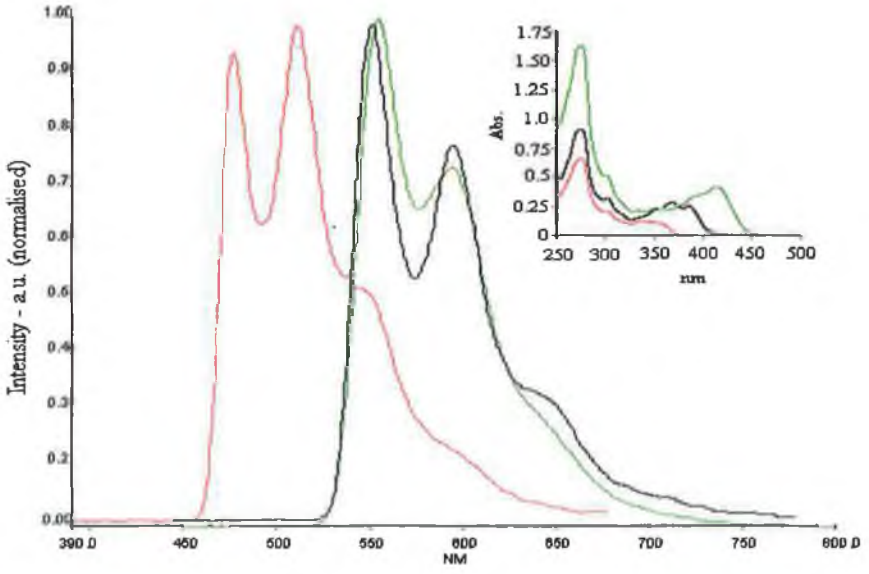

Figure 6.11 Emission spectra of $[Rh(phen)_2(PIP)]^{3+}$(——), $[Rh(phen)_2(MePIP)]^{3+}$ (——) and $[Rh(phen)_2(PTP)]^{3+}$(——) measured in ethanol:methanol 4:1 at 77K. Inset shows the respective UV spectra.

It can be seen that the spectra of $[Rh(phen)_2(PIP)]^{3+}$ and $[Rh(phen)_2(MePIP)]^{3+}$ are quite similar in position with a shoulder at 640 nm being more prominent in the spectrum of $[Rh(phen)_2(PIP)]^{3+}$. The spectrum of $[Rh(phen)_2(PTP)]^{3+}$ occurs at higher energy. The behaviour of this complex is much more like that observed for the pyridine triazole based complex with a structured emission with maxima in the same region. If the emission spectra of these phen complexes are compared with those of the analogous bpy complexes, Figure 6.12, then it can be seen that the emission of $[Rh(phen)_2(PIP)]^{3+}$ and $[Rh(bpy)_2(PIP)]^{3+}$ are virtually identical as are those of $[Rh(phen)_2(MePIP)]^{3+}$ and $[Rh(bpy)_2(MePIP)]^{3+}$.

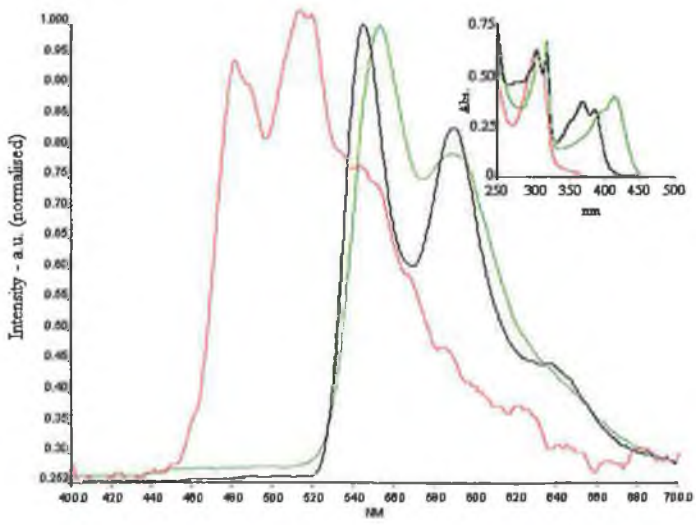

Figure 6.12 Emission spectra of $[Rh(bpy)_2(PIP)]^{3+}$(——), $[Rh(bpy)_2(MePIP)]^{3+}$ (——) and $[Rh(bpy)_2(PTP)]^{3+}$(——) measured in ethanol:methanol 4:1 at 77K. Inset shows the respective UV spectra of each.

This behaviour would imply that the emission exhibited by $[Rh(phen)_2(PIP)]^{3+}$, $[Rh(bpy)_2(PIP)]^{3+}$ is located on the PIP ligand and similarly on the MePIP ligand for $[Rh(phen)_2(MePIP)]^{3+}$ and $[Rh(bpy)_2(MePIP)]^{3+}$. In contrast to this, the structure of the emission of $[Rh(phen)_2(PTP)]^{3+}$ and $[Rh(bpy)_2(PTP)]^{3+}$ differ with that of $[Rh(phen)_2(PTP)]^{3+}$ being structurally similar to $[Rh(phen)_3]^{3+}$ and that of $[Rh(bpy)_2(PTP)]^{3+}$ being structurally similar to $[Rh(bpy)_3]^{3+}$. Based on these results it is concluded that the emission is these cases is located on the phen and bpy ligands. As already discussed, whilst the PTP ligands contain a fused ring similar to the PIP and MePIP ligands this ligand is in fact triazole based and appears to behave

in a manner similar to the pyridine triazole ligands in that emission is phen / bpy based as opposed to being based on the ligand with the fused ring as was seen for complexes with PIP and MePIP. The emission behaviour of all of the complexes detailed in this chapter will be discussed further in Chapter 8.

6.2.3 Photochemical Studies

It should be noted that none of the complexes detailed in this thesis showed any evidence for photochemical activity. Although detailed studies were not carried out on all of the complexes discussed it was found that ^{1}H NMR spectra and absorption and emission spectra did not change over time or with exposure to light. Complexes incorporating the PIP, Me PIP and PTP ligands were however studied as several their Ru(II) and Os(II) analogues had previously exhibited photochemical activity when exposed to light on a timescale of 0 to 150 minutes.[7] The Rh(III) complexes were exposed to light over a 6 hour period and their absorption spectra were monitored over this time period. In contrast to the behaviour of the analogous Ru(II) and Os(II) complexes none of the Rh(III) complexes studied showed any evidence to suggest that they are photochemically active.

6.2.4 Low Temperature Lifetimes

As can be seen from the absorption spectra of the complexes discussed in this chapter the complexes in question absorb at 355 nm thus allowing for the measurement of low temperature lifetimes using both methods detailed in Chapter 2. TCSPC was used with λ_{ex} = 337 nm to obtain lifetimes on a scale shorter than 30μs and the Nd-Yag laser, at the third harmonic λ_{ex} = 355 nm, was used to measure lifetimes in the ms region. The errors using the laser are estimated to be slightly higher than those of TCSPC at ±10% as compared with ±5%. In both cases the quality of the data was judged the χ^2 value and for TCSPC the residuals plot was also examined. Table 6.3 details the excited state lifetime data obtained.

Table 6.3 ***77K lifetimes for $[Rh(phen)_3]^{3+}$, $[Rh(bpy)_3]^{3+}$ and complexes containing the ligands Hpztr, HPhpztr, Hbpzt, Hppt, dppt, PIP, MePIP and PTP measured in ethanol:methanol 4:1.***

Complex	τ^1 (μs)	τ^2 (ms)	Complex	τ^1 (μs)	τ^2 (ms)
$[Rh(phen)_3]^{3+}$	-	48.4 [a]	$[Rh(bpy)_3]^{3+}$	-	2.2 [a]
$[Rh(phen)_2(pztr)]^{2+}$	b	b	$[Rh(bpy)_2(pztr)]^{2+}$	5.7	1.4
$[Rh(phen)_2(Phpztr)]^{2+}$	1.5	0.9	$[Rh(bpy)_2(Phpztr)]^{2+}$	1.5	0.9
$[Rh(phen)_2(bpzt)]^{2+}$	5.3	1.0	$[Rh(bpy)_2(bpzt)]^{2+}$	b	b
$[Rh(phen)_2(ppt)]^{2+}$	5.5	1.1	$[Rh(bpy)_2(ppt)]^{2+}$	5.0	1.2
$[Rh(phen)_2(dppt)]^{3+}$	-	7.1 16.0	$[Rh(bpy)_2(dppt)]^{3+}$	-	8.2 27.3
$[Rh(phen)_2(d_{10}\text{-dppt})]^{3+}$	-	5.7	$[Rh(bpy)_2(d_{10}\text{-dppt})]^{3+}$	-	7.3 18.3
$[Rh(phen)_2(PIP)]^{3+}$	-	5.7	$[Rh(bpy)_2(PIP)]^{3+}$	-	6.5
$[Rh(phen)_2(MePIP)]^{3+}$	-	4.3	$[Rh(bpy)_2(MePIP)]^{3+}$	-	7.2
$[Rh(phen)_2(PTP)]^{3+}$	-	2.7	$[Rh(bpy)_2(PTP)]^{3+}$	-	-

[1] – measurements carried out using TCSPC. [2] – measurements carried out using Nd-Yag laser set-up.
a - values taken from ref. 8 and 9 b – pure complex not isolated.

A typical decay profile can be seen in Figure 6.13 with that of $[Rh(phen)_2(bpzt)]^{2+}$. As was seen for the pyridine triazole complexes the decay here is not completely linear. This deviation from linearity is attributed to a combination a build up of the excited state and the presence of the long-lived π-π* excited state.

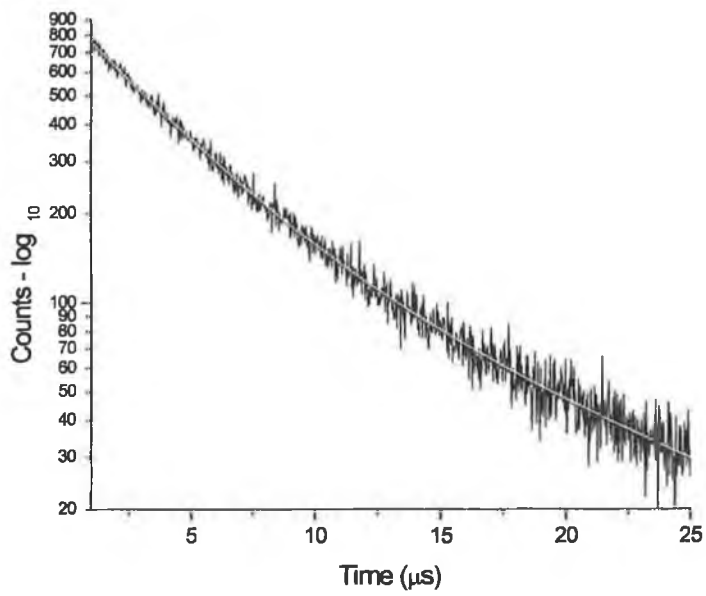

Figure 6.13 The decay profile of $[Rh(phen)_2(bpzt)]^{2+}$ measured using SPC in an ethanol:methanol glass at 77K.

The d-d* excited state lifetimes of the pyrazine triazole complexes were found to be in the range of 1.5 μs - 5.5 μs. No significant difference between the d-d* excited state lifetimes of these pyrazine triazole based complexes and the pyridine triazole complexes detailed in Chapter 4 was observed. The π-π* excited state lifetimes were found to be between 0.91 ms and 27.31 ms and when compared with the excited state lifetimes of the tris homoleptic complexes $[Rh(phen)_3]^{3+}$ and $[Rh(bpy)_3]^{3+}$ it was found that all of the heteroleptic complexes incorporating the phen ligand exhibited excited state lifetimes shorter than that of $[Rh(phen)_3]^{3+}$. The pyrazine triazole complexes incorporating the bpy ligand exhibited excited state lifetimes shorter than that of $[Rh(bpy)_3]^{3+}$ whereas bpy based complexes with the triazine and fused ligands PIP, MePIP and PTP exhibited excited state lifetimes longer than that of $[Rh(bpy)_3]^{3+}$.

6.2.5 Electrochemical Properties

The electrochemical behaviour of Rh(III) complexes has been detailed in both Chapters 1 and 4. It is expected that the variation in ligands will be reflected to some degree in the reduction potentials exhibited. All of the complexes discussed were studied using both cyclic voltammetry and differential pulse voltammetry. The electrochemical results obtained for all of the complexes detailed in this chapter can be seen in Table 6.4 and Table 6.5.

Table 6.4 ***Electrochemical data obtained for $[Rh(phen)_3]^{3+}$ and all phen based complexes detailed in this chapter measured in acetonitrile with 0.1M $TBABF_4$.***

Complex	E_{pc}, V vs. Fc/Fc^+	E_{pa}, V vs. Fc/Fc^+
$[Rh(phen)_3]^{3+}$		
CV	-1.171, -1.343, -1.87, -2.015 [a]	-1.107
$[Rh(phen)_2(Phpztr)]^{2+}$		
CV	-1.26, -1.76, -2.06	-0.88
DPV	-1.22, -1.76, -2.01, -2.15	
$[Rh(phen)_2(bpzt)]^{2+}$		
CV	-1.70, -1.89	-
DPV	-1.15, -1.40, -1.84	-
$[Rh(phen)_2(ppt)]^{2+}$		
CV	-1.23, -1.35, -2.04	+0.68
DPV	-0.95, -1.19, -1.30, -1.71, -2.02	-2.16, -1.96, -1.79, -1.41, -0.86
$[Rh(phen)_2(dppt)]^{3+}$		
CV	-0.91, -1.22, -1.94	0.63, -0.98, -1.36, -1.83
DPV	-0.79, -1.02, -1.24, -1.47	-1.38, -0.76
$[Rh(phen)_2(d_{10}\text{-dppt})]^{3+}$		
CV	-0.92, -1.21, -1.90	-0.84, -1.83
DPV	+0.62, -0.88, -1.17, -1.45, -1.68, -1.86	+0.61, -0.88, -1.16, -1.47, -1.66,-1.85
$[Rh(phen)_2(PIP)]^{3+}$		
CV	-1.25, -1.75, -1.86, -2.06	-1.52, 0.54
DPV	-1.19, -1.37, -1.77, -1.88, -2.02	-
$[Rh(phen)_2(MePIP)]^{3+}$		
CV	-1.20, -1.81, -2.05	-1.50
DPV	-1.16, -1.80, -2.01	-0.97, -1.15, -1.71, -1.76, -1.96
$[Rh(phen)_2(PTP)]^{3+}$		
CV	-1.07, -1.24, -1.83,	-1.97, -1.52, -0.14
DPV	-2.13	

a= values taken from ref 12 and 13and converted from V vs. SCE to V vs. Fc/Fc^+ using ref 11.

Table 6.5 ***Electrochemical data obtained for $[Rh(bpy)_3]^{3+}$ and all bpy based complexes detailed in this chapter measured in acetonitrile with 0.1M $TBABF_4$.***

Complex	E_{pc}, V vs. Fc/Fc^+	E_{pa}, V vs. Fc/Fc^+
$[Rh(bpy)_3]^{3+}$		
CV	-1.21, -1.84, -1.67 [a]	-1.78, -1.99 [a]
$[Rh(bpy)_2(pztr)]^{2+}$		
CV	-1.26, -1.90	-0.82, -1.77
DPV	-1.22, -1.84, -1.91, -2.19	
$[Rh(bpy)_2(Phpztr)]^{2+}$		
CV	-1.24, -1.87	-0.64, -1.78
DPV	-1.21, -1.82, -2.18	-2.17, -1.81, -1.21
$[Rh(bpy)_2(ppt)]^{2+}$		
CV	-1.33, -2.03	-1.92
DPV	-1.17, -1.29, -1.96, -2.17	-2.17, -1.95, -1.31,
$[Rh(bpy)_2(dppt)]^{3+}$		
CV	-0.89, -1.18, -1.65, -1.88	-0.74, -1.11, -1.60, -1.81
DPV	-0.86, -1.14, -1.40, -1.61, -1.84	-1.38, -0.76
$[Rh(bpy)_2(d_{10}\text{-dppt})]^{3+}$		
CV	-0.90, -1.16, -1.88	-0.16, -0.19, -1.58, -1.82
DPV	-0.86, -1.13, -1.63, -1.85	-1.85, -1.63, -1.41, -1.12, -0.87, -0.52
$[Rh(bpy)_2(PIP)]^{3+}$		
CV	-1.28, -1.76	-1.66
DPV	-1.19, -1.50, -1.69, -1.89	
$[Rh(bpy)_2(MePIP)]^{3+}$		
CV	-1.20, -1.75, -2.02	-1.67, -1.977
DPV	-1.15, -1.71, -1.98	
$[Rh(bpy)_2(PTP)]^{3+}$		
CV	-1.25, -1.75, -2.03	-0.72, -1.67, -1.95
DPV	-1.11, -1.20, -1.71, -1.98, -2.06	

a = values taken from ref 12 and 13and converted from V vs. SCE to V vs. Fc/Fc^+ using ref 11.

The CV (a) and DPV (b) obtained for $[Rh(bpy)_2(pztr)]^{2+}$ can be seen in Figure 6.14. It is known that ligands that are strong σ donors donate electron density into d orbitals causing lower oxidation potentials and more negative reduction potentials. It has been stated previously that the pyridine triazole ligand is a better σ donor than it's pyrazine analogue thus it would follow that the reduction potentials of the pyridine triazole ligands would be more negative. The first reduction potential of

$[Rh(bpy)_2(pztr)]^{2+}$ is observed at -1.26V. If we compare this to the first reduction potential of $[Rh(bpy)_2(pytr)]^{2+}$, which was found at -1.34V it can be seen that, as expected, the pyrazine based complex has a reduction which is 80mV more positive than that of $[Rh(bpy)_2(pytr)]^{2+}$. The shape of the second reduction wave in the CV would imply that this is a composite wave and if we look at the DPV, which is more resolved in this region, it can clearly be seen that two processes are taking place. A fourth reduction wave can be seen at -2.19V in the DPV which is not seen the CV due to the presence of water.

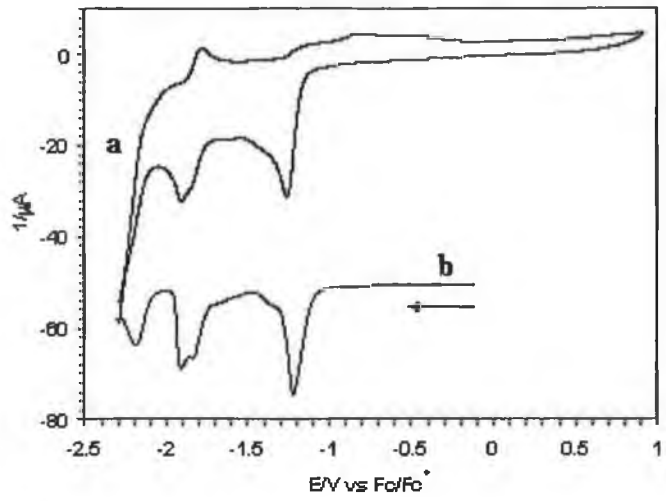

Figure 6.14 CV (a) and DPV (b) of $[Rh(bpy)_2(pztr)]^{2+}$ measured in acetonitrile with 0.1M $TBABF_4$.

Figure 6.15 illustrates the voltammograms obtained for the complexes $[Rh(phen)_2(Phpztr)]^{2+}$ and $[Rh(bpy)_2(Phpztr)]^{2+}$. The CV of $[Rh(phen)_2(Phpztr)]^{2+}$shows three definite reduction waves all of which are irreversible. It should be noted that the CV of $[Rh(phen)_2(Phpztr)]^{2+}$ shown was obtained on the first scan as the definition of the reduction waves deteriorated with successive scanning. The CV and DPV of $[Rh(bpy)_2(Phpztr)]^{2+}$ are more clearly defined than those of $[Rh(phen)_2(Phpztr)]^{2+}$. Two reduction waves can be seen at -1.24V and -1.87V in the CV with a third wave being evident at -2.2V in the DPV. Again this third reduction wave is obscured in the CV due to the presence of water. The CV of $[Rh(bpy)_2(Phpztr)]^{2+}$ remained unchanged with repeated scanning and the CV shown in Figure 6.15 is the third of three scans.

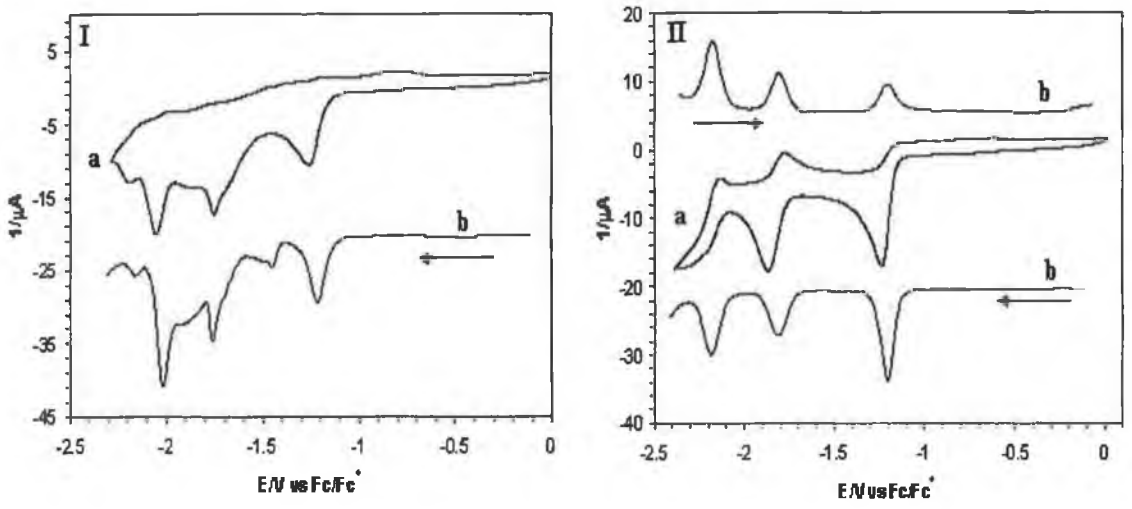

Figure 6.15 CV's (a) and DPV's (b) of (I) $[Rh(phen)_2(Phpztr)]^{2+}$ and (II) $[Rh(bpy)_2(Phpztr)]^{2+}$ measured in acetonitrile with 0.1M $TBABF_4$.

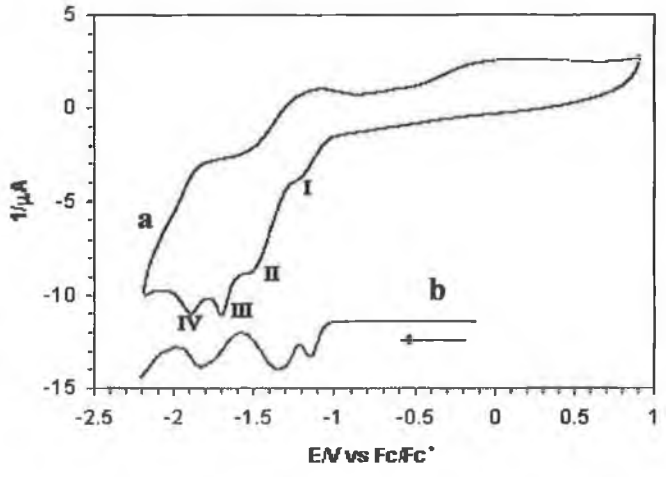

Figure 6.16 CV (a) and DPV (b) of $[Rh(phen)_2(bpzt)]^{2+}$ measured in acetonitrile with 0.1M $TBABF_4$.

Figure 6.16 illustrates the CV and DPV obtained for $[Rh(phen)_2(bpzt)]^{2+}$. Although poorly defined, four irreversible reduction waves (I-IV) can be seen at -1.2V and -1.56V (I and II) and at -1.70V and -1.89V (III and IV). When compared with $[Rh(phen)_2(bpt)]^{2+}$ whose reduction potentials were found at -1.36V, -1.74V, -2.08V

$[Rh(phen)_2(bpzt)]^{2+}$ exhibits more positive reduction potentials. Table 6.6 allows for the comparison of the reduction potentials of all of the pyrazine based complexes studied with their analogous pyridine triazole complexes and it can be seen that the first reduction potentials of the pyrazine triazole compounds are found at 80 mV to 110 mV more positive reduction potentials than the corresponding pyridine triazole compounds.

Table 6.6 ***Electrochemical data obtained for $[Rh(phen)_3]^{3+}$, $[Rh(bpy)_3]^{3+}$ and complexes with Hpztr, Hpytr, HPhpztr, HPhpytr, Hbpzt and Hbpt measured in acetonitrile with 0.1M $TBABF_4$.***

Complex	E_{pc}, V vs. Fc/Fc^+	E_{pa}, V vs. Fc/Fc^+
$[Rh(phen)_3]^{3+}$		
CV	-1.171, -1.343, -1.87, -2.015 [a]	-1.107 [a]
$[Rh(bpy)_3]^{3+}$		
CV	-1.21, -1.84, -1.67 [a]	-1.78, -1.99 [a]
$[Rh(phen)_2(Phpztr)]^{2+}$		
CV	-1.26, -1.76, -2.06	-0.88
DPV	-1.22, -1.76, -2.01, -2.15	
$[Rh(phen)_2(Phpytr)]^{2+}$		
CV	-1.36, -1.72, -2.06	-1.52, -1.94
DPV	-1.32, -1.70, -1.97	-0.87, -1.33, -1.53, -1.97
$[Rh(phen)_2(bpzt)]^{2+}$		
CV	-1.70, -1.89	-
DPV	-1.15, -1.40, -1.84	-
$[Rh(phen)_2(bpt)]^{2+}$		
CV	-1.36, -1.74, -2.08	-1.95
DPV	-0.95, -1.32, -1.77, -2.00	-
$[Rh(bpy)_2(pztr)]^{2+}$		
CV	-1.26, -1.90	-0.82, -1.77
DPV	-1.22, -1.84, -1.91, -2.19	
$[Rh(bpy)_2(pytr)]^{2+}$		
CV	-1.34, -2.03	-1.95
DPV	-0.96, -1.31, 1.65, -2.00	-0.98, -1.32, -1.98
$[Rh(bpy)_2(Phpztr)]^{2+}$		
CV	-1.24, -1.87	-0.64, -1.78
DPV	-1.21, -1.82, -2.18	-2.17, -1.81, -1.21
$[Rh(bpy)_2(Phpytr)]^{2+}$		
CV	-1.35, -2.01	-0.71, -1.94
DPV	-1.31, -1.97	-1.32, -1.97

a – values taken from ref. 12 and 13

The CV's and DPV's of $[Rh(phen)_2(ppt)]^{2+}$ and $[Rh(bpy)_2(ppt)]^{2+}$ can be seen in Figure 6.17. In the case of $[Rh(phen)_2(ppt)]^{2+}$ four irreversible reduction waves can

be seen. Whilst the second reduction wave of $[Rh(bpy)_2(ppt)]^{2+}$ seen at -2.03 V does have a reciprocal wave in the reverse scan the peak potentials separation was found to be 108 mV and is thus considered to be irreversible. The DPV of $[Rh(bpy)_2(ppt)]^{2+}$ shows the presence of four reduction potentials.

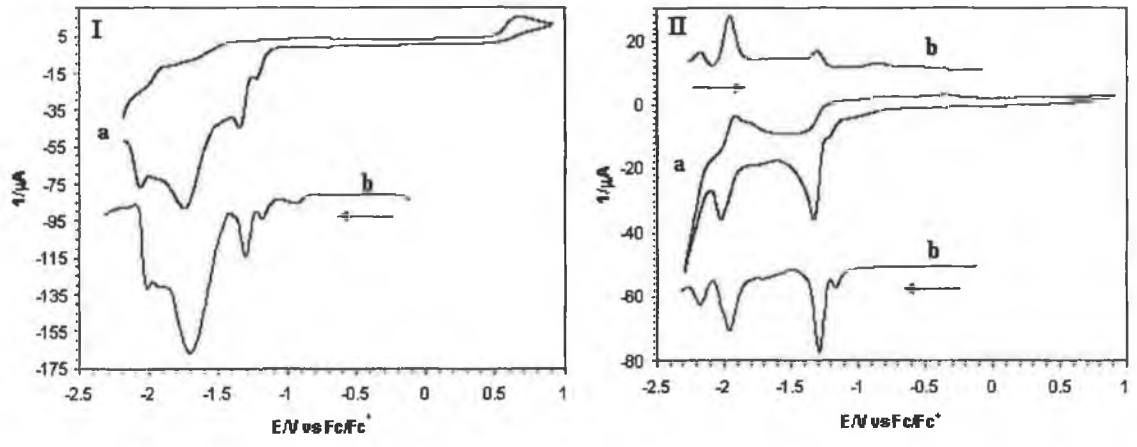

Figure 6.17 CV's (a) and DPV's (b) of (I) $[Rh(phen)_2(ppt)]^{2+}$ and (II) $[Rh(bpy)_2(ppt)]^{2+}$ measured in acetonitrile with 0.1M $TBABF_4$.

As was discussed in Chapter 5 the issue of coordination is quite important for complexes incorporating the Hppt ligand as the metal centre can coordinate either via the pyridine ring or the pyrazine ring. ^1H NMR studies showed that coordination of the Rh(III) metal centre occurs predominantly via the pyridine ring with only a very small amount of the of the pyrazine bound isomer being detected for both the phen and bpy complexes. The mode of coordination of the metal centre to the Hppt ligand is also reflected in the reduction potentials of $[Rh(phen)_2(ppt)]^{2+}$ and $[Rh(bpy)_2(ppt)]^{2+}$ as illustrated by Table 6.7. As shown in Figure 6.17 $[Rh(phen)_2(ppt)]^{2+}$ and $[Rh(bpy)_2(ppt)]^{2+}$ exhibit small reduction waves at -1.23V and -1.17V and more intense reduction waves at -1.35V and -1.33V respectively. When compared with the Hpytr complexes it can be seen that the reduction waves at -1.35V and -1.33V are indicative of coordination via a pyridine ring.

Table 6.7 ***Electrochemical data obtained for the complexes with Hppt, Hpytr and Hpztr measured in acetonitrile with 0.1M $TBABF_4$.***

Complex	E_{pc} -V vs. Fc/Fc^+
$[Rh(phen)_2(ppt)]^{2+}$	-1.23[a], -1.35, -2.04
$[Rh(phen)_2(pytr)]^{2+}$	-1.37, -1.79, -2.04
$[Rh(bpy)_2(ppt)]^{2+}$	-1.17[a], -1.33, -2.03
$[Rh(bpy)_2(pytr)]^{2+}$	-1.34, -2.03
$[Rh(bpy)_2(pztr)]^{2+}$	-1.26, -1.90

a = minor reduction wave

The behaviour of the complexes incorporating the dppt ligands can be seen in Figure 6.18. The potentials of the first reduction waves of these complexes occur at more positive potentials than those incorporating either pyridine or pyrazine based ligands. $[Rh(phen)_2(dppt)]^{3+}$ and $[Rh(bpy)_2(dppt)]^{3+}$ exhibited reduction waves at -0.91V and -0.89V respectively. If we compare these potentials with the potentials exhibited by the complexes incorporating pyridine and pyrazine based ligands then the potentials of $[Rh(phen)_2(dppt)]^{3+}$ and $[Rh(bpy)_2(dppt)]^{3+}$ are found at approximately 450 mV and 350 mV more positive potentials respectively. There does appear to be a species present in the reverse scan which could be associated with these reductions but peak potential separations are >100mV in both cases. The second reduction wave of $[Rh(phen)_2(dppt)]^{3+}$ is found at -1.22V and at -1.18V for $[Rh(bpy)_2(dppt)]^{3+}$. The third reduction wave seen in the CV of $[Rh(phen)_2(dppt)]^{3+}$ does have a reciprocal wave in the reverse scan but the peak potential separation here is 120 mV and is therefore irreversible whereas the third reduction wave of $[Rh(bpy)_2(dppt)]^{3+}$ is quasi reversible with a peak potential separation of 63 mV.

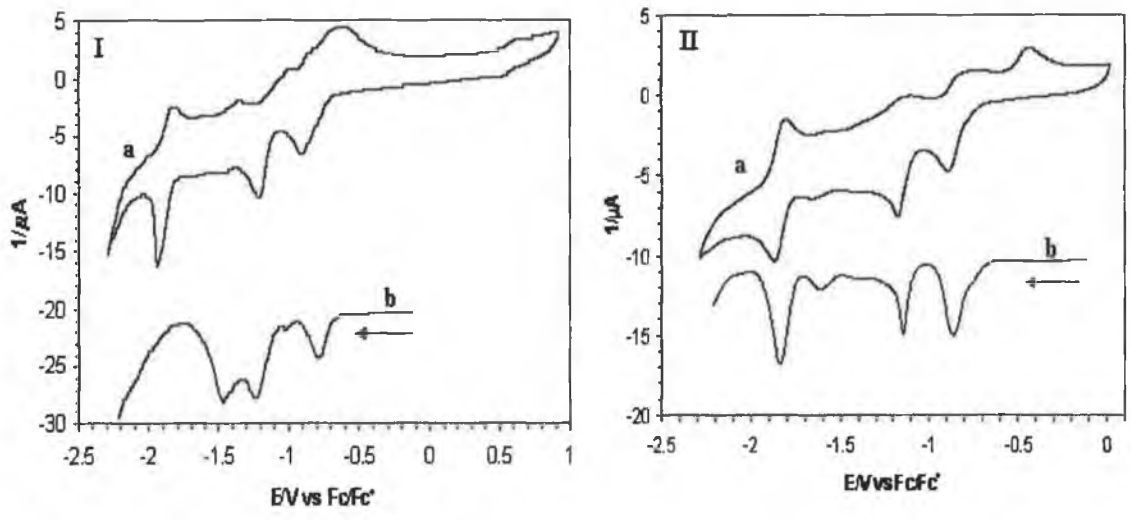

Figure 6.18 CV's (a) and DPV's (b) of (I) $[Rh(phen)_2(dppt)]^{3+}$ and (II)$[Rh(bpy)_2(dppt)]^{3+}$ measured in acetonitrile with 0.1M $TBABF_4$.

The final series of complexes studied incorporated the ligands PIP, MePIP and PTP and the CV's and DPV's of these can be seen in Figure 6.19 to Figure 6.22 .The results of the analysis of the voltammograms can be found in Table 6.4 and Table 6.5. The CV of $[Rh(phen)_2(PIP)]^{3+}$ shows no reversibility of the reduction waves observed.

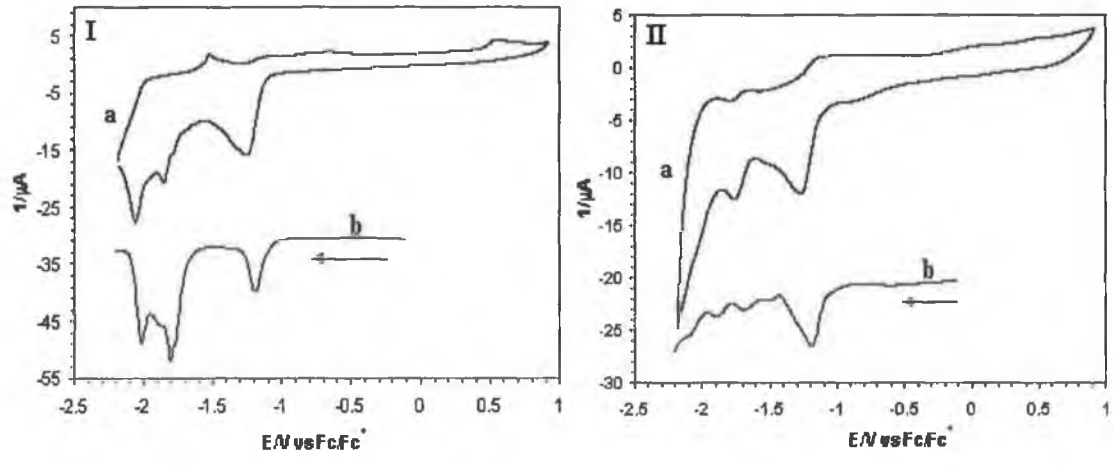

Figure 6.19 CV's (a) and DPV's (2) of (I) $[Rh(phen)_2(PIP)]^{3+}$ and (II) $[Rh(bpy)_2(PIP)]^{3+}$ measured in acetonitrile with 0.1M $TBABF_4$.

Analysis of the CV of $[Rh(bpy)_2(PIP)]^{3+}$ was limited as the reduction waves were very broad and poorly defined. It should be noted that the CV of $[Rh(bpy)_2(PIP)]^{3+}$ shown in Figure 6.19 is the first of three scans. In contrast the CV's of the complexes $[Rh(phen)_2(MePIP)]^{3+}$ and $[Rh(bpy)_2(MePIP)]^{3+}$ are much more defined with $[Rh(bpy)_2(MePIP)]^{3+}$ showing two quasi reversible reduction waves with peak potential separations of 82 mV and 71 mV. The position of these reduction waves and the degree of reversibility they demonstrate would indicate that these are bpy based reductions.

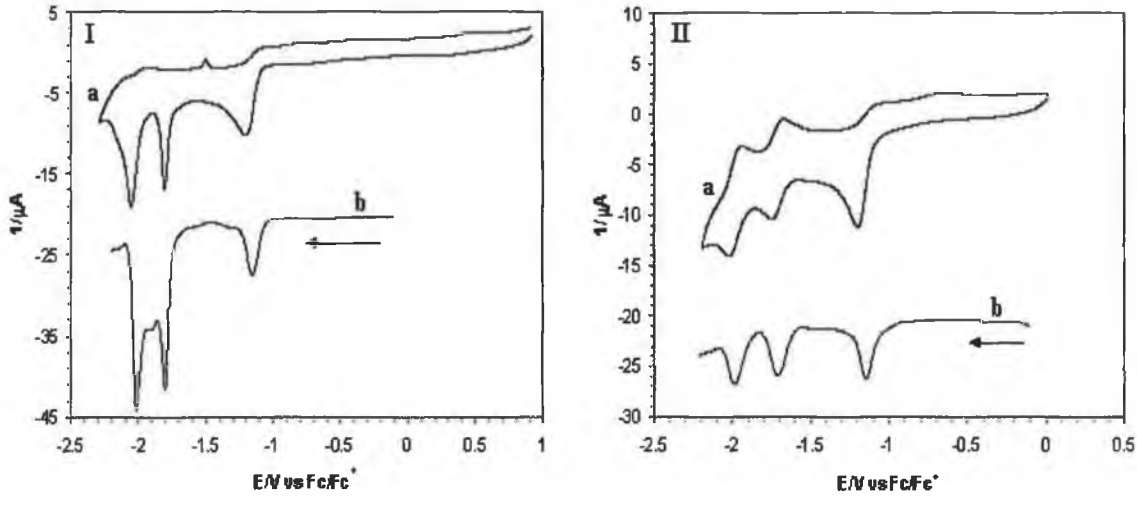

Figure 6.20 CV's (a) and DPV's (b) of (I) $[Rh(phen)_2(MePIP)]^{3+}$ and (II) $[Rh(bpy)_2(MePIP)]^{3+}$ measured in acetonitrile with 0.1M $TBABF_4$.

The CV of $[Rh(phen)_2(PTP)]^{3+}$, Figure 6.21, exhibits four irreversible reduction waves and one sharp peak wave in the reverse scan. Such behaviour was exhibited by several complexes and was attributed to desorption of material from the working electrode. It is likely that the material that adsorbs onto the working electrode is a consequence of the dissociation of the complex upon reduction. If this were the case it would be expected that the intensity of this peak would increase with successive cycling of the potential and with increasing negativity of the switching potential. Figure 6.21 demonstrates that this peak does in fact increase under these conditions.

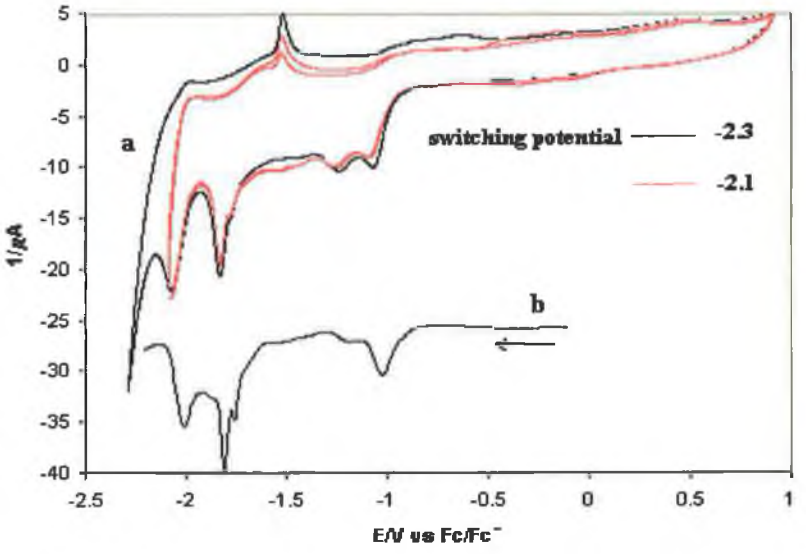

Figure 6.21 CV's (a) and DPV (b) of $[Rh(phen)_2(PTP)]^{3+}$ measured in acetonitrile with 0.1M $TBABF_4$.

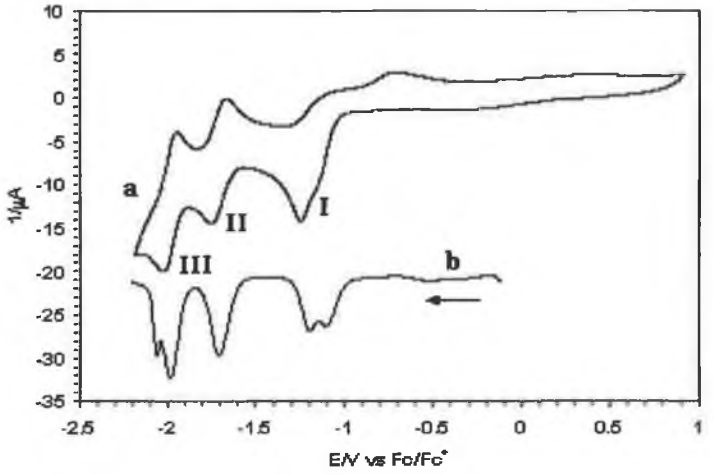

Figure 6.22 CV (a) and DPV(b) of $[Rh(bpy)_2(PTP)]^{3+}$ measured in acetonitrile with 0.1M $TBABF_4$.

$[Rh(bpy)_2(PTP)]^{3+}$ exhibits two quasi reversible waves with peak potential separations of 84 mV and 80 mV. The first reduction wave here is quite broad and if the DPV is studied it can easily be see that this is a composite wave. It also appears from the DPV that the third wave in the CV is a composite wave. The reduction waves II and III are similar in both position and reversibility to the second and third reduction waves observed for $[Rh(bpy)_2(MePIP)]^{3+}$ and it is again probable that these

are bpy based reductions. The electrochemical data for all of the complexes discussed in this chapter can be seen in Table 6.4 and Table 6.5.

6.3 Conclusions

The photophysical and electrochemical properties of the pyridine triazole complexes introduced in Chapter 5 have been investigated in this chapter. The absorption and emission behaviour of the complexes detailed in Chapter 5 were studied and several differences were observed. The pyrazine and triazine based complexes all exhibited strong π-π^* absorption bands between 250 nm and 325 nm whilst weaker shoulders were observed at lower energies, 325 nm to 450 nm depending on the complex and the imidazole based complexes proved to absorb over quite a broad wavelength range. The emission properties of the complexes discussed in this chapter varied quite significantly depending upon the nature of the incorporated ligands. The pyrazine based complexes exhibited a dual emitting behaviour but it was interesting to note that as the σ-donor strength of the ligands decreased so did the intensity of the metal based emission. This point was particularly evident when complexes incorporating the HPhpztr ligand were studied as it was found that their emission was predominantly ligand based with almost no metal based emission being observed. Whilst both the pyridine and the pyrazine complexes exhibited a π-π^* and a d-d* based emission the ligand based emission of the pyrazine complexes was not phen / bpy based, as was the case for the pyridine triazole complexes, but it was found to be located upon the pyrazine moiety. This implies that in the case of the pyrazine triazole complexes the LUMO of the pyrazine triazole ligand is located below that of the bpy ligand and as a result emission is pyrazine based.

A metal based emission was not observed for any of the complexes incorporating the dppt, PIP, MePIP or PTP ligands. These observations can again be related to the σ donor / π acceptor properties of the incorporated ligands. It was found that the metal based emission intensity decreased with decreasing σ-donating strength and it is known that the triazine ligands are weaker σ-donors than bpy thus it is not surprising that these complexes do not exhibit a metal based emission.[5] A decrease in the σ-donor strength of the ligand results in the lowering of the ^{3}MC state

and the absence of a d-d* emission would imply that conversion between the d-d* state and the π-π* state occurs at a rate much faster than emission from the d-d* state. The π-π* based emission detected for $[Rh(phen)_2(dppt)]^{3+}$ was found to be based upon the triazine ligand whereas the emission of $[Rh(bpy)_2(dppt)]^{3+}$ proved particularly interesting as it exhibited a predominantly bpy based emission at λ_{ex} 280 nm compared with a triazine based emission based at 350 nm implying that the LUMO's of the bpy and dppt ligands are quite closely spaced. It was interesting to note that the PIP, MePIP or PTP based complexes did not exhibit a d-d* based emission. Like the triazoles, imidazoles are strong σ-donors however it is known that in their protonated forms the triazoles are weaker σ-donors than their deprotonated forms.[2] It is likely that the absence of a d-d* emission for these complexes it is related to the presence of the fused pyridyl ring in these ligands but it is not known if it is the difference in σ-donor strength or the structural difference which causes this. It is interesting to note that neither $[Rh(phen)_2(NHbpt)]^{2+}$ nor $[Rh(bpy)_2(NHbpt)]^{2+}$, which are structurally quite different from the other pyridine triazole complexes studied, exhibited a d-d* based emission.

The electrochemical properties of the complexes also varied with the σ-donor strength of the incorporated ligands. The dppt ligands are the weakest σ-donating ligands studied and, as would be expected, $[Rh(phen)_2(dppt)]^{3+}$ and $[Rh(bpy)_2(dppt)]^{3+}$ exhibit first reduction waves at more positive potentials than any of the other complexes studied. It was found that the reduction potentials exhibited by the remaining complexes were also related to ligand σ-donor strength. Both the photophysical and the electrochemical properties of the complexes discussed in this chapter will be discussed further in Chapter 8.

References:

1 R.J. Crutchley, A.B.P. Lever, *J. Am. Chem. Soc.*, **1980**, *102*, 7128-7129.

2 R. Hage, *Ph.D. Thesis*, Leiden University, The Netherlands, **1991**.

3 H.A. Nieuwenhuis, J.G. Haasnoot, R. Hage, J. Reedijk. T.L. Snoeck, D.J. Stufkens, J.G. Vos, *Inorg. Chem.*, **1991**, *30*, 48-54.

4 R. Hage, J.G. Haasnoot, H.A. Nieuwenhuis, J. Reedijk, R. Wang, J.G. Vos, *J. Chem. Soc., Dalton Trans.*, **1991**, 3271-3275.

5 R. Hage, J.H. van Diemen, G. Ehrlich, J.G. Haasnoot, D.J. Stufkens, T.L. Snoeck, J.G. Vos, J. Reedijk, *Inorg. Chem.*, **1990**, *29*, 988-993.

6 T.E. Keyes, F. Weldon, E. Müller, P. Pechy, M. Grätzel, J.G. Vos, *J. Chem. Soc., Dalton Transactions*, **1995**, *16*, 2705-2706.

7 Adrian Guckian, *PhD. Thesis*, Dublin City University, 2002.

8 M.K. DeArmond, J.E. Hillis, *J. Chem. Phys.*, **1971**, *54*, 2247-2253.

9 K. Kalyanasundaram, *Photochemistry of Polypyridine and Porphyrin Complexes*, **1992**, Academic Press, London.

10 C. Turro, A. Evenzahav, S.H. Bossmann, J.K. Barton, N.J. Turro, *Inorg. Chim. Acta*, **1996**, *243*, 101-108.

11 V.V. Pavlishchuk, A.W. Addison, *Inorg. Chim. Acta*, **2000**, *298*, 97-102.

12 G. Kew, K. Hanck, K. DeArmond, *J. Phys. Chem.*, **1975**, *79*, 1828-1835.

13 G. Kew, K. DeArmond, K. Hanck, *J. Phys. Chem.*, **1974**, *78*, 727-734.

Chapter 7 – Towards the Synthesis of Rh(III) Dinuclear Complexes.

"If we knew what we were doing, it wouldn't be called research, would it?"
Albert Einstein

"Whenever anyone says 'theoretically', they really mean 'not really'."
Dave Parnas

Abstract: Having synthesised and characterised a number of Rh(III) polypyridyl mononuclear complexes the next stage was the synthesis of dinuclear complexes. A number of the mononuclear complexes detailed in Chapters 3 and 5 are capable of binding a second metal centre and it was hoped that it would be possible to develop a series of homo and hetero-dinuclear complexes. The synthesis of such complexes with the ligands Hbpt, NH_2bpt and Hbpzt proved unsuccessful and as a result the nature of the bridging ligand was changed. Many of the Rh(III) dinuclear complexes reported previously have utilised ligands which contain spacer groups and based upon this, pyridine triazole ligands were used in which two Hpytr units were linked by a benzene spacer. It was with these ligands that Rh(III)/Ru(II) dinuclear complexes were successfully synthesised. The following chapter aims to give a brief overview of the Rh(III) homo and hetero-dinuclear complexes reported to date and details the numerous approaches which were taken in the development of Rh(III) dinuclear complexes with pyridine and pyrazine triazole based ligands.

7.1 Introduction

One of the aims of this work was to progress from mononuclear Rh(III) complexes to the development of dinuclear complexes. Several of the complexes detailed in earlier chapters have the potential to bind a second metal centre and the following chapter is concerned with attempts to synthesise Rh(III)/Ru(II) dinuclear complexes. The following discussion aims to give a brief introduction to Ru(II) polypyridyl chemistry focusing on the properties of $[Ru(bpy)_3]^{2+}$ in particular and provides a brief overview of the types of Rh(III)/Ru(II) complexes which have been developed to date.

Dinuclear complexes are comprised of transition metal centres connected via bridging ligands and in some instances the bridging ligands are linked together by spacers as demonstrated in Figure 7.1. Such transition metal complexes exhibit properties intrinsic to the individual metal centres but importantly they may also demonstrate additional properties, in which case they are referred to as supramolecular systems.[1,2] Supramolecular complexes have generated a great deal of interest with the ultimate aim of designing of multicomponent systems capable of performing useful light and/or redox-induced functions. Numerous homo- and hetero-nuclear complexes have been developed with the ultimate aim of developing functional *Photochemical Molecular Devices* (PMD's).[3]

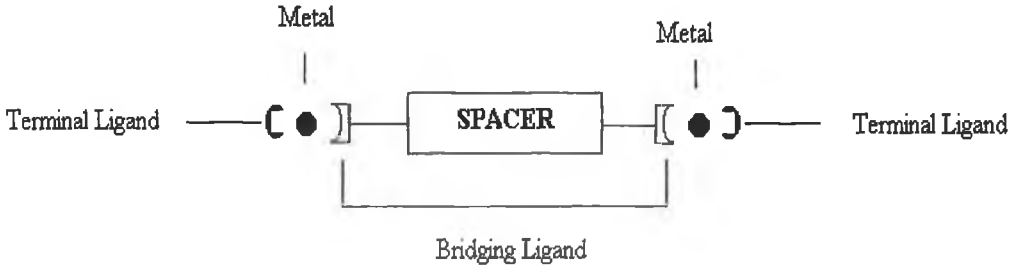

Figure 7.1 Illustration of a dinuclear complex.[3]

The nature of the bridging ligand incorporated in these types of complexes is important, as it tends to contribute to the spectroscopic and redox properties of the active metal-based units. Thus the type of bridging ligand to be integrated into a

system requires careful consideration when trying to produce complexes which are (i) capable of displaying luminescence properties and (ii) give rise to the required photoinduced energy and electron transfer processes.[3] A substantial amount of work has been dedicated in recent years to the fine-tuning of these complexes in attempts to manipulate and improve their ground and excited state properties. When the molecular arrays are assembled correctly with respect to spatial organisation it is possible to control and direct the flow of electrons in the array.[3,4]

Early research in the field of polypyridyl transition metal complexes focused primarily on complexes incorporating a Ru(II) metal centre.[3,4] Ruthenium is one of the six platinum group metals and has nine known oxidation states, with the Ru(II) state being the most stable. The compound which has attracted the most attention over the years, $[Ru(bpy)_3]^{2+}$, is often referred to as the "parent complex". Interest in this compound stemmed primarily from its redox properties, which are illustrated in Figure 7.2.[5]

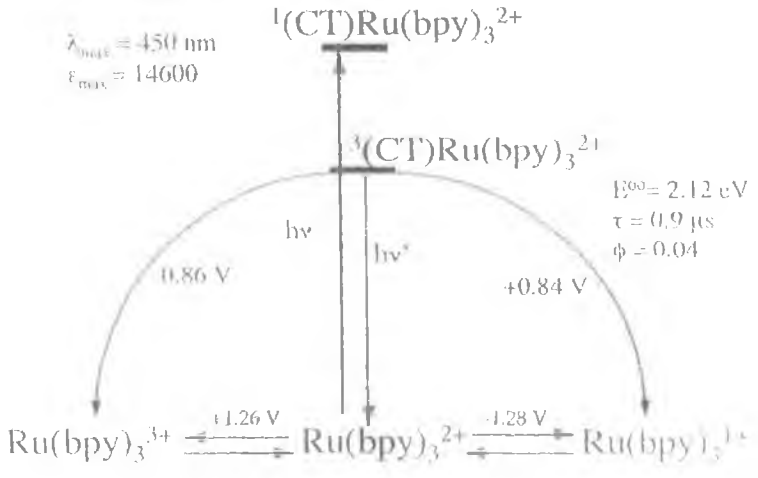

Figure 7.2 Latimer type diagram illustrating the inter-relationships between ground state and excited state redox potentials.[5]

$[Ru(bpy)_3]^{2+}$ was first reported by Burstall *et. al.* in 1936 with the first report of its luminescence being published in 1959 by Paris and Brandt.[6,7] Since then comprehensive investigations have been carried out to understand the intrinsic properties of $[Ru(bpy)_3]^{2+}$.[8,9,10,11] Although the photochemical and photophysical

behaviour demonstrated by the complex $[Ru(bpy)_3]^{2+}$ implied that it was a possible candidate for use as a catalyst for solar energy conversion its application for this purpose was restricted by its ability to absorb only a narrow region of the solar spectrum and by photodecomposition of the complex via a ^{3}MC state. The possibility of overcoming these problems by modifying the ligand systems around the Ru(II) metal centre has led to the development of a wide variety of both mononuclear and polynuclear systems.[3,4]

$[Ru(bpy)_3]^{2+}$ is a remarkably stable low spin d^6 complex with D_3 symmetry and exhibits a significant level of π backbonding between Ru(II) and the π^* orbital of the bipyridyl ligands. The absorbance spectrum of $[Ru(bpy)_3]^{2+}$ exhibits bands at 185 nm and 285 nm which have been assigned as ligand centred π- π^* transitions. Further bands at 238 nm, 250 nm and 452 nm have been assigned as MLCT d- π^* transitions. The shoulders observable at 322 nm and 344 nm are thought to be due to charge transfer or d-d (MC) transitions.[9] Excitation of $[Ru(bpy)_3]^{2+}$ in any of it's absorption bands gives rise to the emission spectra with a maximum at approximately 602 nm.[12,13,14] Upon excitation to the ^{1}MLCT state intersystem crossing occurs with an efficiency of unity to the ^{3}MLCT. This is normally a spin forbidden transition but possible in this situation as a result spin orbit coupling. This ^{3}MLCT consists of four closely spaced triplet states and it is from these that emission occurs. Figure 7.3 illustrates the photophysical processes exhibited by $[Ru(bpy)_3]^{2+}$.

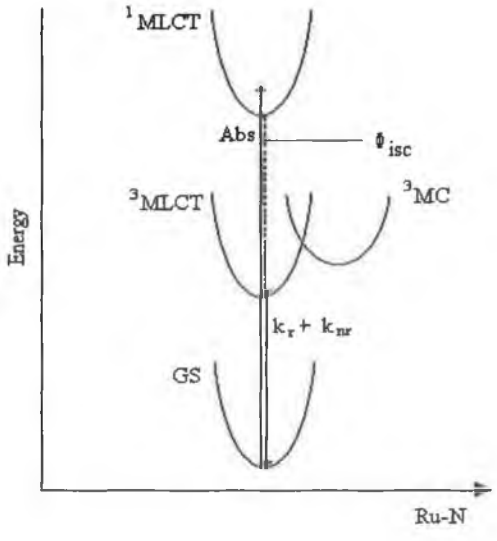

Figure 7.3 Illustration of the photophysical processes of $[Ru(bpy)_3]^{2+}$.[15]

The decay of these species occurs mostly through low-lying dd states and through MLCT (4^{th}) upper states. Once the dd states are populated they tend to be short lived and may result in the loss of ligands and decomposition of the complex. It is possible to reduce this effect by using mixed chelates.[16] Another approach in the effort to eliminate unwanted decomposition has been to trap the ruthenium-polypyridine complexes within zeolite-Y supercages.[17] The result of using supercages is to raise the energy of the ^{3}dd state hence raising the magnitude of ΔE_{dd} thus eliminating the decay route. Ligand photodissociation of $[Ru(bpy)_3]^{2+}$ can also occur from the luminescent triplet ^{3}MLCT level to a distorted triplet ^{3}MC level. This transition gives rise to the loss of one Ru-N bond. In order to eliminate this the energy gap between these two levels has to be altered. This is accomplished by decreasing the energy of the ^{3}MLCT level, however, lowering of the energy of the ^{3}MLCT level increases the decay to the ground state which gives rise to a reduction in the lifetime of the excited state and in the quantum yield.[18]

Numerous efforts have been made to refine / fine-tune $[Ru(bpy)_3]^{2+}$ in order to create systems with desired properties.[3,4] As already discussed modification of the ligands in a complex such as $[Ru(bpy)_3]^{2+}$ affects the absorption, emission and electrochemical properties of the complex. With this in mind both homoleptic and heteroleptic complexes have been synthesised and characterised and the introduction of bridging ligands has allowed for the synthesis of multinuclear complexes.[3,4] Fine tuning of the parent $[Ru(bpy)_3]^{2+}$complex has not been restricted solely to modifying the bridging and peripheral ligands. The introduction of other transition metals such as osmium, iridium and rhodium has led to the development of a number of interesting systems which have led to a better understanding of electron transfer processes and has allowed the production of molecular level devices.[4,19,20]

The Ru(II)-Rh(III) type systems are of particular interest as both the Ru(II) electron donating polypyridyl unit and the Rh(III) electron accepting polypyridyl unit are photoexcitable. As a result it is possible, in theory, to observe (i) electron transfer from excited donor to acceptor, (ii) electron transfer from donor to excited acceptor (iii) back electron transfer from reduced acceptor to oxidised donor and (iv)

energy transfer from excited acceptor to the donor. These intercomponent processes are depicted in Figure 7.4.[20]

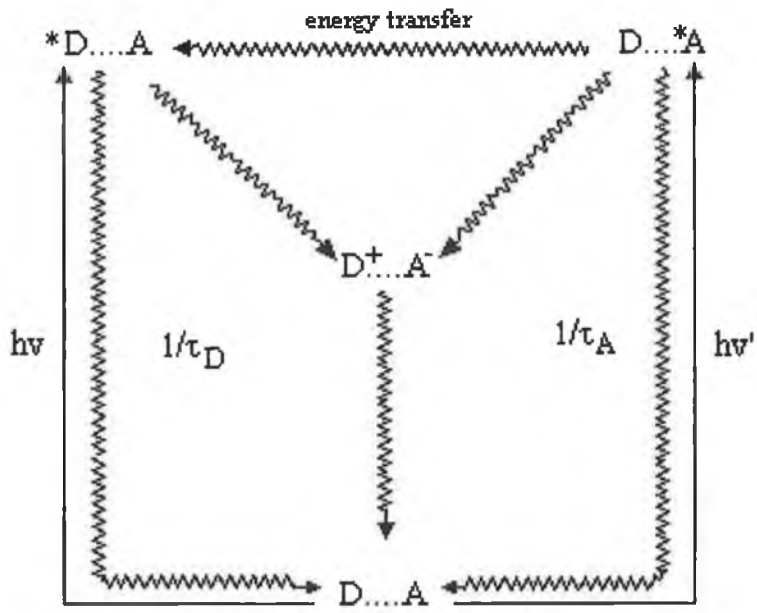

Figure 7.4 Intercomponent processes taking place in a dinuclear system where both the electron donor and the electron acceptor are photoexcitable.[20]

Indelli *et. al.* have synthesised a number of dinuclear Ru(II)-Rh(III) complexes, an example of which is the complex $[Ru(II)(4,7\text{-}Me_2phen)_2\text{-}(4\text{-}Mebpy\text{-}CH_2\text{-}CH_2\text{-}4\text{-}Mebpy)\text{-}Rh(III)(4,4'\text{-}Me_2bpy)_2]^{5+}$, where 4-Mebpy = 4-methyl-2,2'-bipyridine, 4,4'-Me_2bpy = 4,4'-dimethyl-2,2'-bipyridine and 4,7-Me_2phen = 4,7-dimethyl-2,2'-bipyridine, Figure 7.5.[20] Indelli *et. al.* were able to selectively excite the chromophoric units within the complex and it was found that at room temperature Ru(II)— $Rh(III)^* \rightarrow {}^*Ru(II)$— Rh(III) energy transfer did not occur. Instead energy transfer was much more efficient in a rigid medium (i.e. in a glass at 77K) as under these conditions the electron transfer processes which occur at room temperature are blocked due to restricted solvent repolarisation.[20]

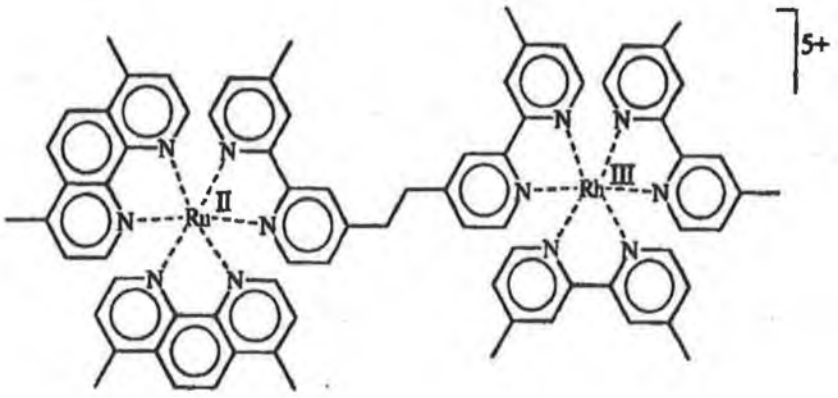

Figure 7.5 Structural formula of a Ru(II)-Rh(III) dinuclear complex developed by Indelli et. al. [20]

Indelli *et. al.* have also reported a series of ruthenium(II)-rhodium(III) dinuclear complexes where 2,2':6'2''-terpyridine units are either directly linked together or connected through phenyl spacers in the 4' position - Figure 7.6.[21] In this series of complexes, of the general formula (ttpy)Ru-tpy-$(ph)_n$-tpy-Rh(ttpy) where ttpy = 4'-*p*-tolyl-2,2':6,2''-terpyridine, ph = phenyl and n = 0-2, no quenching of the Ru(II)-based emission was observed whereas energy transfer from excited Rh(III) to Ru(II) was observed for all complexes at 77K.[21]

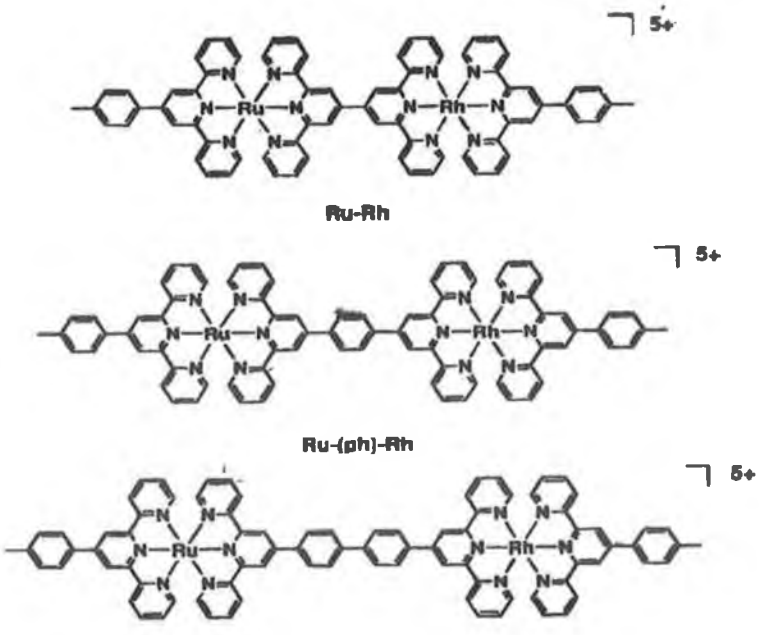

Figure 7.6 Structural formula of Ru(II)-Rh(III) complex.[21]

Ohno *et. al.* have studied electron transfer reactions in a number of systems including systems incorporating benzimidazole type ligands, Figure 7.7.[22,23,24] These ligands are of interest partly due to their asymmetry as this potentially affords a significant difference between the donor and the acceptor sites and facilitates the flow of electrons. Other important features of these types of ligands are that they possess σ/π-donor properties and they contain a dissociable NH proton. In 1992 Ohno *et. al.* reported intramolecular electron transfer in photoexcited Ru(II)-Rh(III) complexes in which the two chelating moieties of either 2-(2'-pyridyl)imidazole or 2-(2'-pyridyl)benzimidazole were linked in various manners.[22] In these systems, emission from (^{3}CT)Ru occurred upon excitation of either the ruthenium or the rhodium chromophore. This was interpreted to be due to a fast intramolecular electron transfer. Rapid quenching of the (^{3}CT)Ru state was attributed to an intramolecular electron transfer giving rise to a Ru(III)-Rh(II) state. It was found that this was followed by a fast backward electron transfer to regenerate the ground state.[22]

A later report by Ohno *et. al.* related the synthesis and study of the proton-coupled redox properties of mononuclear and asymmetric dinuclear complexes of Ru(II) and either Rh(III) or Os(II) with the ligand 2,2'-bis(2-pyridyl)-6,6'-bibenzimidazole.[23] It should be noted that for such a ligand geometrical isomers become an issue, as does the presence of optical isomers (Figure 7.7).

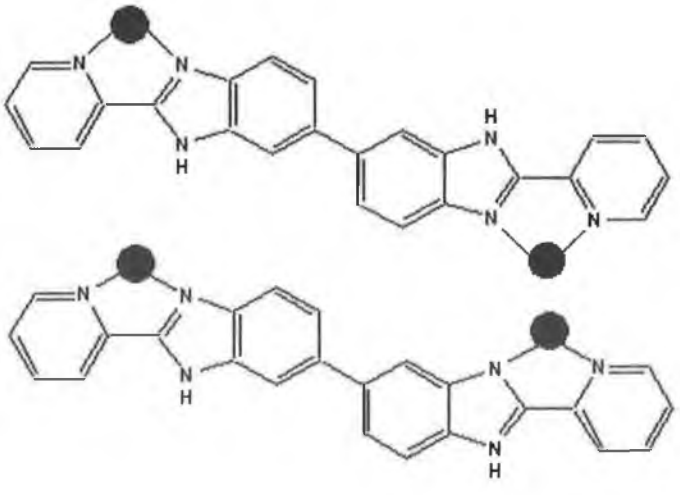

Figure 7.7 Possible geometrical isomers for dinuclear species with the ligand, 2'-bis(2-pyridyl)-6,6'-bibenzimidazole.[23]

The protonation state of these complexes is dependent upon the pH of the solution and as expected, the absorption spectra and the oxidation potentials were found to be strongly pH dependent with oxidation potentials being shifted to more negative potentials with increasing pH. Upon proton transfer a change in the electronic structure of the complex occurs and from this, by shrewd selection of ligands and metals, the desired potential difference.[23] Ohno *et. al.* have also been involved with studies of the inner-sphere reorganisation of photo-induced electron transfers on the laser excitation of Ru(II)-Rh(III) and Ru(II)-Co(III) complexes (Figure 7.8).[24]

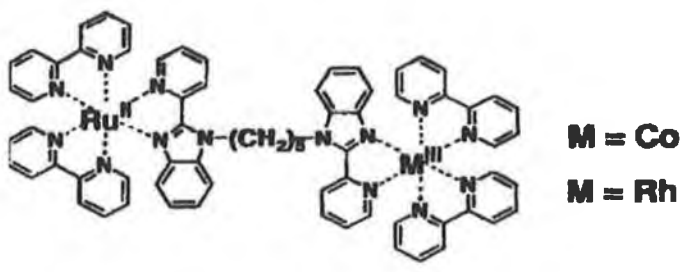

Figure 7.8 Ru(II)-Rh(III) dyad reported by Ohno et. al.[24]

Various other research groups have been involved with the development of ruthenium(II)-rhodium(III) dinuclear systems. Kalyanasundaram *et. al.* studied excited state interactions in ligand bridged chromophore-quencher complexes containing Rh(III) and Ru(II) polypyridyl units. Excitation of one of the complexes discussed, a mixed metal complex Ru(II)-dpp-Rh(III) where dpp is the ligand 2,3-bis(2-pyridyl)pyrazine, led to the formation of the CT excited state of the ruthenium chromophore. The short lifetime of this excited state in fluidic solution was attributed primarily to electron transfer involving the adjacent Rh(III) unit.[25] Furue *et. al* reported evidence for the Marcus inverted region in their study of intermolecular electron transfer in the covalently linked Ru(II)/Rh(III) dinuclear complex seen in Figure 7.9.[26]

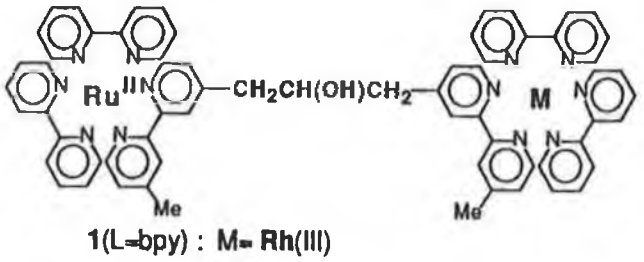

Figure 7.9 Ru(II)-Rh(III) dyad reported by Furue et. al.[26]

Brewer *et. al.* have investigated a tridentate bridged ruthenium – rhodium complex as a stereochemically defined light-absorber-electron-acceptor dyad, Ziegler *et. al.* have reported Rh(III) and Ru(II) complexes with chiral terpyridyl ligands and Kim *et. al.* have recently reported the crystal structure and electrochemical behaviour of the complexes $[Rh(tpy)(bpy)(Cl)](ClO_4)_2$ and $[Rh(tpy)(phen)(Cl)](PF_6)_2$.[27,28] Other mixed metal complexes incorporating rhodium and ruthenium, iridium and osmium have been investigated by Brewer *et. al.*, Seroni *et. al.* and Nallas *et. al.* and a number of rhodium(III) porphyrin systems have also been reported.[29,30, 31, 32, 33, 34, 35,36]

Earlier chapters have outlined the synthesis and characterisation of a number of mononuclear Rh(III) polypyridyl complexes. Of the various ligands studied Hbpt, NH_2bpt, Hbpzt and Hppt are capable of binding a second metal centre as illustrated by Figure 7.10.

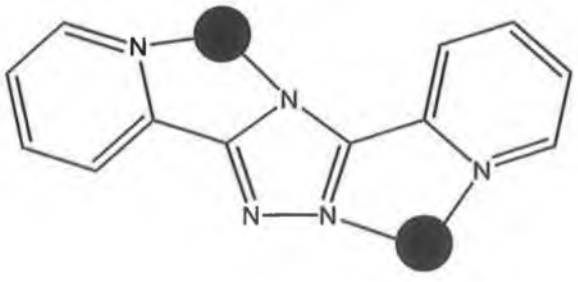

Figure 7.10 Dinuclear complex with the ligand Hbpt.

As discussed in Chapter 1, Section 1.5, heterobimetallic ruthenium-rhodium and ruthenium-iridium complexes incorporating the Hbpt ligand have previously been studied.[37] The complexes $[(bpy)_2Ru(bpt)Rh(ppy)_2]^{2+}$ and $[(bpy)_2Ru(bpt)Ir(ppy)_2]^{2+}$ were obtained by heating the mononuclear complex $[Ru(bpy)_2(bpt)]^+$ with $[M(ppy)_2Cl_2]$ where M = Rh or Ir in 2-methoxyethanol to reflux for 48 hours. The homobimetallic complexes, $[(Rh(ppy)_2)_2(bpt)]^+$ and $[(Ir(ppy)_2)_2(bpt)]^+$ were obtained by heating the Hbpt ligand to reflux with $[M(ppy)_2Cl_2]$, where M = Rh or Ir, in CH_2Cl_2:EtOH 2:1 for 6 hours.[37]

The following discussion focuses upon attempts made to synthesise Rh(III)/Ru(II) dinuclear complexes using pyridine and pyrazine triazole based ligands. Initial attempts concentrated upon synthesising complexes with the ligands Hbpt and Hbpzt. Subsequent efforts involved the NH_2bpt ligand and finally ligands containing a benzene spacer group were investigated. The ligands, which will be discussed in this chapter, can be seen in Figure 7.1.

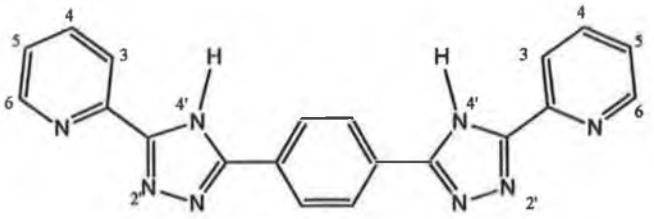

p-pytbzpyt - 1,4 -bis(5-(pyridin-2-yl)-1,2,4-triazol-3-yl)benzene

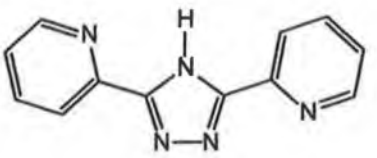

Hbpt - 3,5-bis(pyridin-2-yl)-1,2,4-triazole

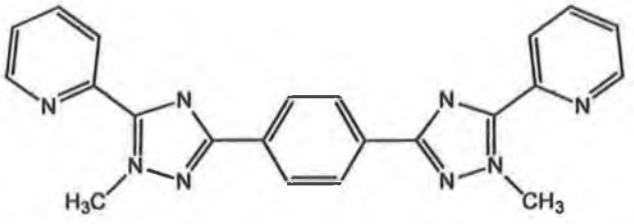

Me-*p*-pytbzpyt - 1,4-bis(5-(pyridin-2-yl)-1,2,4-triazol-3-yl)benzene

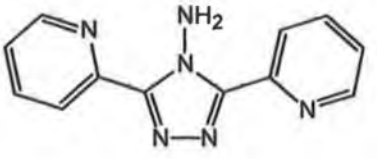

NH_2bpt - 4-amino-3,5-bis(pyridin-2-yl)-1,2,4-triazole

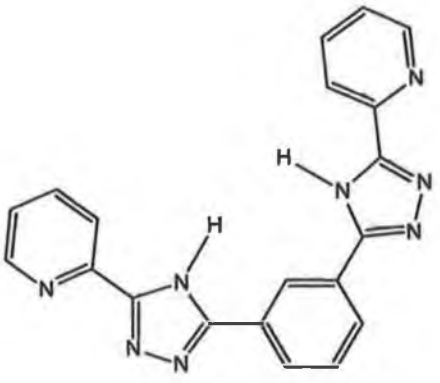

m-pytbzpyt 1,3-bis(5-(pyridin-2-yl)-1,2,4-triazol-3-yl)benzene

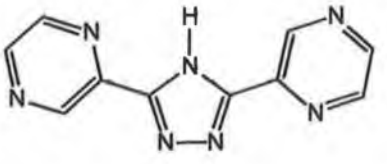

Hbpzt - 3,5-bis(pyrazin-2-yl)-1,2,4-triazole

Figure 7.11 Ligands cited in the following discussion.

7.2 Experimental

$[Ru(mebpy)_2)Cl_2]$ where mebpy = 4,4'-dimethyl-2,2'-bipyridine was obtained from M.T. Indelli and the complexes $[Ru(bpy)_2(m\text{-pytbzpyt})]^+$ and $[Ru(bpy)_2(p\text{-pytbzpyt})]^+$ were obtained from Frances Weldon. Numerous attempts were made to synthesise Rh(III)/Ru(II) dinuclear complexes and Table 7.1 details the work carried out. Of the reactions carried out only two were successful and the method by which these complexes were synthesised and purified is also detailed.

Table 7.1 Reactions carried out in attempts to synthesise dinuclear complexes.

Target Complex	Starting Materials	Solvent System	Reaction Time (hrs)
$[(Rh(phen)_2)_2(bpt)]^{5+}$	$[Rh(phen)_2(bpt)]^{2+}$ and $[Rh(phen)_2Cl_2]Cl$ 1:1	$EtOH:H_2O$ 1:1	96
$[Ru(bpy)_2(bpt)Rh(phen)_2]$	$[Ru(bpy)_2(bpt)]^{2+}$ and $[Rh(phen)_2Cl_2]^+$ 1:1	$EtOH:H_2O$ 1:1	96
$[Rh(phen)_2)_2(NHbpt)]^{5+}$	$[Rh(phen)_2(NHbpt)]^2$ and $[Rh(phen)_2Cl_2]Cl$ 1:1	$EtOH:H_2O$ 1:1	1 week
$[Rh(phen)_2(NHbpt)Ru(mebpy)_2]^{5+}$	$[Rh(phen)_2(NHbpt)]^{2+}$ and $[Ru(mebpy)_2Cl_2]^+$ 1:1	$EtOH:H_2O$ 1:1	72
$[Rh(phen)_2(NHbpt)Ru(mebpy)_2]^{5+}$	$[Rh(phen)_2(NHbpt)]^{2+}$ and $[Ru(mebpy)_2Cl_2]^+$ 1:1	$EtOH:H_2O$ 1:1	96
$[Rh(phen)_2(NHbpt)Ru(mebpy)_2]^{5+}$	$[Rh(phen)_2(NHbpt)]^{2+}$ and $[Ru(mebpy)_2Cl_2]^+$ 1:1	DMF	24
$[Rh(phen)_2(NHbpt)Ru(bpy)_2]^{5+}$	$[Rh(phen)_2(NHbpt)]^{2+}$ and $[Ru(bpy)_2Cl_2]^+$ 1:1	DMF: H_2O 2:1	1 week
$[(Rh(phen)_2)_2(bpzt)]^{5+}$	Hbpzt and $[Rh(phen)_2Cl_2]^+$ 2.2:1	H_2O	72
$[(Rh(phen)_2)_2(bpzt)]^{5+}$	Hbpzt and $[Rh(phen)_2Cl_2]^+$ 2.2:1	$EtOH:H_2O$ 2:1	5 days
$[(Rh(phen)_2)_2(bpzt)]^{5+}$	$[Rh(phen)_2(bpzt)]^{2+}$ and $[Rh(phen)_2Cl_2]^+$ 1:1	$EtOH:H_2O$ 2:1	5 days
$[(Rh(phen)_2)_2(bpzt)]^{5+}$	$[Rh(phen)_2(bpzt)]^{2+}$ and $[Rh(phen)_2Cl_2]^+$ 1:1	H_2O pH9	72
$[(Rh(phen)_2)_2(bpzt)]^{5+}$	$[Rh(phen)_2(bpzt)]^{2+}$ and $[Rh(phen)_2(OH_2)_2]^+$ 1:1	H_2O pH9	96
$[Rh(phen)_2(bpzt)Ru(mebpy)_2]^{4+}$	$[Rh(phen)_2(bpzt)]^{2+}$ and $[Ru(mebpy)_2Cl_2]^+$ 1:1	$EtOH:H_2O$ 2:1	72
$[Rh(phen)_2(bpzt)Ru(mebpy)_2]^{4+}$	$[Rh(mebpy)_2(bpzt)]^+$ and $[Rh(phen)_2Cl_2]^+$ 1:1.2	$EtOH:H_2O$ 2:1	72
$[Ru(bpy)_2(m\text{-pytbzpyt})Rh(phen)_2]^{3+}$	$[Ru(bpy)_2(m\text{-pytbzpyt})]^+$ and $[Rh(phen)_2Cl_2]Cl$ 1:2	DCM	24
$[Ru(bpy)_2(m\text{-pytbzpyt})Rh(phen)_2]^{3+}$	$[Ru(bpy)_2(m\text{-pytbzpyt})]^+$ and $[Rh(phen)_2Cl_2]Cl$ 1:2	$EtOH:H_2O$ 2:1	12
$[Ru(bpy)_2(m\text{-pytbzpyt})Rh(phen)_2]^{3+}$	$[Ru(bpy)_2(m\text{-pytbzpyt})]^+$ and $[Rh(phen)_2Cl_2]Cl$ 1:2	DMF: H_2O 2:1	96
$[Ru(bpy)_2(p\text{-pytbzpyt})Rh(phen)_2]^{3+}$	$[Ru(bpy)_2(p\text{-pytbzpyt})]^+$ and $[Rh(phen)_2Cl_2]Cl$ 1:2	$EtOH:H_2O$ 2:1	96
$[Ru(bpy)_2(p\text{-pytbzpyt})Rh(phen)_2]^{3+}$	$[Ru(bpy)_2(p\text{-pytbzpyt})]^+$ and $[Rh(phen)_2Cl_2]Cl$ 1:2	$EtOH:H_2O$ 2:1	24
$[Ru(bpy)_2(p\text{-pytbzpyt})Rh(bpy)_2]^{3+}$	$[Ru(bpy)_2(p\text{-pytbzpyt})]^+$ and $[Rh(bpy)_2Cl_2]Cl$ 1:2	DMF: H_2O 2:1	96

$[Rh(phen)_2(OH_2)_2]^+$

A 0.099g (0.17mmol) of $[Rh(phen)_2Cl_2]Cl$ and 0.1g NaOH were dissolved in a $15cm^3$ of water. This was allowed to heat and 5μL of hydrazine hydrate were added and the solution was heated for 10 minutes. The volume of the reaction mixture was reduced to $5cm^3$ and allowed to cool to room temperature. The pH of the solution was then adjusted to 7 using HNO_3. The solution was then cooled in an ice bath for 2 hours upon which a white precipitate was observed. Yield 0.072g (68% yield).[38]

$[Rh(phen)_2(p\text{-pytbzpyt})Ru(bpy)_2]^{3+}$

0.034g (0.03mmol) of $[Ru(bpy)(p\text{-pytbzpyt})]^{2+}$ were dissolved in $15cm^3$ DMF : H_2O 2:1 with heating. To this 0.045g (0.08mmol) of $[Rh(phen)_2Cl_2]^+$ were added and the solution was then heated to reflux for 24 hours after which the solution was allowed to cool to room temperature. The solution was then reduced using a rotary evaporator to remove any of the ethanol, cooled and loaded directly onto a Sephadex C-25 ion exchange column. Unreacted $[Rh(phen)_2Cl_2]^+$ was eluted using 0.1M NaCl and the product was eluted with 0.5M NaCl. The 0.5M fraction was then reduced to approximately $10cm^3$ and the complex was isolated as a PF_6^- salt by adding aqueous NH_4PF_6. A red powder was obtained with a yield of 0.011g (22%).

$[Rh(bpy)_2(p\text{-pytbzpyt})Ru(bpy)_2]^{3+}$

0.021g (0.02mmol) of $[Ru(bpy)(p\text{-pytbzpyt})]^{2+}$ Were dissolved in $15cm^3$ DMF : H_2O 2:1 with heating. To this 0.025g (0.04mmol) of $[Rh(bpy)_2Cl_2]^+$ were added and the solution was then heated to reflux for 96 hours after which the solution was allowed to cool to room temperature. The solution was then reduced using a rotary evaporator to remove any of the ethanol, cooled and loaded directly onto a Sephadex C-25 ion exchange column. Unreacted $[Rh(bpy)_2Cl_2]^+$ was eluted using 0.1M NaCl and the product was eluted with 0.5M NaCl. The 0.5M fraction was then reduced to approximately $10cm^3$ and the complex was isolated as a PF_6^- salt by adding aqueous NH_4PF_6. A red powder was obtained with a yield of 0.015g (47%).

7.3 Results and Discussion

7.3.1 Synthetic Aspects

Numerous approaches were taken in the attempted synthesis of both homo and heterodinuclear complexes all of which are detailed in Table 7.1. As can be seen a number of different approaches were tried (i) starting from Rh(III) mononuclear complexes, (ii) starting from the free ligands (iii) starting from Ru(II) mononuclear complexes, (iv) using the bis aqua complex $[Rh(phen)_2(OH_2)_2]^+$, (v) various solvent systems and (vi) extending the type of ligands used to those incorporating spacers. Initially the synthesis focused upon complexes that would incorporate the ligands Hbpt, NH_2bpt and Hbpzt. These were ligands of which Rh(III) mononuclear complexes had been synthesised and purified and Ru(II) and Os (II) dinuclear complexes with Hbpt and Hbpzt had previously been reported.[15,39,40] Dinuclear complexes had also been reported with NH_2bpt but these had incorporated the cyclometallated $[Rh(ppy)_2]^{3+}$ metal centre.[41]

Generally reactions were first attempted in EtOH:H_2O 1:1, the same solvent system used by Hage *et. al.* when synthesising Ru/Os dimers with the ligands Hbpt and Hbpzt.[15] Reactions were carried out in two ways (i) using the free ligands and $[Rh(phen)_2Cl_2]^+$ and (ii) using the Rh(III) monomeric complexes and $[Rh(phen)_2Cl_2]^+$ or $[Ru(L)_2Cl_2]$ where L = bpy or mebpy = 4,4'-dimethyl-2,2'-bipyridine. Such reactions were heated to reflux for between 4 to 7 days but there was never any indication, via tlc, for the formation of a dinuclear complex. When these attempts proved fruitless a different approach was used. It was felt that the problem might be that the coordinated chlorides of $[Rh(phen)_2Cl_2]^+$ were not fully displaced, therefore the starting material $[Rh(phen)_2Cl_2]^+$ was converted to its analogous bis aqua complex $[Rh(phen)_2(OH_2)_2]^+$ which tends to be more reactive, however $[Rh(phen)_2(OH_2)_2]^+$ did not prove to be reactive with the Rh(III) mononuclear complexes.[42,43]

When attempts to introduce a second metal centre, either Rh(III) or Ru(II), were unsuccessful another approach was tried. Instead of starting from a Rh(III) mononuclear complex and attempting to introduce a Ru(II)/Rh(III) metal centre, attempts were made to bind a Rh(III) metal centre to a Ru(II) mononuclear complex. Of the syntheses tried no reaction was observed even after heating to reflux for a week. With the lack of success with the ligands Hbpt, NH_2bpt and Hbpzt it was felt that the type of ligand being used should be varied. Many of the Rh(III)/Ru(II) complexes which have been reported previously have included a bridging ligand which contains a spacer moiety. Thus the ligands *p*-pytbzpyt and Me-*p*-pytbpzyt were chosen. These are essentially two Hpytr σ-donating units connected via a benzene spacer, Figure 7.1. The Ru(II) mononuclear complexes with these ligands have been synthesised and characterised previously as have dinuclear complexes.[44] The Ru(II) mononuclear complexes with the *p*-pytbzpyt and Me-*p*-pytbpzyt ligands were obtained in their pure form from Frances Weldon.[44] Reactions using these complexes were carried out on a small scale as only a very limited quantity of the pure Ru(II) precursors were available. Reactions with the *p*-pytbzpyt ligand proved to be successful. As can be seen from Table 7.1 a number of solvent systems were employed but it was found that the reactions tended to be most successful when carried out in DMF:H_2O, 2:1 whilst a Sephadex C-25 column proved suitable for their purification. Isomers are an issue with complexes such as these and as a result it is quite important to know the (i) the mode of coordination of the starting material and (b) more importantly that only a single isomer is present in the starting material. It had previously been shown that both Ru(II) mononuclear complexes used were coordinated via the N2' position of the triazole ring.[44]

7.3.2 ^{1}H NMR Spectroscopy

The ^{1}H NMR spectra of $[Rh(phen)_2(p\text{-pytbzpyt})Ru(bpy)_2]^{3+}$ and $[Rh(bpy)_2(p\text{-pytbzpyt})Ru(bpy)_2]^{3+}$ can be seen in Figure 7.12 and Figure 7.13.

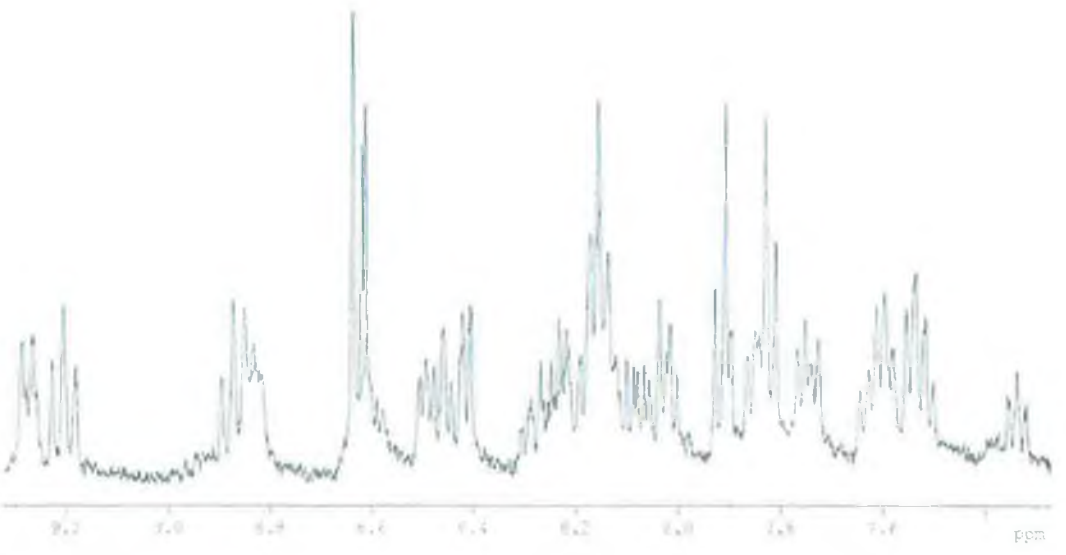

Figure 7.12 ^{1}H NMR spectrum of $[Rh(phen)_2(p\text{-pytbzpyt})Ru(bpy)_2]^{3+}$ measured in d_6-DMSO.

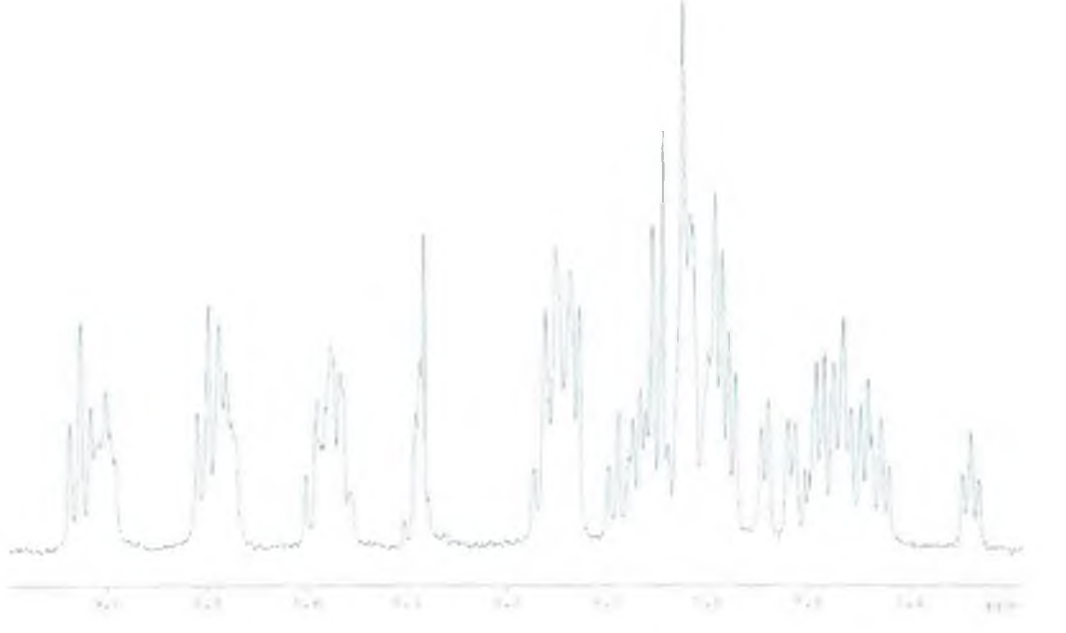

Figure 7.13 ^{1}H NMR spectrum of $[Rh(bpy)_2(p\text{-pytbzpyt})Ru(bpy)_2]^{3+}$ measured in d_6-DMSO.

The spectra of the complex $[Rh(phen)_2(p\text{-pytbzpyt})Ru(bpy)_2]^{3+}$ and $[Rh(bpy)_2(p\text{-pytbzpyt})Ru(bpy)_2]^{3+}$ are particularly complicated, however it was found that both spectra integrate to 44 protons as expected. It was possible to identify the H3, H4, H5 and H6 protons associated with both the Ru(II) and the Rh(III) metal centres using the ^1H-^1H COSY NMR spectrum of $[Rh(bpy)_2(p\text{-pytbzpyt})Ru(bpy)_2]^{3+}$ seen below in Figure 7.14 and by comparison with the spectra of $[Rh(L)_2(pytr)]^{2+}$ where L = phen / bpy discussed in Chapter 3 and the spectrum of the complex $[Ru(bpy)_2(p\text{-pytbzpyt})Ru(bpy)_2]^{3+}$ which was studied previously (Figure 7.15).[44]

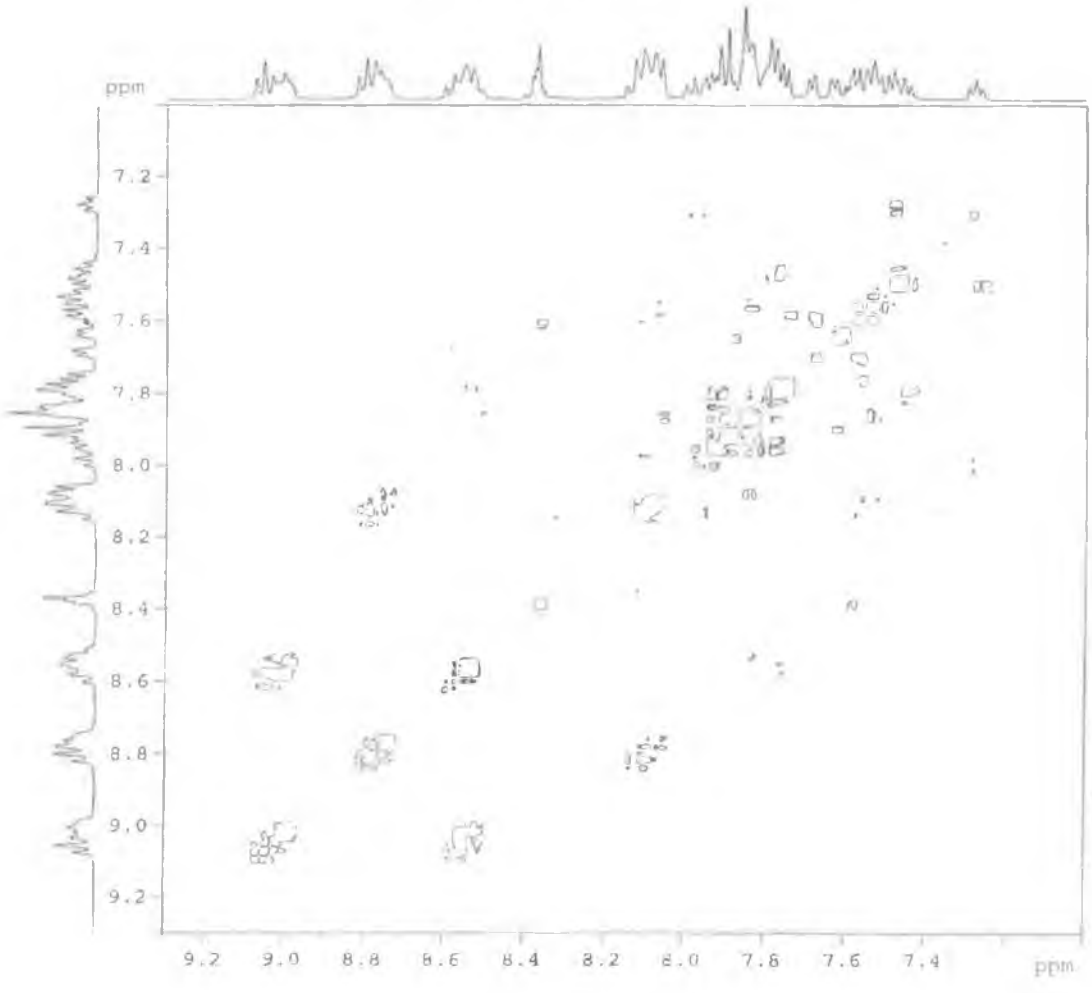

Figure 7.14 ^1H-^1H COSY spectrum of $[Rh(bpy)_2(p\text{-pytbzpyt})Ru(bpy)_2]^{3+}$ measured in d_6-DMSO.

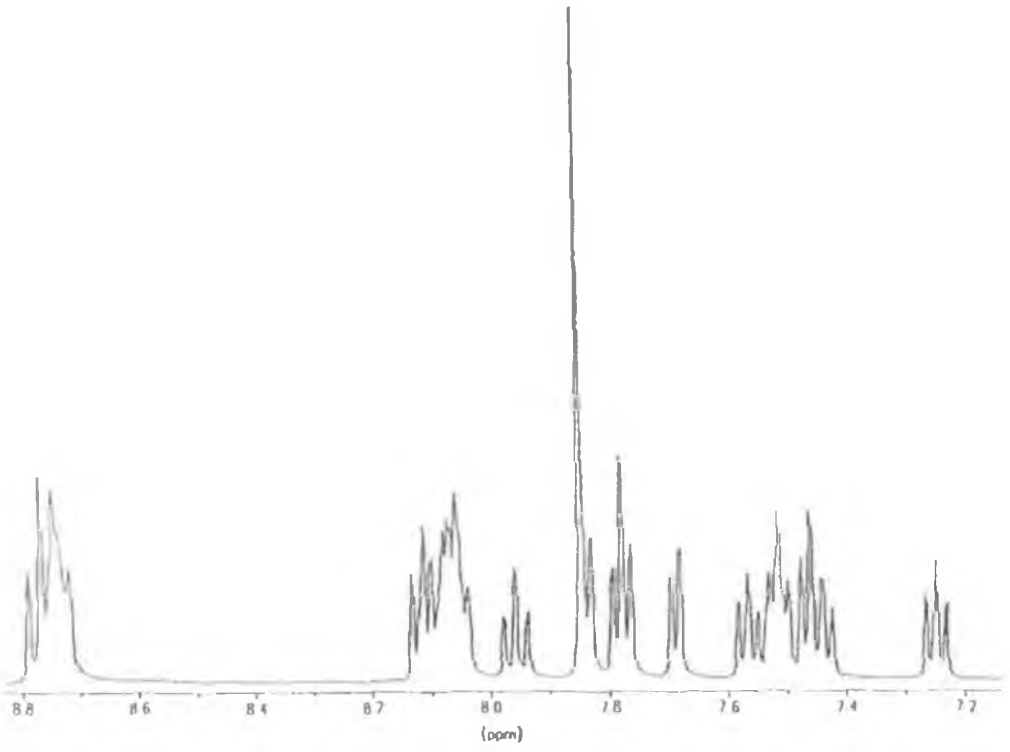

Figure 7.15 ^{1}H NMR spectrum of [Ru(bpy)$_2$(p-pytbzpyt)Ru(bpy)$_2$]$^{2+}$ measured in d_6-DMSO.[44]

The homodinuclear complex [Ru(bpy)$_2$(*p*-pytbzpyt)Ru(bpy)$_2$]$^{2+}$ exhibits a relatively simple ^{1}H NMR spectrum in comparison to the spectra of the heterobimetallic seen in Figure 7.12 and Figure 7.13 which reflects the symmetric environment of the two Ru(II) metal centres. The ^{1}H NMR spectrum of [Ru(bpy)$_2$(*p*-pytbzpyt)Ru(bpy)$_2$]$^{2+}$ was assigned as follows; H3 – 8.12 ppm, H4 – 7.96 ppm, H5 – 7.25 ppm, H6 – 7.69 ppm and the phenyl protons were found at 7.85 ppm.[44] If we consider the behaviour of the complexes [Rh(phen)$_2$(pytr)]$^{2+}$ and [Rh(bpy)$_2$(pytr)]$^{2+}$ detailed in Chapter 3 it is possible to assign the spectra of [Rh(phen)$_2$(*p*-pytbzpyt)Ru(bpy)$_2$]$^{3+}$ and [Rh(bpy)$_2$(*p*-pytbzpyt)Ru(bpy)$_2$]$^{3+}$ as detailed in Table 7.2.

Table 7.2 *^1H NMR data for $[Rh(phen)_2(pytr)]^{2+}$, $[Rh(bpy)_2(pytr)]^{2+}$, $[Ru(bpy)_2(p\text{-}pytbzpyt)Ru(bpy)_2]^{2+}$, $[Rh(phen)_2(p\text{-}pytbzpyt)Ru(bpy)_2]^{3+}$ and $[Rh(bpy)_2(p\text{-}pytbzpyt)Ru(bpy)_2]^{3+}$ measured in d_6-DMSO.*

	H3	H4	H5	H6	Phenyl
$[Rh(phen)_2(pytr)]^{2+}$	8.33	8.33	7.46	7.68	
$[Rh(bpy)_2(pytr)]^{2+}$	8.30	8.36	7.58	7.74	
$[Ru(bpy)_2(p\text{-}pytbzpyt)Ru(bpy)_2]^{2+}$ [a]	8.12	7.96	7.25	7.69	7.85
$[Rh(phen)_2(p\text{-}pytbzpyt)Ru(bpy)_2]^{3+}$					7.92-7.80
Ru metal centre	8.22	8.02	7.33	7.65-7.50	
Rh metal centre	8.65-8.60	8.65-8.60	7.65-7.50	7.72-7.78	
$[Rh(bpy)_2(p\text{-}pytbzpyt)Ru(bpy)_2]^{3+}$					7.92-7.82
Ru metal centre	8.15-8.04	7.98	7.28	7.49	
Rh metal centre	8.38	8.38	7.6-7.5	7.69	

a – values taken from ref. 44

Due to the small amount of the heterodinuclear complexes obtained it was not possible to carry out any further characterisation on these complexes and due to time constraints it was not possible to synthesise and purify the Ru(II) mononuclear precursor in order to attempt any further synthesis.

7.4 Conclusions

It can be seen from the variety of approaches taken that such complexes are not trivial to synthesise. A great deal of time and effort was directed to the synthesis of dinuclear complexes with disappointing results, however, the isolation of the complexes $[Rh(phen)_2(p\text{-pytbzpyt})Ru(bpy)_2]^{3+}$ and $[Rh(bpy)_2(p\text{-pytbzpyt})Ru(bpy)_2]^{3+}$, even if it was not possible to characterise them, is of importance to the future development of such dinuclear complexes with the prevailing result from this study being the identification of the type of ligand necessary for the formation of dinuclear complexes.

It is clear from all of the attempts made to synthesise dinuclear complexes with the ligands Hbpt, Hbpzt and NH_2bpt that such ligands are unsuitable for development of dinuclear complexes incorporating a $[Ru(bpy)_2]^{2+}$ and a $[Rh(phen)_2]^{3+}$ / $[Rh(bpy)_2]^{3+}$ unit. Analysis of the synthesis of the Rh(III) mononuclear complexes detailed in Chapter 3 and 5 indicates that complex formation in these cases is influenced by the σ-donor / π-accepting properties of the ligands. Syntheses with ligands such as PIP, MePIP and PTP in particular required very short reaction times and gave very high yields. Thus it would seem that the $[Rh(phen)_2]^{3+}$ / $[Rh(bpy)_2]^{3+}$ units require an electron rich environment for complex formation. This observation explains to a degree the difficulty observed in synthesising dinuclear complexes with the Hbpt, Hbpzt and NH_2bpt ligands. The formation of dinuclear complexes with these ligands would require the metal centres to share the σ-donating ligand and based upon the results obtained this is not a situation conducive to the formation of dinuclear complexes.

Based upon the outcome of the attempted synthesis of dinuclear complexes with the Hbpt, Hbpzt and NH_2bpt ligands it was felt that a different type of ligand was required to generate such complexes. Thus the synthetic endeavour progressed to incorporate ligands that essentially incorporate two σ-donating units separated by a spacer. The ligands were chosen due to their similarity to the pyridyl triazole complexes discussed in Chapter 3 and 4 and due to the availability of a limited

amount of the purified Ru(II) mononuclear complex. As was seen in 7.2.2 the ligand *p*-pytbzpyt proved to be suitable for the synthesis of the desired Ru(II)/Rh(III) dinuclear complexes. The successful formation of Ru(II)/Rh(III) dinuclear complexes with this ligand is attributed to the increased σ-donating ability of this ligand. The *p*-pytbzpyt ligand essentially incorporates two separate Hpytr units meaning that, unlike the situation with ligands such as Hbpt, Hbpzt and NH_2bpt, there is sufficient electron density available to stabilise both metal centres.

References

1 J.M. Lehn, *Science*, **1993**, *260*, 1762-1763.

2 J.M. Lehn, *Angew. Chem. Int. Ed. Eng.*, **1988**, *27*, 89-112.

3 V. Balzani, A. Juris, M. Venturi, S. Campagna, S. Serroni, *Chem. Rev.*, **1996**, *96*, 759-833.

4 J.P. Sauvage, J.P. Collin, J.C. Chambron, S. Guillerez, C. Coudret, *Chem. Rev.*, **1994**, *94*, 993-1019.

5 V. Balzani and F. Scandola, *Supramolecular Photochemistry*, **1991**, Ellis Horwood: Chichester, UK.

6 F.H. Burstall, *J. Chem. Soc.*, **1936**, 173.

7 J.P. Paris, W.W. Brandt, *J. Am. Chem. Soc.*, **1959**, *81*, 5001-5002.

8 F.E. Lytle, D.M. Hercules, *J. Am. Chem. Soc.*, **1969**, *91*, 253-257.

9 P.S. Braterman, A. Harriman, G.A. Heath, L.J. Yellowlees, *J. Chem. Soc. Dalton Trans.*, **1983**, 1801-1803.

10 F. Felix. J. Ferguson, H.U. Güdel, A. Ludi, *J. Am. Chem. Soc.*, **1980**, *102*, 4096-4106.

11 J.V. Casper, T.J. Meyer, *J. Am. Chem. Soc.*, **1983**, *105*, 5583-5590.

12 K. Kalyanasundaram, *Coord. Chem. Rev.*, **1982**, *46*, 159-244.

13 K. Kalyanasundaram, *Photochemistry of Polypyridine and Porphyrin Complexes*, **1992**, Academic Press, London.

14 R.J. Watts, *J. Chem. Ed.*, **1983**, *60*, 864-842.

15 R. Hage, *Ph.D. Thesis*, Leiden University, The Netherlands, **1991**.

16 T.J. Meyer, *Acc. Chem. Res.*, **1989**, *22*, 163-170.

17 K. Maruszewski, P.D. Strommem, J.R. Kincaid, *J. Am. Chem. Soc.*, **1993**, *115*, 8345-8350.

18 F. Bargelletti, L.De Cola, V. Balzani, A. Von Zelewsky, F. Vogtle, F. Ebmeyer, S.Geammenudi, *J. Am. Chem. Soc.*, **1989**, *111*, 4662-4668.

19 L.Flamigni, F. Barigelletti, N. Armaroli, J.P. Collin, I.M. Dixon, J.P. Sauvage, J.A.G. Williams, Coord. Chem. Rev., 1999, 190-192, 671-682.

20 M.T. Indelli, C.A. Bignozzi, A. Harriman, J.R. Schoonover, F. Scandola, *J. Am. Chem. Soc.*, **1994**, *116*, 3768-3779.

21 M.T. Indelli, F. Scandola, L. Flamigni, J.P. Collin, J.P. Sauvage, A. Sour, *Inorg. Chem.*, **1996**, *35*, 303-312.

22 K. Nozaki, T. Ohno, M. Haga, *J. Phys. Chem.*, **1992**, *96*, 10880-10888.

23 M. Haga, T. Ano, T. Ishizaki, K. Kano, K. Nozaki, T. Ohno, *J. Chem. Soc., Dalton Trans.*, **1994**, 263-272.

24 A. Yoshimura, K. Nozaki, T. Ohno, *Coord. Chem. Rev.*, **1997**, *159*, 375-383.

25 K. Kalyanasundaram, M. Graëtzel, M.K. Nazeeruddin, *J. Phys. Chem.*, **1992**, *96*, 5865-5872.

26 M. Furue, M. Hirata, S. Kinoshita, T. Kusida, M. Kamachi, *Chem. Soc. Jpn., Chemistry Lett.*, **1990**, 2065-2068.

27 M. Ziegler, V. Monney, H. Stoeckli-Evans, A. Von Zelewsky, I. Sasaki, G. Dupic, J.C. Daran, G.G.A. Balavoine, *J. Chem. Soc., Dalton Trans.*, **1999**, 667-675.

28 M.Y. Kim, W.K. Seok, Y. Dong, H. Yun, *Inorg. Chim. Acta*, **2001**, *319*, 194-198.

29 S. Serroni, A. Juris, S. Campagna, M. Venturi, G. Denti, V. Balzani, *J. Am. Chem. Soc.*, **1994**, *116*, 9086-9091.

30 S.M. Molnar, G.E. Jensen, L.M. Vogler, S.W. Jones, L. Laverman, J.S. Bridgewater, M.R. Richter, K.J. Brewer, *J. Photochem. Photobiol. A: Chem.*, **1994**, *80*, 315-322.

31 G.N.A. Nallas, S.W. Jones, K.J. Brewer, *Inorg. Chem.*, **1996**, *35*, 6974-6980.

32 V. Grass, D. Lexa, M. Momenteau, J.M. Savéant, *J. Am. Chem. Soc.*, **1997**, *119*, 3536-3542.

33 W. Leung, W. Lai, I.D. Williams, *J. Organomet. Chem.*, **2000**, *604*, 197-201.

34 F. Odobel, J.P. Sauvage, A. Harriamn, *Tetrahedron Lett.*, **1993**, *34*, 8113-8116.

35 J. Yang, R. Breslow, *Tetrahedron Letts.*, **2000**, *41*, 8063-8067.

36 J.E. Redman, N. Feeder, S.J. Teat, J.K.M. Sanders, *Inorg. Chem.*, **2001**, *40*, 2486-2499.

37 J.H. Van Diemen, R. Hage, J.G. Haasnoot, H.E.B. Lempers, J. Reedijk, J.G. Vos, L.De Cola, F. Barigelletti, V. Balzani, *Inorg. Chem.*, **1992**, *31*, 3518-3522.

38 P.M. Gidney, R.D. Gillard, B.T. Heaton, *J. Chem. Soc., Dalton Trans.*, **1972**, 2621-2628.

39 R. Hage, J.G. Haasnoot, J. Reedijk, R. Wang, J.G. Vos, *Inorg. Chem.*, **1991**, *30*, 3263-3269.

40 H.P. Hughes, *Ph.D. Thesis*, Dublin City University, **1993**.

41 G. Calogero, G. Giuffrida, S. Serroni, V. Ricevuot, S. Campagna, *Inorg. Chem.*, **1995**, *34*, 541-545.

42 R.D. Gillard, J.A. Osborn, G. Wilkinson, *J. Chem. Soc.*, **1965**, 1951-1965.

43 A.M. Pyle, M.Y. Chiang, J.K. Barton, *Inorg. Chem.*, **1990**, *29*, 4487-4495.

44 F. Weldon, *Ph.D. Thesis*, Dublin City University, **1998**.

Chapter 8 – Final Remarks and Future Work.

Abstract: Having detailed the results of the synthesis and characterisation of a series of novel Rh(III) mononuclear complexes and the synthesis of novel Ru(II)/Rh(III) dinuclear complexes in previous chapters it is the aim of the following chapter to take all of the results obtained into consideration and to relate the behaviour exhibited by these complexes to the σ-donor / π-acceptor properties of the incorporated ligands.

8.1 Final Remarks

8.1.1 Synthetic Aspects

The synthesis and characterisation of a series of novel heterotrischelated Rh(III) complexes have been detailed in this study. The complexes studied were of the form $[Rh(L)_2(L')]^{n+}$ where L = phen / bpy and L' = a pyridine triazole / pyrazine triazole/ triazine or imidazole based ligand and n = 2/3. The most significant difference between these L' ligands is their varying σ-donating / π-accepting abilities and it is of interest to determine if this variation is reflected in the behaviour of complexes into which these ligands are incorporated. Differences between the complexes first became apparent in their preparation, with significant variations in reaction times and yields being observed. Table 8.1 allows for the immediate comparison of the synthetic behaviour of the complexes detailed in Chapter 3 and 5.

Table 8.1 ***Reaction times and yields for all novel Rh(III) complexes discussed in this thesis.***

Complex	Rxn. Time EtOH:H_2O	Rxn. Time H_2O pH 9	% Yield	Complex	Rxn. Time EtOH:H_2O	% Yield
$[Rh(phen)_2(pytr)]^{2+}$	24	-	61	$[Rh(phen)_2(pztr)]^{2+}$	72	a
$[Rh(bpy)_2(pytr)]^{2+}$	24	-	59	$[Rh(bpy)_2(pztr)]^{2+}$	24	67
$[Rh(phen)_2(4Mpytr)]^{2+}$	12	-	50	$[Rh(phen)_2(Phpztr)]^{2+}$	17	61
$[Rh(bpy)_2(4Mpytr)]^{2+}$	12	-	80	$[Rh(bpy)_2(Phpztr)]^{2+}$	17	68
$[Rh(phen)_2(1M3pytr)]^{2+}$	12	-	26	$[Rh(phen)_2(bpzt)]^{2+}$	48	37
$[Rh(bpy)_2(1M3pytr)]^{2+}$	12	-	16	$[Rh(bpy)_2(bpzt)]^{2+}$	48	a
$[Rh(phen)_2(bpt)]^{2+}$	48	-	14	$[Rh(phen)_2(ppt)]^{2+}$	24	37
$[Rh(bpy)_2(bpt)]^{2+}$	48	-	32	$[Rh(bpy)_2(ppt)]^{2+}$	24	45
$[Rh(phen)_2(NHbpt)]^{2+}$	-	4	77	$[Rh(phen)_2(dppt)]^{3+}$	17	79
$[Rh(bpy)_2(NHbpt)]^{2+}$	-	5	59	$[Rh(bpy)_2(dppt)]^{3+}$	17	90
$[Rh(phen)_2(NH_2bpt)]^{3+}$	10 days	-	a	$[Rh(phen)_2(PIP)]^{3+}$	3	76
$[Rh(bpy)_2(NH_2bpt)]^{3+}$	24	-	20	$[Rh(bpy)_2(PIP)]^{3+}$	3	89
$[Rh(phen)_2(Phpytr)]^{2+}$	12	-	83	$[Rh(phen)_2(MePIP)]^{3+}$	3	82
$[Rh(bpy)_2(Phpytr)]^{2+}$	12	-	84	$[Rh(bpy)_2(MePIP)]^{3+}$	3	95
				$[Rh(phen)_2(PTP)]^{3+}$	3	78
				$[Rh(bpy)_2(PTP)]^{3+}$	17	51

a – pure complex not isolated

It can be seen that both reaction times and yields change as the L' ligand is varied. In particular complexes incorporating the imidazole based ligands PIP and MePIP require short reaction times and give high yields. Complexes containing the fused ligand PTP also require short reaction times, however, lower yields are observed in these cases. Complexes with the triazine ligands also afford high yields but these require longer reaction times as do the pyridine and pyrazine triazole based complexes, which require relatively long reaction times in comparison to the imidazole based complexes and in most cases gave much lower yields. Thus it can be seen that, with the exception of complexes with the dppt ligand, reactions occur at faster rates with improved yields with the more strongly σ-donating ligands.

The products of the syntheses of complexes incorporating pyridine and pyrazine ligands are particularly interesting as, in each case evidence was only found for the formation of a single isomer and all complexes were obtained in their deprotonated forms. This behaviour is quite unusual as the synthesis of the analogous Ru(II) complexes gives two isomers which can be separated by column chromatography thus allowing for the identification of the mode of coordination of the metal centre in each case, i.e. whether it is N2' bound or N4' bound, via ^{1}H NMR spectroscopy.[1] However, as only a single isomer was obtained for each of the Rh(III) complexes studied and due to the fact that only two of the complexes synthesised yielded crystals suitable for analysis it is not possible to determine unambiguously the mode of coordination for all cases. The crystal structure of $[Rh(bpy)_2(Phpytr)]^{2+}$ was obtained and it was shown conclusively that the N2' isomer is formed in this instance. However, preferential formation of the N2'isomer is anticipated in this instance for steric reasons. Table 8.1 demonstrates that the σ-donating ability of the L' ligand is influential in the formation of complexes of this type thus it is important to note that Hage *et. al.* found that the N2' coordination site is a stronger σ-donor than the N4' site.[1] The synthetic behaviour of the Rh(III) complexes studied indicated a preference for strong σ-donors thus it is likely that the complexes isolated are those in which the metal centre is coordinated via the N2' site of the triazole ring.

Another interesting characteristic of both the pyridine and the pyrazine triazole complexes studied is that all of the complexes isolated were found to be in their deprotonated forms. Despite attempts, using ^{1}H NMR, UV and emission spectroscopy no evidence was found to indicate any pH dependent behaviour. This is in contrast to the behaviour of the analogous Ru(II) complexes whose UV-Vis and emission properties have been shown to be particularly sensitive to pH.[1,2] The difficulties encountered in trying to protonate these complexes may again be explained in terms of the σ-donor / π-acceptor properties of the triazole ligands as complexation of the metal centre to the triazole ligand results in an electron deficient triazole ligand. This results in the ligand becoming more acidic thus lowering the pKa of the complex i.e. the complexes are more difficult to protonate. The strong σ-donor properties of the N2' coordination site and the charge of the Rh(III) metal centre would also contribute to this effect.

As has been demonstrated throughout this thesis the nature of the L' ligand greatly influences the syntheses and behaviour exhibited by Rh(III) polypyridyl complexes. This is particularly evident from attempts to synthesise dinuclear complexes. The necessity for an electron rich environment is apparent from the numerous attempts to synthesise dinuclear complexes incorporating the ligands Hbpt, Hbpzt and NH_2bpt and due to the fact that dinuclear complexes were only obtained when ligands were used in which a large amount of electron density is available i.e. where two separate σ-donor units are available. Whilst it was not possible to characterise the dinuclear complexes isolated, these studies have allowed for the identification of the type of ligand necessary for the formation of dinuclear complexes and has paved the way for the future development of Ru(II)/Rh(III) dinuclear complexes.

8.1.2 Electronic Aspects

The absorption spectra of all of the complexes studied are comprised predominantly of bands associated with ligand based π-π^* transitions. Weak bands are also evident in the spectra of the complexes with the pyridine / pyrazine triazole and triazine ligands and these are tentatively assigned as d-d* bands but this cannot be unequivocally confirmed without further study. The technique of resonance Raman would be particularly useful for this purpose. From an emission perspective several of the complexes studied exhibit a particularly interesting dual emitting behaviour with emissions originating from both ligand based and metal based excited states being observed. It is the complexes incorporating the pyridine and the pyrazine triazole based ligands that exhibit such behaviour and it was found that this behaviour is influenced by the nature of the L' ligand. The lifetimes of these two excited states are well differentiated thus making it possible to isolate each emission via analysis on different time scales. Whilst a quantitative comparison was not carried out trends were observed in the intensity of the MC emissions detected and again these are related to the σ-donor strengths of the incorporated L' ligand. Of the pyridine triazole complexes studied only the complexes with the NH_2bpt ligand coordinated via the amine moiety do not exhibit this dual emitting behaviour. For all of the pyridine triazole complexes studied the ligand based emission is localised on the L ligand, where L = phen / bpy. In contrast to this the pyrazine triazole based complexes exhibit a ligand based emission which, based upon the results obtained, is based on an excited state localised upon the pyrazine triazole ligand. This observation implies that the LUMO of the pyrazine ligand is lower than that of the phen/bpy ligand in these complexes.

In contrast to the dual emitting behaviour demonstrated by the pyridine and pyrazine triazole based complexes those incorporating the dppt, PIP, MePIP and PTP ligands only exhibit a ligand based emission. Complexes with the dppt ligand exhibit a ligand based emission which is observable at a lower energy than emission associated with the phen, bpy, pyridine triazole and pyrazine triazole ligands and is attributable to a π–π^* emission associated with the triazine ligand. PIP, MePIP and

PTP based complexes also exhibit a ligand based emission and in the case of the imidazole based complexes it was found, based on the results obtained, that the excited state is localised on the PIP and MePIP ligands whereas for complexes with the PTP ligand emission is based on the L ligand, where L = phen/bpy.

The photophysical behaviour demonstrated by the complexes detailed in this thesis is related to the σ-donor / π acceptor capabilities of the L' ligand. The pyridine triazole ligands are known to be stronger σ-donors than bpy and as a result donate more electron density into the d orbitals than the bpy ligands do. As a result of this the energy of the excited MC state is raised which in turn results in a situation whereby the rates of conversion between the LC and the MC excited states are slower than the independent deactivation processes to the ground state as evidenced by the observation of two independent emission processes for the Rh(III) complexes incorporating these ligands and, as detailed in Chapters 4 and 6, both the emission energies and intensities of these metal based emissions vary with the σ-donor strength of the L' ligand. It is also interesting to note that the d-d* emissions of complexes having a negative charge on the triazole ring are found at lower energies than those which incorporate a neutral triazole ring i.e. complexes with the ligands 4Mpytr, 1M3pytr and NH_2bpt (Table 4.2). This is due to the fact that the negatively charged triazole moiety is a stronger σ donor than the neutral triazole moiety, donating more electron density into the d orbitals thus causing a shift of the emission spectra to lower energies.

The complexes which do not exhibit a metal based emission are those incorporating the dppt, PIP, MePIP, PTP ligands and $[Rh(phen)_2(NHbpt)]^{2+}$ and $[Rh(bpy)_2(NHbpt)]^{2+}$. The absence of a metal based emission for the triazine based complexes can easily be explained by taking the σ-donor / π acceptor properties of the dppt ligand into consideration. The dppt ligand is known to be a weaker σ-donor and a stronger π–acceptor than bpy and as a result of this both the $^3\pi$-π^* state and the ^{3}d-d* excited state of dppt are lower than $^3\pi$-π^* and the ^{3}d-d* states of bpy. It should be noted that the $^3\pi$-π^* states of dppt and bpy would differ to a greater degree than their ^{3}d-d* excited states. As a result of this the ligand field splitting is expected to

be smaller and it is anticipated that non-radiative deactivation from the MC state would become more efficient. The ligands PIP, MePIP and PTP are all expected to be stronger σ-donors than bpy and from an electrochemical viewpoint their first reduction waves were found to be comparable to those of the pyrazine triazole complexes indicating similar σ-donating abilities. These complexes do not however exhibit any evidence for a d-d* based emission implying that, as was observed for $[Rh(phen)_3]^{3+}$ and $[Rh(bpy)_3]^{3+}$, radiationless deactivation from the excited MC state occurs.

8.1.3 Electrochemical Aspects

The results of the electrochemical studies indicate that it is the first reduction wave which is affected by the nature of the L' ligand incorporated. The complexes incorporating a deprotonated pyridine triazole ligands exhibit the most negative reduction potentials as is expected as these are strongly σ-donating. It is particularly interesting to note that the first reduction potentials of complexes with the 4Mpytr and 1M3pytr ligands are more positive than for those where a negative charge is present on the triazole ring. This indicates that the 4Mpytr and 1M3pytr ligands are weaker σ-donors and is in agreement with the photophysical behaviour exhibited by these complexes. As already detailed the dppt ligand is a weaker σ-donor than bpy and as expected this is reflected in the reduction waves observed as complexes with the dppt based complexes exhibiting first reduction waves at more positive potentials than all of the other complexes studied. By comparison with studies detailed by Kew *et. al.* the first reductions waves observed are attributed to metal based processes.[3,4] Subsequent reduction processes are not as readily identifiable as further metal-based reductions and ligand-based reductions are expected to occur.

8.2 Future Work

The novel Rh(III) heteroleptic complexes detailed in this thesis have demonstrated very interesting properties which merit further investigation as a number issues require further consideration and study. For instance it would be of advantageous to attempt isolate crystals suitable for analysis of the pyridine and pyrazine triazole based complexes thus allowing for the unambiguous identification of the mode of coordination of metal centres. The pyridine and pyrazine complexes isolated were all found to be in their deprotonated forms and, whilst preliminary ^{1}H NMR and UV-VIS and emission experiments showed no evidence for protonation of the triazole ring, further investigation of this behaviour is warranted. It would also be of interest to determine the exact nature of the weak absorption bands in the absorption spectra of the pyridine/pyrazine and triazine based complexes. This could be achieved by determining if these complexes exhibit solvatochromism or via resonance Raman studies.

From the perspective of the emission of these complexes, and particularly for those that are dual emitting, further detailed studies are required to determine the exact origins of the luminescence observed. Studies using resonance Raman, selective ligand deuteration and possibly ODMR would be particularly useful in determining these factors. It would also be of interest to carry out a detailed analysis of the emissive behaviour of these novel Rh(III) complexes over a wide temperature range as some Rh(III) polypyridyl complexes have previously exhibited a temperature dependent behaviour.[5]

Additional studies of the excited state lifetimes could also be carried out. In particular it would be of interest to carry out further deuteration studies, which would aid in the determination of the nature of the excited state. It is also important to study the behaviour of the complexes $[Rh(phen)_2(pytr)]^{2+}$ and $[Rh(phen)_2(d_4\text{-pytr})]^{2+}$ and $[Rh(bpy)_2(pytr)]^{2+}$ and $[Rh(bpy)_2(d_4\text{-pytr})]^{2+}$ further. Variation of the d-d* based excited state lifetimes of $[Rh(phen)_2(pytr)]^{2+}$ and $[Rh(bpy)_2(pytr)]^{2+}$ upon deuteration of the triazole ligands was observed and this unexpected behaviour requires detailed

investigation. Attempts should also be made to obtain the low temperature excited state lifetimes associated with the π-π^* excited states of the pyridine and pyrazine triazole based complexes.

The electrochemical properties of these complexes also need to be investigated in more detail and it would be prudent to study each reduction process individually to determine definitively the nature of the reduction / oxidation waves observed. Studies could also be carried out at higher scan rates, which might allow for improved reversibility of the reduction processes whereas solvent variation might improve complex stability.

The development of Rh(III) homo and hetero-dinuclear complexes should now be relatively straight forward as the behaviour of the mononuclear complexes and dinuclear complexes detailed in this thesis has led to a better understanding of the requirements for formation of dinuclear complexes.

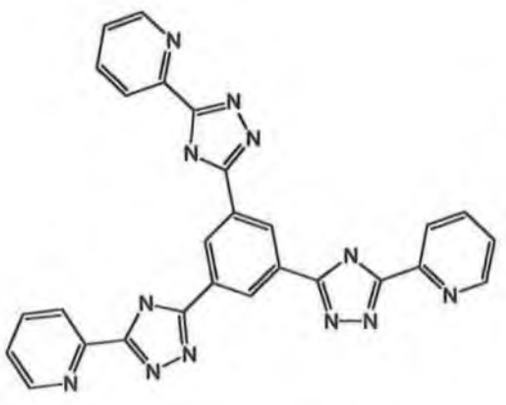

1,3,5-tris(5-(pyrazin-2-yl-1,2,4-triazole)benzene

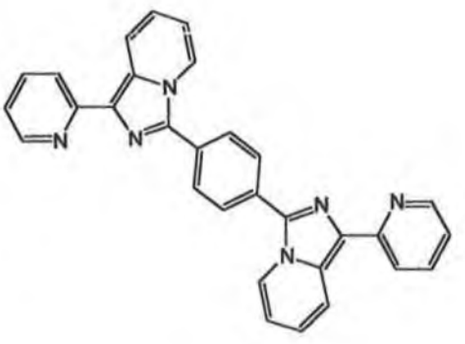

1,4-phenylene-bis(pyridin-2-yl-imidazo[1,5-a]pyridine)

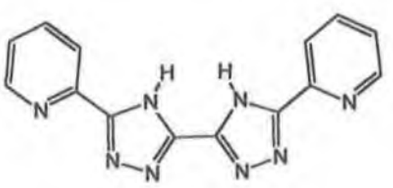

H_2BPBT - 5,5'-bis(pyridin-2-yl)-3,3'-bis(1,2,4-triazole)

Figure 8.1 Structures of ligands that could potentially be used in the development of dinuclear and trinuclear complexes.

The behaviour exhibited by the mononuclear complexes detailed in chapters 3 to 6 will also help in developing systems which will have the desired electrochemical and photophysical properties. It can be seen from the work detailed in Chapter 7 that ligands with more than one sigma donor group are preferable and it was found that synthesis of mononuclear complexes with the ligands imidazole fused ligands were particularly successful thus it would be prudent to progress in this direction. The ligands shown in Figure 8.1 are ligands that could potentially be used in the future development of homo- and hetero-dinuclear and trinuclear complexes.

References:

1 R. Hage, *Ph.D. Thesis*, Leiden University, The Netherlands, **1991**.

2 B.E. Buchanan, J.G. Vos, M. Kaneko, W.J.M. van der Putten, J.M. Kelly, R. Hage, R.A.G de Graaff, R. Prins, J.G. Haasnoot, J. Reedijk, *J. Chem. Soc. Dalton Trans.*, **1990**, 2425-2431.

3 G. Kew, K. Hanck, K. DeArmond, *J. Phys. Chem.*, **1975**, *79*, 1828-1835.

4 G. Kew, K. DeArmond, K. Hanck, *J. Phys. Chem.*, **1974**, *78*, 727-734.

5 A. Islam, N. Ikeda, K. Nozaki, T. Ohno, *J. Photochem Photobiol A: Chem.*, **1997**, *106*, 61-66.

Appendix I

Rhodium Mediated N–O Bond Formation

Helen M. Burke,[a] John F. Gallagher,[b] Maria T. Indelli,[c] Franco Scandola,[c] and Johannes G. Vos*[a]

Keywords: Rhodium / N ligands / Oxygen / Insertion / Crystal structure

Reaction of $[Rh(phen)_2Cl_2]Cl$ (phen = 1,10-phenanthroline) with the ligand 3,5-bis(pyridin-2-yl)-1,2,4-triazole (Hbpt) in H_2O at pH 9 gives rise to the formation of a single stable compound. Single-crystal X-ray analysis of this material reveals that in the product obtained an oxygen atom has been inserted between the $Rh(phen)_2$ moiety and the triazole ring of the bpt ligand yielding a compound of the type $[Rh(phen)_2(Obpt)](PF_6)_2 \cdot 0.767CH_3CN \cdot 0.28H_2O$. Insertion of oxygen in this manner has not been reported previously.

Introduction

A considerable amount of research has been dedicated to the study of ligand-bridged polynuclear transition metal complexes.[1] This particular class of complexes has been used as a basis for studying electron transfer processes with the aim of creating multicomponent systems (supramolecular systems) capable of effecting useful light- and/or redox-induced functions. Most of the initial systems developed incorporated ruthenium(II) polypyridine compounds, although systems incorporating other transition metals such as rhodium(III), osmium(II) and iridium(III) have also been investigated.[2–5]

We have recently started a systematic investigation into the photophysical properties of mixed ligand rhodium(III) complexes. These studies are aimed at achieving a better understanding of the way in which the excited states of rhodium(III) complexes are affected by the introduction of ligands other than polypyridyl ligands. In these studies the ligands investigated are based on substituted 1,2,4-triazole moieties. Through well-established synthetic routes both π accepting and σ donating groupings can be introduced and these triazole based ligands have been shown to promote interactions between metal centres in dinuclear structures via deprotonation of the triazole ring. As a result a wide range of both mononuclear and dinuclear complexes of ruthenium(II) and osmium(II) incorporating these ligands has been reported.[6] An additional interest in these ligands is due to their asymmetry, which allows for different coordination modes. Of particular interest are ligands such as 3,5-bis(pyridin-2-yl)-1,2,4-triazole (Hbpt) (for structure see Figure 1) for which mononuclear and dinuclear Ru^{II} and Os^{II} complexes have been reported.[5] Orthometallated Rh^{III} complexes with Hbpt and the related ligand 4-amino-3,5-bis(2-pyridyl)-4*H*-1,2,4-triazole ($bptNH_2$) have also been reported,[7–9] as have Rh^{I} complexes with the ligands Hbpt and $bptNH_2$.[10–11] In this paper we wish to report on a very unusual reaction product obtained when a rhodium(III) precursor is reacted with Hbpt. In the compound obtained an oxygen atom has inserted into the Rh^{III}-nitrogen bond. To the best of our knowledge this is the first time that such an insertion reaction has been observed.

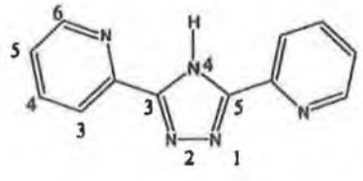

Figure 1. 3,5-bis(pyridin-2-yl)-1,2,4-triazole (Hbpt)

Results and Discussion

$[Rh^{III}$ bis(1,10-phenanthroline)$Cl_2]Cl$ was reacted with Hbpt in aqueous solution at pH 9. The product obtained was purified by column chromatography and precipitated

[a] National Centre for Sensor Research, School of Chemical Sciences, Dublin City University, Dublin 9, Ireland
Fax: (internat.) + 353-1/700-5503
E-mail: johannes.vos@dcu.ie
[b] School of Chemical Sciences, Dublin City University, Dublin 9, Ireland
Fax: (internat.) + 353-1/700-5503
E-mail: john.gallagher@dcu.ie
[c] Dipartimento di Chimica dell'Universita, Universita di Ferrara, 44100 Ferrara, Italy
Fax: (internat.) + 39-0532/240-709
E-mail: snf@unife.it

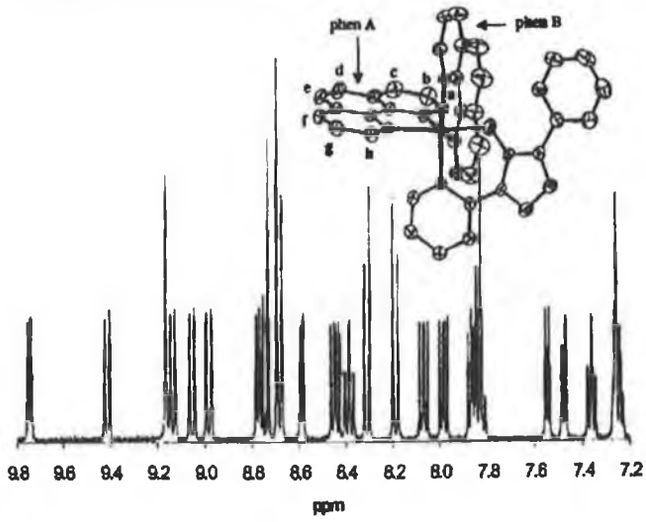

Figure 2. ^1H NMR spectrum $[Rh(phen)_2(Obpt)](PF_6)_2$ in $[D_6]DMSO$

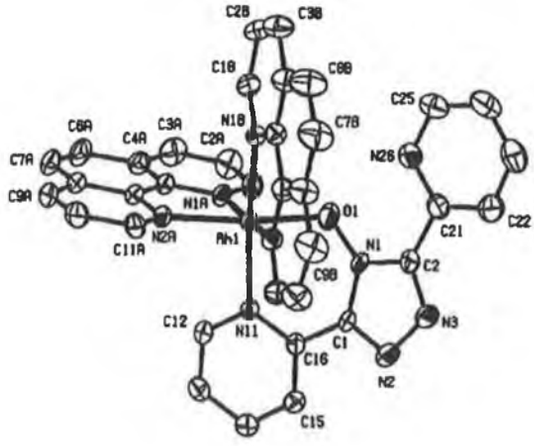

Figure 3. Molecular structure of the cation in $[Rh(phen)_2(Obpt)](PF_6)_2$; hydrogen atoms, counterions and the solvent molecules have been omitted for clarity

as a PF_6^- salt. NMR spectroscopy shows the presence of a single product (see Figure 2). Upon further recrystallisation of the product from acetonitrile/toluene (7:3) yellow needles were obtained. A single crystal X-ray investigation yielded the molecular structure, the cation of which is depicted in Figure 3. X-ray collection parameters are listed in Table 1 and selected bond lengths and angles are given in Table 2 and Table 3, respectively.

The most striking feature of the molecular structure is the presence of an oxygen atom between the metal centre and the triazole nitrogen atom. The rhodium centre is further surrounded by the two 1,10-phenanthroline ligands and the sixth coordination site is taken up by a pyridine ring of the bpt ligand. Two disordered PF_6^- counterions

Table 1. Crystallographic data for $[Rh(phen)_2(Obpt)](PF_6)_2 \cdot 0.767CH_3CN \cdot 0.28H_2O$

Chem formula	$C_{36}H_{26}F_{12}N_9OP_2Rh \cdot 0.767CH_3CN \cdot 0.28H_2O$
Mol. wt.	1029.05
a (Å)	13.2334(12)
b (Å)	20.507(3)
c (Å)	16.0732(15)
β (°)	103.620(6)
Z	4
Volume (Å^3)	4239.3(8)
System, space group	monoclinic, $P2_1/m$
Crystal size	0.43 × 0.10 × 0.08
Temperature	297(2) K
$F(000)$	2059
Radiation, λ (Å)	Mo-K_α, 0.71073
D_{calc}, g·cm^{-3}	1.612
Abs coeff, μ (mm^{-1})	0.577
Abs corr T (min, max)	0.791, 0.958
θ range for data collection	2 to 26°
Reflections collected	8528
Unique, $>2\sigma(I)$	8164, 5460
Parameters	709
Restraints	288
R (F_o)	0.062
R_w (F_o)	0.149
Residual electron density	+0.76, −0.68

Table 2. Selected bond lengths (Å) for $[Rh(phen)_2(Obpt)](PF_6)_2 \cdot 0.767CH_3CN \cdot 0.28H_2O$

Rh1–O1	2.016(4)	Rh1–N11	2.086(5)
Rh1–N1A	2.034(4)	Rh1–N2A	2.105(4)
Rh1–N2B	2.035(5)	N1–O1	1.406(6)
Rh1–N1B	2.039(5)	N1–C1	1.342(7)
		N1–C2	1.372(7)

Table 3. Selected bond angles (°) for $[Rh(phen)_2(Obpt)](PF_6)_2 \cdot 0.767CH_3CN \cdot 0.28H_2O$

O1–Rh1–N1A	91.5(2)	N1A–Rh1–N2B	174.2(2)
O1–Rh1–N2A	171.4(2)	N1A–Rh1–N1B	93.6(2)
O1–Rh1–N1B	88.2(2)	N1B–Rh1–N2B	81.4(2)
O1–Rh1–N2B	91.4(2)	N1B–Rh1–N11	174.8(2)
O1–Rh1–N11	87.2(2)	N1–O1–Rh1	110.1(3)
Rh1–O1–N1–C1	56.3(6)		

and partial site occupancy acetonitrile (0.767) and water solvent molecules (0.28) complete the crystal structure (not depicted). The Rh–O bond length is 2.016(4) Å, in the range expected for Rh–O bond lengths. For example, in the diacetyl monooxime Rh^{III} complex reported by Moszner et. al., typical Rh–O bond lengths are 2.028Å and 2.023Å.[12] The N–O bond length is 1.406(6) Å and typical of an N–O single bond. The presence of the oxygen atom causes a substantial *trans* effect. The Rh–N distance *trans* to the oxygen atom is 2.105(4) Å, which is about 0.07 Å longer than the other three rhodium-nitrogen distances. A number of other rhodium polypyridyl crystal structures have been reported. Paul et al. have reported Rh–N bond lengths of 1.990(5), 2.059(5) and 2.036(5) Å in a rhodium(II) complex with the ligand 2,4,6-tris(2-pyridyl)-1,3,5-triazine and bond lengths of 2.027(10), 2.031(10), 2.083(9) and 2.071(9) Å were found by Brewer et al. in the case of the rhodium(III) complex with the ligand 2,3-bis(2-pyridyl)quinoxaline.[13,14] The X-ray structure of a ruthenium(II) complex with the ligand Hbpt has also been reported.[15]

The NMR spectrum shown in Figure 2 clearly indicates the presence of only one species, indicative of the absence of linkage isomers. This is in contrast with the behaviour of most common triazole complexes.[16,17] 2-D COSY spectroscopic techniques were used to assign the ^1H resonances where possible. The doublets observed at $\delta = 9.75$ and 9.42 can be attributed to the protons at positions a and e of the phenanthroline ring A respectively. These resonances are downfield with respect to the resonances observed for the equivalent protons in the $[Rh(phen)_3]^{3+}$ complex and this can be attributed to the influence of the oxygen in the rhodium complex.[18] The source of the singlet at $\delta = 9.17$ has yet to be determined. Deuteration of the $[Rh(phen)_2(Obpt)](PF_6)_2$ is currently being undertaken in order to unambiguously assign all of the resonances.

The emission spectrum obtained at 77 K in a 4:1 ethanol/methanol glass for $[Rh(phen)_2(Obpt)](PF_6)_2$ can be seen in Figure 4. This structured emission, with maxima at 453 nm, 482 nm and 513 nm, is typical of ligand-centred (LC) phosphorescence of rhodium(III) phenanthroline complexes.[19] This indicates that the lowest LC excited state in this heteroleptic complex lies on the phen ligands.

An insertion of oxygen, as observed in this case, has not been reported previously. The only slightly related compound reported in the literature is a Rh^I complex with the ligand $bptNH_2$.[11] In the complex $[Rh(NHbpt)(diolefin)]$, where the diolefin is for example 2,2,2-octatriene, NMR spectroscopy and elemental analysis suggest that an isoelectronic Rh–NH–N-triazole bond is formed. The mechanism responsible for the formation of $[Rh(phen)_2(Obpt)](PF_6)_2$ can at present only be tentatively formulated. The fact that the reaction described here is carried out in basic solution may indicate that a rhodium hydroxy intermediate is formed by replacement of the chloride atom by water and subsequent deprotonation [Equation (1)]. Interaction between the OH group and the triazole ring may then result in the formation of the N–O bond. In order to account for the oxidative nature of this step, a likely mechanism is the formation of an intermediate Rh^I complex [Equation (2)] which is subsequently reoxidised by oxygen [Equation (3)]. The overall reaction would then amount to a rhodium-mediated oxidation of the ligand by molecular oxygen [Equation (4)].

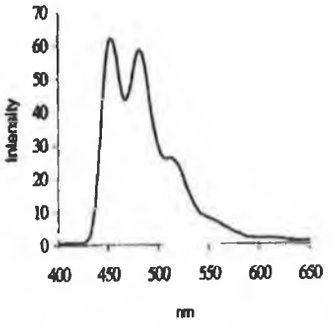

Figure 4. Emission spectra of $[Rh(phen)_2(Obpt)](PF_6)_2$ obtained in an ethanol/methanol 4:1 glass at 77 K

$$[Rh^{III}(phen)_2Cl_2]^+ + Hbpt + H_2O \rightarrow [Rh^{III}(phen)_2(OH)bpt]^+ + 2H^+ + 2Cl^- \quad (1)$$

$$[Rh^{III}(phen)_2(OH)bpt]^+ \rightarrow [Rh^{I}(phen)_2(Obpt)] + H^+ \quad (2)$$

$$[Rh^{I}(phen)_2(Obpt)] + 2H^+ + 1/2O_2 \rightarrow [Rh^{III}(phen)_2(Obpt)]^{2+} + H_2O \quad (3)$$

$$[Rh^{III}(phen)_2Cl_2]^+ + Hbpt + 1/2O_2 \rightarrow [Rh^{III}(phen)_2(Obpt)]^{2+} + 2Cl^- + H^+ \quad (4)$$

Interestingly no *N*-hydroxytriazoles have been reported in the literature. The formation of this N–O bond is therefore clearly dependent on the presence of the rhodium centre. Recently the formation of Rh^I–O–C bond via a Rh-hydroxy intermediate has been reported for the compound $[C_5(CH_3)_5]RhO(C_6F_4)CF_2$.[20]

Conclusion

The reaction product reported upon reaction of $[Rh(phen)_2Cl_2]Cl$ and Hbpt is a very unusual one. In the complex obtained an oxygen atom has been inserted between the rhodium centre and the triazole ring. We are at present engaged in a systematic study of the interaction be-

tween rhodium polypyridyl centres and triazole type ligands. In this investigation we aim to further develop this chemistry and to determine the factors that control this unusual behaviour.

Experimental Section

Materials: Rhodium(III) chloride hydrate and 1,10-phenanthroline were purchased from Aldrich. $[Rh(1,10\text{-phenthroline})_2Cl_2]Cl$ and 3,5-bis(pyridin-2-yl)-1,2,4-triazole (Figure1) were prepared by previously reported procedures.[21,22]

Instrumentation: NMR spectra were obtained on a Bruker AC 400 MHz spectrometer. The peak positions are relative to TMS and the spectra were converted from their FID profiles using a Bruker WINNMR software package. Low temperature emission spectra were obtained at 77 K in a 4:1 ethanol/methanol glass using a Perkin–Elmer LS50B instrument. Elemental analysis on C, H and N was carried out at the Microanalytical Laboratory at University College Dublin (UCD) using an Exador analytical CE440.

Preparation of the Complex: Hbpt (0.3 mmol) was dissolved in H_2O at pH 9. $[Rh(phen)_2Cl_2]Cl$ (0.1 mmol) was then added and the reaction mixture was refluxed for 8 hours. Purification was carried out using a Sephadex C-25 column. Unreacted ligand was removed with distilled water and the product was eluted using 0.1 M NaCl. The complex was precipitated by the addition of a saturated aqueous solution of NH_4PF_6 to the required fraction. Yield: 0.033 g, 32%. Crystals were obtained by recrystallisation from a minimum amount of acetonitrile/toluene (7:3). ^1H NMR spectroscopy was carried in $[(CD_3)_2SO]$ and the resonances observed have been tentatively assigned as follows: **phenanthroline A:** δ = 9.75 (d, 1Ha), 8.45 (dd, 1Hb), 9.41 (d, 1Hc), 8.74 (d, 1Hd), 8.68 (d, 1He), 9.13 (d, 1Hf), 7.98 (dd, 1Hg), 8.59 (d, 1Hh); **phenanthroline B:** δ = 8.98 (d, 1Ha), 8.07 (dd, 1Hb), 8.78 (d, 1Hc), 8.31 (d, 1Hd), 8.19 (d, 1He); bpt: δ = 8.68 (d, 1H6), 8.39 (dd, 1H5), 7.36 (dd, 1H4), 7.48 (d, 1H3). It was not possible to assign the resonances at δ = 9.17 (s, 1 H), 9.05 (d, 1 H), 7.9–7.8 (m, 3 H), 7.55 (d, 1 H), 7.26 (m, 2 H) unambiguously. $[Rh(phen)_2(Obpt)](PF_6)_2 \cdot H_2O$: calcd. C 42.83, H 2.60, N 12.49; found C 42.24, H 2.63, N 12.97. It should be noted that the sample for elemental analysis was recrystallised from ethanol/water.

CCDC-168699 contains the supplementary crystallographic data for this paper. These data can be obtained free of charge at www.ccdc.cam.ac.uk/conts/retrieving.html [or from the Cambridge Crystallographic Data Centre, 12, Union Road, Cambridge CB2 1EZ, UK; fax: (internat.) +44-1223/336-033; E-mail: deposit@ccdc.cam.ac.uk].

Acknowledgments

The authors thank the EU under the TMR programme for financial assistance under contract CT96-0076.

[1] V. Balzani, A. Juris, M. Venturi, S. Campagna, S. Serroni, *Chem. Rev.* **1996**, *96*, 759–833.
[2] J.-P. Sauvage, J.-P. Collin, J.-C. Chambron, S. Guillerez, C. Coudret, V. Balzani, F. Barigelletti, L. De Cola, L. Flamigni, *Chem. Rev.* **1994**, *94*, 993–1019.
[3] M. T. Indelli, C. A. Bignozzi, A. Harriman, J. R. Schnoonover, F. Scandola, *J. Am. Chem. Soc.* **1994**, *116*, 3768–3779.
[4] L. Flamigni, F. Barigelletti, N. Armaroli, J-P. Collin, I. M. Dixon, J.-P. Sauvage, J. A. G. Williams, *Coord. Chem. Rev.* **1999**, *190–192*, 671–682.
[5] R. Hage, J. G. Haasnoot, H. A Nieuwenhuis, J. Reedijk, D. J. A. De Ridder, J. G. Vos, *J. Am. Chem. Soc.* **1990**, *112*, 9245–9251.
[6] J. G. Haasnoot, *Coord. Chem. Rev.* **2000**, *200–202*, 131–185.
[7] J. H. van Diemen, R. Hage, J. G. Haasnoot, H. E. B. Lempers, J. Reedijk, J. G. Vos, L. De Cola, F. Barigelletti, V. Balzani, *Inorg. Chem.* **1992**, *31*, 3518–3522.
[8] J. H. van Diemen, J. G. Haasnoot, R. Hage, J. Reedijk, J. G. Vos, R. J. Wang, *Inorg. Chem.* **1991**, *30*, 4038–4043.
[9] G. Calogero, G. Giuffrida, S. Serroni, V. Ricevuto, S. Campagna, *Inorg. Chem.* **1995**, *34*, 541–545.
[10] M. P. Garcia, M. Martin, L. A. Oro, *Inorg. Chim. Acta* **1992**, *191*, 221–225.
[11] M. P. Garcia, J. A. Manero, L. A. Oro, M. C. Apreda, F. H. Cano, C. Foces-Foces, J. G. Haasnoot, R. Prins, J. Reedijk, *Inorg. Chim. Acta* **1986**, *122*, 235–241.
[12] M. Moszner, T. Glowiak, M. Kubiak, J. J. Ziolkowski, G. Costa, C. Tavagnacco, *Polyhedron* **1997**, *16*, 307–313.
[13] P. Paul, B. Tyagi, A. K. Bilakhiya, M. M. Bhadbhade, E. Suresh, *J. Chem. Soc., Dalton Trans.* **1999**, 2009–2014.
[14] S. C. Rasmussen, M. M. Richter, E. Yi, H. Place, K. Brewer, *Inorg. Chem.* **1990**, *29*, 3926–3932.
[15] R. Hage, R. A. G. de Graaff, J. G. Haasnoot, J. P. Turkenburg, J. Reedijk, J. G. Vos, *Acta Crystallogr., Sect. C* **1989**, *45*, 381–383.
[16] B. E. Buchanan, R. Wang, J. G. Vos, R. Hage, J. G. Haasnoot, J. Reedijk, *Inorg. Chem.* **1990**, *29*, 3263–3265.
[17] B. E. Buchanan, E. McGovern, P. Harkin, J. G. Vos, *Inorg. Chim. Acta* **1988**, *154*, 1–4.
[18] H. M. Burke, J. G. Vos, to be published.
[19] M. T. Indelli, F. Scandola, *Inorg. Chem.* **1990**, *29*, 3056–3058.
[20] R. P. Hughes, D. C. Lindner, L. M. Liable-Sands, A. L Rheingold, *Organometallics* **2001**, *20*, 363–366.
[21] P. M. Gidney, R. D. Gillard, B. T. Heaton, *J. Chem. Soc., Dalton Trans.* **1972**, 2621–2628.
[22] J. F. Geldard, F. Lions, *J. Org. Chem.* **1965**, *30*, 318–319.

Received September 12, 2001
[I01357]

Appendix II – Supplementary X-Ray Crystallographic Data

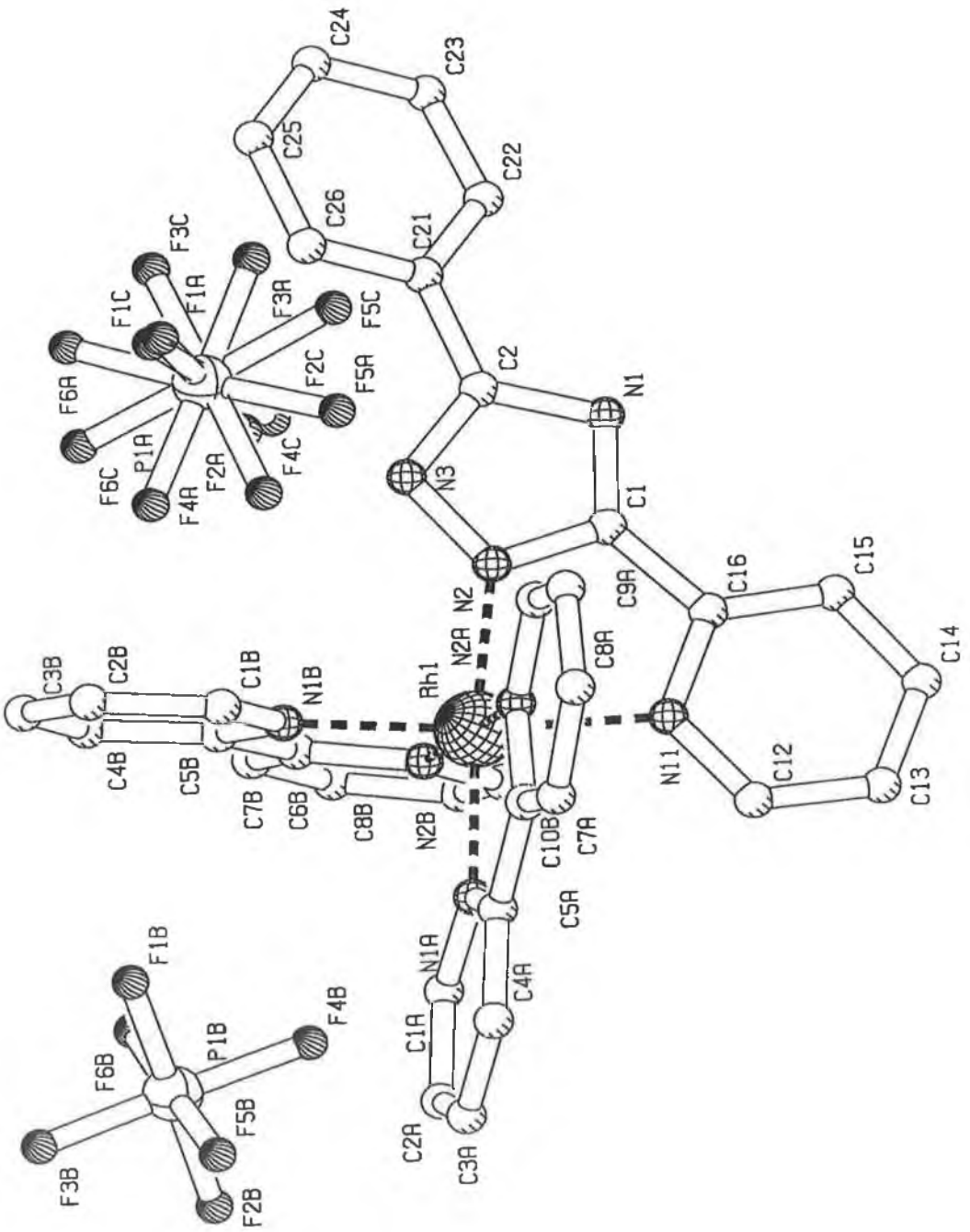

Figure AII.1 Molecular structure of $[Rh(bpy)_2(Phpytr)](PF_6)_2.0.1H_2O$.

Table AII. 1 Crystal data and structure refinement for $[Rh(bpy)_2(Phpytr)](PF_6)_2.0.1H_2O$.

Empirical formula	$C_{33}H_{25}F_{12}N_8P_2Rh$, $0.1(H_2O)$
Formula weight	928.26
Temperature	292(2) K
Wavelength	0.71073 Å
Crystal system, space group	Monocyclic, $P2_1/m$
Unit cell dimensions	a = 13.3893(13) Å
	b = 18.740(2) Å
	c = 14.2650(6) Å
Volume	3562.3(6) A^3
Z, Calculated density	4, 1.731 Mg/m^3
Absorption coefficient	0.672 mm^-1
F(000)	1852
Crystal size	0.28 x 0.17 x 0.13 mm
Theta range for data collection	1.8 to 26.0 deg.
Index ranges	-16<=h<=0, -23<=k<=0, -17<=l<=17
Reflections collected / unique	8278 / 6947 [R(int) = 0.027]
Completeness to 2theta = 25.57	96.0%
Max. and min. transmission	0.921 and 0.837
Refinement method	Full-matrix least-squares on F^2
Data / restraints / parameters	6947/231/642
Goodness-of-fit on F^2	1.01
Final R indices [I>2sigma(I)]	R1 = 0.054, wR2 = 0.083
R indices (all data)	R1 = 0.119, wR2 = 0.101
Largest diff. peak and hole	0.36 and -0.30 e.A^-3

Table AII.2 ***Atomic coordinates ($x10^4$) and equivalent isotropic displacement parameters ($A^2 \times 10^3$) for $[Rh(bpy)_2(Phpytr)](PF_6)_2.0.1H_2O$. U(eq) is defined as one third of the trace of the orthogonalized Uij tensor.***

	x	y	z	U(eq)
Rh(1)	1294(1)	2573(1)	8730(1)	37(1)
P(1)	0	496(2)	7500	34(1)
F(11)	0	-314(5)	7500	120(5)
F(14)	0	1301(5)	7500	195(10)
F(12)	460(1)	505(3)	7753(5)	60(2)
F(13)	75(2)	474(7)	6229(6)	145(5)
P(2)	1950(1)	1730(2)	3564(3)	74(1)
F(21)	1935(3)	1275(5)	4679(8)	127(3)
F(22)	2293(2)	2193(4)	4076(6)	95(2)
F(23)	1631(2)	2239(5)	4038(8)	116(3)
F(24)	1977(2)	2171(4)	2427(7)	96(2)
F(25)	2273(2)	1210(5)	3098(8)	116(3)
F(26)	1617(2)	1235(5)	3035(9)	127(3)
P(3)	2500	5000	3462(2)	36(1)
F(31)	2500	5000	4783(5)	64(2)
F(32)	2032(2)	5065(3)	3459(5)	63(2)
F(33)	2466(2)	4159(2)	3449(4)	51(1)
F(34)	2500	5000	2138(5)	57(2)
P(4)	-390(1)	3476(2)	10523(3)	81(1)
F(41)	-458(2)	3633(5)	11825(6)	104(3)
F(44)	-321(3)	3316(5)	9236(6)	125(3)
F(42)	-848(7)	3470(2)	10170(2)	137(12)
F(43)	-320(7)	4202(10)	10138(17)	90(6)
F(45)	44(6)	3315(14)	10660(16)	93(6)
F(46)	-464(8)	2600(9)	10709(15)	108(6)
F(42X)	-771(6)	3109(13)	10552(15)	85(6)
F(43X)	-625(10)	4227(11)	10370(2)	143(10)
F(45X)	23(10)	3960(2)	10696(18)	178(15)
F(46X)	-134(8)	2883(14)	10860(3)	154(12)
N(1)	1621(2)	1698(4)	9087(7)	47(2)
N(2)	1134(2)	1938(4)	7455(6)	51(2)
N(3)	1159(5)	975(8)	6446(13)	151(8)
N(4)	1681(2)	2992(4)	7621(6)	36(2)
N(5)	981(2)	3425(4)	8217(6)	41(2)
N(6)	903(2)	2197(4)	9879(5)	35(2)
N(7)	1467(2)	3133(4)	10087(6)	36(2)
C(1)	1846(3)	1619(6)	10008(10)	58(3)
C(2)	2042(3)	991(7)	10189(12)	74(3)
C(3)	2010(4)	433(8)	9476(19)	117(7)
C(4)	1779(4)	526(7)	8554(18)	115(7)
C(5)	1581(3)	1144(5)	8365(10)	60(3)
C(6)	1319(3)	1298(6)	7448(11)	69(4)
C(7)	901(4)	2018(7)	6563(8)	63(3)
C(8)	900(4)	1487(7)	5905(10)	75(4)

C(9)	734(6)	1284(12)	4992(13)	164(11)
C(10)	780(7)	646(12)	4510(2)	169(9)
C(11)	991(5)	205(10)	4911(15)	113(5)
C(12)	1229(4)	283(10)	6044(16)	153(10)
C(13)	2018(4)	2718(6)	7327(9)	80(2)
C(14)	2238(3)	2969(6)	6444(9)	62(3)
C(15)	2098(3)	3522(6)	5848(9)	67(3)
C(16)	1740(3)	3817(5)	6130(8)	55(2)
C(17)	1535(3)	3547(5)	7016(7)	45(2)
C(18)	1158(3)	3828(5)	7442(7)	44(2)
C(19)	985(4)	4458(6)	7056(10)	70(3)
C(20)	640(4)	4676(7)	7547(13)	94(4)
C(21)	461(4)	4287(6)	8334(12)	82(4)
C(22)	636(3)	3649(5)	8659(10)	58(3)
C(23)	1741(2)	3638(5)	10086(8)	44(2)
C(24)	1831(3)	4009(5)	11069(9)	56(3)
C(25)	1628(3)	3856(5)	12024(9)	52(2)
C(26)	1337(2)	3341(5)	12041(8)	47(2)
C(27)	1259(2)	3003(4)	11033(7)	36(2)
C(28)	964(2)	2430(5)	10925(7)	41(2)
C(29)	765(3)	2150(5)	11819(8)	52(2)
C(30)	490(3)	1635(6)	11618(8)	62(3)
C(31)	419(3)	1399(6)	10565(8)	59(3)
C(32)	635(3)	1694(5)	9691(7)	44(2)

TableAII.3 Bond lengths [A] and angles [deg] for [Rh(bpy)$_2$(Phpytr)](PF$_6$)$_2$.0.1H$_2$O.

Rh(1)-N(2)	2.016(8)	N(5)-C(18)	1.344(10)
Rh(1)-N(7)	2.026(7)	N(5)-C(22)	1.357(12)
Rh(1)-N(4)	2.031(6)	N(6)-C(32)	1.340(9)
Rh(1)-N(5)	2.031(7)	N(6)-C(28)	1.342(10)
Rh(1)-N(6)	2.040(6)	N(7)-C(23)	1.339(10)
Rh(1)-N(1)	2.048(8)	N(7)-C(27)	1.355(10)
P(1)-F(14)	1.528(11)	C(1)-C(2)	1.384(15)
P(1)-F(11)	1.538(9)	C(2)-C(3)	1.36(2)
P(1)-F(13)	1.539(7)	C(3)-C(4)	1.37(2)
P(1)-F(13)#1	1.539(7)	C(4)-C(5)	1.373(17)
P(1)-F(12)	1.598(5)	C(5)-C(6)	1.443(17)
P(1)-F(12)#1	1.598(5)	C(7)-C(8)	1.277(15)
P(2)-F(23)	1.562(9)	C(8)-C(9)	1.287(19)
P(2)-F(25)	1.579(8)	C(9)-C(10)	1.35(3)
P(2)-F(22)	1.584(7)	C(10)-C(11)	1.21(2)
P(2)-F(21)	1.587(9)	C(11)-C(12)	1.59(2)
P(2)-F(24)	1.598(8)	C(13)-C(14)	1.379(13)
P(2)-F(26)	1.603(8)	C(14)-C(15)	1.356(15)
P(3)-F(31)	1.577(7)	C(15)-C(16)	1.384(14)
P(3)-F(34)	1.582(7)	C(16)-C(17)	1.366(12)
P(3)-F(32)#2	1.599(5)	C(17)-C(18)	1.482(12)
P(3)-F(32)	1.599(5)	C(18)-C(19)	1.412(14)
P(3)-F(33)#2	1.601(5)	C(19)-C(20)	1.377(17)
P(3)-F(33)	1.601(5)	C(20)-C(21)	1.340(17)
P(4)-F(43)	1.472(19)	C(21)-C(22)	1.405(15)
P(4)-F(42X)	1.47(2)	C(23)-C(24)	1.403(12)
P(4)-F(46X)	1.48(2)	C(24)-C(25)	1.365(14)
P(4)-F(45)	1.52(2)	C(25)-C(26)	1.392(12)
P(4)-F(44)	1.584(8)	C(26)-C(27)	1.391(11)
P(4)-F(41)	1.600(8)	C(27)-C(28)	1.487(10)
P(4)-F(42)	1.62(3)	C(28)-C(29)	1.371(12)
P(4)-F(43X)	1.64(2)	C(29)-C(30)	1.376(12)
P(4)-F(45X)	1.69(2)	C(30)-C(31)	1.357(13)
P(4)-F(46)	1.697(16)	C(31)-C(32)	1.395(11)
F(42)-F(42X)	0.87(3)		
F(42)-F(43X)	1.64(4)		
F(43)-F(43X)	1.08(3)		
F(43)-F(45X)	1.42(4)	N(2)-Rh(1)-N(7)	174.9(3)
F(45)-F(46X)	1.05(3)	N(2)-Rh(1)-N(4)	85.2(3)
F(45)-F(45X)	1.22(3)	N(7)-Rh(1)-N(4)	97.3(3)
F(46)-F(46X)	1.26(3)	N(2)-Rh(1)-N(5)	96.2(3)
F(46)-F(42X)	1.44(3)	N(7)-Rh(1)-N(5)	88.6(3)
N(1)-C(1)	1.349(13)	N(4)-Rh(1)-N(5)	80.4(3)
N(1)-C(5)	1.367(13)	N(2)-Rh(1)-N(6)	97.0(3)
N(2)-C(7)	1.337(13)	N(7)-Rh(1)-N(6)	80.5(3)
N(2)-C(6)	1.368(14)	N(4)-Rh(1)-N(6)	177.4(3)
N(3)-C(12)	1.42(2)	N(5)-Rh(1)-N(6)	98.0(3)
N(3)-C(6)	1.450(17)	N(2)-Rh(1)-N(1)	79.5(4)
N(3)-C(8)	1.46(2)	N(7)-Rh(1)-N(1)	95.8(3)
N(4)-C(13)	1.308(14)	N(4)-Rh(1)-N(1)	95.7(3)
N(4)-C(17)	1.371(11)	N(5)-Rh(1)-N(1)	174.5(3)

N(6)-Rh(1)-N(1)	86.0(3)	F(42X)-P(4)-F(41)	86.4(8)
F(14)-P(1)-F(11)	180.000(1)	F(46X)-P(4)-F(41)	88.1(12)
F(14)-P(1)-F(13)	91.5(5)	F(45)-P(4)-F(41)	94.3(9)
F(11)-P(1)-F(13)	88.5(5)	F(44)-P(4)-F(41)	179.7(6)
F(14)-P(1)-F(13)#1	91.5(5)	F(43)-P(4)-F(42)	94.4(14)
F(11)-P(1)-F(13)#1	88.5(5)	F(42X)-P(4)-F(42)	32.2(11)
F(13)-P(1)-F(13)#1	176.9(10)	F(46X)-P(4)-F(42)	129.5(17)
F(14)-P(1)-F(12)	89.4(2)	F(45)-P(4)-F(42)	165.2(16)
F(11)-P(1)-F(12)	90.6(2)	F(44)-P(4)-F(42)	83.5(10)
F(13)-P(1)-F(12)	91.4(3)	F(41)-P(4)-F(42)	96.7(10)
F(13)#1-P(1)-F(12)	88.7(3)	F(43)-P(4)-F(43X)	39.9(11)
F(14)-P(1)-F(12)#1	89.4(2)	F(42X)-P(4)-F(43X)	89.0(14)
F(11)-P(1)-F(12)#1	90.6(2)	F(46X)-P(4)-F(43X)	167.5(12)
F(13)-P(1)-F(12)#1	88.7(3)	F(45)-P(4)-F(43X)	131.3(14)
F(13)#1-P(1)-F(12)#1	91.4(3)	F(44)-P(4)-F(43X)	97.7(10)
F(12)-P(1)-F(12)#1	178.8(5)	F(41)-P(4)-F(43X)	82.7(9)
F(23)-P(2)-F(25)	179.3(5)	F(42)-P(4)-F(43X)	60.3(14)
F(23)-P(2)-F(22)	91.7(5)	F(43)-P(4)-F(45X)	53.0(14)
F(25)-P(2)-F(22)	88.3(5)	F(42X)-P(4)-F(45X)	170.3(11)
F(23)-P(2)-F(21)	90.5(5)	F(46X)-P(4)-F(45X)	83.7(17)
F(25)-P(2)-F(21)	88.8(5)	F(45)-P(4)-F(45X)	44.4(14)
F(22)-P(2)-F(21)	90.1(5)	F(44)-P(4)-F(45X)	95.7(7)
F(23)-P(2)-F(24)	91.3(5)	F(41)-P(4)-F(45X)	84.3(7)
F(25)-P(2)-F(24)	89.3(5)	F(42)-P(4)-F(45X)	147(2)
F(22)-P(2)-F(24)	89.7(4)	F(43X)-P(4)-F(45X)	87.1(17)
F(21)-P(2)-F(24)	178.1(5)	F(43)-P(4)-F(46)	169.3(10)
F(23)-P(2)-F(26)	90.7(5)	F(42X)-P(4)-F(46)	53.3(11)
F(25)-P(2)-F(26)	89.4(5)	F(46X)-P(4)-F(46)	46.0(12)
F(22)-P(2)-F(26)	177.6(5)	F(45)-P(4)-F(46)	86.2(12)
F(21)-P(2)-F(26)	89.4(5)	F(44)-P(4)-F(46)	87.8(7)
F(24)-P(2)-F(26)	90.7(5)	F(41)-P(4)-F(46)	91.9(7)
F(31)-P(3)-F(34)	180.000(2)	F(42)-P(4)-F(46)	83.5(14)
F(31)-P(3)-F(32)#2	90.1(2)	F(43X)-P(4)-F(46)	142.3(15)
F(34)-P(3)-F(32)#2	89.9(2)	F(45X)-P(4)-F(46)	129.7(19)
F(31)-P(3)-F(32)	90.1(2)	F(42X)-F(42)-P(4)	65(2)
F(34)-P(3)-F(32)	89.9(2)	F(42X)-F(42)-F(43X)	118(4)
F(32)#2-P(3)-F(32)	179.7(5)	P(4)-F(42)-F(43X)	60.6(13)
F(31)-P(3)-F(33)#2	90.6(2)	F(43X)-F(43)-F(45X)	133(2)
F(34)-P(3)-F(33)#2	89.4(2)	F(43X)-F(43)-P(4)	78.8(18)
F(32)#2-P(3)-F(33)#2	90.3(3)	F(45X)-F(43)-P(4)	71.3(13)
F(32)-P(3)-F(33)#2	89.7(3)	F(46X)-F(45)-F(45X)	138(3)
F(31)-P(3)-F(33)	90.6(2)	F(46X)-F(45)-P(4)	67.4(15)
F(34)-P(3)-F(33)	89.4(2)	F(45X)-F(45)-P(4)	75.2(19)
F(32)#2-P(3)-F(33)	89.7(3)	F(46X)-F(46)-F(42X)	112.4(16)
F(32)-P(3)-F(33)	90.3(3)	F(46X)-F(46)-P(4)	57.7(11)
F(33)#2-P(3)-F(33)	178.9(4)	F(42X)-F(46)-P(4)	55.4(10)
F(43)-P(4)-F(42X)	126.2(14)	F(42)-F(42X)-F(46)	146(3)
F(43)-P(4)-F(46X)	134.7(16)	F(42)-F(42X)-P(4)	83(3)
F(42X)-P(4)-F(46X)	98.8(15)	F(46)-F(42X)-P(4)	71.3(12)
F(43)-P(4)-F(45)	93.8(11)	F(43)-F(43X)-F(42)	112(2)
F(42X)-P(4)-F(45)	139.5(14)	F(43)-F(43X)-P(4)	61.4(15)
F(46X)-P(4)-F(45)	40.9(11)	F(42)-F(43X)-P(4)	59.1(11)
F(43)-P(4)-F(44)	81.5(8)	F(45)-F(45X)-F(43)	111(2)
F(42X)-P(4)-F(44)	93.6(8)	F(45)-F(45X)-P(4)	60.4(12)
F(46X)-P(4)-F(44)	91.6(13)	F(43)-F(45X)-P(4)	55.7(11)
F(45)-P(4)-F(44)	85.5(9)	F(45)-F(46X)-F(46)	145(3)
F(43)-P(4)-F(41)	98.7(9)		

F(45)-F(46X)-P(4)	71.7(19)	C(7)-C(8)-N(3)	104.5(12)
F(46)-F(46X)-P(4)	76.3(13)	C(9)-C(8)-N(3)	116.1(17)
C(1)-N(1)-C(5)	119.1(9)	C(8)-C(9)-C(10)	126(3)
C(1)-N(1)-Rh(1)	124.7(7)	C(11)-C(10)-C(9)	121(3)
C(5)-N(1)-Rh(1)	116.0(8)	C(10)-C(11)-C(12)	126(2)
C(7)-N(2)-C(6)	111.6(10)	N(3)-C(12)-C(11)	107(2)
C(7)-N(2)-Rh(1)	133.9(8)	N(4)-C(13)-C(14)	123.1(11)
C(6)-N(2)-Rh(1)	114.4(8)	C(15)-C(14)-C(13)	118.5(11)
C(12)-N(3)-C(6)	127(2)	C(14)-C(15)-C(16)	119.8(9)
C(12)-N(3)-C(8)	124.6(17)	C(17)-C(16)-C(15)	119.1(10)
C(6)-N(3)-C(8)	108.0(12)	C(16)-C(17)-N(4)	120.8(9)
C(13)-N(4)-C(17)	118.8(8)	C(16)-C(17)-C(18)	125.0(9)
C(13)-N(4)-Rh(1)	126.2(6)	N(4)-C(17)-C(18)	114.2(7)
C(17)-N(4)-Rh(1)	114.2(5)	N(5)-C(18)-C(19)	121.3(9)
C(18)-N(5)-C(22)	118.6(8)	N(5)-C(18)-C(17)	114.9(8)
C(18)-N(5)-Rh(1)	115.1(6)	C(19)-C(18)-C(17)	123.8(9)
C(22)-N(5)-Rh(1)	125.9(6)	C(20)-C(19)-C(18)	118.2(11)
C(32)-N(6)-C(28)	119.7(7)	C(21)-C(20)-C(19)	121.3(13)
C(32)-N(6)-Rh(1)	125.5(6)	C(20)-C(21)-C(22)	118.5(12)
C(28)-N(6)-Rh(1)	114.2(5)	N(5)-C(22)-C(21)	121.9(10)
C(23)-N(7)-C(27)	119.8(7)	N(7)-C(23)-C(24)	120.8(8)
C(23)-N(7)-Rh(1)	125.3(6)	C(25)-C(24)-C(23)	118.7(8)
C(27)-N(7)-Rh(1)	114.8(5)	C(24)-C(25)-C(26)	121.5(9)
N(1)-C(1)-C(2)	119.8(12)	C(27)-C(26)-C(25)	116.6(8)
C(3)-C(2)-C(1)	122.2(14)	N(7)-C(27)-C(26)	122.5(7)
C(4)-C(3)-C(2)	116.7(14)	N(7)-C(27)-C(28)	114.5(7)
C(3)-C(4)-C(5)	121.8(16)	C(26)-C(27)-C(28)	122.8(7)
N(1)-C(5)-C(4)	120.3(14)	N(6)-C(28)-C(29)	121.4(7)
N(1)-C(5)-C(6)	112.7(10)	N(6)-C(28)-C(27)	115.2(7)
C(4)-C(5)-C(6)	127.0(13)	C(29)-C(28)-C(27)	123.4(8)
N(2)-C(6)-C(5)	117.3(9)	C(28)-C(29)-C(30)	118.5(9)
N(2)-C(6)-N(3)	102.1(13)	C(31)-C(30)-C(29)	121.2(9)
C(5)-C(6)-N(3)	140.6(13)	C(30)-C(31)-C(32)	117.8(8)
C(8)-C(7)-N(2)	113.8(14)	N(6)-C(32)-C(31)	121.4(8)
C(7)-C(8)-C(9)	139(2)		

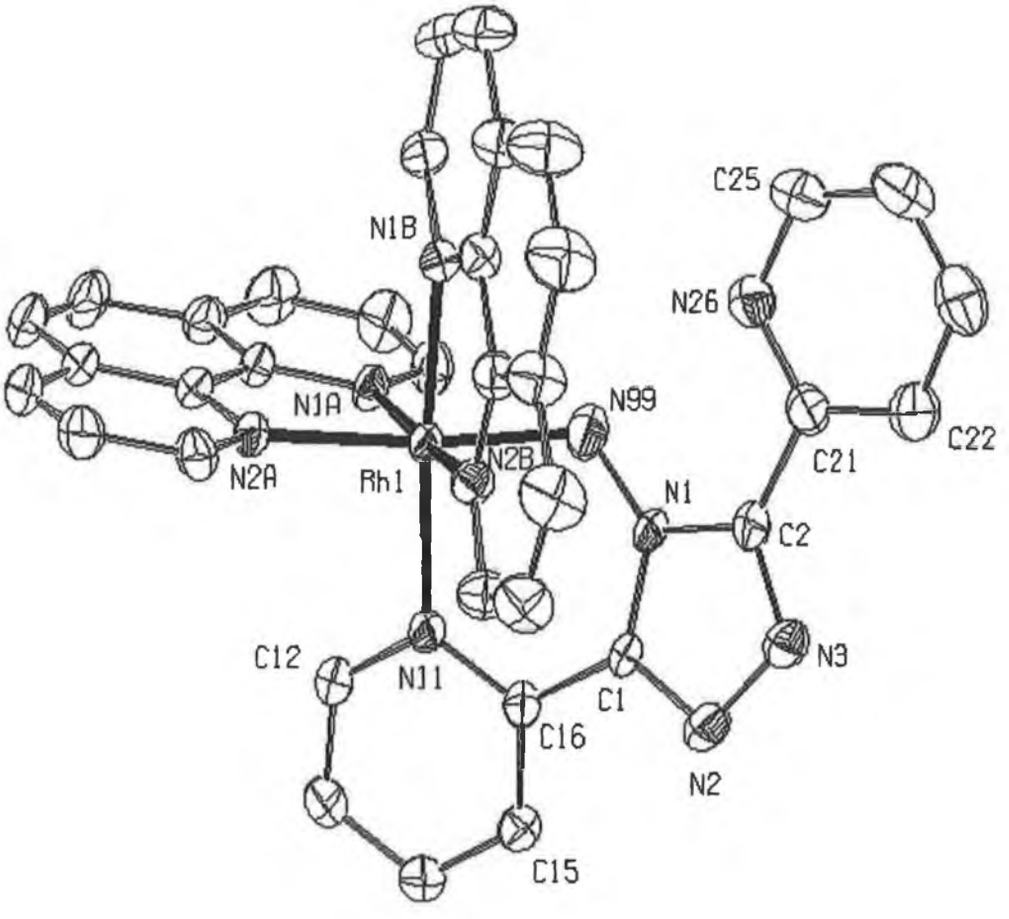

Figure AII.2 Molecular structure of the cation in $[Rh(phen)_2(NHbpt)](PF_6)_2 \cdot 0.767 CH_3CN \cdot 0.28 H_2O$. Counter ions and the solvent molecules have been omitted for clarity.

Table AII.4 Crystal data and structure refinement for $[Rh(phen)_2(NHbpt)](PF_6)_2 \cdot 0.767\ CH_3CN \cdot 0.28\ H_2O$.

Empirical formula	C37.53 H27.86 F12 N10.77 O0.28 P2 Rh
Formula weight	1027.06
Temperature	297(2) K
Wavelength	0.71073 A
Crystal system, space group	Monocyclic, $P2_1/m$
Unit cell dimensions	a = 13.2334(12) A alpha = 90 deg.
	b = 20.507(3) A beta = 103.620(6) deg.
	c = 16.0732(15) A gamma = 90 deg.
Volume	4239.3(8) A^3
Z, Calculated density	4, 1.609 Mg/m^3
Absorption coefficient	0.575 mm^-1
F(000)	2055
Crystal size	0.43 x 0.10 x 0.08 mm
Theta range for data collection	1.87 to 25.57 deg.
Index ranges	-16<=h<=0, -24<=k<=0, -18<=l<=19
Reflections collected / unique	8528 / 8164 [R(int) = 0.0298]
Completeness to 2theta = 25.57	99.6%
Max. and min. transmission	0.9581 and 0.7921
Refinement method	Full-matrix least-squares on F^2
Data / restraints / parameters	8164 / 288 / 705
Goodness-of-fit on F^2	1.030
Final R indices [I>2sigma(I)]	R1 = 0.0614, wR2 = 0.1467
R indices (all data)	R1 = 0.1014, wR2 = 0.1732
Largest diff. peak and hole	1.111 and -0.689 e.A^-3

Table AII.5 ***Atomic coordinates (x 10^4) and equivalent isotropic displacement parameters (A^2 x 10^3) [Rh(phen)$_2$(NHbpt)](PF$_6$)$_2$·0.767 CH$_3$CN·0.28 H$_2$O. U(eq) is defined as one third of the trace of the orthogonalized Uij tensor.***

	x	y	z	U(eq)
Rh(1)	2398(1)	262(1)	2062(1)	33(1)
N(1A)	3296(3)	-194(2)	1373(3)	37(1)
C(1A)	3025(5)	-687(3)	831(4)	50(2)
C(2A)	3745(6)	-983(4)	443(5)	63(2)
C(3A)	4744(5)	-766(4)	612(5)	62(2)
C(4A)	5046(5)	-234(3)	1171(4)	49(2)
C(5A)	4294(4)	36(3)	1551(4)	39(1)
N(2A)	3772(3)	811(2)	2458(3)	40(1)
C(6A)	6066(5)	29(4)	1383(5)	61(2)
C(7A)	6315(5)	521(4)	1931(5)	65(2)
C(8A)	5564(5)	805(3)	2340(4)	48(2)
C(9A)	5752(6)	1327(4)	2914(5)	64(2)
C(10A)	4985(6)	1561(3)	3258(5)	63(2)
C(11A)	3984(5)	1292(3)	3017(4)	51(2)
C(12A)	4552(4)	558(3)	2123(4)	40(1)
N(1B)	2893(4)	-323(2)	3105(3)	40(1)
C(1B)	3516(5)	-825(3)	3205(5)	52(2)
C(2B)	3727(6)	-1200(4)	3936(5)	68(2)
C(3B)	3259(7)	-1070(4)	4581(5)	74(2)
C(4B)	2597(6)	-523(4)	4514(5)	62(2)
C(5B)	2413(5)	-171(3)	3751(4)	44(1)
N(2B)	1615(4)	696(2)	2861(3)	42(1)
C(6B)	2036(8)	-327(5)	5148(5)	85(3)
C(7B)	1403(8)	174(5)	5013(6)	88(3)
C(8B)	1219(6)	564(4)	4253(5)	64(2)
C(9B)	561(7)	1094(4)	4071(6)	80(3)
C(10B)	480(6)	1428(4)	3328(5)	69(2)
C(11B)	1018(5)	1225(3)	2730(5)	55(2)
C(12B)	1746(5)	375(3)	3612(4)	46(2)
N(11)	1754(3)	828(2)	991(3)	37(1)
C(12)	2376(5)	1177(3)	624(4)	45(2)
C(13)	2050(5)	1546(3)	-98(4)	56(2)
C(14)	978(5)	1568(3)	-472(4)	57(2)
C(15)	322(5)	1212(3)	-101(4)	49(2)
C(16)	715(4)	835(3)	614(4)	42(1)
C(1)	0(4)	471(3)	996(4)	41(1)
N(1)	263(3)	-47(2)	1513(3)	40(1)
N(99)	1225(3)	-369(2)	1637(3)	40(1)
N(2)	-993(4)	636(3)	927(4)	62(2)
N(3)	-1373(4)	201(3)	1427(4)	65(2)

C(2)	-615(4)	-205(3)	1783(4)	49(2)
C(21)	-675(5)	-719(3)	2399(5)	53(2)
C(22)	-1616(6)	-886(5)	2593(6)	90(3)
C(23)	-1621(8)	-1351(5)	3206(7)	106(4)
C(24)	-712(8)	-1630(4)	3611(6)	82(3)
C(25)	172(8)	-1446(4)	3391(6)	85(3)
N(26)	205(5)	-994(3)	2808(4)	66(2)
P(1A)	8269(10)	2516(17)	4257(6)	33(5)
F(11A)	8323(16)	1759(7)	4433(13)	88(6)
F(12A)	9510(16)	2540(3)	4470(3)	61(10)
F(13A)	7043(14)	2470(2)	4060(2)	99(15)
F(14A)	8300(3)	2630(2)	5224(14)	90(2)
F(15A)	8280(3)	2360(3)	3294(16)	120(2)
P(1B)	8239(12)	2502(17)	4231(11)	69(7)
F(11B)	8158(18)	1751(10)	3978(16)	127(11)
F(12B)	9453(17)	2450(3)	4280(3)	103(14)
F(13B)	7016(17)	2520(3)	4151(19)	77(12)
F(14B)	8410(3)	2290(3)	5186(15)	140(2)
F(15B)	8070(3)	2720(2)	3268(17)	105(17)
P(2A)	4915(2)	2500	801(2)	59(1)
F(21A)	4847(5)	3261(2)	785(4)	112(2)
F(22A)	5764(6)	2500	271(6)	109(3)
F(23A)	3995(8)	2500	1276(6)	130(3)
F(24A)	5712(7)	2500	1674(5)	132(3)
F(25A)	4064(6)	2500	-91(5)	112(3)
P(3A)	2070(3)	-2500	1789(2)	78(1)
F(31A)	2047(11)	-1792(4)	1818(10)	277(7)
F(32A)	2241(14)	-2500	2740(7)	268(10)
F(33A)	1840(2)	-2500	844(8)	374(16)
F(34A)	3204(10)	-2500	1864(16)	323(12)
F(35A)	903(8)	-2500	1728(13)	255(9)
P(4A)	3317(3)	2500	5066(3)	89(1)
F(41A)	3299(9)	3240(4)	5018(9)	238(5)
F(42A)	4475(8)	2500	4960(10)	197(6)
F(43A)	2179(9)	2500	5155(10)	210(7)
F(44A)	2948(11)	2500	4068(7)	192(6)
F(45A)	3742(14)	2500	6015(7)	304(12)
N(1S)	255(18)	2500	1411(15)	143(8)
C(1S)	-631(18)	2500	1280(2)	166(12)
C(2S)	-1795(18)	2500	1210(2)	330(3)
N(2S)	5720(3)	-1230(2)	2910(3)	220(2)
C(3S)	5350(3)	-1680(2)	2510(3)	143(15)
C(4S)	5200(3)	-2221(19)	1840(2)	201(19)
O(1S)	2110(4)	2500	1850(3)	265(18)

Table AII. 6 Selected bond lengths [A] and angles [deg] for $[Rh(phen)_2(NHbpt)](PF_6)_2 \cdot 0.767\ CH_3CN \cdot 0.28\ H_2O$.

Rh(1)-N(99)	2.012(4)	C(8B)-C(12B)	1.428(9)
Rh(1)-N(1A)	2.033(4)	C(9B)-C(10B)	1.358(11)
Rh(1)-N(2B)	2.036(5)	C(9B)-H(9B)	0.9300
Rh(1)-N(1B)	2.040(5)	C(10B)-C(11B)	1.387(10)
Rh(1)-N(11)	2.086(5)	C(10B)-H(10B)	0.9300
Rh(1)-N(2A)	2.106(4)	C(11B)-H(11B)	0.9300
N(1A)-C(1A)	1.328(7)	N(11)-C(12)	1.328(7)
N(1A)-C(5A)	1.369(7)	N(11)-C(16)	1.365(7)
C(1A)-C(2A)	1.394(9)	C(12)-C(13)	1.367(9)
C(1A)-H(1A)	0.9300	C(12)-H(12)	0.9300
C(2A)-C(3A)	1.360(10)	C(13)-C(14)	1.406(9)
C(2A)-H(2A)	0.9300	C(13)-H(13)	0.9300
C(3A)-C(4A)	1.411(10)	C(14)-C(15)	1.374(9)
C(3A)-H(3A)	0.9300	C(14)-H(14)	0.9300
C(4A)-C(5A)	1.398(8)	C(15)-C(16)	1.381(8)
C(4A)-C(6A)	1.419(9)	C(15)-H(15)	0.9300
C(5A)-C(12A)	1.400(9)	C(16)-C(1)	1.450(8)
N(2A)-C(11A)	1.319(8)	C(1)-N(2)	1.336(7)
N(2A)-C(12A)	1.374(7)	C(1)-N(1)	1.343(7)
C(6A)-C(7A)	1.328(11)	N(1)-C(2)	1.370(7)
C(6A)-H(6A)	0.9300	N(1)-N(99)	1.406(6)
C(7A)-C(8A)	1.437(10)	N(99)-H(99)	1.003(5)
C(7A)-H(7A)	0.9300	N(2)-N(3)	1.374(8)
C(8A)-C(9A)	1.397(10)	N(3)-C(2)	1.326(8)
C(8A)-C(12A)	1.398(8)	C(2)-C(21)	1.460(9)
C(9A)-C(10A)	1.353(11)	C(21)-N(26)	1.323(9)
C(9A)-H(9A)	0.9300	C(21)-C(22)	1.396(10)
C(10A)-C(11A)	1.402(9)	C(22)-C(23)	1.373(12)
C(10A)-H(10A)	0.9300	C(22)-H(22)	0.9300
C(11A)-H(11A)	0.9300	C(23)-C(24)	1.353(13)
N(1B)-C(1B)	1.305(8)	C(23)-H(23)	0.9300
N(1B)-C(5B)	1.375(8)	C(24)-C(25)	1.354(12)
C(1B)-C(2B)	1.377(10)	C(24)-H(24)	0.9300
C(1B)-H(1B)	0.9300	C(25)-N(26)	1.326(10)
C(2B)-C(3B)	1.352(11)	C(25)-H(25)	0.9300
C(2B)-H(2B)	0.9300		
C(3B)-C(4B)	1.412(11)	N(99)-Rh(1)-N(1A)	91.30(19)
C(3B)-H(3B)	0.9300	N(99)-Rh(1)-N(2B)	91.7(2)
C(4B)-C(5B)	1.393(9)	N(1A)-Rh(1)-N(2B)	174.11(19)
C(4B)-C(6B)	1.452(11)	N(99)-Rh(1)-N(1B)	88.53(19)
C(5B)-C(12B)	1.409(8)	N(1A)-Rh(1)-N(1B)	93.54(19)
N(2B)-C(11B)	1.330(8)	N(2B)-Rh(1)-N(1B)	81.4(2)
N(2B)-C(12B)	1.350(8)	N(99)-Rh(1)-N(11)	86.85(19)
C(6B)-C(7B)	1.312(12)	N(1A)-Rh(1)-N(11)	89.10(18)
C(6B)-H(6B)	0.9300	N(2B)-Rh(1)-N(11)	96.15(19)
C(7B)-C(8B)	1.430(11)	N(1B)-Rh(1)-N(11)	174.73(18)
C(7B)-H(7B)	0.9300	N(99)-Rh(1)-N(2A)	171.30(19)
C(8B)-C(9B)	1.380(11)	N(1A)-Rh(1)-N(2A)	80.62(19)

N(2B)-Rh(1)-N(2A)	96.11(19)	C(5B)-C(4B)-C(3B)	117.1(7)
N(1B)-Rh(1)-N(2A)	88.75(19)	C(5B)-C(4B)-C(6B)	117.5(7)
N(11)-Rh(1)-N(2A)	96.18(18)	C(3B)-C(4B)-C(6B)	125.2(7)
C(1A)-N(1A)-C(5A)	119.9(5)	N(1B)-C(5B)-C(4B)	122.1(6)
C(1A)-N(1A)-Rh(1)	127.3(4)	N(1B)-C(5B)-C(12B)	116.3(5)
C(5A)-N(1A)-Rh(1)	112.8(4)	C(4B)-C(5B)-C(12B)	121.6(6)
N(1A)-C(1A)-C(2A)	121.2(6)	C(11B)-N(2B)-C(12B)	119.1(5)
N(1A)-C(1A)-H(1A)	119.4	C(11B)-N(2B)-Rh(1)	129.0(5)
C(2A)-C(1A)-H(1A)	119.4	C(12B)-N(2B)-Rh(1)	111.9(4)
C(3A)-C(2A)-C(1A)	120.2(7)	C(7B)-C(6B)-C(4B)	120.8(8)
C(3A)-C(2A)-H(2A)	119.9	C(7B)-C(6B)-H(6B)	119.6
C(1A)-C(2A)-H(2A)	119.9	C(4B)-C(6B)-H(6B)	119.6
C(2A)-C(3A)-C(4A)	119.8(6)	C(6B)-C(7B)-C(8B)	123.6(8)
C(2A)-C(3A)-H(3A)	120.1	C(6B)-C(7B)-H(7B)	118.2
C(4A)-C(3A)-H(3A)	120.1	C(8B)-C(7B)-H(7B)	118.2
C(5A)-C(4A)-C(3A)	117.4(6)	C(9B)-C(8B)-C(12B)	116.8(7)
C(5A)-C(4A)-C(6A)	118.6(7)	C(9B)-C(8B)-C(7B)	126.4(7)
C(3A)-C(4A)-C(6A)	123.9(6)	C(12B)-C(8B)-C(7B)	116.7(7)
N(1A)-C(5A)-C(4A)	121.6(6)	C(10B)-C(9B)-C(8B)	120.0(7)
N(1A)-C(5A)-C(12A)	118.4(5)	C(10B)-C(9B)-H(9B)	120.0
C(4A)-C(5A)-C(12A)	120.1(5)	C(8B)-C(9B)-H(9B)	120.0
C(11A)-N(2A)-C(12A)	119.4(5)	C(9B)-C(10B)-C(11B)	120.7(7)
C(11A)-N(2A)-Rh(1)	129.5(4)	C(9B)-C(10B)-H(10B)	119.7
C(12A)-N(2A)-Rh(1)	110.7(4)	C(11B)-C(10B)-H(10B)	119.7
C(7A)-C(6A)-C(4A)	121.4(7)	N(2B)-C(11B)-C(10B)	121.1(7)
C(7A)-C(6A)-H(6A)	119.3	N(2B)-C(11B)-H(11B)	119.4
C(4A)-C(6A)-H(6A)	119.3	C(10B)-C(11B)-H(11B)	119.4
C(6A)-C(7A)-C(8A)	121.4(6)	N(2B)-C(12B)-C(5B)	118.3(5)
C(6A)-C(7A)-H(7A)	119.3	N(2B)-C(12B)-C(8B)	122.1(6)
C(8A)-C(7A)-H(7A)	119.3	C(5B)-C(12B)-C(8B)	119.7(6)
C(9A)-C(8A)-C(12A)	117.0(6)	C(12)-N(11)-C(16)	117.5(5)
C(9A)-C(8A)-C(7A)	125.3(6)	C(12)-N(11)-Rh(1)	119.4(4)
C(12A)-C(8A)-C(7A)	117.6(6)	C(16)-N(11)-Rh(1)	123.0(4)
C(10A)-C(9A)-C(8A)	120.5(6)	N(11)-C(12)-C(13)	124.8(6)
C(10A)-C(9A)-H(9A)	119.8	N(11)-C(12)-H(12)	117.6
C(8A)-C(9A)-H(9A)	119.8	C(13)-C(12)-H(12)	117.6
C(9A)-C(10A)-C(11A)	119.9(7)	C(12)-C(13)-C(14)	117.8(6)
C(9A)-C(10A)-H(10A)	120.0	C(12)-C(13)-H(13)	121.1
C(11A)-C(10A)-H(10A)	120.0	C(14)-C(13)-H(13)	121.1
N(2A)-C(11A)-C(10A)	121.2(7)	C(15)-C(14)-C(13)	118.3(6)
N(2A)-C(11A)-H(11A)	119.4	C(15)-C(14)-H(14)	120.9
C(10A)-C(11A)-H(11A)	119.4	C(13)-C(14)-H(14)	120.9
N(2A)-C(12A)-C(8A)	122.0(6)	C(14)-C(15)-C(16)	120.4(6)
N(2A)-C(12A)-C(5A)	117.2(5)	C(14)-C(15)-H(15)	119.8
C(8A)-C(12A)-C(5A)	120.8(6)	C(16)-C(15)-H(15)	119.8
C(1B)-N(1B)-C(5B)	118.4(5)	N(11)-C(16)-C(15)	121.1(5)
C(1B)-N(1B)-Rh(1)	129.5(5)	N(11)-C(16)-C(1)	119.7(5)
C(5B)-N(1B)-Rh(1)	111.8(4)	C(15)-C(16)-C(1)	119.0(5)
N(1B)-C(1B)-C(2B)	122.8(7)	N(2)-C(1)-N(1)	111.0(5)
N(1B)-C(1B)-H(1B)	118.6	N(2)-C(1)-C(16)	124.2(6)
C(2B)-C(1B)-H(1B)	118.6	N(1)-C(1)-C(16)	124.7(5)
C(3B)-C(2B)-C(1B)	120.4(7)	C(1)-N(1)-C(2)	105.6(5)
C(3B)-C(2B)-H(2B)	119.8	C(1)-N(1)-N(99)	123.6(5)
C(1B)-C(2B)-H(2B)	119.8	C(2)-N(1)-N(99)	130.5(5)
C(2B)-C(3B)-C(4B)	119.1(7)	N(1)-N(99)-Rh(1)	110.3(3)
C(2B)-C(3B)-H(3B)	120.5	N(1)-N(99)-H(99)	94.9(4)
C(4B)-C(3B)-H(3B)	120.5	Rh(1)-N(99)-H(99)	116.7(4)

C(1)-N(2)-N(3)	106.0(5)	N(3)-C(2)-C(21)	126.0(6)
C(2)-N(3)-N(2)	108.4(5)		
N(3)-C(2)-N(1)	109.1(6)		
N(1)-C(2)-C(21)	124.8(6)		
N(26)-C(21)-C(22)	120.8(7)		
N(26)-C(21)-C(2)	117.6(6)		
C(22)-C(21)-C(2)	121.5(6)		
C(23)-C(22)-C(21)	119.1(8)		
C(23)-C(22)-H(22)	120.4		
C(21)-C(22)-H(22)	120.4		
C(24)-C(23)-C(22)	119.1(8)		
C(24)-C(23)-H(23)	120.5		
C(22)-C(23)-H(23)	120.5		
C(23)-C(24)-C(25)	118.8(8)		
C(23)-C(24)-H(24)	120.6		
C(25)-C(24)-H(24)	120.6		
N(26)-C(25)-C(24)	123.6(9)		
N(26)-C(25)-H(25)	118.2		
C(24)-C(25)-H(25)	118.2		
C(21)-N(26)-C(25)	118.6(7)		

Appendix III

Supplementary NMR Data

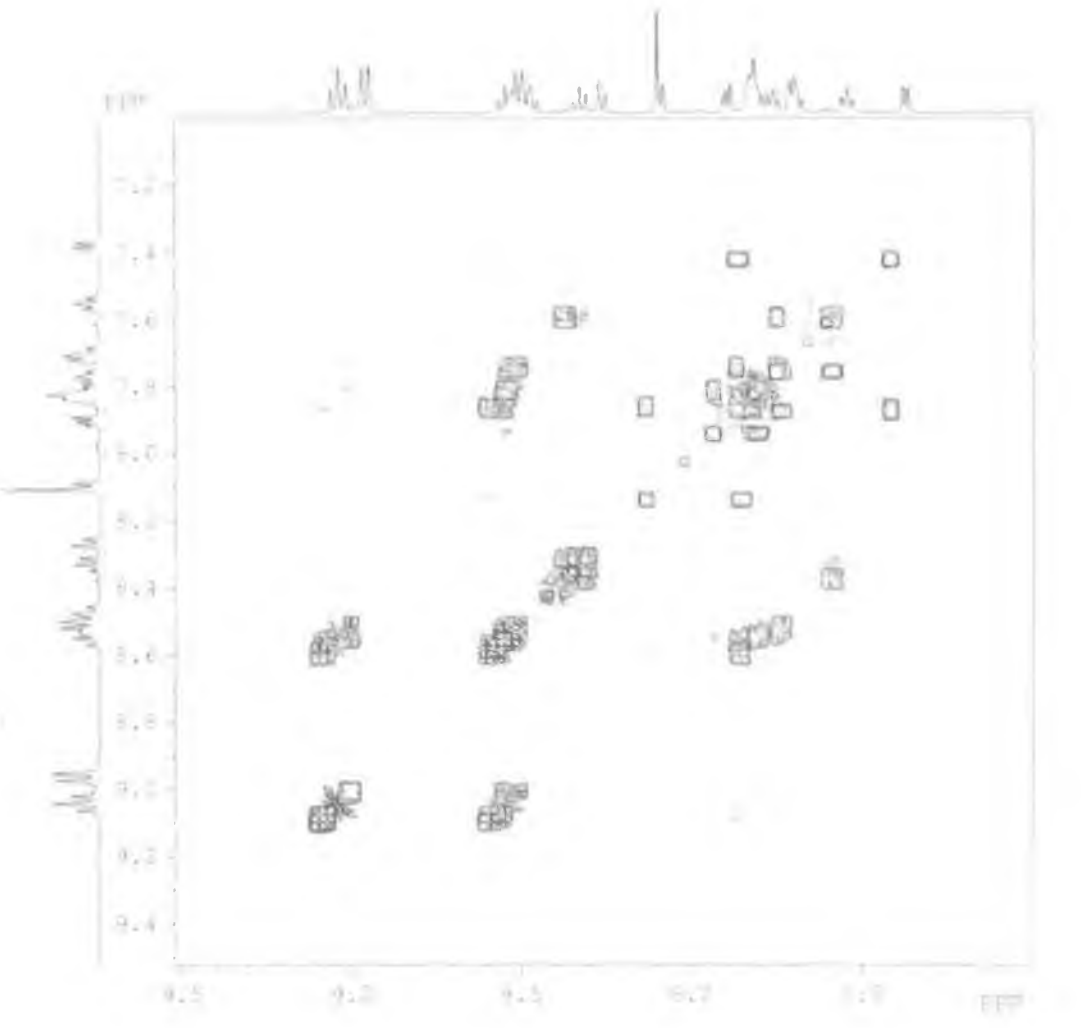

Figure AIII.1 ^{1}H-^{1}H COSY NMR spectrum of $[Rh(bpy)_2(pytr)]^{2+}$ in d_6-DMSO.

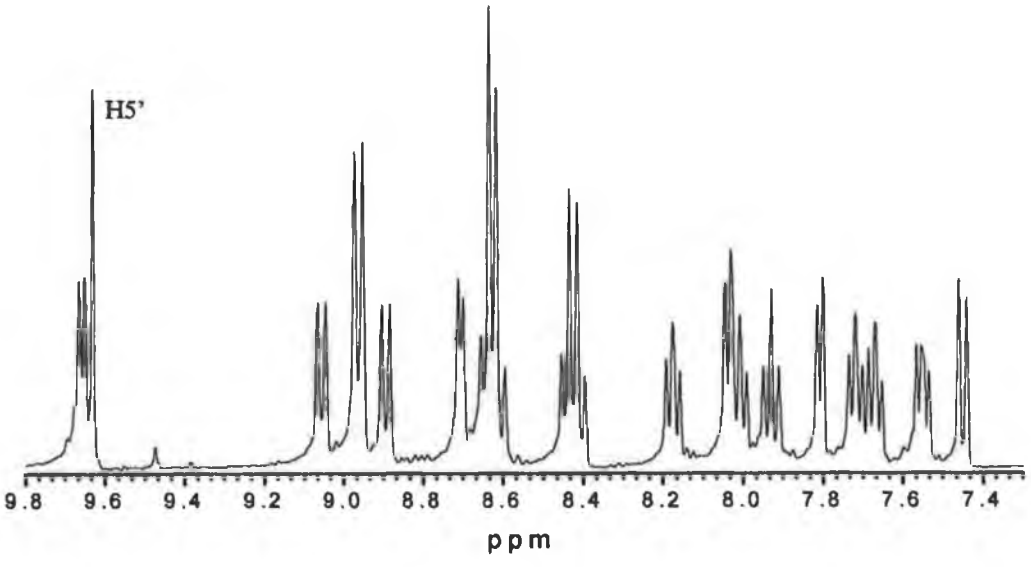

Figure AIII.2 ^{1}H NMR spectrum of $[Rh(bpy)_2(4Mpytr)]^{3+}$ in d_6-DMSO.

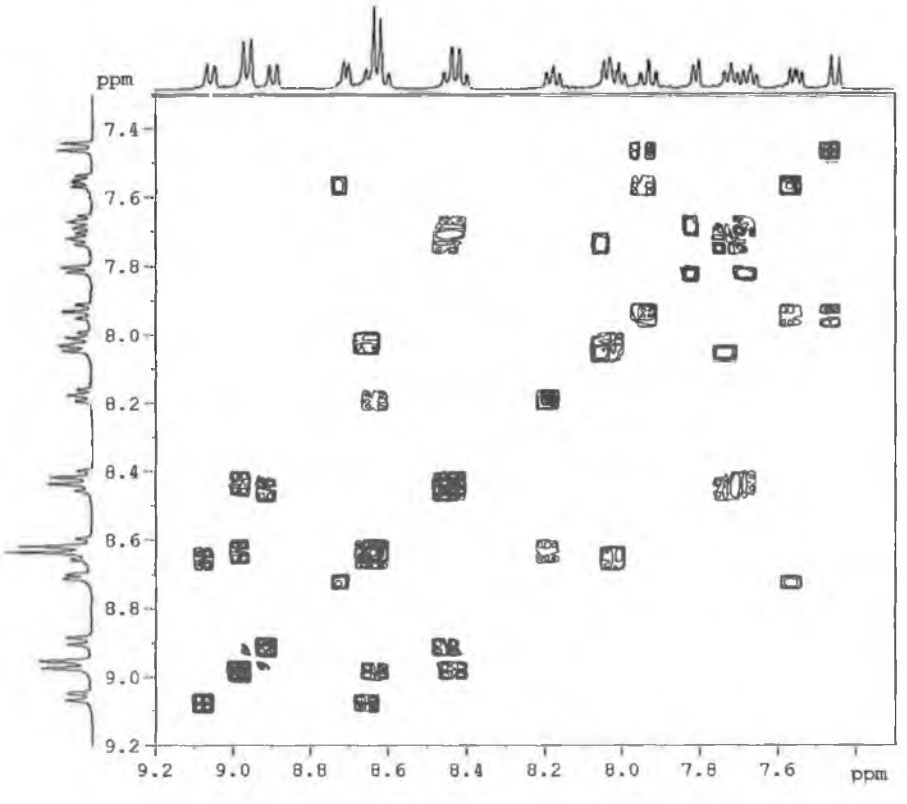

Figure AIII.3 ^{1}H-^{1}H COSY NMR spectrum of $[Rh(bpy)_2(4Mpytr)]^{3+}$ in d_6-DMSO.

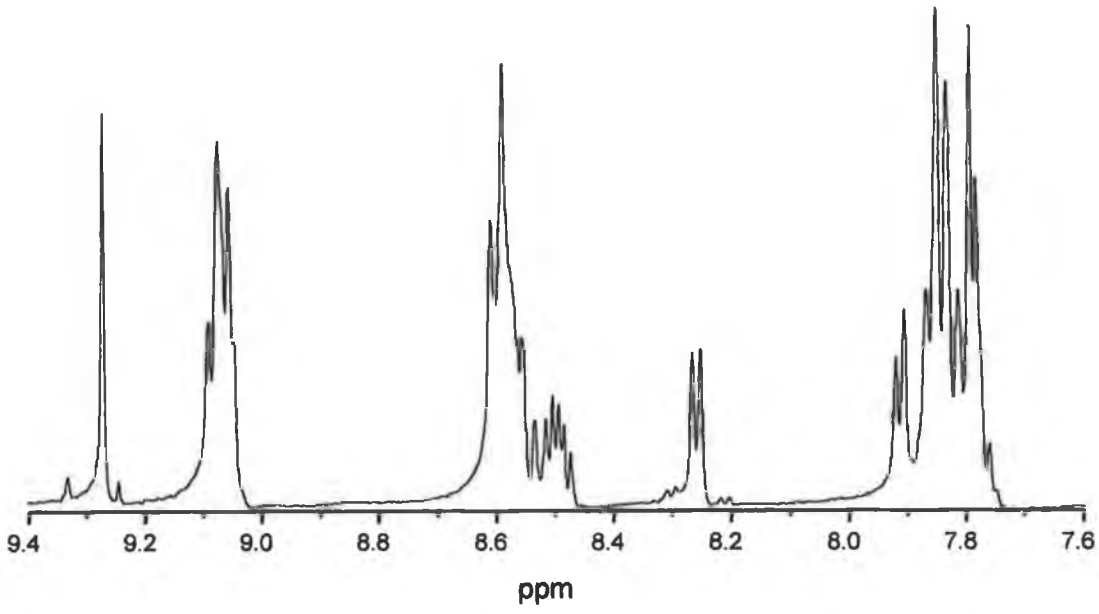

Figure AIII.4 ^{1}H NMR spectrum of $[Rh(bpy)_2(1M3pytr)]^{3+}$ in d_6-DMSO.

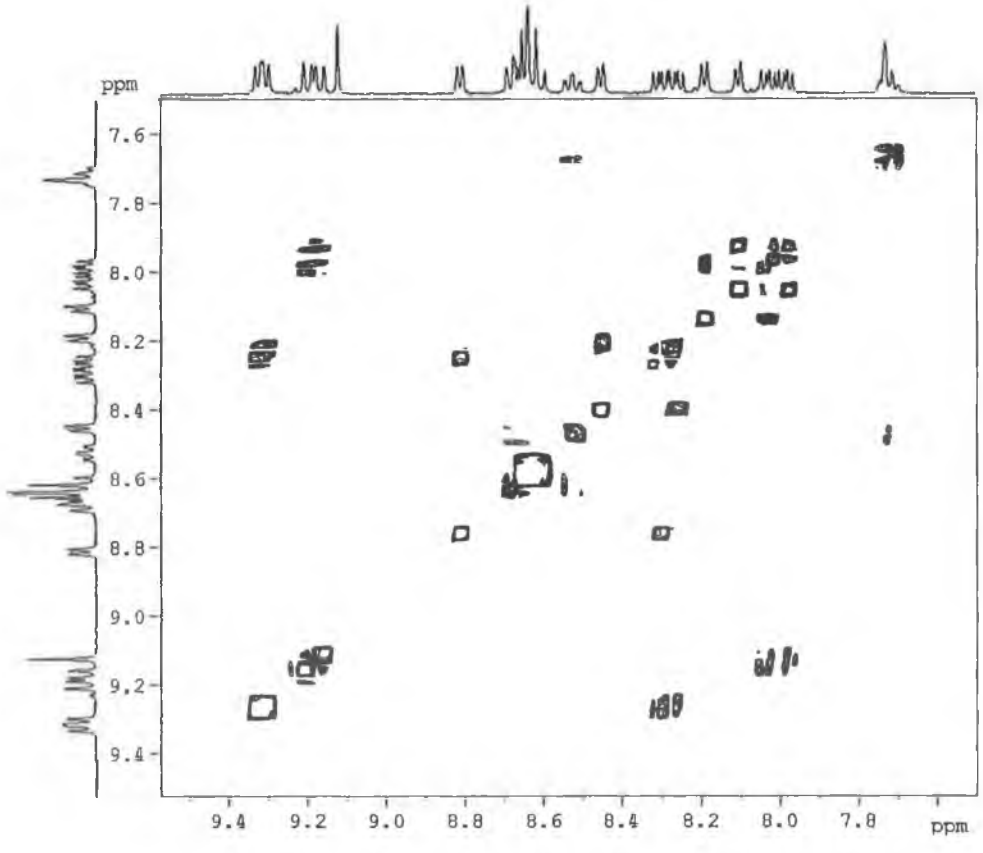

Figure AIII.5 ^{1}H-^{1}H COSY NMR spectrum of $[Rh(bpy)_2(1M3pytr)]^{3+}$ in d_6-DMSO.

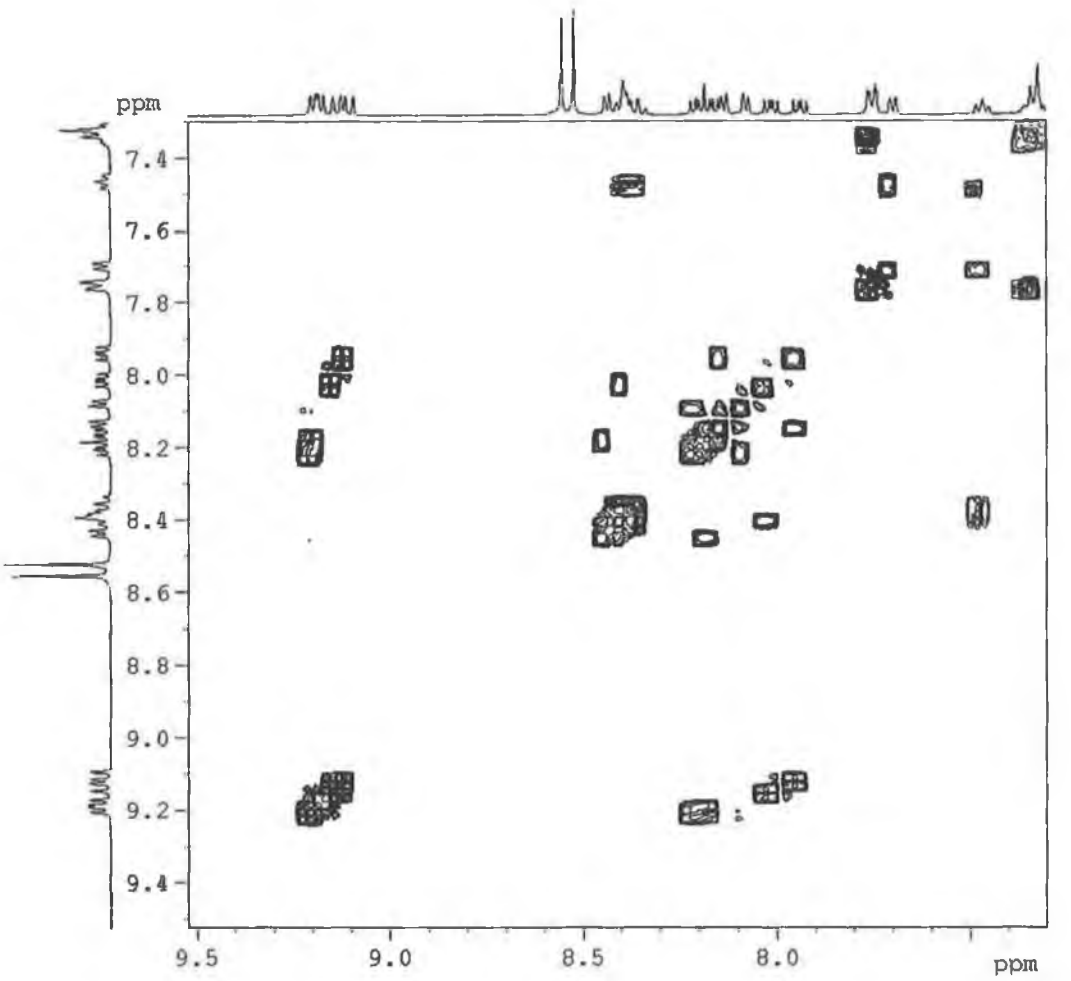

Figure AIII.6 ^{1}H-^{1}H COSY NMR spectrum of $[Rh(phen)_2(Phpytr)]^{2+}$ in d_6-DMSO

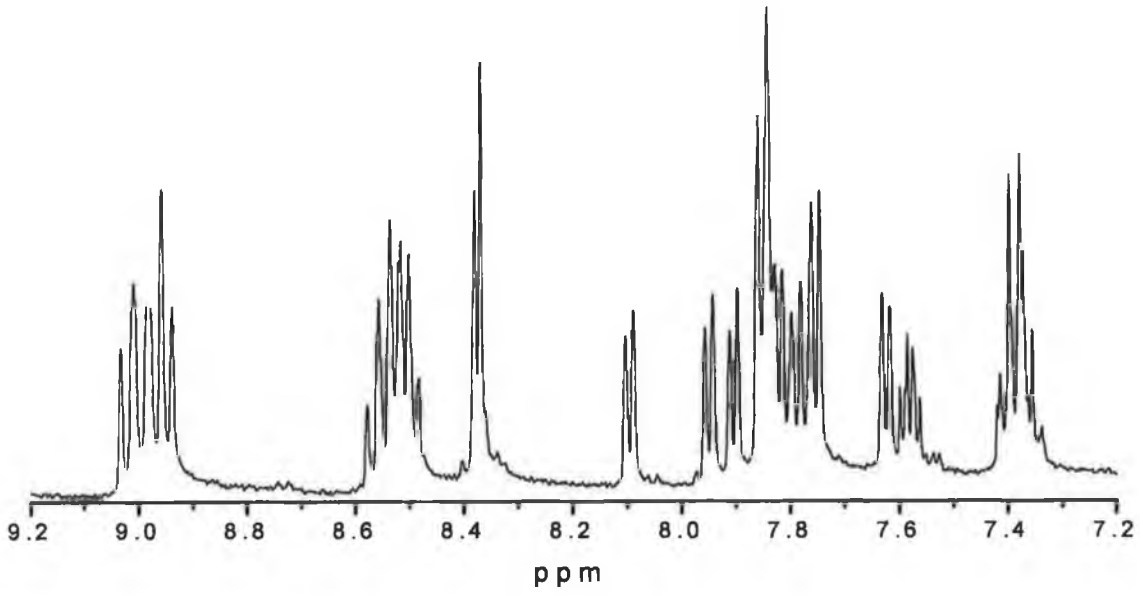

Figure AIII.7 ^{1}H NMR spectrum of [Rh(bpy)$_2$(Phpytr)]$^{2+}$ in d_6-DMSO.

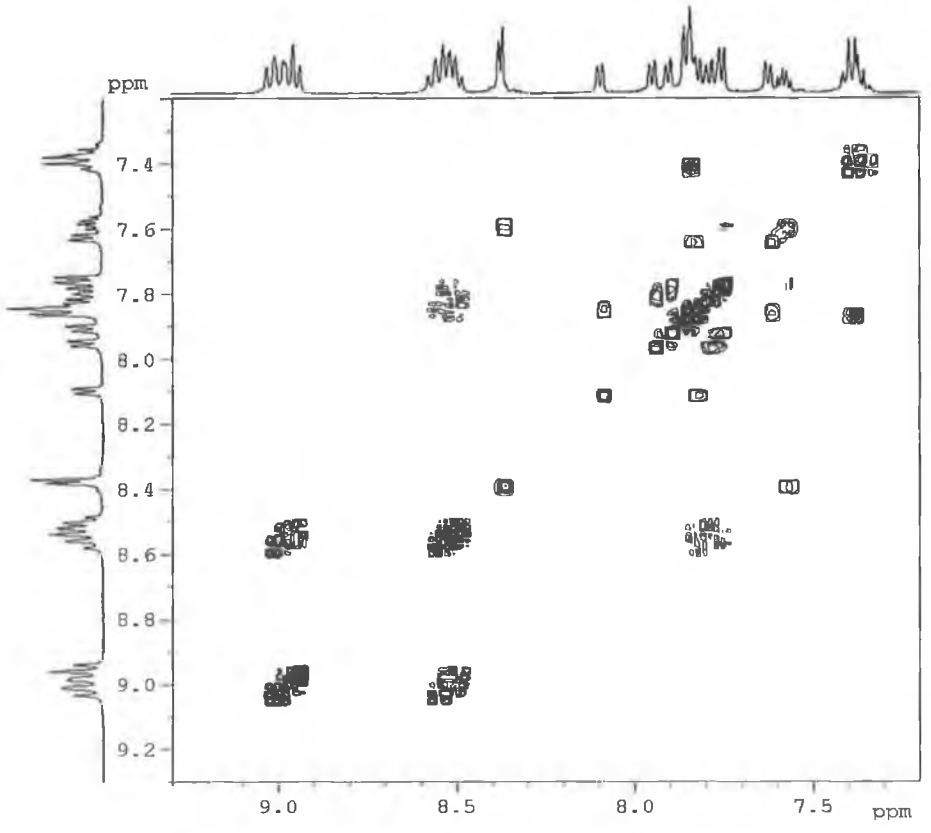

Figure AIII.8 ^{1}H-^{1}H COSY NMR spectrum of [Rh(bpy)$_2$(Phpytr)]$^{2+}$ in d_6-DMSO.

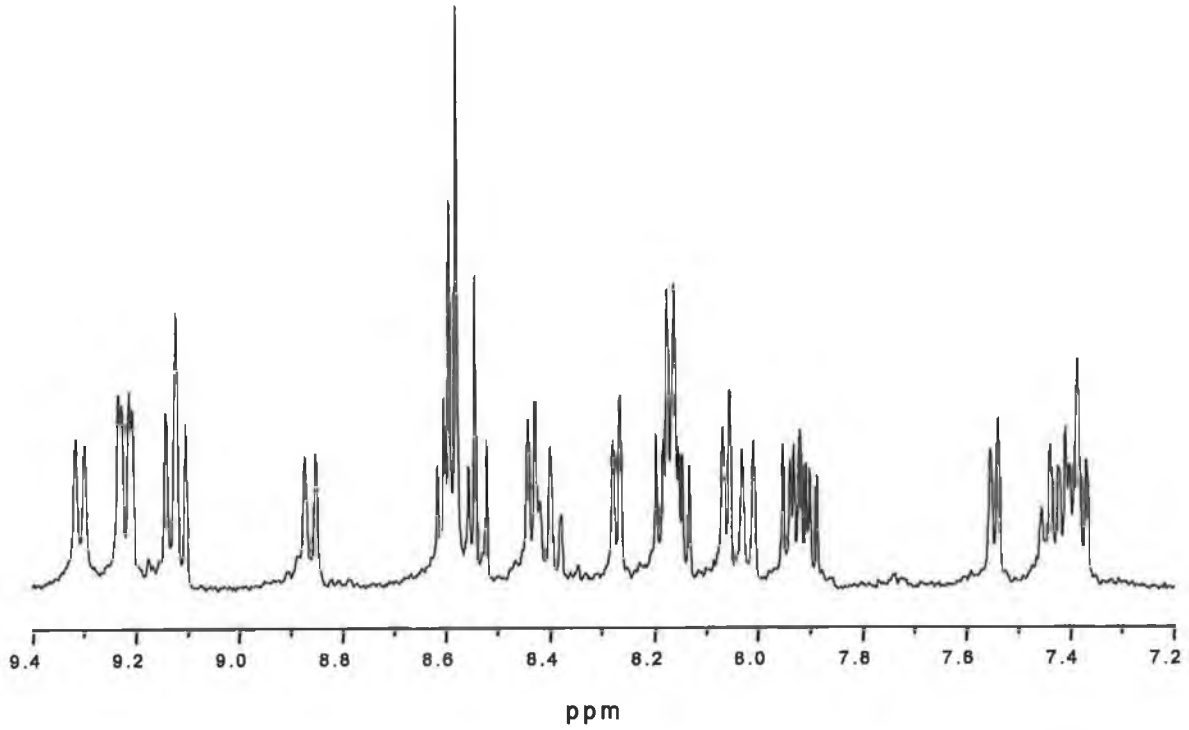

Figure AIII.9 ^{1}H NMR spectrum of [Rh(phen)$_2$(MePIP)]$^{3+}$ in d_6-DMSO.

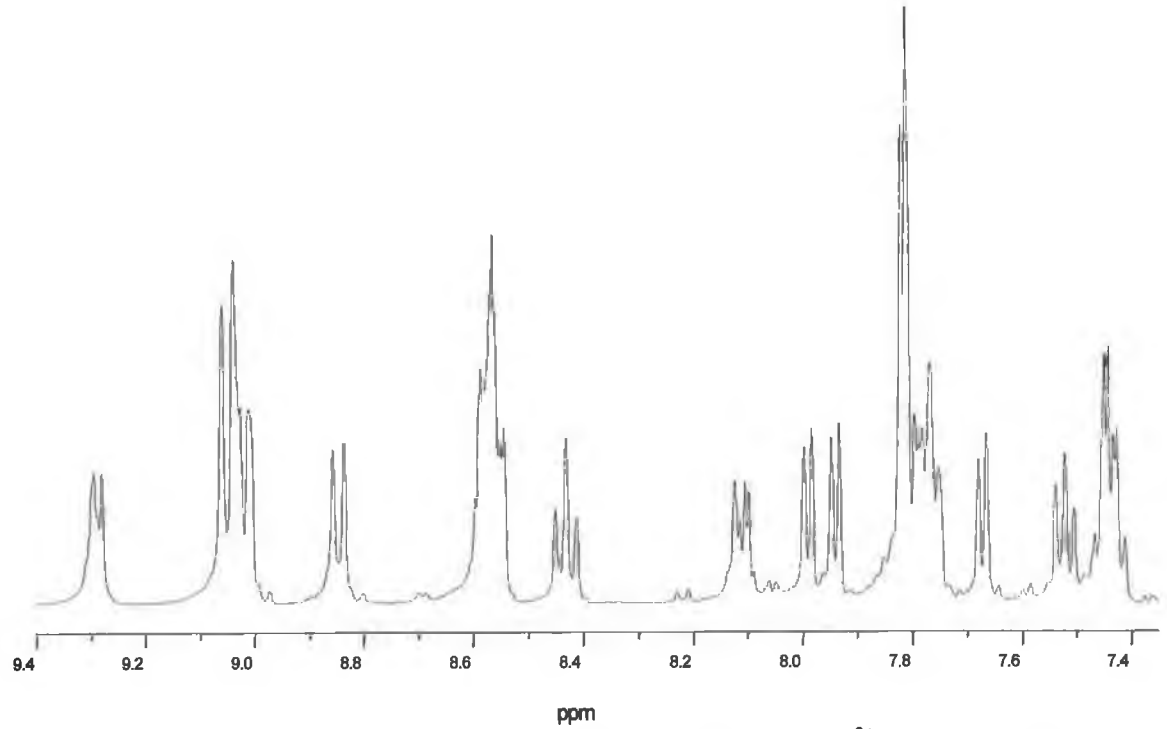

Figure AIII.10 ^{1}H NMR spectrum of [Rh(bpy)$_2$(MePIP)]$^{3+}$ in d_6-DMSO.

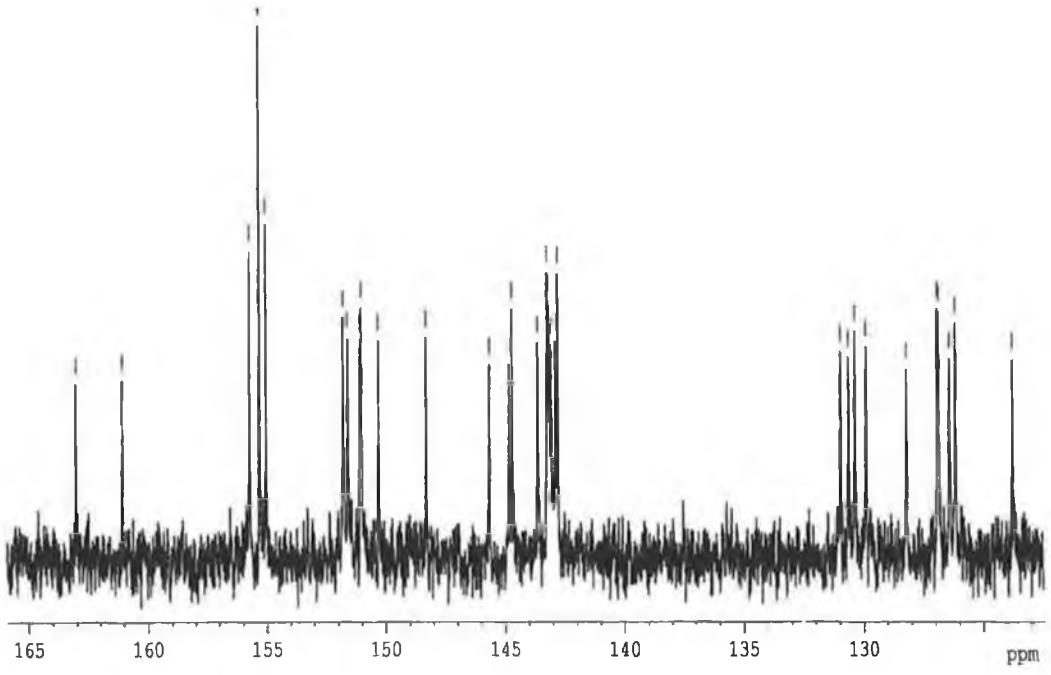

Figure AIII.11 ^{13}C NMR spectrum of $[Rh(bpy)_2(ppt)]^{2+}$ measured in d_6-DMSO.

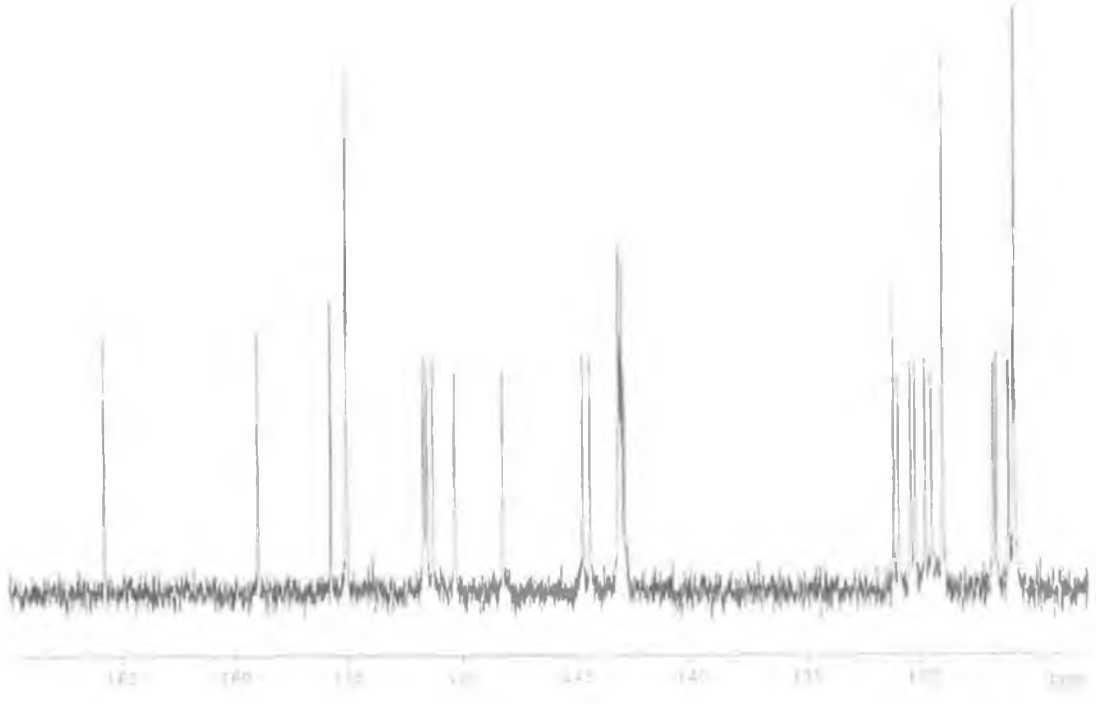

Figure AIII.12 ^{13}C NMR spectrum of $[Rh(bpy)_2(Phpztr)]^{2+}$ measured in d_6-DMSO.

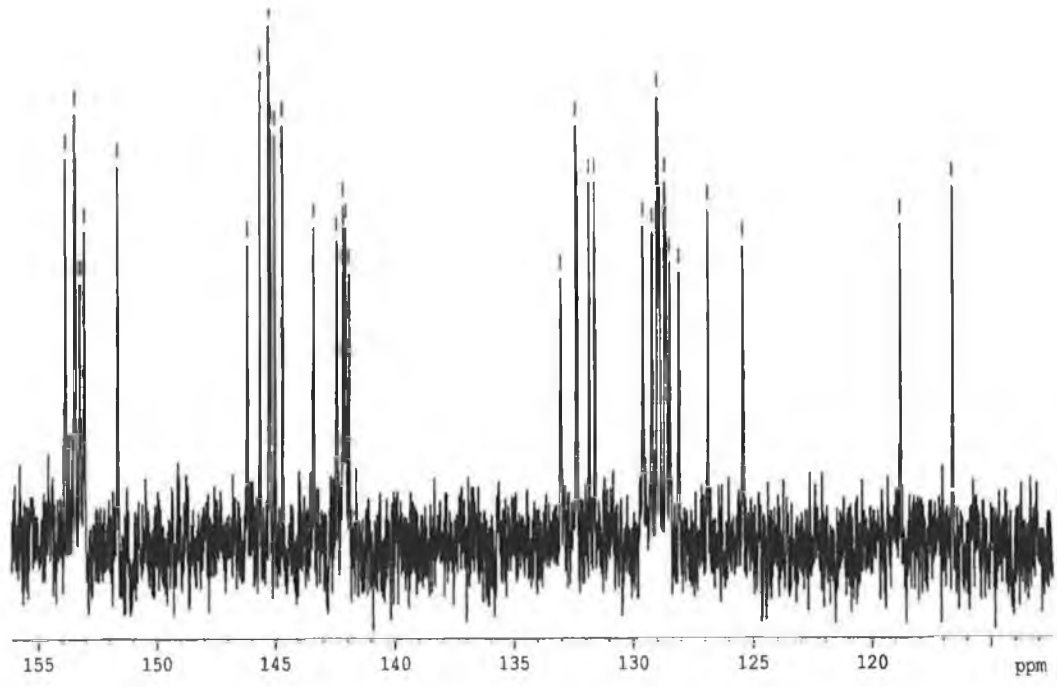

Figure AIII.13 ^{13}C NMR spectrum of $[Rh(phen)_2(PTP)]^{3+}$ measured in d_6-DMSO.

Table AIII. 1 ^{1}H and ^{13}C NMR data for $[Rh(bpy)_2(pztr)]^{2+}$, $[Rh(bpy)_2(Phpztr)]^{2+}$, $[Rh(phen)_2(ppt)]^{2+}$ and $[Rh(bpy)_2(ppt)]^{2+}$ measured in d_6-DMSO.

$[Rh(bpy)_2(pztr)]^{2+}$ (pyrazine ring)	^{1}H chemical shift (ppm)	^{13}C chemical shift (ppm)	**$[Rh(bpy)_2(Phpztr)]^{2+}$** (pyrazine ring)	^{1}H chemical shift (ppm)	^{13}C chemical
3	9.52	144.30	3	9.58	144.90
4	-		4	-	-
5	8.80	130.29	5	8.80	148.40
6	7.85		6	7.89-7.81	
5'	8.23	155.75	5'	-	-
$[Rh(phen)_2(ppt)]^{2+}$ (pyridine ring)	^{1}H chemical shift (ppm)	^{13}C chemical shift (ppm)	**$[Rh(phen)_2(ppt)]^{2+}$** (pyrazine ring)	^{1}H chemical shift (ppm)	^{13}C chemical
3	8.45	*	3	9.10	144.5
4	8.39	*	4	-	-
5	7.51	127.8	5	8.60-8.50	*
6	7.71	135.1	6	8.60-8.50	*
$[Rh(bpy)_2(ppt)]^{2+}$ (pyridine ring)	^{1}H chemical shift (ppm)	^{13}C chemical shift (ppm)	**$[Rh(bpy)_2(ppt)]^{2+}$** (pyrazine ring)	^{1}H chemical shift (ppm)	^{13}C chemical
3	8.45-8.41	143.64-142.78	3	9.13	144.0-142.5
4	8.45-8.41	143.64-142.78	4	-	-
5	7.68-7.61		5	8.64-8.62	*
6	7.90-7.70		6	8.64-8.62	*

* - ^{13}C chemical shift could not be determined unambiguously.

Table AIII.2 ^{1}H and ^{13}C NMR data for $[Rh(phen)_2(PIP)]^{3+}$, $[Rh(bpy)_2(PIP)]^{3+}$, $[Rh(phen)_2(MePIP)]^{3+}$ and $[Rh(bpy)_2(MePIP)]^{3+}$ measured in d_6-DMSO.

$[Rh(phen)_2(PIP)]^{3+}$	^{1}H chemical shift (ppm)	^{13}C chemical shift (ppm)	$[Rh(bpy)_2(PIP)]^{3+}$	^{1}H chemical shift (ppm)	^{13}C chemical shift (ppm)
3	8.67	122.4	3	8.67	122.5
4	8.33	142.60	4	8.33	143.3
5	7.31	125.6	5	7.45	125.8
6	7.52	150.81	6	7.63	151.90-151.00
3'	8.29	126.30	3'	8.52	126.61
4'	7.21	117.51	4'	7.23	116.90
5'	7.59	129.10-128.28	5'	7.61	128.80
6'	8.56-8.62	*	6'	8.60	*
5''	8.62	132.26	5''	8.88	131.80
$[Rh(phen)_2(MePIP)]^{3+}$	^{1}H chemical shift (ppm)	^{13}C chemical shift (ppm)	$[Rh(bpy)_2(MePIP)]^{3+}$	^{1}H chemical shift (ppm)	^{13}C chemical shift (ppm)
3	8.86	133.8	3	8.85	123.35
4	8.40	142.8	4	8.43	143.62-142.89
5	7.47-7.36	*	5	7.52	127.30-126.56
6	7.55	151.40	6	7.67	152.17-151.60
3'	8.02	119.25	3'	8.11	119.29
4'	7.47-7.36	*	4'	7.48-7.40	*
5'	7.47-7.36	*	5'	7.48-7.40	*
6'	9.31	*	6'	9.29	125.12

* - ^{13}C chemical shift could not be determined unambiguously.

Appendix IV

Supplementary Photophysical and Electrochemical Data

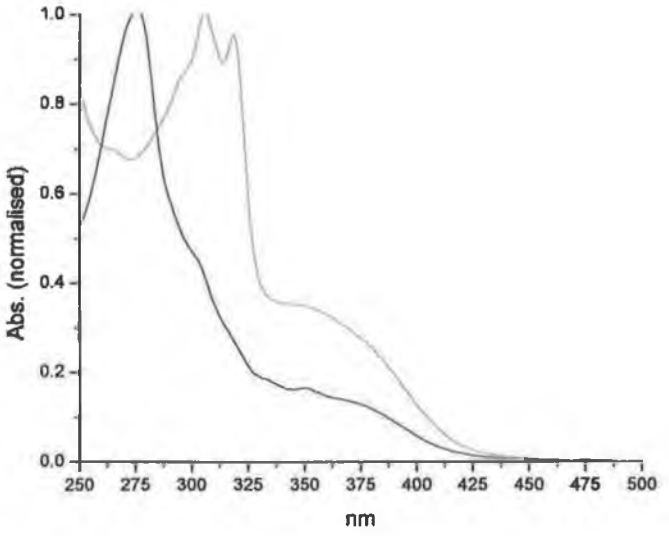

Figure AIV.1Absorption spectra of $[Rh(phen)_2(dppt)]^{3+}$ (——) and $[Rh(bpy)_2(dppt)]^{3+}$ (——) measured in acetonitrile at room temperature.

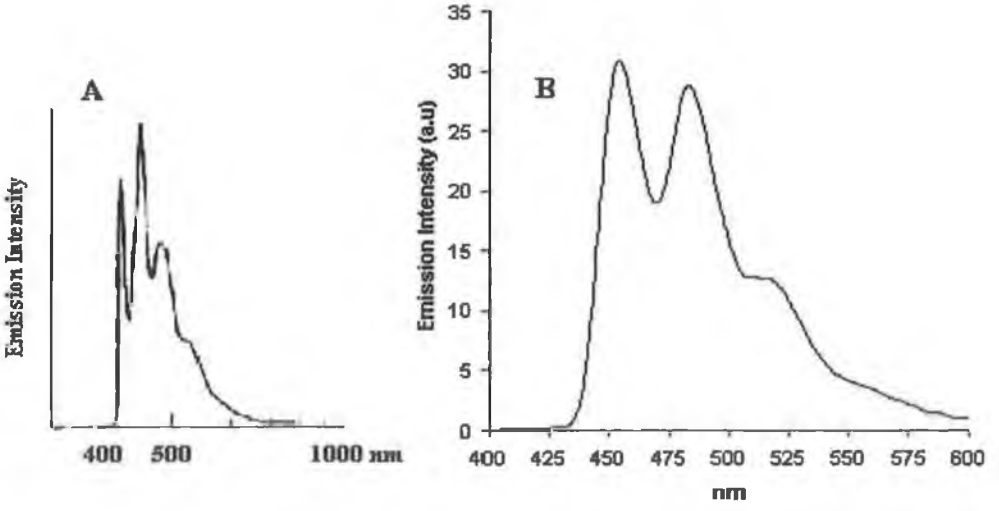

Figure AIV.2Emission spectra of (A) $[Rh(bpy)_3]^{3+}$ and (B) $[Rh(phen)_3]^{3+}$ measured in an ethanol:methanol glass.

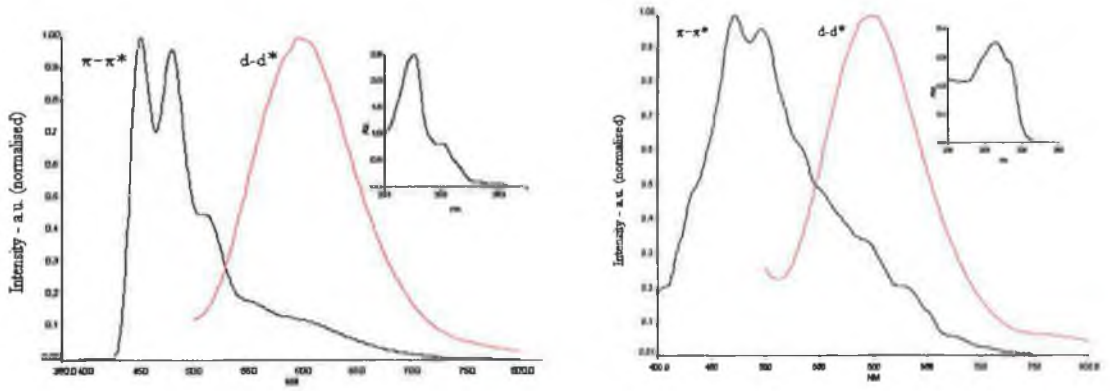

(a) **(b)**

Figure AIV.3 emission spectra of (a) $[Rh(phen)_2(4Mpytr)]^{2+}$ and (b) $[Rh(bpy)_2(4Mpytr)]^{2+}$ measured in ethanol:methanol 4:1 at 77K. Inset shows the UV spectrum of (a) $[Rh(phen)_2(4Mpytr)]^{2+}$ and (b) $[Rh(bpy)_2(4Mpytr)]^{2+}$.

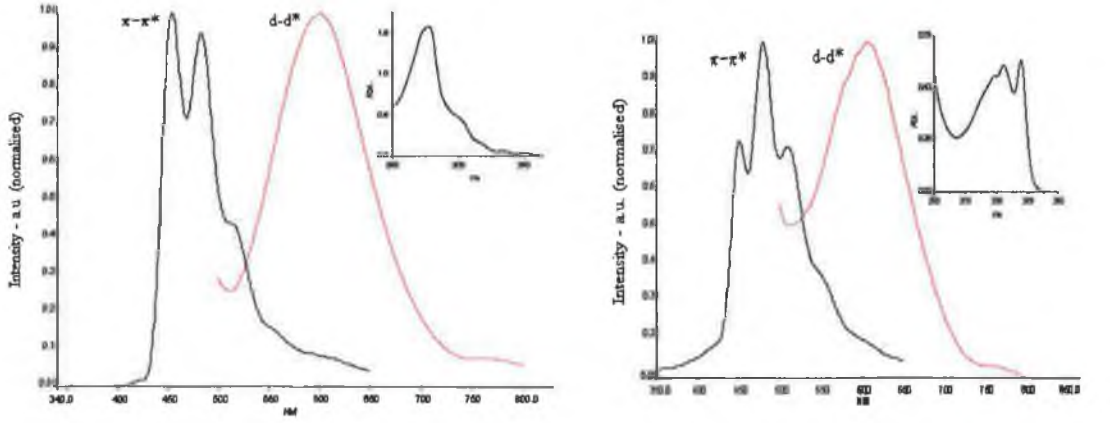

(a) **(b)**

Figure AIV.4 emission spectra of (a) $[Rh(phen)_2(1M3pytr)]^{2+}$ and (b) $[Rh(bpy)_2(1M3pytr)]^{2+}$ measured in ethanol:methanol 4:1 at 77K. Inset shows the UV spectrum of (a) $[Rh(phen)_2(1M3pytr)]^{2+}$ and (b) $[Rh(bpy)_2(1M3pytr)]^{2+}$.

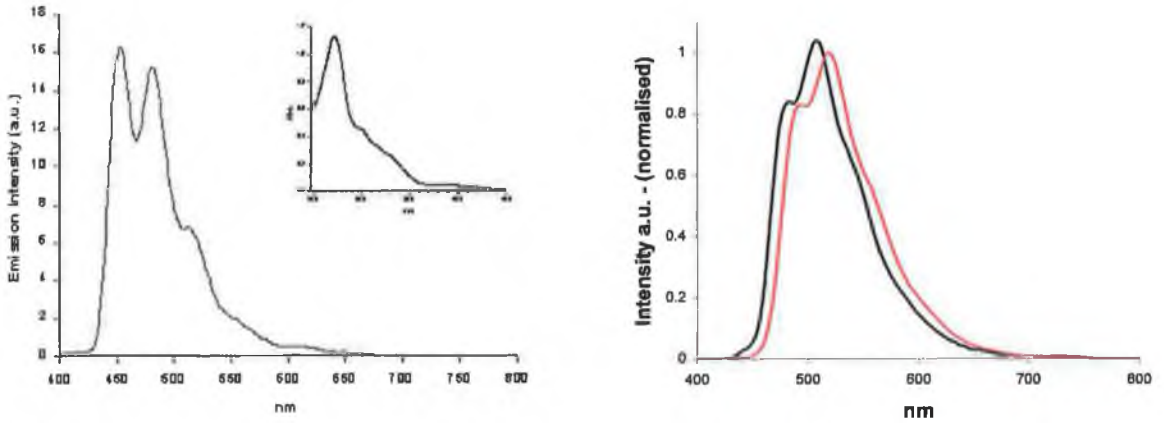

(a) **(b)**

Figure AIV.5 (A) - Emission spectrum of $[Rh(phen)_2(NHbpt)]^{2+}$ with inset illustrating the UV spectrum of $[Rh(phen)_2(NHbpt)]^{2+}$. (B) – Emission spectra of $[Rh(bpy)_2(ppt)]^{2+}$ (——) and of $[Rh(bpy)_2(Phpztr)]^{2+}$ (——). All emission spectra were obtained in ethanol:methanol 4:1 at 77K.

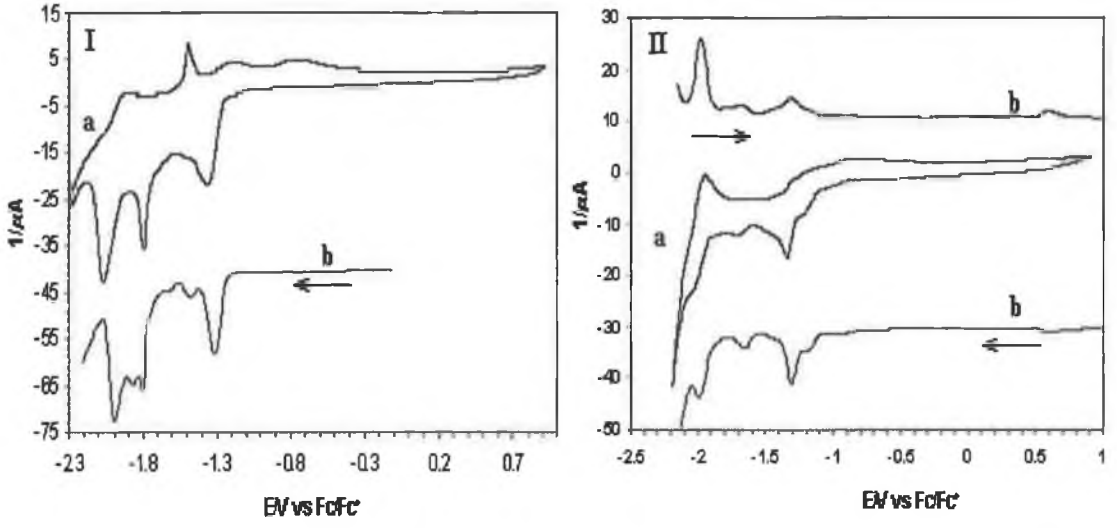

Figure AIV.6 CV's (a) and DPV's (b) of (I) $[Rh(phen)_2(d_4\text{-}pytr)]^{2+}$ and (II) $[Rh(bpy)_2(d_4\text{-}pytr)]^{2+}$ measured in acetonitrile with 0.1M $TBABF_4$.

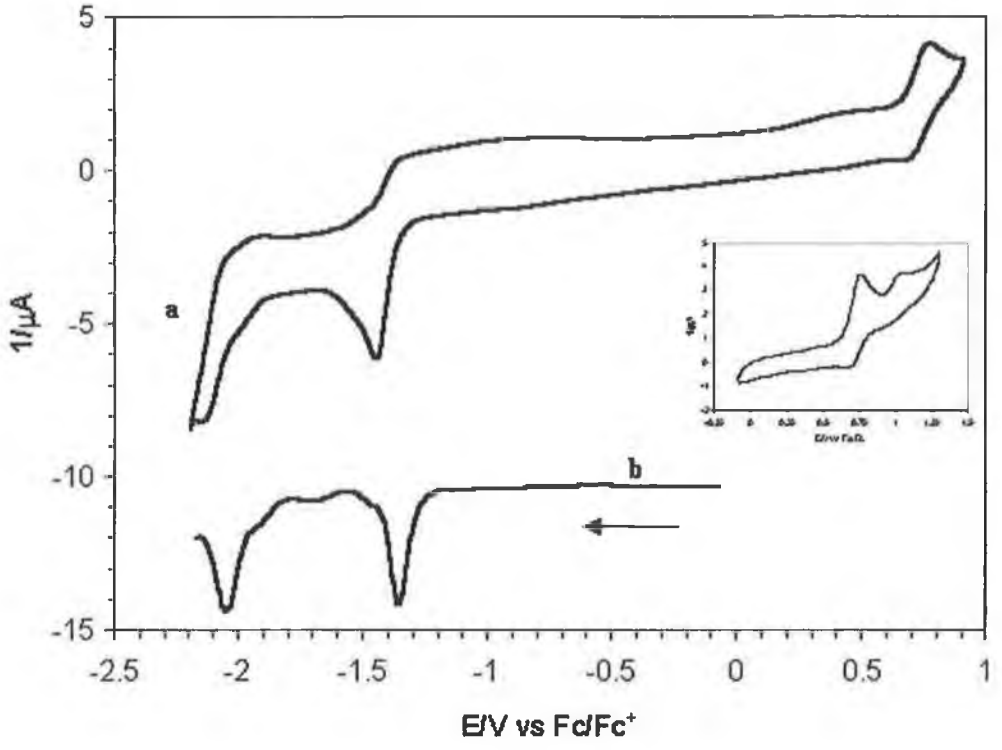

Figure AIV.7 CV (a) and DPV (b) of $[Rh(bpy)_2(NHbpt)]^{2+}$ measured in acetonitrile with 0.1M $TBABF_4$.